People's Democratic Republic of Algeria

Ministry of Higher Education and Scientific Research

University of Larbi Ben M'hidi, Oum El Bouaghi

Faculty of Exact Sciences and Nature and Life Sciences

Dissertation

Submitted to the Department of Mathematics and Computer Science in Candidacy for the Degree of 'Doctorate LMD' in

Applied Mathematics

Submitted by : Amina Aicha Khennaoui

Chaos, Control and Synchronization of Discrete Fractional Systems

Examining Board:

Dr. Adel Ouannas	**MC. A**	University of Larbi Ben M'hidi, Oum El Bouaghi	Supervisor
Dr. Giuseppe Grassi	**Prof**	Universita del Salento, Italy	Co-Supervisor
Dr. Taki Eddine Oussaeif	**MC. A**	University of Larbi Ben M'hidi, Oum El Bouaghi	Chairperson
Dr. Rezzoug Imad	**MC. A**	University of Larbi Ben M'hidi, Oum El Bouaghi	Examiner
Dr. Mohammed-Salah Abdelouahab	**MC. A**	University Center Abdelhafid Boussouf, Mila	Examiner
Dr. Fareh Hannachi	**MC. A**	University of *Larbi Tebessi, Tebessa*	Examiner

Graduation Year : 2020/2021

Acknowledgement

I would like first to express my sincere appreciate to my supervisor **Prof. Adel Ouannas**, who gave me the golden opportunity to do this wonderful dissertation, and which also helped me in doing a lot of research. Without his assistance and dedicated involvement in every step though the process, this project would have never been accomplish. Your insightful feedback pushed me to sharpen my thinking, thank you very much for your support and understanding over these past four yours.

Secondly, I would like to thank my co-supervisor **Prof. Giuseppe Grassi** for providing guidance and feedback throughout this dissertation.

In addition, I would like to thank my parents Ammar Khennaoui and Farida Lahlah for their support and great love. You are always their for me. Finally, I could not have completed this dissertation without the support of my sisters, Roumeissa, Cheima, my brothers, Mohemed Seif, Djellal, and my sweet, Laya. They kept me going and helped me a lot in finalizing this project with in the limited time frame.

Contents

Introduction

Chaotic dynamical systems have been shown to emerge from natural phenomena such as the weather or from designed engineering problems such as the movement of a rigid body in three-dimensional (3D) space. These systems possess different beneficial properties including their random-like trajectories, high sensitivity to initial conditions and ergodicity, chaos theory. Another important property of chaotic systems is that they have attractors characterized by a complicated set of points with a fractal structure commonly referred to as a strange attractor. Such systems have been studies extensively over the last 50 years and have found applications in a wide variety of fields within science and engineering [1]. Depending on the type of calculus involved, these systems can be classified into two main categories: continuous-time and discrete-time. In this thesis, we are interested in discrete-time chaotic systems, which are also referred to as chaotic maps. Over the years, a number of different chaotic maps have been proposed in the literature and applied in different fields including, the Lozi system [2], the generalized Hénon map [3], the Lorenz map [4], the Stefanski map [5], the Rossler map [7], the Arnold map [127] and the Grassi-Miller map [92], etc. All the chaotic attractors in those discrete systems belong to the most common type of attractors with the property that their corresponding initial states are placed close to the unstable periodic orbits or fixed points. Since these attractors can be readily found, they are called "self-excited attractors" [151]. On the other hand, chaotic phenomena, which have been also discovered in discrete-time systems, are distinguished with stable equilibria [154], without equilibrium [13], and hidden attractors with infinite number of equilibrium points [14]. Since the initial conditions in these systems can be only found via massive numerical search, these chaotic attractors are hard to be found. Consequently, this type of attractor has been called "hidden attractor" in literature. Referring to this topic, some papers have been recently published [155–158].

With the discovery of chaos in nonlinear systems, several efforts have been devoted to the study of control methods for effectively stabilizing the chaotic dynamics at the origin; with the purpose to avoid troubles arising from unusual behaviors of a chaotic system. Many control techniques such as adaptive control and fuzzy control methods have been implemented for controlling the chaotic systems. One of the application of this topic is in robotics where the control of the chaotic motion of a rigid study. On the other hand, interest in the chaotic dynamical systems grew exponentially once it became clear that the synchronisation of two chaotic systems is feasible. Chaos synchronization in its simplest form refers to the control of a response chaotic system to force its trajectory towards that of a drive [15]. In this case, the error defined as the difference between the states of the drive and those of the response towards zero as $t \to \infty$. This

means that chaotic systems may be controlled and their path is determined, which highlighted the benefits of the random-like behaviour. Since the pioneering work of Pecora and Carrol, in which they demonstrated chaos synchronisation, chaos synchronization has attracted increasing interests in recent years. There are several different types of synchronization phenomena; such as hybrid synchronization [16], generalized synchronization [17], and inverse full state hybrid projective synchronization [18]. The topics covered by the vast amount of literature include types of synchronisation and the corresponding adaptive control strategies as well as the application of chaos and synchronisation in the fields of science and engineering.

Discrete-time chaotic dynamical systems have been extensively studied over the last few years, and a large number of papers on chaos control, synchronization, and chaos application has been introduced continuously. Chaotic micro-electromechanical resonator model has been analyzed in [19, 20]. Multistability has been observed in a chaotic system with two circles of equilibrium points [21]. The digital chaotic oscillator has been designed and implemented [22]. Complex dynamics of a memristor-based chaotic circuit has been reported in [23]. Perhaps the main application that has recently been considered for such systems and that is closely related to synchronization is in the field of secure communications. In order to achieve secure communication, chaos can be employed in a number of stages. It can be used at the physical layer, either to mask the transmitted message [24], as a modulation carrier [25], or to provide multiple access to the transmission medium [26]. Alternatively, chaos may be used to produce a map based on which data encryption is carried out. Whether secret key or public key encryption is adopted, a set of random keys is required and this is where chaos comes in handy. However, instead of continuous-time chaotic systems, their discrete counterpart is required [27]. At the receiver side, the encryption keys must be reproduced by means of synchronisation, see [28]. This, along with many more applications available for the synchronisation of discrete-time chaotic systems, has motivated many to do research in this subject.

The theory of fractional calculus is old as its inception can be attributed to two of the most prominent figures of modern calculus, L'Hôpital and Leibniz, as early as 1695. The complete framework for this type of calculus was complete by the 1800s. Traditionally the term fractional calculus has referred to studying integration and differentiation of noninteger order. Several definitions of fractional derivatives, including Riemann–Liouville, Caputo, Riesz-Caputo and Grunwald–Letnikov derivatives, are available in the literature. However, the same cannot be said about discrete fractional calculus, which has not seen the light of day until recently. The first definition of a discrete fractional operator was introduced in [31], where the operator was derived by discretizing a continuous-time fractional operator. Successively, several types of difference operators have been proposed, including some fractional *h-difference* operators, which represent further generalizations of the fractional difference operators [32]. The interesting fact about this operator is that it is a generalization of the binomial formula for the $n-th$ difference operator by means of the Gamma function. Efforts have been made to establish a complete framework to study the dynamics and stability of fractional discrete time systems, which have been shown to possess interesting properties that make them more suitable for the modelling of physical phenomena. For example, in [35], Miller and Ross defined the fractional order sum and difference operators, whereas in [39] the author discussed fractional finite difference equations and fractional difference inclusion. Among the most interesting and relevant works on discrete

fractional calculus in the last decade are references [36, 37]. In addition to defining the required notation, operators and numerical methods related to the subject of fractional discrete systems, researchers have paid special attention to the stability of linear and nonlinear systems. Two main methods can be found in the literature for establishing the asymptotic stability of equilibria for fractional discrete systems. The first method is specific to linear systems and works by assessing the eigenvalues of the system matrix [55]. The second method is more generic and is viewed as a natural extension of the direct Lyapunov method for standard systems [56]. More stability results can be found in [57–59].

With the development of science and technology, many complex nonlinear phenomena need to be explained more accurately. Therefore, the fractional-order nonlinear systems which have been updated in recent years are widely applied to describe these phenomena with memory and non-locality. Fractional calculus as a powerful tool for mathematical modelling has been applied in different fields of sciences such as economics, engineering and biologic. In recent years, with the emergence of fractional discrete calculus, some researchers in the field of chaos have found interest in the subject. Many fractional-order continuous-time chaotic systems, such as the fractional-order Lorenz system and the fractional-order Chen system, have been studied, and applied to wide-ranging fields like chaos control, chaotic circuit, image encryption and medicine. However, most researches on chaos based on the theory of fractional calculus are mainly limited to continuous-time chaotic systems, and the study of fractional-order discrete-time chaotic systems is insufficient. In fact, the dynamical behaviors of discrete-time chaotic system are universal and important in the fields ranging from mathematics to information security. Moreover, discrete fractional calculus can avoid the tedious information or calculation error of the numerical discretization for the continuous ones due to the nonlocal property. Thus, researchers turned their attention to apply the theory of discrete fractional calculus to discrete chaotic maps. It is proved that there are abundant dynamical behaviors in the fractional chaotic maps, which lay a foundation for their potential applications. For instance, Wu and Baleanu [103] reported the fractional-order Logistic map using the Caputo like difference operator. They have claimed that the fractional Logistic map have superior characteristics over their integer counterparts, where the chaotic patterns exhibited by the fractional generalized Logistic map depend on the fractional order. This means that the fractional map is more suitable for secure communications and encryption, as it includes a new degree of freedom. These added degrees of freedom can also be used in catching the hidden aspects of real-world phenomena encountered in ecology. Therefore, more and more discrete maps with fractional operators need to be presented, and more abundant and complex dynamics behaviors need to be explored. Besides, it is well known that fractional-order discrete maps are sensitive not only to the small disturbance of parameters and initial conditions but also to the variation of fractional orders, which are the unique advantages of fractional-order systems. Furthermore, fractional-order discrete maps have simple forms and rich dynamics, which are good for system analysis and numerical computation.

In view of the aforesaid motivations, this thesis concerned with different fractional-order discrete time systems. The proposed systems are defined using the Caputo-like difference operator, where the dynamics of the proposed systems are investigated numerically considered from different perspectives. In view of physical interpretation and application, the fractional difference in Caputo sense is more frequently used for the reason that its initial value problems can be

endowed with the same conditions as of integer order case. The main motivation behind this thesis is to assess the benefits of the fractional-order maps, where the asymptotic convergence of the states are established by means of the stability theory of linear fractional discrete systems. We are also interested in the control of this fractional map, including stabilization and synchronization schemes. From these results we find that the proposed fractional order maps has new interesting complex dynamical behaviors.

The thesis is divided into two mains parts:
The first part contain chapter 1, 2 and 3 gives general description of the notation and stability results of discrete fractional calculus that will aid the reader in understanding the analysis to come. Accordingly Chapter 1 contains an introductory overview of the theory of fractional difference operators along with theorems that describe the numerical formula for evaluating a fractional discrete map and the asymptotic stability conditions for the zero equilibrium of a generic fractional discrete map are provided. In addition, chapter 3 provide basic results, concepts and tools on dynamical systems, characteristic Lyapunov exponents and complexity analysis.

The second part contain chapters 4,5,6, 7 and 8, which represent the body of the thesis. This part is concerned with a fractional Caputo-difference form of different families of three-dimensional and two dimensional discrete-time systems with self exited and hidden chaotic attractors. Discrete fractional calculus was employed to analyze the dynamics of the new fractional map. The dynamics of the proposed systems are investigated numerically through, phase plots, bifurcation diagrams, largest Lyapunov exponents and 0-1 test, considered from different perspectives. In addition, we study the existence of chaos and its control and synchronization, where different dimensional nonlinear and linear control laws are proposed for stabilizing at the origin the chaotic dynamics of the proposed systems. The design of these control laws are derived based on the linearisation method. Furthermore, based on the stability theory of linear fractional difference systems, we presents in this part combined synchronization between fractional-order chaotic maps described by the left Caputo difference operator. Some nonlinear controller are designed, which enable synchronization to be achieved between different fractional order chaotic maps with different dimensions. Basically, this part is organized as follows:
Chapter 4 is concerned with fractional Caputo difference form of two dimensional maps with different nonlinearties. The proposed fractional maps are defined as generalization of very well known integer-order maps in the literature. The dynamics of the fractional maps are investigated numerically throught numerical simulations. These fractional models has an ability of a chaotic response which depends on the fractional difference order.

In Chapter 5, novel three dimensional chaotic fractional-order discrete-time systems are presented. Similarly to Chapter 4, the models are described using the Caputo like difference operator. Firstly, three different fractional-order discrete-time systems will be investigated, i.e., Wang's, Rossler's, and Stefanski's maps, while the so-called generalized Hénon map of three dimensions will be studied. Furthermore, the dynamic properties of the fractional-order Grassi-Miller map is illustrated, whereas a three-dimensional Hénon map with Lorenz like attractors is realized in this chapter. Finally, a novel fractional-order triopoly game with bounded rationality, where three firms producing differentiated products compete over a common market. The presence of chaos is confirmed via both the computation of the LEs and the 0-1 test. Also,

ApEn and C_0 algorithm are used to measure the complexity of the proposed models.

Hidden attractor and its presence in fractional-order discrete time systems are presented in Chapter 6. Fractional maps with stable equilibrium, systems with close curve equilibrium points, and systems without equilibrium are reported, respectively. Dynamics of these systems versus parameters are analyzed by LEs, bifurcation diagrams, 0-1 test approximate entropy and C_0 complexity.

Chapter 7 introduces different linear and nonlinear control laws to stabilize the states of these chaotic fractional maps.

In Chapter 8, we discuss chaos synchronization of different classes of fractional maps with "self excited" and "hidden attractors", and establishes the convergence of synchronization errors. Synchronization of fractional order discrete time systems is investigated theoretically and numerically. Numerical simulation are preformed to verify the effectiveness of the proposed synchronization schemes.

Finally, conclusion remarks and future works are drawn in Chapter 9. As a conclusive remark, we would point out that the main contributions and innovations of the thesis can be summarized as follows:

- Novel fractional-order discrete time systems based on the Caputo ν-difference operator.
- Chaos synchronization using linear and nonlinear control laws.
- Chaos stabilization based on very simple controllers.

Part I

Theoretical Study

Chapter 1

Discrete Fractional Calculus

1.1 Introduction

Over the last decade, theory and application of discrete fractional calculus has become an important research topic. The first definition of a discrete fractional operator was introduced in [31], where the operator was derived by discretizing a continuous-time fractional operator. Successively, several types of difference operators have been proposed, including some fractional h-difference operators, which represent further generalizations of the fractional difference operators [34, 41]. Various papers and books exist where some of the key properties of the Caputo operators have been described, see, e.g., [29].

It is well known that the fractional difference calculus have the superiority of the first-order operator linearity, but the basic properties of discrete calculus are not naturally consistent with the integer-order nature discrete calculus. Unlike the integer operator, which is local, the fractional one has infinite memory. To this end, this chapter is dedicated to presenting some definitions, theorems and preliminary facts of fractional difference operators of different types. We begin this chapter by recalling some notation and properties of time scales so that this chapter is self contained. This followed by some detailed analysis of one general class of discrete fractional calculus operators of interest namely "ν-*th fractional sum*", which is equivalent to the standard fractional integral on time scale. In the next sections, the Riemann-Liouville, Caputo and Grunwald-Letnikov fractional order difference operators and their properties are discussed. We see that the Caputo and the earlier defined Riemann-Liouville fractional discrete analogue are related to each other. The commutativity properties of the fractional sum and the fractional difference operators are given and discussed. As for Caputo fractional difference operator, we illustrate a very general Taylor difference formula. This is then applied to transform the initial value problem into an equivalent Voltera difference equation. Moreover, the h-difference operators and their properties are presented. Finally, Z-transform and *Laplace* methods in discrete fractional calculus are reported.

Numerous properties and some not so elementary, are given. Such inequalities are used to state and solve some initial value problems with the Riemann-Liouville and Caputo like difference operators.

1.2 Preliminary considerations

We exhibit here certain definitions and functions in mathematical analysis necessary for our purposes.

Definition 1. Here we restrict our attention to the time scale $\mathbb{N}_a = \{a, a+1, a+2\dots\}$ where $a \in \mathbb{R}$. Let $f : \mathbb{N}_a \to \mathbb{R}$, the forward difference operator is given by:

$$\Delta f(t) = f(t+1) - f(t). \tag{1.1}$$

Higher order differences are defined by composing the difference operator with itself. By using equation (1.1) twice, we obtain the second order difference operator of function $f(t)$ in the form

$$\Delta^2 f(t) = \Delta f(t+1) - \Delta f(t) = f(t+2) - 2f(t+1) + f(t). \tag{1.2}$$

Respectively, we can write a general formula for the n-th order forward difference operator of the function $f(t)$ for $n \in \mathbb{N}$ in the following form:

$$\Delta^n f(t) = \Delta(\Delta^{n-1} f(t)) = \sum_{k=0}^{n} \binom{n}{k} (-1)^{n-k} f(t+k), \qquad t \in \mathbb{N}_a, \tag{1.3}$$

where $\binom{n}{k}$ is a binomial coefficients, for positive value of n are defined as:

$$\binom{n}{k} = \frac{n(n-1)(n-2)\dots(n-k+1)}{k!} = \frac{n!}{k!(n-k)!}. \tag{1.4}$$

The fundamental properties of difference operator Δ are given in the following book [52].

Theorem 1.1.

1. $\Delta^m(\Delta^n x(t)) = \Delta^{m+n} x(t)$ *for all positive integers* m *and* n.
2. $\Delta(x(t) + y(t)) = \Delta x(t) + \Delta y(t)$.
3. $\Delta(Cy(t)) = C\Delta y(t)$ *if* C *is a constant.*
4. $\Delta(x(t)y(t)) = x(t)\Delta y(t) + Ey(t)\Delta x(t)$, *where* E *is the shift operator and is defined by* $Ey(t) = y(t+1)$.
5. $\Delta\left(\frac{x(t)}{y(t)}\right) = \frac{y(t)\Delta x(t) - x(t)\Delta y(t)}{y(t)Ey(t)}$.

In order to give a reasonable treatment of the topic, we begin by recalling the most important function used in fractional calculus "*Euler's Gamma function*", which is defined as follows.

Definition 2. The *Euler's Gamma function* is given by

$$\Gamma(n) = \int_0^\infty t^{n-1} \exp^{-t} dt. \tag{1.5}$$

This function is generalization of a factorial in the following form:

$$\Gamma(n) = (n-1)! \tag{1.6}$$

and it has the following basic properties:

- $\Gamma(\nu) > 0$ for $\nu > 0$.
- $\Gamma(\nu+1) = \nu\Gamma(\nu)$ for $\nu \in \mathbb{C}\backslash(-\mathbb{N}_0)$, with the normalizing condition $\Gamma(1) = 1$.
- $\Gamma(n+1) = n!$ for $n \in \mathbb{N}_0$.
- $\frac{\Gamma(\nu+k)}{\Gamma(\nu)} = (\nu+k-1)\dots(\nu-1)\nu = \prod_{i=0}^{k-1}(\nu-i)$, for $\nu \in \mathbb{C}\backslash(-\mathbb{N}_0)$ and $k \in \mathbb{N}$.

We shall also need the "*falling factorial power function*"which is an elementary function that is often used in conjunction with the discrete fractional calculus, and has the same role of functions t^n in differential and integral calculus.

Definition 3. For a positive integer n, we define the falling factorial power by

$$t^{(n)} = t(t-1)(t-2)..(t-n+1) = \frac{\Gamma(t+1)}{\Gamma(t+1-n)}, \tag{1.7}$$

where the product is zero if $t+1-j = 0$ for some j, where Γ satisfying the factorial equation $\Gamma(n+1) = n\Gamma(n)$. Generaly, for arbitrary ν, we define the generalized falling function as

$$t^{(\nu)} = \frac{\Gamma(t+1)}{\Gamma(t+1-\nu)}. \tag{1.8}$$

The following properties of this factorial function and their proofs can be found in a paper by the authors [32] .

Theorem 1.2. *Assume that the following factorial functions are well defined*

1. $\Delta t^{(\nu)} = \nu t^{(\nu-1)}$.
2. *The following (generalized) power rule*

$$\Delta(t-a)^{(\nu)} = \nu(t-a)^{(\nu-1)}. \tag{1.9}$$

3. $(t-\nu)^{(\nu)} = t^{(\nu+1)}$, *where* $\nu \in \mathbb{R}$.
4. $\nu^{(\nu)} = \Gamma(\nu+1)$.
5. *If* $t \le r$, *then* $t^{(\nu)} \le r^{(\nu)}$ *for any* $\nu > r$.

6. *If* $0 < \nu < 1$ *then* $t^{(\alpha\nu)} \geq (t^{(\alpha\nu)})^{\nu}$, *where* $\alpha \in \mathbb{R}$.

7. $t^{(\alpha+\beta)} = (t-\beta)^{(\alpha)} t^{(\beta)}$.

It is understood that the following identities are only holding whenever the generalized falling functions are well defined.

Notice that when $n \geq k \geq 0$, then the binomial coefficient can be written as

$$\binom{n}{k} = \frac{n!}{(n-k)!k!} = \frac{n^{(k)}}{\Gamma(k+1)}.$$

This relationship between the binomial coefficients and the falling factorial power suggests the following definition of an generalized binomial coefficient.

Definition 4. The "*generalized binomial coefficient* "is defined by

$$\binom{t}{r} = \frac{t^{(r)}}{\Gamma(r+1)}. \tag{1.10}$$

Note that the following relations hold:

- symmetry $\binom{t}{r} = \binom{t}{t-r}$,
- moving out of parentheses $\binom{t}{r} = \frac{t}{r}\binom{t-1}{r-1}$,
- addition formula $\binom{t}{r} = \binom{t-1}{r} + \binom{t-1}{r-1}$.

Here we also use the convention that if the denominator is undefined, but the numerator is defined, then $\binom{n}{k} = 0$.

Now we have the following result, which contains a power rule for differences and closely related formulas for the difference of binomial coefficients.

Theorem 1.3. *The following hold*

- $\Delta_t t^{(r)} = r t^{(r-1)}$.
- $\Delta_t \binom{t}{r} = \binom{t}{r-1}, \quad (r \neq 0)$.
- $\Delta_t \binom{r+t}{t} = \binom{r+t}{t+1}$.

1.3 Fractional difference summation

To make effective use of the fractional difference calculus, we introduce in this section the right inverse operator of the fractional difference operator, which is called the "fractional sum". For expression the definition of the fractional sum, we will first consider the definition of the n-th integer sum. The basic idea behind the definition is intimately related to the unique solution of the the n-th order initial value problem of the form:

$$\begin{cases} \Delta^n y(t) = f(t), \\ y(a+j-1) = 0, \quad j = 1, \ldots, n. \end{cases} \tag{1.11}$$

In a similar way to the indefinite integral in the differential calculus, one can define the solution $y(t) = \Delta^{-n} f(t)$ of the initial value problem 1.11 as:

$$y(t) = \Delta^{-n} f(t) = \sum_{s=a}^{t-1} \sum_{\delta_1=a}^{s-1} .... \sum_{\delta_{n-1}=a}^{\delta_{n-2}-1} f(\delta_{n-1}) = \sum_{s=a}^{t-1} \frac{(t-\sigma(s))^{(n-1)}}{(n-1)!} f(s), \tag{1.12}$$

that is easily proved by induction. Since the Cauchy function $\frac{(t-s-1)^{(n-1)}}{(n-1)!}$ is equal to zero for $s = t-1, t-2, \ldots, t-n+1$, the n-th integer sum of the function $f(t)$ is expressed from equation (1.12) as follows:

$$\Delta_a^{-n} f(t) = \sum_{s=a}^{t-n} \frac{(t-\sigma(s))^{(n-1)}}{(n-1)!} f(s), \quad t \in \mathbb{N}_a. \tag{1.13}$$

It is obvious that the right side of equation (1.13) can be generalized for any positive real number $\nu > 0$ using the Gamma function to remove the discrete nature of the factorial. Based on this observation we give the definition of the ν-th fractional summation as follows.

Definition 5. Assume $f : \mathbb{N}_a \to \mathbb{R}$ and $\nu > 0$, then the ν-th fractional sum of f is defined by

$$\Delta_a^{-\nu} f(t) = \frac{1}{\Gamma(\nu)} \sum_{s=a}^{t-\nu} (t-\sigma(s))^{(\nu-1)} f(s), \qquad \textit{for } t \in \mathbb{N}_{a+\nu}. \tag{1.14}$$

Let us discuss this definition. We see from Eq. (1.14), that the fractional sum $\Delta_a^{-\nu}$ with $n-1 < \nu \leq n$ is identically zero under the assumption that:

$$\Delta_a^{-\nu} f(a+\nu-n) = \Delta_a^{-\nu} f(a+\nu-n+1) = \ldots = \Delta_a^{-\nu} f(a+\nu-1) = 0, \tag{1.15}$$

because the relevant sum vanish at this point. We conclude that the domain of $\Delta_a^{-\nu}$ is $\mathbb{N}_{a+\nu}$, which means that the fractional sum (1.13) maps every function defined on $\mathbb{N}_a$ into function defined on $\mathbb{N}_{a+\nu}$.

Accordingly to the definition of factorial function the fractional sum given in Definition 5 can be rewritten as in the following binomial formula.

Proposition 1. For a function $f : \mathbb{N}_a \to \mathbb{R}$ and $\nu > 0$ be given with $n-1 < \nu \leq n$. For each $t \in \mathbb{N}_{a+\nu}$ the fractional sum is defined as

$$\Delta_a^{-\nu} f(t) = \sum_{k=0}^{-\nu+t-a} (-1)^k \binom{-\nu}{k} f(t-\nu-k). \tag{1.16}$$

Proof. Let f, ν and n be given as in the statement of the theorem and let $t \in \mathbb{N}_{a+\nu}$ be given by $t = a + \nu + n$, for $n \in \mathbb{N}_0$. Recall that the binomial expression

$$\binom{-n}{k} = (-1)^k \binom{n+k-1}{k}, \tag{1.17}$$

may be generalized for $\nu > 0$ to

$$\binom{-\nu}{k} = (-1)^k \binom{\nu+k-1}{k}. \tag{1.18}$$

Then, we have

$$\begin{aligned}
\Delta_a^{-\nu} f(t) &= \frac{1}{\Gamma(\nu)} \sum_{s=a}^{t-\nu} (t - \sigma(s))^{(\nu-1)} f(s) \\
&= \frac{1}{\Gamma(\nu)} \sum_{s=a}^{t-\nu} \frac{\Gamma(t-s)}{\Gamma(t-s-\nu+1)} f(s) \\
&= \frac{1}{\Gamma(\nu)} \sum_{s=a}^{a+n} \frac{\Gamma(a+\nu+n-s)}{\Gamma(a+n-s+1)} f(s) \\
&= \sum_{s=0}^{n} \frac{\Gamma(\nu+n-s)}{\Gamma(\nu)\Gamma(n+1-s)} f(s+a) \\
&= \sum_{s=0}^{n} \binom{n-s+\nu-1}{n-s} f(s+a) \\
&= \sum_{j=0}^{n} (-1)^j \binom{-\nu}{j} f(a-j),
\end{aligned}$$

for $t = a + \nu + n$, $n \in \mathbb{N}_0$. For each $t \in \mathbb{N}_{a+\nu}$, we have:

$$\Delta_a^{-\nu} f(t) = \sum_{k=0}^{-\nu+t-a} (-1)^k \binom{\nu}{k} f(t+\nu-k). \tag{1.19}$$

□

Example 1. From the definition of fractional sum we derive the following sum:

$$\begin{aligned}
\Delta_0^{-\frac{1}{2}} 1 &= \frac{1}{\Gamma(\frac{1}{2})} \sum_{s=0}^{t-\frac{1}{2}} (t-s-1)^{-\frac{1}{2}} \times 1 \\
&= \frac{1}{\Gamma(\frac{3}{2})} \left(- (t-s)^{\frac{1}{2}} \Big|_{s=0}^{t+\frac{1}{2}} \right) \\
&= \frac{1}{\Gamma(\frac{3}{2})} \left(-(-\frac{1}{2})^{\frac{1}{2}} + t^{\frac{1}{2}} \right) \\
&= \frac{2}{\sqrt{\pi}} t^{\frac{1}{2}}.
\end{aligned}$$

1.3.1 Power rule formula

In the fractional order calculus, the power rule functions plays an important rule in the analysis of difference equations with fractional order. Firstly, let us evaluate the fractional sum $\Delta_{a+\mu}^{-\nu}$ of the power function $f(t) = (t-a)^{(\mu)}$, where $\mu \geq 0$ and $\nu > 0$ for $\nu, \mu \notin \mathbb{N}$. To illustrate the previous assertions, we will show that $\Delta_{a+\mu}^{-\nu}(t-a)^{(\mu)}$ is equal to:

$$\Delta_{a+\mu}^{-\nu}(t-a)^{(\mu)} = \frac{\Gamma(\mu+1)}{\Gamma(\mu+\nu+1)}(t-a)^{(\mu+\nu)}. \tag{1.20}$$

The formula (1.20) can be also presented as

$$\Delta_{a+\mu}^{-\nu}(t-a)^{(\mu)} = \mu^{(-\nu)}(t-a)^{(\mu+\nu)} \tag{1.21}$$

for $t \in \mathbb{N}_{a+\nu+\mu}$. In particular, if $f(t) = C$ where C is a constant; then (1.20) implies that

$$\Delta_{a}^{-\nu}C = \frac{C}{\Gamma(\nu+1)}(t-a)^{(\nu)}, \quad \textit{for} \quad t \in \mathbb{N}_{a+\nu}. \tag{1.22}$$

Proof. To demonstrate (1.20), we consider the two cases $\nu = 1$ and $\nu \in (0,1) \cup (1,\infty)$ separately. First let us consider the case $\nu = 1$, then we have by direct calculation:

$$\Delta_{a-\mu}^{-1}(t-a)^{(\mu)} = \Delta_{a-\mu}^{-1}\Delta\left(\frac{(t-a)^{(\mu+1)}}{(\mu+1)}\right),$$

by the classical equality in Theorem 1.2, $\Delta(t-a)^{(\mu)} = \mu(t-a)^{(\mu-1)}$, and therefore:

$$\begin{aligned}
\Delta_{a}^{-1}(t-a)^{(\mu)} &= \sum_{s=a+\mu}^{t-1}\left(\frac{(s+1-a)^{(\mu+1)}}{\mu+1} - (s-a)^{(\mu+1)}\mu + 1\right) \\
&= \frac{(t-a)^{(\mu+1)}}{\mu+1} - \frac{\mu^{(\mu+1)}}{\mu+1} \\
&= \mu^{-1}(t-a)^{(\mu+1)} \\
&= \frac{\Gamma(\mu+1)}{\Gamma(\mu+2)}(t-a)^{(\mu+1)}.
\end{aligned}$$

Secondly, for $\nu \in (0,1) \cup (1,\infty)$; we set the left hand side of equation (1.20) as:

$$\begin{aligned}
g_1(t) = \Delta_{a+\mu}^{-\nu}(t-a)^{(\mu)} &= \frac{1}{\Gamma(\nu)}\sum_{s=a+\mu}^{t-\nu}\frac{\Gamma(t-s)}{\Gamma(t-s-\nu+1)}(s-a)^{(\mu)} \\
&= \frac{1}{\Gamma(\nu)}\sum_{s=\mu+a}^{t-\nu}\frac{\Gamma(t-s)\Gamma(s-a+1)}{\Gamma(t-s-\nu+1)\Gamma(s-a-\mu+1)},
\end{aligned}$$

and for the right term, we set:

$$g_2(t) = \frac{\Gamma(\mu+1)}{\Gamma(\mu+\nu+1)}(t-a)^{(\mu+\nu)}. \tag{1.23}$$

For the two functions g_1 and g_2, we show if both satisfy:

$$g(a+\mu+\nu) = \Gamma(\mu+1) \tag{1.24}$$
$$(t-a-(\mu+\nu)+1)\Delta g(t) = (\mu+\nu)g(t), \quad \textit{for } \ t \in \mathbb{N}_{a+\mu+\nu}. \tag{1.25}$$

In the next steps of the proof, the formula (3) and (4) in Theorem 1.2 are used repeatedly. First, consider g_1; apply $\mu^{(\mu)} = \Gamma(\mu+1)$ to see that:

$$g_1(a+\nu+\mu) = \frac{1}{\Gamma(\nu)} \sum_{s=a+\mu}^{a+\mu} \frac{\Gamma(\mu+\nu-1)}{\Gamma(\mu+\nu-s-\nu+1)} s^{(\mu)} = \frac{\Gamma(\nu)\mu^{(\mu)}}{\Gamma(\nu)} = \Gamma(\mu+1). \tag{1.26}$$

In the case of function g_2, analogously to (1.26), we apply (4) in Theorem 1.2 to see that:

$$g_2(a+\nu+\mu) = \frac{\Gamma(\mu+1)(\mu+\nu)^{(\mu+\nu)}}{\Gamma(\mu+\nu+1)} = \frac{\Gamma(\mu+1)\Gamma(\mu+\nu+1)}{\Gamma(\mu+\nu+1)} = \Gamma(\mu+1), \tag{1.27}$$

both functions g_1 and g_2 satisfy the first condition (1.24).
We now present a tedious calculation to show that g_1 and g_2 satisfies the difference equation in (1.25). Use $(t-\mu)t^{(\mu)} = t^{(\mu+1)}$ and add and subtract μ to write:

$$\begin{aligned}
g_1(t) &= \frac{1}{\Gamma(\nu)} \sum_{s=a+\mu}^{t-\nu} (t-\sigma(s))^{(\nu-1)}(s-a)^{(\mu)} \\
&= \frac{1}{\Gamma(\nu)} \sum_{s=a+\mu}^{t-\nu} (t-\sigma(s)-(\nu-2))(t-\sigma(s))^{(\nu-2)}(s-a)^{(\mu)} \\
&= \frac{1}{\Gamma(\nu)} \sum_{s=a+\mu}^{t-\nu} [(t-a-(\nu+\mu)+1)-(s-a-\mu)](t-\sigma(s))^{(\nu-2)}(s-a)^{(\mu)} \\
&= \frac{(t-a-(\nu+\mu)+1)}{\Gamma(\nu)} \sum_{s=a+\mu}^{t-\nu} (t-\sigma(s))^{(\nu-2)}(s-a)^{(\mu)} \\
&\qquad\qquad - \frac{1}{\Gamma(\nu)} \sum_{s=a+\mu}^{t-\nu} (t-\sigma(s))^{(\nu-2)}(s-a-\mu)(s-a)^{(\mu)} \\
&= h_1(t) - h_2(t),
\end{aligned}$$

where

$$\begin{cases} h_1(t) = \frac{(t-a-(\nu+\mu)+1)}{\Gamma(\nu)} \sum_{s=a+\mu}^{t-\nu} (t-\sigma(s))^{(\nu-2)}(s-a)^{(\mu)} \\ h_2(t) = \frac{1}{\Gamma(\nu)} \sum_{s=a+\mu}^{t-\nu} (t-\sigma(s))^{(\nu-2)}(s-a-\mu)(s-a)^{(\mu)}. \end{cases}$$

Then, taking the difference with respect to $t \in \mathbb{N}_{a+\mu+\nu}$ of the function $g_1(t)$, we get:

$$\begin{aligned}\Delta g_1(t) &= \Delta\left[\frac{1}{\Gamma(\nu)}\sum_{s=a+\mu}^{t-\nu}(t-\sigma(s))^{(\nu-1)}(s-a)^{(\mu)}\right]\\ &= \frac{\nu-1}{\Gamma(\nu)}\sum_{s=a+\mu}^{t-\nu}(t-\sigma(s))^{(\nu-2)}(s-a)^{(\mu)} + \frac{(\nu-1)^{(\nu-1)}(t+1-\nu-a)^{(\mu)}}{\Gamma(\nu)}\\ &= \frac{\nu-1}{\Gamma(\nu)}\sum_{s=a+\mu}^{t-\nu}(t-\sigma(s))^{(\nu-2)}(s-a)^{(\mu)} + (t+1-\nu-a)^{(\mu)}.\end{aligned}$$

Consider now the function $h_2(t)$, sum by parts and note that $\Delta((t-s)^{\nu-1}(s-a)^{(\mu+1)}) = (t-\sigma(s))^{(\nu-1)}(\nu+1)(s-a)^{(\mu)} - (\nu-1)(t-\sigma(s))^{(\nu-2)}(s-a)^{(\mu+1)}$. Also recall $(s-a)^{(\mu+1)} = (s-a-\mu)(s-a)^{(\mu)}$. Thus:

$$\begin{aligned}h_2(t) &= \frac{1}{\Gamma(\nu)}\sum_{s=a+\mu}^{t-\nu}(t-\sigma(s))^{(\nu-2)}(s-a-\mu)(s-a)^{(\mu)}\\ &= \frac{1}{\nu-1}\left(\frac{\mu+1}{\Gamma(\nu)}\sum_{s=a+\mu}^{t-\nu}(t-\sigma(s))^{\nu-1}(s-a)^{(\mu)} - (\nu-1)^{(\nu-1)}(t-a+1-\nu)^{(\mu+1)}\right).\end{aligned}$$

Combining all the results, we derive

$$\begin{cases}\text{-}\,(t-a-(\mu+\nu)+1)\Delta g_1(t) = (\nu-1)h_1(t) + (t+1-\nu-a)^{(\nu+1)}.\\ \text{-}\,(\mu+1)g_1(t) - (\nu-1)h_2(t) = (t+1-\nu-a)^{(\nu+1)}.\end{cases}$$

In summary we have shown

$$\begin{aligned}(t-a-(\mu+\nu)+1)\Delta g_1(t) &= (\nu-1)h_1(t) + (\mu+1)g_1(t) - (\nu-1)h_2(t)\\ &= (\nu-1)g_1(t) + (\mu+1)g_1(t)\\ &= (\mu+\nu)g_1(t).\end{aligned}$$

Using the generalized rule formula (3) of Theorem 1.2 we obtain for g_2:

$$\begin{aligned}(t-a-(\mu+\nu)+1)\Delta g_2(t) &= \frac{(\mu+\nu)\Gamma(\mu+1)(t-a-(\mu+\nu)+1)(t-a)^{(\mu+\nu-1)}}{\Gamma(\mu+\nu+1)}\\ &= \frac{(\mu+\nu)\Gamma(\mu+1)(t-a)^{(\mu+\nu)}}{\Gamma(\mu+\nu+1)}\\ &= (\mu+\nu)g_2(t).\end{aligned}$$

By uniqueness of solutions to the well-posed initial value problem (1.24)-(1.25), we conclude that $g_1 \equiv g_2$ on $\mathbb{N}_{a+\mu+\nu}$. This complete the proof. □

In [58] the authors prove the previous results using different approach. Observe that the n power factorial of $(\nu+n)$ for $n \in \mathbb{N}_0$ is:

$$(\nu+n)^{(\nu)} = \frac{\Gamma(\nu+n+1)}{\Gamma(n+1)} = \frac{\Gamma(\nu)}{n!}\prod_{j=0}^{n}(\nu+j). \tag{1.28}$$

Let $t \in \mathbb{N}_{a+\mu+\nu}$ be given and $t_n = a+\mu+\nu+n$, then

$$\begin{aligned}
\Delta_{a+\mu}^{-\nu}(t-a)^{(\mu)}\Big|_{t=t_n} &= \frac{1}{\Gamma(\nu)}\sum_{s=a+\mu}^{t-\nu}(t-\sigma(s))^{(\nu-1)}(s-a)^{(\mu)} \\
&= \frac{1}{\Gamma(\nu)}\sum_{s=a+\mu}^{a+\mu+n}(a+\mu+\nu+n-s-1)^{(\nu-1)}(s-a)^{(\mu)} \\
&= \frac{1}{\Gamma(\nu)}\sum_{s=0}^{n}(\nu-1+n-s)^{(\nu-1)}(s-a)^{(\mu)} \\
&= \frac{1}{\Gamma(\nu)}\sum_{s=0}^{n}\frac{\Gamma(\nu-1)}{(n-s)!}\prod_{j=0}^{n-s}(\nu-1+j)(s+\mu)^{(\mu)} \\
&= \sum_{s=0}^{n}\frac{(s+\mu)^{(\mu)}}{(n-s)!}\prod_{j=1}^{n-s}(\nu-1+j) = \Gamma(\mu+1)\sum_{s=0}^{n}\frac{1}{(n-s)!}\prod_{j=1}^{n-s}(\nu+j-1)\frac{1}{s!}\prod_{j=1}^{s}(\mu+j) \\
&= \frac{\Gamma(\mu+1)}{n!}\sum_{s=0}^{n}\binom{n}{s}\prod_{j=1}^{n-s}(\nu+j-1)\prod_{j=1}^{s}(\mu+j).
\end{aligned}$$

We notice that for $\nu > 0$ one can have

$$\prod_{j=1}^{n-s}(\nu+j-1) = (-1)^{n-s}\frac{d^{n-s}x^{-\nu}}{dx^{n-s}}\bigg|_{x=1} \qquad \text{and} \qquad \prod_{j=1}^{s}(\nu+j) = (-1)^{s}\frac{d^{s}x^{-\nu-1}}{dx^{s}}\bigg|_{x=1}.$$

Hence

$$\begin{aligned}
\Delta_{a+\mu}^{-\nu}(t-a)^{(\mu)}\Big|_{t=t_n} &\frac{\Gamma(\mu+1)}{n!}\sum_{s=0}^{n}\binom{n}{s}(-1)^{n-s}\left.\frac{d^{n-s}x^{-\nu}}{dx^{n-s}}\right|_{x=1}(-1)^{s}\left.\frac{d^{s}x^{-\nu-1}}{dx^{s}}\right|_{x=1} \\
&= \frac{\Gamma(\mu+1)}{n!}(-1)^{n}\left.\frac{d^{n}x^{-\nu-\mu-1}}{dx^{n}}\right|_{x=1} \\
&= \frac{\Gamma(\mu+1)}{n!}(\nu+\mu+1)\dots(\nu+\mu+1+n-1) \\
&= \frac{\Gamma(\mu+1)}{\Gamma(n+1)}\frac{\Gamma(\nu+\mu+n+1)}{\Gamma(\nu+\mu+1)} \\
&= \frac{\Gamma(\mu+1)}{\Gamma(\nu+\mu+1)}(\nu+\mu+n)^{(\nu+\mu)} \\
&= \left.\frac{\Gamma(\mu+1)}{\Gamma(\nu+\mu+1)}(t-a)^{(\nu+\mu)}\right|_{t=t_n}.
\end{aligned}$$

Let us apply the above lines of reasoning to the fractional sum of function $g(t) = (1+\mu)^{t-a}$ where $t \in \mathbb{N}_{a+\nu}$, $a, \mu \in \mathbb{R}$ and $\nu > 0$. Proceeding as above, we obtain:

$$\begin{aligned}\Delta_a^{-\nu}(1+\mu)^{t-a}\Big|_{t=a+\nu+n} &= \frac{1}{\Gamma(\nu)}\sum_{s=a}^{t-\nu}(t-s-1)^{(\nu-1)}(1+\mu)^{s-a}\\ &= \frac{1}{\Gamma(\nu)}\sum_{s=a}^{a+n}(a+\nu+n-s-1)^{(\nu-1)}(1+\mu)^{s-a}\\ &= \frac{1}{\Gamma(\nu)}\sum_{s=0}^{n}(\nu-1+n-s)^{(\nu-1)}(1+\mu)^{s}\\ &= \sum_{s=0}^{n}\frac{(1+\mu)^s}{(n-s)!}\prod_{j=1}^{n-s}(\nu-1+j). \end{aligned} \tag{1.29}$$

In particular, we have

$$(1+\mu)^s = \frac{(-1)^s}{s!}\frac{d^s h(x)}{dx^s}\Big|_{x=1}, \qquad \text{where} \quad h(x) = \frac{1}{1+(1+\mu)(x-1)},$$

and we have

$$\begin{aligned}\Delta_a^{-\nu}(1+\mu)^{t-a}\Big|_{t=a+\nu+n} &= \frac{(-1)^n}{n!}\sum_{s=0}^{n}\binom{n}{s}\frac{d^{n-s}x^{-\nu}}{dx^{n-s}}\Big|_{x=1}\frac{d^s h(x)}{dx^s}\Big|_{x=1}\\ &= \frac{(-1)^n}{n!}\frac{d^n\left(h(x)x^{-\nu}\right)}{dx^n}\Big|_{x=0}.\end{aligned}$$

The above results allows us to obtain a compact form for the fractional sum. The following definition of the fractional sum was proposed by R. Abu saris and Q. Al-Mdallal in [58].

Theorem 1.4. *For arbitrary $a \in \mathbb{R}$ and $\nu > 0$, the ν-th fractional sum is defined by*

$$\Delta_a^{-\nu}y(t)|_{t=a+\nu+n} = \frac{(-1)^n}{n!}\frac{d^n(h(x)x^{-\nu})}{dx^n}\Big|_{x=1}, \tag{1.30}$$

where $h(x)$ is the generating function defined by

$$h(x) = \sum_{k=0}^{\infty}(-1)^k y(k+a)(x-1)^k, \quad |x-1| < L,\ L > 0.$$

1.3.2 Composing two fractional sums

The results obtained in above subsection allow us to state and prove the commutativity property of the fractional sum. This result plays important role.

Theorem 1.5. *Let f be a real-valued function defined on $\mathbb{N}_a$, where $\mu, \nu > 0$. Then the following equalities hold:*

$$\Delta_{a+\mu}^{-\nu}\Delta_a^{-\mu}f(t) = \Delta_a^{-(\nu+\mu)}f(t) = \Delta_{a+\nu}^{-\mu}\Delta_a^{-\nu}f(t), \quad t \in \mathbb{N}_{a+\nu+\mu}. \tag{1.31}$$

Proof. Let $f : \mathbb{N}_a \to \mathbb{R}$ and $\nu, \mu > 0$. Then, for $t \in \mathbb{N}_{a+\nu+\mu}$ one can right

$$\begin{aligned}
\psi(t) = \Delta_{a+\nu}^{-\mu}\Delta_a^{-\nu} f(t) &= \frac{1}{\Gamma(\nu)}\Delta_{a+\nu}^{-\mu}\left(\sum_{r=a}^{t-\nu}(t-\sigma(r))^{(\nu-1)}f(r)\right) \\
&= \frac{1}{\Gamma(\nu)\Gamma(\mu)}\sum_{s=a+\nu}^{t-\mu}(t-\sigma(s))^{(\mu-1)}\left(\sum_{r=a}^{s-\nu}(s-\sigma(r))^{(\nu-1)}f(r)\right) \\
&= \frac{1}{\Gamma(\nu)\Gamma(\mu)}\sum_{s=a+\nu}^{t-\mu}\sum_{r=a}^{s-\nu}(t-\sigma(s))^{(\mu-1)}(s-\sigma(r))^{(\nu-1)}f(r) \\
&= \frac{1}{\Gamma(\nu)\Gamma(\mu)}\sum_{r=a}^{t-(\mu+\nu)}\sum_{s=r+\nu}^{t-\mu}(t-\sigma(s))^{(\mu-1)}(s-\sigma(r))^{(\nu-1)}f(r).
\end{aligned}$$

Let $x = s - \sigma(r) = s - r - 1$, then

$$\begin{aligned}
\psi(t) &= \frac{1}{\Gamma(\nu)\Gamma(\mu)}\sum_{r=a}^{t-(\mu+\nu)}\left[\sum_{x=\nu-1}^{t-\sigma(r)-\mu}(t-\sigma(r)-\sigma(x))^{(\mu-1)}x^{(\nu-1)}\right]f(r) \\
&= \frac{1}{\Gamma(\nu)}\sum_{r=a}^{t-(\mu+\nu)}\left[\frac{1}{\Gamma(\mu)}\sum_{x=\nu-1}^{(t-\sigma(r))-\mu}((t-\sigma(r))-\sigma(x))^{(\mu-1)}x^{(\nu-1)}\right]f(r) \\
&= \frac{1}{\Gamma(\nu)}\sum_{r=a}^{t-(\mu+\nu)}\left[\Delta_{\nu-1}^{-\mu}(t)^{(\nu-1)}\right]\Big|_{t-r-1}f(r) \qquad (1.32) \\
&= \frac{1}{\Gamma(\nu)}\sum_{r=a}^{t-(\mu+\nu)}\frac{\Gamma(\nu)}{\Gamma(\nu+\mu)}(t-\sigma(r))^{(\nu+\mu-1)}f(r)
\end{aligned}$$

and using formula (1.20)

$$\psi(t) = \frac{1}{\Gamma(\nu+\mu)}\sum_{r=a}^{t-(\mu+\nu)}(t-\sigma(r))^{(\mu+\nu)-1}f(r) = \Delta_a^{-(\mu+\nu)}f(t) = \Delta_a^{-\mu-\nu}f(t).$$

Since ν and μ were chosen arbitrary, the last equality in formula (1.31) also holds. □

1.3.3 Composing fractional sums and differences

Before considering the general composition of ν-th fractional sum with fractional difference operator, we shall state and prove the commutative type properties of the fractional sum and difference operator [34]. Let us now recall a result that will be used later in finding solutions to the boundary value problems originated from the fractional difference calculus.

Proposition 2. For any $\nu > 0$, the following equality holds

$$\Delta^{-\nu}\Delta f(t) = \Delta\Delta^{-\nu}f(t) - \frac{(t-a)^{\nu-1}}{\Gamma(\nu)}f(a), \qquad (1.33)$$

for f is defined on $\mathbb{N}_a$.

Proof. We first calculate the left part of the inequality. Using the summation by part formula [33], given by

$$\sum_{l=a}^{t-1} f(l)\Delta g(l) = f(l)g(l)|_{l=a}^{t} - \sum_{l=a}^{t-1} \Delta f(l)g(l+1), \tag{1.34}$$

we get

$$\begin{aligned}
\Delta_a^{-\nu}\Delta f(t) &= \frac{1}{\Gamma(\nu)}\sum_{s=a}^{t-\nu}(t\sigma(s))^{(\nu-1)}\Delta_s f(s) \\
&= \frac{(t-s)^{(\nu-1)}f(s)}{\Gamma(\nu)}\Big|_a^{t-\nu+1} + \frac{\nu-1}{\Gamma(\nu)}\sum_{s=a}^{t-\nu}(t-\sigma(s))^{(\nu-2)}f(s) \\
&= \frac{(\nu-1)^{(\nu-1)}f(t+1-\nu)}{\Gamma(\nu)} - \frac{(t-a)^{(\nu-1)}}{\Gamma(\nu)}f(a) + \frac{\nu-1}{\Gamma(\nu)}\sum_{s=a}^{t-\nu}(t-\sigma(s))^{(\nu-2)}f(s) \\
&= \frac{1}{\Gamma(\nu-1)}\sum_{s=a}^{t-(\nu-1)}(t-\sigma(s))^{(\nu-2)}f(s) - \frac{(t-a)^{(\nu-1)}}{\Gamma(\nu)}f(a).
\end{aligned} \tag{1.35}$$

We now compute $\Delta\Delta_a^{-\nu}f(t)$. To accomplish this, we need the following version of Leibniz Rule, which is proved in [39]. Let $f : \mathbb{N}_{a+\nu} \times \mathbb{N}_a \to \mathbb{R}$, then for $t \in \mathbb{N}_{a+\nu}$

$$\Delta\left(\sum_{s=a}^{t-\nu} f(t,s)\right) = \sum_{s=a}^{t-\nu}\Delta_t f(t,s) + f(t+1, t+1-\nu). \tag{1.36}$$

Hence

$$\begin{aligned}
\Delta\Delta_a^{-\nu}f(t) &= \frac{1}{\Gamma(\nu)}\left[\sum_{s=a}^{t-\nu}\left(\Delta_t\left((t-\sigma(s))^{(\nu-1)}f(s)\right)\right) + (\nu-1)^{(\nu-1)}f(t-\nu+1)\right] \\
&= \frac{1}{\Gamma(\nu)}\left[\sum_{s=a}^{t-\nu}\left((\nu-1)(t-\sigma(s))^{(\nu-2)}f(s)\right) + (\nu-1)^{(\nu-1)}f(t-\nu+1)\right] \\
&= \frac{1}{\Gamma(\nu-1)}\sum_{s=a}^{t-(\nu-1)}(t-\sigma(s))^{(\nu-2)}f(s).
\end{aligned} \tag{1.37}$$

From (1.35) and (1.37) the desired equality follows. □

In particular if we replace ν by $\nu+1$. In view of the commutativity property of the fractional sum in the previous subsection, the following expression is obtained.

Corollary 1. Assume f is defined on $\mathbb{N}_a$ and let $\nu > 0$, then

$$\Delta_a^{-\nu-1}\Delta f(t) = \Delta_a^{-\nu}f(t) - \frac{(t-a)^{(\nu)}}{\Gamma(\nu+1)}f(a). \tag{1.38}$$

This implies

$$\Delta^{-\nu}f(t) = \Delta^{-\nu-1}\Delta f(t) + \frac{(t-a)^{(\nu)}}{\Gamma(\nu+1)}f(a). \tag{1.39}$$

We can extend proposition 2 to an arbitrary positive integer order. The following version of proposition has been proved in [34].

Proposition 3. For any real number $\nu > 0$ and any positive integer p, the following equality holds

$$\Delta^{-\nu}\Delta^{p} f(t) = \Delta^{p}\Delta^{-\nu} f(t) - \sum_{k=0}^{p-1} \frac{(t-a)^{\nu-p+k}}{\Gamma(\nu+k-p+1)} \Delta^{k} f(a), \tag{1.40}$$

where f is defined on $\mathbb{N}_a$.

Proof. We prove formula (1.40) by induction. Firstly, we would check if it works if we replace f by Δf in formula (1.33)

$$\begin{aligned}
\Delta^{-\nu}\Delta^{2} f(t) &= \Delta\Delta^{-\nu}\Delta f(t) - \frac{(t-a)^{(\nu-1)}}{\Gamma(\nu)}\Delta f(a) \\
&= \Delta\left[\Delta\Delta^{-\nu} f(t) - \frac{(t-a)^{(\nu-1)}}{\Gamma(\nu)} f(a)\right] - \frac{(t-a)^{(\nu-1)}}{\Gamma(\nu)}\Delta f(a) \\
&= \Delta^{2}\Delta^{-\nu} f(t) - \frac{(t-a)^{(\nu-2)}}{\Gamma(\nu-1)} f(a) - \frac{(t-a)^{(\nu-1)}}{\Gamma(\nu)}\Delta f(a) \\
&= \Delta^{2}\Delta^{-\nu} f(t) - \sum_{k=0}^{1} -\frac{(t-a)^{(\nu-2+k)}}{\Gamma(\nu+k-1)}\Delta^{k} f(a).
\end{aligned}$$

Repeated iteration gives the desired results. □

Corollary 2. It is quite easy to notice that if we replace ν by $\nu + p$ and employ Proposition 3, the formula (1.40) can be rewritten as

$$\Delta^{-\nu} f(t) = \Delta^{-\nu-p}\Delta^{p} f(t) + \sum_{k=0}^{p-1} \frac{(t-a)^{(\nu+k)}}{\Gamma(\nu+k+1)}\Delta^{k} f(a). \tag{1.41}$$

We now state and prove the composition property of the ν-th fractional sum with difference operator of integer order p. Note that, the following property has been discussed by Atici and Eloe in [34] for the case $\nu > p$.

Proposition 4. Let p be a positive integer and let $\nu > 0$ with $n - 1 < \nu \leq n$. Then for the function $f : \mathbb{N}_a \to \mathbb{R}$, we have

$$\Delta^{p}[\Delta^{-\nu} f(t)] = \Delta^{-(\nu-p)} f(t), \tag{1.42}$$

for $t \in \mathbb{N}_{a+\nu}$.

Proof. Let f, ν, n and p be as given in the statement of the theorem. Firstly, we should check if it works for $\nu = n$. We have for any $p \in \mathbb{N}$ and $t \in \mathbb{N}_{a+p}$

$$\begin{aligned}
\Delta^{p}\Delta^{-p} f(t) &= \Delta^{p-1}\left[\Delta\Delta_{a+p-1}^{-1}\left(\Delta_{a}^{-(p-1)} f(t)\right)\right] \\
&= \Delta^{p-1}\Delta_{a}^{-(p-1)} f(t) \\
&= f(t).
\end{aligned}$$

Therefore, when $p \geq n$ for any $t \in \mathbb{N}_{a+n}$ we have

$$\Delta^p \Delta^{-n} f(t) = \Delta^{p-n} \left[\Delta^n \Delta_a^{-n} f(t)\right] = \Delta^{p-n} f(t),$$

and when $p < n$

$$\Delta^p \Delta_a^{-n} f(t) = \Delta^p \Delta_{a+n-p}^{-p} \left[\Delta^{-(n-p)} f(t)\right] = \Delta_a^{p-n} f(t).$$

Now, we consider the case $n-1 < \nu < n$. For simplicity, we first show that $\Delta\Delta^{-\nu} f(t) = \Delta^{-(\nu-1)} f(t)$ for $t \in \mathbb{N}_{a+\nu}$. The proof follows by applying the definition of fractional sum and the Leibniz rule as in proof of proposition 2, then we get

$$\begin{aligned}
\Delta\Delta^{-\nu} f(t) &= \frac{1}{\Gamma(\nu)} \Delta \left[\sum_{s=a}^{t-\nu} (t-\sigma(s))^{(\nu-1)} f(s)\right] \\
&= \frac{\nu-1}{\Gamma(\nu)} \sum_{s=a}^{t-\nu} (t-\sigma(s))^{\nu-2} f(s) + f(t+1-\nu) \\
&= \frac{1}{\Gamma(\nu-1)} \sum_{s=a}^{t-(\nu-1)} (t-\sigma(s))^{(\nu-1)-1} f(s) \\
&= \Delta^{-(\nu-1)} f(t).
\end{aligned}$$

Apply the operator to both sides of the last equality we have for any $p \in \mathbb{N}$

$$\Delta^p \Delta_a^{\nu} f(t) = \Delta^{p-1} \left[\Delta \Delta_a^{\nu} f(t)\right] = \Delta^{p-1} \Delta^{-(\nu-1)} f(t) = \Delta^{-(\nu-p)} f(t).$$

This complete the proof. □

1.3.4 Leibenitz formula

Next, we would like to be able to compute the fractional summation of products of two functions. This is possible according to the following theorem. An alternative proof to this formula for ν-sum with carefully stating the domain of the function is given by Atici and Sengul [36].

Theorem 1.6. *Let f be a real-valued function defined on $\mathbb{N}_0$ and g be a real-valued function defined on $\mathbb{N}_a \cup \mathbb{N}_0$, where ν is a real number between 0 and 1. Then the following equality holds*

$$\Delta_0^{-\nu}(fg)(t) = \sum_{k=0}^{\infty} \binom{-\nu}{k} [\Delta^k g(t)][\Delta_0^{-(\nu+k)} f(t+k)], \tag{1.43}$$

where $t \equiv \nu \, (mod\ 1)$ and

$$\binom{-\nu}{k} = \frac{\Gamma(-\nu+1)}{\Gamma(k+1)\Gamma(-\nu-k+1)}.$$

Proof. By the definition of discrete fractional sum, we have

$$\Delta_0^{-\nu}(fg)(t) = \frac{1}{\Gamma(\nu)} \sum_{s=0}^{t-\nu} (t-\sigma(s))^{(\nu-1)} f(s) g(s) \tag{1.44}$$

where $t \equiv \nu \pmod 1$.
By Taylor expansion of $g(s)$, which is given by [33]

$$f(t) = \sum_{i=0}^{n-1} \frac{(t-a)^{(i)}}{i!} \Delta^i f(a) + \frac{1}{(n-1)!} \sum_{l=a}^{t-n} (t-l-1)^{(n-1)} \Delta^n f(l). \tag{1.45}$$

Therefore, we have

$$g(s) = \sum_{k=0}^{\infty} \frac{(s-t)^{(k)}}{k!} \Delta^k g(t) = \sum_{k=0}^{\infty} (-1)^k \frac{\Delta^k g(t)}{k!} (t-\sigma(s)+k)^{(k)}. \tag{1.46}$$

Thus by substituting Taylor series expansion of $g(s)$ in the sum, we have

$$\Delta_0^{-\nu}(fg)(t) = \frac{1}{\Gamma(\nu)} \sum_{s=0}^{t-\nu} (t-\sigma(s))^{\nu-1} f(s) \sum_{k=0}^{\infty} (-1)^k \frac{\Delta^k g(t)}{k!} (t-\sigma(s)+k)^{(k)}. \tag{1.47}$$

Since $(t-\sigma(s))^{(\nu-1)}(t-\sigma(s)+k)^k = (t+k-\sigma(s))^{(\nu+k-1)}$, we have

$$\Delta_0^{-\nu}(fg)(t) = \frac{1}{\Gamma(\nu)} \sum_{k=0}^{\infty} (-1)^k \frac{\Delta^k g(t)}{k!} \sum_{s=0}^{(t+k)-(\nu+k)} (t-\sigma(s)+k)^{(\nu+k-1)} f(s). \tag{1.48}$$

Since $(-1)^k = \frac{\Gamma(-\nu+1)\Gamma(\nu)}{\Gamma(-\nu-k+1)\Gamma(k+\nu)}$ for any nonnegative integer k, the above expression on the right becomes

$$\sum_{k=0}^{\infty} \binom{-\nu}{k} [\Delta^k g(t)][\Delta^{-(\nu+k)} f(t+k)]. \tag{1.49}$$

This completes the proof of the theorem. □

1.4 Riemann difference operator

Having established these fundamental definition and properties of the ν-th fractional sum, we are now in a position to give a first definitions of fractional difference operators as used to be done in usual fractional calculus. Till now, there are three known definitions of fractional difference operators that are the so-called Riemann operator, Caputo-left operator and Grunwald-Letnikov operator. First, let us consider the definition of the Riemann-left difference operator. The definition of the operator can be found in [41].

Definition 6. (Riemann left fractional difference). Let $\nu > 0$, $f : \mathbb{N}_a \to \mathbb{R}$ and $n-1 < \nu < n$, where n denotes a positive integer. The Riemann left fractional operator is defined as

$${}^{RL}\Delta_a^{\nu} f(t) = \Delta^n \Delta_a^{-(n-\nu)} f(t) = \frac{1}{\Gamma(n-\nu)} \Delta^n \left(\sum_{s=a}^{t-(n-\nu)} (t-\sigma(s))^{(n-\nu-1)} f(t) \right). \tag{1.50}$$

Remark 1. Naming this functional the Riemann-left difference operator, in case of integer ν, $\nu = n$, it coincides with the n-order difference operator.

Remark 2. From the fractional sum domaine, it is claire that the fractional Riemann operator maps evry function defined on $\mathbb{N}_a$ into functions defined on $\mathbb{N}_{a+n-\nu}$.

The next theorem unified fractional sum and differences where it was proved in [39].

Theorem 1.7. *Let $f : \mathbb{N}_a \to \mathbb{R}$ and $\nu > 0$ be given, with $n-1 < \nu \leq n$. The following formula for the fractional difference is equivalent to (1.50)*

$$ {}^{RL}\Delta_a^{\nu} f(t) = \begin{cases} \frac{1}{\Gamma(-\nu)} \sum_{s=a}^{t+\nu} (t-\sigma(s))^{-\nu-1} f(s), & n-1 < \nu < n, \\ \Delta^n f(t), & \nu = n. \end{cases} \tag{1.51} $$

Proof. Let f and ν be as in the statement of the theorem. We show that (1.50) is equivalent to (1.51) on $\mathbb{N}_{a+n-\nu}$.
The case $\nu = n$ is obvious, since

$$ {}^{RL}\Delta_a^{\nu} f(t) = \Delta^n \Delta^{-(n-\nu)} f(t) = \Delta^n \Delta_a^{-0} f(t) = \Delta^n f(t). \tag{1.52} $$

Now we discuss the remaining case $n-1 < \nu < n$. Then the direct application of (1.50) yields

$$ \begin{aligned} {}^{RL}\Delta_a^{\nu} f(t) = \Delta^n \Delta_a^{-(n-\nu)} f(t) &= \Delta^n \left[\frac{1}{\Gamma(n-\nu)} \sum_{s=a}^{t-(n-\nu)} (t-\sigma(s))^{n-\nu-1} f(s) \right] \\ &= \frac{\Delta^{n-1}}{\Gamma(n-\nu)} . \Delta \left[\sum_{s=a}^{t-(n-\nu)} (t-\sigma(s))^{n-\nu-1} f(s) \right]. \end{aligned} $$

Recalling the Leibni'z rule:

$$ \Delta \left(\sum_{s=a}^{t-\nu} f(t,s) \right) = \sum_{s=a}^{t-\nu} \Delta_t f(t,s) + f(t+1, t+1-\nu). \tag{1.53} $$

Then applying the Leibni'z rule with respect to the function $\Delta \left[\sum_{s=a}^{t-(n-\nu)} (t-\sigma(s))^{n-\nu-1} f(s) \right]$, we get

$$ \begin{aligned} &= \frac{\Delta^{n-1}}{\Gamma(n-\nu)} \left[\sum_{s=a}^{t-(n-\nu)} \Big((n-\nu-1)(t-\sigma(s))^{n-\nu-2} f(s) \Big) \right. \\ &\qquad \left. + (t+1-\sigma(t+1-(n-\nu)))^{n-\nu-1} f(t+1-(n-\nu)) \right] \\ &= \Delta^{n-1} \left[\sum_{s=a}^{t-(n-\nu)} \frac{(t-\sigma(s))^{n-\nu-2}}{\Gamma(n-\nu-1)} f(s) + f(t+1-(n-\nu)) \right] \end{aligned} $$

$$= \Delta^{n-1}\left[\frac{1}{\Gamma(n-\nu-1)}\sum_{s=a}^{t+1-(n-\nu)}(t-\sigma(s))^{n-\nu-2}f(s)\right]$$
$$= \Delta^{n-1}\left[\frac{1}{\Gamma(n-\nu-1)}\sum_{s=a}^{t-(n-\nu-1)}(t-\sigma(s))^{n-\nu-2}f(s)\right].$$

Repeating the similar procedure $n-2$ times we get

$$\begin{aligned}
{}^{RL}\Delta_a^{\nu}f(t) &= \Delta^{n-1}.\left[\frac{1}{\Gamma(n-\nu-1)}\sum_{s=a}^{t-(n-\nu-1)}(t-\sigma(s))^{n-\nu-2}f(s)\right]\\
&= \Delta^{n-2}\left[\frac{1}{\Gamma(n-\nu-2)}\sum_{s=a}^{t-(n-\nu-2)}(t-\sigma(s))^{n-\nu-3}f(s)\right]\\
&= \ldots \quad \ldots \quad \ldots\ldots \quad \ldots \quad \ldots \quad \ldots \quad \ldots \quad \ldots \quad \ldots\\
&= \Delta^{n-n}\left[\frac{1}{\Gamma(n-\nu-n)}\sum_{s=a}^{t-(n-\nu-n)}(t-\sigma(s))^{n-\nu-(n+1)}f(s)\right]\\
&= \frac{1}{\Gamma(-\nu)}\sum_{s=a}^{t+\nu}(t-\sigma(s))^{-\nu-1}f(s).
\end{aligned}$$

In the sequel we use equalities (1.51) for each point $t \in \mathbb{N}_{a+n-\nu}$ (say $t = a+n-\nu+m$ for some $m \in \mathbb{N}_0$), we see that

$$(t-\sigma(s))^{n-\nu-k-1} = \frac{\Gamma(t-s)}{\Gamma(t-s-n+\nu+k+1} = \frac{\Gamma(a+n-\nu+m-s)}{\Gamma(a+m+k+1-s)},$$

which exists for each $k \in \{1,2,\ldots,n\}$ and for each

$$s \in \{a, a+1, \ldots, t-(n-\nu-k)\} = \{a, a+1, \ldots, a+m+k\}.$$

Finally, note that (1.51) at first glance appears to be valid for all $t \in \mathbb{N}_{a-\nu}$, it only define the ν^{th}-fractional difference on $\mathbb{N}_{a+n-\nu}$. □

Example 2. Let us derive the ${}^{RL}\Delta^{\frac{4}{3}}$ of the function $f(t) = t^{\frac{1}{3}}$, it follows

$${}^{RL}\Delta^{\frac{4}{3}}f(t) = \Delta^2\left(\Delta^{-\frac{2}{3}}t^{\frac{1}{3}}\right) = K\Delta^2 t^{\frac{2}{3}+\frac{1}{3}} = 0.$$

Example 3. As an example, we compute the ν-th order difference of the product $tf(t)$, where f and t are defined on $\mathbb{N}_0$ and on $\mathbb{N}\cup\mathbb{N}_0$ respectively, and $0<\nu<1$. It follows from Leibiniz formula, given in Theorem 1.6, that

$${}^{RL}\Delta^{\nu}(tf(t)) = \Delta\Delta^{-(1-\nu)}(tf(t)) = \Delta\sum_{k=0}^{\infty}\binom{-1+\nu}{k}\Delta^k t\Delta^{-(1+\nu+k)}f(t+k), \tag{1.54}$$

for $t \equiv \nu \pmod 1$.

Since $\Delta^k t = 0$ for $k \geq 2$, we have

$$\begin{aligned} {}^{RL}\Delta^{\nu}(tf(t)) &= \Delta\left[t\Delta^{-(1-\nu)}f(t) + (\nu-1)\Delta^{-(2-\nu)}f(t+1)\right] \\ &= \Delta^{-(1-\nu)}f(t+1) + t\ {}^{RL}\Delta^{\nu}f(t) + (\nu-1)\Delta^{-(1-\nu)}f(t+1) \\ &= \nu\Delta^{-(1-\nu)}f(t+1) + t\ {}^{RL}\Delta^{\nu}f(t), \end{aligned}$$

for $t \equiv \nu \pmod 1$. If the domaine of function $g(t) = t$ is $\mathbb{Z}$, then the Leibiniz formula implies that:

$${}^{RL}\Delta^{\nu}(tf(t)) = \nu\Delta^{-(1-\nu)}f(t) + (t+\nu)\ {}^{RL}\Delta^{\nu}f(t). \tag{1.55}$$

Example 4. Let us now calculate the fractional difference of the power rule function $(t-a)^{\nu}$ for $t \in \mathbb{N}_{a+\mu+n-\nu}$

$$\begin{aligned} \Delta^{\nu}_{a+\mu}(t-a)^{(\mu)} &= \Delta^n\left[\Delta^{-(n-\nu)}_{a+\mu}(t-a)^{(\mu)}\right] \\ &= \Delta^n\left[\frac{\Gamma(\mu+1)}{\Gamma(\mu+1+n-\nu)}(t-a)^{(\mu+n-\nu)}\right] \\ &= \frac{\Gamma(\mu+1)}{\Gamma(\mu+1+n-\nu)}\left((\mu+n-\nu)\dots(\mu+1-\nu)\right)(t-a)^{(\mu-\nu)}. \end{aligned}$$

Using the fractional sum of the power formula (1.20)

$$\Delta^{\nu}_{a+\mu}(t-a)^{(\mu)} = \frac{\Gamma(\mu+1)}{\Gamma(\mu+1+n-\nu)}\frac{\Gamma(\mu+n-\nu+1)}{\Gamma(\mu+1-\nu)}(t-a)^{(\mu-\nu)}.$$

In the next proposition, the binomial coefficient is used to define the Riemann like operator of order $\nu > 0$ for a real valued function.

Proposition 5. (see [39]). For a function $f : \mathbb{N}_a \to \mathbb{R}$ the Riemann like operator of order $\nu > 0$ is given by

$$\Delta^{\nu}_{a}f(t) = \sum_{k=0}^{\nu+t-a}(-1)^k\binom{\nu}{k}f(t+\nu-k), \tag{1.56}$$

with $t \in \mathbb{N}_{a+n-\nu}$.

Proof. Similar to the proof of Proposition 1. Let $f : \mathbb{N}_a \to \mathbb{R}$ and $\nu > 0$ such that $\nu \notin \mathbb{N}$, then

the fractional sum for $t = a + n - \nu + m$, for some $m \in \mathbb{N}_0$, is given by:

$$\begin{aligned}
\Delta_a^{\nu} f(t) &= \frac{1}{\Gamma(-\nu)} \sum_{s=a}^{t+\nu} (t - \sigma(s))^{(-\nu-1)} f(s) \\
&= \sum_{s=a}^{t+\nu} \frac{\Gamma(t-s)}{\Gamma(t-s+\nu+1)\Gamma(-\nu)} f(s) \\
&= \sum_{s=a}^{a+n+m} \frac{\Gamma(a+n-\nu+m-s)}{\Gamma(a+n+m-s+1)\Gamma(-\nu)} f(s) \\
&= \sum_{s=0}^{n+m} \frac{\Gamma(n+m-s-\nu)}{\Gamma(n+m-s+1)\Gamma(-\nu)} f(s+a) \\
&= f(a+n+m) + \sum_{s=0}^{n+m-1} \frac{(n+m-1-s-\nu)\dots(-\nu)}{\Gamma(n+m-s+1)} f(s+a) \\
&= f(a+n+m) + \sum_{s=0}^{n+m-1} (-1)^{n+m-s} \frac{\nu\dots(\nu-(n+m-s)+1)}{\Gamma(n+m-s+1)} f(s+a) \\
&= \sum_{s=0}^{n+m} (-1)^{n+m-s} \binom{\nu}{n+m-s} f(s+a) \\
&= \sum_{k=0}^{n+m} (-1)^{k} \binom{\nu}{k} f(a+n+m-k) \\
&= \sum_{k=0}^{n+m} (-1)^{k} \binom{\nu}{k} f\left((a+n-\nu+m)+\nu-k\right) \\
&= \sum_{k=0}^{\nu+t-a} (-1)^{k} \binom{\nu}{k} f(t+\nu-k),
\end{aligned}$$

which complete the proof. □

Remark 3. Note that when $\nu = n$, the formula (1.56) reduces to the traditional binomial formula:

$$\Delta^n = \sum_{k=0}^{n} (-1)^k \binom{n}{k} f(t+n-k), \qquad \text{for } t \in \mathbb{N}_a.$$

In the next theorem of this section we discuss another important property of fractional difference operators, namely the continuity with respect to the order of the operators. A proof of this result may be found in [39].

Theorem 1.8. *Let $f : \mathbb{N}_a \to \mathbb{R}$, $\nu > 0$ and let $t_{\nu,m} = a + \lceil \nu \rceil - \nu + m$ be a fixed but arbitrary point in domain of operator $\Delta_a^{\nu} f$ where $m \in \mathbb{N}_0$. Then for each fixed $m \in \mathbb{N}_0$, $\nu \to \Delta_a^{\nu} f(t_{t,m})$ is continuous on $[0, \infty)$.*

Proof. Let $f : \mathbb{N}_a \to \mathbb{R}$ be given, and fix $n \in \mathbb{N}$ and $m \in \mathbb{N}_0$. It is easy to show that:

$$\Delta_a^\nu f(a+n-\nu+m) \quad \textit{is continuous with respect to } \nu \textit{ on } (n-1,n) \tag{1.57}$$
$$\Delta_a^\nu f(a+n-\nu+m) \to \Delta^n f(a+m) \textit{ as } \nu \to n^- \tag{1.58}$$
$$\Delta_a^\nu f(a+n-\nu+m) \to \Delta^{n-1} f(a+m+1) \textit{ as } \nu \to (n-1)^+ \tag{1.59}$$

We begin with the case (1.57), for any fixed $\nu \in (n-1,n)$ we have

$$\begin{aligned}
\Delta_a^\nu f(a+n-\nu+m) &= \frac{1}{\Gamma(-\nu)} \sum_{s=a}^{t+\nu} (t-\sigma(s))^{-(\nu+1)} f(s)\Big|_{t=a+n-\nu+m} \\
&= \frac{1}{\Gamma(-\nu)} \sum_{s=a}^{a+n+m} (a+n-\nu+m-\sigma(s))^{-(\nu+1)} f(s) \\
&= \frac{1}{\Gamma(-\nu)} \sum_{s=a}^{a+n+m} \frac{\Gamma(a+n-\nu+m-s)}{\Gamma(a+n+m-s+1)} f(s) \\
&= \sum_{s=a}^{a+n+m} \frac{1}{\Gamma(a+n+m-s+1)} \frac{\Gamma(a+n-\nu+m-s)}{\Gamma(-\nu)} f(s) \\
&= \sum_{s=a}^{a+n+m+1} \left(\frac{(a+n-\nu+m-s-1)\dots(-\nu)}{(a+n+m-s)} f(s) \right) + f(a+n+m) \\
&= \sum_{i=1}^{n+m} \left(\frac{(i-1-\nu)\dots(-\nu)}{i!} f(a+n+m-i) \right) + f(a+n+m).
\end{aligned} \tag{1.60}$$

Since (1.60), an expression for $\Delta_a^\nu f(a+n-\nu+m)$, is clearly continuous with respect to ν on $(n-1,n)$. Thus we have demonstrated (1.60).

In the case (1.58) we take the limit of (1.60) as $\nu \to n^-$:

$$\begin{aligned}
&\lim_{\nu \to n^-} \Delta_a^\nu f(a+n-\nu+m) \\
&= \lim_{\nu \to n^-} \left[\sum_{i=1}^{n+m} \left(\frac{(i-1-\nu)\dots(-\nu)}{i!} f(a+n+m-i) \right) + f(a+n+m) \right] \\
&= \sum_{i=1}^{n+m} \left(\frac{(i-1-n)\dots(-n)}{i!} f(a+n+m-i) \right) + f(a+n+m) \\
&= \sum_{i=1}^{n} \left(\frac{(i-1-\nu)\dots(-\nu)}{i!} f(a+n+m-i) \right) + f(a+n+m)
\end{aligned} \tag{1.61}$$

$$
\begin{aligned}
&= \sum_{i=1}^{n} \left((-1)^i \frac{(n)\dots(\nu-i+1)}{i!} f(a+n+m-i) \right) + f(a+n+m) \\
&= \sum_{i=1}^{n} \left((-1)^i \binom{n}{i} f(a+n+m-i) \right) + f(a+n+m) \\
&= \sum_{i=1}^{n} (-1)^i \binom{n}{i} f(a+n+m-i) \\
&= \sum_{i=1}^{n} (-1)^i \binom{n}{i} f((a+m)+n-i) \\
&= \Delta^n f(a+m),
\end{aligned}
$$

and hence it remains to prove (1.59). Similarly, we take the limit of (1.59) as $\nu \to (n-1)^+$; we obtain:

$$
\begin{aligned}
&\lim_{\nu \to (n-1)^+} \Delta_a^{\nu} f(a+n-\nu+m) \\
&= \lim_{\nu \to (n-1)^+} \left[\sum_{i=1}^{n+m} \left(\frac{(i-1-\nu)\dots(-\nu)}{i!} f(a+n+m-i) \right) + f(a+n+m \right] \\
&= \sum_{i=1}^{n+m} \left(\frac{(i-n)\dots(-n+1)}{i!} f(a+n+m-i) \right) + f(a+n+m) \\
&= \sum_{i=1}^{n-1} \left((-1)^i \frac{(n-1)\dots(n-i)}{i!} f(a+n+m-i) \right) + f(a+n+m) \\
&= \sum_{i=1}^{n-1} \left((-1)^i \binom{n-1}{i} f(a+n+m-i) \right) + f(a+n+m) \\
&= \sum_{i=0}^{n-1} \left((-1)^i \binom{n-1}{i} f(a+m+1+(n-1)-i) \right) \\
&= \Delta^{n-1} f(a+m+1).
\end{aligned}
$$

as desired. □

1.4.1 Relation between Riemann difference operator and fractional sum

Having established a theory of Riemann difference operator and ν-th fractional sum separately, we now investigate how they interact. With the help of Proposition 4 and Theorem 1.5, we obtain the composing rule of fractional differences with fractional sums which was proved in [39].

Proposition 6. Let $f : \mathbb{N}_a \to \mathbb{R}$ be given and suppose $\nu, \mu > 0$ with $n-1 < \nu \leq n$. Then

$$
{}^{RL}\Delta_{a+\mu}^{\nu} \Delta_a^{-\mu} f(t) = \Delta_a^{\nu-\mu} f(t), \quad \text{for } t \in \mathbb{N}_{a+\mu+n-\nu}. \tag{1.62}
$$

Proof. Let f, ν, n and ν be given as in the statement of the theorem and let $t \in \mathbb{N}_{a+\mu+n-\nu}$. Then

$$\begin{aligned}\Delta_{a+\mu}^{\nu}\Delta_{a}^{-\mu}f(t) &= \Delta^{n}\Delta_{a+\mu}^{-(n-\nu)}\Delta_{a}^{-\mu}f(t)\\ &= \Delta^{n}\Delta_{a}^{-(n-\nu+\mu)}f(t).\end{aligned}$$

By the composition rule presented in Theorem 1.5, one can get

$$\begin{aligned}&= \Delta_{a}^{n-(n-\nu+\mu)}f(t), \textit{ by Proposition 4},\\ &= \Delta_{a}^{\nu-\mu}f(t).\end{aligned}$$

□

When $\nu > 0$ and $f \in \mathbb{N}_a$, the left Riemann difference operator ${}^{RL}\Delta_{a+\nu}^{\nu}$ provide operations inverse to the ν-th fractional sum operator $\Delta^{-\nu}$, given in (1.14) from the left and right. More precisely, we have the following situations.

Proposition 7. [40] For $\nu > 0$ and f defined in a suitable domain $\mathbb{N}_a$, we have for $t \in \mathbb{N}_{a+n} \subset \mathbb{N}_a$

$${}^{RL}\Delta_{a+\nu}^{\nu}\Delta^{-\nu}f(t) = f(t), \tag{1.63}$$

and

$$\Delta_{a+n-\nu}^{-\nu}\,{}^{RL}\Delta^{\nu}f(t) = f(t), \;\; \nu \notin \mathbb{N}. \tag{1.64}$$

Remark 4. If the fractional order ν is not as required in the assumptions of Proposition 7, then equation (1.64) is not true.

If $t \in \mathbb{N}_{a+n-\mu+\nu}$, then we obtain a different representation for fractional sum and fractional Riemann operator.

Proposition 8. [39] Let $f : \mathbb{N}_a \to \mathbb{R}$ be given and suppose $\nu > 0$, $\mu > 0$ with $0 < \mu \leq n$, then for $t \in \mathbb{N}_{a+n-\mu+\nu}$

$$\Delta_{a+n-\mu}^{-\nu}\Delta_{a}^{\mu}f(t) = \Delta_{a}^{\mu-\nu}f(t) - \sum_{j=0}^{n-1}\frac{\Delta^{j-(n-\mu)}f(a+n-\mu)}{\Gamma(\nu-n+j+1)}(t-a-n+\mu)^{(\nu-n+j)}. \tag{1.65}$$

Proof. Suppose that ν, $\mu > 0$ with $n-1 < \mu \leq$. Defining

$$g(t) = \Delta_{a}^{-(n-\mu)}f(t) \quad \textit{and} \quad b = a+n-\mu, \tag{1.66}$$

where b is the first point of the g function, we have for $t \in \mathbb{N}_{a+n-\mu+\nu}$, and by Proposition 4

$$\begin{aligned}\Delta_{a+n-\mu}^{-\nu}\Delta_{a}^{\mu}f(t) = \Delta_{a+n-\mu}^{-\nu}\Delta^{n}(g(t)) &= \Delta_{a+n-\mu}^{n-\nu}g(t) - \sum_{j=0}^{n-1}\frac{\Delta^{j}g(b)}{\Gamma(\nu-n+j+1)}(t-b)^{\nu-n+j}\\ &= \Delta_{a+n-\mu}^{n-\nu}\Delta_{a}^{-(n-\mu)}f(t) - \sum_{j=0}^{n-1}\frac{\Delta^{j}\Delta^{-(n-\mu)}f(b)}{\Gamma(\nu-n+j+1)}(t-b)^{\nu-n+j}\\ &= \Delta_{a}^{\mu-\nu}f(t) - \sum_{j=0}^{n-1}\frac{\Delta_{a}^{j-n+\mu}f(a+n-\mu)}{\Gamma(\nu-n+j+1)}(t-a-n+\mu)^{\nu-n+j},\end{aligned}$$

where in this last step we applied Proposition 6 and in the case $\nu > n$, Theorem 1.5. □

1.4.2 Composing two fractional difference operators

We now consider the concatenation properties of two fractional difference operators. Unlike fractional sum operator, fractional difference operators do not commute always, i.e. $\Delta^{\nu}\Delta^{\mu} \neq \Delta^{\nu+\mu} \neq \Delta^{\mu}\Delta^{\nu}$. To show this, we begin with the commutativity property of integer difference operator and fractional difference operator ν.

Lemma 1. Let $f : \mathbb{N}_a \to \mathbb{R}$ be given. For any integer number p and $\nu > 0$ with $n-1 < \nu \leq n$, we have

$$\Delta^{p}\Delta_a^{\nu} = \Delta_a^{p+\nu} f(t), \quad \textit{for } t \in \mathbb{N}_{a+n-\nu} \tag{1.67}$$

Under Theorem 1.5, Proposition 2 and that $\Delta^{-(n-\nu)} f(a+n-\nu-1) = 0$, the following result can be directly stated.

Proposition 9. [32] Let $p-1 < \nu < p$ where p is a positive integer Proposition 2 implies that

$$\Delta\, {}^{RL}\Delta^{\nu} f(t) = {}^{RL}\Delta^{\nu}\Delta f(t) + \frac{(t-a)^{(-\nu-1)}}{\Gamma(-\nu)} f(a). \tag{1.68}$$

We extend the previous result here to the fully fractional case with μ any positive real number.

Theorem 1.9. *[39] Let $f : \mathbb{N}_a \to \mathbb{R}$ be given and suppose $\nu, \mu > 0$ with $n-1 < \nu \leq n$ and $m-1 < \mu \leq m$. Then for $t \in \mathbb{N}_{a+m-\mu+n-\nu}$*

$$\Delta_{a+m-\mu}^{\nu}\Delta_a^{\mu} f(t) = \Delta^{\nu+\mu} f(t) - \sum_{j=0}^{m-1} \frac{\Delta_a^{j-(n-\mu)} f(a+m-\mu)}{\Gamma(-\nu-m+j+1)} (t-a-m+\mu)^{-\nu-m+j}. \tag{1.69}$$

Proof. Let f, ν and μ be given as in the statement of theorem. If $n-1 < \nu < n$, then we have for $t \in \mathbb{N}_{a+m-\mu+n-\nu}$

$$\begin{aligned}
\Delta_{a+m-\mu}^{\nu}\Delta_a^{\mu} f(t) &= \Delta^{n}\left[\Delta_{a+m-\mu}^{-(n-\nu)}\Delta_a^{\mu} f(t)\right] \\
&= \Delta^{n}\left[\Delta_a^{-n+\nu+\mu} f(a+m-\nu) - \sum_{j=0}^{m-1} \frac{\Delta^{j-m+\mu} f(a+m-\mu)}{\Gamma(n-\nu-m+j+1)} (t-a-m+\mu)^{(n-\nu-m+j)}\right] \\
&= \Delta^{\nu+\mu} f(t) - \sum_{j=0}^{m-1} \frac{\Delta^{j-m+\mu} f(a+m-\mu)}{\Gamma(\nu-m+j+1)} (t-a-m+\mu)^{(-\nu-m+j)}.
\end{aligned}$$

□

By the same token as in the Theorem 1.9, we may write in reverse order

$$\Delta_{a+n-\nu}^{\mu}\Delta_a^{\nu} f(t) = \Delta^{\mu+\nu} f(t) - \sum_{j=0}^{n-1} \frac{\Delta_a^{j-(m-\nu)} f(a+m-\mu)}{\Gamma(-\mu-n+j+1)} (t-a-n+\nu)^{-\mu-m+j}, \tag{1.70}$$

where the terms in the summation vanish if $\mu \in \mathbb{N}_0$.

Combining the above theorem with formula (1.70) we obtain the following composition rule

Corollary 3. [39] Let $f : \mathbb{N}_a \to \mathbb{R}$ and $\nu, \mu > 0$ be given with $n-1 < \nu \leq n$ and $m-1 < \nu \leq m$. Then for $t \in \mathbb{N}_{a+m-\mu+n-\nu}$, we have

$$\Delta^{\nu}_{a+m-\nu}\Delta^{\mu}_{a} f(t) = \Delta^{\mu}_{a+n-\nu}\Delta^{\nu}_{a} f(t) + \sum_{j=0}^{n-1} \frac{\Delta_a^{j-(m-\nu)} f(a+m-\mu)}{\Gamma(-\mu-n+j+1)}(t-a-n+\nu)^{-\mu-n+j} - \sum_{j=0}^{m-1} \frac{\Delta_a^{j-(m-\mu)} f(a+m-\mu)}{\Gamma(-\nu-m+j+1)}(t-a-m+\mu)^{-\nu-m+j}.$$

1.4.3 Summation by pats formula

The summation by parts formula is the discrete analogue of the integration by parts formula, and it can be used to compute certain indefinite sums as the integration by parts formula is used to compute integrals. In the classical case we have the following well knows result (that we have already used in the proof of Theorem 1.6).

Lemma 2. [33] Let $f(k)$ and $g(k)$ be defined on $\mathbb{N}_a$. Then, for all $t \in \mathbb{N}_a$

$$\sum_{l=a}^{t-1} f(l)\Delta g(l) = f(l)g(l)|_{l=a}^{t} - \sum_{l=a}^{t-1} \Delta f(l) g(l+1). \tag{1.71}$$

The following theorem transfers the summation by parts formula to the fractional setting.

Theorem 1.10. *[36] Let f and g be real be real-valued functions and $0 < \nu < 1$. $f(b+\nu-2) = 0$ and $f(a+\nu-2) = 0$ or $g(a+\nu-1) = 0$ and $g(b+\nu-1) = 0$, then the following equality holds*

$$\sum_{s=a}^{b-1} f(s+\nu-1)\, {}_s\Delta^{\nu}_{a+\nu-1} g(s) = \sum_{s=a}^{b-1} g(s+\nu-1)_{b+\nu-1}\Delta^{\nu}_{s} f^{\rho}(s+2(\nu-1)), \tag{1.72}$$

where $f^{\rho} = f \circ \rho$ with $\rho(t) = t-1$.

Proof. To prove formula (1.72) we use the definition of fractional difference on the left side of the equality (1.72) to obtain

$$\sum_{s=a}^{b-1} f(s+\nu-1)\, {}_s\Delta^{\nu}_{a+\nu-1} g(s) = \sum_{s=a}^{b-1} f(s+\nu-1)\Delta\Delta^{-(1-\nu)} g(s). \tag{1.73}$$

Applying summation by parts formula for Δ-operator (1.71), we get

$$\begin{aligned}
&\sum_{s=a}^{b-1} f(s+\nu-1)\Delta_s\, \Delta_{a+\nu-1}^{-(1-\nu)} g(s) \\
&= f(s+\nu-2)\, {}_s\Delta_{a+\nu-1}^{-(1-\nu)} g(s)\big|_a^b - \sum_{s=a}^{b-1} {}_s\Delta_{a+\nu-1}^{-(1-\nu)} g(s)\Delta_s f(s+\nu-2) \\
&= \frac{-1}{\Gamma(1-\nu)} \sum_{s=a}^{b-1} \sum_{\tau=a+\nu-1}^{s-(1-\nu)} (s-\sigma(\tau))^{(-\nu)} g(\tau)\Delta_s f(s+\nu-2) \\
&= \frac{-1}{\Gamma(1-\nu)} \sum_{\tau=a+\nu-1}^{b-2+\nu} \sum_{s=\tau+1-\nu}^{b-1} (s-\sigma(\tau))^{-\nu} g(\tau)\Delta_s f(s+\nu-2) \\
&= \frac{-1}{\Gamma(1-\nu)} \sum_{u=a}^{b-1} \sum_{s=u}^{b-1} (s-\nu-u)^{-\nu} g(u+\nu-1)\Delta_s f(s+\nu-2). \qquad (1.74)
\end{aligned}$$

Now, we apply the summation by parts formula for Δ-operator to the equation (1.74) to get

$$\begin{aligned}
&\sum_{s=u}^{b-1} (s-\nu-u)^{-\nu}\Delta_s f(s+\nu-2) \\
&\qquad = \left[(s-\nu-u-2)^{-\nu} f(s+\nu-2)\right]\big|_u^b - \sum_{s=u}^{b-1} \Delta_s (s-\nu-u-1)^{-\nu} f(s+\nu-2). \qquad (1.75)
\end{aligned}$$

Since $[(s-\nu-1)^{\nu} f(s+\nu-2)]|_u^b = 0$, then (1.75) becomes

$$\begin{aligned}
\frac{-1}{\Gamma(1-\nu)} \sum_{s=u}^{b-1} (s-\nu-u)^{-\nu}\Delta_s f(s+\nu-2) &= \frac{1}{\Gamma(1-\nu)} \sum_{s=u}^{b-1} \Delta_s (s-\nu-u-1)^{-\nu} f(s+\nu-2) \\
&= \frac{1}{\Gamma(1-\nu)} (-\nu) \sum_{s=u}^{b-1} (s-\nu-u-1)^{-1-\nu} f(s+\nu-2). \qquad (1.76)
\end{aligned}$$

It follows from [Theorem 8.50 in [38]]

$$\Delta_u \sum_{s=u}^{b-1} (s-\nu-u)^{-\nu} f(s+\nu-2) = \nu \sum_{s=u}^{b-1} (s-\nu-\sigma(u))^{(-1-\nu)} f(s+\nu-2). \qquad (1.77)$$

Hence the expression in (1.76) becomes

$$\begin{aligned}\frac{-1}{\Gamma(1-\nu)}\sum_{s=u}^{b-1}(s-\nu-u)^{-\nu}\Delta_s f(s+\nu-2) &= \frac{-1}{\Gamma(1-\nu)}\Delta_u\sum_{s=u}^{b-1}(s-\nu-u)^{-\nu}f(s+\nu-2)\\ &= \frac{-1}{\Gamma(1-\nu)}\Delta_u\sum_{s=u}^{b-1}(s-\sigma(u+\nu-1))^{-\nu}f^{\rho}(s+\nu-1)\\ &= \frac{1}{\Gamma(1-\nu)}(-\Delta_u)\sum_{s=u-1+\nu}^{b+\nu-1}(s-\sigma(u+2\nu-2))^{-\nu}f^{\rho}(s)\\ &=_{b+\nu-1}\Delta_s^{\nu}f^{\rho}(u+2(\nu-1)).\end{aligned}$$

Putting this into equation (1.74) we have the desired result. □

1.4.4 Initial value problem

In this section, we discuss initial value problem for orders $\nu \in]0,1]$ and obtain the existence and uniqueness of a solution. Consider the following nonlinear fractional difference equation with an initial condition

$$\begin{cases}{}^{RL}\Delta_a^{\nu}y(t) = f(t+\nu-1, y(t+\nu-1)), \quad t = 0,1,2,\dots,\\ \Delta^{\nu-1}|_{t=0} = a_0,\end{cases} \tag{1.78}$$

where $\nu \in (0,1]$, f is a real-valued function, and a_0 is a real number. Note that the solution, $y(t)$, if it exists, is defined on $\mathbb{N}_{\nu-1}$.

First, we construct a summation equation that is equivalent to the initial value problem (1.78). Apply the $\Delta^{-\nu}$ operator to each side of (1.78) to obtain

$$\Delta^{-\nu}\Delta^{\nu}y(t) = \Delta^{-\nu}f(t+\nu-1, y(t+\nu-1)), \quad t = \nu, \nu+1, \dots \tag{1.79}$$

Apply Theorem 1.5 to the right-hand side of (1.79) to obtain

$$\Delta^{-\nu}\Delta^{\nu}y(t) = \Delta^{-\nu}\Delta\Delta^{-(1-\nu)}y(t) = \Delta\Delta^{-\nu}\Delta^{-(1-\nu)}y(t) - \frac{t^{(\nu-1)}}{\Gamma(\nu)}y(\nu-1) = \Delta^{-\nu}f(t+\nu-1, y(t+\nu-1)). \tag{1.80}$$

So, for $t \in \mathbb{N}_{\nu-1}$ we have

$$y(t) = \frac{t^{(\nu-1)}}{\Gamma(\nu)}a_0 + \frac{1}{\Gamma(\nu)}\sum_{s=0}^{t-\nu}(t-\sigma(s))^{(\nu-1)}f(s+\nu-1, y(s+\nu-1)). \tag{1.81}$$

The recursive iteration to this sum equation implies that (1.81) represents the unique solution of the initial value problem (1.78).

Example 5. Consider

$$\begin{cases} {}^{RL}\Delta_a^{\nu} y(t) = \lambda y(t+\nu-1), & t = 0, 1, 2, \dots, \\ \Delta^{\nu-1}|_{t=0} = a_0. \end{cases} \tag{1.82}$$

Note that the solution is defined on $\mathbb{N}_{\nu-1}$ and $\Delta^{\nu-1} y(t)|_{t=0} = y(\nu-1)$ since $(-\nu)^{(-\nu)} = \Gamma(1-\nu)$. So the initial value problem (1.82) is equivalent to the initial value problem

$$\begin{cases} {}^{RL}\Delta_a^{\nu} y(t) = \lambda y(t+\nu-1), & t = 0, 1, 2, \dots, \\ \Delta^{\nu-1}|_{t=0} = a_0. \end{cases} \tag{1.83}$$

By (1.81), the solution of the initial value problem (1.82) is a solution of the summation equation

$$y(t) = \frac{t^{(\nu-1)}}{\Gamma(\nu)} a_0 + \frac{\nu}{\Gamma(\nu)} \sum_{s=0}^{t-\nu} (t - \sigma(s))^{(\nu-1)} y(s+\nu-1). \tag{1.84}$$

We employ the method of successive approximations. Set

$$y_0(t) = \frac{t^{(\nu-1)}}{\Gamma(\nu)} a_0,$$

$$y(t) = y_0(t) + \frac{\nu}{\Gamma(\nu)} \sum_{s=0}^{t-\nu} (t - \sigma(s))^{(\nu-1)} y_{m-1}(s+\nu-1) = y_0(t) + \lambda \Delta^{-\nu} y_{m-1}(t+\nu-1).$$

Apply the power rule to show that

$$y(t) = y_0(t) + \lambda \Delta^{-\nu} y_0(t+\nu-1) = a_0(t) + \left(\frac{t^{(\nu-1)}}{\Gamma(\nu)} + \lambda \frac{(t+\nu-1)^{(2\nu-1)}}{\Gamma(2\nu)} \right).$$

With repeated applications of the power rule it follows inductively that

$$y_m(t) = a_0(t) + \sum_{i=0}^{m} \frac{\lambda^i}{\Gamma((i+1)\nu)} (t + (i-1)(\nu-1))^{(i\nu+\nu-1)}, \quad m = 0, 1, 2, \dots$$

Formally, take the limit $m \to \infty$ to obtain

$$y_m(t) = a_0(t) + \sum_{i=0}^{\infty} \frac{\lambda^i}{\Gamma((i+1)\nu)} (t + (i-1)(\nu-1))^{(i\nu+\nu-1)}, \quad m = 0, 1, 2, \dots \tag{1.85}$$

One immediate observation can be made. Set $\nu = 1$. Then $y(t) = a_0 \sum_{i=0}^{\infty} \frac{\lambda^i}{i!} t^{(i)}$ Since the initial value problem with $\nu = 1$ has the unique solution $a_0(1+\lambda)t$, we obtain $(1+\lambda)^t = \sum_{i=0}^{\infty} \frac{\lambda^i}{i!} t^{(i)}$.

1.5 Caputo fractional difference operator

It turns out that the Riemann–Liouville left operator have certain disadvantages when trying to model real-world phenomena with fractional difference equations. We shall therefore now discuss a modified concept of a fractional difference operator. Analogue to the usual fractional calculus we can define the left Caputo fractional difference of order ν. The first definition of a discrete fractional operator was introduced in [41], where the operator was derived by a natural discretization of the traditional Caputo operator in fractional calculus. The original continuous Caputo operator was introduced by the mathematician Caputo in 1967 [42]. The main advantage of using the Caputo difference operator is that the initial condition of the fractional order does not need to be specified in order to solve an equation or a system of equations.

Definition 7. Let $\nu > 0$ and $n-1 < \nu < n$, where n denotes a positive integer, $n = [\nu] + 1$ and $[.]$ ceiling of number. The ν-th fractional Caputo like difference is defined as

$$ {}^{C}\Delta_a^{\nu} = \Delta_a^{-(n-\nu)}\Delta^n f(t) = \frac{1}{\Gamma(n-\nu)} \sum_{s=a}^{t-(n-\nu)} (t-\sigma(s))^{(n-\nu-1)} (\Delta_s^n f)(s), \quad \forall\, t \in \mathbb{N}_{a+\nu}. \tag{1.86} $$

If $\nu = n \in \mathbb{N}$, then ${}^{C}\Delta_a^{\nu} f(t) = \Delta^n f(t)$.

Since

$$ \Delta^n f(t) = \sum_{r=0}^{n} (-1)^{r+1} \binom{n}{r} f(r+k). \tag{1.87} $$

In thsi traditional definition fractional-order Caputo difference operator is defined as the next higher whole-order difference acting on a small order sum. Newt, from relation (1.87) we get the equivalent formula for the Caputo fractional difference of order ν whose use is essential in many applications.

Proposition 10. Let $n-1 < \nu \leq n$ and set $\mu = n - \nu$, where $n \in \mathbb{N}$. The following formula is equivalent to (1.86):

$$ {}^{C}\Delta_a^{\nu} f(t) = \begin{cases} \frac{1}{\Gamma(n-\nu)} \sum_{s=a}^{t-(n-\nu)} (t-\sigma(s))^{(n-\nu-1)} \\ \qquad \times \sum_{r=0}^{n} (-1)^{r+1} \binom{n}{r} f(r+k), & \nu \in (n-1, n) \\ \Delta^n f(t), & \nu = n. \end{cases} \tag{1.88} $$

Example 6. We start by computing the left Caputo difference operator of the constant function. Let then $f(t) = C$, where C is a constant, from (1.86) we have:

$$ {}^{C}\Delta_a^{\nu} C = 0, \quad \nu > 0,\ a \in \mathbb{R}. \tag{1.89} $$

These formulae is straight and may be proved by direct evaluation.

Example 7. For the power rule function $f(t) = (t-a)^{(\mu)}$ we have

$$ \Delta_{a+\mu}^{\nu} (t-a)^{(\mu)} = \frac{\Gamma(\mu+1)}{\Gamma(\mu-\nu+1)} (t-a)^{(\mu-\nu)}, \quad t \in \mathbb{N}_{a+\mu+n-\nu}, \tag{1.90} $$

where $n = \lceil \nu \rceil$ and $\mu > n$. One may obtain (1.90) by direct generalization of Δ^n difference of f. The classical method of proving that is as follows. First note that $\Delta(t-a)^{(\mu)} = \mu(t-a)^{(\mu-1)}$. Furthermore,

$$\begin{aligned}\Delta^n(t-a)^{(\mu)} &= \mu(\mu-1)\dots(\mu-(n-1))(t-a)^{(\mu-n)},\\ &= \frac{\Gamma(\mu+1)}{\Gamma(\mu-n+1)}(t-a)^{(\mu-n)}.\end{aligned}$$

Introducing the Caputo-like delta difference defined in (1.86) leads to

$$\begin{aligned}\Delta^\nu(t-a)^{(\mu)} &= \Delta_{a+\mu}^{-(n-\nu)}\Delta^n(t-a)^{(\mu)}\\ &= \frac{\Gamma(\mu+1)}{\Gamma(\mu-n+1)}\Delta^{-(n-\nu)}(t-a)^{(\mu-n)}\\ &= \frac{\Gamma(\mu+1)}{\Gamma(\mu-n+1)}\frac{\Gamma(\mu-n+1)}{\Gamma(\mu-\nu+1)}(t-a)^{(\mu-\nu)},\end{aligned}.$$

where $t \in \mathbb{N}_{a+\nu-n+\mu}$. This complete the proof.

The following theorem relates the Caputo and the Riemann fractional operators.

Theorem 1.11. *The relation between the Riemann and Caputo fractional difference operators for any $\nu > 0$ is given by:*

$$ {}^{C}\Delta_a^\nu f(t) = {}^{RL}\Delta_a^\nu f(t) - \sum_{k=0}^{n-1}\frac{(t-a)^{(k-\nu)}}{\Gamma(k-\nu+1)}\Delta^k f(a). \tag{1.91}$$

Proof. We mentioned in Proposition 3 that for $\nu > 0$ and a positive integer p we have

$$\Delta^{-\nu}\Delta^p f(t) = \Delta^p\Delta^{-\nu}f(t) - \sum_{k=0}^{p-1}\frac{(t-a)^{\nu-p+k}}{\Gamma(\nu+k-p+1)}\Delta^k f(a). \tag{1.92}$$

If we replace ν by $n-\nu$ and p by n, and we let $n = [\nu]+1$. Then we can establish

$$\Delta^{-(n-\nu)}\Delta^n f(t) = \Delta^n\Delta^{-(n-\nu)}f(t) - \sum_{k=0}^{n-1}\frac{(t-a)^{(k-\nu)}}{\Gamma(k-\nu+1)}\Delta^k f(a). \tag{1.93}$$

Consequently from equation(1.93) we obtain

$$ {}^{C}\Delta_a^\nu f(t) = {}^{RL}\Delta_a^\nu f(t) - \sum_{k=0}^{n-1}\frac{(t-a)^{(k-\nu)}}{\Gamma(k-\nu+1)}\Delta^k f(a). \tag{1.94}$$

In particular, when $0 < \nu < 1$, the relation (1.94) takes the following form:

$$ {}^{C}\Delta_a^\nu f(t) = {}^{RL}\Delta_a^\nu f(t) - \frac{(t-a)^{(-\nu)}}{\Gamma(1-\nu)}f(a). \tag{1.95}$$

□

1.5.1 Properties of the fractional Caputo left operator

As for the Riemann fractional difference operator, it is natural to introduce the left Caputo operator as an operation inverse to fractional summation. Similarly to what we have earlier, we have the following proposition.

Proposition 11. [37] Assume $\nu > 0$ and f is defined on suitable domains $\mathbb{N}_a$. Then

$$\Delta^{-\nu}_{a+(n-\nu)} \, {}^{C}\Delta^{\nu}_{a} f(t) = f(t) - \sum_{k=0}^{n-1} \frac{(t-a)^k}{k!} \Delta^k f(a). \tag{1.96}$$

In particular, if $0 < \nu \leq 1$, then

$$\Delta^{-\nu}_{a+(n-\nu)} \, {}^{C}\Delta^{\nu}_{a} f(t) = f(t) - f(a). \tag{1.97}$$

Proof. The proof of equation (1.96) is followed by applying the definition and then using Theorem 1.5 and the relation between Riemann left operator and sum reported in Proposition 7. □

1.5.2 Summation by pats for Caputo fractional difference

Analogously to Theorem 1.10, in the case of Caputo fractional difference the integration by parts has the following form.

Theorem 1.12. *[37] Let $0 < \nu < 1$ and let f, g be functions defined on $\mathbb{N}_a \cap b_{\mathbb{N}}$ where $a \equiv b$ (mod 1). Then*

$$\sum_{s=a+1}^{b+1} g(s) \, {}^{C}\Delta^{\nu}_{a} f(s-\nu) = f(s)_{b-1}\Delta^{-(1-\nu)} g(s-(1-\nu))\big|_a^{b-1} + \sum_{a}^{b-2} f(s) \, b-1\Delta^{\nu} g(s+\nu). \tag{1.98}$$

Equation (1.98) may obtained similarly to the Riemann-left formula in Theorem 1.10. It may be achieved with the aid of Theorem [Theorem 8.50 in [38]] analogously to the proof of equation (1.77).

1.5.3 Taylor difference formula

Another important basic result in classical analysis is Taylor's theorem. In the following we will introduce a new generalization of Taylor's formula that involving Caputo-like difference operator along with its proprieties. Moreover, these formulas turn out to be of fundamental importance in the analysis of initial value problems, as we will see later. All the following results were reported in [43].

Theorem 1.13. *For $\mu > 0$, μ non-integer, $m = [\mu]$, $\nu = m - \mu$, it holds*

$$f(t) = \sum_{k=0}^{m-1} \frac{(t-a)^k}{k!} \Delta^k f(a) + \frac{1}{\Gamma(\mu)} \sum_{s=a+\nu}^{t-\mu} (t-s-1)^{(\mu-1)} \Delta^{\mu} f(s), \quad \forall t \in \mathbb{N}_{a+m}, \tag{1.99}$$

where f is defined on $\mathbb{N}_a$ with $a \in \mathbb{Z}^+$, $\mathbb{Z}^+ := \{0, 1, 2, \ldots\}$.

In case of $0 < \nu < 1$, *the Caputo generalized Taylor's formula (1.99) reduces to*

$$f(t) = f(0) + \frac{1}{\Gamma(\nu)} \sum_{s=1-\nu}^{t-\nu} (t-s-1)^{(\nu-1)} \Delta^{\nu} f(s). \tag{1.100}$$

Proof. From the definition of Caputo-left operator (1.86) and the commutativity property in Theorem 1.5, we have

$$\Delta^{-\nu}\Delta^{\nu} f(t) = \Delta^{-\nu}\Delta^{-(m-\nu)}(\Delta^m f(t)) = \Delta^{-(\nu+(m-\nu))}(\Delta^m f(t)) = \Delta^{-m}(\Delta^m f(t)), \ \ \forall t \in \mathbb{N}_{a+\nu+\mu}, \tag{1.101}$$

that is

$$\Delta^{-\nu}\Delta^{\nu} f(t) = \Delta^{-m}(\Delta^m f(t)), \quad \forall t \in \mathbb{N}_{a+m}. \tag{1.102}$$

It been noticed that

$$(t-s-1)^{(m-1)} = \frac{\Gamma(t-s)}{\Gamma(t-s-m+1)} = (t-s-1)(t-s-2).....(t-s-m+1), \tag{1.103}$$

the falling factorial, here we have $t-s-m+1 > 0$. Therfore we obtain

$$\Delta^{-m}(\Delta^m f(t)) = \frac{1}{(m-1)!} \sum_{s=a}^{t-m} (t-s-1)^{(m-1)} \Delta^m f(s). \tag{1.104}$$

Using the discrete Taylor formula reported before in equation (1.45), one can get

$$f(t) = \sum_{k=0}^{n-1} \frac{(t-a)^{(k)}}{k!} \Delta^k f(a) + \frac{1}{(m-1)!} \sum_{s=a}^{t-n} (t-s-1)^{(m-1)} \Delta^m f(s), \tag{1.105}$$

where $t^{(k)} = t(t-1).....(t-k+1)$. From the last we derive the Taylor formula

$$f(t) = \sum_{k=0}^{n-1} \frac{(t-a)^{(}k)}{k!} \Delta^k f(a) + \Delta^{-\nu}\Delta^{\nu} f(t), \tag{1.106}$$

where f is defined on $\mathbb{N}_a$, $\forall\ t \in \mathbb{N}_{a+m}$. □

Remark 5. Here $[a,b]$ denotes the discrete interval $[a,b] = [a, a+1, a+2, \ldots, b]$, where $a < b$ and $a, b \in \{0, 1, \ldots\}$.

Let $\nu > 0$ be non integer such that $n-1 < \nu < n$, i.e, $n = \lceil \nu \rceil$. Consider a function f defined on $[a,b]$. Then clearly the fractional discrete Taylor's formula (1.99) is only valid for $t \in [a+n, b]$, $a+n < b$.

By using the fact that $\Delta^p \left(\frac{(t-a)^k}{k!} \right) = \frac{(t-a)^{k-p}}{(k-p)!}$, we obtain the following Caputo type fractional extended Taylor's formula.

Theorem 1.14. *Let* $\mu > p$, $p \in \mathbb{N}$, μ *not integer,* $n = \lceil \mu \rceil$, $\nu = n - \mu$. *Then*

$$\Delta^p f(t) = \sum_{k=p}^{n-1} \frac{(t-a)^{(k-p)}}{(k-p)!} \Delta^k f(a) + \frac{1}{\Gamma(\mu-p)} \sum_{s=a+\nu}^{t-\mu+p} (t-s-1)^{(\mu-p-1)} \Delta_*^{\mu} f(s), \tag{1.107}$$

$\forall t \in \mathbb{N}_{a+n-p}$, f *is defined on* $\mathbb{N}_a$, $a \in \mathbb{Z}^+$.

Proposition 12. Notice for $p = 0$ applied on (1.107) we get for $\mu > 0$, μ not an integer, $n = \lceil \mu \rceil$, $\nu = n - \mu$, f is defined on $\mathbb{N}_a$, $a \in \mathbb{Z}^+$; and $\Delta^k f(a) = 0$, for $k = 0, \ldots, n-1$, we get

$$f(t) = \frac{1}{\Gamma(\mu)} \sum_{s-a+\nu}^{t-\mu} (t - s - 1)^{(\mu-1)} \Delta_*^{\mu} f(s), \quad \forall\, t \in \mathbb{N}_{a+n}. \tag{1.108}$$

Proposition 13. Let $\mu > p$, $p \in \mathbb{N}$, μ non-integer, $n = \lceil \mu \rceil$, $\nu = n - \mu$; f is defined on $\mathbb{N}_a$, $a \in \mathbb{Z}^+$. Assume that $\Delta^k f(a) = 0$, $k = p, \ldots n-1$. Then

$$\Delta^p f(t) = \frac{1}{\Gamma(\mu - p)} \sum_{s=a+\nu}^{t-\mu+p} (t - s - 1)^{(\mu-p-1)} \Delta_*^{\mu} f(s), \quad \forall\, t \in \mathbb{N}_{a+n-p}. \tag{1.109}$$

1.5.4 Initial value problem

We discuss now the problem of resolvability of initial value problems fractional-order systems defined by difference equations with the Caputo-type operator. We begin once again with a brief overview of the results of existence and uniqueness theorems for the left Caputo difference equations. We shall first transform the initial value problem into an equivalent Volterra difference equation (Theorem 1.15) and then we are going to prove the existence and uniquence of the solution. Recalling that the Caputo version is usually preferred when physical model is described because its initial condition is the same as one of the integer order difference equations.

Theorem 1.15. *[48] For the left-Caputo difference operator consider the initial value problem*

$$\begin{cases} {}^{C}\Delta_a^{\nu} x(t) = f(t - 1 + \nu, x(t - 1 + \nu)), \quad t \in \mathbb{N}_{a+1-\nu}, \ 0 < \nu \leq 1, \\ x_0(t) = x(a), \end{cases} \tag{1.110}$$

where f is the continue function define by $f : [0, +\infty) \times \mathbb{R} \to \mathbb{R}$. The function $x(t)$ is a solution of the initial value problem (1.110) if and only if it is a solution of the following discrete Volterra equation

$$x(t) = x_0(t) + \frac{1}{\Gamma(\nu)} \sum_{s=a+1-\nu}^{t-\nu} (t - s - 1)^{(\nu-1)} f(s + \nu - 1, x(s + \nu - 1)), \tag{1.111}$$

where $0 < \nu \leq 1$ and $t \in \mathbb{N}_{a+1}$.

Proof. Suppose first that the function $x(t)$ for $t \in \mathbb{N}_a$ is a solution of the IVP (1.110). Then, we may write this solution using Taylor formula in Theorem 1.13, as follows

$$x(t) = x_0(t) + \frac{1}{\Gamma(\nu)} \sum_{s=a+1-\nu}^{t-\nu} (t - s - 1)^{(\nu-1)} f(s + \nu - 1, x(s + \nu - 1)). \tag{1.112}$$

Conversely, we assume that $x(t)$ verify the discrete Voltera equation (1.111). Hence, we have

$$x(t) = x_0(t) + \frac{1}{\Gamma(\nu)} \sum_{s=a+1-\nu}^{t-\nu} (t - s - 1)^{(\nu-1)} f(s + \nu - 1, x(s + \nu - 1)). \tag{1.113}$$

Similarly, using the Taylor formula in Theorem 1.13, we get

$$x(t) = x_0(t) + \frac{1}{\Gamma(\nu)} \sum_{s=a+1-\nu}^{t-\nu} (t-s-1)^{(\nu-1)} \, {}^{C}\Delta_a^{\nu} x(s). \tag{1.114}$$

Comparing equation (1.112) with equation (1.113) yields

$$\frac{1}{\Gamma(\nu)} \sum_{s=a+1-\nu}^{t-\nu} (t-s-1)^{(\nu-1)} \left[{}^{C}\Delta_a^{\nu} x(s) - f(s+\nu-1, x(s+\nu-1)) \right] = 0. \tag{1.115}$$

Therefore, for all $t \in \mathbb{N}_a$, we have that ${}^{C}\Delta_a^{\nu} x(t) = f(t-1+\nu, x(t-1+\nu))$ which implies that $x(t)$ is a solution of IVP (1.110). □

Remark 6. Let $n = t - a$, since $(t-s-1)^{(\nu-1)}/\Gamma(\nu)$ is equal to $\Gamma(t-s)/\Gamma(t-s-\nu+1)$ and for $a = 0$, the numerical formula of (1.111) can be described as [103]

$$x_1(n) = x(0) + \frac{1}{\Gamma(\nu)} \sum_{j=0}^{n-1} \frac{\Gamma(n-j+\nu)}{\Gamma(n-j+1)} f(j-1, x(j-1)). \tag{1.116}$$

where $x(0)$ is the initial conditions. According to the numerical equation (1.116), the proposed fractional discrete-time system has memory effect; which means that the iterated solutions are determined by all the previous states.

Theorem 1.16. *[48] Let $(X, ||.||)$ real Banack space where $||x|| = sup\{||x(t), t \in \mathbb{N}_a\}$, and assume that the function f is continuous in X and that is globally Lipshitz with constant L. Then, the IVP (1.110) has a unique solution $x(t)$ provided that $0 < L < \frac{1}{1+\nu}$.*

Proof. We define the operator $T : X \to X$ by

$$Tx(t) = x_0(a) + \frac{1}{\Gamma(\nu)} \sum_{s=a+1-\nu}^{t-\nu} (t-s-1)^{(\nu-1)} f(s+\nu-1, x(s+\nu-1)). \tag{1.117}$$

For any $x, y \in X$ it follows from definition of the operator A and the Lipschitz condition on f, that

$$\begin{aligned}
&||Tx(t) - Ty(t)|| \\
&\quad \leq \frac{1}{\Gamma(\nu)} \sum_{s=1+a-\nu}^{t-\nu} (t-s-1)^{(\nu-1)} ||f(s+\nu-1, x(s+\nu-1)) - f(s+\nu-1, y(s+\nu-1))|| \\
&\quad \leq \frac{L}{\Gamma(\nu)} (\nu-1)^{(\nu-1)} ||x-y|| \\
&\quad = \frac{L}{\Gamma(\nu)} \Gamma(\nu) ||x-y|| \\
&\quad = L||x-y||.
\end{aligned}$$

Since $L < \frac{1}{(1+\nu)} < 1$, by applying Banach contraction principle, T has a fixed point $x_1(t)$ which is a unique solution of the IVP (1.110) on $t \in \{a, a+1\}$.

Since$x_1(t)$ exists, for $t \in \{a+1, a+2\}$, we may define the following mapping $T_1 : X \to X$:

$$T_1x(t) = x_1(a+1) + \frac{1}{\Gamma(\nu)} \sum_{s=a+2-\nu}^{t-\nu} (t-s-1)^{(\nu-1)} f(s+\nu-1, x(s+\nu-1)). \tag{1.118}$$

In this case we have

$$\begin{aligned}
&||T_1x(t) - T_1y(t)|| \\
&\quad \leq \frac{1}{\Gamma(\nu)} \sum_{s=2+a-\nu}^{t-\nu} (t-s-1)^{(\nu-1)} ||f(s+\nu-1, x(s+\nu-1)) - f(s+\nu-1, y(s+\nu-1))|| \\
&\quad \leq \frac{L}{\Gamma(\nu)} \sum_{s=2+a-\nu}^{t-\nu} (t-s-1)^{(\nu-1)} ||x-y|| \\
&\quad = \frac{L}{\Gamma(\nu)} \left[\sum_{s=2+a-\nu}^{2+a-\nu} (2+a-s-1)^{(\nu-1)} \right] ||x-y|| \\
&\quad = \frac{L}{\Gamma(\nu)} \left[\nu^{(\nu-1)} + (\nu-1)^{(\nu-1)} \right] ||x-y|| \\
&\quad = \frac{L}{\Gamma(\nu)} \left[\frac{\Gamma(\nu+1)}{\Gamma(2+a)} + \frac{\Gamma(\nu)}{\Gamma(1+a)} \right] ||x-y|| \\
&\quad = L(1+\nu)||x-y||.
\end{aligned}$$

Since $L(1+\nu) < 1$, by applying Banach contraction principle, T_1 has a fixed point $x_2(t)$ which is a unique solution of the IVP (1.110) on $t \in \{1+a, 2+a\}$. Hence, in order to prove the desired result, it is sufficient to show that the operator T has unique fixed points which are unique solutions $x_{m+1}(t)$ of the IVP (1.110) on the $t \in \{m+a, m+a+1\}$. For this purpose, we write operator T_m as follows

$$T_mx(t) = x_m(a+m) + \frac{1}{\Gamma(\nu)} \sum_{s=a+m-\nu}^{t-\nu} (t-s-1)^{(\nu-1)} f(s+\nu-1, x(s+\nu-1)). \tag{1.119}$$

Similarly, we may obtain that the IVP (1.110) has a unique solution $x_m(t)$ on $t \in \{m+a, m+a+1\}$ exists.

Hence, define $x(t)$ as follows

$$x(t) \begin{cases} x_0, & t = a, \\ x_1, & t = a+1, \\ \vdots & \\ x_m(t), & t = a+m, \\ \vdots & \end{cases} \tag{1.120}$$

then $x(t)$ is the unique solution of (1.110) on $t \in N_a$. □

Example 8. Consider the following linear left Caputo fractional difference equation

$$ {}^{C}\Delta_{a}^{\nu}x(t) = \lambda x(t+\nu-1), \quad t \in \mathbb{N}_{a+1-\nu}, \tag{1.121} $$

with the initial condition $x(a) = x_a$. Thus, according to Theorem 1.15 the solution is given by

$$ y(t) = a_0 + \frac{\lambda}{\Gamma(\nu)} \sum_{s=a+1-\nu}^{t-\nu} (t-\sigma(s))^{(\nu-1)} y(s+\nu-1). $$

Abdeljawad in [41] have given an explicit clear solution by applying the method of successive approximation. Set $x_0(t) = a_0$ and

$$ x_m(t) = a_0 + \lambda \Delta_{a+1-\nu}^{-\nu} x(s+\nu-1), \quad m = 1, 2, 3, \ldots $$

For $m = 1$, by the power formula (1.20) one can get

$$ x_1(t) = a_0 \left[1 + \frac{\lambda t^{(\nu)}}{\Gamma(\nu+1)} \right]. $$

For $m = 2$,

$$ x_2(t) = a_0 + \lambda \Delta_{a+1-\nu}^{-\nu} \left[a_0 + \frac{(t+\nu-1)^{(\nu)}}{\Gamma(\nu+1)} \right] = a_0 \left[1 + \frac{\lambda t^{(\nu)}}{\Gamma(\nu+1)} + \frac{\lambda^2 (t+\nu-1)^{(2\nu)}}{\Gamma(2\nu+1)} \right]. $$

If we proceed inductively and let $m \to \infty$ we obtain

The last operator that we take under our consideration is the fractional Grunwald like operator and the definition of operator can be found for example in [60].

1.6 Grunwald-Letnikov fractional difference operator

In this paragraph, as a definition of fractional discrete difference operator, a following *fractional order Grunwald-Letnikov* definition will be used.

Definition 8. The *fractional order Grunwald-Letnikov* is given by

$$ \Delta^{\nu} f(k) = \frac{1}{h^{\nu}} \sum_{j=0}^{k} (-1)^j \binom{\nu}{j} f(k-j), \tag{1.122} $$

where the fractional order $\nu \in \mathbb{R}^{*+}$, i.e., the set of strictly positive real numbers, $h \in \mathbb{R}^{*+}$ is a sampling time will be taken equal to unity in all what follows, and $k \in \mathbb{N}$ represents the discrete time. The term $\binom{\nu}{j}$ can be obtain from the following relation:

$$ \binom{\nu}{j} = \begin{cases} 1 & for \quad j = 0, \\ \frac{\nu(\nu-1)\ldots(\nu-j+1)}{j!} & for \quad j > 0. \end{cases} \tag{1.123} $$

1.7 $h-$Difference fractional operators

In this section, some basic concepts related to the fractional h-difference operators are briefly summarized. In this context, we first introduce some definitions and notation [49]. Let $h > 0$ and put $(h\mathbb{N})_a = \{a, a+h, a+2h, \ldots\}$ with $a \in \mathbb{R}$.

Definition 9. Let h be a strictly real positive number and $f : (h\mathbb{N})_a \to \mathbb{R}$, the forward h-difference operator is introduced as:

$$\Delta_h f(t) = \frac{f(\sigma_h(t)) - f(t)}{h}, \tag{1.124}$$

where $\sigma(sh) = (t+1)h$.

Definition 10. The *h-falling factorial function* of real order ν is defined by

$$t_h^{(\nu)} = h^\nu \frac{\Gamma\left(\frac{t}{h}+1\right)}{\Gamma\left(\frac{t}{h}+1-\nu\right)}, \tag{1.125}$$

in which $t \in \mathbb{R}$. As one can see when $h = 1$, the *h-falling factorial function* is equivalent to the falling factorial function defined by equation (1.8). One also expects to see that $t_h^{(\nu)}$ converges to $t^{(\nu)}$ when h tends to zero. This is illustrated in the next proposition.

Proposition 14. [44] For $t \geq 0$ and $\nu \in \mathbb{R}$,

$$\lim_{h\to 0} t_h^{(\nu)} = t^{(\nu)}. \tag{1.126}$$

Definition 11. [44] Let $f : (h\mathbb{N})_a \to \mathbb{R}$ and $0 < \nu$ be given. a is a starting point. The ν-th order *fractional h–summation* is given by

$${}_h\Delta_a^{-\nu} f(t) = \frac{h}{\Gamma(\nu)} \sum_{s=\frac{a}{h}}^{\frac{t}{h}-\nu} (t - \sigma(sh))_h^{(\nu-1)} f(sh), \quad \sigma(sh) = (s+1)h,\ a \in \mathbb{R},\ t \in (h\mathbb{N})_{a+\nu h}, \tag{1.127}$$

where the h–falling factorial function, in which $(h\mathbb{N})_{a+(1-\nu)h} = \{a+(1-\nu)h, a+(2-\nu)h, \ldots\}$.

Remark 7. The fractional h-difference summation ${}_h\Delta_a^{-\nu}$ maps every function defined from $(h\mathbb{N})_a$ into function defined $(h\mathbb{N})_{a+\nu h}$.

Accordingly to the definition of h-factorial function the formula given in Definition 11 can be rewritten as

$$\begin{aligned}
\left({}_h\Delta_a^{-\nu} f\right)(t) &= h^\nu \sum_{k=0}^{n} \frac{\Gamma(\nu+n-k)}{\Gamma(\nu)\Gamma(n-k+1)} f(a+kh) \\
&= h^\nu \sum_{k=0}^{n} \binom{n-k+\nu-1}{n-k} f(a+kh) \\
&= h^\nu \sum_{j=0}^{n} (-1)^j \binom{-\nu}{j} f(\nu-jh),
\end{aligned} \tag{1.128}$$

for $t = a + (\nu + n)h$, $n \in \mathbb{N}_0$.

Next, the h-power rule and the commutative property of the fractional h-difference summation operator are reported. The proof for the case $h > 0$ one can find in [45].

Lemma 3. Let ν be real number such that. Then

$$ {}_a\Delta_h^{-\nu}(t-a+\mu h)_h^{(\mu)} = \frac{\Gamma(\mu+1)}{\Gamma(\mu+\nu-1)}(t-a+\mu h)_h^{(\mu+\nu)}. \tag{1.129} $$

Proposition 15. Let f be a real valued function defined on $(h\mathbb{N})_a$, where $a, h \in \mathbb{R}$, $h > 0$. For $\nu, \mu > 0$ the following equalities hold

$$ {}_h\Delta_{a+\mu h}^{-\nu}\, {}_h\Delta_a^{-\mu} f(t) = {}_h\Delta_a^{-(\nu+\mu)} f(t) = {}_h\Delta_{a+\nu h}^{-\mu}\, {}_h\Delta_a^{-\nu} f(t), \quad t \in (h\mathbb{N})_{a+(\nu+\mu)h}. \tag{1.130} $$

Based on the above definition of the h- fractional sum, it is possible to define the fractional h-difference operators.

Definition 12. Let $\nu \in (0, 1]$, the *Riemann-like fractional h-difference operator*

$$ {}_a^{RL}\Delta_h^{\nu} f(t) = \left(\Delta_h \left({}_h\Delta_a^{-(1-\nu)} f\right)\right)(t), \quad t \in (h\mathbb{N})_{a+(1-\nu)h}. \tag{1.131} $$

Remark 8. Not that the the *Riemann-like fractional h-difference operator* maps every function defined from $(h\mathbb{N})_a$ into $(h\mathbb{N})_{a+(1-\nu)h}$.

Definition 13. [41] For $f(t)$ defined on $(h\mathbb{N})_a$ and $0 < \nu,\ \mu \notin \mathbb{N}$, the Caputo–like difference is defined by

$$ {}_h^C\Delta_a^{\mu} f(t) = \Delta_a^{-(n-\mu)} \Delta^n f(t), \quad t \in (h\mathbb{N})_{a+(n-\mu)h}, \tag{1.132} $$

where $n = \lceil \nu \rceil + 1$. If $\nu = 1$, then we have:

$$ {}_h^C\Delta_a^{\nu} f = \Delta^m f, \qquad t \in (h\mathbb{N})_a. \tag{1.133} $$

The last operator that we take under our consideration is fractional h-difference Grunwald-Letnikov like operator.

Definition 14. Let $\nu \in \mathbb{R}$, the *Grunwald-Letnikov like h-difference operator* Δ_h^{ν} of order ν for a function $f : (h\mathbb{N})_a \to \mathbb{R}$ is defined by

$$ \Delta_h^{\nu} f(t) = \frac{1}{h^{\nu}} \sum_{s=0}^{\frac{t-a}{h}} (-1)^s \binom{\nu}{j} f(t - sh), \tag{1.134} $$

where the term $\binom{\nu}{s}$ can be obtain from the following relation

$$ \binom{\nu}{s} = \begin{cases} 1 & \text{for} \quad s = 0, \\ \frac{\nu(\nu-1)\ldots(\nu-s+1)}{s!} & \text{for} \quad s \in \mathbb{N}. \end{cases} \tag{1.135} $$

Remark 9. The *Grunwald-Letnikov like h-difference operator* maps every function defined from $(h\mathbb{N})_a$ into the same domain $(h\mathbb{N})_a$.

1.8 The Z-Transform method

Here we attempt to review the *Z-transform* of the expressed fractional h-difference summation and operators. The following definition describes the *Z-transform* of a discrete sequence.

Definition 15. [46] The Z-transform of a sequence $x(n)$, which is identically zero for negative integers n (i.e., $x(n) = 0$ for $n = -1, -2, \ldots$), is defined by

$$Z(x(n)) = \sum_{j=0}^{\infty} x(j) z^{-j}, \tag{1.136}$$

where z is a complex number.

The set of numbers z in the complex plane for which series (1.136) converges is called the region of convergence of $x(z)$. The most commonly used method to find the region of convergence of the series (1.136) is the ratio test. Suppose that

$$\lim_{j\to\infty} \left| \frac{x(j+1)}{x(j)} \right| = R.$$

Then by the ratio test, the infinite series (1.136) converges if

$$\lim_{j\to\infty} \left| \frac{x(j+1)z^{-j-1}}{x(j)z^{-j}} \right| < 1,$$

and diverges if

$$\lim_{j\to\infty} \left| \frac{x(j+1)z^{-j-1}}{x(j)z^{-j}} \right| > 1.$$

Hence the series (1.136) converges in the region $|z| > R$ and diverges for $|z| < R$.

1.8.1 The Z-Transform of the fractional difference summation

Let us now evaluate a Z-transform of the fractional difference summation. Considering the binomial functions defined on $\mathbb{Z}$, parametrized by $\nu \in \mathbb{R}$, and given by values $\varphi_\nu(n) = \binom{n+\nu-1}{n}$. For $n \in \mathbb{N}_0$ and $\varphi_\nu(n) = 0$ with $n < 0$, we can use

$$\varphi_\nu(n) = \binom{n+\nu-1}{n} = (-1)^n \binom{-\nu}{n},$$

and write the fractional difference operator (1.19) in the form of the convolution of φ_ν and $x(a+th)$, as

$$\left({}_a\Delta_h^{-\nu} x\right)(t) = h^\nu \left(\varphi_\nu * x(a+th)\right)(n), \tag{1.137}$$

where $*$ denotes a convolution operator, that is,

$$(\varphi * x(a+nh))(n) = \sum_{s=0}^{n} \binom{n-s+\nu-1}{n-s} \bar{x}(s).$$

According to this, we now establish a general formula of the fractional sum as reported in reference [47].

Proposition 16. For $t = a + \nu h + nh \in (h\mathbb{Z})_{a+\nu h}$ let one denote $y(n) = \left({}_a\Delta_h^{-\nu} x\right)(t)$ and $\bar{x}(n) = x(a + nh)$. Then

$$\mathcal{Z}[y](z) = \left(\frac{hz}{z-1}\right)^{\nu} X(z), \tag{1.138}$$

where $X(z) = \mathcal{Z}[\bar{x}](z)$.

1.8.2 The Z-Transform of the fractional Riemann fractional difference operator

We also formulate the similar family of functions that are used in solutions of systems with Riemann- Liouville-type operator. Let us define the family of functions $\varphi_{k,\nu} : \mathbb{Z} \to \mathbb{R}$ parametrized by $k \in \mathbb{N}_0$ and by $\nu \in (0, 1]$ with the following values

$$\varphi_{k,\nu} = \begin{cases} \binom{n-k+k\nu+\nu-1}{n-k} & \text{for } n \in \mathbb{N}_k, \\ 0 & \text{for } n < k. \end{cases} \tag{1.139}$$

Proposition 17. Let $\varphi_{k,\nu}$ be the function defined by (1.139). Then

$$\mathcal{Z}[\varphi_{k,\nu}](z) = \frac{1}{z^k}\left(\frac{z}{z-1}\right)^{k\nu+\nu}, \tag{1.140}$$

for z such that $|z| > 1$.

Proposition 18. For $a \in \mathbb{R}$, $\nu \in (0, 1]$, let one define $y(n) = \left({}_a^{RL}\Delta_h^{\nu} x\right)(t)$, where $t \in (h\mathbb{N})_{a+(1-\nu)h}$ and $t = a + (1-\nu)h + nh$. Then

$$\mathcal{Z}[y](z) = z\left(\frac{hz}{z-1}\right)^{-\nu} X(z) - zh^{-\nu}x(a), \tag{1.141}$$

where $X(z) = \mathcal{Z}[x(a + nh)](z)$.

1.8.3 The Z-Transform of the fractional Caputo fractional difference operator

Firstly, let us consider the Caputo-type h-difference operator ${}_a\Delta_h^{\nu}$ given in (1.132). Using the binomial function φ given by (1.8.1) we can write the Caputo type difference in the following way

$$\left({}_a^{C}\Delta_h^{\nu} x\right)(t) = h^{-\nu}\left(\varphi_{1-\nu} * \Delta x(a + nh)\right)(n), \tag{1.142}$$

where $t = a + (1-\nu)h + nh$.

Proposition 19. For $a \in \mathbb{R}$, $\nu \in (0,1]$ let one define $y(n) = \left({}_a^C\Delta_h^\nu x\right)(t)$, where $t \in (h\mathbb{N})_{a+(1-\nu)h}$ and $t = a + (1-\nu)h + nh$. Then

$$\mathcal{Z}[y](z) = h^{-\nu}\left(\frac{z}{z-1}\right)^{1-\nu}\left((z-|1)X|(z) - zx(a)\right), \tag{1.143}$$

where $X(z) = \mathcal{Z}[x(a+nh)]$.

1.8.4 The Z-Transform of the Fractional Grunwald-Letnikov-Type Operator

The third type of the operator, which we take under our consideration, is the Grunwald-Letnikov-type fractional h-difference operator.

Proposition 20. For $a \in \mathbb{R}$, $\nu \in (0,1]$, let one define $y(n) = \left(\Delta_h^\nu x\right)(t)$, where $t \in (h\mathbb{N})_a$ and $t = a + nh$, $n \in \mathbb{N}_0$. Then

$$\mathcal{Z}[y](z) = z\left(\frac{hz}{z-1}\right)^{-\nu} X(z), \tag{1.144}$$

where $X(z) = \mathcal{Z}[x(a+nh)](z)$.

1.9 Laplace transform method

The Laplace transform method is a very frequently used tool for solving engineering problems. In this section we will recall some basic facts about the Laplace transform method for integer order and then we will show this method for fractional order as well. One should not that the Z-transform, which is reported in the previous section, is a similar but with distinct transform form.

Definition 16. [50] Assume that $f : \mathbb{T}_a \to \mathbb{R}$ is a regular function. Then the *Laplace transform* of f on an unbounded time scale $\mathbb{T}_a$, is given by

$$\mathcal{L}_a\{f\}(s) = \int_a^\infty \exp_{\ominus}^{\sigma}(t,a) f(t)\Delta t, \forall s \in \mathcal{D}\{f\}, \tag{1.145}$$

where $\mathcal{D}\{f\}$ is the set for all regressive, complex constants for which the integral converges.

For the time scale $\mathbb{N}_a$, the *Laplace transform* is reduced to the so-called *Discrete Laplace Transform*; which is reported in the following theorem.

Theorem 1.17. *[51] The discrete Laplace transform of a regular function $f : \mathbb{T}_a \to \mathbb{R}$ is given by*

$$\mathcal{L}_a\{f\}(s) = \int_0^\infty \frac{f(t)}{(s+1)^{t-a+1}}\Delta t = \int_0^\infty \frac{f(t+a)}{(s+1)^{t+1}}\Delta t = \sum_{k=0}^{\infty}\frac{f(k+a)}{(s+1)^{k+1}}, \tag{1.146}$$

for all complex number $s \neq -1$ such that this improper integral (infinite series) converges.

Proof. Let $f : \mathbb{N}_a \to \mathbb{R}$, given any $s \in \mathbb{C}\{-1\}$; the *Laplace transform formula* (1.145) can be written as

$$\begin{aligned}
\mathcal{L}_a\{f\}(s) &= \int_a^{\infty} \exp_{\ominus}^{\sigma}(t,a) f(t) \Delta t \\
&= \sum_a^{\infty} \exp_{\ominus s}(\sigma(t),a) f(t) \\
&= \sum_{t=a}^{\infty} [1 + \ominus s]^{\sigma(t)-a} f(t) \\
&= \sum_{t=a}^{\infty} \frac{f(t)}{(1+s)^{t-a+1}} \\
&= \sum_{k=0}^{\infty} \frac{f(a+k)}{(1+s)^{k+1}}.
\end{aligned}$$

□

To proof the convergence of the *discrete Laplace transform* (1.146), the function $f(t)$ must be of *exponential order*. Basically, we make the following definition.

Definition 17. We say that a function $f : \mathbb{N}_a \to \mathbb{R}$ is of *exponential order* $r > 0$ if there exists a constant $A > 0$ such that

$$|f(t)| \leq A r^t, \quad \text{for} \quad t \in \mathbb{N}_a, \quad \text{sufficiently large} \quad t \in \mathbb{N}_a. \tag{1.147}$$

In other words, the function $f(t)$ must not grow faster than a certain exponential function when $t \to \infty$.

Now we can prove the following existence theorem.

Theorem 1.18. *[29] Suppose $f : \mathbb{N}_a \to \mathbb{R}$ is of exponential order $r > 0$. Then $\mathcal{L}_a\{f\}(s)$ converges absolutely $|s+1| > r$.*

Example 9. We start by computing the Laplace transform of the generalized exponential function $\exp_p(t,a) = (1+p)^{t-a}$, $p \neq -1$. Therefore, we have

$$\begin{aligned}
\mathcal{L}_a\{\exp_p(t,a)\}(s) &= \mathcal{L}_a\{(1+p)^{t-a}\}(s) \\
&= \sum_a^{\infty} \frac{(1+p)^k}{(s+1)^{k+1}} \\
&= \frac{1}{s+1} \sum_{k=0}^{\infty} \left(\frac{p+1}{s+1}\right)^k \\
&= \frac{1}{s+1} \left(\frac{1}{1-\frac{p+1}{s+1}}\right) \\
&= \frac{1}{s-p}.
\end{aligned}$$

An important special case ($p = 0$) of the above formula is

$$\mathcal{L}_a\{1\}(s) = \frac{1}{s}, \quad \text{for} \quad |s+1| > 1.$$

1.9.1 The exponential order of discrete fractional operators

In the following section, we develop the Laplace transform of fractional operators "fractional sum" and "difference operator". First, we must determine how the exponential order of f relates to the exponential orders of $\Delta_a^{-\nu} f$ and Δ_a^{ν}. The following lemma, which was reported by Holm [51], describes this relationship.

Lemma 4. Suppose that $f : \mathbb{N}_a \to \mathbb{R}$ is of exponential order $r \geq 1$ and let $\nu > 0$ be given. Then for each fixed $\epsilon > 0$, $\Delta_a^{-\nu} f$ and $\Delta_a^{\nu} f$ are of exponential order $r + \epsilon$.

Corollary 4. Suppose that $f : \mathbb{N}_a \to \mathbb{R}$ is of exponential order $r \geq 1$ and let $\nu > 0$ be given with $n - 1 < \nu \leq n$. Then both $\mathcal{L}_{a+\nu-n}\{\Delta_a^{-\nu} f\}(s)$ and $\mathcal{L}_{a+\nu-n}\{\Delta_a^{\nu} f\}(s)$, converge for all $s \in \mathbb{C}/\overline{B_{-1}(r)}$.

1.9.2 The Laplace transform of fractional difference summation

We will start with the Laplace transform of the fractional sum of fractional order ν, where the Corollary 4 is used to ensure the correct domain of convergence for the Laplace transform of any fractional operator.

Theorem 1.19. *Suppose $f : \mathbb{N}_a \to \mathbb{R}$ is of exponential order $r \geq 1$ and let $\nu > 0$ be given with $n - 1 < \nu \leq n$. Then for $s \in \mathbb{C}/\overline{B_{-1}(r)}$,*

$$\mathcal{L}_{a+\nu}\{\Delta_a^{-\nu} f\}(s) = \frac{(s+1)^{\nu}}{s^{\nu}} \mathcal{L}_a\{f\}(s), \tag{1.148}$$

and

$$\mathcal{L}_{a+\nu-n}\{\Delta_a^{-\nu} f\}(s) = \frac{(s+1)^{\nu-n}}{s^{\nu}} \mathcal{L}_a\{f\}(s). \tag{1.149}$$

1.9.3 Laplace transform of fractional difference operator

Now let us turn to the evaluation of the Laplace transform of the Riemann-left fractional difference operator. Readers are refereed to reference [39] for more analysis details.

Theorem 1.20. *Let $f : \mathbb{N}_a \to \mathbb{R}$ with exponential order $r \geq 1$ and let $\nu > 0$ be given with $n - 1 < \nu \leq n$. Then for $s \in \mathbb{C}/\overline{B_{-1}(r)}$, we have*

$$\mathcal{L}_{a+\nu-n}\{\Delta_a^{\nu} f\}(s) = s^{\nu}(s+1)^{n-\nu} \mathcal{L}_a\{f\}(s) - \sum_{j=0}^{n-1} s^j \Delta_a^{\nu-1-j} f(a+n-\nu). \tag{1.150}$$

Chapter 2

Stability of Fractional-order Difference equations

2.1 Introduction

The asymptotic stability of discrete fractional systems is an important subject since it brings us a step closer to establishing the existence of chaos and serves as a basis for proving the convergence of a system's states to zero (or some other equilibrium) as time approaches infinity. This is particularly important when dealing with the stabilization and synchronization of discrete fractional dynamical systems.

In this chapter, a brief overview on the recent stability results of fractional difference equations and the analytical methods used are provided. These equations include linear fractional difference equations and nonlinear fractional difference equations. Some conclusions for stability are similar to that of classical integer-order difference equations. However, not all of the stability conditions are parallel to the corresponding classical integer-order difference equations because of the non-locality of fractional calculus. Some remarks and examples are also included.

2.2 Stability notions

Let us consider the vector difference equation

$$x(n+1) = f(n, x(n)), \quad x(n_0) = x_0, \tag{2.1}$$

where $x(n) \in \mathbb{R}^k$ $f : \mathbb{Z}^+ \times \mathbb{R}^k \to \mathbb{R}^k$. assume that $f(n, x)$ is continous in x.

The following definitions are associated with the stability problem in the paper.

Proposition 21. A point x^* in $\mathbb{R}^k$ is called equilibrium point of (2.1) if $f(n, x^*) = x^*$ for all $n \geq n_0$.

Remark 10. In most of the literature x^* is assumed to be the origin 0 and is called zero solution. The justification for this assumption is as follows:

Let $y(n) = x(n) - x^*$. Then (2.1) becomes

$$y(n+1) = f(n, y(n) + x^*) - x^* = g(n, y(n)). \tag{2.2}$$

Notice that $y = 0$ corresponds to $x = x^*$. Since in many cases it is not convenient to make this change of coordinates, we will not assume that $x^* = 0$ unless it is more convenient to do so.

Without loss of generality, let the equilibrium point be $x^* = 0$, we introduce the following definitions.

Definition 18. The zero solution of fractional difference system (2.1) is said to be stable if, for all $\epsilon > 0$, there exist $\delta = \delta(t_0, \epsilon) > 0$ such that if $||x(t_0)|| < \delta$ then any solution $x(t)$ of (2.1) satisfies $||x(t)|| < \epsilon$ for all $t > t_0$ where $t \in \mathbb{N}_{t_0}$.

Definition 19. The zero solution is said to be asymptotically stable if there exist a $\delta = \delta(t_0) > 0$ such that $||x(t_0)||$ implies $||x(t)|| \to$ as $t \to +\infty$.

As indicated above, we begin with the integer order case.

2.3 Stability of integer order difference systems

2.3.1 Stability of linear difference system

Consider the following integer order difference system

$$\begin{cases} \Delta x(k) = Ax(k), & k \in \mathbb{N}, \\ x(0) = x_0, & x_0 \in \mathbb{R} \end{cases} \tag{2.3}$$

where A is a $n \times n$ constant matrix defined on $\mathbb{Z}^+$ and $x(k) = (x_1(k), x_2(k), \dots x_n(k)) \in \mathbb{R}^n$. The system (2.3) has an equilibrium point in the origin ($x^* = 0$). The solution of the linear system (2.3) starting from x_0 has the form

$$x(n) = (A + I)^k x_0, \tag{2.4}$$

where I is the identity matrix. We are now ready to introduce the various stability notions of the linear difference systems.

Theorem 2.1. *The solution of (2.3) is said to be:*

- *Globally asymptotically stable on $\mathbb{N}$, if all the eigenvalues λ_j of A satisfy $|\lambda_j + 1| < 1$, $1 \le j \le n$.*
- *Unstable on $\mathbb{N}$, if there is an eigenvalue λ of A satisfying the condition $|\lambda + 1| > 1$.*

Example 10. We consider a discrete system with matrix A for system (2.3), given by

$$A = \begin{bmatrix} 0 & 1/2 \\ -1 & -1 \end{bmatrix}.$$

The characteristic equation of matrix A is $\lambda^2 + \lambda + \frac{1}{2} = 0$, with equilibrium points $\lambda_1 = \frac{-1-i}{2}$ and $\lambda_2 = \frac{-1+i}{2}$. Then,

$$|\lambda_1 + 1| = |\lambda_2 + 1| < 1.$$

Hence by Theorem 2.1, the solution of system is asymptotically stable on $\mathbb{N}$.

Example 11. Now, we consider the following system

$$\Delta x(n) = \begin{bmatrix} 1 & -1 \\ -1 & 1.5 \end{bmatrix} x(n), \quad n \in \mathbb{N}. \tag{2.5}$$

Similarly, the characteristic equation of the matrix is $\lambda^2 - 2.5\lambda + 1.5 = 0$, with equilibrium points $\lambda_1 = \frac{2.5-i\sqrt{3.75}}{2}$ and $\lambda_2 = \frac{2.5+i\sqrt{3.75}}{2}$. Since $|\lambda_2 + 1| = 2.58$, therefore from Theorem 2.1 the trivial solution of (2.5) is unstable in $\mathbb{N}$.

2.3.2 Stability of nonlinear systems

Consider the nonlinear discrete-time system

$$\begin{cases} \Delta x(n) = f\left(x(n)\right), & n \in \mathbb{N}, \\ x(0) = x_0, & x_0 \in \mathbb{R}. \end{cases} \tag{2.6}$$

where $x(k) \in \mathbb{R}$ is the state and $f : \mathbb{R}^n \to \mathbb{R}^n$ is a continuously differentiable function. In the following, we suppose that $f(0) = 0$, hence, $x^* = 0$ is an equilibrium point for system (2.6).

2.3.2.1 Linearisation method

The most fundamental tool involved in the analysis of nonlinear discrete dynamical systems is *linearisation* of the system about a trivial solution. The *linearization* associated with the system given by equation (2.6) is determined by the Jacobian matrix as illustrated in the following theorem.

Theorem 2.2. *Let J be the Jacobian matrix of $f = (f_1, f_2, \ldots, f_n)^T$ at the point zero. The trivial solution of nonlinear system (2.6) is said to be:*

- *Asymptotically stable on $\mathbb{N}$, if all the eigenvalues λ of J satisfy $|\lambda_j + 1| < 1$, $1 \leq j \leq n$.*
- *Unstable on $\mathbb{N}$, if there is an eigenvalue λ of A satisfying $|\lambda + 1| > 1$.*

Example 12. We consider the Nicholson-Bailey predator prey model as example, which is given by

$$\begin{cases} \Delta x(n) = ax(n) \exp^{-by(n)} \\ \Delta y(n) = cx(n) \left(1 - \exp^{-by(n)}\right), \end{cases} \tag{2.7}$$

where x is prey population size at discrete time n and y is predator population size at time discrete time n. Let $f = (f_1, f_2)$, where $f_1 = ax(n)\exp^{-by(n)}$ and $f_2 = cx(n)\left(1-\exp^{-by(n)}\right)$, then the Jacobian matrix is given by

$$J = \begin{pmatrix} a\exp^{-by(0)} & -abx(0)\exp^{-by(0)} \\ c\left(1-\exp^{-by(0)}\right) & bcx(0)\exp^{-by(0)} \end{pmatrix} = \begin{pmatrix} a & 0 \\ 0 & 0 \end{pmatrix}, \tag{2.8}$$

the characteristic equation of J is equal to $\lambda^2 - a\lambda = 0$, hence, by Theorem 2.2 the trivial solution of (2.7) is unstable on $\mathbb{N}$ when $|a+1| < 1$.

2.3.2.2 Lyapunov direct method

The *Lyapunov direct method* allows one to investigate the qualitative nature of solutions without actually determining the solutions themselves, which is regard as one of the major tools in stability theory. We now follow [46] and illustrate the method with Theorem 2.3.

Theorem 2.3. *If there exists a function $V : \mathbb{R}^n \to \mathbb{R}^+$, (Lyapunov function) which is continuous and such that*

$$\begin{aligned} &V(0) = 0 \quad \text{and} \quad V\left(x(n)\right) > 0, \quad \forall\, x(n) \neq 0, \\ &\Delta V\left(x(n)\right) = V\left(x(n+1)\right) - V\left(x(n)\right) \leq 0, \quad \forall k \in \mathbb{N}. \end{aligned} \tag{2.9}$$

Then the trivial solution of (2.6) is stable. Moreover if

$$\Delta V\left(x(k)\right) = V\left(x(k+1)\right) - V\left(x(k)\right) < 0, \quad \forall k \in \mathbb{N}. \tag{2.10}$$

Then the trivial solution of (2.6) is asymptotically stable. One should not that, there is no specific way to generate Lyapunov functions.

Example 13. Consider the non-linear system given by

$$\begin{cases} \Delta x(n) = \frac{y(n)}{1+y^2(n)} - x(n), \\ \Delta y(n) = \frac{x(n)}{1+y^2(n)} - y(n), \end{cases} \tag{2.11}$$

which has its only equilibrium point in the origin. Our first choice of a Lyapunov function will be

$$V(x) = x^2 + y^2$$

this is clearly continuous and positive definite on $\mathbb{R}$. Hence, we find

$$\Delta V(x(n)) = V(x(n))\left(\frac{1}{[1+x_2^2(n)]^2} - 1\right) \leq 0.$$

From Theorem 2.3, we can conclude that the trivial solution is stable. This example is taken from the reference [54].

2.4 Stability of fractional order difference systems

2.4.1 Stability of fractional order linear systems

In this section, we will conceder the stability notions for the fractional order - difference systems involving the Caputo-like difference operator.

Consider the following general type of linear fractional difference equation involving Caputo left operator

$$ {}^{C}\Delta_a^{\nu} y(n+1-\nu) = Ay(n), \tag{2.12}$$

where matrix $A \in \mathbb{R}^{n\times n}$ and ${}^{C}\Delta_a^{\nu}$ is the Caputo left difference operator, where $0 < \nu < 1$. Then we have the following result, which was introduced in [55].

Theorem 2.4. *Let $\nu \in (0,1]$ and $A \in \mathbb{R}^{n\times n}$. Then (2.12) is asymptotically stable if and only if the isolated zeros, off the non-negative real axis, of $det(1-z^{-1}(1-z^{-1})^{-\nu}A)$ lie inside the unit circle.*

Remark 11. If $\nu \to 1^{-}$, then Theorem 2.4 simplifies to the isolated zeroes, the *non-negative real axis*, of

$$ det\left(I - \frac{1}{z-1}A\right) = \frac{1}{z-1} det((z-1)I - A), \tag{2.13}$$

lie inside the unit disk, this means all the eigenvalues $\lambda = (z-1)$ of A satisfies $|(z-1)+1| = |z| < 1$, which is the same results of integer order results reported in Theorem 2.1.

First, we start by righting the discrete solution of system (2.12). Using the Taylor formula, reported in Chapter 1 Theorem 1.13, we get

$$ y(t) = \sum_{k=0}^{m-1} \frac{(t-a-\nu+m)^{(k)}}{k!}\Delta^k y(a+\nu-m) + \frac{1}{\Gamma(\nu)}\sum_{s=a}^{t-\nu}(t-s-1)^{(\nu-1)}\Delta_{a+\nu-m}^{\nu} y(s), \quad t \in \mathbb{N}_{a+\nu} \tag{2.14}$$

$$ = \sum_{k=0}^{m-1} \frac{(t-a-\nu+m)^{(k)}}{k!} a_k + \frac{1}{\Gamma(\nu)}\sum_{s=a}^{t-\nu}(t-s-1)^{(\nu-1)} F(y(s+\nu-m)). \tag{2.15}$$

For $t = a+n+1$, $n = 0,1,2,\ldots$, and following the same steps in formula (1.29); the previous equation reduces to

$$ y(a+\nu+n) = y_{-1} + \sum_{s=0}^{n} B(n-s)y(a+\nu+s-1), \tag{2.16}$$

where the kernel function $B(n-s)$ is given, by

$$ B(n-s) = \frac{A}{(n-s)!}\prod_{j=1}^{n-s}(\nu+j-1).$$

Notice that (2.16) is a non-homogeneous Volterra difference equation of the convolution type.

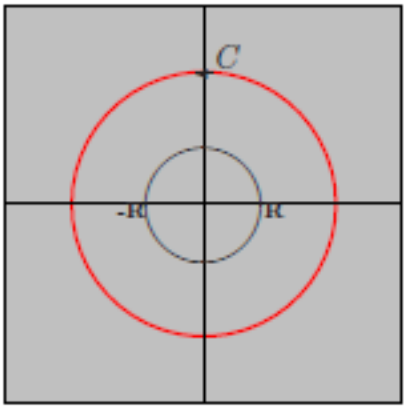

Figure 2.1: Region of analyticity of $\bar{y}$ and the contour C.

Firstly, we focus on the *scalar case*, i.e, we will proof Theorem 2.4 when $A = \lambda$.

Proof. Let $y(a+\nu+s-1) = y_{s-1}$ and $A = \lambda$. The scalar equation (2.16) is simplified to

$$y_n = y_{-1} + \lambda \sum_{s=0}^{n} \frac{1}{(n-s)!} \left(\prod_{k=1}^{n-s} (\nu + k - 1) \right) y_{s-1}, \quad n = -1, 0, 2, \dots \tag{2.17}$$

Likewise, we shall take $y_{-1} = 1$.

Cas 1 . $\lambda = 0$, then $y_n = y_{-1}$ for $k = 0, 1, 2, \cdots$, and we discuss the sign of λ.

Cas 2 . $\lambda > 0$, then $y_n > 1$ for $n \leq 0$,

$$y_n > 1 + \lambda \sum_{s=0}^{n} \frac{1}{(n-s)!} \left(\prod_{k=1}^{n-s} (\nu + k - 1) \right) = 1 + \lambda \sum_{s=0}^{n} \frac{1}{s!} \left(\prod_{k=1}^{s} (\nu + k - 1) \right). \tag{2.18}$$

Since $\frac{\prod_{k=1}^{s}(\nu+k-1)/s!}{1/(\nu+s)} = \nu \frac{\prod_{k=1}^{s}(\nu+k)}{s!} > \nu$ and $\prod_{k=1}^{s} \frac{(\nu+k)}{s!}$ is monotonic increasing. Therefore, y_n diverges to infinity.

Cas 3 . If we assume $\lambda < 0$, let $\bar{y} = \mathcal{Z}(\{y_n\})$. Then

$$\bar{y} = (1 - z^{-1})^{-1} + \lambda (1 - z^{-1})^{-\nu} (1 + z^{-1} \bar{y}); \quad |z| > R \geq 1. \tag{2.19}$$

Solving for $\bar{y}$ yields

$$\bar{y} = \frac{(1 - z^{-1})^{-1} + \lambda (1 - z^{-1})^{-\nu}}{1 - \lambda z^{-1} (1 - z^{-1})^{-\nu}} = \frac{\frac{z}{z-1} + \lambda \left(\frac{z}{z-1} \right)^{\nu}}{1 - \lambda \frac{1}{z} \left(\frac{z}{z-1} \right)^{\nu}}. \tag{2.20}$$

That says

$$y_n = \int_C z^{n-1} \bar{y}(z) dz,$$

where C, see Figure 2.1, is any positively-oriented simple-closed contour in the analyticity region of $\bar{y}$ that encircles all singular points of $\bar{y}(z)$. The function $\left(\frac{z}{z-1}\right)^{\nu} = \frac{z^{\nu}}{(z-1)^{\nu}}$ is multi-valued. We introduce the branch cut

$$\begin{cases} |z| > 0, & -\pi \leq \theta < \pi, \\ |z-1| > 0, & -\pi \leq \theta < \pi. \end{cases} \tag{2.21}$$

With that in mind, we consider the contour C_ρ, depicted in Figure 2.2. The inner circles are of radius ρ which we take it small enough so that all isolated singularities of $\bar{y}$ are inside the C_ρ.
Since the line integrals of $z^{n-1}\bar{y}(z)$ over the inner circles in Figure 2.2 tend to zero as $\rho \to \infty$, we have

$$\begin{aligned} \int_C z^{n-1}\bar{y}(z)\,dz &= \lim_{\rho\to 0}\int_{C_\rho} z^{n-1}\bar{y}(z)\,dz \\ &= 2\pi i \sum_i Res\left(z^{n-1}\bar{y}(z), z_i\right) \\ &= 2\pi i \sum_i z_i^{n-1} Res(\bar{y}(z), z_i), \end{aligned}$$

where the z_i's are the isolated singularities $\bar{y}(z)$. Indeed, the singularities of $\bar{y}(z)$ are

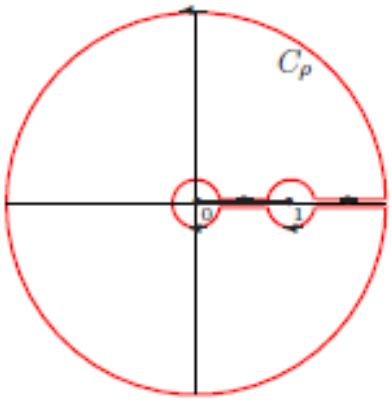

Figure 2.2: The contour C_ρ.

simple poles given by the zeros of

$$Q(z) = 1 - \lambda \frac{1}{z}\left(\frac{z}{z-1}\right)^{\nu}.$$

To see this, suppose z_i is a zero of $Q(z)$. Then

$$\lambda\left(\frac{z_i}{z_i-1}\right)^{\nu} = z_i, \quad \text{and so} \quad Q'(z_i) = \frac{1-\nu-z_i}{z_i(1-z_i)} \neq 0$$

because $Q(1-\nu) \neq 0$ if $0 < \nu < 1$. Furthermore, with $P(z) = \frac{z}{z-1} + \lambda\left(\frac{z}{z-a}\right)^{\nu}$, where $P(z_i) = \frac{z_i}{z_i-1} + z_i \neq 0$.
Given the branch cat depicted in (2.21), let $z = |z|\exp^{i\theta}$ and $z-1 = |z-1|\exp^{i\phi}$, where $|z|, |z-1| > 0$ and $-\pi \leq \phi, \theta < \pi$. Hence,

$$Q(z) = 0 \Leftrightarrow \lambda \frac{|z|^{\nu-1}}{|z-1|^{\nu}} \exp^{-i[(1-\nu)\theta+\nu\phi]} = 1 \Leftrightarrow (1-\nu)\theta + \nu\phi = -\pi \ \& \ \lambda \frac{|z|^{\nu-1}}{|z-1|^{\nu}}. \quad (2.22)$$

Moreover, since $-\pi \leq \theta$, $\theta = \phi = -\pi$ and, consequently $|z-1| = |z|+1$. Therefore, there are finitely many poles inside C_ρ and the residue of each is finite, which complete the proof.

□

Corollary 5. If $\nu = \frac{1}{2}$, then the zero solution of equation (2.12) is asymptotically stable if and only if $-\sqrt{2} < \lambda < 0$.

Example 14. Consider the following $\frac{1}{2}$-order difference system

$$\begin{cases} \Delta^{\frac{1}{2}}_{a-\frac{1}{2}} y(t) = \lambda y(t-\frac{1}{2}), \quad t \in \mathbb{N}_a, \text{ and } \lambda \in \mathbb{R}, \\ y(a-\frac{1}{2}) = 1. \end{cases} \quad (2.23)$$

Recall that Corollary 5 asserts that the zero solution of equation (2.23) is asymptotically stable if $-\sqrt{(2)} < \lambda < 0$. This, as can be seen, is evident in Figure 2.3, which depicts the solution $\{yn\}$ for different values of λ.

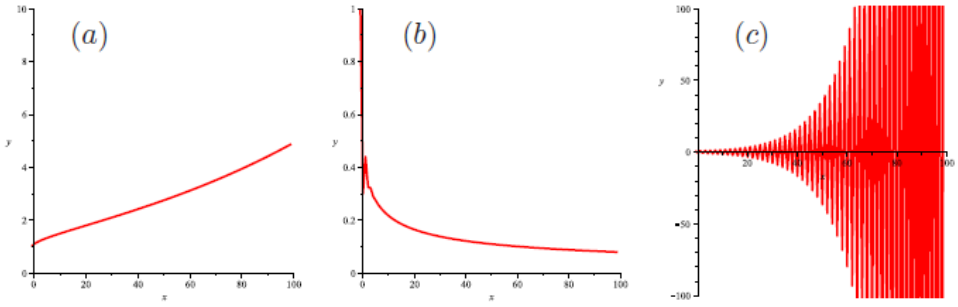

Figure 2.3: The first 100 iterates of the solution yn of Example 14, for (a) $\lambda = 0.1$, (b) $\lambda = -0.7$, and (c) $\lambda = -1.5$.

On the other hand, it has been shown by [58], that for the matrix case we have the following result.

Theorem 2.5. *Let $\nu \in (0,1]$ and $A \in \mathbb{R}^{n\times n}$. Then (2.12) is asymptotically stable if and only if the isolated zeros, off the non-negative real axis, of $det(1-z^{-1}(1-z^{-1})^{-\nu}A)$ lie inside the unit circle.*

Proof. Following the same lines of reasoning employed in the scalar case and applying the Z-transform to (2.16), one obtains

$$\bar{y}(z) = (1 - z^{-}1)^{-1} y_{-1} + A(1 - z^{-1})^{-\nu}(y_{-1} + z^{-1}\bar{y}(z)),$$

by simple calculation, one gets

$$\bar{y}(z) = \left(I_p - z^{-1}(1 - z^{-1})^{-\nu} A\right)^{-1} \left((1 - z^{-1})^{-1} + (1 + z^{-1})^{-\nu} A\right) y_{-1},$$

where I_p is the identity matrix of order p. □

Example 15. Consider the following $\frac{1}{2}$-order systems of difference equations

$$\Delta^{\frac{1}{2}}_{a-\frac{1}{2}} y(t) = \begin{bmatrix} \lambda_1 & 1 \\ 0 & \lambda_2 \end{bmatrix} y\left(t - \frac{1}{2}\right), \quad t \in \mathbb{N}_a,\ a \in \mathbb{R},\ \text{and}\ \lambda_1, \lambda_2 \in \mathbb{R}, \tag{2.24}$$

subject to the initial condition

$$y\left(a - \frac{1}{2}\right) = \begin{bmatrix} 1 \\ 1 \end{bmatrix}.$$

Recall that Corollary 5 asserts that the zero solution of (2.24) is asymptotically stable if $-\sqrt{2} < \lambda_1, \lambda_2 < 0$. This, for different values of λ_i, is confirmed in Figure 2.4 below. The figure depicts the 2-norm of the solution $\{y_n\}$ for the first 100 iterates.

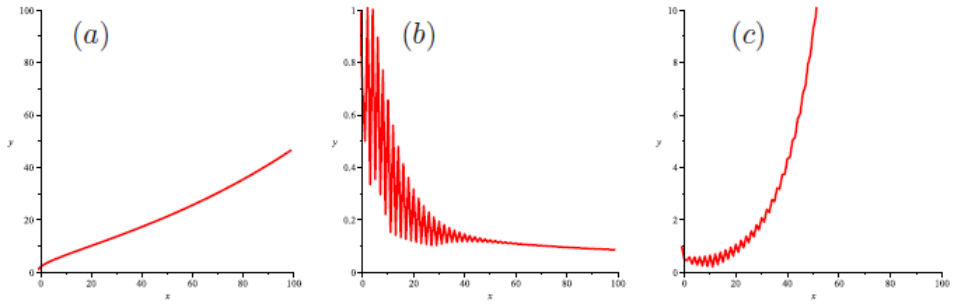

Figure 2.4: The first 100 iterates of 2-norm of the solution y_n of Example 15, for (a) $\lambda_1 = 0.1$, $\lambda_2 = 0.01$, (b) $\lambda_1 = -1.3$, $\lambda_2 = -1$, and (c) $\lambda_1 = -1.5$, $\lambda_2 = -0.7$.

A direct extension of stability theorem of linear difference equations with integer order was given by Cermak. et al in manuscript [55] and is given as follows.

Theorem 2.6. *Let $\nu \in (0, 1)$ and A is an $n \times n$ constant matrix. Then the trivial solution of (2.12) is asymptotically stable, if*

$$\lambda \in= S^{\nu} \left\{ z \in \mathbb{C} : \ |z| < \left(2 \cos \frac{|\arg z| - \pi}{2 - \nu}\right)^{\nu} \ \textit{and}\ |\arg z| > \frac{\nu\pi}{2} \right\}, \tag{2.25}$$

for all the eigenvalues λ of A. In this case, the solutions of (2.12) decay towards zero algebraically (and not exponentially), more precisely

$$||y(n)|| = O\left(n^{-\nu}\right) \quad as\ n \to \infty, \tag{2.26}$$

for any solution x of (2.12). Furthermore, if $\lambda \in \mathbb{C}(S^{\nu})$ for an eigenvalue λ of A, the zero solution of (2.12) is not stable.

As we can see, in case $\nu = 1$, the above stability result shows that roots of the equation $det(diag(\lambda, \lambda, \ldots, \lambda) - A) = 0$ lie outside the closed angular sector $|arg(\lambda)| \leq 2$, thus generalizing the result for the integer case $\alpha = 1$ reported in the previous section. In [55] the authors used z-transform and the stability definitions for linear Volterra difference systems to prove Theorem 2.6.

Remark 12. The assertions of Theorems 2.6 and 2.5 describe the same stability region, but these analytical descriptions are different. In particular, the condition stated in Theorem 2.6 seems to be more convenient for practical purposes due to the explicit form of S^{ν}. Also, it enables us to collect the following basic properties of S^{ν}.

Example 16. Consider the following fractional linear difference system

$$\begin{cases} {}^{C}\Delta_{a}^{\nu} x(t) = -x(t-1+\nu) + y(t-1+\nu), \\ {}^{C}\Delta_{a}^{\nu} y(t) = -y(t-1+\nu) + z(t-1+\nu), \\ {}^{C}\Delta_{a}^{\nu} z(t) = z(t-1+\nu), \end{cases} \tag{2.27}$$

where $a = 0$ and $t \in \mathbb{N}_{1+\nu}$, and the matrix A is given by

$$A = \begin{pmatrix} -1 & 1 & 0 \\ 0 & -1 & 1 \\ 0 & 0 & 1 \end{pmatrix}.$$

We can see that the characteristic equation of the matrix A is given by $(-1-\lambda)^2(1-\lambda) = 0$. One can observe that the eigenvalues λ_i of the matrix A satisfy

$$|\arg \lambda_i| = \pi \frac{\nu\pi}{2} \quad \text{and} \quad |\lambda_i| = 1\left(2\cos\frac{|\arg \lambda_i| - \pi}{2-\nu}\right).$$

Therefore, by Theorem 2.6 the trivial solution is asymptotically stable. The state evolution of the linear fractional system are depicted in Figure 2.5.

2.4.2 Stability of fractional order nonlinear systems

In the following we will investigate stability of the Caputo left fractional order h-difference systems by using the discrete fractional Lyapunov direct method. Consider the following nonlinear vector fractional order h-difference equations

$$\begin{cases} {}^{C}_{h}\Delta_{a}^{\nu} y(t) = f(t+\nu h, y(t+\nu h)), \quad t \in (h\mathbb{N})_{a+(1-\nu)h}, \\ y(a) = y_0 \in \mathbb{R}^n, \end{cases} \tag{2.28}$$

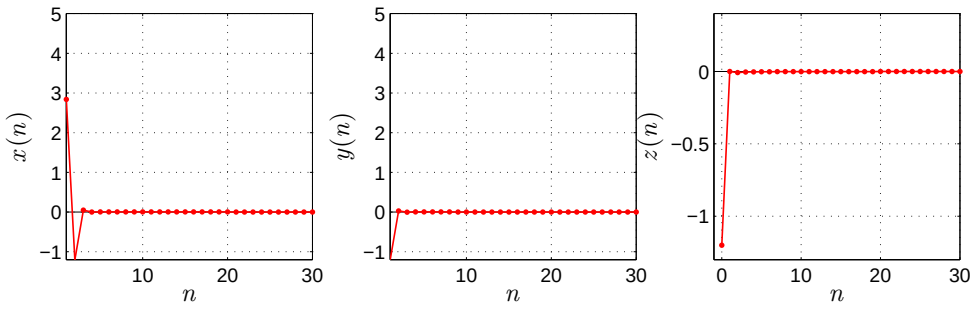

Figure 2.5: The evolution of the solution yn of Example 16, for $\nu = 0.98$.

where f is continuous with respect to y, and $\nu \in (0, 1]$. First, we present the following simple definitions and important facts.

Definition 20. [61] A function $\gamma(t)$ is said to belong to the class $\mathcal{K}$ if and only if $\gamma \in C[(0, \gamma), \mathbb{R}_+]$, $\gamma(0) = 0$, and $\gamma(t)$ is strictly monotonically increasing in t.

Definition 21. A real valued function $V(t, y)$ defined on $(h\mathbb{N})_a \times S_\gamma$, where $S_\gamma = \{y \in \mathbb{R}^n : ||y|| \leq \gamma$, is said to be decrecent if and only if $V(t, 0) = 0$ for all $t \in (h\mathbb{N})_a$ and there exists $\gamma(t) \in \mathcal{K}$ such that $V(t, y) \leq \gamma(t)$, $||y|| = t$, $(t, x) \in (h\mathbb{N})_a \times S_\gamma$.

Then we present the following theorem of a discrete fractional Lyapunov direct method for system (2.28).

Theorem 2.7. *[61] Let $y = 0$ be an equilibruim point of the system (2.28). If there exists a positive definite and decrescent scalar function $V(t, y)$, discrete class-$\mathcal{K}$ γ_1, γ_2, γ_3 such that*

$$\gamma_1 \left(||y(t)|| \right) \leq V(t, y(t)) \leq \gamma_2 \left(||y(t)|| \right), \quad t \in (h\mathbb{N})_a \tag{2.29}$$

and

$${}_h^C\Delta_a^\nu V(t, y(t)) \leq -\gamma_3 \left(||y(t + \nu h|| \right), \quad t \in (h\mathbb{N})_{a+(1-\nu)h}. \tag{2.30}$$

Then the system (2.28) is asymptotically stable.

Proof. From equations (2.29) and (2.30) we have

$${}_h^C\Delta_a^\nu V(t, y(t)) \leq -\gamma_3(\gamma_2^{-1} \left(V(t + \nu h, x(t + \nu h)) \right), \quad t \in (h\mathbb{N})_{a+(1-\nu)h}, \tag{2.31}$$

where γ_2^{-1} denotes the inverse of γ_2. It is evident that $\gamma_3 \circ \gamma_2^{-1}$ is a discrete class $\mathcal{K}$-function. Considering a fractional difference equation

$${}_h^C\Delta_a^\nu U(t, y(t)) = -\gamma_3 \left(\gamma_2^{-1}(U(t + \nu h, y(t + \nu h))) \right), \quad t \in (h\mathbb{N})_{a+(1-\nu)h}.$$

Before we proceed we need the following lemma.

Lemma 5. Let $u(t)$ and $g(t)$ satisfy

$$ {}^{C}_{h}\Delta^{\nu}_{a}u(t) = \lambda u - t + \nu h), \quad 0 < \nu \leq 1, \tag{2.32} $$

and the inequality

$$ {}^{C}_{h}\Delta^{\nu}_{a}g(t) \leq \lambda g(t + \nu h), \tag{2.33} $$

respectively. If $\lambda < 0$ and $g(a) = u(a) > 0$, then $g(t) \leq u(t)$ for all $t \in (h\mathbb{N})_a$.

Therefore, $V(t, y(t))$ is bounded by the solution $U(t, y(t))$ from the previous lemma. $V(t, y(t))$ is a positive scalar function and we can derive $\lim_{t\to\infty} V(t, y(t)) = 0$. Since γ_1 is a discrete class $\mathcal{K}$-function, it follows that $\lim_{t\to\infty} y(t) = 0$ due to the fact $\gamma_1(||y(t)||) \leq V(t, y(t)),\ t \in (h\mathbb{N})_a$. This completes the proof. □

One should note that the construction of γ_i functions it's not easy. In this section, we present another Lemma and sufficient condition. We start by presenting the following lemma.

Lemma 6. (*Discrete comparison principal*)
For $\nu \in (0, 1]$, ${}^{C}_{h}\Delta^{\nu}_{a}y(t) \geq C_h\Delta^{\nu}_{a}y(t), \quad \forall t \in (h\mathbb{N})_{a+(1-\nu)h}$ and $x(a) = y(a)$. Then

$$ x(t + \nu h) \geq y(t + \nu h). $$

Proof. Let $F(t) = x(t) - y(t)$. Due to ${}^{C}_{h}\Delta^{\nu}_{a}y(t) \geq C_h\Delta^{\nu}_{a}y(t)$, we have ${}^{C}_{h}\Delta^{\nu}_{a}F(t) \geq 0$, which can be written explicitly

$$ \frac{h}{\Gamma(1-\nu)} \sum_{s=a/h}^{t/h+\nu-1} (t - \sigma(sh))^{(-\nu)}_{h}\Delta_s F(sh) \geq 0, t \in (h\mathbb{N})_{a+(1-\nu)h}. \tag{2.34} $$

Using the summation by parts, let $g(sh) = \frac{(t-sh)^{-\nu}}{\Gamma(1-\nu)}$ and $f(sh) = F(sh)$. We derive

$$ \frac{(t - sh)^{-\nu}_{h}}{\Gamma(1-\nu)} F(sh)|^{t/h+\nu}_{s=a/h} - \frac{h}{\Gamma(1-\nu)} \sum_{s=a/h}^{t/h+\nu-1} (t - \sigma(sh))^{(-\nu-1)}_{h} F(sh) \geq 0. $$

Considering $F(sh)|_{s=1/h} = x(a) - y(a) = 0$ and $\frac{(t-sh)^{-\nu}_{h}}{\Gamma(1-\nu)}|_{s=t/h+\nu} = h^{-\nu}$, we can obtain

$$ F(t + sh) \geq \frac{1}{\Gamma(1-\nu)} \sum_{s=a/h}^{t/h+\nu-1} \frac{\Gamma(t/h - s)}{\Gamma(t/h - s + \nu + 1)} F(sh). $$

For $t = a + (1-\nu)h$, we have $F(t + \nu h) = F(a + h) \geq \frac{F(a)}{\Gamma(2)} = 0$. Since the discrete kernel holds

$$ \frac{\Gamma(t/h - s)}{\Gamma(1-\nu)\Gamma(t/h - s + \nu + 1)} > 0, \quad t \in (h\mathbb{N})_{a+(1-\nu)h}, $$

it successively follows that

$$ x(t + \nu h) - y(t + \nu h) = F(t + \nu h) \geq \frac{1}{\Gamma(1-\nu)} \sum_{s=a/h}^{t/h+\nu-1} \frac{\Gamma(t/h - s)}{\Gamma(t/h - s + \nu + 1)} F(sh) \geq 0, $$

and this completes the proof. □

A useful inequality for Lyapunov functions is now provided.

Lemma 7. For any discrete time $t \in (h\mathbb{N})_{a+(1-\nu)h}$, the following inequality holds

$$ {}_h^C\Delta_a^\nu x^2(t) \leq 2x(t+\nu h)\, {}_h^C\Delta_a^\nu x(t), \quad 0 < \nu \leq 1. \tag{2.35}$$

Remark 13. For $\mathbf{y} = (y_1(t), \ldots, y_m(t))^T$, $t \in (h\mathbb{N})_{a+(1-\nu)h}$, Lemma 7 still hold. For example, we can have Lemma 7 as

$$ {}_h^C\Delta_a^\nu (x^T(t)x(t)) \leq 2x^T(t+\nu h)\, {}_h^C\Delta_a^\nu x(t), \quad t \in (h\mathbb{N})_{a+(1-\nu)h}$$

Example 17. Consider the following nonlinear fractional difference system

$$\begin{cases} {}_h^C\Delta_a^\nu x_1(t) = -x_1(t+\nu h) + x_2^3(t+\nu h), \ 0 < \nu \leq 1, \\ {}_h^C\Delta_a^\nu x_2(t) = -x_1(t+\nu h) - x_2(t+\nu h), \ t \in (h\mathbb{N})_{a+(1-\nu)h}, \end{cases} \tag{2.36}$$

with the initial conditions $x_1(0) = 0.4$ and $x_2(0) = 0.8$.
We use the Lyapunov function $V = \frac{1}{2}x_1^2(t) + \frac{1}{4}x_2^4(t)$. According to Lemma 7, we have

$$\begin{aligned} {}_h^C\Delta_a^\nu V \leq & x_1(t+\nu h) {}_h^C\Delta_a^\nu x_1(t) + \frac{1}{2}x_1^2(t+\nu) {}_h^C\Delta_a^\nu x_2^2(t) && (2.37)\\ \leq & \, x_1(t+\nu h) {}_h^C\Delta_a^\nu x_1(t) + x_2^3(t+\nu) {}_h^C\Delta_a^\nu x_2(t) && (2.38)\\ = & -x_1^2(t+\nu h) - x_2^4(t+\nu h) < 0. && (2.39) \end{aligned}$$

As a result, the system is asymptotically stable from Theorem 2.7. Using the h-fractional sum operator reported in Chapter 1, we can derive numerical formula of fractional nonlinear system (2.36). Note that, the numerical formula obtained is implicit formula. To plot the states of the system, we use the Newton method to transfer it into explicit one. Results are illustrated in Figure 2.6 which proof the theoretical results.

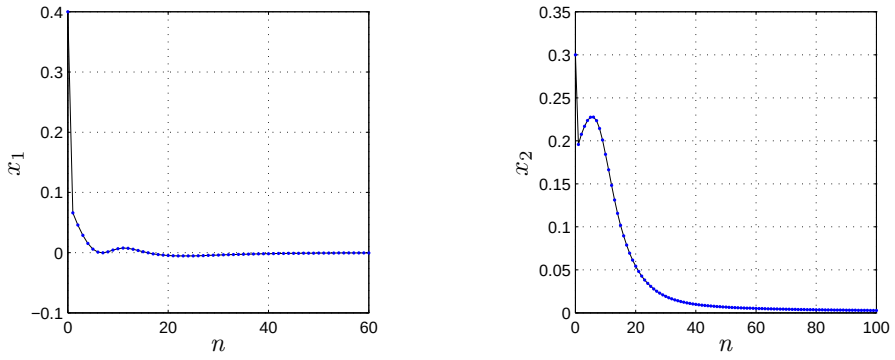

Figure 2.6: Asymptotic stability of states x_1 and x_2 for $\nu = 0.9$.

Chapter 3

Introduction to Chaos and Complexity Analysis of Fractional Order Maps

3.1 Introduction

Nonlinear systems are very interesting to engineers, physicists and mathematicians because most real physical systems are inherently nonlinear in nature [62]. In mathematics, a nonlinear system is any problem, where the variables to be solved cannot be written as a linear combination of independent components. If the equation contains a nonlinear function (power or cross product), the system is nonlinear as well. The system is nonlinear if there is some typical nonlinearity as, for instance, saturation, hysteresis, etc. These characteristics are basic properties of the nonlinear systems.

Nonlinear equations are difficult to be solved by analytical methods and give rise to interesting phenomena such as bifurcation and chaos. Even simple nonlinear (or piecewise linear) dynamical systems can exhibit completely a unpredictable behavior, the so-called deterministic chaos. Dynamical systems constitute a mathematical framework common to many disciplines, among which ecology and population dynamics. Chaos theory has been so surprising because it can also be found within trivial systems. Discrete chaotic systems have been around for a while. Hence we are forced to resort to different means in order to understand these behavior. This Chapter is meant to provide a simple and heuristic illustration of some basic features of chaos theory in nonlinear discrete dynamical systems with fractional order ν. Basically, this chapter introduces the basic mathematical concepts and numerical tools to analyze such irregular geometrical entities, in order to be able to carry out the analysis and numerical simulations required for discrete fractional system in our thesis. To this aim, the theoretical background needed for this research is presented. The concept of Lyapunov Exponents will be introduced first. Next, the 0-1 test algorithm for fractional discrete time systems will be presented. Then, two methods for calculating the complexity of fractional order maps will be discussed. We consider two systems which played a crucial role in the development of dynamical systems the-

ory: the integer-order logistic map and the integer order Hénon map and their fractional-order counterpart, to illustrate and demonstrate the methods.

3.2 Discrete time dynamical systems: maps

A *dynamical system* may be defined as a deterministic mathematical description for evolving the state of a system forward in time. Dynamical systems may be continuous time or discrete time outlined by differential equations or difference equations, respectively, or stochastic process. It is worth remarking from the outset that there is no specific difference between continuous and discrete time dynamical systems; as a continue system of dimension N can be reduced to a discrete time map of dimension $N-1$ via the Poincaré map [63] . Referring to discrete-time dynamical systems, such systems provide accurate models for natural physical phenomena in the field of biology, chemistry and physics. Moreover, discrete-time systems can avoid the calculation error of the numerical discretization of continuous ones.

Discrete-time dynamical systems can be written as the map [64]

$$\mathbf{x}(n+1) = f\left(\mathbf{x}(n)\right), \tag{3.1}$$

where $\mathbf{x}_n$ is N-dimensional, $\mathbf{x}(n) = (x_1(n), x_2(n), \ldots, x_N(n))$, which is a shorthand notation for

$$\begin{cases} x_1(n+1) = f_1(x_1(n), x_2(n), \ldots, x_N(n)), \\ \quad\vdots \\ x_N(n+1) = f_N(x_1(n), x_2(n), \ldots, x_N(n)), \end{cases} \tag{3.2}$$

with n denoting the discrete-time variable. Given initial values $(x_1(0), \ldots, x_N(0))$ we can compute $(x_1(n), \ldots, x_N(n))$ successively for all positive n using (3.1). Thus, the trajectory of $\mathbf{x}(0)$ is the sequence

$$\mathbf{x}(0), \quad \mathbf{x}(1) = f(\mathbf{x}(0)), \quad \mathbf{x}(2) = f^2(\mathbf{x}(0)), \ldots, \mathbf{x}(n) = f^n(\mathbf{x}(0)), \ldots$$

3.3 Chaotic dynamical systems

Chaos theory is a branch of mathematics which is focused on the behaviour of non-linear dynamic systems that are highly *sensitive to initial conditions*. Sensitive dependence here means that even a small change in one state of a deterministic non-linear system can result in large differences in a later state. Thus, although deterministic, the evolution in time of these systems cannot be predicted analytically and cannot be even approximated due to the finite resolution of any computational system that make it become complex. However, there is still order in this complex system because while the momentary behaviours appears random and chaotic, the general pattern of the system over time and space will display some type of order which can be modelled [70].

In the most used sense, chaotic dynamics are dynamics originated by regular dynamical equations with no stochastic coefficients, but at the same time, with trajectories that are similar

or indistinguishable from some stochastic processes [67]. Yorke et al., 1976, concluded that period three implies chaos. They discussed how a dynamical system with period three orbits gives an assurance that the system is chaotic. Several approaches and conditions are factored before the construction of any definition of chaos. One of the most popular definition of chaos, is the one given by Devaney [68], in which includes three fundamental parts. In addition to sensitivity to the variation of the initial conditions, a map $f : \mathbf{U} \to \mathbf{U}$ is chaotic then: f is topological transitive and f has a dense set of periodic points. Today, the chaos defined in this way is said to be the *Devaney chaos* or the *chaos in the sense of Devaney*. Later Banks et al. in [69] proved that if a system is transitive with dense periodic orbits then obviously sensitivity dependence to initial condition is guaranteed [71].

Ever since the disclose of Lorenz system in one of the Lorenz paper's on climatic expectation [72], chaos has become a hot research topic and a large number of chaotic systems were proposed over the last 50 years. The advancements in this area have been greatly influenced by the advancement of technology and personal computers, which makes it easier to follow the trajectories of chaotic systems for a longer time period and with higher precision. It is important to note that, for chaotic systems, trajectories cannot escape to infinity. Thus the theoretical analysis of chaos has been assisted by the numerical simulation of such chaotic systems, made possible by the use of computers [73]. Many tools, both qualitative and quantitative, have been developed to investigate this chaotic behavior using computer programs.

3.3.1 Characterisation of chaotic dynamical system

3.3.1.1 Sensitive initial condition

The sensitive dependence to initial condition also knows as the *butterfly effect* describes how a small change in one state of a deterministic non-linear system may lead to dramatic change in the behavior of the system over time. This makes prediction of future behavior impossible but this does not mean the system is not deterministic. The mathematical definition is given as follows.

Definition 22. Let $\mathbf{X}$ be a compact metric space and f a continuous map. A dynamical system $(\mathbf{X}, f)$ has sensitivity dependence on initial conditions if $\exists\, \delta > 0$ *such that, for* $x \in \mathbf{X}$ *and each* $\epsilon > 0$, *there is* $y \in \mathbf{X}$ *with* $d(x, y) < \epsilon$ *and* $n \in \mathbb{N}$ *such that* $d(f^n x, f^n y) > \delta$.

Numerically, sensitivity is measured by *Lyapunov exponent* such that a positive value implies the system is really sensitive to initial conditions. We will discuss this point later.

3.3.1.2 Strange attractors

A strange attractor is an *attractor* which displays sensitive dependence on initial conditions. We note that an *attractor* is a bounded region of phase space to which all sufficiently close trajectories from the so-called *basin of attraction* are attracted asymptotically for long enough times. In particular, the basin of attraction of attractor $\mathbf{A}$ is defined to be set of initial points $\mathbf{x}$ such that $f^n\mathbf{x}$ approaches $\mathbf{A}$ as $n \to \infty$, i.e, $\cup_{n<0} f^n\mathbf{U}$. We note that the basin of attraction can have a very complicated structure. Therefore, a strange attractor consistent of set of a infinity

points, in N dimensional space which is invariant under the dynamics, i.e if a point belongs to $\mathbf{A}$, its evolution also belongs to $\mathbf{A}$. This points correspond to the state of a chaotic system.

Apart from this definition, there exists no generally accepted formal definition of a strange attractors. Ruelle in [66] tries to give mathematical definition which is summarized as follows.

Definition 23. A bounded set $\mathbf{A}$ in N-dimensional space, of a discrete dynamical system described by the equation (3.1), is a *strange attractor* if there is a set $\mathbf{U}$ with the following properties [65]:

(a) *Attractor:* $\mathbf{U}$ is a N-dimensional neighbourhood of $\mathbf{A}$, i.e, $\mathbf{A}$ is contained in $\mathbf{U}$.

(b) *The bounded set $\boldsymbol{A}$ is attracting*: for every initial point $\mathbf{x}(0)$ in $\mathbf{U}$, the point $\mathbf{x}(n)$ with coordinates $x_1(n), \ldots, x_N(n)$ remains in $\mathbf{U}$ for positive n; it becomes and stays as close as one wants to A for n large enough.

(c) There is sensitive to dependence on initial condition.

(d) One can a choose point $\mathbf{x}(0)$ in $\mathbf{A}$ such that, arbitrary close to each other point in $\mathbf{A}$, there is a point $\mathbf{x}(n)$ for some positive n. This indecomposability condition implies that $\mathbf{A}$ cannot be spilt into two different attractors.

Strange attractor are relatively abstract mathematical objects, but computers gives them some life; and draw picture of them by plot the points $\mathbf{x}(n) = f^n(\ \mathbf{x}(0))$ with almost any initial value in $\mathbf{U}$ [72]. Thus, they give us a global description of the asymptotic behaviour of dynamical systems.

Remark 14. The property of sensitive dependence on initial conditions makes the attractor strange .

3.3.2 Example of discrete chaotic dynamical systems

We consider two systems which played a crucial role in the development of dynamical discrete systems theory: the logistic map and the Hénon map.

3.3.2.1 The Logistic map

The logistic map can be obtained by the discretization of logistic differential equation that was initially proposed in the population growth model by Verhulst [75]. This differential equation is

$$\frac{dx}{dt} = rx(1-x), \tag{3.3}$$

where, x denotes the total number of the population. The discretized logistic equation or logistic map:

$$x(n+1) = rx(n)\left(1 - x(n)\right), \quad n = 1, 2, \cdots . \tag{3.4}$$

This is an example of a first-order difference equation but non-invertible. Unlike its continuous version, the logistic map exhibits a complex dynamic behaviour and presents numerous applications. The value of x lies in the $[0, 1]$ interval and changes over time according to the parameter

$r \in (0, 4]$. This map will go through a whole spectrum of possible dynamical behaviour. In particular, when $r > 3$ the logistic map (3.8) has an attracting periodic orbit of period 2^n, with n tending to infinity as r tends to 3.57. When the latter value is reached there is the attractor shown in Figure 3.1.

To demonstrate the sensitivity to initial conditions, we plot two very close trajectories as shown in Figure 3.2 with $r = 4$. The blue curve stars from $x_1(0) = 0.1$ and the red curve stars from $x_2(0) = 0.099999$. The difference at the initial condition, 10^{-6}, is very tiny. It can be observed that at the beginning the time series are undistinguishable, but after a number of iterations, the difference between them builds up rapidly and becomes totally different. This a consequence of sensitivity, which is the characteristics of chaotic systems.

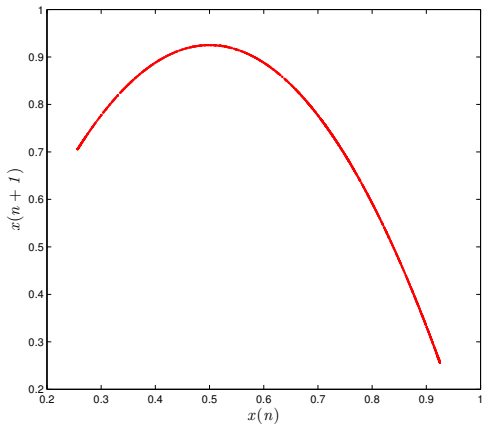

Figure 3.1: The chaotic attractor of the logistic map (3.8) with $r = 3.57$.

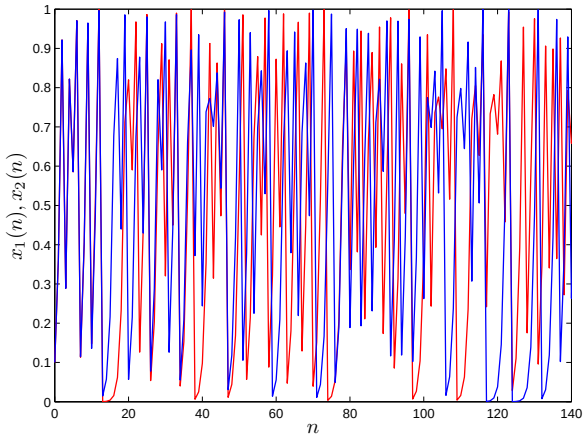

Figure 3.2: The trajectory portraits of states x_1 and x_2 starting from 0.1 and 0.10001 respectively, with $r = 4$.

3.3.2.2 The Hénon map

On of the most commonly studied and applied discrete chaotic system is the Hénon map, which was introduced in 1976 [3] as a discretization of the Poincaré section of the famous continuous-time Lorenz system. This can be considered as a two-dimensional extension of the logistic map:

$$\begin{cases} x_1(n+1) = 1 - \alpha x_1^2(n) + x_2(n), \\ x_2(n+1) = \beta x_1(n), \end{cases} \tag{3.5}$$

where α and $|\beta| \leq 1$ are external parameters. Because of its simplicity it lends itself to computer studies and numerous investigations followed. Set $\alpha = 1.4$, $\beta = 0.3$ the generated attractor is presented in Figure 3.3. Moreover the gently swirling boomerang-like shape of the attractor that arises through the dynamics is very appealing aesthetically. This object is now known as the ***Hénon attractor***. In fact it has become another icon of chaos theory next to the Lorenz attractor.

Remark 15. [76] Up to now no one knows whether the attractor in Hénon's transformation for $\alpha = 1.4$ and $\beta = 0.3$ really is a strange attractor according to the above or a similar definition even though very extensive numerical checks have been performed which all indicate a positive answer. This underlines the incomplete state of affairs. For example we could speculate that the experimental observations are due to an attractive periodic orbit with a very long period.

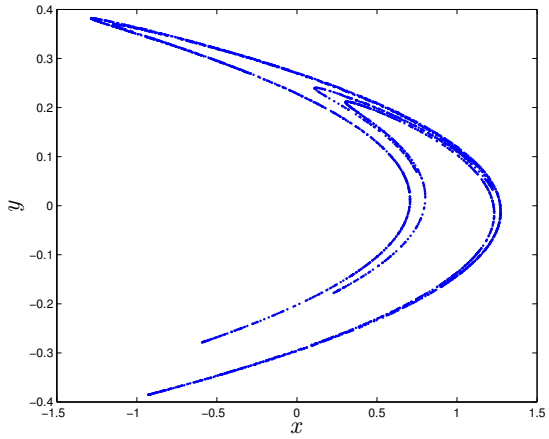

Figure 3.3: The chaotic attractor of the Hénon map (3.5)

3.3.3 Bifurcation Diagrams

With the discovery of chaotic dynamics, the theory has become even more important, as researchers try to find mechanisms by which systems change from simple to highly complicated behavior. Consider an n^{th}-order discrete-time system

$$x(n+1) = f\left(x(n), \alpha\right), \tag{3.6}$$

with a parameter $\alpha \in \mathbb{R}$. As α changes, the dynamic behavior of the system is also change. Typically, a small change in α produces small quantitative changes in the states of the system. Such change in specifc behavior of the map is known as a *bifurcation*. Accordingly, the bifurcation phenomenon describes the fundamental alteration in the dynamics of nonlinear systems under parameter variation. For this reason it is considered as a tool that help to understand equilibrium loss and its consequences for complex behavior. Moreover, bifurcation diagrams display some characteristic property of the asymptotic solution of a dynamical system as a function of a control parameter, allowing one to see at a glance where qualitative changes in the asymptotic solution occur. We call the parameter at which the dynamic behaviour changes the *bifurcation parameter*.

There are many types of periodic orbit local bifurcation, in the following will describe the most common bifurcations.

Example 18. ***Period Doubling Bifurcation***

As a prime example, we are going to analyse in details the bifurcation diagram of the logistic map (3.8). It is easy to verify that the logistic map has tow fixed point $x_{f1} = 0$ and $x_{f2} = 1 - \frac{1}{4r}$. The origin changes its stability with x_{f2} when it enters to the interval $[0, 1]$. Thus, it is stable for $0 < r < 0.25$. The second fixed point $x_{f2} = 1 - \frac{1}{4r}$ is stable for $0.25 < r < 0.75$, while it becomes unstable and spawns a stable period-two closed orbit when r passes through 0.75. Observe that the period-one fixed point still exists after the period-two orbit is created, though it has become unstable. As r is increased further, the period-two closed orbit becomes unstable and spawns a stable period-four closed orbit. This period- four orbit spawns a period-eight orbit and so on. This bifurcation is called the *period-doubling bifurcation* (or, sometimes, the ***flip bifurcation***). In Figure 3.4, the period- doubling bifurcations accumulate at a bifurcation value r at which the system becomes chaotic.

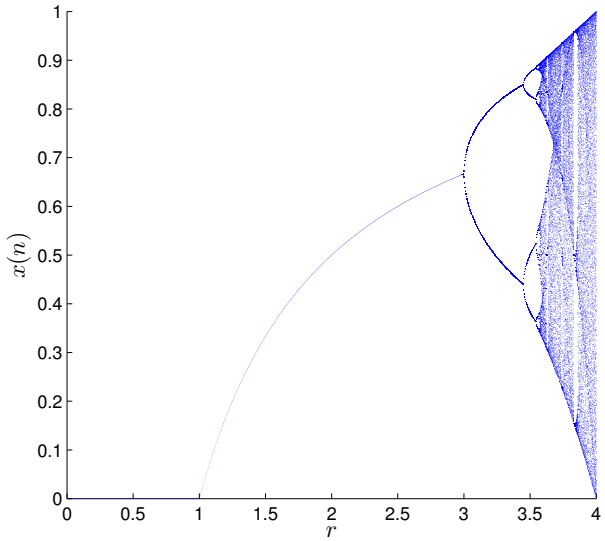

Figure 3.4: Period doubling route to chaos of the Logistic map.

Period-doubling bifurcation also occurs in the 2D Hénon map

$$\begin{cases} x_1(n+1) = 1 - \alpha x_1^2(n) + x_2(n), \\ x_2(n+1) = \beta x_1(n). \end{cases} \tag{3.7}$$

A bifurcation diagram for Hénon's map is shown in Figure 3.5

Example 19. ***Hopf bifurcation***
Hopf bifurcation in a discrete-time system: As a final example of the different types of bifurcation, we present the Hopf bifurcation of a fixed point of a map. This bifurcation is the discrete-time analogue of the Hopf bifurcation of an equilibrium point. In a discrete-time Hopf bifurcation, an invariant closed curve is created as a stable fixed point loses stability when the real parts of its (complex conjugate pair of) characteristic multipliers pass through the unit circle.

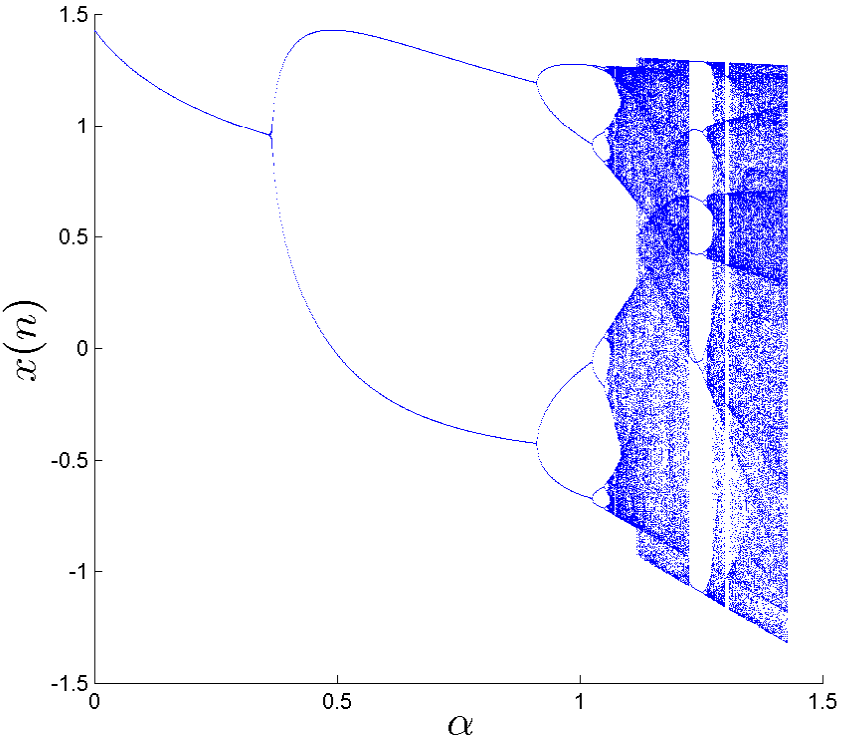

Figure 3.5: The bifurcation diagram of the Hénon map.

3.4 Fractional order discrete-time systems: fractional maps

Even the theory and applications of discrete fractional calculus may be considered as a novel topic, some recent contributions have been developed to deal with discrete analogues of conti-

inuous fractional calculus and fractional difference equations. Very recently, some literature has studied the dynamics, including chaotic behavior of discrete-time fractional order systems using the Caputo fractional difference operator type, introduced in Section 1.5. The first such system is the fractional-order logistic map which was proposed by Wu and Baleanu [103] where chaotic behaviors and a synchronization method of the fractional map were numerically illustrated. Over time, the dynamics of more discrete-time fractional-order systems, such as the fractional-order Hénon map have been investigated [171].

The literature seems to agree that fractional chaotic maps possess superior properties as compared to their standard counterpart. For instance, the general dynamics of fractional maps are heavily dependent on variations in the fractional order [103]. This adds new degrees of freedom to the map's states making them more suitable for data encryption, for example. In addition, Edelman [106] showed that the convergence speed as well as the convergence route depend on the initial conditions, which leads to richer dynamics. The fractional difference provides us a new powerful tool to characterize the dynamics of discrete complex systems more deeply. Recently, Peng et al. revised the fractional logistic map reported by Wu, et. al, based on Edelman's work and presented the correct simulation results for bifurcation diagrams in [107].

Motivated by the works mentioned above, we will report in our thesis different dimensional fractional order discrete-time systems with self-exited and hidden attractors. For that we start by reporting both of the fractional Logistic and Hénon maps to clarify the method used here in.

3.4.1 The fractional Logistic map

For the famous logistic map reported in Section 3.3.2.1, as

$$x(n+1) = rx(n)\left(1 - x(n)\right), \quad n = 1, 2, \cdots . \tag{3.8}$$

First, we take the difference form of (3.8) to obtain

$$\Delta x(n) = rx(n)\left(1 - x(n)\right) - x(n), \quad n = 1, 2, \cdots . \tag{3.9}$$

We may replace the standard difference in (3.9) with the Caputo-difference operator defined in Section 1.5, which yields

$${}^{C}\Delta_a^{\nu} x(t) = rx(t-1+\nu)\left(1 - x(t-1+\nu)\right) - x(t-1+\nu), \quad \text{for} \;\; t \in \mathbb{N}_{a+1-\nu} \tag{3.10}$$

where a is the starting point. The case $\nu = 1$ corresponds to the non fractional scenario. To investigate the dynamics of the logistic map (3.10), we will need a discrete numerical formula that allows us to evaluate the states of the map in fractional discrete time. According to Wu et.al and other similar studies, we can obtain the following equivalent discrete integral from of equation (3.10), using Theorem 1.15 reported in the first chapter as

$$x(t) = x(a) + \frac{1}{\Gamma(\nu)} \sum_{s=1-\nu}^{t-\nu} (t-s-1)^{(\nu-1)} (rx(s-1+\nu)\left(1 - x(s-1+\nu)\right) - x(s-1+\nu)), \tag{3.11}$$

for $t \in \mathbb{N}_1$. As a result, the numerical formula can be presented accordingly

$$x(n) = x(0) + \frac{1}{\Gamma(\nu)} \sum_{s=1}^{n} \frac{\Gamma(n-j+\nu)}{\Gamma(n-j+1)} (rx(j-1)\,(1-x(j-1)) - x(j-1)). \tag{3.12}$$

Where $x(0)$ is the initial condition. Compared with the map of the integer order, the fractionalized one (3.10) has a discrete kernel function. $x(n)$ depends on the past information $x(0), \ldots, x(n-1)$. As a result, the memory effects of the discrete maps means that their present state of evolution depends on all past states.

3.4.2 The fractional Hénon map

Similarly to the previous section we right the fractional Hénon map with Caputo-like difference operator. The Hénon map is given by the following pair of first-order difference equations

$$\begin{cases} x_1(n+1) = 1 - \alpha x_1^2(n) + x_2(n), \\ x_2(n+1) = \beta x_1(n), \end{cases} \tag{3.13}$$

where α, β are bifurcation parameters. We can rewrite above equation:

$$\begin{cases} \Delta x_1(t) = 1 - \alpha x_1^2(n) + x_2(n) - x_1(n), \\ \Delta x_2(t) = \beta x_1(n) - x_2(n). \end{cases} \tag{3.14}$$

From the discrete fractional calculus, we modify the standard map as a fractional one

$$\begin{cases} \Delta_a^{\nu} x_1(t) = 1 - \alpha x_1^2(t-1+\nu) + x_2(t-1+\nu) - x_1(t-1+\nu), \\ \Delta_a^{\nu} x_2(t) = \beta x_1(t-1+\nu) - x_2(t-1+\nu). \end{cases} \tag{3.15}$$

From the previous equation, we can obtain the following discrete integral form from $0 < \nu \leq 1$

$$\begin{cases} x_1(t) = x_1(0) + \frac{1}{\Gamma(\nu)} \sum_{s=1-\nu}^{t-\nu} (t-s-1)^{(\nu-1)} (1 - \alpha x_1^2(s-1+\nu) + x_2(s-1+\nu) - x_1(s-1+\nu)), \\ x_2(t) = x_2(0) + \frac{1}{\Gamma(\nu)} \sum_{s=1-\nu}^{t-\nu} (t-s-1)^{(\nu-1)} (\beta x_1(s-1+\nu) - x_2(s-1+\nu)). \end{cases} \tag{3.16}$$

As a result, the numerical formula can be presented explicitly

$$\begin{cases} x_1(n) = x_1(0) + \frac{1}{\Gamma(\nu)} \sum_{j=1}^{n} \frac{\Gamma(n-j+\nu)}{\Gamma(n-j+1)} \left(x_2(j-1) + 1 - \alpha x_1^2(j-1) - x_1(j-1)\right), \\ x_2(n) = x_2(0) + \frac{1}{\Gamma(\nu)} \sum_{j=1}^{n} \frac{\Gamma(n-j+\nu)}{\Gamma(n-j+1)} \beta x_1(j-1) - x_2(j-1). \end{cases} \tag{3.17}$$

where $x_1(0)$ and $x_2(0)$ are the initial states.

3.5 Lyapunov exponents

Perhaps the most important qualitative measure of chaos is the method of Lyapunov exponents, which was originally developed by the russian mathematician Aleksander Lyapunov in his research paper [77]. The basic idea of Lyapunov exponents or Lyapunov characteristic exponents

(LEs) is to evaluate the average growth rate of a small perturbation introduces in the orbit of a dynamical system. One exponent is defined for each dimension, representing the average rate of growth or decay along each of the principal axes in the d_E-dimensional state space. Since then, different methods have been developed to calculate the Lyapunov exponents of dynamical systems. Oseledec in [78] was the first to establish a solid theoretical background on calculating the LEs. Benettin et al. [79, 80] in their two part paper developed a complete set of theoretical as well as numerical framework to compute these exponent. Unfortunately, this algorithm is not very robust and may lead to wrong results. Geist et al. [85] made a thorough comparison of several methods for computing LEs and also presented the main ideas published in the previous decade [81, 82].

In this section, we consider problem of estimating the Lyapunov exponents of the fractional order discrete-time systems. The concept of Lyapunov exponents (LEs) in discrete-time systems is introduced first. Then the Jacobian matrix algorithm for the fractional order discete-time systems is discussed. This algorithm is employed to estimate the LEs of the one-dimensional fractional Logistic method and the two-dimensional fractional Hénon map, respectively.

3.5.1 Definition of Lyapunov exponents

Consider the discrete dynamical system of dimension m, defined by the following difference equations

$$x_{n+1} = f\left(x_n\right), \tag{3.18}$$

in which x is the phase space vector and f is generally a nonlinear continuous differentiable function. To define what is understood by Lyapunov exponents we start from an initial condition belongs to the trajectory $\mathbf{x}$ of the discrete dynamical system (3.18), and a nearby point of the trajectory $\mathbf{x}'$, where the initial distance $(\delta\mathbf{x}_0)$ is extremely small. Let $(\delta\mathbf{x}_n)$ be the distance after n iteration. The sensitivity to initial conditions can be quantified as

$$||\delta\mathbf{x}_n|| \approx ||\delta\mathbf{x}_0||e^{n\lambda}, \tag{3.19}$$

where λ is treated as the *maximum Lyapunov exponent (MLE)*, that characterizes the rate of divergence or convergence of two nearby initial points of a dynamical system; which can be estimated for long iteration as

$$\lambda = \lim_{n\to\infty} \frac{1}{n} ln \frac{||\delta\mathbf{x}_n||}{||\delta\mathbf{x}_0||}. \tag{3.20}$$

A positive exponent implies divergence of the orbits and indicates global instability and sensitivity to initial conditions that define the presence of chaos. A negative one indicates convergence of the orbits. A zero exponent indicates the temporally continuous nature of the phase space (i.e. the orbits show periodic motion). Figure 3.6 provides a visual example of divergent orbits.

The maximum LE alone does not fully characterize the instability of a d-dimensional dynamical system. There are m-exponents (equal to the dimension of the phase space) which are customarily ranked from largest to smallest [83], as

$$\lambda_1 \geq \lambda_2 \geq \ldots \lambda_m. \tag{3.21}$$

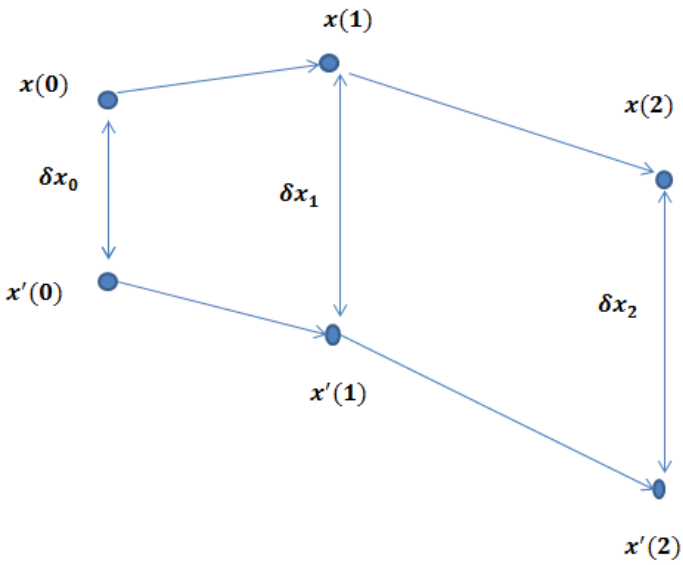

Figure 3.6: Illustration of a typical example of divergent orbits. $\delta\mathbf{x}(0)$ is the initial difference state vectors given by $\delta\mathbf{x}(0) = ||\mathbf{x}(0) - \mathbf{x}'(0)||$.

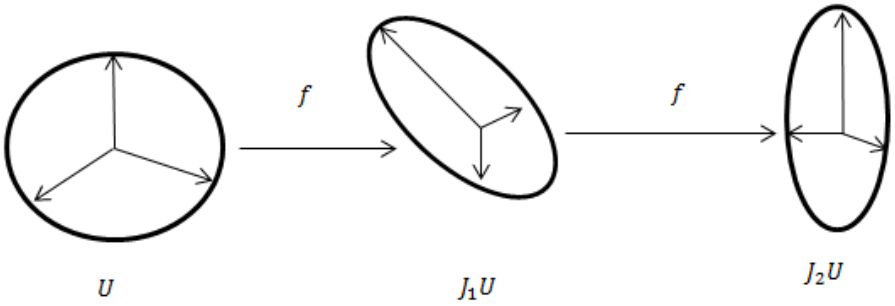

Figure 3.7: This figure illustrates change in a sphere of initial condition under a map.

We can go beyond equation (3.20) to determine all m-Lyapunov exponents by considering not just one nearby initial condition, but rather a small m-dimensional sphere of initial conditions in the phase space of the discrete dynamical system (3.18). An example of the change in the sphere of initial conditions is given in Figure 3.7. As the discrete time n increases, the sphere evolves into an ellipsoid whose principal axes expand or contract at rates given by the Lyapunov exponents. This is reflected by the "tangent space" given by the Jacobian matrix of the system (3.18), $D_x f^n = (\partial f_i / \partial x_j)$, that describes these deformations after a finite time n. For the n-th composition of f with itself n times, f^n, the corresponding matrix partial derivatives is given by the chain rule

$$D_x f^n\left(x(0)\right) = J\left(f^{n-1}\left(x(0)\right)\right) \times J\left(f^{n-2}\left(x(0)\right)\right) \ldots J\left(f\left(x(0)\right)\right) \times J(x(0)), \tag{3.22}$$

in which $J(x(0)) = D_x f\left(x\right)|_{x=x(0)}$. Consequently, the separation of two initial points $\mathbf{x}(0)$ and $\mathbf{x}'(0)$ after discrete-time n is then become

$$\delta\ \mathbf{x}_n \simeq D_{x(0)} f^n\left(x(0)\right) \delta \mathbf{x}_0. \tag{3.23}$$

Then, according to Oseledec (1968) in [78] we can define the average rate of growth as

$$\lambda_1 = \lim_{N\to\infty} \frac{1}{N} ln||J^n\left(x(0)\right) u||. \tag{3.24}$$

By the theorem of Oseledec (1968) [78], the limit exists for almost all $x(0)$ and for almost all tangent vectors u it is equal to the maximum Lyapunov exponent λ_1. Furthermore, if we denote by $a_i(n,x)$ the i^{th} eigenvalue of J^n, ordered so that $a_1(n,x) \geq \ldots \geq a_m(n,x)$. Then, we define the i^{th} Lyapunov exponent $\lambda_i(x)$ as

$$\lambda_i = \lim_{n\to\infty} \frac{1}{n} ln|a_i(n,x)|, \quad i = 1, \ldots, m. \tag{3.25}$$

Determining the Lyapunov exponents analytically is extremely difficult since we can not compute the matrix J^n which required the calculation of the product (3.22). Even for few iteration the components of matrix J^n become very large for chaotic attractors and null for the periodic attractors. Consequently, the numerical calculation become important to avoid this difficulty [81]. There are different kinds of methods used for estimating Lyapunov exponents: *direct methods* and Jacobian methods. For example, in [82] a QR decomposition is proposed for extracting the eigenvalues of the Jacobian matrix J^n. In this method, J^n is transformed in product of the upper right triangular matrices. Another method proposed by Wolf [83], in principle permits the estimation of all the positive Lyapunov exponents. The method proposed by is most widely used where the vectors are repeatedly renormalized using the Gram-Shmidt procedure. However, it was observed that the Wolf method does not works, since the linearized fractional order discrete dynamical systems due to the fractional order nature which takes into account all past variables values, that were previously modified by GSR procedure. This discovery motivated a search for new algorithmic designs to estimate Lyapunov exponents (LEs), which are necessary and more convenient for detecting chaos in fractional-order discrete time systems. Recently, Wu *et.al* [86] considered the extension of the Jacobian matrix algorithm to discrete fractional maps. We sketch the algorithm and numerical computation in the remainder of this section with more details.

3.5.2 Algorithm for computing Lyapunov spectrum

In order to calculate the Lyapunov exponents (LEs) for nonlinear dynamical fractional order discrete time systems (FODT), we consider the extended Jacobian matrix algorithm which was proposed in reference [86] by Wu and Balaneau.

Given a vector-valued nonlinear function $f(t) = (f_1(t), \ldots, f_m(t))^T$, the fractional order difference equations with the ν-Caputo-left operator is given by

$$\begin{cases} {}^C\Delta_a^{\nu}\mathbf{x}(t) = f(\mathbf{x}(t+\nu-1)), \\ \Delta^k(a) = \mathbf{x}_k, \quad m = [\nu]+1, \quad k = 0, 1, \ldots, m-1, \end{cases} \tag{3.26}$$

where $\mathbf{x}(t) = \{x_1(t), x_2(t), \ldots, x_m(t)\}$ are the state vector and the fractional order value $0 < \nu \leq 1$. To set up the tangent map corresponding to he above system we would need at first the Jacobian matrix of the right side which is given by

$$F(n) = \begin{pmatrix} \frac{\partial f_1}{\partial x_1}(n), & \frac{\partial f_1}{\partial x_2}(n), & \ldots, & \frac{\partial f_1}{\partial x_m}(n) \\ \vdots & \vdots & \vdots & \vdots \\ \frac{\partial f_m}{\partial x_1}(n), & \frac{\partial f_m}{\partial x_2}(n), & \ldots, & \frac{\partial f_m}{\partial x_m}(n) \end{pmatrix}. \tag{3.27}$$

Then, the Jacobian matrix $J(n)$ is defined by

$$J(n) = \begin{pmatrix} a_{11}(n), & a_{12}(n), & \ldots, & a_{1m}(n) \\ \vdots & \vdots & \vdots & \vdots \\ a_{m1}(n), & a_{m2}(n), & \ldots, & a_{mm}(n) \end{pmatrix}, \tag{3.28}$$

where $J(0) = I$ is the identity matrix. Each element of the matrix J can be calculated by multiplying the matrix F with the matrix J, ie:

$$J = \begin{pmatrix} \frac{\partial f_1}{\partial x_1}, & \frac{\partial f_1}{\partial x_2}, & \ldots, & \frac{\partial f_1}{\partial x_m} \\ \vdots & \vdots & \vdots & \vdots \\ \frac{\partial f_m}{\partial x_1}, & \frac{\partial f_m}{\partial x_2}, & \ldots, & \frac{\partial f_m}{\partial x_m} \end{pmatrix} \times \begin{pmatrix} a_{11}, & a_{12}, & \ldots, & a_{1m} \\ \vdots & \vdots & \vdots & \vdots \\ a_{m1}, & a_{m2}, & \ldots, & a_{mm} \end{pmatrix}. \tag{3.29}$$

This lead to the following set of tangent map system

$$\begin{cases} a_{11}(n+1) = a_{11}(0) + \frac{1}{\Gamma(\nu)} \sum_{j=0}^{n} \frac{\Gamma(n-j+\nu)}{\Gamma(n-j+1)} a_{11}(j) \frac{\partial f_1}{\partial x_1}(j) + a_{21}(j) \frac{\partial f_1}{\partial x_2}(j) + \ldots + a_{m1}(j) \frac{\partial f_1}{\partial x_m}(j), \\ a_{12}(n+1) = a_{12}(0) + \frac{1}{\Gamma(\nu)} \sum_{j=0}^{n} \frac{\Gamma(n-j+\nu)}{\Gamma(n-j+1)} a_{12}(j) \frac{\partial f_1}{\partial x_1}(j) + a_{22}(j) \frac{\partial f_1}{\partial x_2}(j) + \ldots + a_{m2}(j) \frac{\partial f_1}{\partial x_m}(j), \\ \vdots \qquad\qquad \vdots \qquad\qquad \vdots \quad \ldots\ldots\ldots\ldots\ldots \quad \vdots \qquad\qquad \vdots \\ a_{mm}(n+1) = a_{m1}(0) + \frac{1}{\Gamma(\nu)} \sum_{j=0}^{n} \frac{\Gamma(n-j+\nu)}{\Gamma(n-j+1)} a_{m1}(j) \frac{\partial f_m}{\partial x_1}(j) + a_{m2}(j) \frac{\partial f_m}{\partial x_2}(j) + \ldots + a_{mm}(j) \frac{\partial f_m}{\partial x_m}(j). \end{cases} \tag{3.30}$$

According to the discrete equation (3.30), the tangent map holds discrete memory effect. Therefore, the LEs of the fractional order discrete-time system can be derived from the following equation

$$\lambda_i = \lim_{N \to \infty} \frac{1}{N} ln|a_i^{(N)}|, \qquad i = 1, \ldots, m. \tag{3.31}$$

We can continue this method successfully and identify the stability of the FODT system with the sign of the spectrum. If all the lyapunov exponents λ_i are negative this indicates that the system has an attractive fixed point. If there is one positive Lyapunov exponent then the system is define to be chaotic. For a one-dimensional system, the Lyapunov spectrum clearly consists of one value. For a three-dimensional system the spectra can only show up in three possible types, $(0,-,-)$ for a limit cycle, $(+,0,-)$ for a strange attractor, and finally $(-,-,-)$ for a fixed point [87]. For a given FODT system a change in parameters and fractional order will generally change the Lyapunov spectrum and may also change both the type of spectrum and the type of attractor. Due to the exponential divergence of chaotic orbits, the trajectory of any dynamical system can not be accurately predicted on times scales much greater than system's Lyapunov time. They indicate the dynamical freedom of the system, because a larger exponent means a larger freedom, in the sense that small changes in the past lead to larger changes in the future [84]. This determines the importance of methods for estimating the Lyapunov exponents.

3.5.3 Results and discussion

3.5.3.1 Estimating Lyapunov exponents in the fractional logistic map

As a very simple initial example we will briefly analyse the behaviour of the Lyapunov exponents in the fractional logistic map. The discrete equation of the fractional logistic map is the following

$$x(n) = x(0) + \frac{1}{\Gamma(\nu)} \sum_{j=1}^{n} \frac{\Gamma(n-j+\nu)}{\Gamma(n-j+1)} \times \left(rx(j-1)(1-x(j-1)) - x(j-1) \right), \tag{3.32}$$

where r is the bifurcation parameter and ν is the fractional order in which $0 < \nu \leq 1$.

For the computation of the Lyapunov exponents, we will follow the Jacobian matrix algorithm in the previous section. The tangent map of the fractional logistic map (3.32) is given by [105],

$$a(i) = a(0) + \frac{1}{\Gamma(\nu)} \sum_{j=1}^{i} \frac{\Gamma(i-j+\nu)}{\Gamma(i-j+1)} \times \left(ra(j-1)(1-2x(j-1)) - a(j-1) \right), \tag{3.33}$$

where $a(0) = 1$. In the numerical experiments, we can select $x(0) = 0.3$ and $a = 0$. The first 100 points of the time series were abandoned to avoid the transient process and the length of the series of data is $n = 17500$. The parameter r and the fractional order ν are varied. In Figure 3.8, we plot the phase plane of a periodic attractor for $\nu = 0.75$ and $r = 3$. For this behaviour the estimated LE is negative where the convergence is occurs with good precision.

As an example of chaotic behavior, we present in Figure 3.9 a chaotic phase portraits of the fractional logistic map for $\nu = 0.75$ and $r = 3.5$, with the test of the convergent series of the Lyapunov exponent of this attractor. As can be seen, the one Lyapunov exponent is positive which confirms the chaotic behaviour of the attractor. Besides, the convergence occurs with good precision.

To show the efficiency of the Jacobian matrix algorithm in FODT systems for a wide range of a control parameter, we plot a bifurcation diagram (Figure 3.10-(a)) and the corresponding Lyapunov exponents (Figure 3.10-(b)). We can note there is an excellent agreement between the

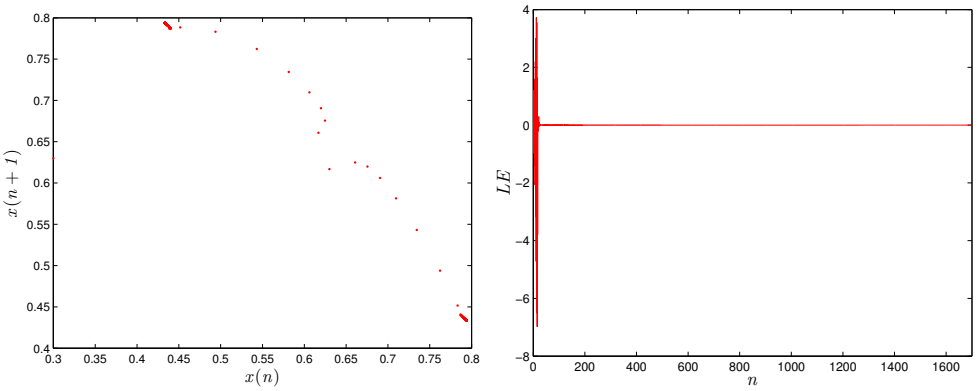

Figure 3.8: The periodic attractor of the fractional logistic map (3.32) and the estimated LE for fractional order $\nu = 0.75$ and $r = 3$.

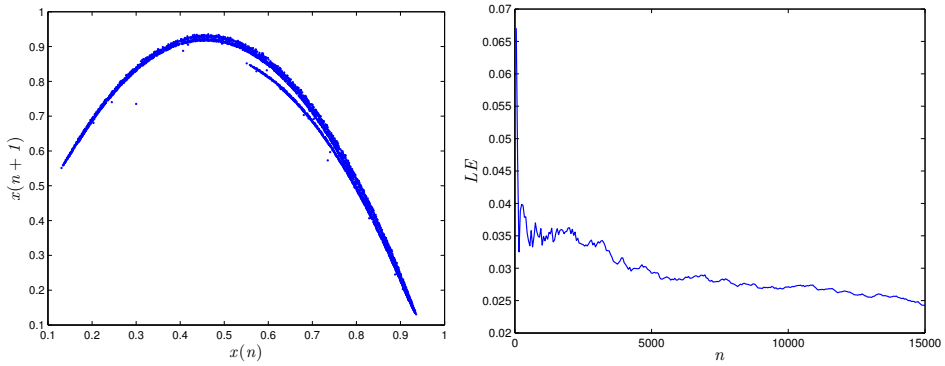

Figure 3.9: The chaotic attractor of the fractional logistic map (3.32) and the estimated LE for fractional order $\nu = 0.75$ and $r = 3.5$.

attractor behavior shown in bifurcation diagram and their corresponding Lyapunov exponent values. This diagrams are constructed by varying $r \in [0, 4]$ and $\nu = 0.9$. It is thus clear that for fractional logistic map, the positive value will appear early when the systems parameter takes larger values, which means that the fractional order affects the chaotic window. Thus, using Lyapunov exponents we can discriminate regions characterized by periodic or chaotic motion.

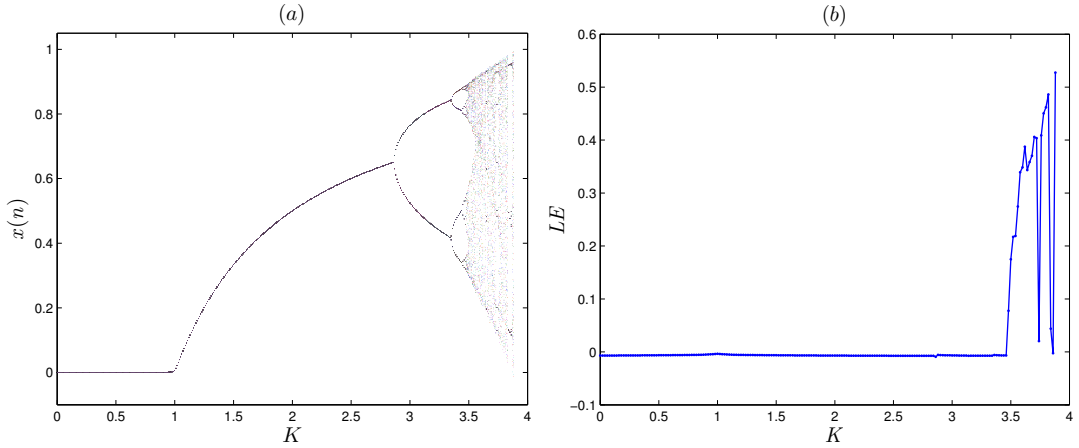

Figure 3.10: (a) Bifurcation diagram of the fractional the fractional Logistic map (3.32) with $\nu = 0.9$ and $r = 3.7$. (b) Lyapunov exponent diagram corresponding to (a).

3.5.3.2 Estimating Lyapunov exponents in the fractional Hénon map

Now, we will analyse a more complex system that presents chaotic behavior, which is described by

$$\begin{cases} x_1(n) = x_1(0) + \frac{1}{\Gamma(\nu)} \sum_{j=1}^{n} \frac{\Gamma(n-j+\nu)}{\Gamma(n-j+1)} \left(x_2(j-1) + 1 - \alpha x_1^2(j-1) - x_1(j-1)\right), \\ x_2(n) = x_2(0) + \frac{1}{\Gamma(\nu)} \sum_{j=1}^{n} \frac{\Gamma(n-j+\nu)}{\Gamma(n-j+1)} \left(\beta x_1(j-1) - x_2(j-1)\right). \end{cases} \tag{3.34}$$

The system of equations (3.42) is the numerical formula of the two-dimensional fractional Hénon map with x_1, x_2 as the states variables. The system display chaotic behaviour for some values of fractional order and displays periodic for other values [171].

For this specific system the Jacobian is

$$J(n) = \begin{pmatrix} a(n) & b(n) \\ c(n) & d(n) \end{pmatrix}, \tag{3.35}$$

where

$$\begin{cases} a(n) = a(0) + \frac{1}{\Gamma(\nu)} \sum_{j=1}^{n} \frac{\Gamma(n-j+\nu)}{\Gamma(n-j+1)} \left(-2\alpha a(j-1)x(j-1) - a(j-1) + c(j-1)\right), \\ b(n) = b(0) + \frac{1}{\Gamma(\nu)} \sum_{j=1}^{n} \frac{\Gamma(n-j+\nu)}{\Gamma(n-j+1)} \left(-2\alpha b(j-1)x(j-1) - b(j-1) + d(j-1)\right), \\ c(n) = c(0) + \frac{1}{\Gamma(\nu)} \sum_{j=1}^{n} \frac{\Gamma(n-j+\nu)}{\Gamma(n-j+1)} \left(\beta a(j-1) - c(j-1)\right), \\ d(n) = d(0) + \frac{1}{\Gamma(\nu)} \sum_{j=1}^{n} \frac{\Gamma(n-j+\nu)}{\Gamma(n-j+1)} \left(\beta b(j-1) - d(j-1)\right), \end{cases} \tag{3.36}$$

in which $a(0) = b(0) = c(0) = d(0) = 1$. Let $\beta = 1.3$, $\alpha = 0.3$, the phase portrait and the Lyapunov exponents estimation of the fractional Hénon map with different system parameters and fractional order values are shown in Figure 3.11. As shown in Figure 3.11(a) and Figure 3.11(b), when $\nu = 0.98$ and $a = 1.02$ the system is periodic since there are few points in the phase portraits and the largest Lyapunov exponent converge to zero confirming the regular dynamics. Successfully, Figure 3.12(a) and Figure 3.12(b) depicts chaotic attractor and one positive Lyapunov exponent for and $a = 1.3$, $\nu = 0.96$.

Let the parameter α vary from 0 to 1.5 with step size of 0.0015 with the fractional order value $\nu = 0.96$. Largest Lyapunov exponents values are shown in Figure 3.13. The high complexity region marked as α increases. It also shows that the proposed algorithm is effective for detecting chaos in the fractional-order discrete chaotic systems. Changes in LLEs coincide with the bifurcation diagrams constructed for the same intervals of changes in the control parameters α.

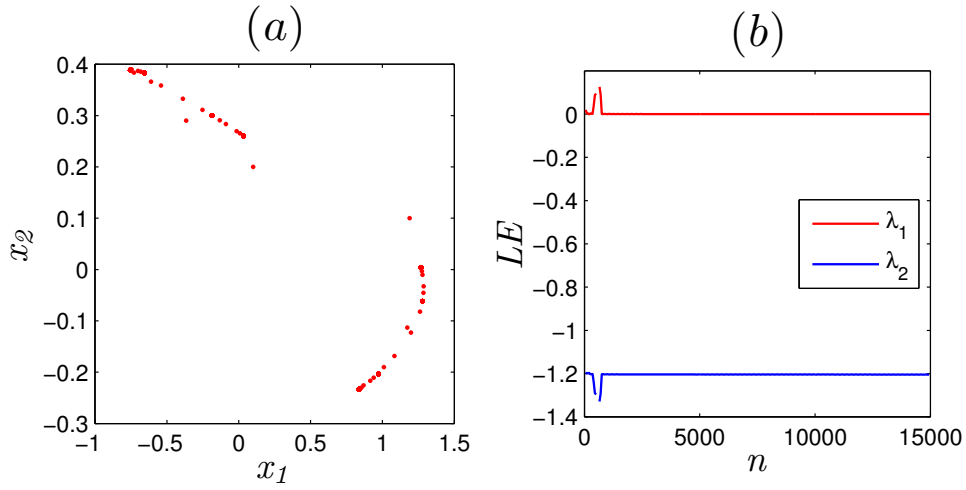

Figure 3.11: (a) Periodic attractor of the fractional Hénon map for fractional order value $\nu = 0.98$ and $a = 1.02$. (b) The corresponding Lyapunov exponents estimation.

3.6 0-1 test method

To reflect the sensitivity of the fractional order discrete-time systems, the 0-1 test for chaos is considered. This test was proposed by Gottwald and Melbourne in [89] to distinguish between regular and chaotic dynamics in deterministic dynamical systems. As opposed to the Lyapunov exponents method the 0-1 test is applied to known and unknown systems regarding the phase plane. Thus it is able to identify the chaos in a series of data where the phase space reconstruction is not necessary. This avoids any difficulty related to the choice of the embedding dimension and the delay parameter inherent to the phase space reconstruction. Moreover, the test is a binary test (i.e. 0 or 1) and, consequently, yields a definite conclusion about the system dynamics, so

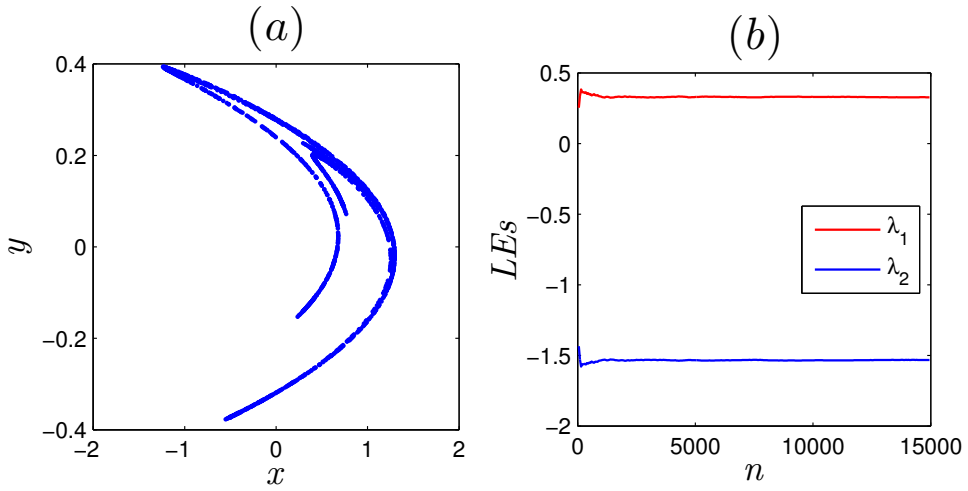

Figure 3.12: (a) Chaotic attractor of the fractional Hénon map for fractional order value $\nu = 0.96$ and $a = 1.3$. (b) The corresponding Lyapunov exponents estimation.

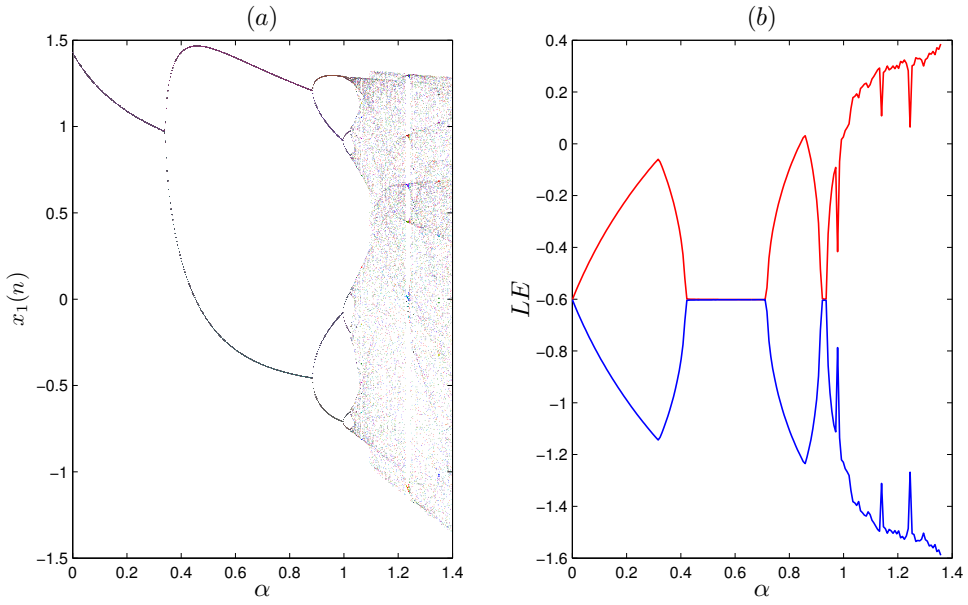

Figure 3.13: (a) Chaotic attractor of the fractional Hénon map for fractional order value $\nu = 0.96$ and $a = 1.3$. (b) The corresponding Lyapunov exponents estimation.

a numerically computed value, say 0.01, yields a definite conclusion, whereas such a value for the maximal Lyapunov exponent would not. One can found more about 0-1 test theory and application in [90] and [91].

Among the reasons of its success, there is the extreme simplicity of its numerical implementation and the fact that it can be applied directly on the output of the system, independently on the features of the system itself. Recently, Cafagna and Grassi in [92] extended the method to fractional-order systems. In particular, for the finite time series of data $(x_i)_{i=1,\dots,N}$ and a suitable choice of c ; one can define the two terms for $m = \overline{1, N}$ as

$$p_m = \sum_{i=1}^{m} x_i \cos(ic) \qquad and \qquad q_m = \sum_{i=1}^{m} x_i \sin(ic). \tag{3.37}$$

Such terms are called the translation components. In order to study the boundedness or unboundedness of the functions p_m and q_m we calculate the time-averaged mean-square displacement, which can be defined as

$$M_m = \lim_{N\to+\infty} \frac{1}{N} \sum_{j=1}^{N} \left((p_{j+m} - p_j)^2 + (q_{j+m} - q_j)^2 \right). \tag{3.38}$$

If the behaviour of the translation function $p(n)$ ($q(n)$ behaves in the same way) is Brownian, then $M(n)$ grows linearly in time. If the behaviour of $p(n)$ is bounded, then $M(n)$ is bounded. The 0-1 result is given by

$$K_c = corr(\xi, \Delta) = \frac{cov(\xi, \Delta)}{\sqrt{var(\xi)var(\Delta)}} \in [-1, 1]. \tag{3.39}$$

In practice, the fractional-order system is evaluated to be chaotic if the plot of p and q in the $p - q$ plane present a Brownian–like trajectories and if K approaches 1, while it becomes regular as K approaches 0 and p and q display bounded–like trajectories.

Remark 16. The 0-1 test algorithm depends on three parameters, c, m and the length of data points N. The following illustrates the selection of parameters of this algorithm by numerical experiments.

- Nevertheless, there is zero probability of making a bad choice in theory. In practice, numerical experimentation shows that even for short data series, the bad choices of c are rare but do occur from time to time. For example, if the signal is 2-periodic and we choose c as an integer, then a simple argument using the Fourier series shows that typically $p(n)$ will grow linearly yielding $K = 2$. The resolution of this problem is to choose several values of c at random, and compute K for each choice of c. Then we take the median value of K. Finally, we obtain the asymptotic growth rate K via

$$K = median(K_c). \tag{3.40}$$

- For the selection of N, it should tend to infinity in theory, but this is not feasible in practice. As the algorithm is achieved with the loop, and there are nested loops. The greater the sequence length selected, the longer the loop will increase, and the execution time of the algorithm will significantly increase. Therefore, the sequence length N should be selected long enough.

- For the selection of n, there is no special requirement. Based on the principle of $n \ll N$, any choice of n is sufficient. Thus an appropriate value of n should be selected as small as possible.

Applications of the 0-1 test on the fractional-order discrete time systems

To demonstrate the reliability and universality of the test, we apply the test to the fractional-order logistic map and the fractional Hénon map.

Detecting chaos in the fractional-order logistic map

The discrete fractional-order logistic map is considered

$$x(n) = x(0) + \frac{1}{\Gamma(\nu)} \sum_{j=1}^{n} \frac{\Gamma(n-j+\nu)}{\Gamma(n-j+1)} \times \left(rx(j-1)(1-x(j-1)) - x(j-1)\right). \tag{3.41}$$

By taking into account the results illustrated in Subsection 3.5.3.1, at first the 0-1 test is applied to the series of point $x(n)$ where r is the bifurcation parameter and $\nu = 0.9$. The results are shown in Figure 3.14. Figure 3.14 illustrates the asymptotic growth rate K versus parameter $r \in [0, 4]$. As the bifurcation parameter r increases the fractional-order logistic map (3.41) becomes chaotic as the growth rate K asymptotically approaches 1. Furthermore, Figure 3.15 depicts the Brownian-like trajectories for , confirming that the fractional logistic map (3.41) is chaotic for $\nu = 0.75$ and $r = 3.5$. On the other hand, Figure 3.16 depicts the bounded-like trajectories for $r = 3$ and $\nu = 0.75$ confirming the existence of periodic attractors.

Based on this figures, one can observe that the output K have appeared in a similar manner to the results of bifurcation diagram and Lyapunov exponents shown in Section 3.5.3.1. It is conclude that the 0-1 test prove to be a valuable tool for cheeking the existence of difference chaotic attractors as well as periodic attractors.

Detecting chaos in the fractional-order Hénon map

We apply the test to fractional-order Hénon map, which it's numerical solution is given by

$$\begin{cases} x_1(n) = x_1(0) + \frac{1}{\Gamma(\nu)} \sum_{j=1}^{n} \frac{\Gamma(n-j+\nu)}{\Gamma(n-j+1)} \left(x_2(j-1) + 1 - \alpha x_1^2(j-1) - x_1(j-1)\right), \\ x_2(n) = x_2(0) + \frac{1}{\Gamma(\nu)} \sum_{j=1}^{n} \frac{\Gamma(n-j+\nu)}{\Gamma(n-j+1)} \beta x_1(j-1) - x_2(j-1). \end{cases} \tag{3.42}$$

Here, the test has been applied directly to the solution $x(n)$ for system parameter $\beta = 0.3$ and for different fractional order values. The results are reported in Figure 3.18 and Figure 3.17 for

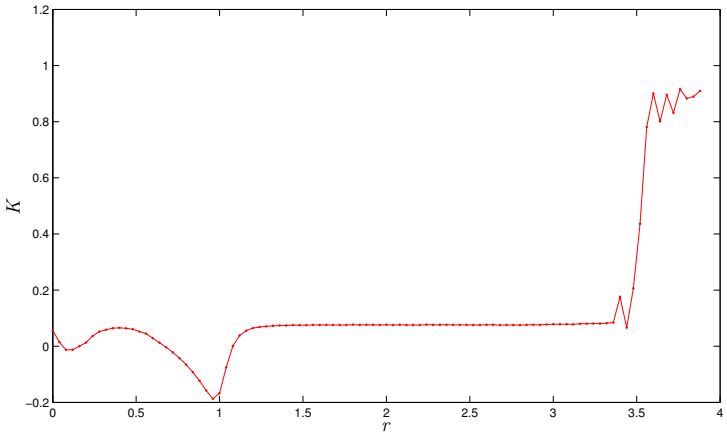

Figure 3.14: The asymptotic growth rate of fractional logistic map versus n

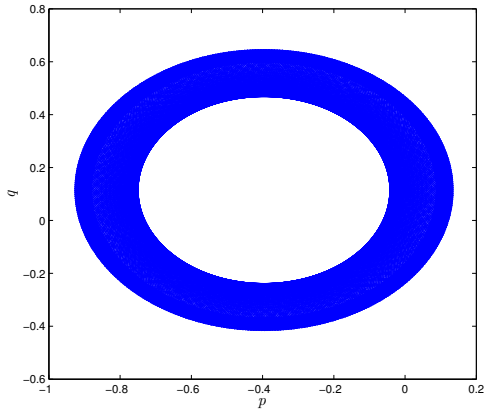

Figure 3.15: Bounded like trajectories of the translation components p and q in the $p-q$ plane

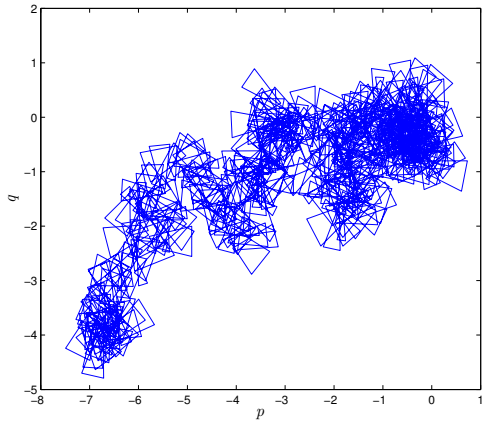

Figure 3.16: Browlian-like like trajectories of the translation components p and q in the $p-q$ plane

$\nu = 0.98$, $\alpha = 1.02$ and $\nu = 0.96$, $\alpha = 1.3$, respectively. In particular, Figure 3.17 depicts the asymptotic growth rate K as a function of the length n, and the dynamics of the translation components in the $p - q$ plane. Since the asymptotic growth rate K approaches one and the $p - q$ plane highlights Brownian-like trajectories, the fractional Hénon map is chaotic.

On the other hand, Figure 3.18 shows that K approaches zero, whereas bounded trajectories in the $p - q$ plane are depicted, indicating the periodic dynamic of the map.

Successively, the 0-1 test is carried out by varying the parameter α from 0 to 1.40. The step size for α is 0.001. The plot of the asymptotic growth rate K versus α is shown in Figure 3.19. It shows that the fractional Hénon map (3.42) is chaotic over most of the range $a \in (1.07, 1.40)$ where K approaches 1. On the other hand Figure 3.18 depicts Brownian-like trajectories confirming the chaotic dynamics of the system for $\alpha = 1.3$.

All the results reported in this section indicate the effectiveness of the 0-1 test in detecting chaos. This figures are in good agreement with the Lyapunov exponents results reported in the previous section. Although the 0-1 test has many advantages over calculating the largest Lyapunov exponent, and it avoids certain well-documented drawbacks of traditional tests, it will not replace traditional methods completely.

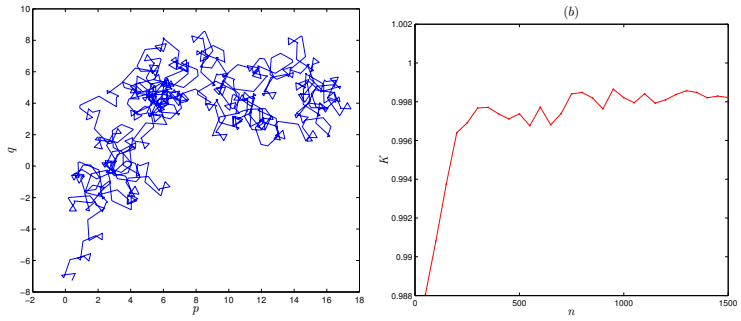

Figure 3.17: Brownian like trajetories of translation component in the $p - q$ plane of the fractional Hénon map and the corresponding translation component versus n

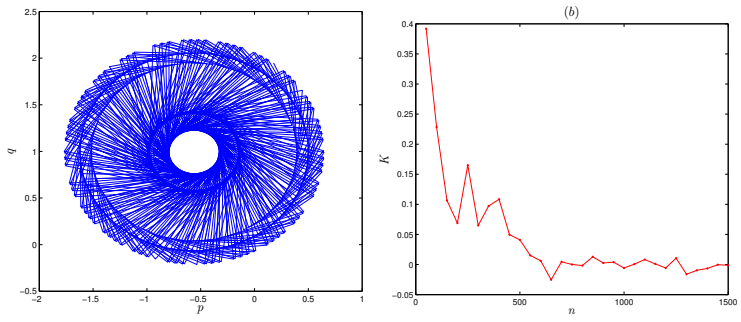

Figure 3.18: Bounded like trajetories of translation component in the $p - q$ plane of the fractional Hénon map for$\nu = 0.98$, $\alpha = 1.02$ and the corresponding translation component versus n.

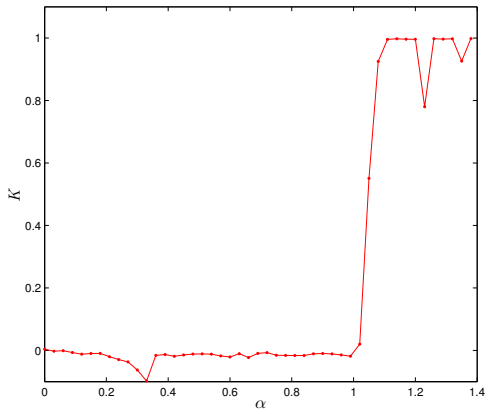

Figure 3.19: Asymptotic growth rate of the fractional Hénon map versus α corresponding to the bifurcation diagram and LEs in Figure 3.10

3.7 Complexity measure

A complexity measure plays important role in analyzing dynamic properties of chaotic systems. It can reflect the security of the system to some extent, if it is used in information security. It has the same effect as the Lyapunov exponent and bifurcation diagram. The larger the complexity values, the closer the sequence is to the random sequence. Currently, there are several methods to measure complexity of time series, including permutation entropy (PE), statistical complexity measure (SCM), sample entropy (SampEn), fuzzy entropy (FuzzyEn), approximate entropy ($ApEn$), and C_0 algorithm. Among them, C_0 algorithms and approximate entropy ($ApEn$) [93,102] are proper choices to estimate the complexity of a time series accurately and rapidly without any over-coarse graining preprocessing. The approximate entropy finds its origins in Kolmogorov-Sinai Entropy (K-S Entropy), defined as the mean rate of information generated by a process [102]. This measure is recognized for being a meaningful parameter to describe the behavior of dynamical systems. On the other hand, the C_0 complexity is calculated by the fast Fourier transform and through of the new spectra to obtain a new signal. The corresponding complexity value is obtained by the ratio of the area between the difference of the original signal and the new signal and its mean value over the area between the original signal and its mean values. The mathematical foundation of this complexity measure was given in [93].

3.7.1 C_0 complexity algorithm description

C_0 complexity (C_0), is a measure of complexity under the meaning of randomness, was first introduced by Shen et al [93], to overcome the over-coarse graining preprocessing problem. The C_0 algorithm is a method that aimed to devide the original serie of data into two components, the regular component and irregular part, the proposition of irregular part is what we need. Consider a set of discrete data $x(n)$, $n = \overline{1.N}$ with a length of N, representing a one dimensional observable data set. Description of the C_0 algorithm is as follows [130].

Step 1. In order to get the amplitude of spectrum, construct the fast Fourier transform of the original time series. Denote the fast Fourier transform of $x(n)$ by X_N, then we have

$$X_N(j) = \frac{1}{N}\sum_{n=0}^{N-1} x(n)\exp^{-2\pi\frac{nj}{N}}, \quad n = 0, 1, \ldots, N-1 \tag{3.43}$$

where $j = \sqrt{-1}$ is the unit imaginary. Note that the power spectrum contains essential information about the nature of x.

Step 2. Calculate the mean square value of the amplitude spectrum

$$G_N = \frac{1}{N}\sum_{j=0}^{N-1} |X_N(j)|^2. \tag{3.44}$$

Import a control parameter $\bar{r}$. Replace the spectrum component with zero if their square values are plus than $\bar{r}G_N$, while keep the irregular parts, i.e. the parts which their square are less or equal to $\bar{r}G_N$, changed as follows

$$\bar{X}_N(n) = \begin{cases} X_N(n), & \textit{if} \quad |X_N(n)|^2 > \bar{r}G_N, \\ 0, & \textit{if} \quad |X_N(n)|^2 \leq \bar{r}G_N. \end{cases} \tag{3.45}$$

Step 3. Then, construct inverse fast Fourier transform for the new component $\bar{X}_N$ and get a new time series $\bar{x}$

$$\bar{x}(n) = \sum_{j=0}^{N-1} \bar{X}_N(j)\exp^{-2\pi\frac{nj}{N}}, \qquad n = 0, 1, 2 \ldots, N-1. \tag{3.46}$$

$\bar{x}(n)$ is considered as the regular time series of original time series.

Step 4. Define the C_0 complexity as

$$C_0 = \frac{\sum_{n=0}^{N-1} |x(n) - \bar{x}(n)|^2}{\sum_{n=0}^{N-1} |x(n)|^2}. \tag{3.47}$$

Note that, the difference between the original time series and it regular component is considered as the disorder components of the original series. Therefore, from equation (3.47) one can see that the regular part of the domain is removed; leaving the irregular part. The larger the proportion of the non-regular part of the spectrum in the sequence, the closer the corresponding time series spectrum is to the random sequence, the greater the complexity.

Some important properties of C_0 complexity were proved in [93] mathematically. It has been proved that:

1. If the time series is constant, then $C_0 = 0$;
2. If $x(n)$ is a periodic time series, then $\lim_{N\to\infty} C_0 = 0$;
3. For any time series the C_0 complexity ranges between 0 and 1.

Hence, C_0 complexity can be used as a randomness finding complexity of a time series.

3.7.1.1 Choice of parameters of the C_0 complexity algorithm

From the definition of C_0 complexity, two parameters need to be chosen; which are control parameter $\bar{r}$ and length N. To illustrate the selection of parameter of the C_0 complexity algorithm, fractional logistic map was taken as an example [103], which the equivalent discrete integral equation can be obtained as

$$x(x) = x(0) + \frac{1}{\Gamma(\nu)} \sum_{j=1}^{n} \frac{\Gamma(n-j+\nu)}{\Gamma(n-j+1)} \left(rx(j-1)(1-x(j-1))x(j-1) \right). \tag{3.48}$$

As reported in Section 3.5.3.1, when $r = 3.5$ and $\nu = 0.75$, the fractional logistic map is in a chaotic state. Here, the parameter r is taken as $r = 3.5$, and the result of calculating the complexity of C_0 is shown in Figure 3.20. In Figure 3.20-(a), N is 2000, r first starts from 0.1 and gradually increases with a step value of 0.1, and then increases by 0.5 when it is greater than 2, and the initial value $x_0 = 0.1$; Figure 3.20(b). Where the value of r is 4, the sequence length N starts from 100, the step length is 200. It can be seen from Figure 3.20(a) that as the parameter $\bar{r}$ increases, the measured value of C_0 gradually increases, which shows that as $\bar{r}$ increases, the less regular parts are removed, and the measured value will increase accordingly. When $\bar{r}$ is greater than 2. After that, the measured value is stable, so it is recommended that the value range of $\bar{r} \in [5, 10]$, which is consistent with the analysis result of the literature [94]; in Figure 3.20-(b) when $N > 2000$, the measured value is stable. In view of the fast calculation speed of the C_0 algorithm, it is recommended that he sequence length is greater than 2000.

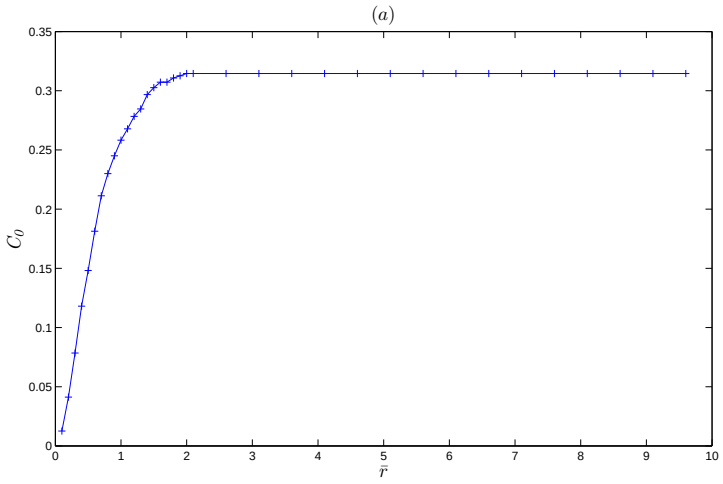

Figure 3.20: Asymptotic growth rate of the fractional Hénon map versus α corresponding to the bifurcation diagram and LEs in Figure 3.10

3.7.2 Aprroximate entropy

In information theory, entropy is a logarithmic measure that quantifies the rate of transfer or generation of information in a particular system. For discrete-time dynamical systems in general, Kolmogorov-Sinai (KS) entropy is an interesting measure. A direct time-series approximation of the KS entropy was developed in [97], termed Eckmann-Ruelle (ER) entropy, which quickly became appealing as a way of quantifying the level of chaos present in a particular system. The idea is that instead of looking at the phase plots of bifurcation diagrams, an exact measure of the information generated in a sequence is more indicative of the level of chaos. Calculating the exact ER entropy experimentally is impossible. Rather, the "approximate entropy" (ApEn) was proposed by Pincus to present the complexity or irregularity of a serie of data from multi-dimensional perspective [98, 99]. Larger values of ApEn indicate higher complexity and irregularity of the current data. Approximate entropy measurement is helpful and applied to discover different chaotic systems. It has been used extensively in the literature to investigate chaos in discrete dynamical systems [97,100]. The brief computation of the approximate entropy is presented as follows.

Step 1. Consider a set of discrete points $x(1)$, $x(2), \dots, x(n)$, define $n-m+1$ vectors as follows

$$X(i) = [x(i), ..., x(i+m-1)]. \tag{3.49}$$

These vectors represent m consecutive x values which starts with the $i-$th data.

Step 2. Define the maximum distance between the vectors $X(i)$ and the vector $X(j)$ as

$$d\left(X(i), X(j)\right) = \max ||x(i+k) - x(j+k)||, \tag{3.50}$$

for all k values from 0 to $m-1$. Then calculate the distance for all possible pairs $(X(i), X(j))$ if $i \neq j$.

Step 3. Let K be the number of vectors $X(i)$ such that the maximum absolute difference $d(X(i), X(j))$ of two vectors $X(i)$ and $X(j)$ is lower or equal to the tolerance $\bar{r}$.

Step 4. With tolerance $\bar{r}$ and for each $i \in [1, n-m+1]$, define the following equation

$$C_i^m(r) = \frac{K}{n-m+1}, \tag{3.51}$$

where K is the number of $X(i)$ having $d(X(i), X(j)) \leq \bar{r}$.

Step 5. Define the approximate entropy by

$$ApEn = \phi^m(\bar{r}) - \phi^{m+1}(\bar{r}), \tag{3.52}$$

where $\phi^m(r)$ is considered as

$$\phi^m(\bar{r}) = \frac{1}{n-m-1} \sum_{i=1}^{n-m+1} \log C_i^m(\bar{r}). \tag{3.53}$$

As reported in [98], the value of the approximate entropy depends on three important parameters, i.e., the length of the serie of sata N, the embedding dimension m and the similar tolerance $\bar{r}$. In practice N cannot be infinity, we can only estimate it if N is big enough. According to the experience of Pincus in his research paper [99], the tolerance r is suitable to be chosen as

$$\bar{r} = 0.2std(x), \tag{3.54}$$

where $std(x)$ denotes the standard deviation of the data x. It has pointed out also that for a robust estimation it would proper if the embedding dimension equal to $m = 2$. Based on the research paper of Pincus [99], it has been found that the $ApEn$ is a very convenient method to choose parameters for the discrete fractional order discrete-time systems.

3.8 Conclusion remarks

The concept of the behavior of chaos in fractional order discrete time systems with Caputo like difference operator is successfully captured in this chapter. Firstly, the Jacobian matrix algorithm is presented in form of discrete fractional maps where it has been applied to one and two dimensional maps of fractional order. With the different fractional difference orders, the LEs are plotted together with the bifurcation diagrams from which the chaotic areas of the systems are clearly derived. The results show the efficiency of calculating the LEs. Secondly, this Chapter identified chaos of the fractional order Hénon and logistic maps by using the 0-1 test, which is different from the Lyapunov exponent method. These results show that the 0–1 test is a convenient tool to diagnose chaos in fractional chaotic map.

We have seen that, in addition to the standard calculation of the asymptotic Lyapunov exponent, we can extract more information about the dynamical system by calculating the complexity of the fractional order discrete time systems. Two methods are reported: The C_0 algorithm and the $ApEn$. Complexity analysis provides a parameter choice basis for application of fractional order chaotic systems. Furthermore, one should not that complexity results cannot distinguish chaos and hyperchaos bur it can be used as for parameter choice in the practical application.

In the following chapters (Chapter 4, 5 and 6) we will define and discuss the chaotic behaviour of novel fractional order maps with ”self excited and "hidden attractors" using numerical tools reported in this chapter.

Part II

Application Study

Chapter 4

Two Dimensional Fractional Order Maps

4.1 Introduction

Over the past decades, the study of fractional-order systems has become an active field and has simulated the interest of researchers due to its existence in different fields of science and engineering. Significantly, it was reported that fractional-order systems, as fractional extensions of many well-known established systems, can realize chaotic attractors such as the fractional-order modified Duffing system [108], the fractional-order Chua's system [109]. However, the dynamics of such fractional-order systems have mostly been explored where the fractional derivatives have been described on a continuous time scale.

Recently, some literature has studied the chaotic behavior of discrete-time fractional order systems. The first such system is the fractional-order logistic map which was proposed by Wu and Baleanu and has been reported in Chapter 3. Similar to the integer-order difference systems (maps), fractional order discrete-time systems can exhibit chaotic behaviours (see Chapter 3). By considering the theory and application of discrete fractional calculus, which have been mentioned in the first part of the thesis, this Chapter presents different fractional discrete time systems, i.e, maps, in the fractional ν-Caputo seance with different nonlinearities terms, such as rational terms, trigeometrical terms, absolute function terms and unified functions. The novel fractional maps are defined as generalization of very well known integer-order maps in the literature, such as Lozi map, Ikeda map, Duffing map, discrete double scroll map, Arnold map and rational maps (Chang et al., Rulkov, Zeraoulia Sprott maps). For the different fractional order values and system parameters, the dynamics of the fractional order maps are studied. Complex dynamics with interesting characteristics are presented by means of Lyapunov exponents, bifurcation diagrams, 0-1 test C_0 algorithm and approximate entropy. Namely, the influence of both fractional order ν and system parameters on the dynamical behaviour of the novel fractional maps are investigated in detail, with the aim to highlight the existence of different chaotic attractors. Both the system parameter and fractional order can be taken as bifurcation parameters, and the range of existing chaos is different for different parameters.

4.2 The fractional–order chaotic Lozi map

Among the many chaotic maps introduced over the years is the Hénon map [3], which was proposed in 1976 as a simplified version of the discretization of the Poincaré section resulting from the well-known continuous time Lorenz system. More recently, Lozi developed a new discrete chaotic system by replacing the quadratic term in the Hénon map with quasi linear term [2]. The equation for the iterated Lozi chaotic map is given by

$$\begin{cases} x(n+1) = -\alpha |x(n)| + y(n) + 1, \\ y(n+1) = \beta x(n), \end{cases} \tag{4.1}$$

where $x(n)$ and $y(n)$ are the states of the map, n denotes the iteration number and α and β are some parameters. This map is a piecewise linear model with non-differentiable function. Under some typical control parameter settings, the Lozi map (4.1) admits a singular hyperbolic chaotic attractor, for instance, with the parameter values $(\alpha, \beta) = (1.7, 0.5)$ we can derive the strange attractor as seen in Figure 4.1. Zooming into a particular part of the map reveals that each curved line consists of multiple components. By changing the control parameters, the Lozi map can display complex behaviors such as border collision bifurcations [112]. A detailed collection of works regarding Lozi map can be seen in in the reference [113].

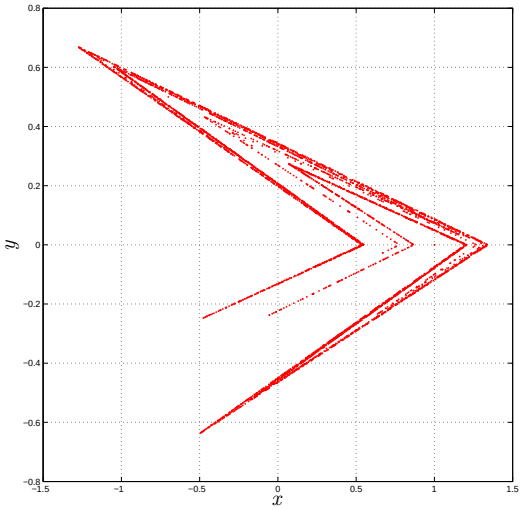

Figure 4.1: The chaotic attractor of the standard Lozi map (4.1) with $[x(0), y(0)] = [0, 0]$ and $(\alpha, \beta) = (1.7, 0.5)$.

In this section, we aim to study the fractional form of the Lozi map (4.1) by replacing the integer order difference operator with the left Caputo-like difference. As has been reported, this type of operators are able to include memory and filter effects into the ordinary Lozi map, which makes it more suitable to application in cryptography, image encryption, and secure

communication. We first rewrite the Lozi map (4.1) in the first difference order form, using the standard forward difference operator, $\Delta x(t) = x(t+1) - x(t)$, as

$$\begin{cases} \Delta x\left(n\right) = -\alpha|x\left(n\right)| + y\left(n\right) + 1 - x\left(n\right), \\ \Delta y\left(n\right) = \beta x\left(n\right) - y\left(n\right). \end{cases} \tag{4.2}$$

Then, by replacing the first–order difference by the Caputo–like delta difference as defined in (4.2), we get

$$\begin{cases} {}^{C}\Delta_{a}^{\nu} x\left(t\right) = -\alpha\left|x\left(t-1+\nu\right)\right| + y\left(t-1+\nu\right) + 1 - x\left(t-1+\nu\right), \\ {}^{C}\Delta_{a}^{\nu} y\left(t\right) = \beta x\left(t-1+\nu\right) - y\left(t-1+\nu\right), \end{cases} \tag{4.3}$$

for $0 < \nu \leq 1$ and $t \in \mathbb{N}_{a+1-\nu}$. If $\nu = 1$, this fractional system degenerates into the integer-order Lozi map (4.1). From now on, we shall refer to (4.3) as the fractional Lozi map.

Now that we have the fractional Lozi map we must determine a suitable numerical formula for its evaluation. Following the same steps reported in Section 3.4, we employ Theorem 1.15 to obtain a numerical formula for system (4.3). We start by taking the equivalent discrete integral for $0 < \nu \leq 1$ and $t \in \mathbb{N}_{a+1-\nu}$ yielding

$$\begin{cases} x\left(t\right) = x\left(a\right) + \frac{1}{\Gamma(\nu)} \sum_{s=a+1}^{t-\nu} \left(t - \sigma\left(s\right)\right)^{(\nu-1)} \\ \qquad\qquad \left(-\alpha|x\left(t-1+\nu\right)| + y\left(t-1+\nu\right) + 1 - x\left(t-1+\nu\right)\right), \\ y\left(t\right) = y\left(a\right) + \frac{1}{\Gamma(\nu)} \sum_{s=a-\nu}^{t-\nu} \left(t - \sigma\left(s\right)\right)^{(\nu-1)} \\ \qquad\qquad \left(\beta x\left(t-1+\nu\right) - y\left(t-1+\nu\right)\right). \end{cases} \tag{4.4}$$

The reciprocal $\frac{(t-\sigma(s))^{(\nu-1)}}{\Gamma(\nu)}$ represents a discrete kernel function and can be simply taken as

$$\frac{\left(t - \sigma\left(s\right)\right)^{(\nu-1)}}{\Gamma\left(\nu\right)} = \frac{\Gamma\left(t-s\right)}{\Gamma\left(\nu\right)\Gamma\left(t-s-\nu+1\right)}. \tag{4.5}$$

Hence, by choosing a zero starting point, i.e. $a = 0$, the numerical formula is defined as

$$\begin{cases} x\left(n\right) = x\left(0\right) + \frac{1}{\Gamma(\nu)} \sum_{j=1}^{n} \frac{\Gamma(n-j+\nu)}{\Gamma(n-j+1)} \\ \qquad\qquad \left(-\alpha\left|x\left(j-1\right)\right| + y\left(j-1\right) + 1 - x\left(j-1\right)\right), \\ y\left(n\right) = y\left(0\right) + \frac{1}{\Gamma(\nu)} \sum_{j=1}^{n} \frac{\Gamma(n-j+\nu)}{\Gamma(n-j+1)} \left(\beta x\left(j-1\right) - y\left(j-1\right)\right). \end{cases} \tag{4.6}$$

We mentioned earlier that fractional calculus brings the major addition of an infinite memory. This can be clearly observed in (4.6) where the solution $x\left(n\right)$ depends on all previous values $x\left(0\right), \ldots, x\left(n-1\right)$. This, of course, is not the case with the integer order system (4.1). A Matlab program was implemented based on the numerical formula (4.6). For $\nu = 1$, Figure 4.2 (a) shows the bifurcation plot with α as the critical parameter and Figure 4.2 (b) shows the largest Lyapunov exponent as a function of α calculated by means of the Jacobian method. These plots confirm the existence of chaos and agree with previous results reported in the literature for the classical Lozi map.

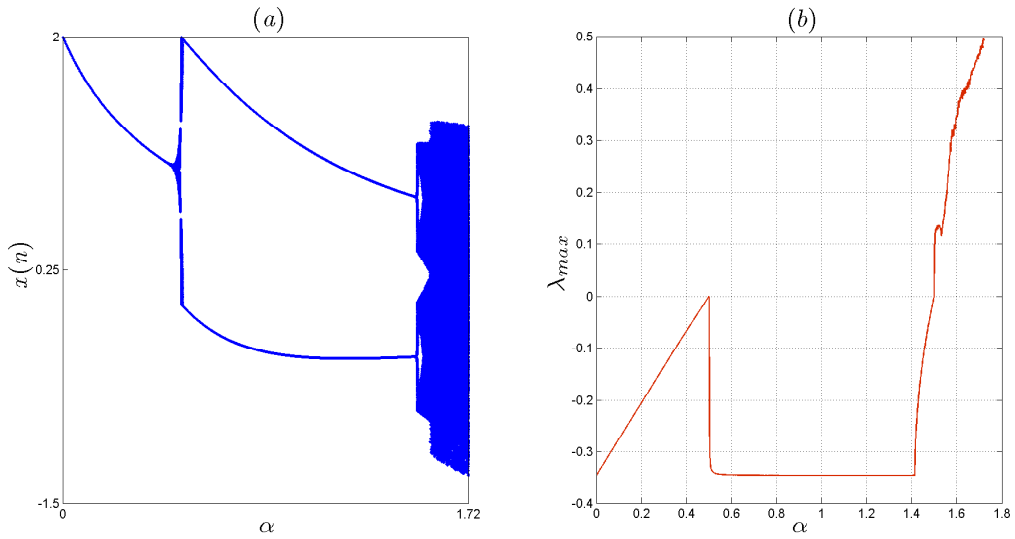

Figure 4.2: (a) Bifurcation diagram of the standard Lozi map with $x(0) = y(0) = 0$ and $(\alpha, \beta) = (1.7, 0.5)$ and (b) the largest Lyapunov exponent calculated by means of the Jacobian method.

Dynamics of the fractional Lozi map

In the following part, we present the dynamics of the fractional Lozi map by considering numerical simulation. Such simulation contain bifurcation diagrams, maximum Lyapunov exponents (MLE), phase portraits and transient states. Namely, the influence of both fractional order ν and system parameter α on the dynamical behaviour of the novel map are investigated in detail, with the aim to highlight the existence of different chaotic attractors.

To ensure the existence of chaos, we choose to fix $x(0) = y(0) = 0$ and $(\alpha, \beta) = (1.7, 0.5)$ and vary the fractional order ν in the interval $]0, 1]$. We ran the numerical formula for 6000 points and plotted the solution $(x(n), y(n))$ in the $x - y$ plane for the fractional order values $\nu \in \{0.98, 0.93, 0.9, 0.8, 0.86\}$. Here, the Lozi map with fractional order ν exhibits a new type of chaotic motion called the fractional chaotic attractor. As can be observed from Figure 4.3 , the attractors change whenever the fractional order ν does. In all cases, the phase space converges to an attractor that remains bounded. As ν decreases, we can see that the solution approaches some set points until a minimum number of iterations n_0 and then generally diverges towards infinity. For example, when $\nu = 0.654$, $n_0 = 1854$ (see Figure 4.4). From the numerical solutions depicted in Figures 4.3 and 4.4, it is clear that the numerical solution $(x(n), y(n))$ depends on the fractional order ν. In order to understand more about the behavior of the fractional Lozi map (4.3), we employ bifurcation diagrams with α as the critical parameter. We vary α over the interval $[0, 1.72]$ in steps of $\Delta\alpha = 0.001$ and choose initial conditions $x(0) = y(0) = 0$ and $\beta = 0.5$. The bifurcation diagrams are shown in Figure 4.5 for $\nu \in \{0.98, 0.8, 0.77, 0.66\}$. When $\nu = 1$, the Lozi map exhibits the dynamical behavior shown in Figure 4.2(a), which

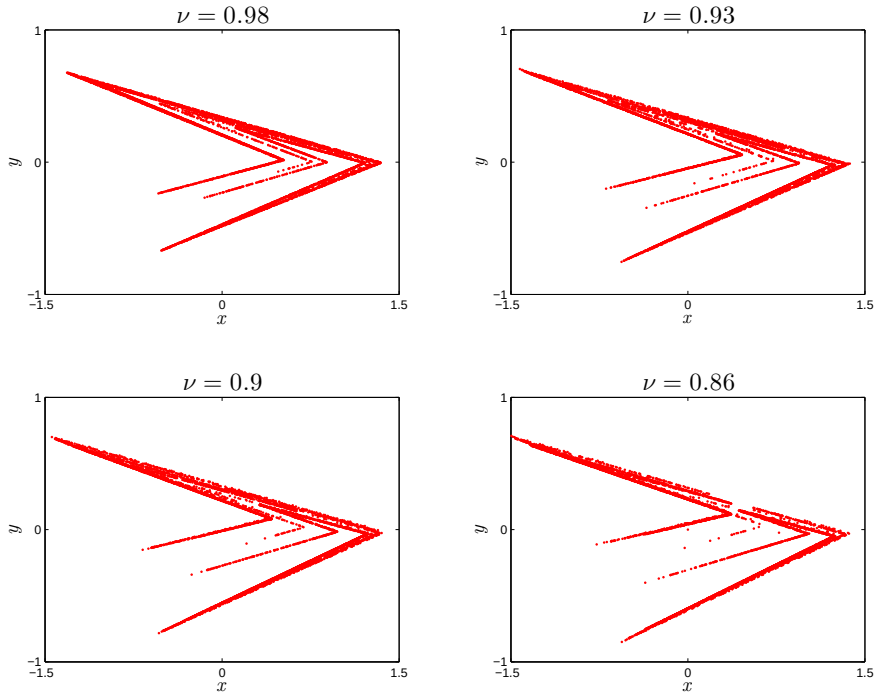

Figure 4.3: Solutions of the fractional Lozi map in the $x - y$ plane with $x(0) = y(0) = 0$, $(\alpha, \beta) = (1.7, 0.5)$ and different fractional orders.

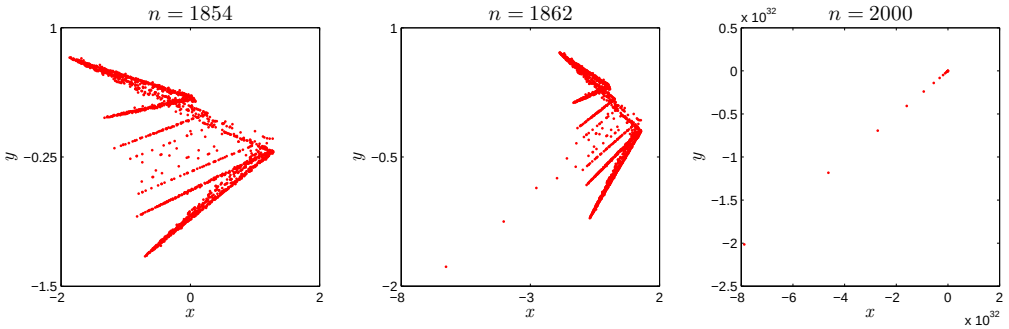

Figure 4.4: Snapshots of the $x - y$ plane belonging to the fractional Lozi map with $\nu = 0.65$ taken at $n = 954$, $n = 957$, and $n = 1000$.

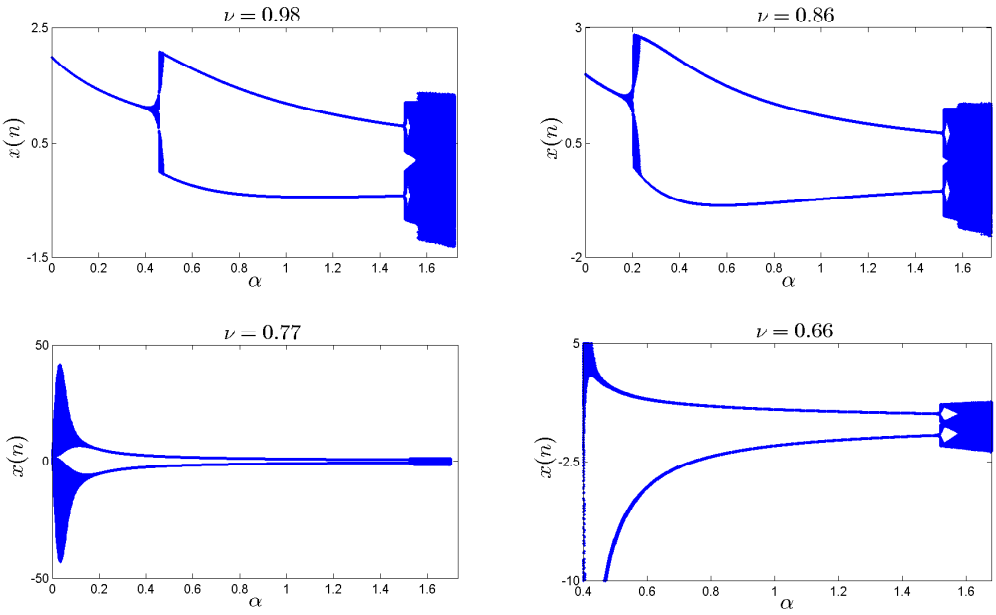

Figure 4.5: Bifurcation diagrams of the fractional Lozi map with α as the bifurcation diagram, $\beta = 0.5$, and $x(0) = y(0) = 0$ for different factional orders ν.

as expected coincides with the standard bifurcation result reported in the literature. In the interval $0 \leq \alpha \leq 0.5$, the map converges to a single fixed point. Then, as $0.5 < \alpha \leq 1.503$, we observe a two point periodic solution. It is well known that the dynamics of the Lozi map change directly from a stable periodic orbit of period 4 to a fully developed chaotic regime, which is supported by Figure. 4.2(a). As shown in Figure 4.5, the value of the fractional order ν affects the bifurcation diagram both in terms of its general shape and the duration of the chaotic interval. For $\nu = 0.98$, the bifurcation diagram is similar to the corresponding integer diagram except for a small broadening in the interval where the chaos is observed. As ν decreases further, we find that when $0 \leq \alpha \leq 0.5$, the orbit no longer goes to a fixed point. In fact, as n increases, we observe that the trajectory becomes unbounded (see Figure 4.3 for $\nu = 0.77, 0.66$). A major difference between the bifurcation diagram of the integer and fractional Lozi maps is in the interval over which chaos is observed. The interval becomes slightly smaller as ν decreases. Figure 4.6 shows the maximum Lyapunov exponent of the fractional Lozi map calculated by means of the fractional Jacobian method. This plot is obtained using the same previous parameters and initial conditions and with $\nu = 0.98$. The result agrees completely with the corresponding bifurcation plot. For completeness, Figure 4.7 shows the states of the fractional Lozi map with $x(0) = y(0) = 0$, $(\alpha, \beta) = (1.7, 0.5)$ and $\nu = 0.98$.

It can be seen from the simulation results that the fractional Lozi map undergoes chaos when the parameter α and fractional-order ν vary. Fractional order ν should be treated as a bifurcation parameter as it also determines dynamics of the system.

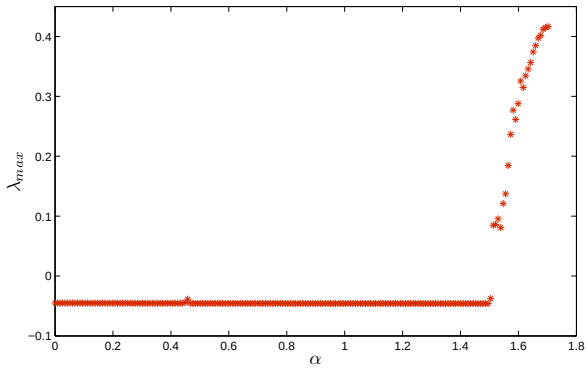

Figure 4.6: The largest Lyapunov exponent of the fractional Lozi map obtained for the same parameters, initial conditions and fractional order of Figure 4.5.

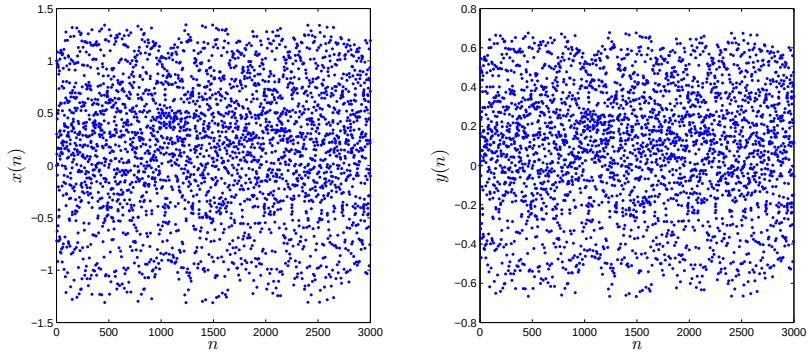

Figure 4.7: Discrete time evolution of states for the fractional Lozi map with $x(0) = y(0) = 0$, $(\alpha, \beta) = (1.7, 0.5)$ and $\nu = 0.98$.

Needless to say, fractional calculus has superior characteristics compared to conventional calculus including the endless memory effect, which leads to a higher level of dynamics, that it can be used in encryption and secure communication.

4.3 The fractional-order discrete-time Unified system

Since the Hénon and Lozi maps are the earliest discrete-time chaotic systems, they have been studied extensively by a vast number of researchers. One of the interesting studies is that of Zeraoulia and Sprott [110], where the authors proposed a new chaotic map as a combination of the the Hénon and Lozi maps named the unified map. The unified map with a single adjustable parameter α is described by

$$\begin{cases} x\,(n+1) = 1 - 1.4 f_\alpha(x(n)) + y(n), \\ y\,(n+1) = 0.3x(n), \end{cases} \tag{4.7}$$

where they limited the bifurcation parameter α is in the range $0 \leq \alpha \leq 1$ and function f_α is defined as

$$f_\alpha\left(x(n)\right) = \alpha|x(n)| + (1-\alpha)x^2(n). \tag{4.8}$$

The importance of this unified map stems from the fact that setting α to zero yields the classical Hénon map depicted in Figure 4.8-(a) and given by

$$\begin{aligned} x(n+1) &= 1 - 1.4x^2(n) + y(n), \\ y(n+1) &= 0.3x(n). \end{aligned}$$

On the other hand, when $\alpha = 1$, we end up with the classical Lozi map depicted in Figure 4.8-(b) and defined as:

$$\begin{aligned} x(n+1) &= 1 - 1.4|x(n)| + y(n), \\ y(n+1) &= 0.3x(n). \end{aligned}$$

This map do not only bridge the gap between Hénon map and Lozi map, but it also presents the entire family of chaotic maps among them, for $0 < \alpha < 1$. Figure 4.9 shows the bifurcation diagram with the critical parameter α being changed in steps of $\Delta\alpha = 0.001$. Therefore it is meaningful to investigate the dynamic characteristic of its fractional formula.

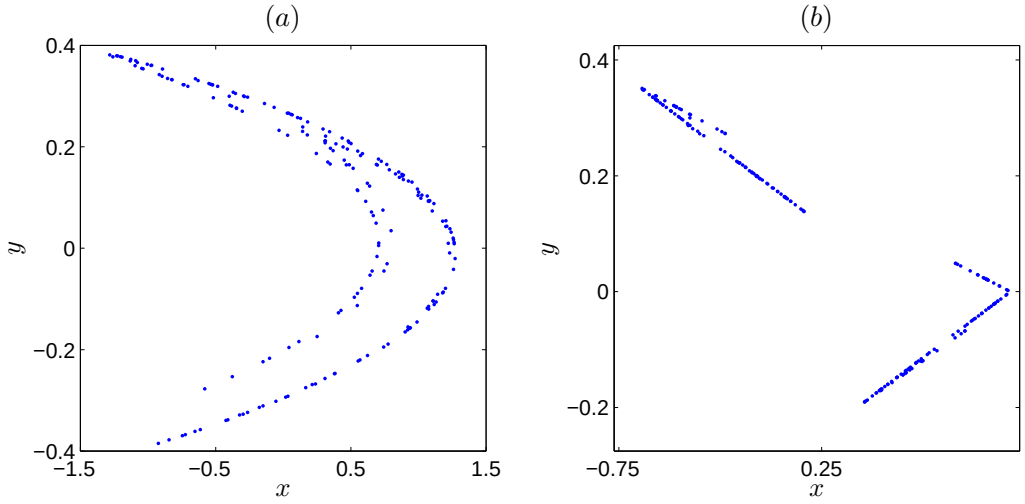

Figure 4.8: (a) The original Hénon chaotic attractor obtained from the unified chaotic map for $\alpha = 0$. (b) The original Lozi chaotic attractor obtained from the unified chaotic map for $\alpha = 1$.

System (4.7) may be rewritten in the form

$$\begin{cases} \Delta x\left(n\right) = 1 - 1.4f_\alpha\left(x(n)\right) + y(n), -x(n) \\ \Delta y\left(n\right) = 0.3x(n) - y(n). \end{cases} \tag{4.9}$$

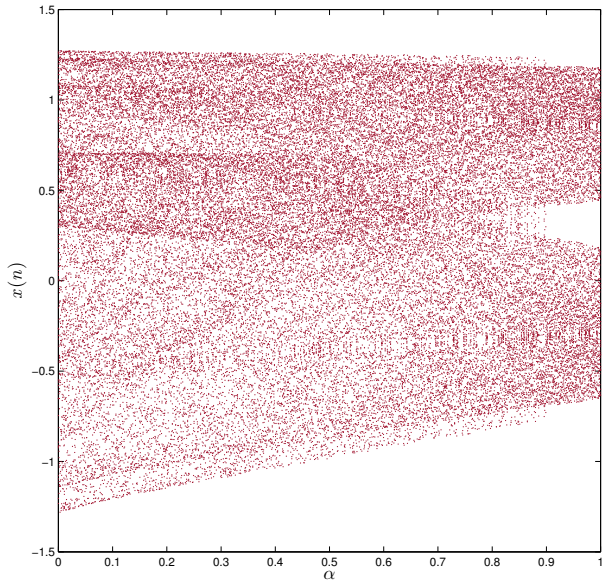

Figure 4.9: The bifurcation diagram of the unified chaotic map with the critical parameter $0 \leq \alpha \leq 1$ being changed in steps of $\Delta\alpha = 0.001$.

The fractional Unified map can be obtained by replacing the integer order difference operator Δ with the Caputo difference operator ${}^{C}\Delta_{a}^{\nu}$ and it described, as it has been reported in our research paper [111], by

$$\begin{cases} {}^{C}\Delta_{\alpha}^{\nu}x(t) = 1 - 1.4f_{\alpha}(x(t-1+\nu)) + y(t-1+\nu) - x(t-1+\nu), \\ {}^{C}\Delta_{\alpha}^{\nu}y(t) = 0.3x(t-1+\nu) - y(t-1+\nu), \qquad t \in N_{a+1-\nu}. \end{cases} \tag{4.10}$$

Following Theorem 1.15, the numerical formulas for the fractional unified map (4.10) may be obtained as

$$\begin{cases} x(n) = x(0) + \frac{1}{\Gamma(\nu)}\sum_{j=1}^{n}\frac{\Gamma(n-j+\nu)}{\Gamma(n-j+1)}\left(1 - 1.4f_{\alpha}(x(j-1)) + y(j-1) - x(j-1)\right), \\ y(n) = y(0) + \frac{1}{\Gamma(\nu)}\sum_{j=1}^{n}\frac{\Gamma(n-j+\nu)}{\Gamma(n-j+1)}\left(0.3x(j-1) - y(j-1)\right). \end{cases} \tag{4.11}$$

In [110], it was reported that while the bifurcation parameter α is close to zero, the function f_{α} defined in (4.10) behaves similar to the term $x^2(n)$ and when α is close to one it behaves similar to the absolute function $|x(n)|$. Since the values $\alpha = 0$ and $\alpha = 1$ belong to the fractional Hénon and Lozi maps, which have been studied previously, we choose to ignore them and investigated the numerical Formula (4.11) over the range $0 < \alpha < 1$. Results are reported in the following subsections.

Bifurcation diagrams and chaotic attractors

Considering the values $\alpha = 0.8$ and $\alpha = 0.2$, Figure 4.10 depicts the phase space for $n = 200$ and $\nu = 1$ with initial conditions $x(0) = y(0) = 0$. Observe that in this case, the fractional

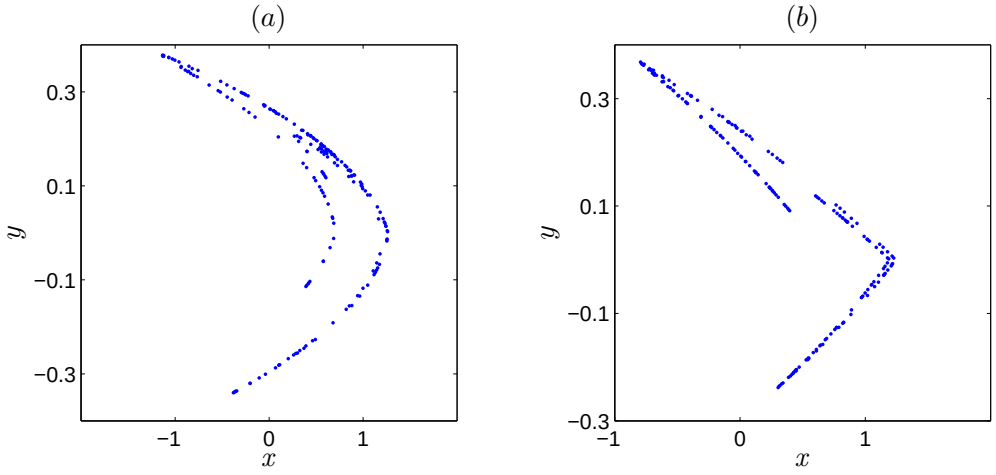

Figure 4.10: (a) A chaotic attractor obtained from the unified chaotic map for $\alpha = 0.2$. (b) A chaotic attractor obtained from the unified chaotic map for $\alpha = 0.8$.

unified map (4.10) refers to the classical map.

With the same parameters and the same initial condition, using numerical Formula (4.11), the fractional unified map is shown in Figure 4.11 for different fractional order values ν. As ν decreases, the phase plane of the fractional maps changes its shape until it completely disappears. For $\alpha = 0.2$, the minimum fractional order that produced a bounded attractor is $\nu = 0.88$. On the other hand, when $\alpha = 0.8$, we see that we obtain a bounded attractor as far as $\nu = 0.4$.

To investigate the chaotic behavior of the fractional unified map, we study the bifurcation of the parameter α with the step size $\Delta\alpha = 0.001$. Figure 4.12 illustrates the results. The figure demonstrates clearly the chaotic behavior of the fractional map. When $\nu = 1$, chaos is observed in the interval $[0, 1]$. A decrease in the fractional order ν leads to a decrease in the interval, where chaos is apparent. As shown in For $\nu = 0.4$, chaos is seen in the interval $\alpha \in [0.799, 0.95]$. A better understanding of the route to chaos can be seen, where the range of α is increased to 1.8. However, for $\alpha \in [0, 1.8]$, a border-collision bifurcation scenario is observed. The map begins with a fully-developed chaotic regime, and increasing a leads to the disappearance of the chaotic band and the appearance of a four-period orbit. Experiments have also shown that even with fractional orders ν less than one, the fractional map still behaves in a similar manner to the standard case with the one exception that the chaotic interval varies with ν.

Approximate entropy

We have calculated the approximate entropy $(ApEn)$ for the fractional-order unified map, and the results are reported in Table 4.1. For $\alpha = 0.2$, the complexity of the fractional-order unified map is reduced when the value of ν is decreased to 0.88. For $\alpha = 0.8$, when reducing the value of ν from 0.98 to 0.88, the complexity of the map varies. The results display the changes of the phase portraits in Figure 4.11. At practical applications, we should choose low values of system

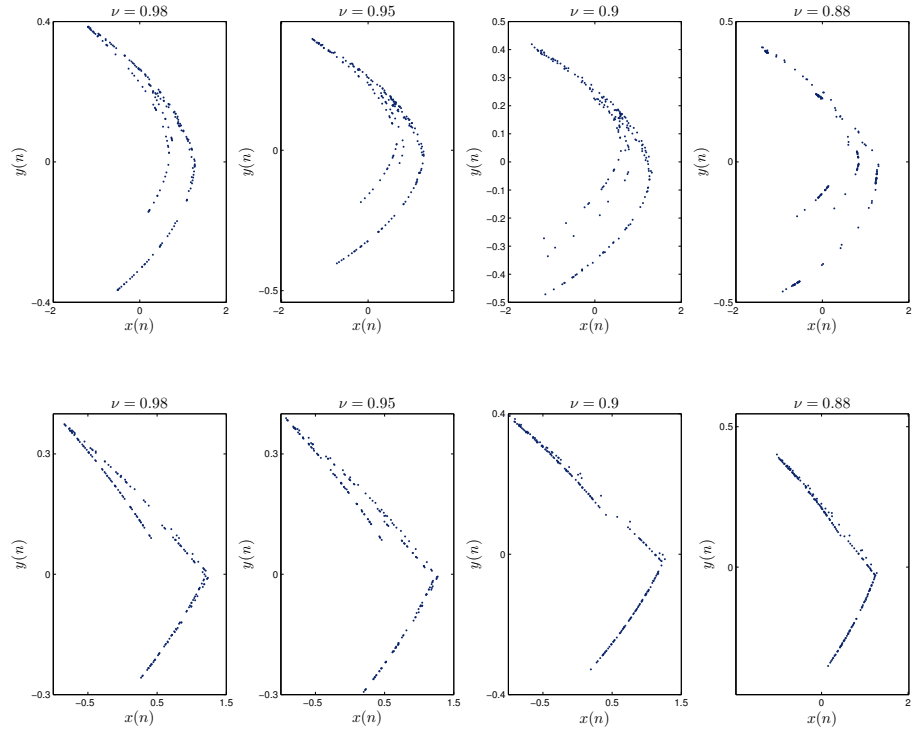

Figure 4.11: Phase portraits of the fractional unified map for: $(a)\,\alpha = 0.2$ and $(b)\,\alpha = 0.8$ with different fractional order values.

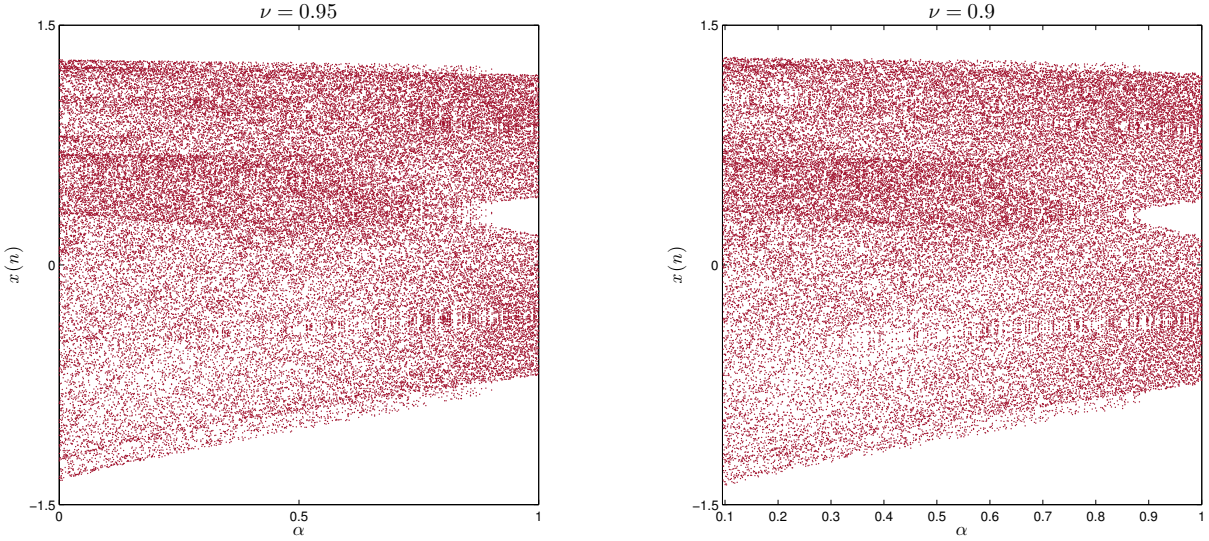

Figure 4.12: The bifurcation diagram of the unified chaotic map with α as the critical parameter for $\nu = 0.95$ and $\nu = 0.9$.

parameters α and fractional order ν, because their corresponding complexity are larger.

Table 4.1: Approximate entropy calculation of the fractional-order unified map for different fractional orders

α	ν	ApEn	α	ν	ApEn
0.2	0.98	0.4037	0.8	0.98	0.2451
0.2	0.95	0.4511	0.8	0.95	0.2571
0.2	0.9	0.4511	0.8	0.9	0.2304
0.2	0.88	0.0981	0.8	0.88	0.2530

4.4 the fractional form of the discrete Double Scroll

We consider here the 2D piecewise-linear map proposed in [114]. The map uses the same nonlinearity adopted in the Chua circuit and can exhibit chaos subject to specific parameter values. The so-called discrete hyperchaotic double scroll is of the form

$$\begin{cases} x(n+1) = x(n) - \alpha h\left(y(n)\right), \\ y(n+1) = \beta x(n), \end{cases} \tag{4.12}$$

where α and β are the bifurcation parameters and h is the characteristic function defined as

$$h(x) = \frac{1}{2}\left(2m_1 x + (m_0 - m_1)\left(|x+1| - |x-1|\right)\right), \tag{4.13}$$

with m_0 and m_1 denoting the slopes of the inner and outer sets of the original Chua circuit, respectively. This map exhibits chaos, for instance, when $x(0) = y(0) = 0.1$, $(\alpha, \beta) = (3.36, 1.04)$, and $(m_0, m_1) = (-0.43, 0.41)$, as demonstrated by the phase portraits shown in Figure 4.13. It is always helpful to examine the bifurcation diagram corresponding to a specific critical parameter in order to gain a comprehensive understanding of the dynamics of a chaotic system.

System (4.12) can be rewritten in the first difference order form given by

$$\begin{cases} \Delta x(n) = -\alpha h(y(n)), \\ \Delta y(n) = \beta x(n) - y(n). \end{cases} \tag{4.14}$$

Results reported here where considered in our paper [195]. Similarly, introducing the Caputo-like delta difference defined in Chapter 1 leads to the fractional-order map

$$\begin{cases} {}^{C}\Delta_a^{\nu} x(t) = -\alpha h(y(t-1+\nu)), \\ {}^{C}\Delta_a^{\nu} y(t) = \beta x(t-1+\nu) - y(t-1+\nu), \end{cases} \tag{4.15}$$

for $t \in \mathbb{N}_{a+1-\nu}$, where $0 < \nu \leq 1$ denotes the fractional order, and a is the starting point. The discrete integral formula described in Theorem 1.15, with starting point $a = 0$, we end up with the numerical formulas gives as

$$\begin{cases} x(n) = x(0) + \frac{1}{\Gamma(\nu)} \sum_{j=1}^{n} \frac{\Gamma(n-j+\nu)}{\Gamma(n-j+1)} \left(-ah(y(j-1))\right), \\ y(t) = y(0) + \frac{1}{\Gamma(\nu)} \sum_{j=1}^{n} \frac{\Gamma(n-j+\nu)}{\Gamma(n-j+1)} \left(bx(j-1) - y(j-1)\right), \end{cases} \tag{4.16}$$

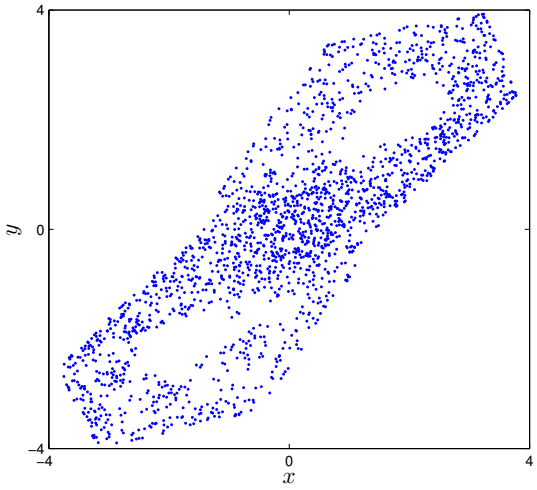

Figure 4.13: The discrete double scroll attractor for $\alpha = 3.36$, $\beta = 1.04$, $m_0 = -0.43$, and $m_1 = 0.41$.

With the same initial conditions and the bifurcation parameter values adopted for Figure 4.13 above, computer simulations were used to evaluate the numerical formulas (4.16) in order to gain a perspective on the dynamics of fractional double scroll map (4.15).

Dynamics of the fractional Double Scroll map

First, for $\nu = 1$, (4.15) becomes identical to the classical map, whose phase portraits are depicted in Figure 4.13. The corresponding bifurcation diagram is displayed in Figure 4.14 as a result of varying the parameter α in the interval $[-3.4, 3.8]$ with a step size $\Delta\alpha = 0.007$. Figure 4.14 shows that over the critical parameter range $-3.4 \leq \alpha \leq 3.8$, the double scroll map goes from border-collision bifurcation to a stable period-3 orbit and then collapses to a point as stable period-3 orbit goes to chaos band. As ν decreases, experiments show that the chaotic band decreases with it until the stable period-3 orbit disappears and a stable period-1 orbit shows up. As ν drops below 0.7, the system becomes stable. Some attractors belonging to the fractional double scroll map are plotted in Figure 4.15 for different values of ν. We notice the strong effect of the fractional order ν on the dynamics of the map. The bifurcation diagrams corresponding to the two different fractional order values $\nu = 0.93$ and $\nu = 0.8$ are depicted in Figure 4.16. The chaotic nature of the states is apparent.

Although the bifurcation diagrams presented earlier give a good indication of the dynamics of the proposed fractional map, they do not tell us how the map behaves for every fractional order. As can be seen in Figure, the value of the fractional order has a very diverse effect on the dynamics. The results agree with the phase plots discussed earlier. It is shown that the fractional order of the map has a considerable impact on its dynamics and the range of parameter values over which chaos is observed. In addition, we notice that even with reasonably low fractional orders, one can find parameter values that lead to a chaotic behavior.

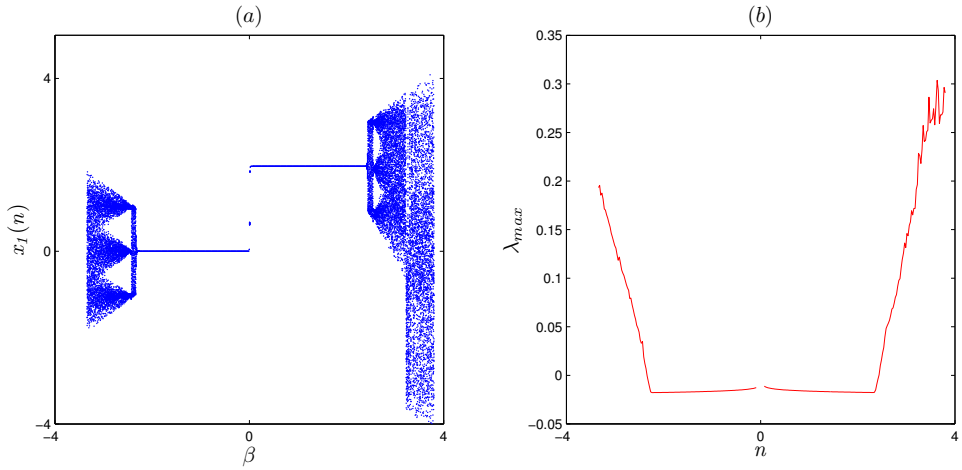

Figure 4.14: Bifurcation diagram of the discrete double scroll attractor with α as the critical parameter and $\beta = 1.04$, $m_0 = -0.43$, and $m_1 = 0.41$.

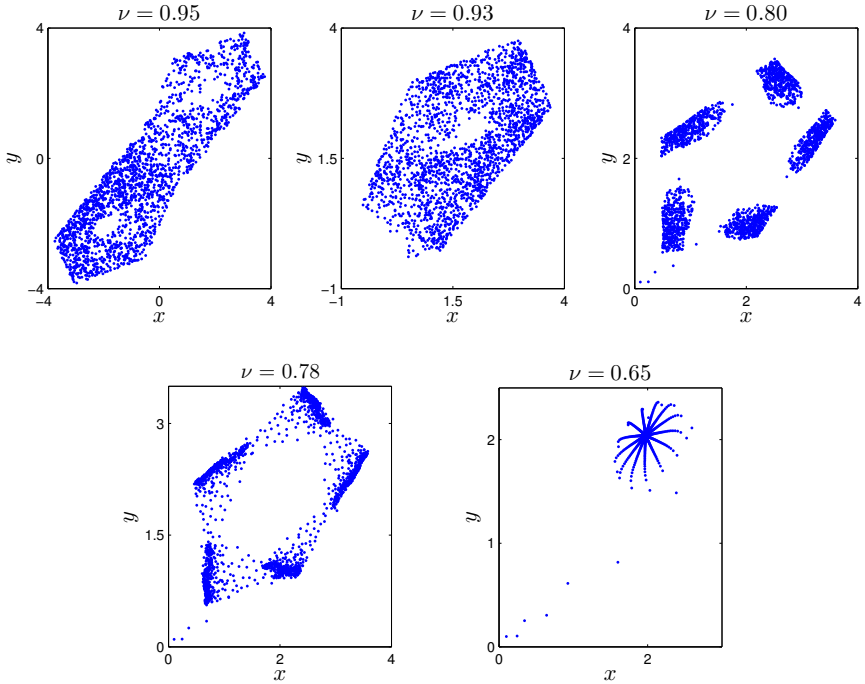

Figure 4.15: Different phase portraits with fixed parameters $\alpha = 3.36$, $\beta = 1.04$, $m_1 = -0.43$, and $m_2 = 0.41$ for various values of ν.

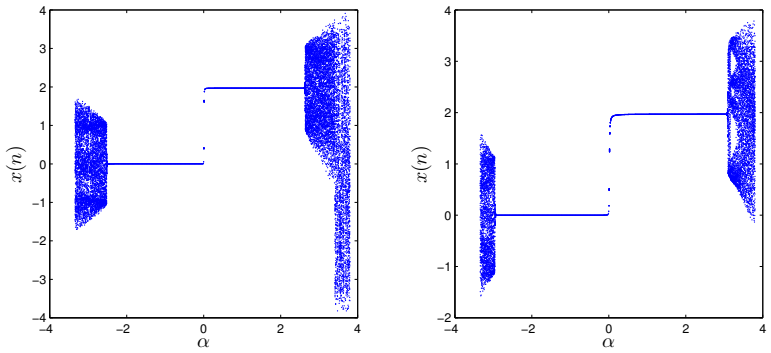

Figure 4.16: Different phase portraits with fixed parameters $\alpha = 3.36$, $\beta = 1.04$, $m_1 = -0.43$, and $m_2 = 0.41$ for various values of ν.

4.5 The fractional Hénon-Lozi map

Motivated by the Lozi work, Alaoui et al. [10] proposed and analyzed a new two dimensional chaotic piecewise map with a very similar form to the Hénon map, but with C^1 smooth function. This map is not only better in mathematical analysis, but it also can process the characteristic of the Hénon dynamics. Therefore, it is meaningful to extend the Hénon-Lozi type map into the fractional case and investigate the resulting system's dynamics. We first present the integer order Hénon-Lozi map given by

$$\begin{cases} x\left(n+1\right) = 1 - \alpha S_{\varepsilon}\left(x\left(n\right)\right) + y\left(n\right), \\ y\left(n+1\right) = \beta x\left(n\right), \end{cases} \tag{4.17}$$

where $\alpha, \beta \in \mathbb{R}$, $\beta \neq 0$ and S_{ε} is defined by

$$S_{\varepsilon} : \mathbb{R} \to \mathbb{R}, \qquad x \to S_{\varepsilon}(x) = \begin{cases} |x| & \text{if } |x| \geq \varepsilon, \\ (\frac{x^2}{2\varepsilon}) + (\frac{\varepsilon}{2}) & \text{if } |x| \leq \varepsilon, \end{cases} \tag{4.18}$$

in which ε satisfies $0 < \varepsilon < 1$. The only difference between Lozi (or Hénon's) map is that the term $|x|$ (or x^2) is replaced by $S_{\varepsilon}(x)$. It was found that this map shares many of the qualitative features of both Lozi's and Hénon map. The chaotic attractor of the Hénon-Lozi map under system parameters $(\alpha, \beta) = (1.7, 0.5)$ with initial conditions $(x\left(0\right), y\left(0\right)) = (1, 0)$ is shown in Figure 4.17. As with the Lozi map, zooming into particular part of the attractors reveals clearly the fractal structure of the map. It is always helpful to examine the bifurcation diagram corresponding to a specific critical parameter in order to gain a comprehensive understanding of the dynamics of a chaotic system. We have produced the bifurcation diagram of (4.17) with $\alpha \in [0, 1.8], \beta = 0.5$, and $\varepsilon = 0.1$ as shown in Figure 4.18. As it can be seen, the Hénon-Lozi map enters into chaos via period doubling bifurcation.

In this section, we consider the fractional version of the Hénon-Lozi map based on the Caputo

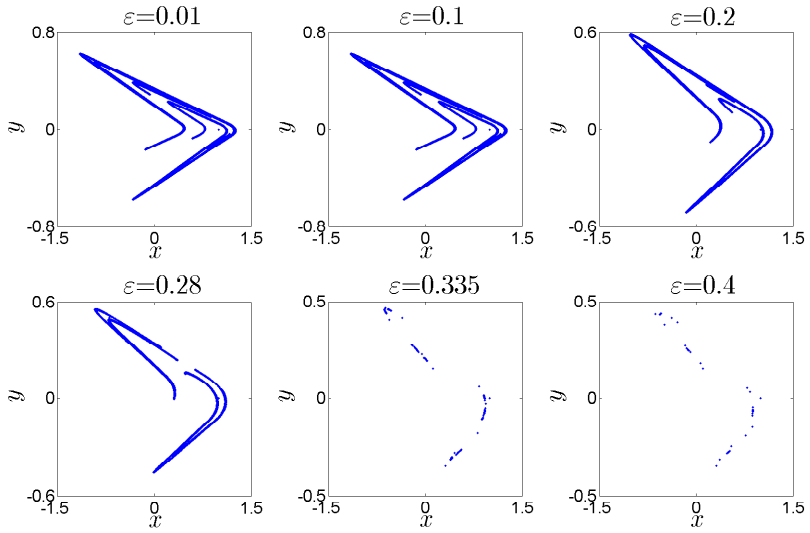

Figure 4.17: Phase plots of the map (4.17) for different values of ε.

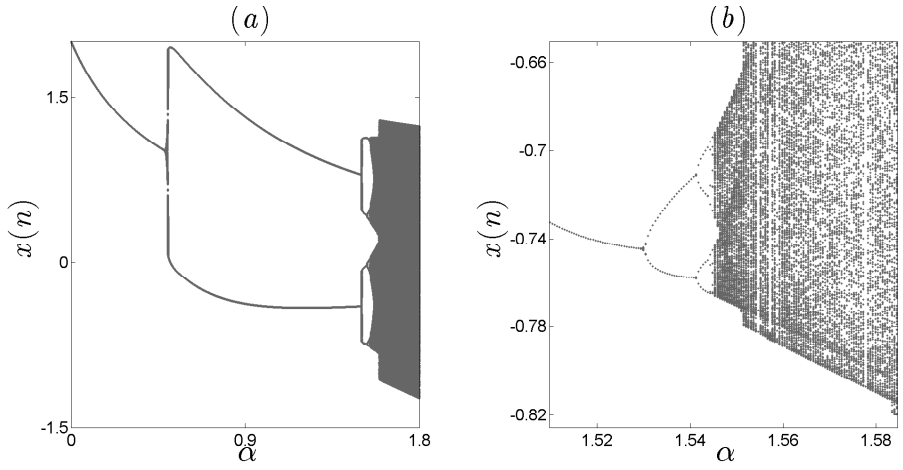

Figure 4.18: (a) Bifurcation diagram of the Hénon-Lozi map (4.17), (b) The local amplifications of bifurcation diagram for $\alpha \in (1.51, 1.583)$.

left difference operator. The fractional form of the map (4.17) can be defined by

$$\begin{cases} {}^{C}\Delta_a^{\nu} x(t) = 1 - \alpha S_{\varepsilon}\left(x\left(t-1+\nu\right)\right) + y(t-1+\nu) - x(t-1+\nu), \\ {}^{C}\Delta_a^{\nu} y(t) = \beta x(t-1+\nu) - y(t-1+\nu), \end{cases} \tag{4.19}$$

where $t \in \mathbb{N}_{a+1-\nu}$ and $0 < \nu < 1$. This fractional form has been reported in our research paper [118]. Following the same steps as in the previous section, we can express the numerical formula of the fractional Hénon-Lozi map (4.19) as

$$\begin{cases} x(n) = x(0) + \frac{1}{\Gamma(\nu)} \sum\limits_{j=1}^{n} \frac{\Gamma(n-j+\nu)}{\Gamma(n-j+1)} \left(1 - \alpha S_{\varepsilon}\left(x\left(j-1\right)\right) + y(j-1) - x(j-1)\right), \\ y(n) = y(0) + \frac{1}{\Gamma(\nu)} \sum\limits_{j=1}^{n} \frac{\Gamma(n-j+\nu)}{\Gamma(n-j+1)} (\beta x(j-1) - y(j-1)), \end{cases} \tag{4.20}$$

where $x(0)$ and $y(0)$ are the initial conditions. These numerical formula will allow us to examine the sensitivity of the fractional Hénon-Lozi map throughout the remainder of this section.

Dynamics of the fractional Hénon-Lozi map

To fully understand the properties of fractional order Hénon-Lozi map (4.19), simulation experiments, including largest Lyapunov exponents, bifurcation diagrams, phase portraits and 0-1 test are preformed. We look at the bifurcation graphs and give rough experimental bounds on the fractional order to separate between the asymptotically stable range and the chaotic range. Our numerical simulation reveals that the Hénon-Lozi map with fractional order show coexistence attractors. Regions of the fractional order spaces corresponding to the occurrence of coexisting attractors are illustrated using bifurcation diagrams that were computed based on forward and backward construction strategy. A detailed investigation is presented in the following.

Bifurcations and largest Lyapunov exponents

Bifurcation and largest Lyapunov exponents (LEs) are effective tools that are used to identify the complex dynamics of the nonlinear systems (4.19). By definition, the fractional order Hénon-Lozi map display sensitive dependence on initial conditions when two trajectories that are starting from infinitesimally close initial conditions can diverge exponentially with the rate given by LLE. Lyapunov exponents can be approximated using the Jacobian matrix, which in the case of fractional order maps is calculated in a similar manner to the states of the logistic map in Chapter 3. The Jacobian matrix J_i of the fractional Hénon-Lozi map (4.19) is defined as

$$J_i = \begin{pmatrix} a_i & b_i \\ c_i & d_i \end{pmatrix},$$

where

$$\begin{aligned} a_i &= a_0 + \tfrac{1}{\Gamma(\nu)} \textstyle\sum_{j=1}^{i} \frac{\Gamma(i-j+\nu)}{\Gamma(i-j+1)} \left(a_i \left(-\alpha \frac{\delta S_{\varepsilon}}{\delta x}(x) - 1\right) + c_i\right), \\ b_i &= b_0 + \tfrac{1}{\Gamma(\nu)} \textstyle\sum_{j=1}^{i} \frac{\Gamma(i-j+\nu)}{\Gamma(i-j+1)} \left(b_i \left(-\alpha \frac{\delta S_{\varepsilon}}{\delta x}(x) - 1\right) + d_i\right), \\ c_i &= c_0 + \tfrac{1}{\Gamma(\nu)} \textstyle\sum_{j=1}^{i} \frac{\Gamma(i-j+\nu)}{\Gamma(i-j+1)} \left(\beta a_i - c_i\right), \\ d_i &= d_0 + \tfrac{1}{\Gamma(\nu)} \textstyle\sum_{j=1}^{i} \frac{\Gamma(i-j+\nu)}{\Gamma(i-j+1)} \left(\beta b_i - d_i\right), \end{aligned}$$

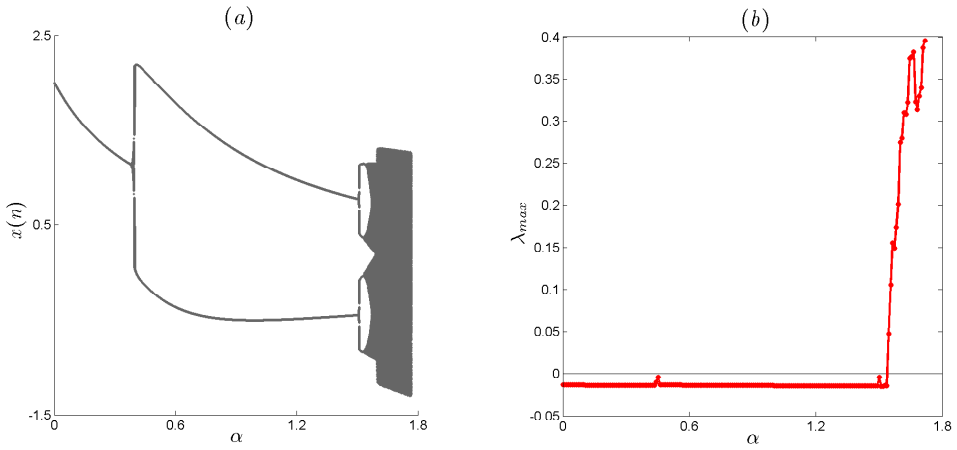

Figure 4.19: (a) Bifurcation diagram of the fractional order Hénon-Lozi (4.19) versus α with $\nu = 0.95$, (b) Largest Lyapunov exponent of the fractional map corresponding to (a).

in which

$$\frac{\delta S_\varepsilon}{\delta x}(x) = \begin{cases} 1 & \text{if } x \geq \varepsilon, \\ \frac{x}{\varepsilon} & \text{if } |x| \leq \varepsilon. \\ -1 & \text{if } x \leq -\varepsilon. \end{cases} \tag{4.21}$$

By changing the system parameters, the fractional map (4.19) can undertake different dynamic scenarios. As can be seen in the standard case of Figure 4.18, the Hénon-Lozi map enters into chaos via period doubling bifurcation. Hence, it is more interesting to visualize the effect of the fractional order ν on its dynamic behavior when α is varied. The bifurcation diagram and the largest Lyapunov exponent in the $x - \alpha$ plane are shown in Figure 4.19, where the parameters β, ε are set to $\varepsilon = 0.1$, $\beta = 0.5$ and $\nu = 0.95$. When $\nu = 0.95$, the bifurcation diagram is similar to the one observed in Figure 4.18. As ν passes into the range $(1.556, 1.74)$ the largest Lyapunov exponent becomes positive which confirms the existence of chaos. The phase portraits of the fractional Hénon-Lozi map (4.19) for different values of ε with $\alpha = 1.7$, $\beta = 0.5$ and fractional order $\nu = 0.95$ are shown in Figure 4.20. In all the six cases, the states $x(n)$, $y(n)$ approach a bounded attractor. The corresponding bounded attractors resemble to the ones obtained in Figure 4.17.

Now we reduce the value of ν to 0.84, the resulting bifurcation diagram and the largest Lyapunov exponent are given in Figure 4.21 (a)-(c). The local amplifications of the bifurcation diagram for $\alpha \in (1.4, 1.646)$ is shown in Figure 4.21 (b). Regardless the value of ν, the period doubling route to chaos is always observed. As α is increased, the fractional order Hénon-Lozi map (4.19) turns into chaos along with periodic orbits at $\alpha \simeq 1.62$. Obviously, as the fractional order ν decreases the bifurcation diagram gradually shifted to the left, which indicates that the fractional order ν is another bifurcation parameter.

To get further informations about the complex dynamics, we plot some bifurcation diagrams of the fractional order Hénon-Lozi map versus order ν when the other parameters are taken as

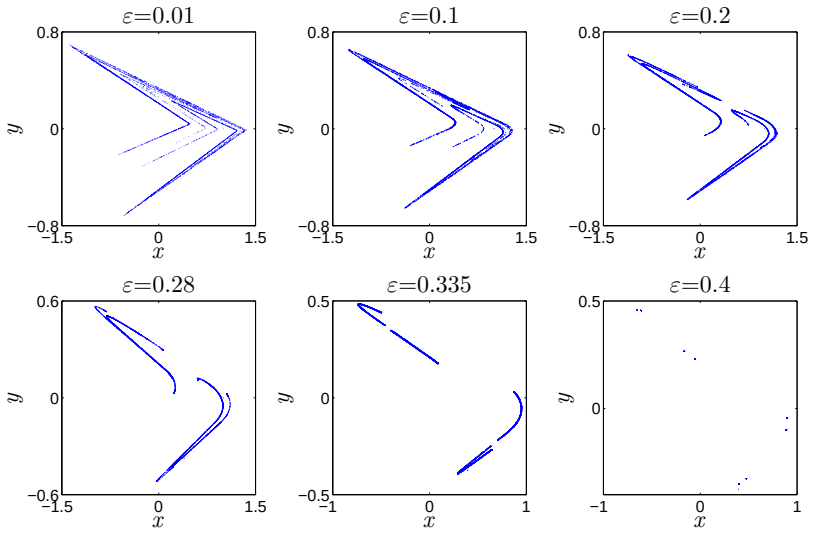

Figure 4.20: Phase plots of the fractional order Hénon-Lozi map (4.19) for different values of ε.

$\alpha = 1.7$ and $\beta = 0.6$. The bifurcation diagrams are obtained by presenting local maxima of the state $x(n)$ in terms of fractional order ν, which is increased or decreased. Figures 4.22 (a), (b) and (c) display the bifurcation diagrams for $\varepsilon = 0.2$, $\varepsilon = 0.3$ and $\varepsilon = 0.335$, respectively. The coexisting bifurcation diagrams have been plotted in blue and red colours. The trajectories coloured in red correspond to increasing value of ν while the trajectories coloured in blue correspond to decreasing value of ν. This gives us a better understanding of the effect of ν on the map's dynamics. It shows that the fractional order Hénon-Lozi map (4.19) experiences periodic and chaotic states with the variation of order ν. It is interesting that the fractional order Hénon-Lozi map (4.19) has coexisting chaotic and periodic attractors. As we increase the value of ε to 0.335, the fractional order Hénon-Lozi map exhibits two different types of chaotic and periodic attractors when $\nu \in [0.964, 0.9712]$. It is worth noting that when $\varepsilon = 0.335$, the Hénon-Lozi map with fractional order generates chaotic behavior while its integer order counterpart is periodic. The coexisting attractors with different values of ν and ε are shown in Figure 4.23.

0-1 test method

In order to further confirm the influence of the fractional order ν on the properties of the fractional order Hénon-Lozi map, we apply the 0-1 test method. Consider the translation components (p, q) of the system (4.19) with two different values $\alpha = 1.65$, $\alpha = 1.6$ and with fractional order $\nu = 0.95$. The (p, q) trajectories are shown in Figure 4.24. Clearly, the trajectories of the translation components p and q shows Brownian behavior in the $(p - q)$ plane. On the other hand, the asymptotic growth rate corresponding to Figure 4.24 converges to 1 as $n \longrightarrow \infty$ as shown in Figure 4.25. Based on these results we prove that the attractors for the two different

values $\alpha = 1.65$ and $\alpha = 1.6$ are chaotic.

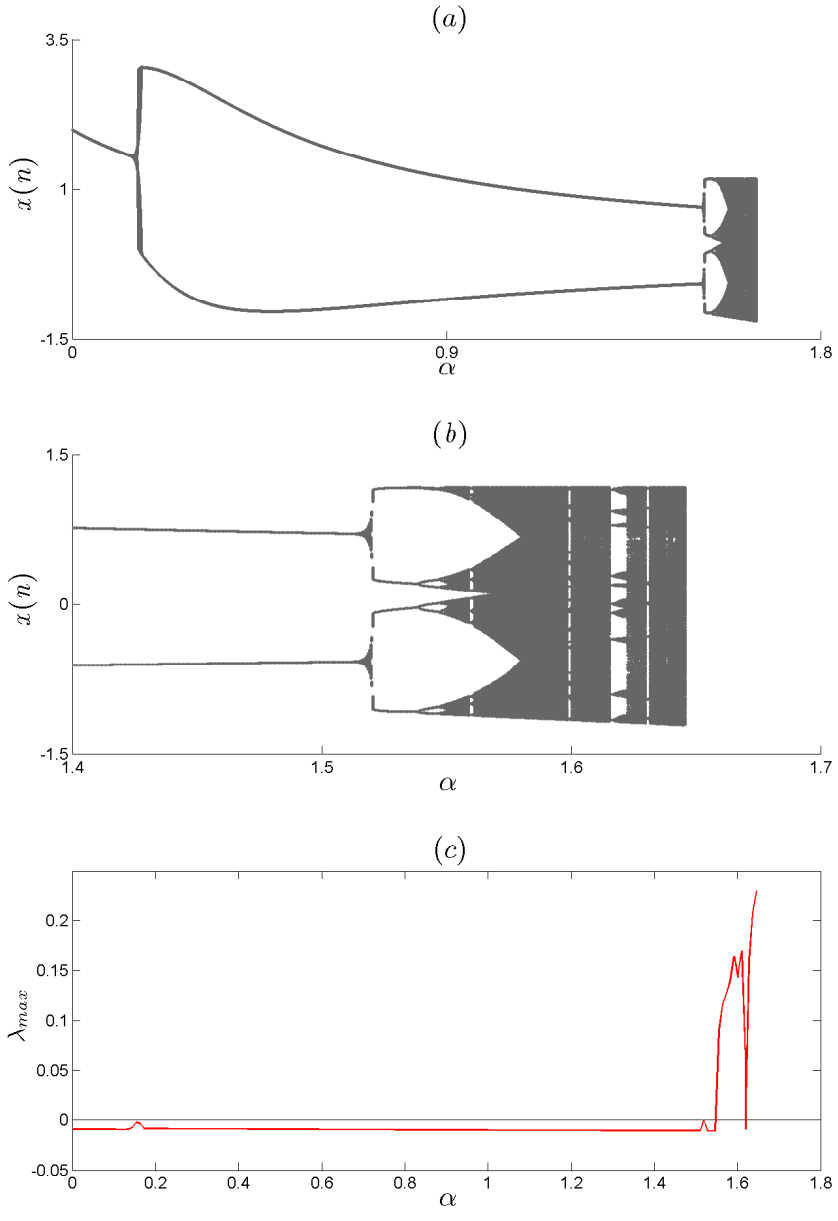

Figure 4.21: (a) Bifurcation diagram for $\nu = 0.84$, $\beta = 0.5$ and $\varepsilon = 0.1$; (b) Zoom in on the bifurcation diagram; (c) Largest Lyapunov exponent.

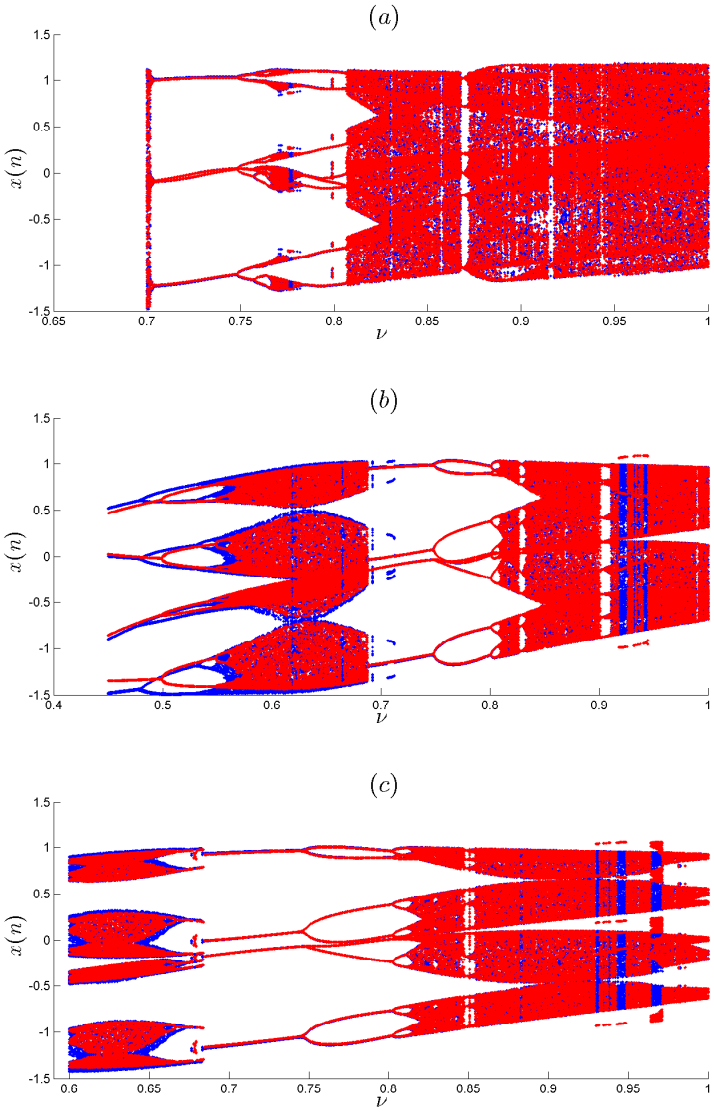

Figure 4.22: Bifurcation diagrams with ν increases and decreases with $\alpha = 1.7$ and $\beta = 0.5$. (a) $\varepsilon = 0.2$, (b) $\varepsilon = 0.3$, (c) $\varepsilon = 0.335$.

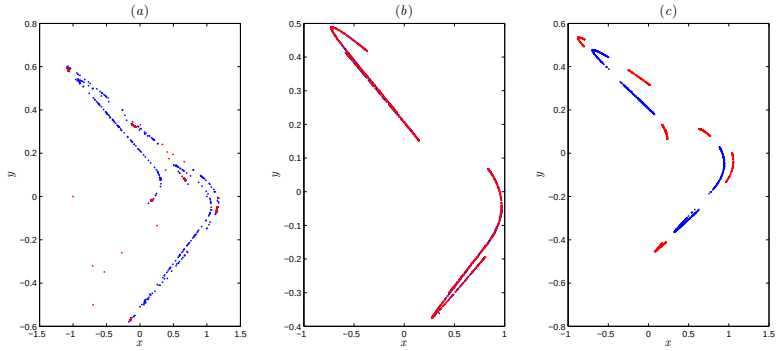

Figure 4.23: (a) Coexisting chaotic attractor and periodic orbit for $\varepsilon = 0.2$ and fractional order $\nu = 0.9418$. (b) Chaotic attractors for $\varepsilon = 0.3$ and fractional order $\nu = 0.9774$. (c) Coexisting chaotic attractors for $\varepsilon = 0.335$ and fractional order $\nu = 0.9688$.

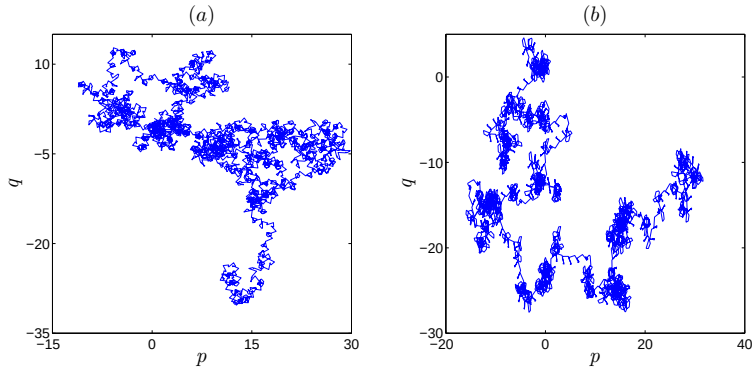

Figure 4.24: Brownian-like trajectories in the $p - q$ plane for the fractional order map (4.19) when $\nu = 0.95$, (a) for $\alpha = 1.65$, (b) for $\alpha = 1.6$.

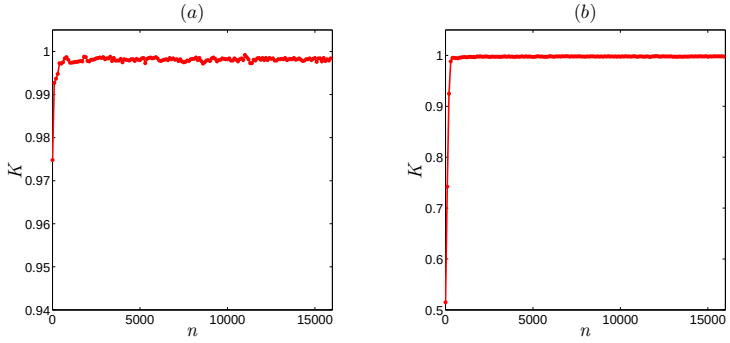

Figure 4.25: Dependence of the asymptotic growth rate K on the number of iteration n for the fractional- order Hénon-Lozi map.

4.6 The fractional sine map

Similarly, by replacing the term x^2 from the Hénon map with the trigonometry $sin(x)$ term, a new two–dimensional iterated map [12] was proposed

$$\begin{cases} x(n+1) = 1 - \alpha \sin x(n) + \beta y(n), \\ y(n+1) = x(n), \end{cases} \tag{4.22}$$

where x and y denote the states of the discrete–time system and α and β are some bifurcation parameters. This resulted in richer dynamics as the map was found to yield a C^{∞} mapping that can be considered as a generalization of the chaotic attractor with "multifolds" by means of a period–doubling bifurcation route to chaos. According to [12], the map exhibits a chaotic behavior when α falls in the interval $[-150, 200]$ and $\beta = 0.3$. Namely, for $\alpha = 3.8$, the phase space is plotted in Figure 4.26 confirming the existence of chaos.

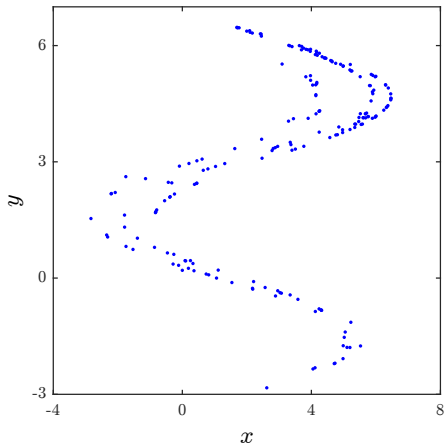

Figure 4.26: Phase portrait of the sine map for parameter values $(\alpha, \beta) = (3.8, 0.3)$.

In what follows, we aim to study the dynamics of the Caputo-type fractional map corresponding to the sine map (4.22). We will present some numerical simulation to gain an understanding of the types of behavior and the effect of the fractional order on the dynamics of the integer order map. Similar to the previous sections to derive the fractional Caputo–type version of (4.22), we start by taking the delta–differences as

$$\begin{cases} \Delta x(n) = 1 - \alpha \sin x(n) + \beta y(n) - x(n), \\ \Delta y(n) = x(n) - y(n). \end{cases} \tag{4.23}$$

Using the Caputo–like delta difference, the fractional–order sine map can be given by

$$\begin{cases} {}^{C}\Delta_a^{\nu} x(t) = 1 - \alpha \sin x(t+\nu-1) + \beta y(t+\nu-1) - x(t+\nu-1), \\ {}^{C}\Delta_a^{\nu} y(t) = x(t+\nu-1) - y(t+\nu-1), \end{cases} \tag{4.24}$$

where $t \in \mathbb{N}_{a+1-\nu}$, $0 < \nu < 1$ and a is the starting point.

Dynamics of the fractional sine map

Now, we consider the equivalent discrete formula for system (4.24), with $0 < \nu \leq 1$, as

$$\begin{cases} x(n) = x(0) + \frac{1}{\Gamma(\nu)} \sum_{j=1}^{n} \frac{\Gamma(n-j+\nu)}{\Gamma(n-j+1)} \\ \qquad\qquad (1 - \alpha \sin x(j-1) + \beta y(j-1) - x(j-1)), \\ y(n) = y(0) + \frac{1}{\Gamma(\nu)} \sum_{j=1}^{n} \frac{\Gamma(n-j+\nu)}{\Gamma(n-j+1)} (x(j-1) - y(j-1)). \end{cases} \tag{4.25}$$

According to the discrete equation (4.25), the proposed fractional map (4.24) highlights memory effects, indicating that the iterated solutions x_n and y_n are determined by all the previous states. For numerical simulation purposes, we consider the same bifurcation parameter values used previously. Using numerical formula (4.25), we study the effect of the fractional order ν on the dynamics of the fractional sine map (4.24).

Bifurcation diagrams, Lyapunov exponents and phase portraits

First, with $\nu = 1$, the resulting bifurcation diagram is depicted in Figure 4.27 whereby α is kept within the interval $[-1, 4]$ and varied in steps of $\Delta\alpha = 0.003$. Since $\nu = 1$, it is expected that our fractional map reduces to the standard one with the solution $x(n)$ depending on all past information $x(n-1), x(n-2), ..., x(0)$. Once the fractional order ν is varied from 1 to smaller values, it has an impact on the dynamics of the map. The phase portraits for $\nu = 0.976$, $\nu = 0.78$, and $\nu = 0.65$ are shown in Figure 4.28. The corresponding bifurcation diagrams are depicted in Figure 4.29 for $\alpha \in [-1, 4]$. It is observed that if we fix the bifurcation parameters α and β and change the value of the fractional order ν, the bounded attractor of the fractional map distributes in larger regions. When $\nu = 0.63$, a transient state is observed as shown in Figure

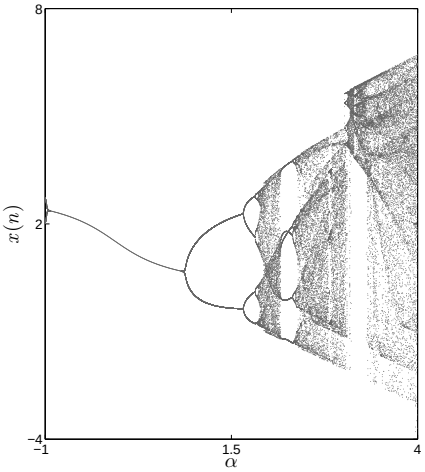

Figure 4.27: Bifurcation diagram of the sine map with $-1 \leq \alpha \leq 4$ as the critical parameter and $\nu = 1$.

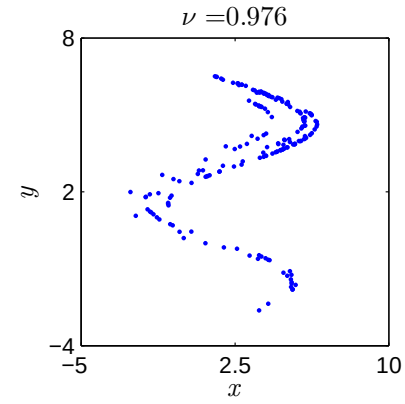

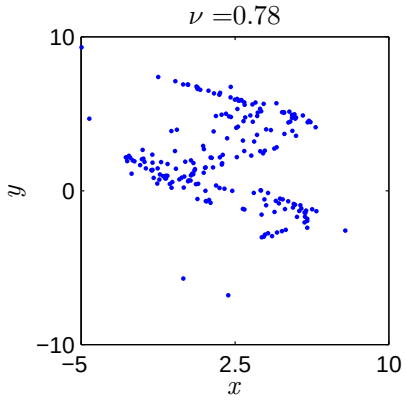

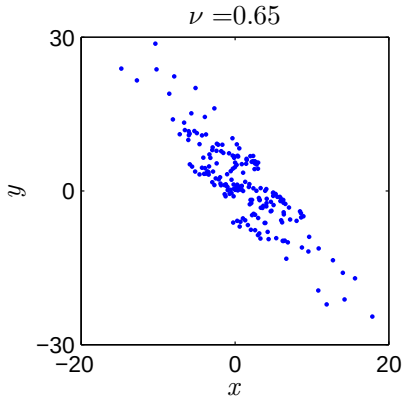

Figure 4.28: Attractors of the fractional sine map for different fractional orders ν.

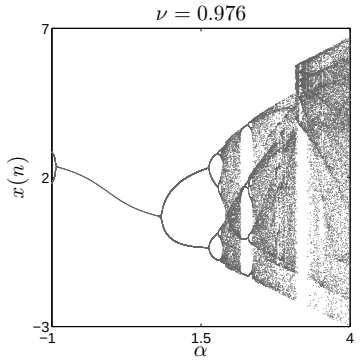

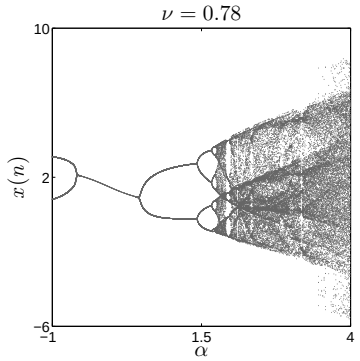

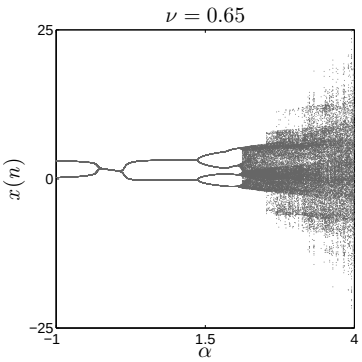

Figure 4.29: Bifurcation diagrams of the fractional sine map for different fractional orders ν.

4.30. The solution converges to a bounded attractor at the beginning and then diverges gradually to infinity in a different direction. Going back to the bifurcation plot of the standard sine map as shown in Figure 4.27, it agrees with what was reported in [12]. The standard map goes from a fixed point to a series of period–doubling bifurcations throughout the interval $(0.76, 1.86]$. Then, it exhibits a chaotic attractor for $\alpha \in (1.86, 2.16]$. Once ν passes to the interval $(2.16, 2.27]$, the map goes back to a fixed point for $\alpha \in (2.27, 2.39]$. There are also periodic windows for $\alpha > 2.92$. In Figure 4.29, we observe that as ν is made smaller, the fixed point and periodic orbit phases in intervals $(2.16, 2.27]$ and $(2.27, 2.39]$ disappear. In addition, an increase is observed in the chaotic attractors. For completeness, Figure 4.31 shows the time evolution of the chaotic states for $\nu = 0.78$. To further visualize the influence of the fractional order ν on the dynamic

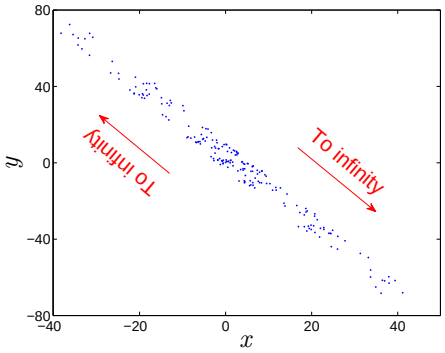

Figure 4.30: Transient state of the fractional sine map for $\nu = 0.63$.

behavior of the new map (4.24), the dynamics of the fractional sine map is analyzed by varying the fractional order ν. Since the Lyapunov exponent is a good indicator for existence of chaos, we compute the Lyapunov characteristic exponents (LEs) via the householder Jacobian method described in Chapter 3. For the parameter set $(\alpha, \beta) = (3, 0.3)$, the corresponding bifurcation and LLE diagrams taken over the range $\nu \in [0.65, 1]$ are shown in Figure 4.32. As ν decreases below 1, the fractional–order sine map (4.24) is observed to undergo a translation from chaotic to periodic states and then gradually becomes chaotic again at 0.7124. As ν continues to decrease, the system eventually converges to an unbounded attractor. All of the results above lead to the conclusion that the fractional order ν can be taken as a bifurcation parameter.

0-1 test

In order to prove the existence of a chaotic behavior in the fractional–order sine map for system parameters $(\alpha, \beta) = (3.8, 0.3)$, the 0-1 test method is considered. The 0-1 test is a binary test that works by constructing a random walk type process from a time series data. A simple visual test is provided by plotting the trajectories of the translation component in the p–q plane. Generally, unbounded trajectories in the p–q plane imply a chaotic behavior whereas bounded trajectories imply a regular behavior. Here, we applied the test directly to the solution $x(n)$. The results are depicted in Figures 4.33 and 4.34. Figure 4.33 illustrates the dynamics of the

translation components (p, q). The unbounded trajectories in the p–q plane correspond to the chaotic state. Figure 4.34 shows that the asymptotic growth rate K approaches 1 as n increases indicating a chaotic behavior.

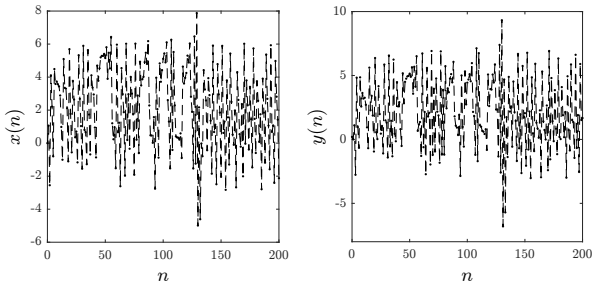

Figure 4.31: Time evolution of states for the fractional sine map with $\nu = 0.78$.

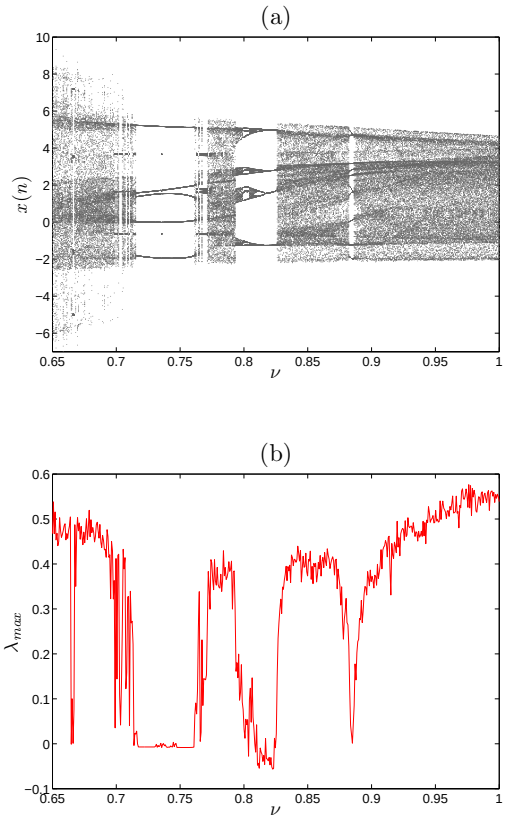

Figure 4.32: Bifurcation (a) and LLE (b) diagrams with respect to ν for the fractional order sine map with $\alpha = 3$ and $\beta = 0.3$.

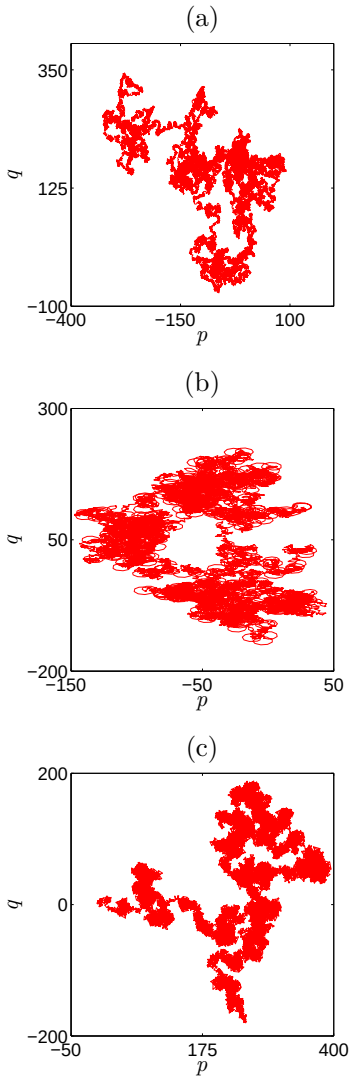

Figure 4.33: The 0-1 test (Dynamics of translation components p and q) of the fractional sine map for different fractional orders (a) $\nu = 0.976$, (b) $\nu = 0.78$, (c) $\nu = 0.65$.

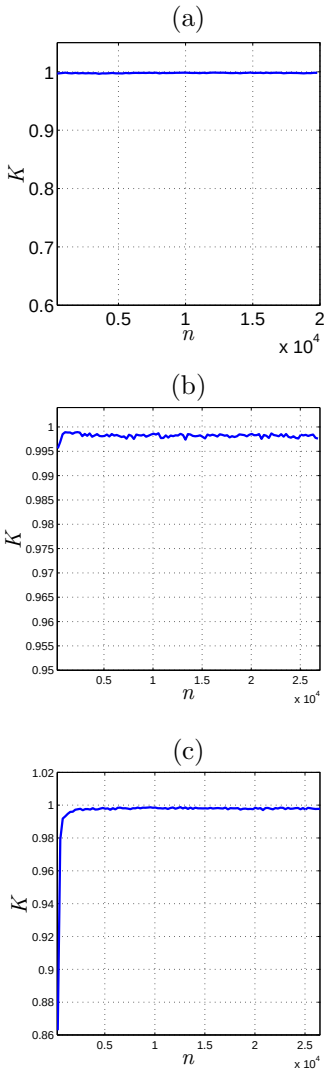

Figure 4.34: The 0-1 test (asymptotic growth rate versus n) of the fractional sine map for different fractional orders (a) $\nu = 0.976$, (b) $\nu = 0.78$, (c) $\nu = 0.65$.

4.7 The fractional Duffing map

During the last years a large number of maps were proposed. One map that has recently attracted some attention due to its interesting dynamics is the Duffing map, which is based on the Duffing oscillator [115]. The Duffing oscillator is a well known second order differential equation that describes a class of damped and driven oscillators, which is described by

$$\ddot{x} + \delta\dot{x} + \alpha x + \beta x^3 = \gamma \cos(\omega t), \tag{4.26}$$

where x, $\dot{x}$, and $\ddot{x}$ denote the displacement, velocity, and acceleration and δ, α, β, γ, and ω are parameters. Equation (4.26) is extremely important in many fields including mechanical engineering as it can model the motion of a spring pendulum where Hooke's law, which states that the displacement of a spring is linearly proportional to the force applied to it, does not apply. In such a case, $\gamma \cos(\omega t)$ represents the sinusoidal driving force for the pendulum with γ and ω being the amplitude and angular frequency, respectively, and δ, α, and β represent the damping, stiffness, and restoring force nonlinearity of the spring, respectively. This Duffing oscillator (4.26) has received considerable attention over the years due to its interesting chaotic behavior with a double strange attractor. Figure 4.35 depicts the phase space of the oscillator.

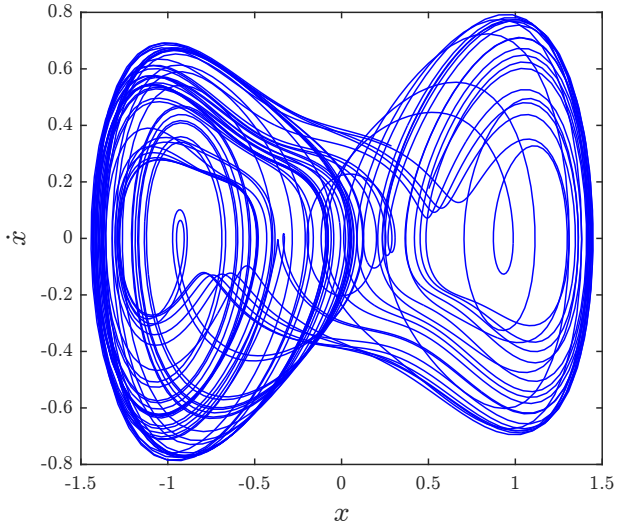

Figure 4.35: Phase space of the Duffing oscillator (4.26) with $\delta = 0.5$, $\alpha = -1$, $\beta = 1$, $\gamma = 0.42$, and $\omega = 1$.

The Duffing map is a discrete–time system based on equation (4.26), and given by

$$\begin{cases} x(n+1) = y(n), \\ y(n+1) = -\beta x(n) + \alpha y(n) - y^3(n), \end{cases} \tag{4.27}$$

where α and β are bifurcation parameters. This map was first introduced in [116] to describe the transformation required by a certain laser ray represented by its discrete-time distance to

the optical axis $x(n)$ and its angle $y(n)$ after one round trip inside the laser cavity. The Duffing map has been shown to exhibit a chaotic behavior for certain values of α and β. Figure 4.36 shows the attractor of the Duffing map (4.27) along with its bifurcation plots with respect to α and β and the estimation of the Lyapunov exponents. The attractor shown in Figure 4.36(a) is produced given initial conditions $[x(0), y(0)] = [0.3, 0.1]$ and system parameters $[\alpha, \beta] = [2.77, 0.2]$. Figure 4.36(b) depicts the estimation of the Lyapunov exponents by means of the Jacobian method, which yields $\lambda_1 = 0.4682$ and $\lambda_2 = -2.0776$. Clearly, since $\lambda_1 > 0$, the map is chaotic. Figures 4.36(c) and 4.36(d) show the bifurcation plots produced when fixing one of the parameters and varying the second. We see that the maximum chaotic range is observed for $\alpha \approx 2.77$ and $\beta \approx -0.116$. In addition to its application in the modelling of lasers, this map has also found applications in the digital scrambling of voice [117] and biometric encryption [119].

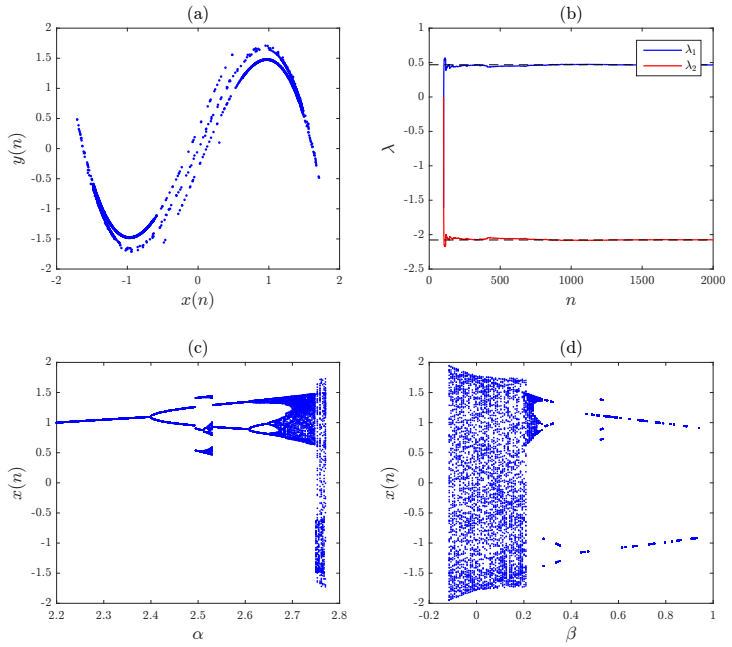

Figure 4.36: (a) Attractor of the standard Duffing map (4.27) with $(\alpha, \beta) = (2.77, 0.2)$ and initial conditions $[x(0), y(0)] = [0.3, 0.1)]$. (b) estimates Lyapunov exponents by means of the Jacobian matrix method. (c) Bifurcation plot with $\alpha \in [2.2, 2.8]$ as the critical parameter and $\beta = 0.2$. (d) Bifurcation plot with $\beta \in [-0.2, 1]$ as the critical parameter and $\alpha = 2.77$.

Now, we would like to produce a fractional difference form of the Duffing map (4.27) and investigate the effect of fractional order on its chaotic behaviour. First, we take the difference

form, which is given by

$$\begin{cases} \Delta x\left(n\right) = y\left(n\right) - x\left(n\right), \\ \Delta y\left(n\right) = -\beta x\left(n\right) + \left(\alpha - 1\right) y\left(n\right) - y^{3}\left(n\right). \end{cases} \tag{4.28}$$

Then, we can state the Caputo–type fractional form as

$$\begin{cases} {}^{C}\Delta_{a}^{\nu} x\left(t\right) = y\left(t - 1 + \nu\right) - x\left(t - 1 + \nu\right), \\ {}^{C}\Delta_{a}^{\nu} y\left(t\right) = -\beta x\left(t - 1 + \nu\right) + \left(\alpha - 1\right) y\left(t - 1 + \nu\right) - y^{3}\left(t - 1 + \nu\right), \end{cases} \tag{4.29}$$

for $t \in \mathbb{N}_{a+1-\nu}$, $0 < \nu \leq 1$, a is the starting point, and ${}^{C}\Delta_{a}^{\nu}$ is Caputo–like difference operator. The fractional duffing map (4.29) remains invariant under the transformation $(x, y) \to (-x, -y)$ for all values of parameters α, β and order ν. Hence this system could display coexisting attractors for appropriate choice of initial conditions and fractional order as well. For numerical analysis purposes, we define the numerical formula as

$$\begin{cases} x\left(n\right) = x\left(0\right) + \frac{1}{\Gamma(\nu)} \sum\limits_{j=1}^{n} \frac{\Gamma(n-j+\nu)}{\Gamma(n-j+1)} \left(y\left(j-1\right) - x\left(j-1\right)\right), \\ y\left(n\right) = y\left(0\right) + \frac{1}{\Gamma(\nu)} \sum\limits_{j=1}^{n} \frac{\Gamma(n-j+\nu)}{\Gamma(n-j+1)} \left(-\beta x\left(j-1\right) + \left(\alpha - 1\right) y\left(j-1\right)\right. \\ \qquad\qquad\qquad\qquad\qquad\qquad \left. - y^{3}\left(j-1\right)\right). \end{cases} \tag{4.30}$$

Particularly, the case of $\nu = 1$ can be reduced to the standard fractional Duffing map (4.27) where we have show that the integer-order map produced chaotic attractor given initial conditions $\left[x\left(0\right), y\left(0\right)\right] = \left[0.3, 0.1\right]$ and system parameters $\left[\alpha, \beta\right] = \left[2.77, 0.2\right]$. It is interesting to see the wide variety of dynamics as ν changes. The following results where reported in reference [120].

Dynamics of The Fractional Duffing Map

In this part, complex dynamical behaviors of the fractional Duffing map (4.29) including coexisting of different attractors are broadly investigated by phase portraits, bifurcation diagrams, largest Lyapunov exponent and 0-1 test. Then, complexity of the fractional map (4.29) is investigated using C_0 algorithm and approximate entropy ($ApEn$).

Bifurcation analysis and coexisting attractors

As we saw in the standard case of Figure 4.36, the range of α for which we obtain a chaotic behavior is very short. Hence, it is more interesting to visualize the effect of β on the map's dynamics. We have produced the bifurcation plots of (4.29) with $\beta \in \left[-0.2, 1\right]$ and $\alpha = 2.77$. Varying the fractional order ν between 0.6 and 1 yields the bifurcation diagrams depicted in Figure 4.37. It is interesting to see the wide variety of dynamics as ν changes. Next, we assess the behavior of the fractional Duffing map with ν as the bifurcation parameter. Figure 4.38 depicts the resulting bifurcation when $\left(\alpha, \beta\right) = \left(2.77, 0.2\right)$ and $\nu \in \left[0, 1\right]$, in which the red diagram begins with the initial condition $\left(-0.3, -0.1\right)$ and the blue diagram begins with the initial condition $\left(0.3, 0.1\right)$. This gives us a better understanding of the effect of ν on the map's

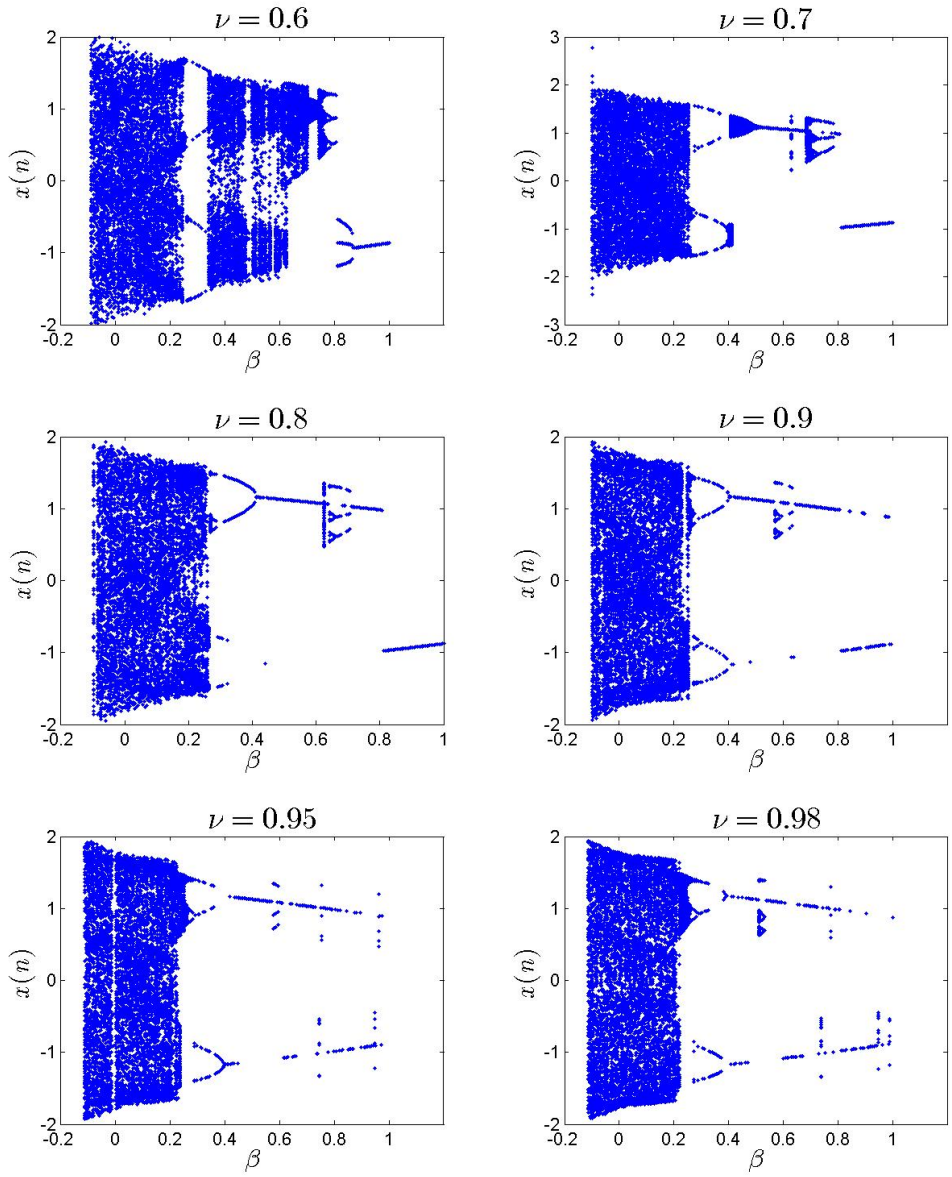

Figure 4.37: Bifurcation diagrams of the fractional Duffing map (4.29) with $\beta \in [-0.2, 1]$ as the critical parameter, $\alpha = 2.77$, $[x(0), y(0)] = [0.3, 0.1]$, and different fractional orders ν.

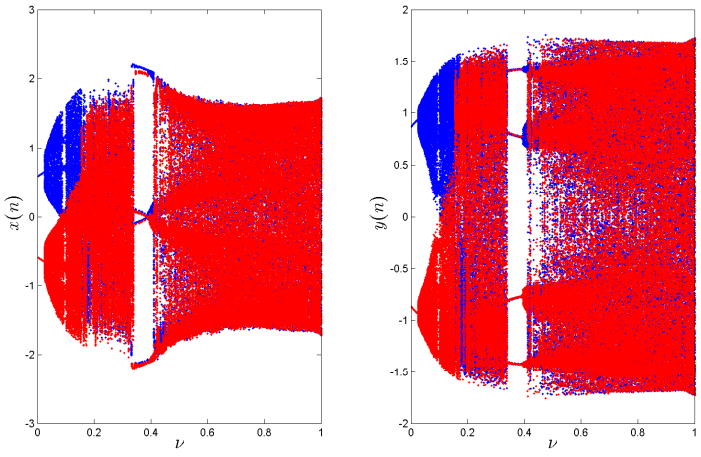

Figure 4.38: Bifurcation diagrams of the fractional Duffing map (4.29) with $\nu \in]0,1]$ as critical parameter, $(\alpha,\beta) = (2.77, 0.2)$, $(x(0), y(0)) = (-0.3, -0.1)$ for red diagram and $(x(0), y(0)) = (0.3, 0.1)$ for blue diagram.

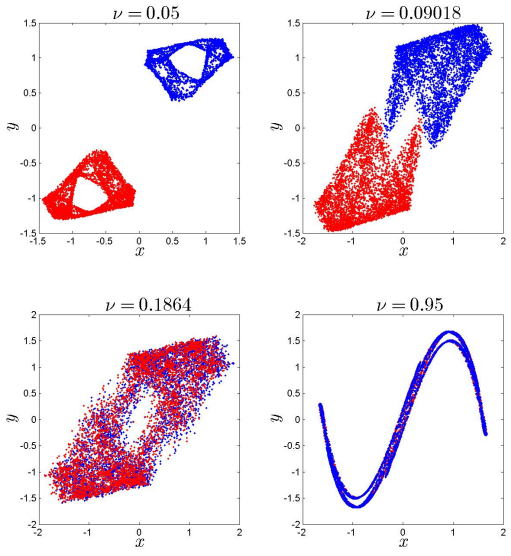

Figure 4.39: The coexisting attractors of the fractional Duffing map (4.29) for $(\alpha,\beta) = (2.77, 0.2)$, with initial condition $[x(0), y(0)] = [0.3, 0.1]$ for blue attractors and with $[x(0), y(0)] = [-0.3, -0.1]$ for red attractors.

dynamics. When $\nu \in]0, 0.1543] \cup [0.3367, 0.4289]$, the fractional Duffing map (4.29) has two coexisting periodic and chaotic attractors as shown in Figure 4.39. When ν is in the interval $[0.1663, 0.3307[\cup[0.4489, 1]$, the fractional Duffing map (4.29) become totally chaotic (see Figure 4.39).

Now, we present the tangent map to get the Lyapunov exponent from which we can get corresponding ν to distinguish the chaotic state of the fractional Duffing map (4.29)

$$J_i = \begin{pmatrix} a_i & b_i \\ c_i & d_i \end{pmatrix},$$

where

$$\begin{aligned}
a_i &= a_0 + \tfrac{1}{\Gamma(\upsilon)} \textstyle\sum_{j=1}^{i} \tfrac{\Gamma(i-j+\upsilon)}{\Gamma(i-j+1)} \left(-a_i + c_i\right), \\
b_i &= b_0 + \tfrac{1}{\Gamma(\upsilon)} \textstyle\sum_{j=1}^{i} \tfrac{\Gamma(i-j+\upsilon)}{\Gamma(i-j+1)} \left(-b_i + d_i\right), \\
c_i &= c_0 + \tfrac{1}{\Gamma(\upsilon)} \textstyle\sum_{j=1}^{i} \tfrac{\Gamma(i-j+\upsilon)}{\Gamma(i-j+1)} \left(-\beta a_i + \left(\alpha - 3y^2 - 1\right) c_i\right), \\
d_i &= d_0 + \tfrac{1}{\Gamma(\upsilon)} \textstyle\sum_{j=1}^{i} \tfrac{\Gamma(i-j+\upsilon)}{\Gamma(i-j+1)} \left(-\beta b_i + \left(\alpha - 3y^2 - 1\right) d_i\right).
\end{aligned}$$

Figure 4.41 shows the the largest LE as functions of ν. By direct comparison, the largest Lyapunov exponents are consistent with the corresponding bifurcation diagram. In addition to these particular snapshots, we have also estimated largest LE for the same bifurcation constants, initial states, and fractional orders from Figure 4.37 as depicted in Figure 4.40. This, again, is consistent with the previous results in Figure 4.37.

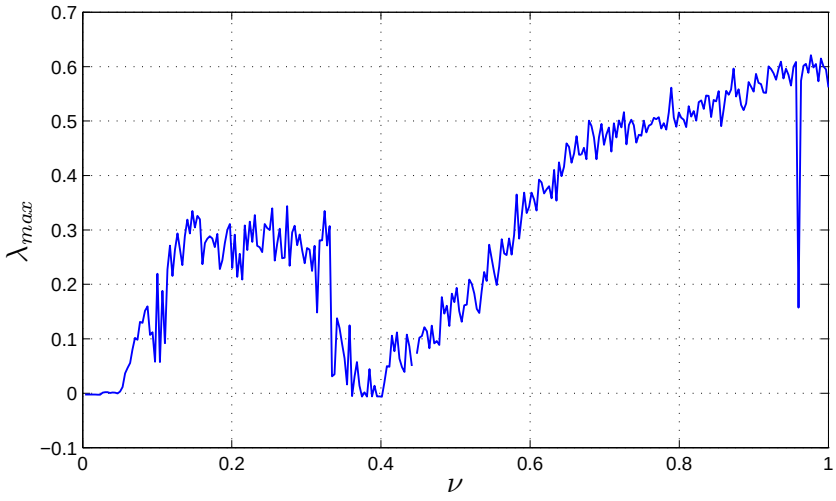

Figure 4.40: Largest Lyapunov exponents of the fractional Duffing map with $\nu \in]0, 1]$ as critical parameter, $(\alpha, \beta) = (2.77, 0.2)$ and $(x_0, y_0) = (0.3, 0.1)$.

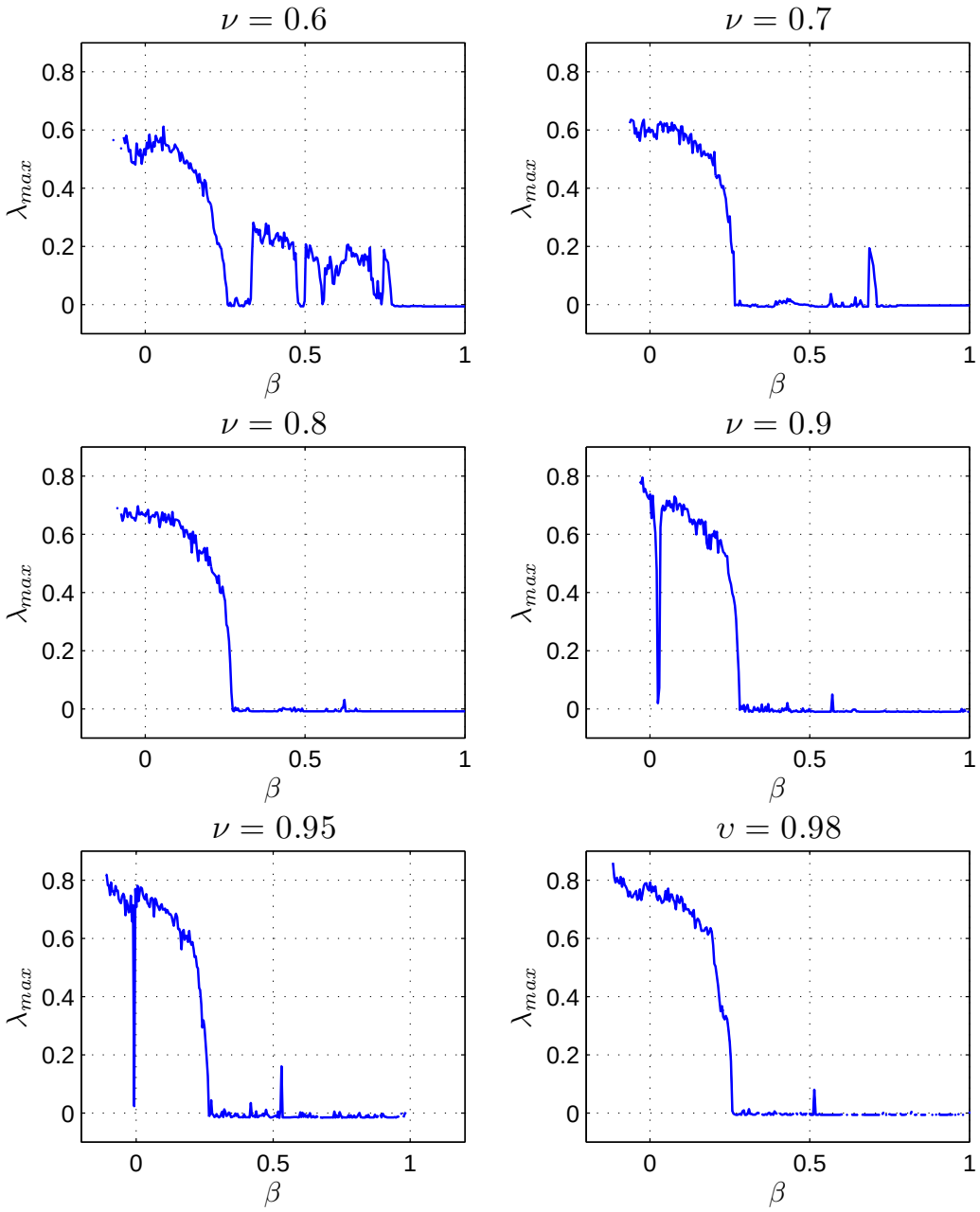

Figure 4.41: Estimated Lyapunov exponents for the same parameters, initial conditions, and fractional orders adopted in Figure 4.37.

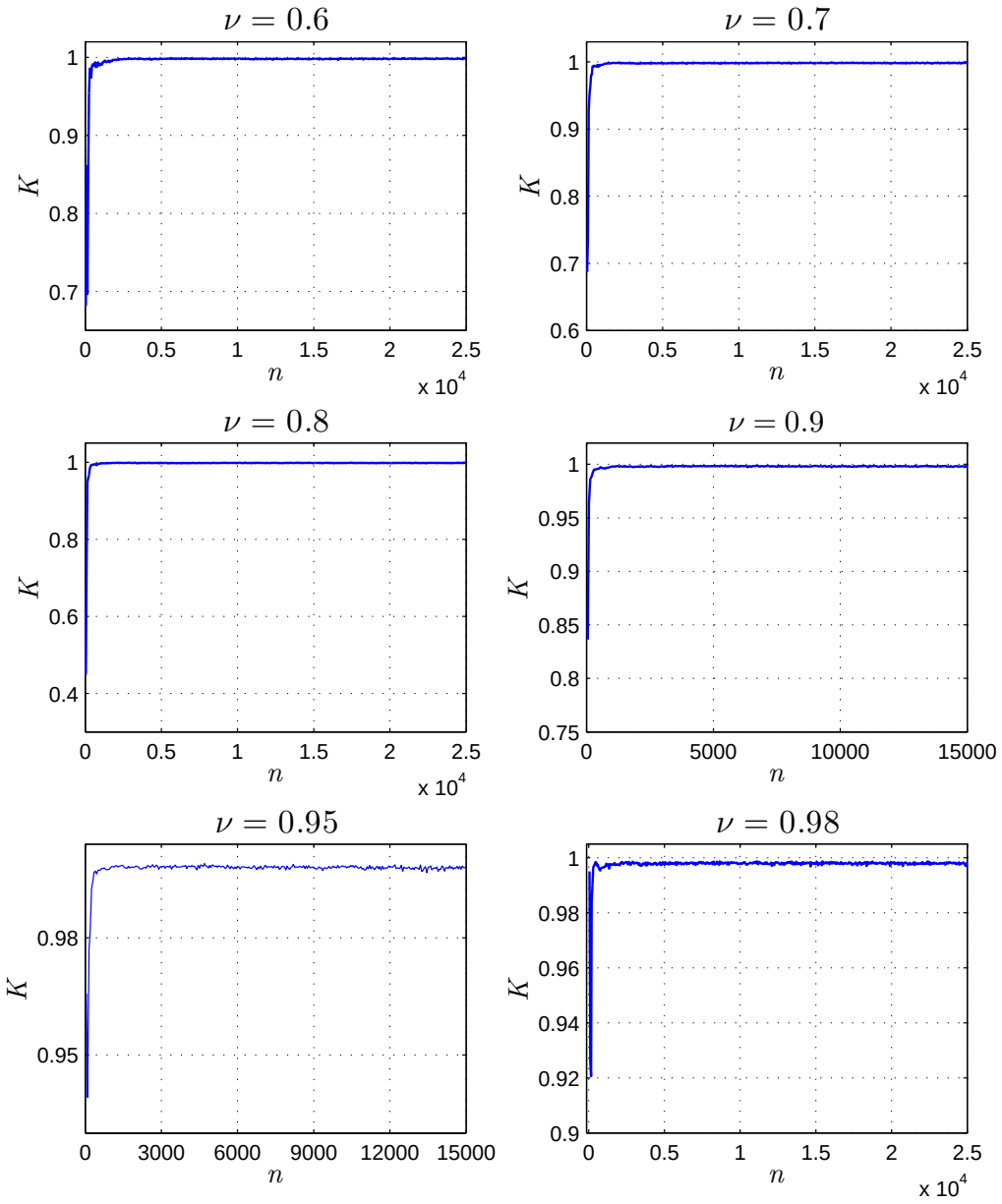

Figure 4.42: The 0-1 test of chaos for the fractional Duffing map (4.29); dependence of the asymptotic growth rate K on the length of N, with parameters, $\alpha = 2.77, \beta = 0.2$, $[x(0), y(0)] = [0.3, 0.1]$, and different fractional orders ν.

0-1 test

To validate the chaotic behavior of the fractional Duffing map, Figure 4.42 illustrates the asymptotic growth rate K of the $0-1$ test method with different values of ν. The solution $x(n)$ is obtained under the same system parameters as in Figure 4.37, and for the initial values $[x(0), y(0)] = [0.3, 0.1]$. In these cases the asymptotic growth rate K of the fractional-order duffing map approaches one, which indicates the presence of chaos. These results agree well with the bifurcation and largest Lyapunov exponent diagrams in Figure 4.37 and Figure 4.41, respectively. We also treat the fractional order ν as a bifurcation parameter, the asymptotic growth rate K versus $\nu \in]0, 1]$ is shown in Figure 4.43. As ν increases, the asymptotic growth rate approaches 1 for most values of ν at the interval $]0, 1]$. We conclude that the Duffing map shows chaotic behavior for most values of ν.

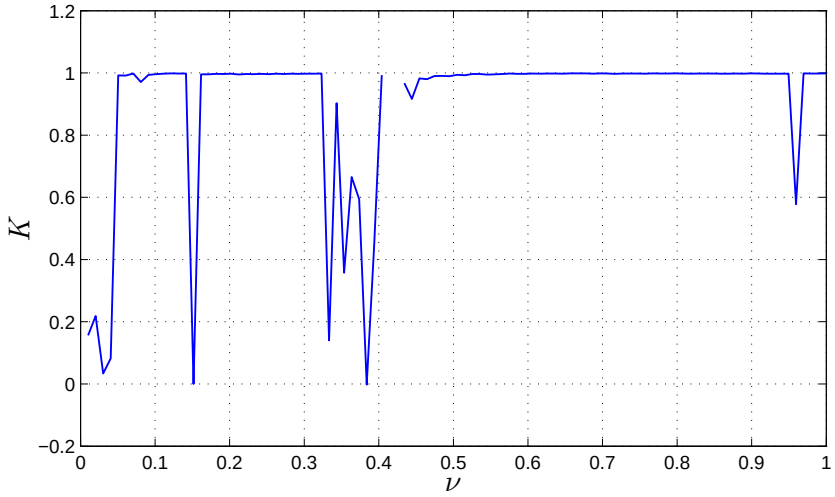

Figure 4.43: Dependence of the asymptotic growth rate K of the fractional Duffing map with $\nu \in]0, 1]$ as critical parameter, $(\alpha, \beta) = (2.77, 0.2)$ and $[x(0), y(0)] = [0.3, 0.1]$.

C_o complexity analysis

In this section the complexity of the fractional order Duffing map is analyzed by means of C_0 complexity algorithm. Complexity of the fractional Duffing map is calculated under the same conditions as above, and the results are shown in Figure 4.45 and Figure 4.44. These results consist with the previous diagrams and it shows that the fractional Duffing map has higher complexity when $\nu \in (0.8485, 0.9495)$.

Approximate entropy (ApEn)

Now, the complexity of the fractional Duffing map (4.29) is described by employing the approximate entropy ($ApEn$). Figure 4.46 shows the $ApEn$ of the proposed fractional Duffing

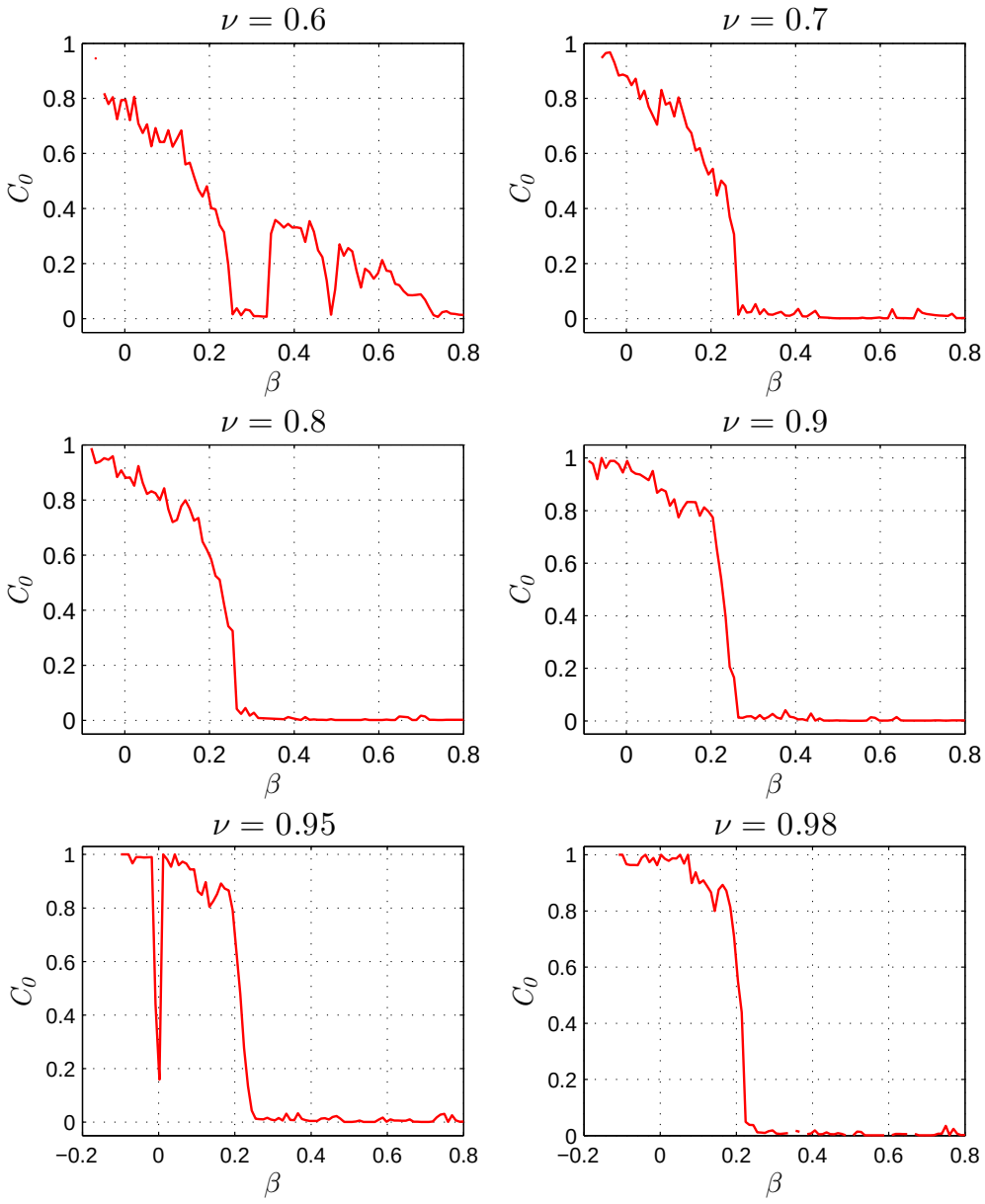

Figure 4.44: C_0 complexity analysis of the fractional Duffing map (4.29) with $\beta \in [-0.2, 1]$ as critical parameter, $\alpha = 2.77$, $[x(0), y(0)] = [0.3, 0.1]$, and different fractional orders ν.

map (4.29) for different values of fractional order and when $\alpha = 2.75$, $\beta = 0.2$, $x(0) = 0.3$, $y(0) = 0.1$. As one can see, the complexity of the fractional Duffing map (4.29) varied as we vary ν. Therefore, we must be aware of the value of the fractional order in the fractional duffing map (4.29) in order to have a relatively high structural complexity.

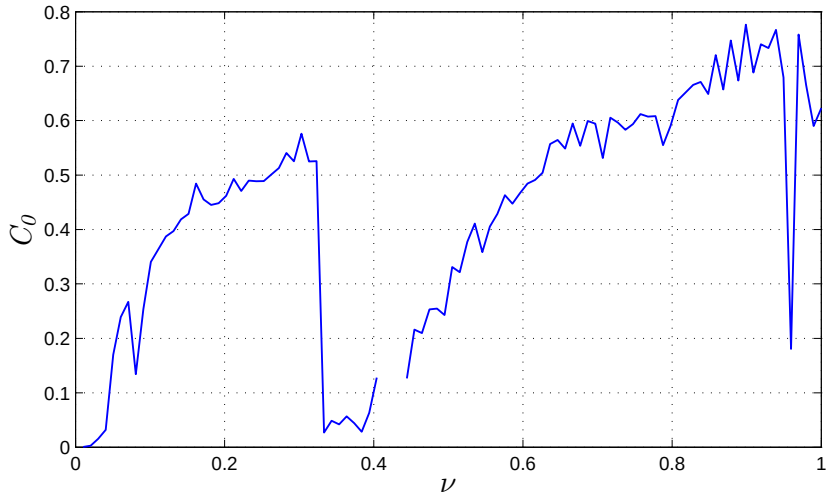

Figure 4.45: C_0 complexity analysis of the fractional Duffing map with $\nu \in]0, 1]$ as the critical parameter, $(\alpha, \beta) = (2.77, 0.2)$ and $[x(0), y(0)] = [0.3, 0.1]$.

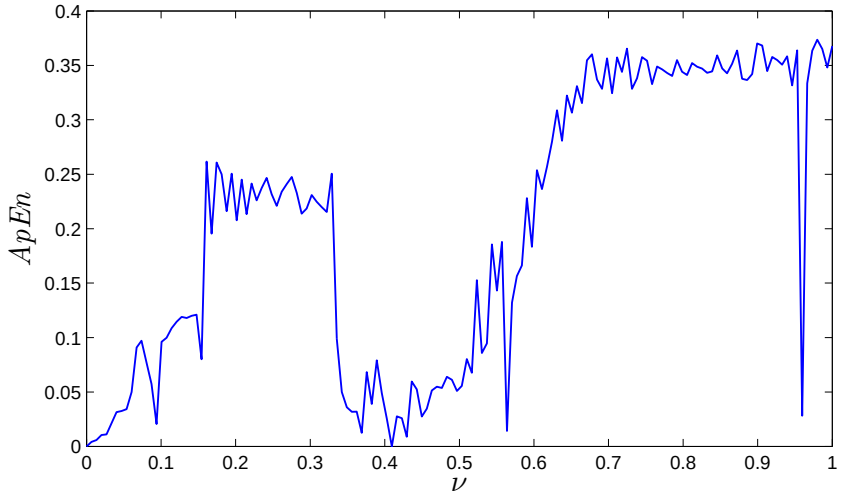

Figure 4.46: $ApEn$ of the fractional Duffing map with $\nu \in]0, 1]$ as critical parameter, $(\alpha, \beta) = (2.77, 0.2)$ and $[x(0), y(0)] = [0.3, 0.1]$.

4.8 The fractional sine–sine map

We now move to a new two dimensional chaotic map that includes two sine terms, which was proposed and studied in [121]. The so called sine–sine map is defined by

$$\begin{cases} x\left(n+1\right) = \sin x\left(n\right) - \sin 2y\left(n\right), \\ y\left(n+1\right) = x\left(n\right), \end{cases} \tag{4.31}$$

where x and y are the dependent state variables. Although this map is simpler than the previous one, it was shown to exhibit richer dynamics with a class 1 type of basin excluding a set of measure zero. The phase space for initial conditions $\left[x\left(0\right), y\left(0\right)\right] = \left[1, 1\right]$ is shown in Figure 4.47. The shape of the attractor agrees with the results reported in [121].

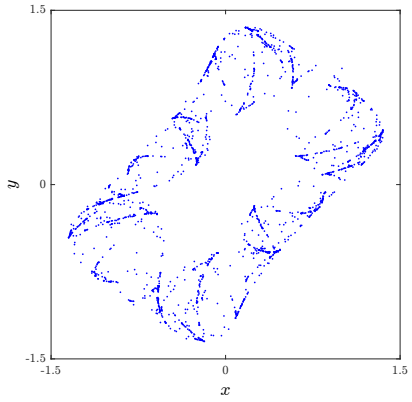

Figure 4.47: Phase portrait of the standard sine–sine map with initial conditions $\left[x\left(0\right), y\left(0\right)\right] = \left[1, 1\right]$.

Similar to the the previous sections, using the fractional discrete calculus notation described in Chapter 1, we can write the fractional sine–sine map for $t \in \mathbb{N}_{a+1-\nu}$ as

$$\begin{cases} {}^{C}\Delta_{a}^{\nu} x(t) = \sin x\left(t+\nu-1\right) - \sin 2y\left(t+\nu-1\right) - x\left(t+\nu-1\right), \\ {}^{C}\Delta_{a}^{\nu} y(t) = x\left(t+\nu-1\right) - y\left(t+\nu-1\right), \end{cases} \tag{4.32}$$

where $0 < \nu < 1$. Also, the numerical formula can be represented as

$$\begin{cases} x\left(n\right) = x\left(0\right) + \frac{1}{\Gamma(\nu)} \sum_{j=1}^{n} \frac{\Gamma(n-j+\nu)}{\Gamma(n-j+1)} \left(\sin x\left(j-1\right) - \sin 2y\left(j-1\right) - x\left(j-1\right)\right), \\ y\left(n\right) = y\left(0\right) + \frac{1}{\Gamma(\nu)} \sum_{j=1}^{n} \frac{\Gamma(n-j+\nu)}{\Gamma(n-j+1)} \left(x\left(j-1\right) - y\left(j-1\right)\right), \end{cases} \tag{4.33}$$

where $x(0)$, $y(0)$ are the initial conditions. The following results are reported in reference [122].

Dynamics of the Fractional Sine-Sine map

Using numerical formula (4.33) with two different fractional orders $\nu = 0.989$ and $\nu = 0.976$ yields the phase space portraits shown in Figure 4.48. The largest Lyapunov exponent for these

two orbits are illustrated in Figure 4.49. Since the fractional order map has a positive largest Lyapunov exponent, the phase portrait in Figure 4.48 are therefore a chaotic attractors. The calculated values K of the 0-1 test for these two orbits are also presented in Figure 4.50. We observe that K approaches 1 for $\nu = 0.989$ and $\nu = 0.976$. Therefore, the 0-1 test confirms the existence of chaos. Setting $\nu = 0.976$ and varying parameter p in the interval $[0, 2.5]$ in steps of $\Delta p = 0.001$ yields the bifurcation diagram shown in Figure 4.51.

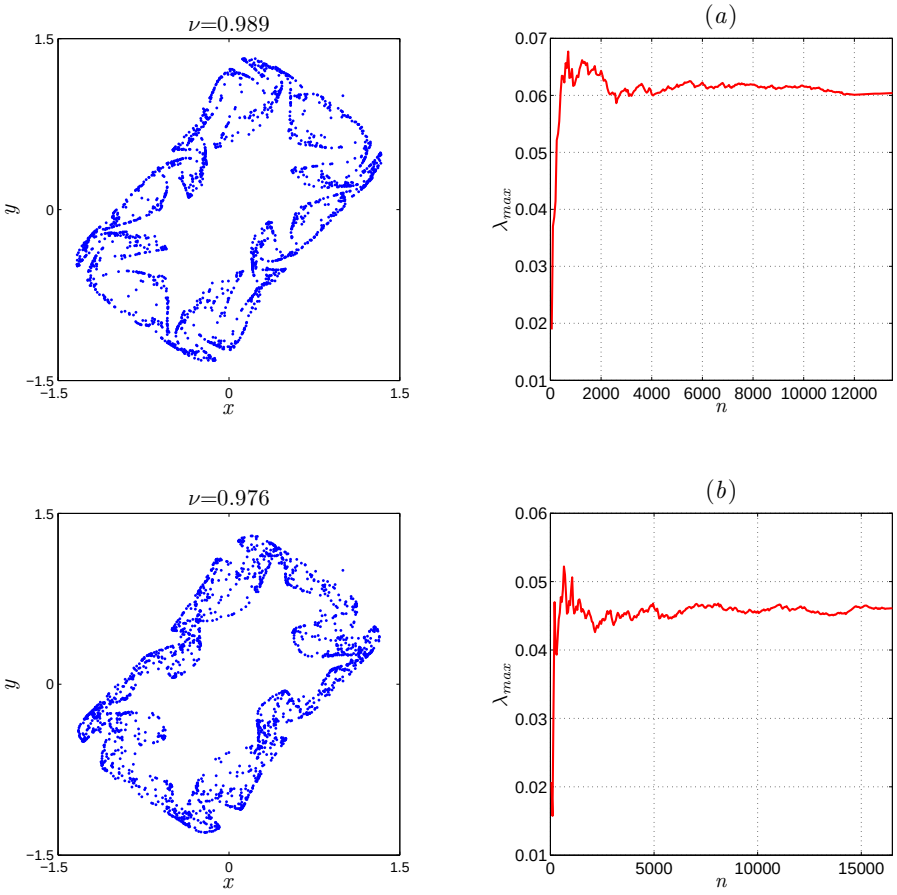

Figure 4.48: Attractors of the fractional sine–sine map for two different fractional orders $\nu = 0.989$ and $\nu = 0.976$.

Figure 4.49: LLE of the fractional sine–sine map for different fractional orders: (a) $\nu = 0.989$, and (b) $\nu = 0.976$.

To analyze further the effect of the fractional–order ν on the dynamic behavior of the fractional–order sine–sine map (4.31), we chose to vary ν from 0 to 1 in steps of 0.001 and observe the behavior of the map. The bifurcation diagrams for two different initial conditions

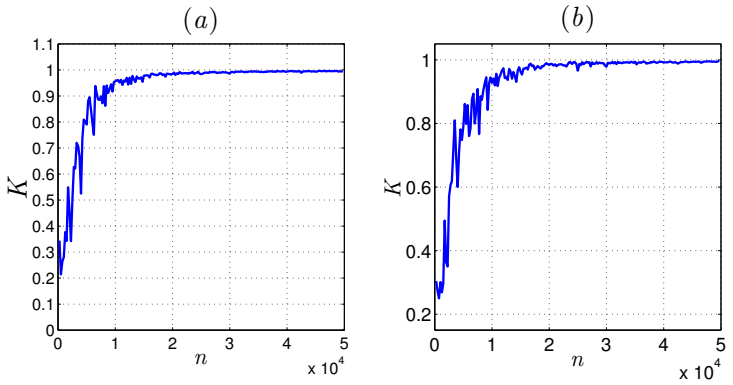

Figure 4.50: The 0-1 test of the fractional sine–sine map for different fractional orders: (a) $\nu = 0.989$ and (b) $\nu = 0.976$.

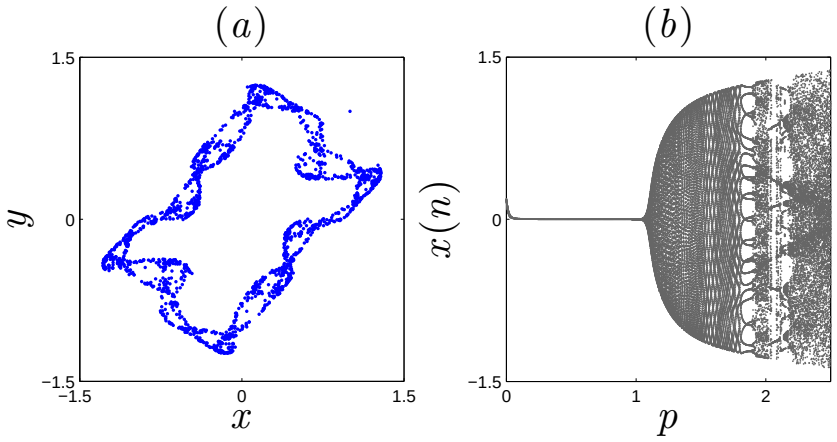

Figure 4.51: Chaotic attractor and bifurcation diagram of the fractional sine–sine map for $\nu = 0.976$ and critical parameter p varying from 0 to 2.5: (a) chaotic attractor, (b) bifurcation diagram

are shown in Figure 4.52. The red diagram corresponds to initial conditions $(-1, -1)$ while the blue diagram corresponds to initial conditions $(1, 1)$. It is clear that the fractional order map (4.31) is invariant under the transformation from (x, y) to $(-x, -y)$. From Figure 4.52, we find that even with a fractional order, the map still exhibits a chaotic behavior. The chaotic properties of the map disappear in the interval $\nu \in [0.952, 0.967]$ and reappear for $\nu \in [0.939, 0.951]$ as seen in Figure 4.52. Finally, when $\nu \leq 0.03$, chaos disappears once more and the system becomes stable.

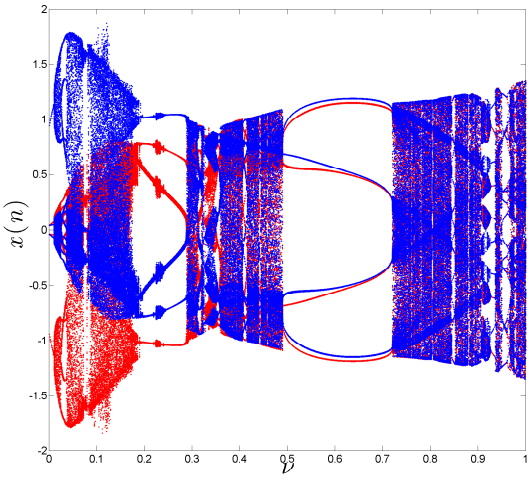

Figure 4.52: Bifurcation diagram of the fractional sine-sine map with ν as the critical parameter for two different initial conditions: (red) $(x_0, y_0) = (-1, -1)$ and (blue) $(x_0, y_0) = (1, 1)$.

4.9 The fractional form of the Ikeda map

The Ikeda map was introduced firstly by Ikeda [11] as a physical model to exhibit the dynamics of light in the ring cavity (a model of light going around across a nonlinear optical resonator). In [123], this model has been reduced to the following discrete-time dynamical system

$$\mathbf{z}(n+1) = A + B\mathbf{z}(n) \exp\left[i\left(|\mathbf{z}(n)|^2 + C\right)\right], \tag{4.34}$$

where $\mathbf{z}(n)$ represents the electric field inside the resonator at the n-th step of rotation in the resonator, the parameter A indicates laser light applied form the outside, the parameter C indicates linear phase across the resonator, and the dissipation parameter B characterizing the loss of resonator. If $B = 1$ then the Ikeda map reduces to a conservative map. In mathematics, the real valued two-dimensional Ikeda map can be expressed as a discrete-time dynamical system in the form

$$\begin{cases} x(n+1) = 1 + \{x(n)\cos\varphi(n) - y(n)\sin\varphi(n)\}\delta, \\ y(n+1) = \{x(n)\sin\varphi(n) + y(n)\cos\varphi(n)\}\delta. \end{cases} \tag{4.35}$$

where δ is a parameter and

$$\varphi(n) = 0.4 - \frac{6}{1 + x^2(n) + y^2(n)}. \tag{4.36}$$

In Figure 4.53, we display the bifurcation diagram, when δ varying from 0 to 0.9, Lyapunov exponents and the phase space of the Ikeda map. It is clear from Figure 4.53 that this map exhibits chaotic behavior for almost all values of $0.6 \leq \delta \leq 0.9$. Now, before we introduce the

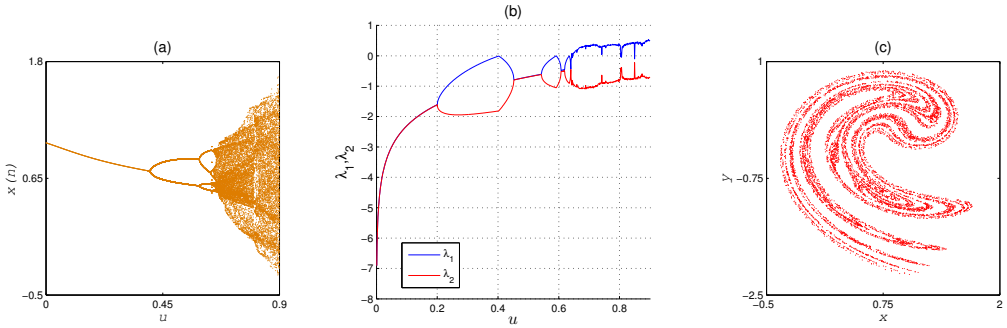

Figure 4.53: (a) Bifurcation diagram for δ varying from 0 to 0.9 in the $\delta - x$ plane, (b) Lyapunov exponents corresponding to the bifurcation diagram in the $\delta - x$ plane, (c) Phase space of Ikeda map

fractional-order form of Ikeda map, we use the standard forward difference operator, $\Delta u(n) = u(n+1) - u(n)$, to rewrite the system (4.35) into the difference form

$$\begin{cases} \Delta x\left(n\right) = 1 + \left\{x\left(n\right)\cos\varphi\left(n\right) - y\left(n\right)\sin\varphi\left(n\right)\right\}\delta - x\left(n\right), \\ \Delta y\left(n\right) = \left\{x\left(n\right)\sin\varphi\left(n\right) + y\left(n\right)\cos\varphi\left(n\right)\right\}\delta - y\left(n\right). \end{cases} \tag{4.37}$$

In the above system, if we replace the difference operator Δ by the Caputo-like difference operator ${}^{C}\Delta_{a}^{\nu}$ and n by $\omega = t - 1 + \nu$ then we get the fractional-order difference system

$$\begin{cases} {}^{C}\Delta_{a}^{\nu}x(t) = 1 + \left\{x(\omega)\cos\varphi(\omega) - y(\omega)\sin\varphi(\omega)\right\}\delta - x(\omega), \\ {}^{C}\Delta_{a}^{\nu}y(t) = \left\{x(\omega)\sin\varphi(\omega) + y(\omega)\cos\varphi(\omega)\right\}\delta - y(\omega), \end{cases} \tag{4.38}$$

where $t \in N_{a+1-\nu}$, $\nu \in]0,1]$ is the fractional order parameter and a is the starting point. The fractional Ikeda map expressed by the fractional order difference system given in (4.38) can been seen as an extension or a generalization of the integer order Ikeda map given in the difference system.

Dynamics of the fractional Ikeda map

This subsection employs numerical tools to assess the dynamics of the proposed fractional Ikeda map given in system (4.38). For this purpose, we define the discrete numerical formula, as

$$\begin{cases} x(t) = x(a) + \frac{1}{\Gamma(\nu)}\sum_{s=a+1-\nu}^{t-\nu}(t-s-1)^{\nu-1}\left(1 + \left\{x(\omega)\cos\varphi(\omega) \quad -y(\omega)\sin\varphi(\omega)\right\}\delta - x(\omega)\right), \\ y(t) = y(a) + \frac{1}{\Gamma(\nu)}\sum_{s=a+1-\nu}^{t-\nu}(t-s-1)^{\nu-1}\left(\left\{x(\omega)\sin\varphi(\omega) + y(\omega)\cos\varphi(\omega)\right\}\delta - y(\omega)\right), \end{cases} \tag{4.39}$$

$t \in N_{a+1}$, since $(t-s-1)^{\nu-1} = \frac{\Gamma(t-s)}{\Gamma(t-s+1-\nu)}$, and for $a = 0$, we have

$$\begin{cases} x(n) = x(0) + \frac{1}{\Gamma(\nu)} \sum_{j=1}^{n} \frac{\Gamma(n-j+\nu)}{\Gamma(n-j+1)} \left(1 + \{x(j-1)\cos\varphi(j-1) \right. \\ \qquad\qquad \left. -y(j-1)\sin\varphi(j-1)\}\,\delta - x(j-1)\right), \\ y(n) = y(0) + \frac{1}{\Gamma(\nu)} \sum_{j=1}^{n} \frac{\Gamma(n-j+\nu)}{\Gamma(n-j+1)} \left(\{x(j-1)\sin\varphi(j-1) + y(j-1) \right. \\ \qquad\qquad \left. \cos\varphi(j)\}\,\delta - y(j-1)\right). \end{cases} \tag{4.40}$$

Now, using the above numerical formula, we are going to explore numerically the action of the fractional order ν the behavior of the fractional Ikeda map (4.38) . For simplicity we take $[x(0), y(0)] = [0, 0]$. The attractors of the map (4.38) for different fractional order values ν are listed in Figure 4.54, where the variable x is located horizontally and the variable y is located vertically. From Figure 4.54, it has been noticed that decreasing the fractional order ν leads to a change of the shape of the fractional Ikeda attractor, as ν decreases further the chaotic attractor transitioned to stable one. The evolution of the states in discrete time for the fractional Ikeda map is illustrated in Figure 4.55 for the case of $\nu = 0.95$. The random like nature of the solutions shown in Figure 4.55 confirms the existence of chaos when $\nu = 0.95$.

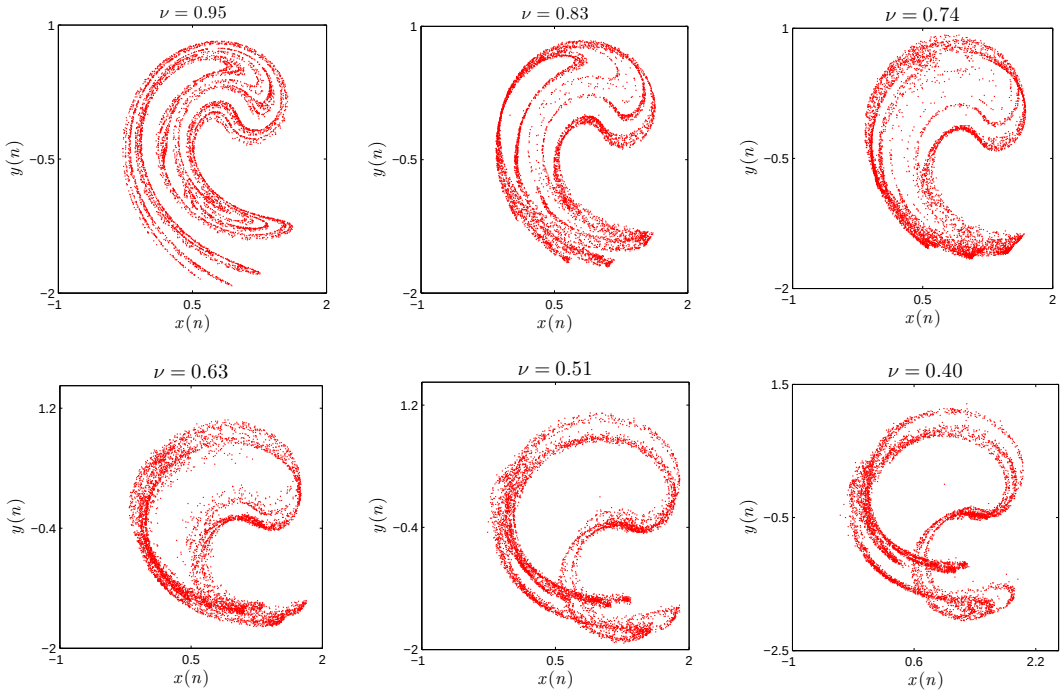

Figure 4.54: Attractors of the fractional Ikeda map for different fractional orders

Figure 4.56 shows the bifurcation diagrams of the fractional Ikeda map when $\nu = 0.95, 0.83, 0.51$ and 0.4. Form these bifurcation diagrams one can see that fractional Ikeda map is chaotic for almost all values of the fractional order ν. However, in order to gain a better explanation of the

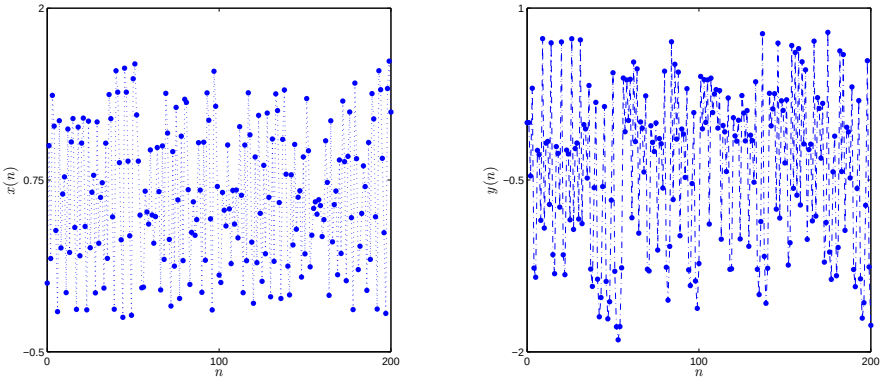

Figure 4.55: Evolution of the fractional Ikeda map states when $\nu = 0.95$

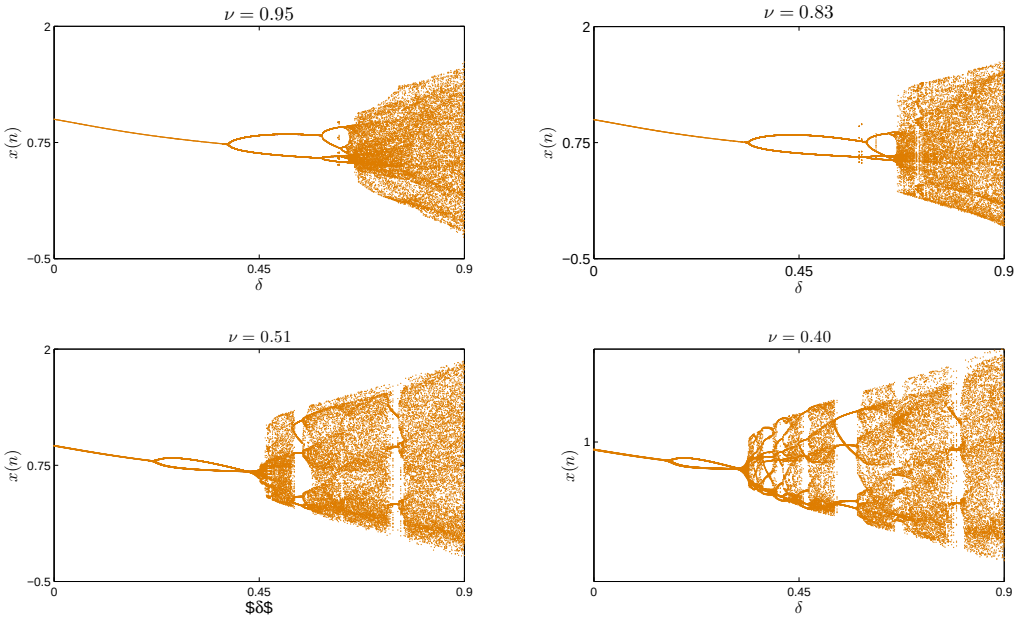

Figure 4.56: Bifurcation diagrams of the fractional Ikeda map obtained when $\nu = 0.95$, $\nu = 0.83$, $\nu = 0.51$ and $\nu = 0.4$.

dynamics of the proposed fractional Ikeda map, we use some additional tools. Figure 4.57(a) shows the largest Lyapunov exponent and Figure 4.57(b) shows the bifurcation diagram of the fractional Ikeda map when $\nu \in [0, 1]$, where the fractional order is used as the critical parameter and with the same initial conditions and parameters used previously. As expected, from the agreement between the results shown in Figure 4.57, we can see that the map remains chaotic for almost all values of the fractional order $\nu \in [0.3, 1]$. All the above results where reported in [124].

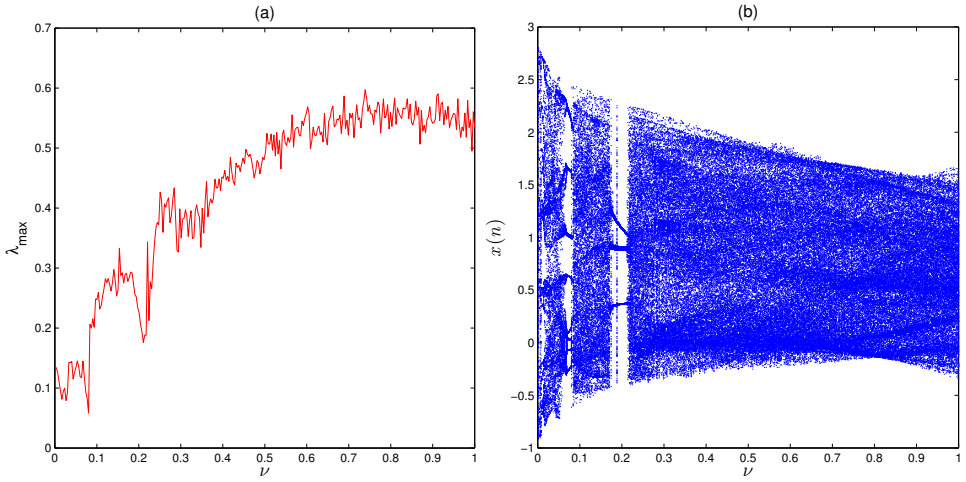

Figure 4.57: (a) Largest Lyaponov exponent and (b) bifurcation diagram of the fractional Ikeda map when $\nu \in [0, 1]$.

4.10 The fractional generalized Arnold map

In this section, we are interested in the generalized Arnold map, which is of the form

$$\begin{cases} x(n+1) = x(n) + Ay(n), \ mod\ 1, \\ y(n+1) = Bx(n) + (AB+1)y(n), \ mod\ 1, \end{cases} \tag{4.41}$$

where $x(n), y(n) \in [0, 1]$, A, B are system parameters and n represents the discrete iteration step. It is clear that when $A = B = 1$ the integer-order map (4.41) can be reduced to the classical Arnold map. A more comprehensive study of the generalized Arnold map was performed in [127]. The phase-space portraits of the map (4.41) are depicted in Figure 4.58 for three typical examples.

In the following, we aim to report the results obtained in our manuscript [129], where this map has been extended into the fractional case and the resulting system dynamic has been

investigated. Taking the Caputo-difference of (4.41) , yields

$$\begin{cases} {}^{C}\Delta_a^{\nu} x(t) = Ay(t-1+\nu),\ mod\ 1, \\ {}^{C}\Delta_a^{\nu} y(t) = Bx(t-1+\nu) + ABy(t-1+\nu),\ mod\ 1, \end{cases} \tag{4.42}$$

in which $t \in N_{a+1-\nu}$, $0 < \nu \leq 1$ is the fractional order, and a is the starting point. Following

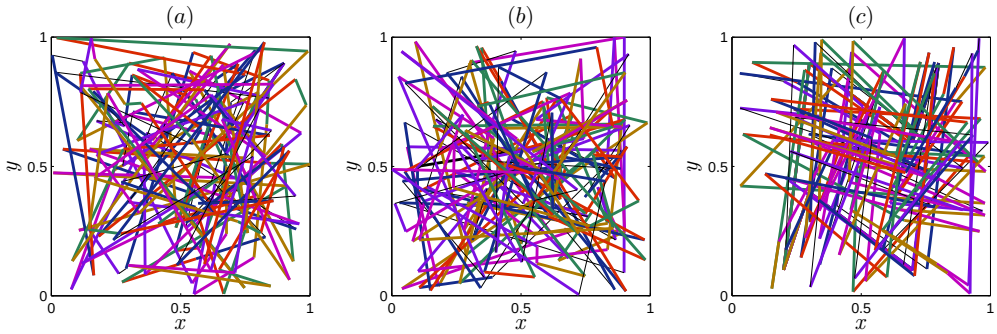

Figure 4.58: Chaotic attractors of the integer-order generalized Arnold map (4.41): (a) $(A, B) = (12, 7)$; (b) $(A, B) = (24, 9)$; (c) $A = B = 1$.

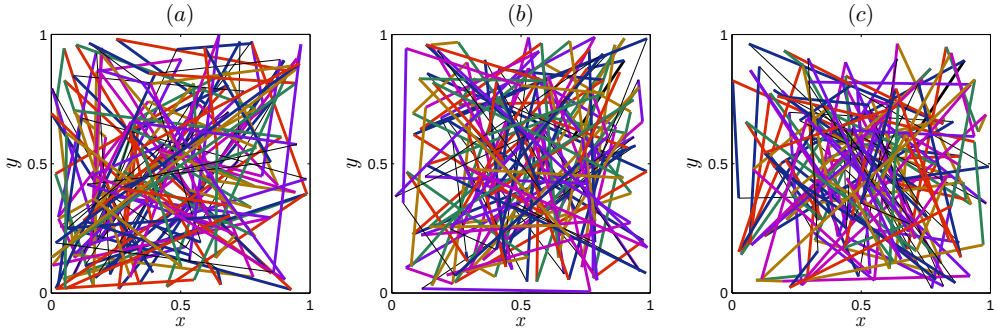

Figure 4.59: Attractors of the fractional-order generalized Arnold map (4.42) with different values of the fractional order: (a) $\nu = 0.95$; (b)$\nu = 0.73$; (c) $\nu = 0.4$.

Section 4.2, we obtain the corresponding numerical formula as

$$\begin{cases} x(n) = x(0) + \frac{1}{\Gamma(\nu)} \sum_{j=1}^{n} \frac{\Gamma(n-j+\nu)}{\Gamma(n-j+1)} (Ay(j-1)), \\ y(n) = y(0) + \frac{1}{\Gamma(\nu)} \sum_{j=1}^{n} \frac{\Gamma(n-j+\nu)}{\Gamma(n-j+1)} (Bx(j-1) + ABy(j-1)). \end{cases} \tag{4.43}$$

Using formula (4.43), we may obtain the states of the fractional generalized Arnold map (4.42) and consequently produce time series plots of the states and phase-space plots.

Dynamics of the fractional generalized Arnold map

In order to explain the dynamics of the proposed fractional generalized Arnold map (4.42), similarly, numerical analysis is considered using Matlab software. In the following, the initial condition are assigned to $[x_0, y_0] = [0.7, 0.6]$, the bifurcation parameters A, B are fixed as $A = 12$, $B = 7$ and ν is varied from 0 to 1. The phase portraits for $\nu = 0.95$, $\nu = 0.73$ and $\nu = 0.4$ are depicted in Figure 4.59. From Figure 4.59, we can observe that, for each value of the fractional order ν, the trajectories converges to bounded attractors with quite different shapes and irregular motion, that is chaotic attractors. As a next step of the investigation, the evolution of states at $\nu = 0.73$ is shown in Figure 4.60. As might be seen there is sensitive change in the initial condition which in general implies the existence of chaos.

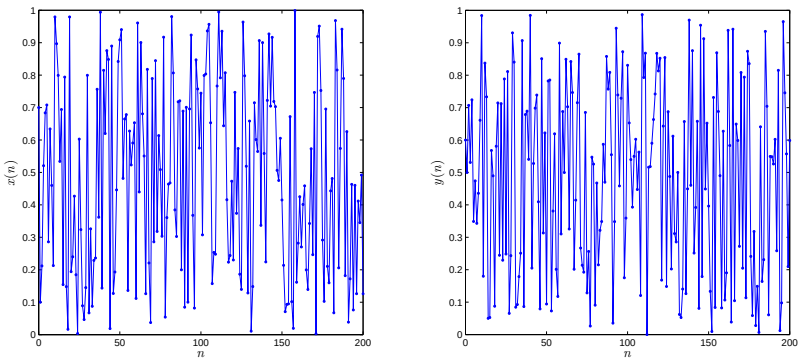

Figure 4.60: Evolution of states of the fractional-order map (4.42) for $(A, B) = (12, 7)$ and $\nu = 0.7$.

To provide more informations about the chaotic behavior of the fractional generalized Arnold map (4.42), the largest Lyapunov exponent (LLE) will be computed. In this case, the tangent map J_i is defined as

$$J_i \equiv \begin{pmatrix} a_i & b_i \\ c_i & d_i \end{pmatrix} \tag{4.44}$$

where

$a_i = a_0 + \frac{1}{\Gamma(\nu)} \sum_{j=1}^{i} \frac{\Gamma(i-j+\nu)}{\Gamma(i-j+1)} A c_{j-1},$

$b_i = b_0 + \frac{1}{\Gamma(\nu)} \sum_{j=1}^{i} \frac{\Gamma(i-j+\nu)}{\Gamma(i-j+1)} A d_{j-1},$

$c_i = c_0 + \frac{1}{\Gamma(\nu)} \sum_{j=1}^{i} \frac{\Gamma(i-j+\nu)}{\Gamma(i-j+1)} (B a_{j-1} + AB c_{j-1}),$

$d_i = d_0 + \frac{1}{\Gamma(\nu)} \sum_{j=1}^{i} \frac{\Gamma(i-j+\nu)}{\Gamma(i-j+1)} (B b_{j-1} + AB d_{j-1})$ and $(a_0, b_0, c_0, d_0) = (1, 0, 0, 1)$.

As reported in Chapter 3 the matrix J_i is independent of initial condition and it depends only on the values of the factor $\frac{\Gamma(i-j+\nu)}{\Gamma(\nu)\Gamma(i-j+1)}$. The largest Lyapunov exponents are calculated numerically

against $\nu \in [0,1]$ and plotted in Figure 4.61(a). As shown in Figure 4.61(a), the LLE remain positive for each value of ν which implies that fractional generalized Arnold map (4.42) exhibits chaotic behavior. Also, we notice that the LLE of the fractional map (4.42) are less than the LLE of the integer-order generalized Arnold map (4.41). Figure 4.61(b), 4.61(c) depict the LLE when $(A, B) = (24, 9)$ and $A = B = 1$, respectively. The similar behavior is observed and the fractional order generalized Arnold map remains to be chaotic for every positive parameters A and B.

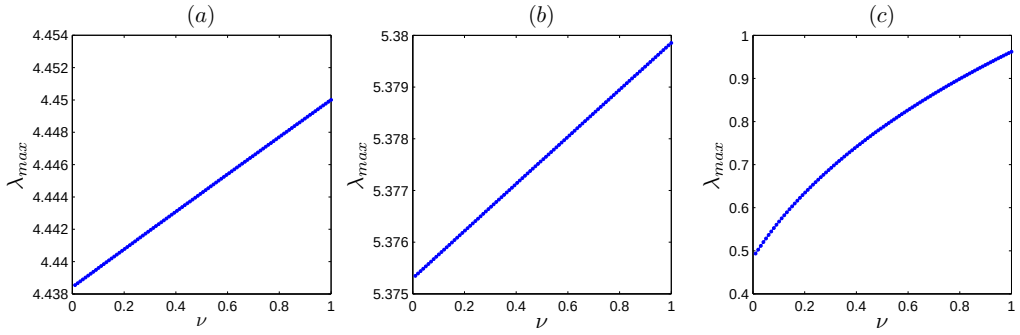

Figure 4.61: Largest lyapunov exponent in the $\lambda_{\max} - \nu$ diagrams: (a)$(A, B) = (12, 7)$; (b) $(A, B) = (24, 9)$; (c) $A = B = 1$.

4.11 The fractional-order modified Arnold map

Based on the Arnold cat map, a new two-dimensional map is proposed as

$$\begin{bmatrix} x(n+1) \\ y(n+1) \end{bmatrix} = \begin{bmatrix} A & B \\ C & D \end{bmatrix} \begin{bmatrix} x(n) \\ y(n) \end{bmatrix} + \begin{bmatrix} E \\ F \end{bmatrix}, \quad mod \quad 1, \tag{4.45}$$

in wich $A = KC + 1$, $B = K(D-1)$, $E \neq KF \neq 0$, $E \in (0,1)$ and $F \in (0,1)$. This map was developed by Wang and Ding in [128] as a modification of the original Arnold cat map. They showed by means of analytical and numerical methods that hidden chaotic attractors exist in the integer-order map (4.45) for certain values of the bifurcation parameters and $|KC + D| > 1$. The phase-space portraits of the map with no fixed point are depicted in Figure 4.62 . The fractional–order map corresponding to (4.45) may be obtained in a similar manner to the fractional map (4.3) as follow

$$\begin{cases} {}^{C}\Delta_a^{\nu} x(t) = Ax(t-1+\nu) + By(t-1+\nu) + E - x(t-1+\nu) \\ \qquad\qquad\qquad\qquad\qquad\qquad\qquad\qquad\qquad\qquad mod\ 1, \\ {}^{C}\Delta_a^{\nu} y(t) = Cx(t-1+\nu) + Dy(t-1+\nu) + F - y(t-1+\nu) \\ \qquad\qquad\qquad\qquad\qquad\qquad\qquad\qquad\qquad\qquad mod\ 1, \end{cases} \tag{4.46}$$

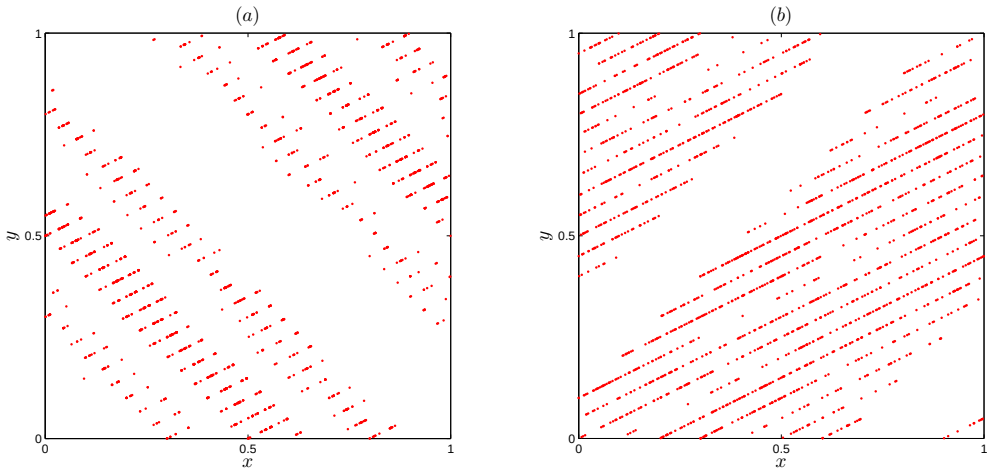

Figure 4.62: Chaotic attractors of the integer-order modified Arnold map (4.45): (a) when $A = 3$, $B = 2$, $C = 1$, $D = 2$, $E = 0.1$, $F = 0.2$; (b) when $A = 0.5$, $B = 0.2$, $C = -0.25$, $D = 2$, $E = 0.1$ and $F = 0.2$.

for $t \in \mathbb{N}_{a-\nu+1}$, where $0 < \nu \leq 1$. The corresponding numerical formulas may be given by

$$\begin{cases} x(n) = x(0) + \frac{1}{\Gamma(\nu)} \sum\limits_{j=1}^{n} \frac{\Gamma(n-j+\nu)}{\Gamma(n-j+1)} \\ \qquad\qquad (Ax(j-1) + By(j-1) + E - x(j-1)) \ \ mod\ 1, \\ y(n) = y(0) + \frac{1}{\Gamma(\nu)} \sum\limits_{j=1}^{n} \frac{\Gamma(n-j+\nu)}{\Gamma(n-j+1)} \\ \qquad\qquad (Cx(j-1) + Dy(j-1) + F - y(j-1)) \ \ mod\ 1. \end{cases} \tag{4.47}$$

This numerical formula will allow us to to analyse the dynamics of the fractional modified Arnold map (4.46) and ensure the existence of chaos.

Dynamics of the fractional Modified Arnold map

Now, phase portraits, largest lyapunov exponent and bifurcation diagram are used to study the dynamical behavior of the fractional-order modified Arnold map (4.46). When $(A, B, C, D, E, F) = (3, 2, 1, 2, 0.1, 0.2)$ and with various values of the fractional order ν, different phase portraits are plotted in Figure 4.63. As the values of ν decreases the phase portraits remains in bounded attractors and a chaotic behavior appears. The bifurcation diagram and the largest Lyapunov exponent are shown in Figure 4.64. When $\nu \in [0.1, 1]$, the fractional-order map (4.46) exhibits chaotic behavior state with positive largest Lyapunov exponent. For $\nu \in]0, 0.1[$, the largest Lyapunov exponent equals to zero, implies that the fractional-order map (4.46) is in periodic state. It worth pointing that for some fractional-order the trajectories of the generalized Arnold

map are not exactly periodic; Figure 4.65 shows that the trajectory never return the same point.

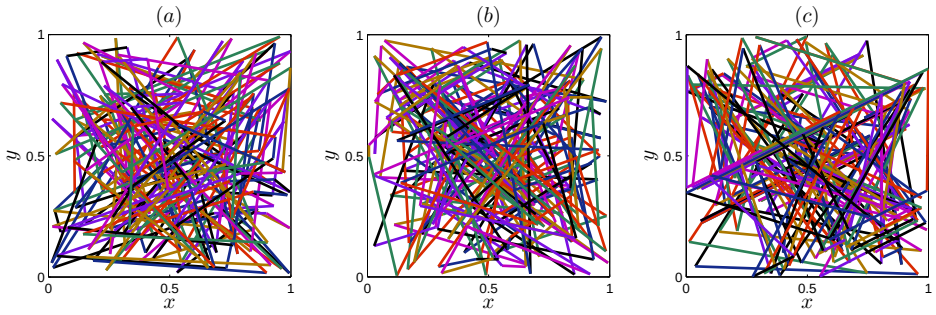

Figure 4.63: Attractors of the fractional-order modified Arnold map (4.46) for different fractional order values: (a) $\nu = 0.9$; (b) $\nu = 0.8$; (c) $\nu = 0.25$

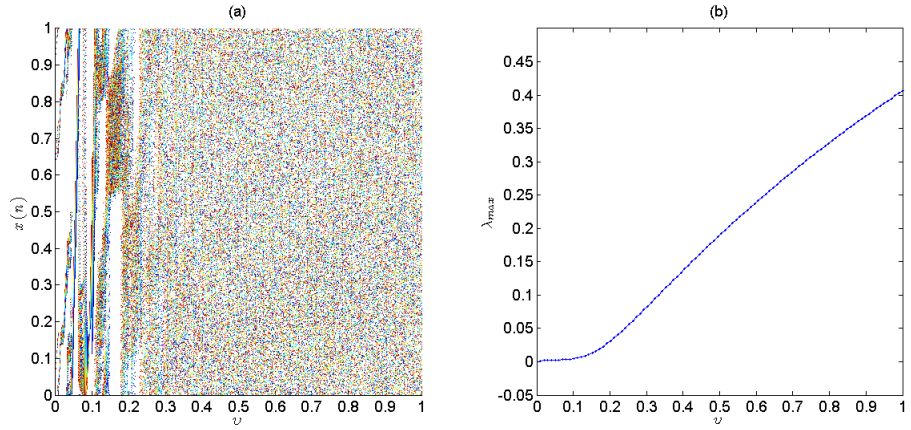

Figure 4.64: (a) Bifurcation diagram in the $x - \nu$ plane; (b) largest Lyapunov exponent versus ν.

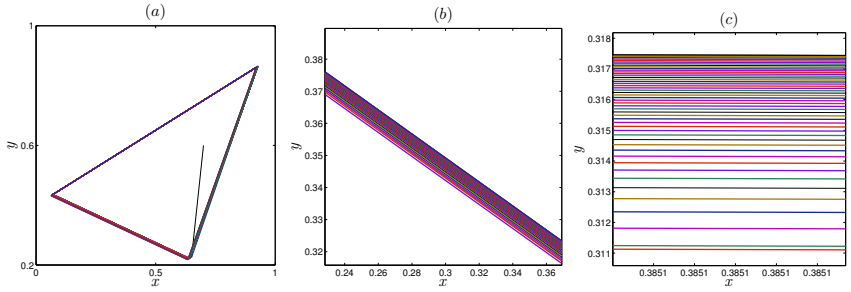

Figure 4.65: Non-chaotic attractor of the fractional-order modified Arnold map for $\nu = 0.001$ (b) and (c) zoom in on.

4.12 The fractional Rulkov map

Chaotic discrete–time systems (maps) have received considerable attention over the last two decades due to their many applications in secure communications and control. Numerous maps have been proposed throughout the years. The many proposed chaotic maps can be classified into categories according to their nonlinearities. For instance, the class of rational chaotic maps comprises of those maps where the nonlinearity is a rational function of the system's states. Rational maps have been an interesting subject due to the fact that exhibit a rich chaotic behavior as demonstrated in numerous studies. Interest in this type of maps started with one-dimensional maps such as that of [125], where the authors showed how the dynamics of a 1D rational map where more complicated than the standard logistic map. Further investigations led to the development of a number of 2D maps. Very recently, a new discrete iterative system with rational fraction has been discovered in the study of evolutionary algorithms. The two dimensional discrete Rulkov model with rational fraction [126], is described by

$$\begin{cases} x\left(n+1\right) = \frac{\mu}{1+x^2(n)} + y\left(n\right), \\ y\left(n+1\right) = y\left(n\right) - \sigma x\left(n\right) - \theta, \end{cases} \tag{4.48}$$

where $x\left(n\right)$ and $y\left(n\right)$ denote the states of the system representing the fast and slow dynamical variables, respectively, and θ and σ are positive parameters in the order 0.001. We fix the parameters σ, θ and vary μ in the interval $[0, 5]$ with a step size $\Delta\mu = 0.007$. The bifurcation diagram is shown in Figure 4.66.

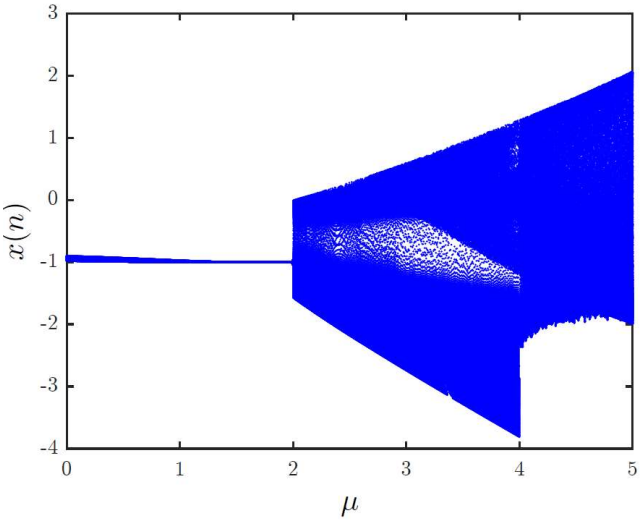

Figure 4.66: Bifurcation diagram of the standard Rulkov rational map with $\sigma = \theta = 0.001$ and $\mu \in [0, 5]$

The fractional version of system (4.48) can be given as in [131]

$$\begin{cases} {}^{C}\Delta_{a}^{\nu}x\left(t\right)=\frac{\mu}{1+x^{2}(t-1+\nu)}+y\left(t-1+\nu\right)-x\left(t-1+\nu\right), \\ {}^{C}\Delta_{a}^{\nu}y\left(t\right)=-\sigma x\left(t-1+\nu\right)-\theta, \end{cases} \tag{4.49}$$

for $t\in N_{a+1-\nu}$. The numerical formula for (4.49) can be expressed as

$$\begin{cases} x\left(n\right)=x\left(0\right)+\frac{1}{\Gamma(\nu)}\sum_{j=1}^{n}\frac{\Gamma(n-j+\nu)}{\Gamma(n-j+1)}\left(\frac{\mu}{1+x^{2}(j-1)}+y\left(j-1\right)-x\left(j-1\right)\right), \\ y\left(n\right)=y\left(0\right)+\frac{1}{\Gamma(\nu)}\sum_{j=1}^{n}\frac{\Gamma(n-j+\nu)}{\Gamma(n-j+1)}\left(-\sigma x\left(j-1\right)-\theta\right), \end{cases} \tag{4.50}$$

Considering the parameter values $\mu=4.3$ and $\sigma=\theta=0.001$, the phase portrait is depicted in Figure 4.67 for $\nu=1$ and $\left[x\left(0\right),y\left(0\right)\right]=\left[0.1,0.2\right]$. In this case, the map is identical to the classical Rulkov model (4.48). Figure 4.68 shows the bifurcation diagram with μ as the critical parameter and $\nu=0.85$. We observe that chaos exists in the fractional map and that the factional order has an effect on the system dynamics. The chaotic nature of the states is apparent.

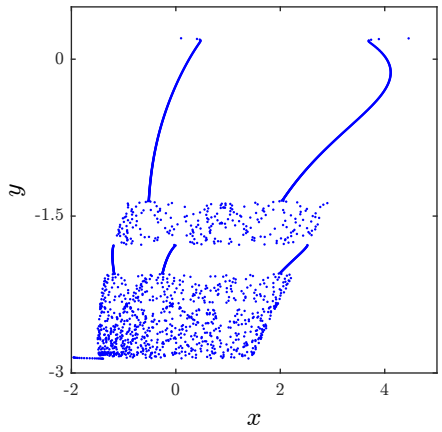

Figure 4.67: Phase space of the fractional Rulkov map for $\nu=1$

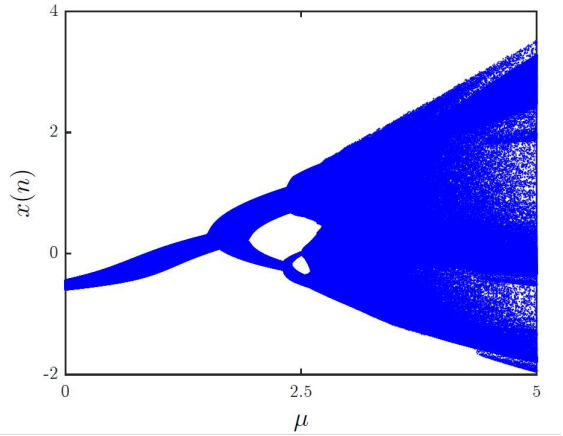

Figure 4.68: Bifurcation diagram of the fractional Rulkov map for $\nu=0.85$

4.13 The fractional Chang *et al.* map

In this section, we consider another rational discrete map that was proposed in [132]. The Chang *et al.* map is given by

$$\begin{cases} x\left(n+1\right)=\frac{1}{x^{2}(n)+0.1}-py\left(n\right), \\ y\left(n+1\right)=\frac{1}{y^{2}(n)+0.1}+qx\left(n\right), \end{cases} \tag{4.51}$$

where $p,q\in\left[0,0.99\right]$ and $x\left(n\right),y\left(n\right)\in\left[-1000,1000\right]$. Numerical analysis showed that for $p=0.99$ and $q=0.9$, the map is chaotic. The bifurcation diagram and phase portraits are

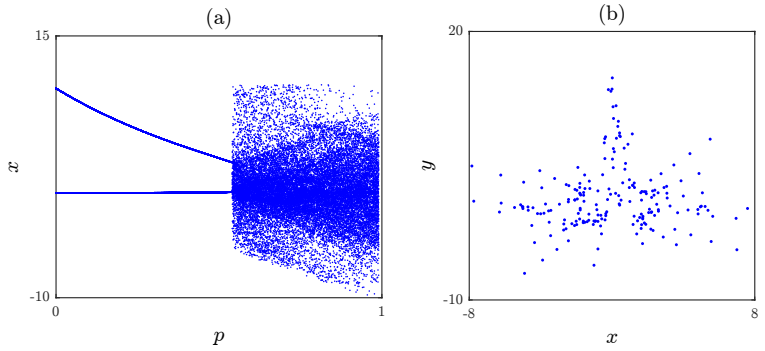

Figure 4.69: (a) Bifurcation diagram with the critical parameter p being varied from 0 to 0.99. (b) Phase portrait for the Chang *et al.* map with parameter values $p = 0.99$ and $q = 0.9$

shown in Figure 4.69. Using the Caputo–like fractional difference, we can formulate the fractional Chang *et al.* map as follows

$$\begin{cases} {}^{C}\Delta_{a}^{\nu} x\left(t\right) = \frac{1}{x^{2}(t-1+\nu)+0.1} - py\left(t-1+\nu\right) - x\left(t-1+\nu\right), \\ {}^{C}\Delta_{a}^{\nu} y\left(t\right) = \frac{1}{y^{2}(t-1+\nu)+0.1} + qx\left(t-1+\nu\right) - y\left(t-1+\nu\right), \end{cases} \tag{4.52}$$

where $t \in N_{a+1-\nu}$ and $0 < \nu \leq 1$. In view of Theorem 1, the discrete solution of the fractional order map (4.52), for $a = 0$, can be obtained as

$$\begin{cases} x\left(n\right) = x\left(0\right) + \frac{1}{\Gamma(\nu)} \sum_{j=1}^{n} \frac{\Gamma(n-j+\nu)}{\Gamma(n-j+1)} \left(\frac{1}{x^{2}(j-1)+0.1} - py\left(j-1\right) - x\left(j-1\right) \right), \\ y\left(n\right) = y\left(0\right) + \frac{1}{\Gamma(\nu)} \sum_{j=1}^{n} \frac{\Gamma(n-j+\upsilon)}{\Gamma(n-j+1)} \left(\frac{1}{y^{2}(j-1)+0.1} + qx\left(j-1\right) - y\left(j-1\right) \right). \end{cases} \tag{4.53}$$

In what follows, we choose to fix $p = 0.99$ and $q = 0.9$ and set the initial conditions to $\left[x\left(0\right), y\left(0\right)\right] = \left[1, 1\right]$. By implementing numerical formula (4.53) as a Matlab script, we have examined the general behavior of the fractional Chang *et al.* map (4.52) in terms of its dependence on the fractional order ν. First, the phase space is shown in Figure 4.70. It provides a general idea about the nonlinearity of the solution. It can be noticed that as we vary the fractional order ν, the attractor changes its shape. Such changes confirm that the fractional order has an effect on the dynamics of the solution. To investigate the chaotic behavior further, the bifurcation diagram is considered. We varied the parameter p in steps of $\Delta p = 0.001$ over the interval $[0, 0.99]$. For $\nu = 0.95, 0.85, 0.7, 0.64$ the bifurcation diagrams are shown in Figure 4.71. This confirms the existence of chaos. In addition, as the fractional order drops below 0.613, chaos disappears completely.

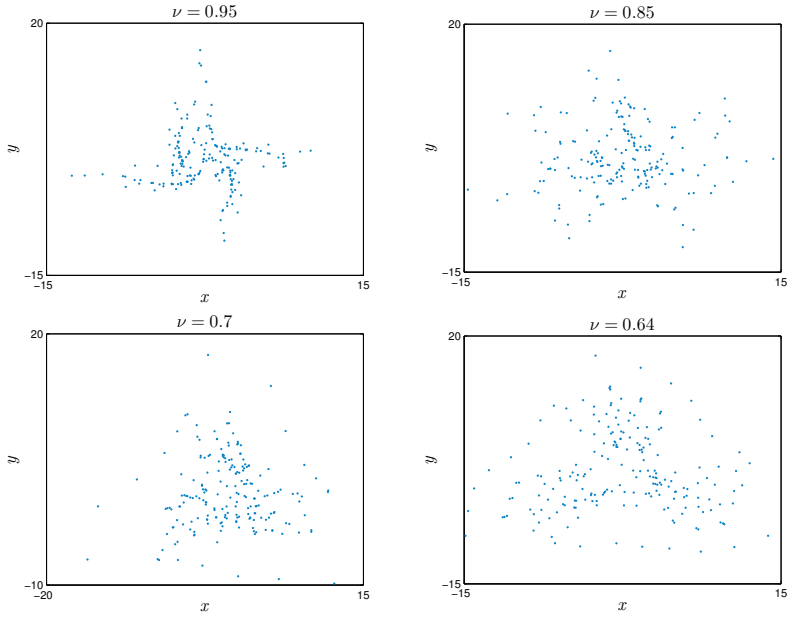

Figure 4.70: Attractors of the fractional Chang *et al.* map for different fractional orders

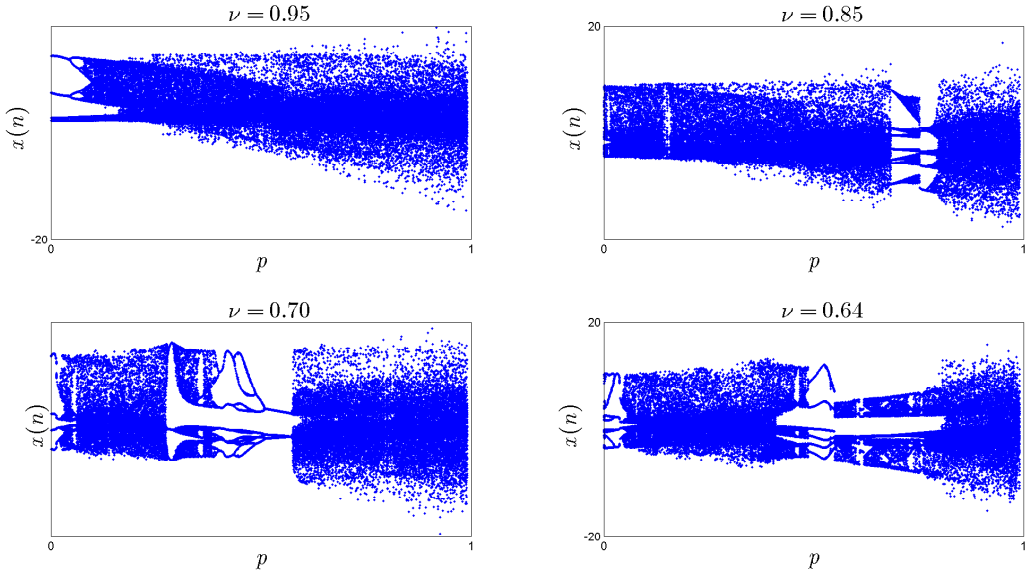

Figure 4.71: Bifurcation diagrams obtained with different fractional orders

4.14 The fractional Zeraoulia–Sprott rational map

Another interesting fractional 2D chaotic map that can be found in the literature is that of Zeraoulia and Sprott [133], which is of the the form

$$\begin{cases} x\left(n+1\right) = \frac{-\alpha x(n)}{1+y^2(n)}, \\ y\left(n+1\right) = x\left(n\right) + \beta y\left(n\right), \end{cases} \tag{4.54}$$

where α and β are bifurcation parameters. This map is more dynamically rich than the previous two maps as it produces several chaotic attractors obtained via the quasi periodic route to chaos. Considering parameter values $\alpha = 3.7$ and $\beta = 0.6$, the resulting chaotic attractor is depicted in Figure 4.72.

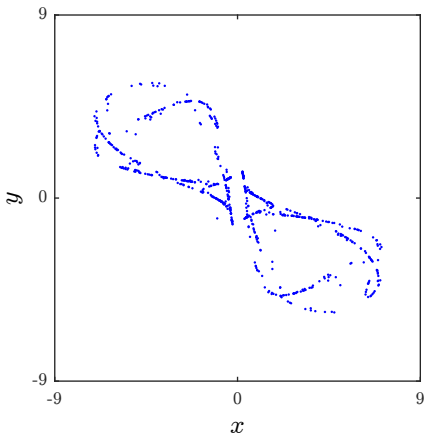

Figure 4.72: Phase portraits of the standard Zeraoulia–Sprott rational map with $\alpha = 3.7$ and $\beta = 0.6$.

The fractional version of this map can be described for $t \in N_{a+1-\nu}$ as

$$\begin{cases} {}^{C}\Delta_{a}^{\nu} x\left(t\right) = \frac{-\alpha x(t-1+\nu)}{1+y^{2}(t-1+\nu)} - x\left(t-1+\nu\right), \\ {}^{C}\Delta_{a}^{\nu} y\left(t\right) = x\left(t-1+\nu\right) + \left(\beta-1\right) y\left(t-1+\nu\right), \end{cases} \tag{4.55}$$

with the corresponding numerical formula

$$\begin{cases} x\left(n\right) = x\left(0\right) + \frac{1}{\Gamma(\nu)} \sum_{j=1}^{n} \frac{\Gamma(n-j+\nu)}{\Gamma(n-j+1)} \left(\frac{-\alpha x(j-1)}{1+y^{2}(j-1)} - x\left(j-1\right) \right), \\ y\left(n\right) = y\left(0\right) + \frac{1}{\Gamma(\nu)} \sum_{j=1}^{n} \frac{\Gamma(n-j+\nu)}{\Gamma(n-j+1)} \left(x\left(j-1\right) + \left(\beta-1\right) y\left(j-1\right) \right). \end{cases} \tag{4.56}$$

In order to assess the dynamics of this fractional map, we use numerical results. We consider the initial conditions $\left(x\left(0\right), y\left(0\right)\right) = \left(-1, -1\right)$ and vary the fractional order ν. Figures 4.73 and 4.74 summarize the results. The phase portraits of the fractional map (4.55) for $\nu = 0.98, 0.95, 0.93, 0.92$ are displayed in Figure 4.73 with $\alpha = 3.7$ and $\beta = 0.6$. Given the same value for β and with $\alpha \in [-1, 4]$, Figure 4.74 depicts the bifurcation diagrams for the four values of the fractional order ν. It is noticed that system (4.55) exhibits a chaotic behavior when $0.93 \leq \nu \leq 1$. As ν takes a value less than 0.93, chaos starts to disappear. We note that when $0.8 \leq \nu \leq 0.88$, the map converges to a quasi periodic orbit as demonstrated by Figure 4.75.

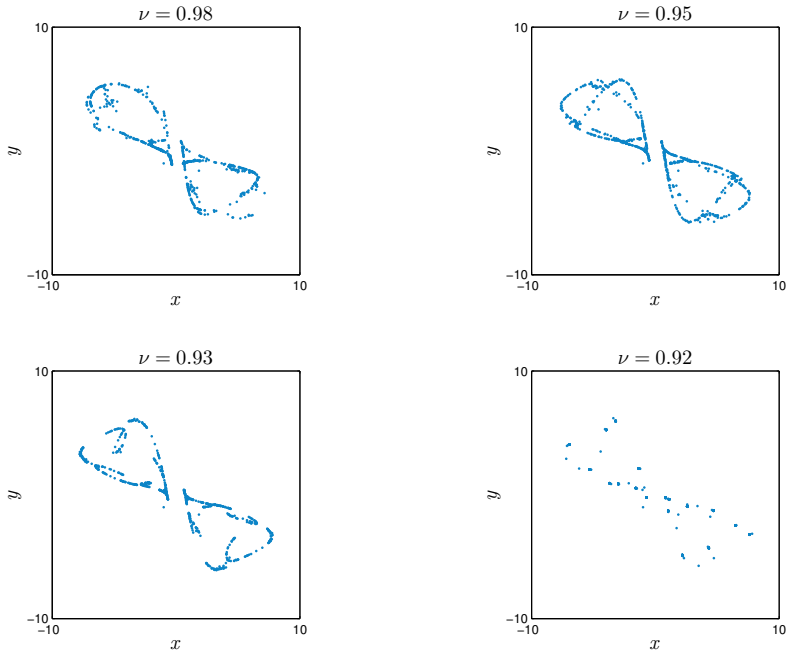

Figure 4.73: Phase space attarctors of the fractional Zeraoulia–Sprott rational map for different fractional orders

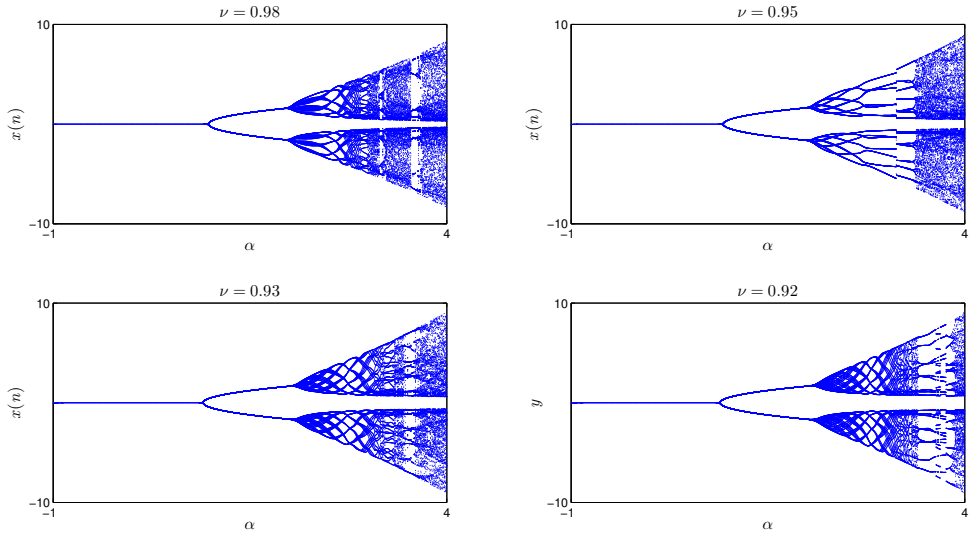

Figure 4.74: Bifurcation diagrams of the fractional Zeraoulia–Sprott rational map for different fractional orders

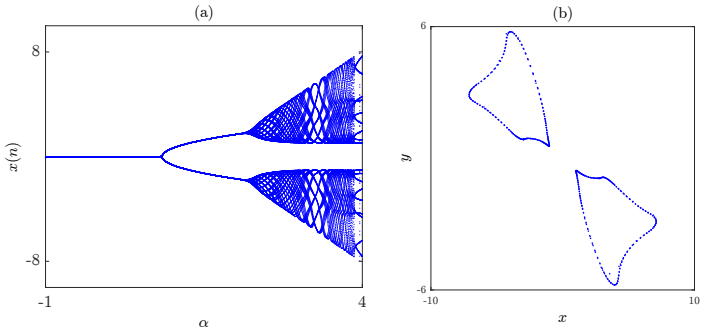

Figure 4.75: Bifurcation diagram of the fractional Zeraoulia–Sprott map (left) and the attractor of the map's Quasi periodic orbit for $\nu = 0.88$ (right)

4.15 The fractional–order Lorenz chaotic map

The discretization of the well known continuous–time Lorenz chaotic system was proposed in [7] and is of the form

$$\begin{cases} x(n+1) = (1+\gamma\delta)\, x(n) - \delta y(n)\, x(n), \\ y(n+1) = (1-\delta)\, y(n) + \delta x^2(n), \end{cases} \tag{4.57}$$

where γ and δ are some parameters that determine the general behavior and dynamics of the system. This system has a chaotic attractor, for instance, when $\gamma = 1.25$ and $\delta = 0.75$. Following the same steps as in Section 4.2 above, we can formulate the fractional Lorenz map as

$$\begin{cases} {}^{C}\Delta_a^{\nu} x(t) = \gamma\delta x(t-1+\nu) - \delta y(t-1+\nu)\, x(t-1+\nu), \\ {}^{C}\Delta_a^{\nu} y(t) = \delta\left(-y(t-1+\nu) + x^2(t-1+\nu)\right), \end{cases} \tag{4.58}$$

for $t \in N_{a-\nu+1}$ and $0 < \nu \leq 1$. The frctional Lorenz map (4.58) is symetrical about the x-axis since it remains unchanged whent the transformation $(-x, y) \to (x, y)$ is applied. Therefore,

The numerical formula of fractional discrete–time systen (4.58) can be given by

$$\begin{cases} x(n) = x(a) + \frac{1}{\Gamma(\nu)} \sum_{j=1}^{n} \frac{\Gamma(n-j+\nu)}{\Gamma(n-j+1)} \\ \qquad\qquad \left(\gamma\delta x(j-1) - \delta y(j-1)\, x(j-1)\right), \\ y(n) = y(a) + \frac{1}{\Gamma(\nu)} \sum_{j=1}^{n} \frac{\Gamma(n-j+\nu)}{\Gamma(n-j+1)} \left(\delta(-y(j-1) + x^2(j-1)\right). \end{cases} \tag{4.59}$$

Given the parameters $(\gamma, \delta) = (1.25, 0.75)$, $\nu = 1$, $a = 0$, and initial conditions $(x(0), y(0)) = (0.1, 0)$, the fractional Lorenz map (4.58) reduces to the standard integer Lorenz map. The solutions approach the strange attractor depicted in Figure 4.76(b). Figure 4.77 shows the trajectories obtained with 9000 points given the same parameters and initial conditions chosen previously and with the fractional order $\nu \in \{0.98, 0.838, 0.837, 0.833, 0.83\}$. In all six cases, solutions are plotted in the $x - y$ plane. We observe that a slight change in the fractional order ν leads to transition from a strange attractor to two invariant circles and then to a seven periodic orbit. These changes denote that the strange attractor is destroyed as ν decreases.

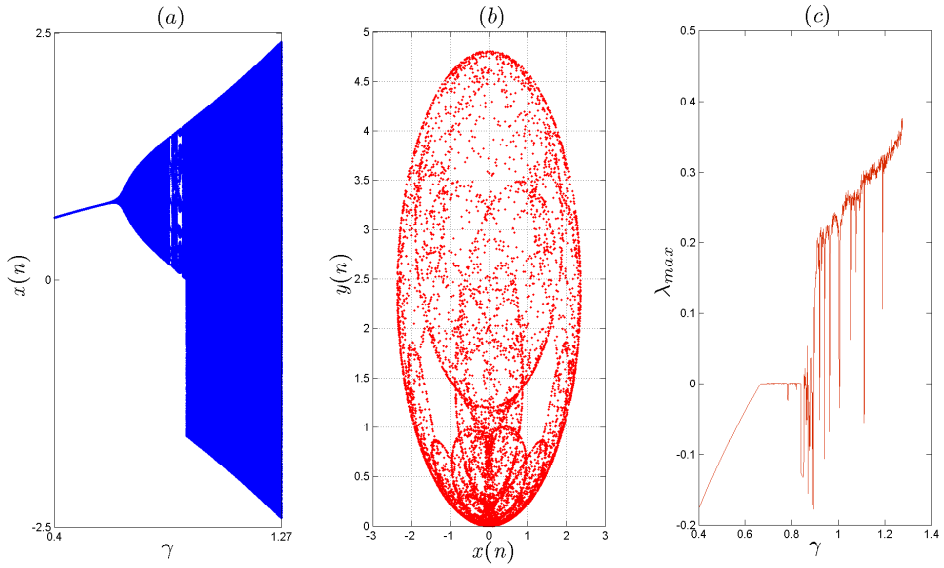

Figure 4.76: (a) Bifurcation diagram of the standard Lorenz map with $(x(0), y(0)) = (0.1, 0)$ and $(\gamma, \delta) = (1.25, 0.75)$ and (b) the solutions in the $x - y$ plane.

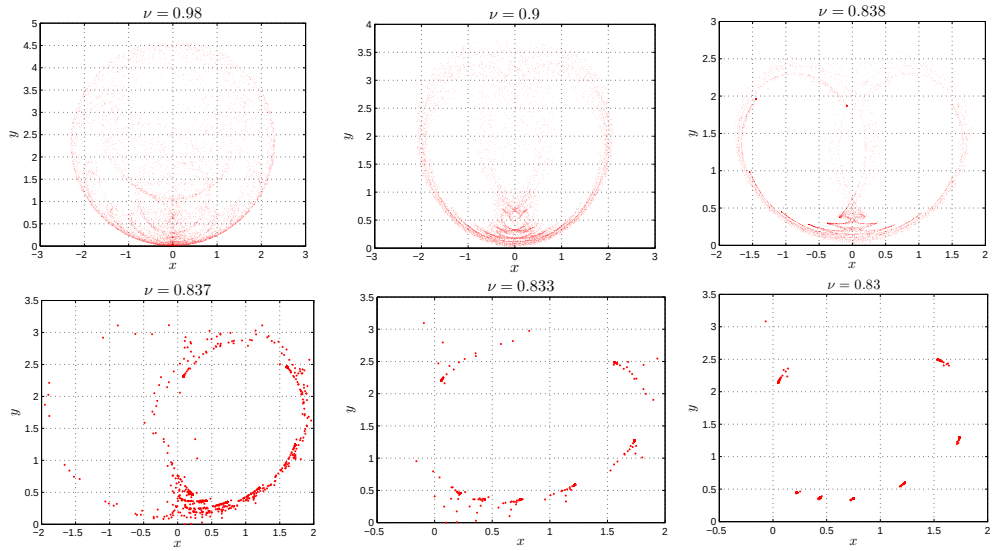

Figure 4.77: Trajectories generated by the fractional Lorenz map after being run for 9000 points with $(x(0), y(0)) = (0.1, 0)$, $(\gamma, \delta) = (1.25, 0.75)$ and different fractional orders ν.

In order to study the effect of the fractional order on the dynamics of the chaotic system, we observe its bifurcation analysis. For accurate and stable outputs, we calculate the bifurcation for 2000 points. The initiale states are again fixed at $(x(0), y(0)) = (0.1, 0)$ and parameter $\delta = 0.75$. Figure 4.78 shows the bifurcation graphs obtained with γ as the critical parameter and different fractional orders. The step size adopted in the variation of γ to produce this graph was set to $\gamma = 0.001$. As ν decreases, the bifurcation diagram changes. Particularly, for $\nu = 0.98$, the fractional map converges to a fixed point over the approximate interval $\gamma \in [0.4, 0.6429]$. For, $\gamma \in [0.92, 1.27]$, the trajectories converge to a chaotic attractor. However, for $\nu = 0.9$, the fixed point convergence and chaotic attractor intervals expand to $\gamma \in [0.4, 0.7726]$ and $\gamma \in [1.1, 1.27]$, respectively. Finally, for $\nu = 0.83$, we see a fixed point convergence for γ between 0.4 and 0.8886 and a small chaotic interval approximately when $\gamma \in [1.255, 1.27]$. Comparing these results to the bifurcation diagram obtained for $\nu = 1$ as shown in Figure 4.77(a), we conclude that that the bifurcation diagrams of the fractional map are stretched along the γ axis.

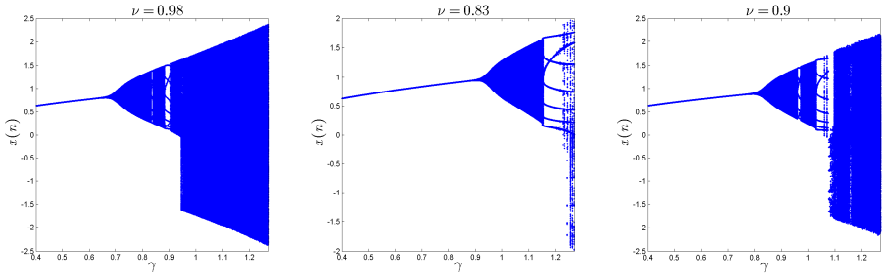

Figure 4.78: Bifurcation diagrams of the fractional Lorenz map with $(x(0), y(0)) = (0.1, 0)$ and $\delta = 0.75$ for fractional orders $\nu = 0.98$, $\nu = 0.9$, and $\upsilon = 0.83$.

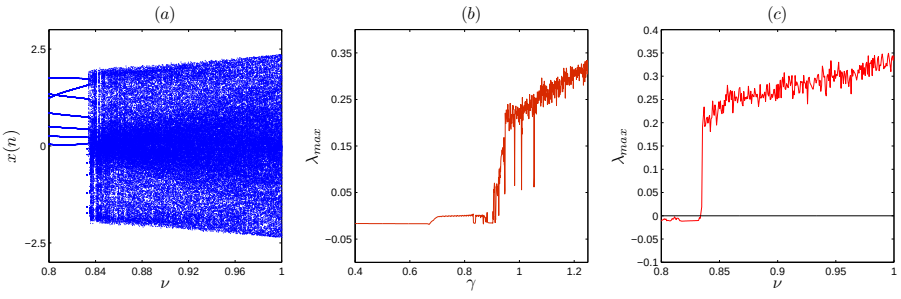

Figure 4.79: (a) Bifurcation of the fractional lorenz map with $(x(0), y(0)) = (0.1, 0)$, $(\gamma, \delta) = (1.25, 0.75)$, and ν as the critical parameter; (b) Largest Lyaponov exponent with fractional order ν as the bifurcation parameter; (c) Largest Lyapunov exponent with γ as the bifurcation parameter and $\nu = 0.98$.

4.16 The fractional–order Flow chaotic map

We move now to study a generalized flow map model and is described by

$$\begin{cases} {}^{c}\Delta_{a}^{\nu}x\left(t\right)=y\left(t+\nu-1\right)+\left(\theta-1\right)x\left(t+\nu-1\right), \\ {}^{c}\Delta_{a}^{\nu}y\left(t\right)=\lambda+x^{2}\left(t+\nu-1\right)-y\left(t+\nu-1\right),\ t\in N_{a-\nu+1}, \end{cases} \tag{4.60}$$

where x and y stand for state variables of the fractional flow map, θ and λ are the system's parameters, and Δ_{a}^{ν} is the Caputo-like difference operator of fractional-order where $\nu\in]0,1]$. The numerical formula corresponding to (4.60) is given by

$$\begin{cases} x\left(n\right)=x\left(0\right)+\frac{1}{\Gamma(\nu)}\sum_{j=1}^{n}\frac{\Gamma(\nu-j+\nu)}{\Gamma(\nu-j+1)}\left(y\left(j-1\right)+\left(\theta-1\right)x\left(j-1\right)\right), \\ y\left(n\right)=y\left(0\right)+\frac{1}{\Gamma(\nu)}\sum_{j=1}^{n}\frac{\Gamma(\nu-j+\nu)}{\Gamma(\nu-j+1)}\left(\lambda+x^{2}\left(j-1\right)-y\left(j-1\right)\right), \end{cases} \tag{4.61}$$

for $0<\nu\leq1$.

With the same parameter values defined above and with $\left[x\left(0\right),y\left(0\right)\right]=\left[0,1\right]$, when the fractional flow map is run for 9000 points, it generates the trajectories depicted in Figure 4.81 for $\nu=0.98$ and $\nu=0.973$ in the x-y plane. Clearly, map converges to a bounded attractor. Similar to the previous fractional order maps, when the fractional order ν decreases below the threshold 0.973, the trajectories diverge to infinity. Keeping $\lambda=-1.7$, $\nu=0.98$, and $\left[x\left(0\right),y\left(0\right)\right]=\left[0,1\right]$ and varying θ in the interval $[-0.1,0.1]$ in steps of $\Delta\theta=0.001$ yields the bifurcation diagram depicted in Figure 4.82, which shows that the fractional flow map is chaotic in the interval $[-0.1,0.1]$. This agrees completely with the largest Lyapunov exponent in Figure 4.82 (b).

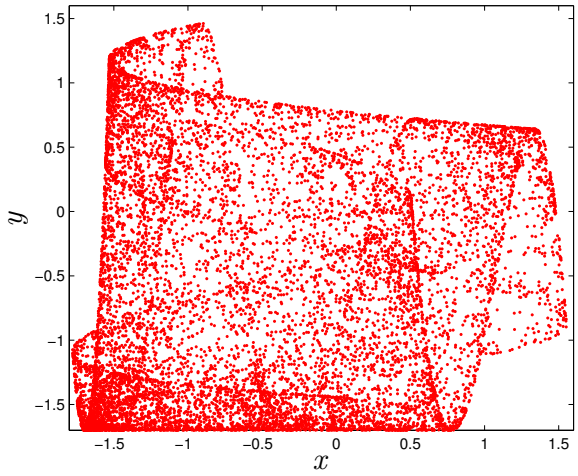

Figure 4.80: The trajectories generated by the standard discrete Flow map with $\theta=-0.1$, $\lambda=-1.7$, and $(x(0),y(0))=(0,1)$.

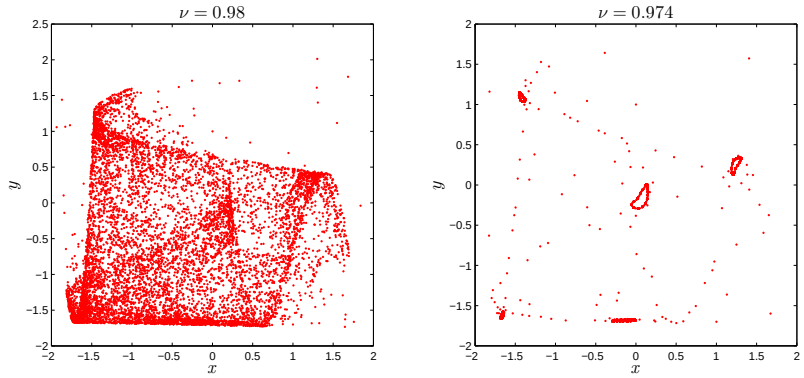

Figure 4.81: Trajectories of the fractional flow map with $\theta = -0.1$, $\lambda = -1.7$, $(x(0), y(0)) = (0, 1)$, and fractional orders $\nu = 0.98$ and $\nu = 0.973$.

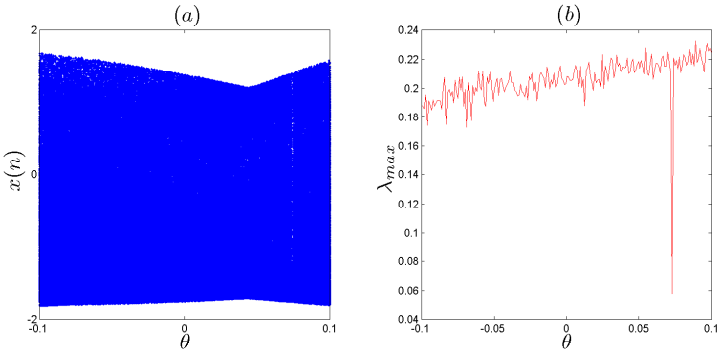

Figure 4.82: Bifurcation diagrams of the fractional flow map with $\lambda = -1.7$, $(x(0), y(0)) = (0, 1)$, and fractional orders $\nu = 0.98$ and $\nu = 0.973$; (b) The corresponding largest Lyapunov exponent.

4.17 Conclusion

In this chapter we have proposed different two dimensional fractional order discrete-time systems corresponding to standard well known maps reported in the literature. The existence of chaos in the proposed maps and the general dynamics are examined experimentally by means of phase portraits, bifurcation diagrams, Lyapunov exponents, 0-1 test, C_0-complexity and approximate entropy. Compared with its integer-order counterpart, the fractional order maps shows different dynamics. The bifurcations and chaos in this system were investigated by varying the system parameters and the fractional-order value ν. It is shown that the fractional order maps has a considerable impact on its dynamics and the range of parameter values over which chaos is observed. Therefore, the fractional order ν is considered as another bifurcation parameter except

for the system parameters.

Several typical bifurcations are observed such as border-collision bifurcation scenario for the fractional unified map and the double scroll map, and period doubling route to chaos for the fractional Hénon-Lozi map and the Sine-Sine map, and cascade of bifurcation for the fractional Lozi map. Moreover, the fractional Hénon-Lozi map, Duffing map, and the Sine-Sine map possesses the interesting property of being characterized by the coexistence of various kinds of chaotic attractors, for various fractional-order values and initial conditions. The coexistence bifurcations and coexisting attractors have been investigated using bifurcation diagrams, phase portraits and 0-1 test. Thus such fractional maps are potential useful in the engineering field. Compared with the integer order maps, the fractional maps has more complexity when fractional order values is smaller. That is the corresponding two-dimensional integer-order maps, i.e, Hénon-Lozi map, Duffing map, and the Sine-Sine map do not have the property of coexisting attractors, while fractional map have it. Meanwhile, the transient state were observed under some specific parameters for the Lozi and the Hénon-Lozi maps. Due to the rich complex dynamical behaviour, the proposed fractional maps are suitable fore secure communication image encryption, just to name few. The $ApEn$ and C_0 complexity algorithms provide a parameter choice criteria for practice applications of fractional-order chaotic discrete-time systems.

Chapter 5

Three Dimensional Fractional Order Discrete-Time Systems

5.1 Introduction

Very recently, study on the chaotic behaviour of three-dimensional (3D) discrete-time systems has considered as one of the most interesting topic in nonlinear dynamical systems. Namely, 3D discrete systems show a higher degree of complexity (with respect to 1D or 2D systems), which can improve their applicability in image encryption and pseudo-random number generation. We have seen in the previous chapter that, compared to classic discrete maps, fractional maps could provide more degree of freedom and own better ability to reflect the evolution of practical problem. Consequently, in this chapter, we introduce new different three dimensional fractional maps, for which a detailed analysis of their dynamics is analyzed via Lyapunov exponents, bifurcation diagrams, 0-1 test approximate entropy and 0-1 test. Chaos does exist for these systems for different range of fractional orders. As a consequence, a number of chaotic attractors appear in the system dynamics, indicating that the behaviour of the maps becomes unpredictable. Futhermore, a novel fractional-order triopoly game is presented and investigated, where three firms producing differentiated products compete over a common market. The proposed game theory model, is characterized by eight equilibria, including the Nash fixed point.

5.2 The fractional–order Stefanski map

In [5], Stefanski introduced a generalization of the standard Hénon map into 3–dimensional space. The system is of the form

$$\begin{cases} x(n+1) = 1 + z(n) - \alpha y^2(n), \\ y(n+1) = 1 + \beta y(n) - \alpha x^2(n), \\ z(n+1) = \beta x(n), \end{cases} \tag{5.1}$$

where $x(n)$, $y(n)$, and $z(n)$ are the states, $\alpha > 0$, and $0 < \beta < 1$. The system has been studied extensively in the literature and is known to exhibit a hyperchaotic behavior for the bifurcation

parameters $\beta = 0.2$, and $\alpha \in [1.22, 1.40]$. The resulting attractor for $\alpha = 1.4$ and $\beta = 0.2$ is depicted in Figure 5.1.

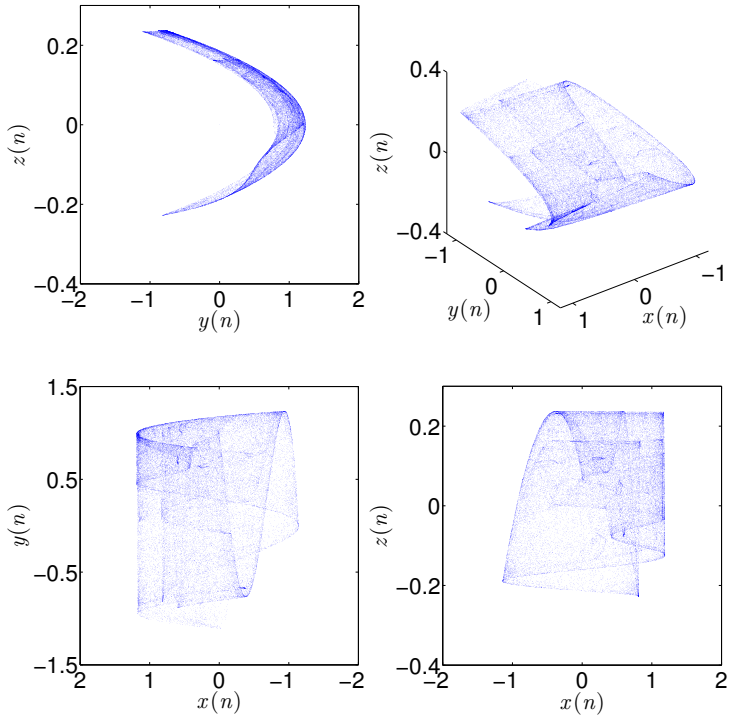

Figure 5.1: Phase portraits of the classical Stefanski attractor.

Using the fractional discrete calculus notation in Chapter 1, we can write the ν–Caputo formula of discrete integer order system (5.1) for time $t \in \mathbb{N}_{a+1-\nu}$ and fractional order $0 < \nu \leq 1$ as

$$\begin{cases} {}^{C}\Delta_{a}^{\nu} x\left(t\right) = 1 + z\left(t-1+\nu\right) - \alpha y^{2}\left(t-1+\nu\right) - x\left(t-1+\nu\right), \\ {}^{C}\Delta_{a}^{\nu} y\left(t\right) = 1 + \left(\beta - 1\right) y\left(t-1+\nu\right) - \alpha x^{2}\left(t-1+\nu\right), \\ {}^{C}\Delta_{a}^{\nu} z\left(t\right) = \beta x\left(t-1+\nu\right) - z\left(t-1+\nu\right). \end{cases} \tag{5.2}$$

We will call system (5.2) the fractional–order Stefanski map. Before we go ahead and present some important dynamics, let us first present a discrete numerical formula .

Suppose that $a = 0$, using Theorem 1.15, the numerical formulas for (5.2), yield

$$\begin{cases} x\left(n\right) = x\left(0\right) + \frac{1}{\Gamma(\nu)} \sum_{j=1}^{n} \frac{\Gamma(n-j+\nu)}{\Gamma(n-j+1)} \left(1 + z\left(j-1\right) - \alpha y^{2}\left(j-1\right) - x\left(j-1\right)\right), \\ y\left(n\right) = y\left(0\right) + \frac{1}{\Gamma(\nu)} \sum_{j=1}^{n} \frac{\Gamma(n-j+\nu)}{\Gamma(n-j+1)} \left(1 + \left(\beta - 1\right) y\left(j-1\right) - \alpha x\left(j-1\right)\right), \\ z\left(n\right) = z\left(0\right) + \frac{1}{\Gamma(\nu)} \sum_{j=1}^{n} \frac{\Gamma(n-j+\nu)}{\Gamma(n-j+1)} \left(\beta x\left(j-1\right) - z\left(j-1\right)\right), \end{cases} \tag{5.3}$$

where $x\left(0\right)$, $y\left(0\right)$, and $z\left(0\right)$ are the initial conditions.

Dynamical analysis of the fractional Stefanski map

Let $a = 0$ and $x(0) = y(0) = z(0) = 0$. The phase portraits are displayed in Figures 5.2 and 5.3 for different fractional orders. For the numerical simulation, we choose the step size $\Delta\alpha = 0.001$. The bifurcation diagrams are plotted in Figure 5.4 for different values of fractional order ν. When $\nu = 0.97$, the bifurcation diagrams show a period doubling cascade route to chaos in the area $\alpha \in [1.1, 1.4]$. As the value of ν decreases, the bifurcation diagram of the fractional Stefanski map (5.2) expands along α axis and gradually shift to the left. In addition

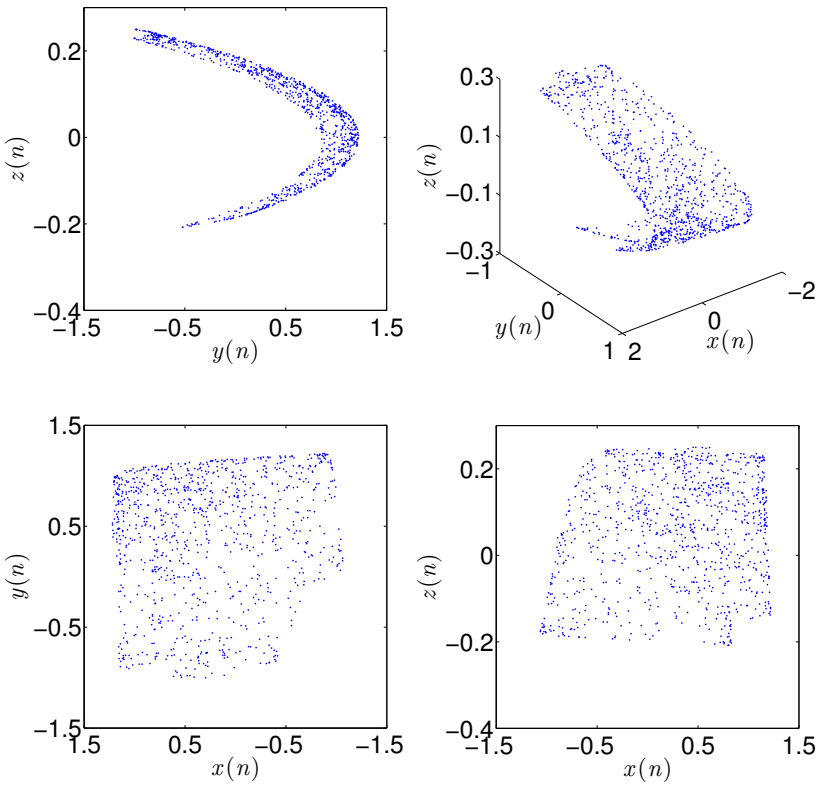

Figure 5.2: Phase portraits of the fractional–order Stefanski map with $\nu = 0.97$.

to visualizing the effect of parameter α on the dynamics of the map, we have seen that the value of the fractional order ν has an impact on the dynamics. This has been further investigated by plotting the bifurcation of the fractional Stefanski map (5.2) taking ν as the critical parameter. The resulting bifurcation diagram when $(\alpha, \beta) = (1.4, 0.2)$ and $[x(0), y(0) z(0)] = [0, 0, 0]$ is depicted in Figure 5.5. We see that chaos is apparent for the interval $\nu \in [0.915, 1]$. As soon as ν drops below 0.915 the states diverge towards infinity.

Although bifurcation plots clearly indicate the existence of chaos in the fractional map, it is usually more convenient to calculate or estimate the map's Lyapunov exponents. A common method to estimate Lyapunov exponents for standard maps is by means of a QR decomposition

of the time–varying Jacobian matrix. For fractional maps, the Jacobian matrix is subject to the same discrete memory effect as the map's states and thus can be calculated in a similar manner, see (Chapter 3, section 3.5.2). Figure 5.6 shows the estimated Lyapunov exponents for different values of the fractional order ν. We see that the results agree with those of the bifurcation in the sense that lowering ν below 1 yields lower exponents to the point where they become negative, which coincides with a stable system.

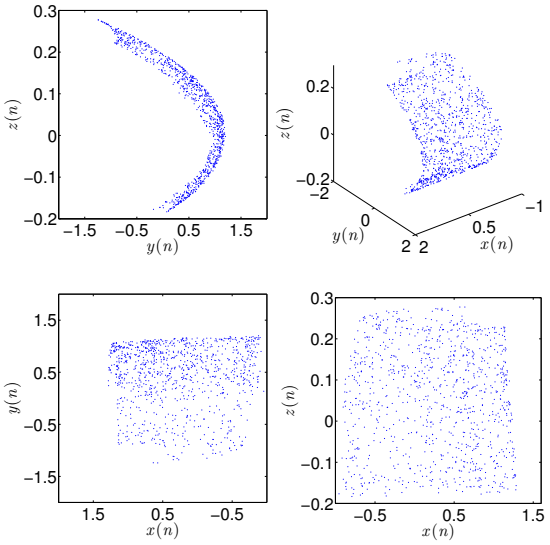

Figure 5.3: Phase space of the fractional–order Stefanski map for $\nu = 0.969$.

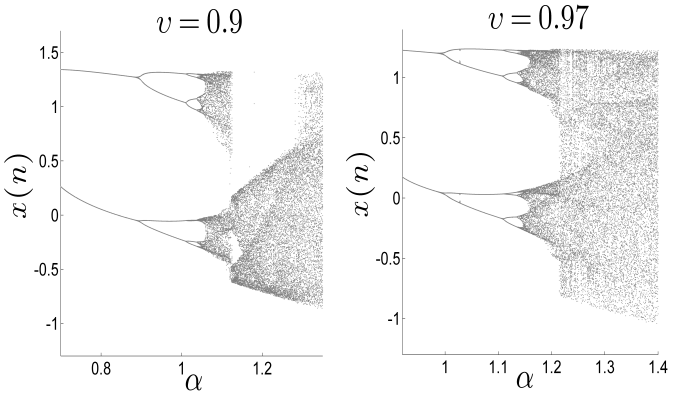

Figure 5.4: Bifurcation diagrams corresponding to the fractional Stefanski map with α as the critical parameter, $\beta = 0.2$, and different fractional orders ν.

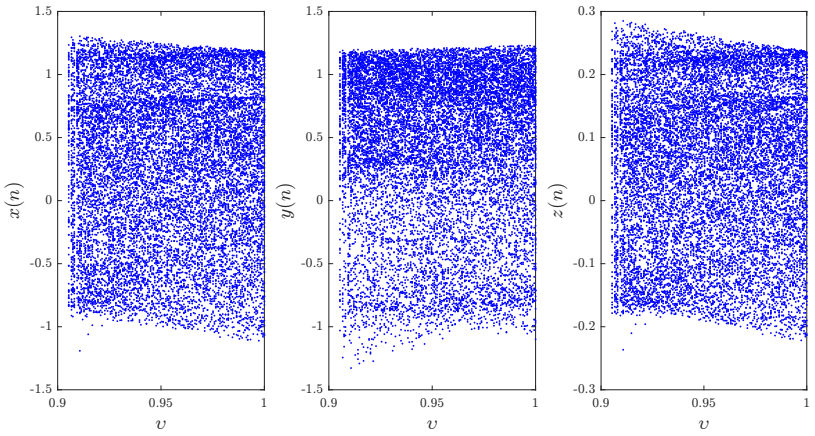

Figure 5.5: Bifurcation diagram of the fractional Stefanski map with $\nu \in [0,1]$ as the critical parameter, $(\alpha,\beta) = (1.4, 0.2)$ and $(x(0), y(0)\, z(0)) = (0,0,0)$.

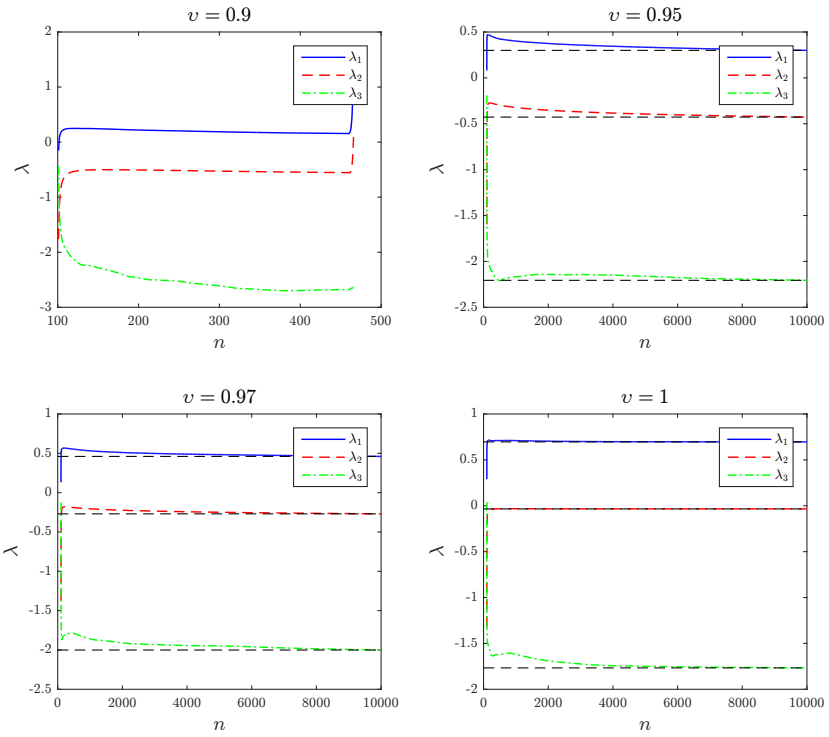

Figure 5.6: Estimated Lyapunov exponents of the fractional Stefanski map for $(\alpha,\beta) = (1.4, 0.2)$, $[x(0), y(0)\, z(0)] = [0,0,0]$, and different fractional orders.

5.3 The fractional–order discrete–time Rössler system

The second map we are going to consider here is the 3D Rössler map introduced in [7] and given by

$$\begin{cases} x\left(n+1\right) = b_1 x\left(n\right)\left(1-x\left(n\right)\right) - b_2\left(z\left(n\right)+b_3\right)\left(1-2y\left(n\right)\right), \\ y\left(n+1\right) = b_4 y\left(n\right)\left(1-y\left(n\right)\right) + b_5 z\left(n\right), \\ z\left(n+1\right) = b_6\left(1-b_7 x\left(n\right)\right)\left[\left(z\left(n\right)+b_3\right)\left(1-2y\left(n\right)\right)-1\right], \end{cases} \tag{5.4}$$

with states $x\left(n\right)$, $y\left(n\right)$, and $z\left(n\right)$ and parameters $b_1 = 3.8$, $b_2 = 0.05$, $b_3 = 0.35$, $b_4 = 3.78$, $b_5 = 0.2$, $b_6 = 0.1$, and $b_7 = 1.9$. The Rössler map is well known and has been examined and applied in countless studies found in the literature. The phase–space portraits of the Rössler map for initial conditions $\left[x\left(0\right), y\left(0\right), z\left(0\right)\right] = \left[0.1, 0.2, -0.5\right]$ are displayed in Figure 5.7.

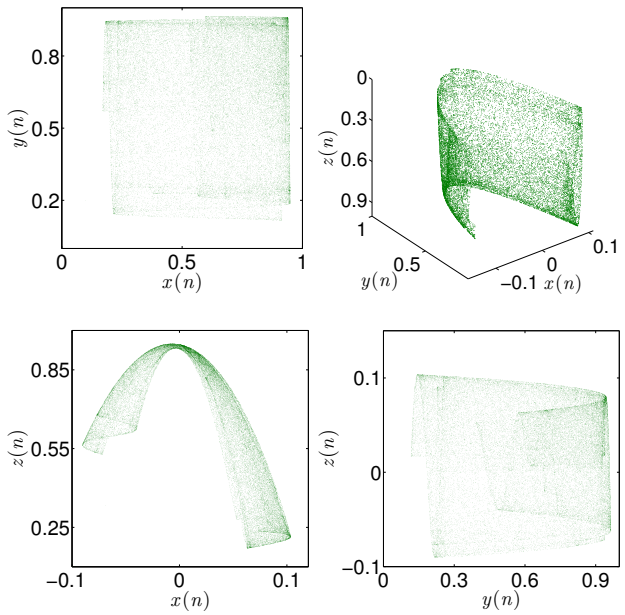

Figure 5.7: Phase space portraits of the standard Rössler map for $b_1 = 3.8$, $b_2 = 0.05$, $b_3 = 0.35$, $b_4 = 3.78$, $b_5 = 0.2$, $b_6 = 0.1$, and $b_7 = 1.9$.

The fractional–order map corresponding to (5.4) may be obtained in a similar manner to the fractional Stefanski map, as

$$\begin{cases} {}^{C}\Delta_a^{\nu} x\left(t\right) = b_1 x\left(t-1+\nu\right)\left(1-x\left(t-1+\nu\right)\right) \\ \qquad\qquad -b_2\left(\left(z\left(t-1+\nu\right)+b_3\right)\left(1-2y\left(t-1+\nu\right)\right)\right) - x\left(t-1+\nu\right), \\ {}^{C}\Delta_a^{\nu} y\left(t\right) = b_4 y\left(t-1+\nu\right)\left(1-y\left(t-1+\nu\right)\right) + b_5 z\left(t-1+\nu\right) \\ \qquad\qquad -y\left(t-1+\nu\right), \\ {}^{C}\Delta_a^{\nu} z\left(t\right) = b_6\left(1-b_7 x\left(t-1+\nu\right)\right) \\ \qquad\qquad \left[\left(z\left(t-1+\nu\right)+b_3\right)\left(1-2y\left(t-1+\nu\right)\right)-1\right] - z\left(t-1+\nu\right), \end{cases} \tag{5.5}$$

for $t \in \mathbb{N}_{a-v+1}$, where $0 < \nu \leq 1$. The corresponding numerical may be given by

$$\begin{cases} x(n) = x(a) + \frac{1}{\Gamma(\nu)} \sum_{j=1}^{n} \frac{\Gamma(n-j+\nu)}{\Gamma(n-j+1)} \\ \qquad (b_1 x(j-1)(1-x(j-1)) - b_2 (z(j-1)+b_3)(1-2y(j-1)) - x(j-1)), \\ y(n) = y(a) + \frac{1}{\Gamma(\nu)} \sum_{j=1}^{n} \frac{\Gamma(n-j+\nu)}{\Gamma(n-j+1)} \\ \qquad (b_4 y(j-1)(1-y(j-1)) + b_5 z(j-1) - y(j-1)), \\ z(n) = z(a) + \frac{1}{\Gamma(\nu)} \sum_{j=1}^{n} \frac{\Gamma(n-j+\nu)}{\Gamma(n-j+1)} \\ \qquad (b_6 (1-b_7 x(j-1)) [(z(j-1)+b_3)(1-2y(j-1))-1] - z(j-1)). \end{cases} \tag{5.6}$$

Dynamical analysis of the fractional order Rössler system

In order to ensure that the fractional Rössler map (5.5) is chaotic, it helps to visualize its bifurcation plot. Let us consider the simple case where $a = 0$ and $[x(0), y(0), z(0)] = [0.1, 0.2, -0.5]$. Figures 5.8 depicts the phase portraits for fractional order values $\nu = 0.97$. Through an ex-

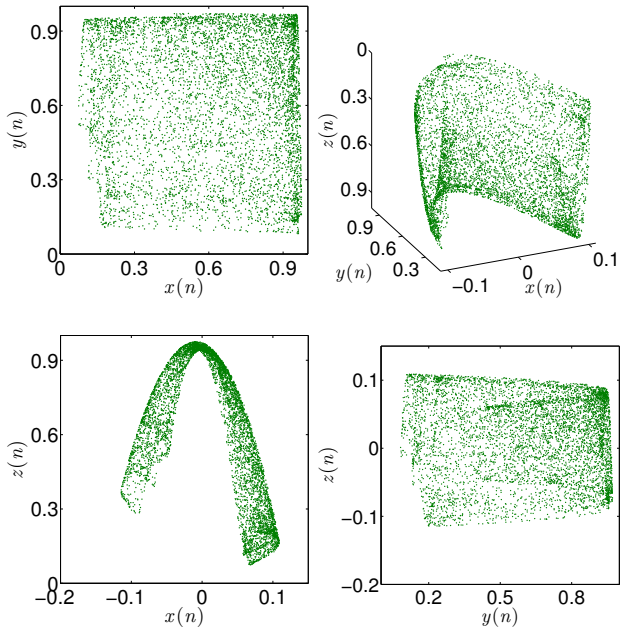

Figure 5.8: Phase portraits of the fractional order Rössler map for $\nu = 0.97$.

perimental sweep of the fractional order, we found that the minimum value of ν for which the system exhibits a chaotic behavior is 0.903. Figure 5.9 shows the bifurcation diagram for $\nu = 0.97$ with b_1 as the critical parameter and $(b_2, b_3, b_4, b_5, b_6, b_7) = (0.05, 0.35, 3.78, 0.2, 0.1, 1.9)$. The critical parameter was varied with the step size $\Delta b_1 = 0.001$. Figure 5.10 shows the bifurcation diagram of the fractional Rössler map with $\nu \in [0.9, 1]$ as the critical parameter, $(b_2, b_3, b_4, b_5, b_6, b_7) = (0.05, 0.35, 3.78, 0.2, 0.1, 1.9)$ and $[x(0), y(0), z(0)] = [0.1, 0.2, -0.5]$. We

see that chaos is only observed for $\nu > \nu_0 \approx 0.933$. Below ν_0, the map becomes unstable and the states diverge towards infinity. Using the same parameters and initial conditions, Figure 5.11 shows the estimated Lyapunov exponents using the Jacobian matrix. For $\nu = 1$, we observe that $\lambda_1 \approx \lambda_2 > 0$ indicating a hyperchaotic nature of the fractional Rössler map. Similar to the Stefanski map, as ν reduces, so do the Lyapunov exponents.

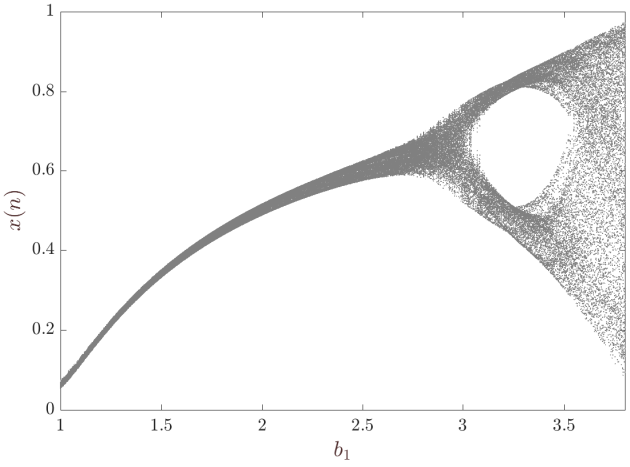

Figure 5.9: Bifurcation diagram of Rössler system with a as the critical parameter and $\nu = 0.97$.

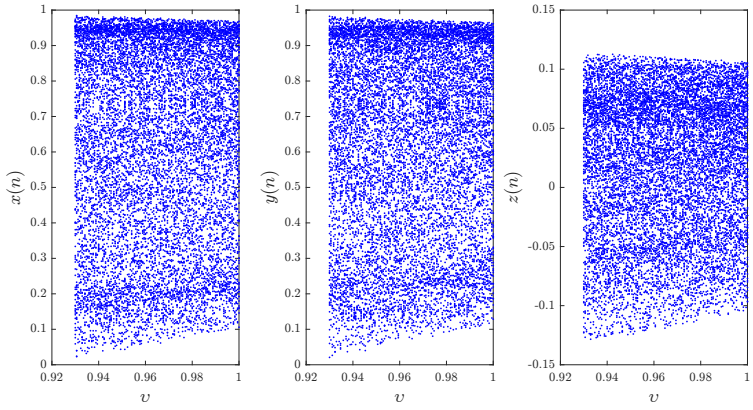

Figure 5.10: Bifurcation diagram of the fractional Rössler map with $\nu \in [0, 1]$ as the critical parameter, $(b_2, b_3, b_4, b_5, b_6, b_7) = (0.05, 0.35, 3.78, 0.2, 0.1, 1.9)$ and $[x(0), y(0), z(0)] = [0.1, 0.2, -0.5]$.

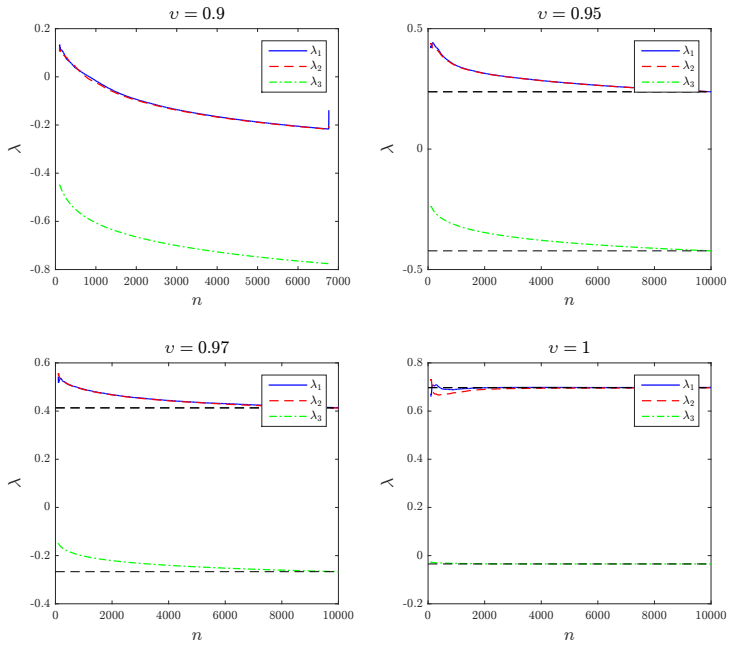

Figure 5.11: Estimated Lyapunov exponents of the fractional Rössler map for with $(b_2, b_3, b_4, b_5, b_6, b_7) = (0.05, 0.35, 3.78, 0.2, 0.1, 1.9)$, $[x(0), y(0), z(0)] = [0.1, 0.2, -0.5]$, and different fractional orders ν.

5.4 The fractional–order Wang map

Another 3D chaotic map that has an interesting attractor is the hyperchaotic Wang map proposed in [9] and given by

$$\begin{cases} x(n+1) = a_3 y(n) + (a_4+1)x(n), \\ y(n+1) = a_1 x(n) + y(n) + a_2 z(n), \\ z(n+1) = (a_7+1)z(n) + a_6 y(n) z(n) + a_5. \end{cases} \tag{5.7}$$

Figure 5.12 shows the phase portraits for the following set of parameters $(a_1, a_2, a_3, a_4, a_5, a_6, a_7) = (-1.9, 0.2, 0.5, -2.3, 2, -0.6, -1.9)$. It is easy to see that the system exhibits chaos, a result that has been reported and studied in the literature.

We follow the same lines of the previous two sections to arrive at the fractional–order discrete–time Wang map given by

$$\begin{cases} {}^{C}\Delta_a^{\nu} x(t) = a_3 y(t-1+\nu) + a_4 x(t-1+\nu), \\ {}^{C}\Delta_a^{\nu} y(t) = a_1 x(t-1+\nu) + a_2 z(t-1+\nu), \\ {}^{C}\Delta_a^{\nu} z(t) = a_7 z(t-1+\nu) + a_6 y(t-1+\nu) z(t-1+\nu) + a_5. \end{cases} \tag{5.8}$$

The numerical formulas can be obtained in a similar fashion to the previous two sections by

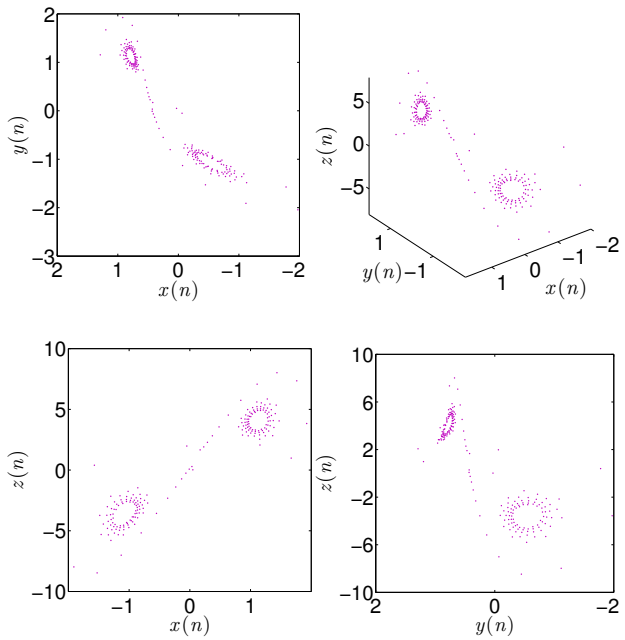

Figure 5.12: Phase portraits of the standard discrete–time Wang system.

means of Theorem 1.15, as

$$\begin{cases} x(n) = x(0) + \frac{1}{\Gamma(\nu)} \sum_{j=1}^{n} \frac{\Gamma(n-j+\nu)}{\Gamma(n-j+1)} \left(a_3 y(j-1) + a_4 x(j-1)\right), \\ y(n) = y(0) + \frac{1}{\Gamma(\nu)} \sum_{j=1}^{n} \frac{\Gamma(n-j+\nu)}{\Gamma(n-j+1)} \left(a_1 x(j-1) + a_2 z(j-1)\right), \\ z(n) = z(0) + \frac{1}{\Gamma(\nu)} \sum_{j=1}^{n} \frac{\Gamma(n-j+\nu)}{\Gamma(n-j+1)} \left(a_7 z(j-1) + a_6 y(j-1) z(j-1) + a_5\right). \end{cases} \tag{5.9}$$

It can be easily shown that the fractional Wang map (5.8) is chaotic. Consider the case $a = 0$ and initial conditions $[x(0), y(0), z(0)] = [0.05, 0.03, 0.02]$. Figures 5.13 and 5.14 show the resulting attractors for the fractional orders $\nu = 0.97$ and $\nu = 0.969$. We have also plotted the bifurcation diagram with the critical parameter a_3 being varied at steps of $\Delta a_{.3} = 0.001$ and the remaining parameters chosen as $(a_1, a_2, a_4, a_5, a_6, a_7) = (-1.9, 0.2, -2.3, 2, -0.6, -1.9)$. The bifurcation duration was set to $n = 200$. The bifurcation diagrams are depicted in Figure 5.15 for different fractional orders ν. In Figure 5.16, we show the bifurcation diagram of the fractional Wang map (5.8) with $\nu \in [0.9, 1]$ as the critical parameter. We see that the map exhibits a chaotic behavior over a short interval of fractional orders . Chaos clearly disappears completely for $\nu < \nu_0 \approx 0.915$. In fact, when $\nu < 0.968$, the chaotic behavior is intermittent and has a very short range.

The Lyapunov exponents of the fractional Wang map (5.8) with the same previous parameters and initial conditions are depicted in Figure 5.17. For $\nu = 1$, we see that $\lambda_1 > \lambda_2 > 0$ indicating hyperchaotic dynamics. This changes as the fractional order is made smaller. In fact, for $\nu = 0.9$, $0 > \lambda_1 > \lambda_2 > \lambda_3$, which leads to a stable map dynamic.

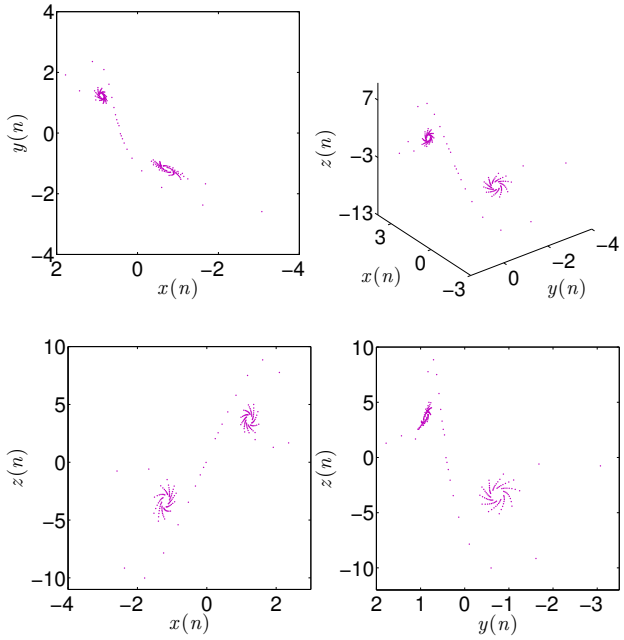

Figure 5.13: Phase space portraits of the fractional–order Wang map for $\nu = 0.97$.

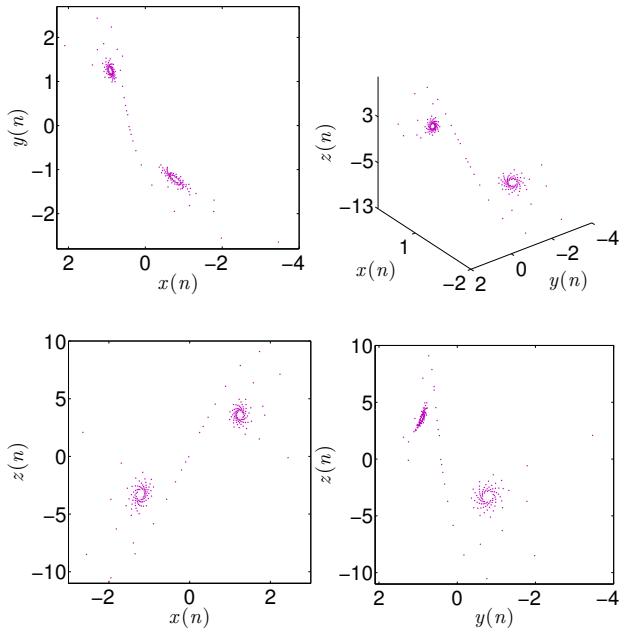

Figure 5.14: Phase space portraits of the fractional–order Wang map for $\nu = 0.969$.

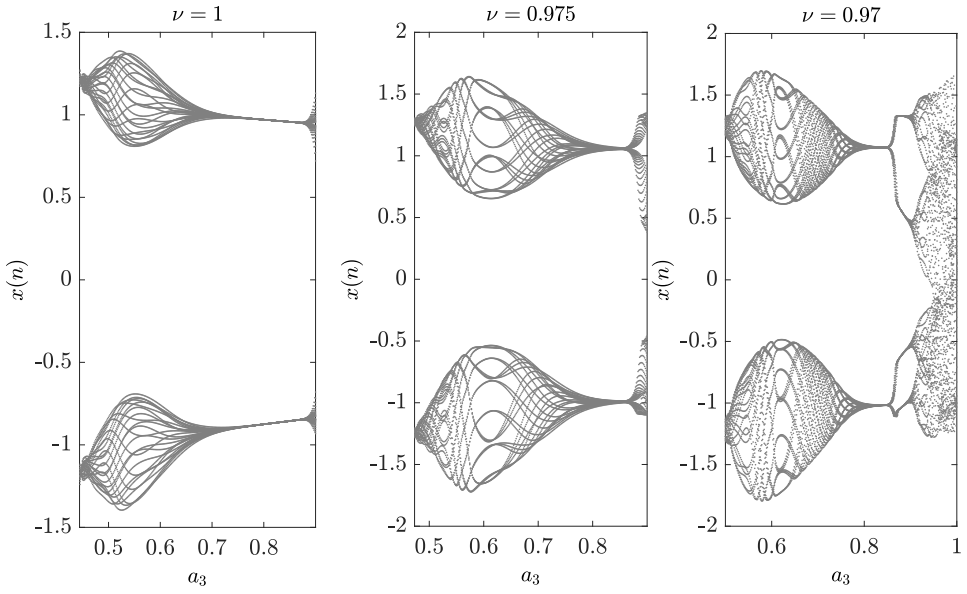

Figure 5.15: Bifurcation diagrams of the fractional–order Wang map for different fractional orders.

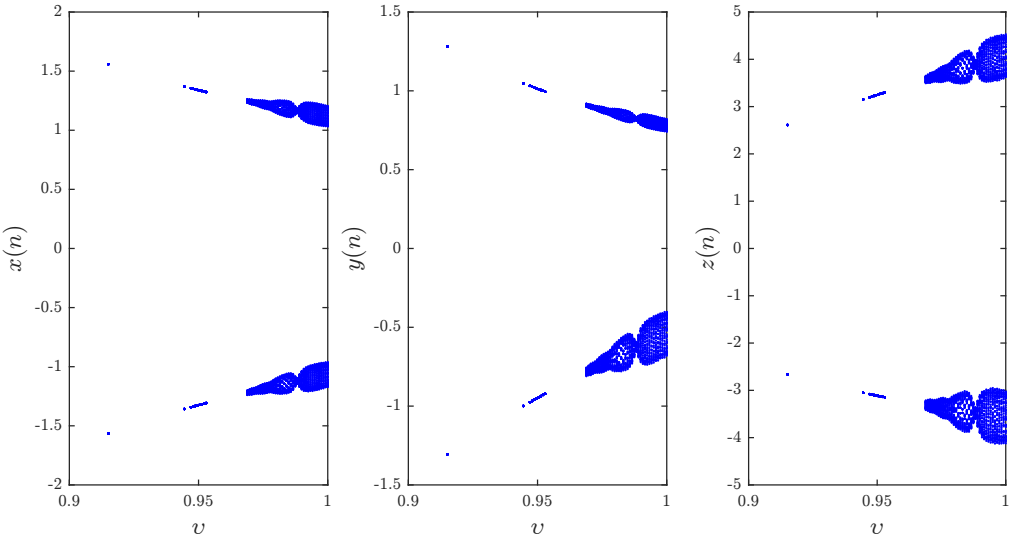

Figure 5.16: Bifurcation diagram of the fractional Wang map with $\nu \in [0,1]$ as the critical parameter, $(a_1, a_2, a_4, a_5, a_6, a_7) = (-1.9, 0.2, -2.3, 2, -0.6, -1.9)$ and $[x(0), y(0), z(0)] = [0.05, 0.03, 0.02]$.

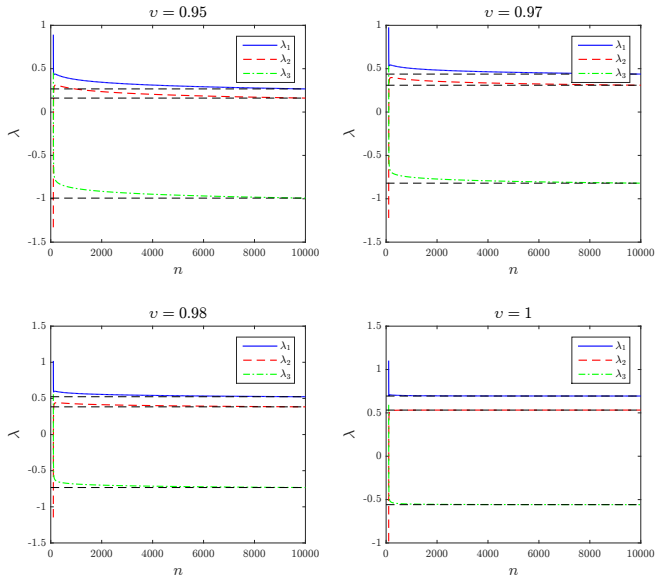

Figure 5.17: Estimated Lyapunov exponents of the fractional Wang map for with $(a_1, a_2, a_4, a_5, a_6, a_7) = (-1.9, 0.2, -2.3, 2, -0.6, -1.9)$, $[x(0), y(0), z(0)] = [0.05, 0.03, 0.02]$, and different fractional orders ν.

5.5 The three dimensional fractional-order Hénon map with Lorenz-Like attractors

One of the most studied models of nonlinear systems is the two dimensional Hénon map reported in Chapter 3. As a generalization of the classical Hénon map, the three-dimensional Hénon map is described by the following system of difference equations

$$\begin{cases} x(n+1) = M_1 + Bz(n) + M_2 y(n) - x^2(n), \\ y(n+1) = x(n), \\ z(n+1) = y(n), \end{cases} \tag{5.10}$$

where B, M_1 and M_2 are system parameters and n represents the discrete iteration step. The three-dimensional map (5.10) is a simple quadratic diffeomorphisms with a constant Jacobian. The map (5.10) can exhibit wild Lorenz-type strange attractors. This kind of attractors persist for open domains in the parameter space. A more comprehensive study was performed in [136]. For instance, its bifurcation subject to different scenarios and initial settings has been studied in [137, 138]. In order to visualize the dynamics of map (5.10), we resort to phase plots, bifurcation diagrams, evolution states and Lyapunov exponent estimation. We assume parameter values $(B, M_1, M_2) = (0.7, 0, 0.85)$ and initial states $[x(0), y(0), z(0)] = [0, 0, 1]$. The the three-dimensional Hénon phase plot is depicted in Figure 5.18. Figure 5.19(a) depicts the bifurcation diagrams of map (5.10) with respect to different parameters by fixing $M_1 = 0$,

$M_2 = 0.85$ and varying B in the interval $[0, 1]$. Figure 5.19(b) shows the largest Lyapunov exponent corresponding to the bifurcation diagram in Figure 5.19(b). Based on these figures, we can see that the estimated Lyapunov exponents of (5.10) are positive, and so the map (5.10) displays chaotic behavior. Based on these figures, we can see that the estimated Lyapunov exponents of (5.10) are positive, and so the map (5.10) displays chaotic behavior.

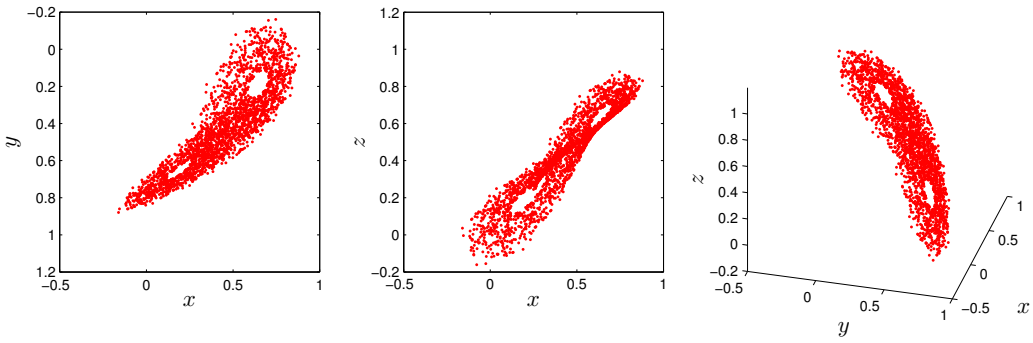

Figure 5.18: Phase plot of the three-dimensional Hénon map (5.10).

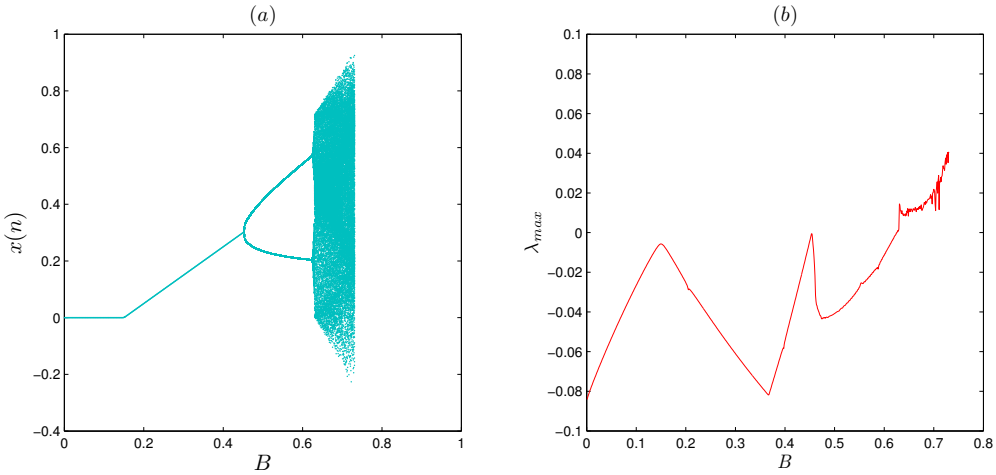

Figure 5.19: (a) Bifurcation diagram of the 3D Hénon map (5.10) and (b) the largest Lyaounov exponent.

This section introduces the formulation of the 3D fractional-order Hénon map, then employs numerical tools to investigate the dynamics of the proposed fractional map [160]. In the first place, let us formulate the difference equations system that represents the fractional-order Hénon-like map as

$$\begin{cases} {}^{C}\Delta_a^{\nu} x\,(t) = M_1 + Bz(t-1+\nu) + M_2 y(t-1+\nu) - x^2(t-1+\nu) - x(t-1+\nu), \\ {}^{C}\Delta_a^{\nu} y\,(t) = x(t-1+\nu) - y(t-1+\nu), \\ {}^{C}\Delta_a^{\nu} z\,(t) = y(t-1+\nu) - z(t-1+\nu), \end{cases} \tag{5.11}$$

where $t \in N_{a+1-\nu} and\ \nu \in]0, 1]$ is the fractional order. The fractional-order Hénon-like map

expressed by the fractional order difference system given in (5.11) introduces a generalization of the integer-order Hénon map given in the difference system (5.10). Next, to deal with fractional-order Hénon-like map and to employ our numerical tools, we define the following discrete formula

$$\begin{cases} x(n) = x(0) + \frac{1}{\Gamma(\nu)} \sum_{j=1}^{n} \frac{\Gamma(n-j+\nu)}{\Gamma(n-j+1)} \left(M_1 + Bz(j-1) + M_2 y(j-1) - x^2(j-1) - x(j-1)\right), \\ y(n) = y(0) + \frac{1}{\Gamma(\nu)} \sum_{j=1}^{n} \frac{\Gamma(n-j+\nu)}{\Gamma(n-j+1)} \left(x(j-1) - y(j-1)\right), \\ z(n) = z(0) + \frac{1}{\Gamma(\nu)} \sum_{j=1}^{n} \frac{\Gamma(n-j+\nu)}{\Gamma(n-j+1)} \Gamma(n-j+1) \left(y(j-1) - z(j-1)\right). \end{cases} \tag{5.12}$$

Now, using the iterative formula (5.12), we are going to investigate the effect of the fractional order ν on the behavior of the fractional Hénon map (5.11).

Bifurcation and chaotic attractors

Setting the system parameters as $M_1 = 0, B = 0.7, M_2 = 0.85$, the initial conditions as $[x(0), y(0), z(0)] = [0, 0, 1]$ and letting $n = 2500$. Also, we consider the first 50 solution as transient. For different values of ν the numerical solution of the fractional-order Hénon map (5.11) are displayed in Figures 5.20, 5.21 and 5.22. It is clear that when $\nu \geq 0.952$ the initial states $[x(0), y(0), z(0)] = [0, 0, 1]$ will converge to kind of bounded attractors. Figures 5.20, 5.21 and 5.22 illustrate that each values of ν generate its own attractor. On the contrary, when ν is less then 0.952 the trajectories diverge to infinity; this is clearly shown in Figure 5.23. Figure 5.23 shows the bifurcation diagram and the largest Lyapunov exponent diagram of $x(n)$ versus ν with respect to the given parameters M_1, M_2, B and initial conditions.

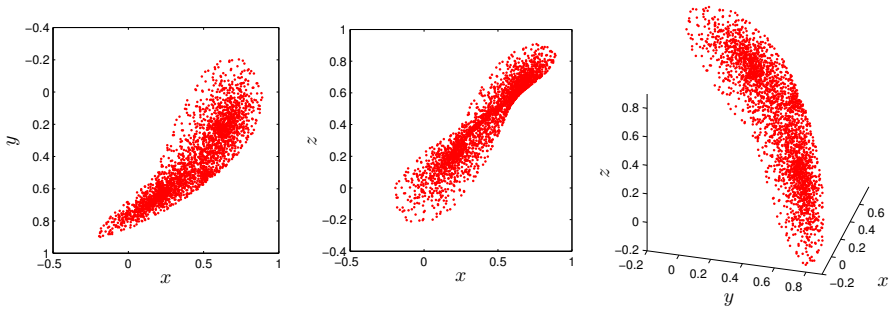

Figure 5.20: Phase plot of the 3D fractional Hénon map (5.11) when $\nu = 0.985$.

Now, let $M_1 = 0$, $M_2 = 0.85$ be fixed and let B be varied from 0 to 1 with the step size $\Delta B = 0.001$, the resulting bifurcation diagrams for the initial point $[x(0), y(0), z(0)] = [0, 0, 1]$ are plotted in Figure 5.24 for the fractional orders $\nu = 0.985$ and $\nu = 0.96$. Additionally, the dynamic behavior of the fractional order map (5.11) can also be illustrated by the largest

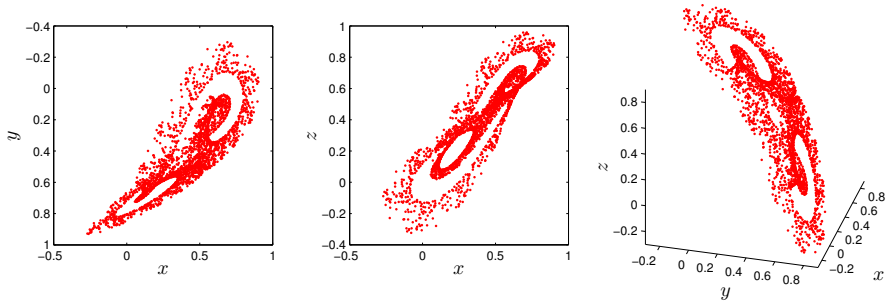

Figure 5.21: Phase plot of the 3D fractional Hénon map (5.11) when $\nu = 0.96$.

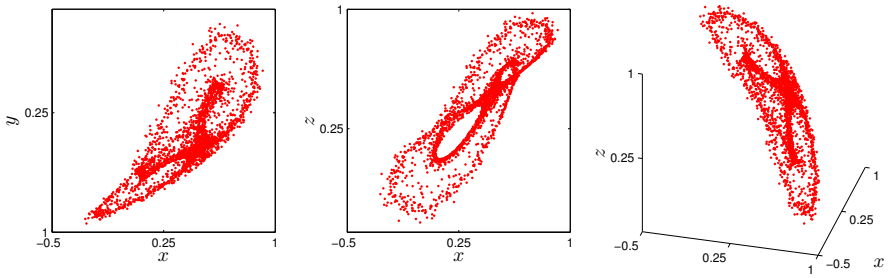

Figure 5.22: Phase plot of the 3D fractional Hénon map (5.11) when $\nu = 0.956$.

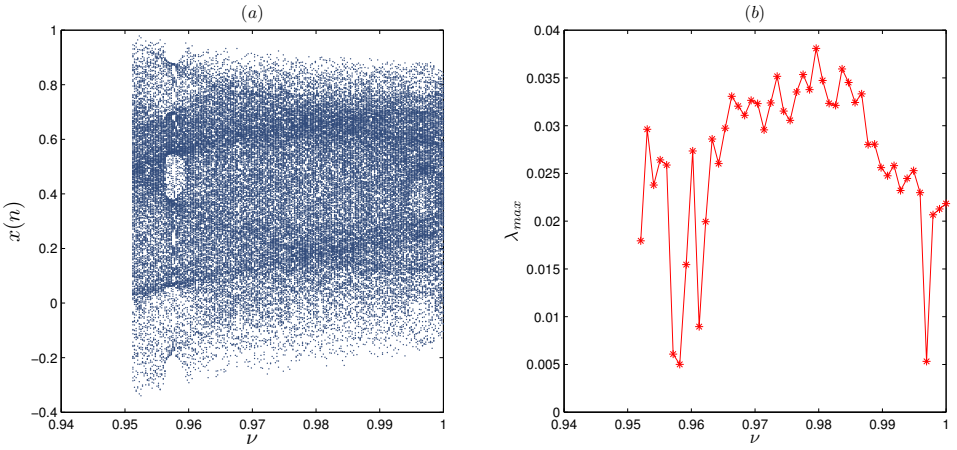

Figure 5.23: (a) Bifurcation diagram of the 3D fractional Hénon map (5.11) as a function of ν and (b) largest Lyapunov exponent corresponding to (a)

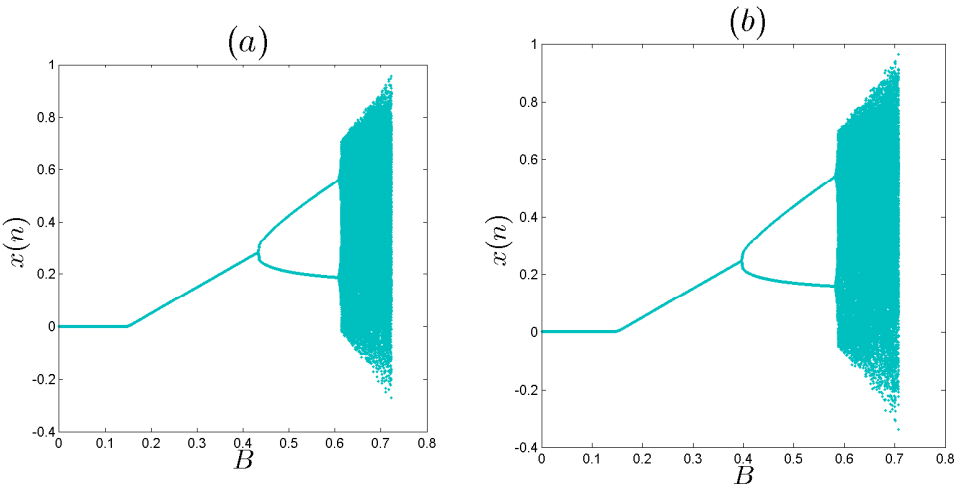

Figure 5.24: (a) Bifurcation diagram of the 3D fractional Hénon map (5.11) as a function of B, when (a) $\nu = 0.985$ and (b) $\nu = 0.96$.

Lyapunov exponent in Figure 5.25 for the same bifurcation parameters and with $\nu = 0.985$, $\nu = 0.96$.

The 0-1 test method

In order to further analyze the influence of the fractional order ν on the properties of the map, we will re-examine the dynamical behavior of the fractional order map (5.11) by means of 0-1 test. With the parameters of the system (5.11) chosen as $M_1 = 0, B = 0.7, M_2 = 0.85$ and for fractional order $\nu = 0.985$ and $\nu = 0.96$ Figure 5.26 shows the asymptotic growth rate K of the fractional order map. For both values, the asymptotic growth rate K approaches 1 as n increase; which indicate the existence of chaos . This result agrees well with the bifurcation diagram and largest lyapunov exponent in Figure 5.24 and 5.25.

From Figure 5.24, we can observe that when ν decreases the bifurcation diagram along the B-axis get shrink, the difference is very small but when ν hit the value 0.951 the unbounded area reach the value $B = 0.7$ which confirm the result above. From the previous numerical results it can be seen clearly that chaos exist in the fractional-order map when ν is in the rang $(0.952, 1)$.

5.6 The three dimensional fractional-order generalized Hénon map

An integer-order discrete-time system called the Generalized Hénon map is proposed in reference [135] which was proposed by Zheng, J.,*et.al* as generalization of the two dimensional Hénon map,

and it is described as

$$\begin{cases} x(n+1) = A - y^2(n) + Bz(n), \\ y(n+1) = x(n), \\ z(n+1) = y(n), \end{cases} \tag{5.13}$$

where A and B are bifurcation parameters. This map exhibits chaos, for instance, when $(A, B) = (0.7281, 0.5)$ and $[x(0), y(0), z(0)] = [1, 0, 0]$, as demonstrated by the phase portraits shown in Figure 5.27. It is always helpful to examine the bifurcation diagram corresponding to a specific critical parameter in order to gain a comprehensive understanding of the dynamics of a chaotic system, see Figure 5.28.

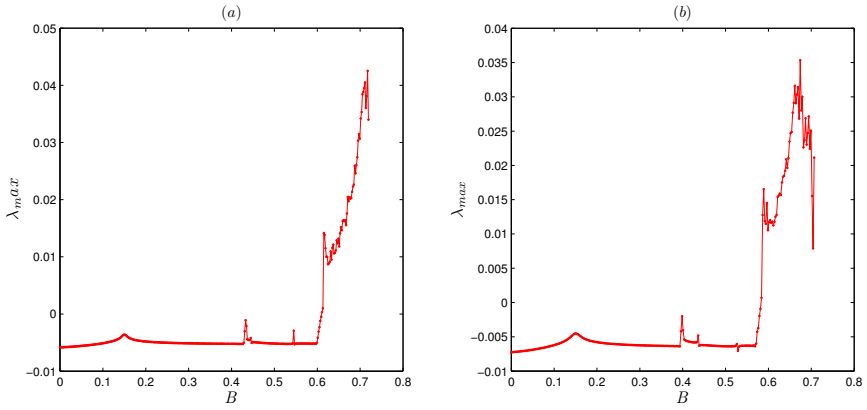

Figure 5.25: Largest Lyapunov exponent of the 3D fractional Hénon map (5.11) as a function of B, when (a) $\nu = 0.985$ and (b) $\nu = 0.96$.

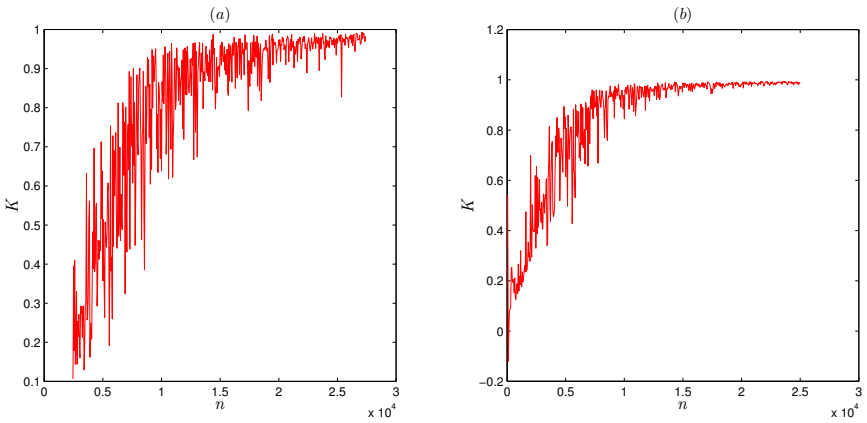

Figure 5.26: The 0-1 test for chaos, when (a) $\nu = 0.985$ and (b) $\nu = 0.96$.

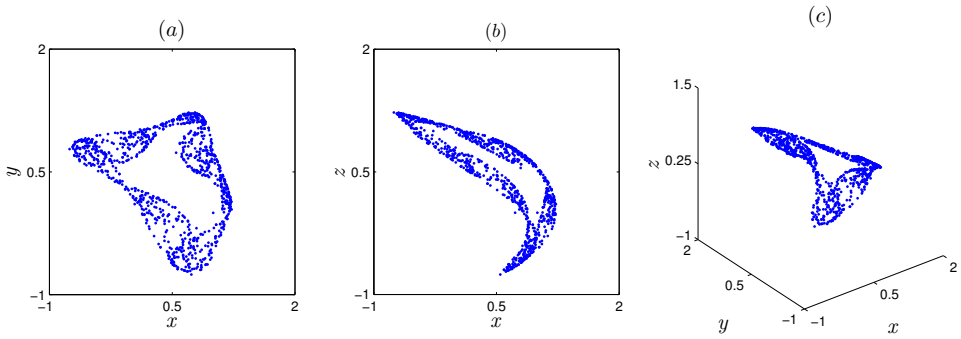

Figure 5.27: Chaotic attractors of the map (5.13) in: $(a)\, x-y$ plane $(b)\, x-z$ plane $(c)\, x-y-z$ space.

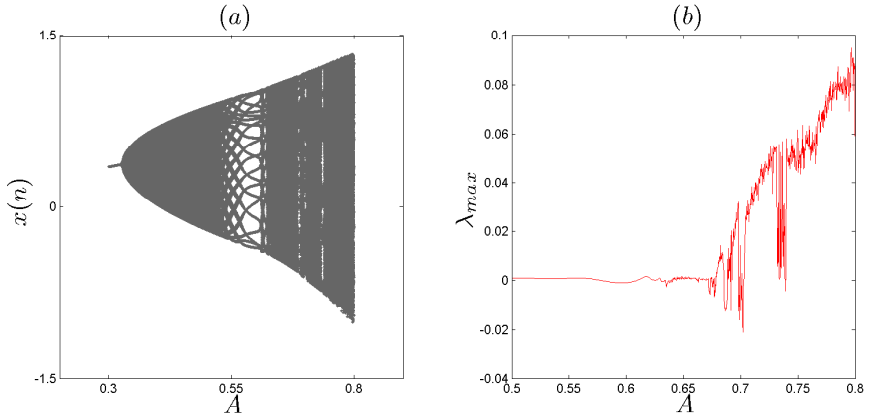

Figure 5.28: (a) Bifurcation diagram of the map (5.13); (b) largest Lyapunov exponent

The map (5.13) can be rewritten in the first difference order form given by

$$\begin{cases} \Delta x\,(n) = A - y^2\,(n) + Bz\,(n) - x(n), \\ \Delta y\,(n) = x\,(n) - y(n), \\ \Delta z\,(n) = y\,(n) - z(n). \end{cases} \tag{5.14}$$

Introducing the Caputo-like delta difference defined in Chapter 1 leads to the fractional-order map

$$\begin{cases} {}^{C}\Delta_a^{\nu} x(t) = A - y^2(t-1+\nu) + Bz(t-1+\nu) - x(t-1+\nu), \\ {}^{C}\Delta_a^{\nu} y(t) = x(t-1+\nu) - y(t-1+\nu), \\ {}^{C}\Delta_a^{\nu} z(t) = y(t-1+\nu) - z(t-1+\nu), \end{cases} \tag{5.15}$$

where $t \in N_{a+1-\nu}$ and $0 < \nu \leq 1$. By means of Theorem 1.15, setting $a = 0$ yields the explicit numerical formula

$$\begin{cases} x(n) = x(0) + \frac{1}{\Gamma(\nu)} \sum_{j=1}^{n} \frac{\Gamma(n-j+\nu)}{\Gamma(n-j+1)} \left(A - y^2(j-1) + Bz(j-1) - x(j-1)\right), \\ y(n) = y(0) + \frac{1}{\Gamma(\nu)} \sum_{j=1}^{n} \frac{\Gamma(n-j+\nu)}{\Gamma(n-j+1)} (x(j-1) - y(j-1)), \\ z(n) = z(0) + \frac{1}{\Gamma(\nu)} \sum_{j=1}^{n} \frac{\Gamma(n-j+\nu)}{\Gamma(n-j+1)} (y(j-1) - z(j-1)), \end{cases} \tag{5.16}$$

where $x(0)$, $y(0)$ and $z(0)$ are the initial conditions. The following results has been reported in [134].

Bifurcation diagram, largest LE and phase portrait

With the same initial conditions and the bifurcation parameter values adopted for Figure 5.27 above, computer simulation were used to evaluate the numerical formulas (5.16) in order to gain a perspective on the dynamics of 3D fractional generalized Hénon map (5.16). The bifurcation diagram and the corresponding largest Lyapunov exponent for $\nu \in [0.96, 1]$ are given in Figure 5.29. In Figure 5.29-(a), we set $n = 700$ and we plot only the last 200, we compute the largest Lyapunov exponent using the Jacobian matrix algorithm reported in Chapter 3. This figures visualizes how the fractional order ν can make effect on the system behavior.First, we note that when $0 \leq \nu \leq 0.969$ the fractional map diverges to infinity. On the contrary, it can be observed that there are vertical lines with a positive largest Lyapunov exponent when $\nu \in]0.969, 0.97[$. In this case, the solution $x(n)$ converges to a chaotic attractor. From the diagrams in Figure 5.29-(a) and (b), we can see that there is transition from chaos to periodic cycles, followed by a series of appearance and disappearance of chaos, meaning, largest Lyapunov exponent change its values between negative numbers and positive as $\nu \in (0.97, 0.986)$. Finally, when $\nu \in [0.986, 1]$ the solution $x(n)$

In what follows, we illustrate the bifurcation diagrams for $A \in [0.3, 0.8]$ in Figure 5.30. To provide this diagrams, we set $n = 2000$ and we fix $B = 0.5$ then we discard away the first 1700 results, the last 300 points are displayed in Figure 5.30 corresponding to fractional order values $\nu = 0.987, 0.975$, respectively. Figure 5.30-(a) is the bifurcation diagram for $\nu = 0.987$. As A passes to the interval $[0.66, 0.7885]$ a periodic cycles and a chaotic regions are apparent. However, when the value of ν is set to 0.975, one can see the jumping behavior from chaotic set to a 3 periodic orbit that suddenly drupes into 3 small-sized attractors at $A = 0.326$. With the increase of parameter A, the fractional map goes directly to a fully developed chaotic regime. It is worth pointing out, that the fractional map never produces the same largest Lyapunov exponent twice, we deduce that each values of ν have its own attractor. An attractor which includes periodic orbit is shown in Figure Figures 5.32 and 5.33 shows the chaotic attractor of the fractional map for $\nu = 0.987$, and for $\nu = 0.9695$, respectively.

5.7 The fractional-order Grassi-Miller map

Throughout the years many integer order chaotic maps have been proposed and have found applications in numerous fields within science and engineering. Here, we interested in the Grassi-Miller map, which was proposed first by Miller and Grassi in [148] as a generalization of the Hénon map. The Grassi-Miller system can be described by the following 3D discrete-time system

$$\begin{cases} x(n+1) = 1 + z(n) - \alpha y^2(n), \\ y(n+1) = 1 + \beta y(n) - \alpha x^2(n), \\ z(n+1) = \beta x(n), \end{cases} \tag{5.17}$$

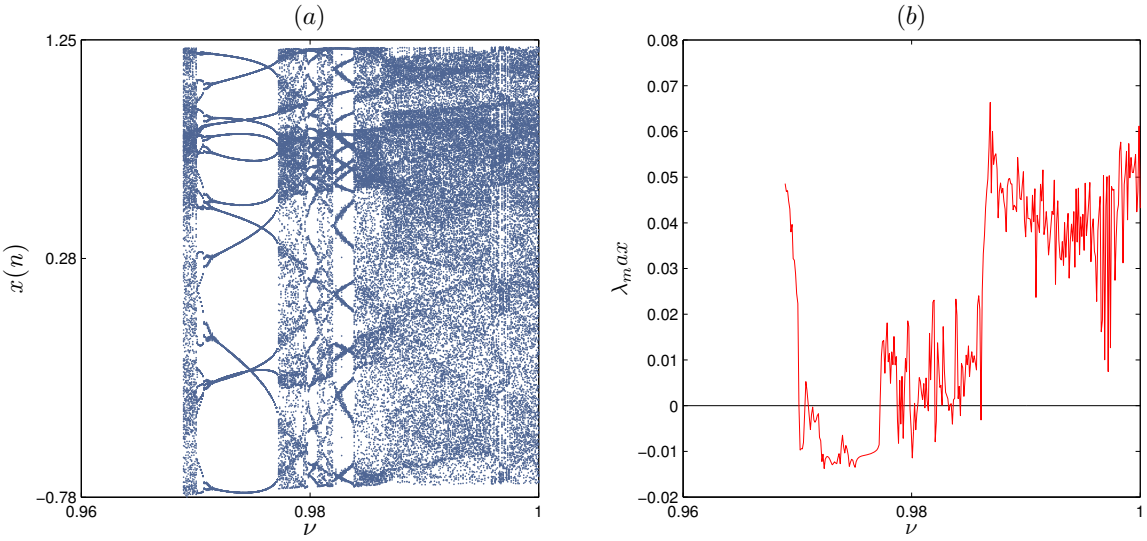

Figure 5.29: (a) Bifurcation diagram of the map (5.15); (b) largest Lyapunov exponent

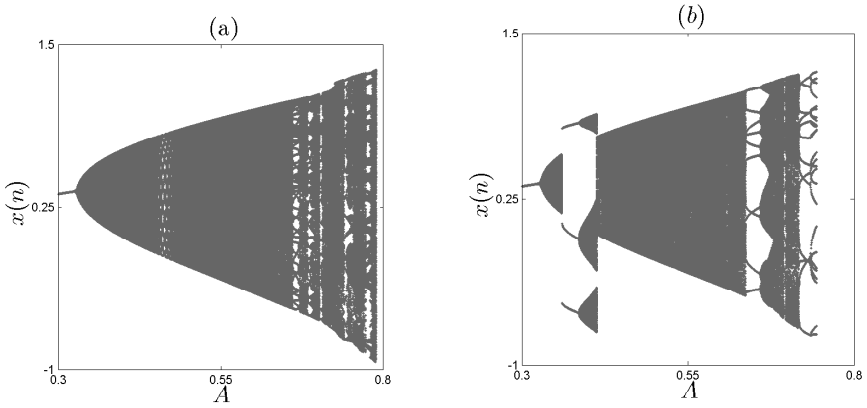

Figure 5.30: (a) Bifurcation of the fractional map (5.15); (b) largest Lyapunov exponent with fractional order ν.

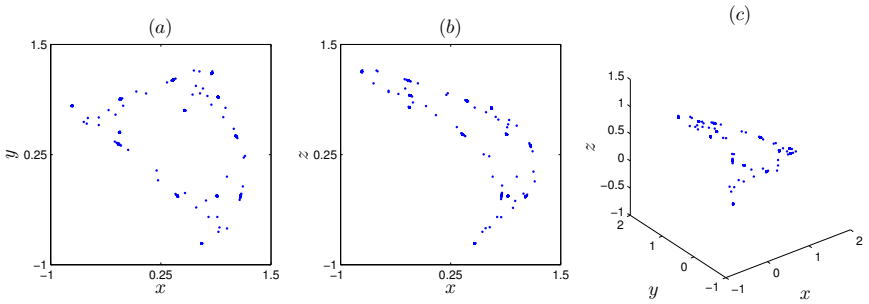

Figure 5.31: Periodic orbit obtained for $n = 2000$ and $\nu = 0.975$ in: $(a)\, x - y$ plane; $(b)\, x - z$ plane; $(c)\, (x, y, z)$ space.

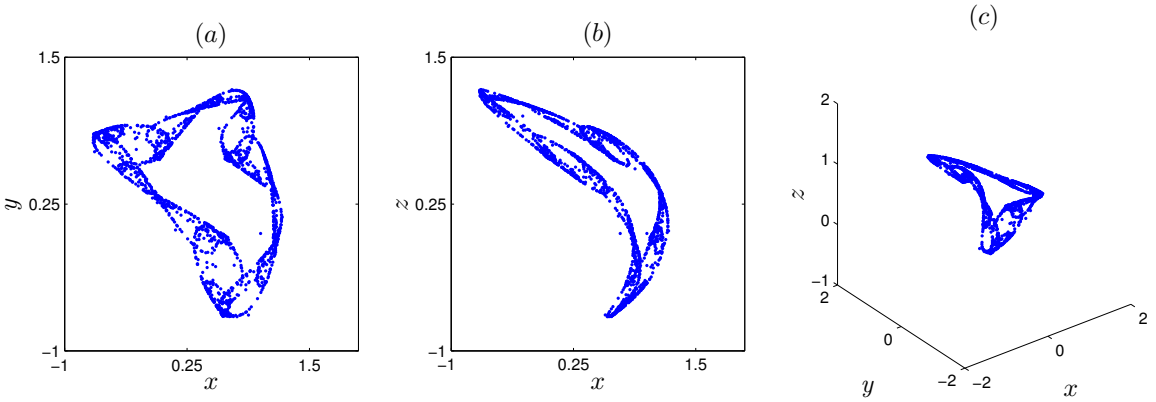

Figure 5.32: Chaotic attractor obtained for $n = 2000$ and $\nu = 0.987$ in: $(a)\, x - y$ plane; $(b)\, x - z$ plane; $(c)\, (x, y, z)$ space.

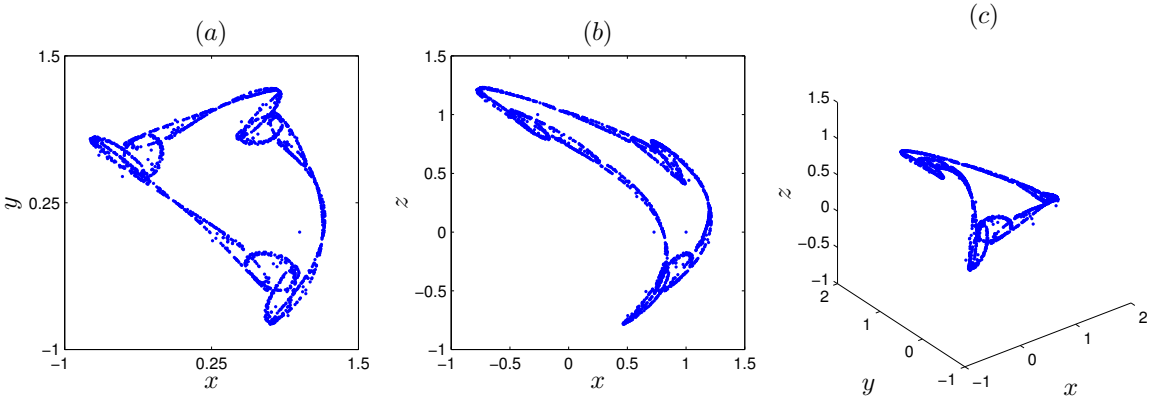

Figure 5.33: Periodic orbit obtained for $n = 2000$ and $\nu = 0.9695$ in: $(a)\, x - y$ plane; $(b)\, x - z$ plane; $(c)\, (x, y, z)$ space.

where $x(n)$, $y(n)$, and $z(n)$ denote the states and α and β are system parameters. As demonstrated in [148], the system exhibits a hyperchaotic behavior, for instance, when $(\alpha, \beta) = (1.76, 0.1)$ given the initial conditions $[x(0), y(0), z(0)] = [1, 0.1, 0]$. Plots of the attractors in the integer-order Grassi-Miller map (5.17), obtained using these parameter values and initial conditions, are reported in Figure 5.34. We propose and examine the fractional form corresponding to the Grassi-Miller integer order discrete-time system. We show experimental phase portraits and bifurcation diagrams to highlight the ranges of parameters and fractional orders over which chaos is observed.

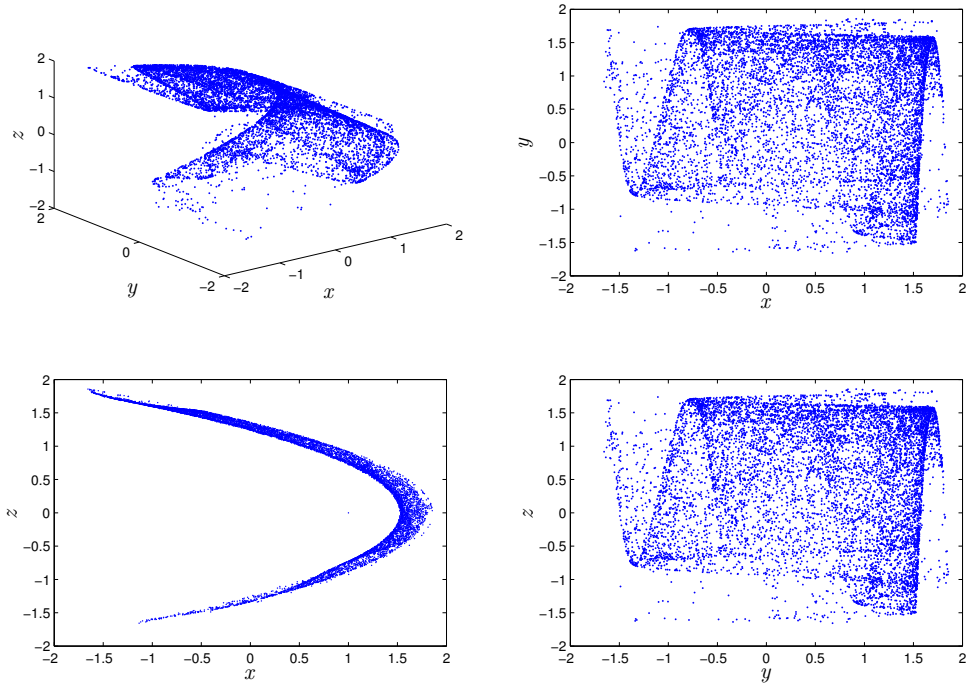

Figure 5.34: Phases portraits of integer-order Grassi-Miller map for $\alpha = 1.76$ and $\beta = 0.1$.

By exploiting the fractional Caputo differences, the fractional-order Grassi chaotic map is obtained

$$\begin{cases} {}^{C}\Delta_a^{\nu} x(t) = 1 + z(t-1+\nu) - \alpha y^2(t-1+\nu) - x(t-1+\nu), \\ {}^{C}\Delta_a^{\nu} y(t) = 1 + \beta y(t-1+\nu) - \alpha x^2(t-1+\nu) - y(t-1+\nu), \\ {}^{C}\Delta_a^{\nu} z(t) = \beta x(t-1+\nu) - z(t-1+\nu), \end{cases} \tag{5.18}$$

where $0 < \nu \leq 1$ is the fractional difference order and a defines the starting point of the set $\mathbb{N}_{a+1-\nu}$. Similarly, the numerical formula of (5.18) is obtained as

$$\begin{cases} x(n) = x(a) + \frac{1}{\Gamma(\nu)} \sum_{j=1}^{n} \frac{\Gamma(n-j+\nu)}{\Gamma(n-j+\nu)} \left(1 + z(j-1) - \alpha y^2(j-1) - x(j-1)\right), \\ y(n) = y(a) + \frac{1}{\Gamma(\nu)} \sum_{j=1}^{n} \frac{\Gamma(n-j+\nu)}{\Gamma(n-j+\nu)} \left(1 + \beta y(j-1) - \alpha x(j-1) - y(j-1)\right), \\ z(n) = z(a) + \frac{1}{\Gamma(\nu)} \sum_{j=1}^{n} \frac{\Gamma(n-j+\nu)}{\Gamma(n-j+\nu)} \left(\beta x(j-1) - z(j-1)\right), \end{cases} \tag{5.19}$$

when a is taken equal to 0. Based on the discrete map equation (5.19), it is easy to get the time series by the way of computer programming. Dynamics under two parameters α and β, and fractional order ν are analyzed in the following subsections.

Dynamics analysis of the fractional-order Grassi-Miller map

For the proposed fractional system (5.18), experimental variation of the fractional order has shown a variety of responses in the form of chaotic states, limit cycles and asymptotic stability. We have used the numerical formula (5.19) along with different sets of parameters and fractional orders, with the aim of observing the phase portraits, bifurcation diagrams and maximum Lyapunov exponent of the system through a Matlab script.

Dynamics with α varying

First, let $\nu = 1$, $[x(0), y(0), z(0)] = [1, 0.1, 0]$, and $(\alpha, \beta) = (1.76, 0.1)$. As expected, since when $\nu = 1$ numerical system (5.19) reduces to the integer-order system (5.17), the resulting phase portraits obtained from system (5.18) are identical to those depicted in Figure 5.34 for system (5.18). Note that for both systems simulations have been carried out for $n = 7000$. More generally, consider the case where $\nu = 0.98$. Figures 5.35 and 5.36 show the portraits given $\alpha = 1.6$ and $\alpha = 1.5$, respectively. It can be noticed that a slight change in system parameters leads to a variation in the strange attractor. The time evolution of the states is depicted in Figure 5.38 for $\alpha = 1.6$. Figure 5.39 depicts the portraits for $\nu = 0.86$ and $\alpha = 1.5$. This confirms that the proposed fractional system (5.18) can exhibit chaotic behaviors for a range of different fractional orders and system parameters. Figure 5.37 shows the phase portraits of the proposed system subject to $\alpha = 0.4$ and $\nu = 0.5$. Obviously, in this scenario, the system does not exhibit chaos. This suggests to us that the existence or absence of chaos is dependent on the fractional order.

Phase portraits are a nice tool for evaluating the nature of solutions but are not sufficient to gain a comprehensive perspective. We may also observe the bifurcation plots with α as the critical parameter. Let us set the step size $\Delta\alpha$ to 0.002 and use numerical formula (5.19) to produce the bifurcation diagrams for different values of the fractional order ν. For $\nu = 0.98$ and $\nu = 0.88$, the bifurcation diagrams are plotted in Figures 5.40(a) and (b), respectively. From these pictures it can be deduced that each time we modify the fractional order considerable changes occur in the chaotic region of the diagram. These observed variations in the shape of the bifurcation plot suggest that the Grassi-Miller fractional map is able to exhibit a variety of chaotic motions.

Let us now conduct a detailed analysis of the obtained plots with the aim of establishing a connection between the changes in the shape of the attractors and the values of the system parameters. If we compare the attractors in the $x-y$ and $y-z$ plots in Figure 5.34 (integer-order case, with $\alpha = 1.76$) with the attractors in the $x-y$ and $y-z$ plots in Figure 5.35 (fractional order $\nu = 0.98$ and $\alpha = 1.6$), we can notice that the slight change in the parameter values (ν from 1 to 0.98 and α from 1.76 to 1.6) generates a reduction in the size of the attractors. Namely, while in Figure 5.34 the attractors in the $x-y$ and $y-z$ plots cover all the area ranging

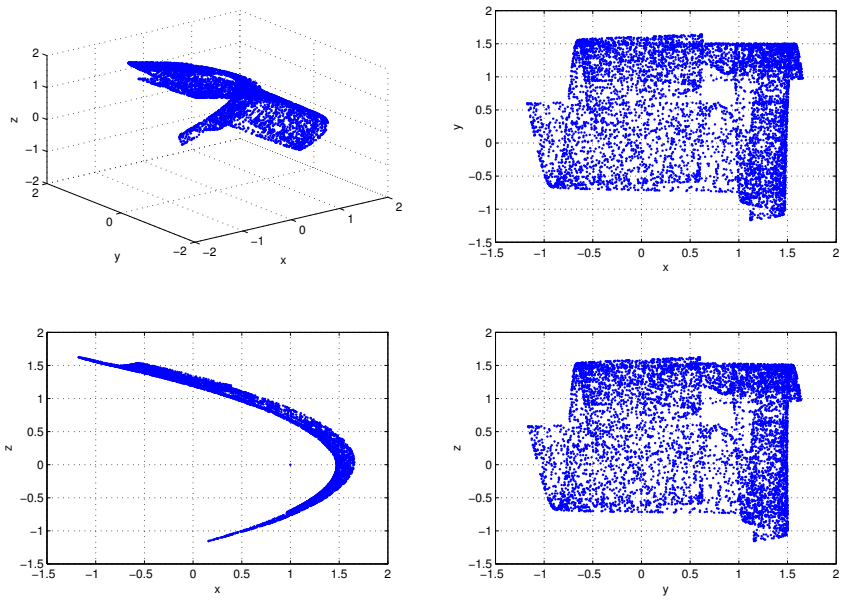

Figure 5.35: Phase portraits of the Grassi-Miller Hypercchaotic map for $\beta = 0.1$, $\alpha = 1.6$ and $\nu = 0.98$.

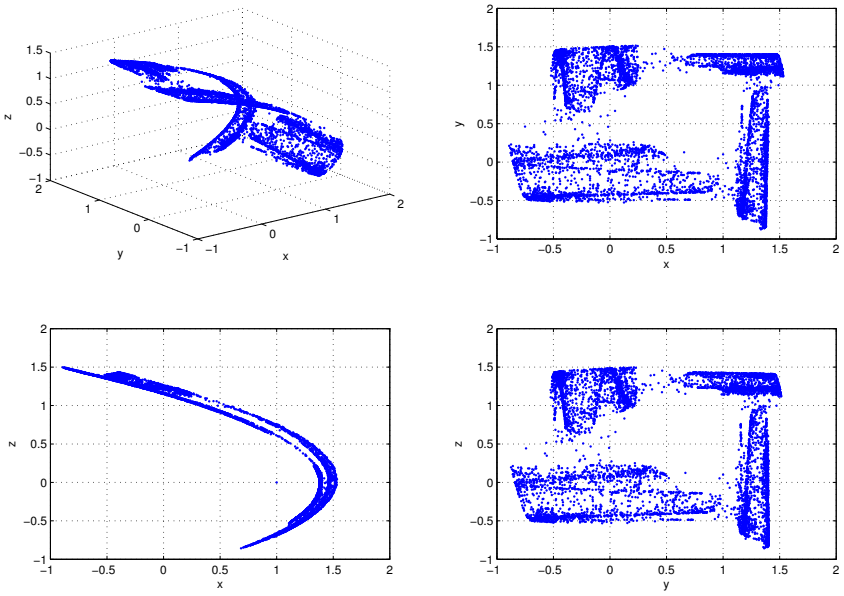

Figure 5.36: Phase portraits of the fractional Grassi-Miller map $\alpha = 1.5$ and $\nu = 0.98$.

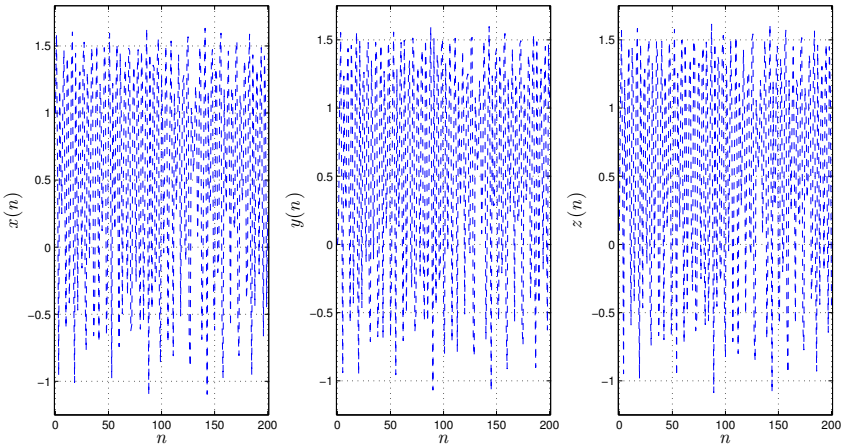

Figure 5.37: Evolution of states for the fractional Grassi-Miller hyperchaotic map with $\alpha = 1.6$ and $\nu = 0.98$.

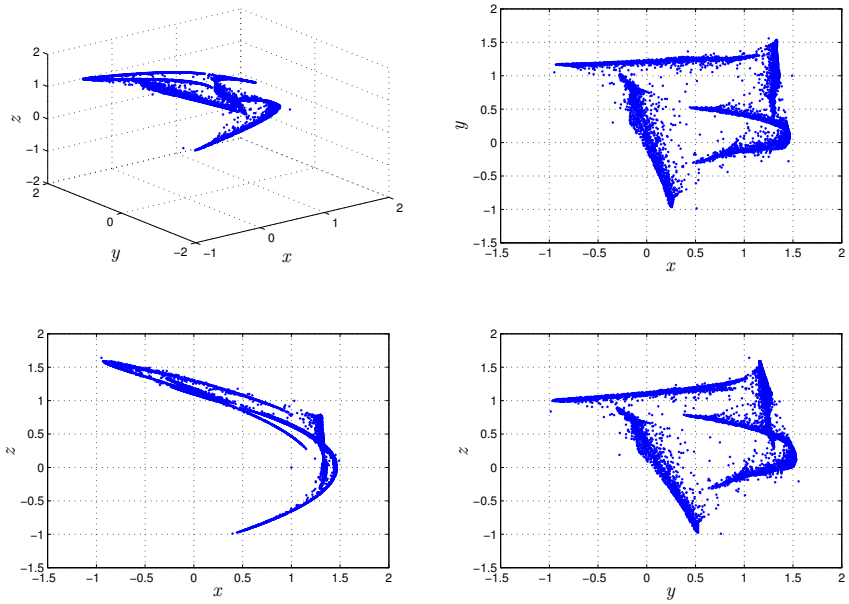

Figure 5.38: Phase portraits of the fractional Grassi-Miller map $\alpha = 1.5$ and $\nu = 0.86$.

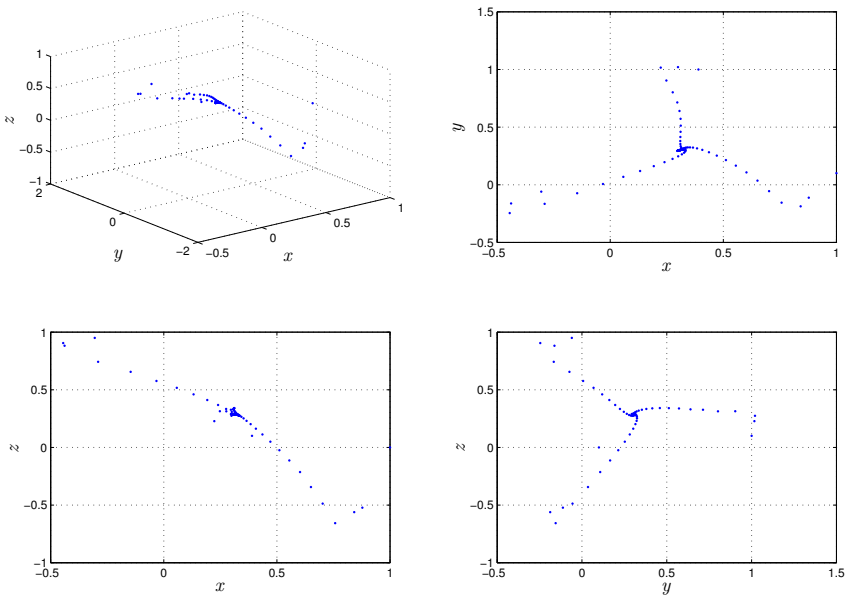

Figure 5.39: Phase portraits of the fractional Grassi-Miller map $\alpha = 0.4$ and $\nu = 0.5$.

from -2 to $+2$ for both the horizontal and the vertical axes, in Figure 5.35 the attractors in the $x-y$ and $y-z$ plots cover the area ranging approximately from -1.5 to $+1.5$ for both the axes, indicating that reducing the system parameters generates a reduction in the size of attractors.

Next, we discuss the results plotted in Figures 5.35 and 5.36. If we compare the attractors in the $x-y$ and $y-z$ plots in Figure 5.35 (fractional order $\nu = 0.98$ and $\alpha = 1.6$) with the attractors in the $x-y$ and $y-z$ plots in Figure 5.36 (fractional order $\nu = 0.98$ and $\alpha = 1.5$), we can notice that the slight change in the parameter values (α from 1.6 to 1.5) generates a further reduction in the size of the attractor as well as its subdivision into four different parts. Specifically, referring to the size, note that in Figure 5.36 the attractors in the $x-y$ and $y-z$ plots cover the area ranging approximately from -1 to $+1.5$ for both the axes, indicating that reducing the parameter α from 1.6 to 1.5 generates a reduction in the size of attractors (besides the appearance of four different parts, with respect to the attractor plotted in Figure 5.35). Going ahead in our analysis, let us discuss the results plotted in Figures 5.36 and 5.39. If we compare the attractors in the $x-y$ and $y-z$ plots in Figure 5.36 (fractional order $\nu = 0.98$ and $\alpha = 1.5$) with the attractors in the $x-y$ and $y-z$ plots in Figure 5.38 (fractional order $\nu = 0.86$ and $\alpha = 1.5$), we can notice that a change in the fractional-order of the system ν from 0.98 to 0.86 while keeping the same value of α does not generate a reduction in the size of the attractor anymore. However, from Figure 5.39 it can be noticed that the shape of the attractor is slightly different from that plotted in Figure 5.36, although the subdivision into four different parts is still present in Figure 5.39. When we further reduce the fractional-order of the system, chaotic phenomena disappear as shown in Figure 5.37 for $\nu = 0.5$. Finally, we analyze the bifurcation diagrams with the aim of clarifying the values of the system parameters for which the fractional Grassi-Miller map shows asymptotic stability, limit cycles or chaotic behaviors.

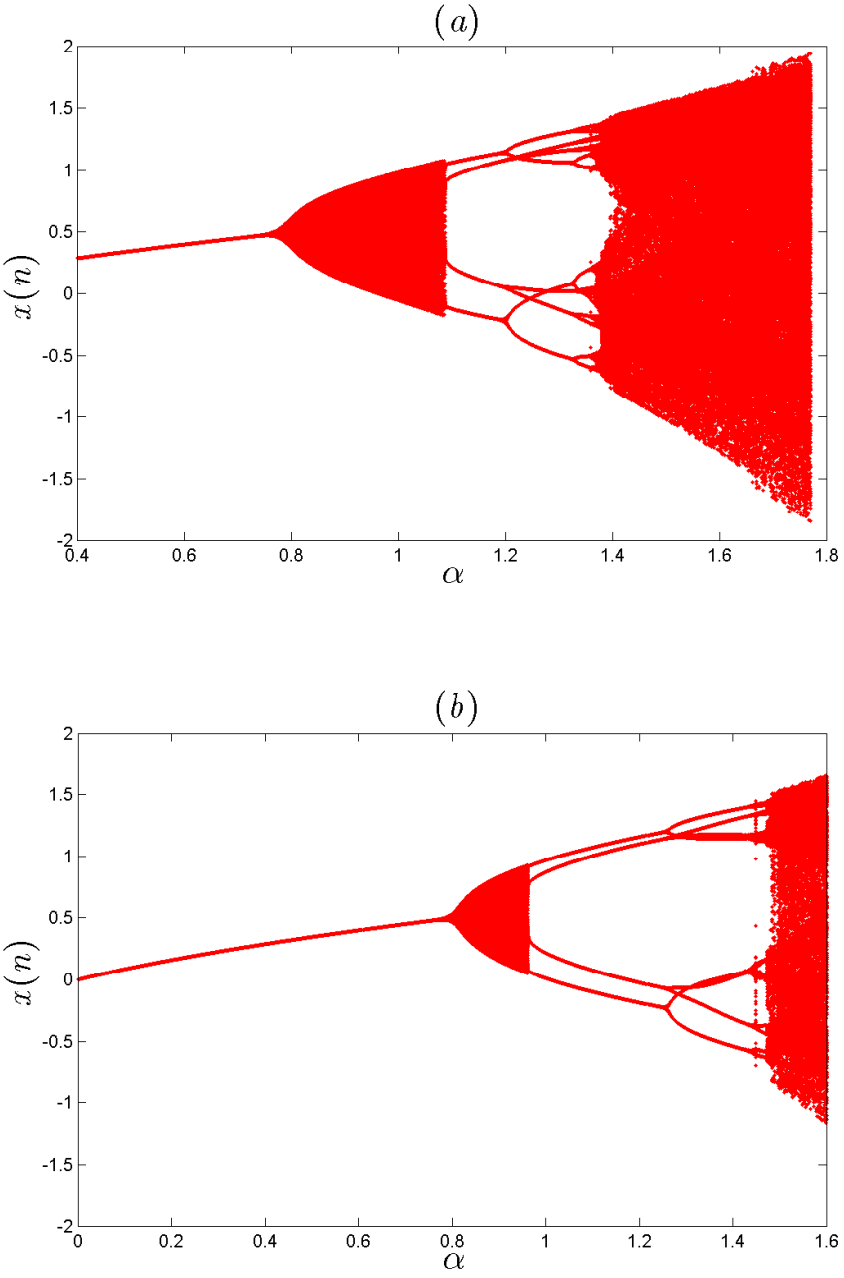

Figure 5.40: The bifurcation diagram versus α for: (a) $\nu = 0.98$, (b) $\nu = 0.88$.

By looking at Figure 5.40(a), which shows the bifurcation diagram obtained for $\nu = 0.98$, it is clear that the map has a stable equilibrium point until the parameter α reaches the value of 0.7. Then, when α assumes values between 0.8 and 0.9, the bifurcation diagram shows the typical shape that indicates the presence of chaotic behaviors. When the value $\alpha = 1$ is reached, the map is characterized by the presence of period-4 limit cycles. Successively, it can be noticed that the map shows period-8 limit cycles when the value $\alpha = 1.3$ is reached. By further increasing the value of α, chaotic behaviors are generated for $\alpha = 1.5$ and beyond. Similar considerations can be done for the bifurcation diagram reported in Figure 5.40(b) for $\nu = 0.88$.

Dynamics with order ν varying

Although the above analysis gives a clear idea of the dynamics of the proposed fractional map, a more comprehensive understanding of the map's dynamics may be obtained through visualizing the bifurcation diagrams and Lyapunov exponents as a function of the fractional order ν. In this last experiment, we keep the initial values as $[x(0), y(0), z(0)] = [1, 0.1, 0]$, set $\beta = 0.1$ and let the fractional order ν vary across the interval $[0, 1]$. Figure 5.41 shows the bifurcation diagrams and largest Lyapunov exponent (LLE) for $\alpha \in \{1.6, 1.5, 1.3\}$. First, for $\alpha = 1.6$, we obtain the results in the top row. Both diagrams show that when $0.92 \leq \nu \leq 1$, fractional map (5.18) generates a chaotic behavior as the LLE remains positive. A transient region is observed over the interval $0.916 \leq \nu \leq 0.92$ and then chaos is observed again until it eventually disappears as $\nu \leq 0.814$ and the states diverge towards infinity. Next, for $\alpha = 1.5$, the results are depicted in the middle row. We see that for $\nu \in [0.8, 1]$, the system exhibits a chaotic behavior along with periodic windows. The lowest fractional order that yields chaos is 0.8. Finally, for $\alpha = 1.3$, the bifurcation diagram and LLE for $\nu \in [0.75, 1]$ are depicted in the bottom row. As can be seen, the LLE diagram matches perfectly with the bifurcation diagram. The fractional Grassi-Miller map remains in periodic motion over the interval $[0.89, 1]$. However, when ν moves to the interval $[0.75, 0.89)$, we notice that the LLE alternates between positive and negative signs, which indicates that the periodic states become chaotic for certain values of ν. This analysis tells us that the minimum fractional order for which chaotic motion is observed depends on the system parameters.

0-1 test

To reflect more the sensitivity of the fractional map, the 0-1 test is considered. Figure 5.42 and 5.43, depict the results of the test for different values of fractional order ν and system parameter α, respectively, in which $[x(0), y(0), z(0)] = [0.5, 0.1, 0]$. In particular, Figure 5.18 depicts the trajectories of the translation function of the fractional Grassi–Miller (5.18) in the $p - q$ plane for $\nu = 0.98$ and $\beta = 0.1$ and by varying α. Clearly, Figure 5.42(a)-(b) and (c) depicts bounded trajectories, indicating that the reported fractional map is periodic. On the other hand, Figure 5.42(d) depicts Brownian–like trajectories, indicating that the suggested fractional map (5.18) is chaotic when $\alpha = 1.55$, which confirms very well the results in Figure 5.41.

Now we apply the 0-1 test by taking $\alpha = 1.3$, $\beta = 0.1$, and by varying the fractional order ν. Figure 5.43 depicts the trajectories of the translation function in the $p - q$ plane. Figure

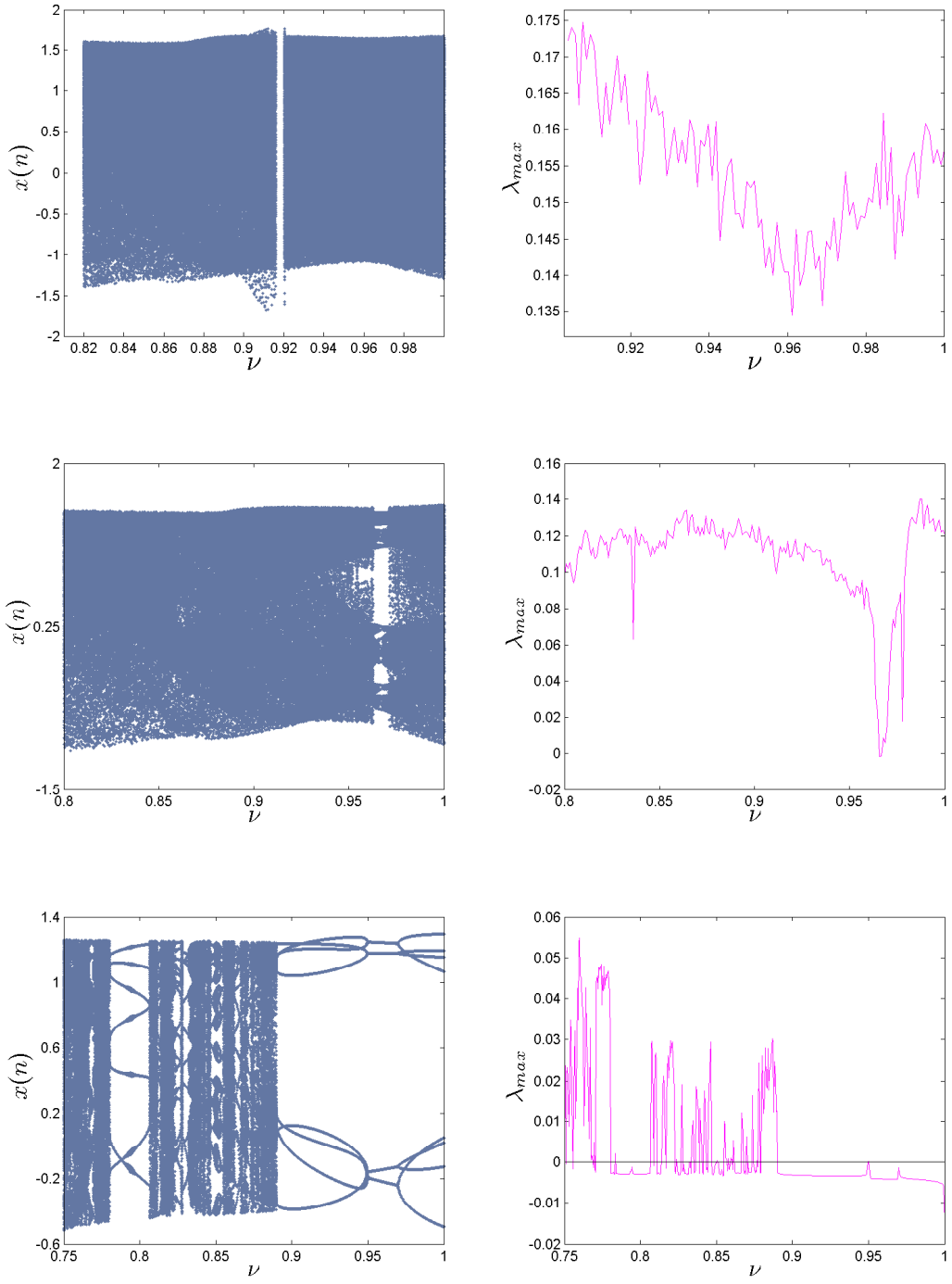

Figure 5.41: Bifurcation diagrams with ν as the critical parameter (left) along with the corresponding largest Lyapunov exponents (right) for different parameter values: $(\alpha, \beta) = (1.6, 0.1)$ (top), $(\alpha, \beta) = (1.5, 0.1)$ (middle), and $(\alpha, \beta) = (1.3, 0.1)$ (bottom).

5.43(a)-(b) depicts bounded like trajectories, indicating that the fractional Grassi–Miller map (5.18) is periodic when $\nu = 1$ and $\nu = 0.755$. When $\nu = 0.775$ the chaotic attractor is confirmed by the Brownian–like trajectories in Figure 5.43(c).

Numerical simulation have shown that the fractional Grassi-Miller map derived from the original integer-order Grassi-Miller map can exhibit chaos for a range of parameter and fractional order values. We have shown that even with a fractional order as low as $\nu = 0.5$, chaos still exists for specific parameters. Generally speaking, the proposed fractional map exhibits different types of attractors with fractional order-dependent chaotic regions. It is interesting that the system with integer-order is periodic, but chaos is observed with the decrease of the fractional-order ν.

5.8 Application of Caputo fractional difference operator on game theory model

Researcher's ever-growing interests in fractional calculus have led the ever-broadening applications in a lot of fields of science and engineering [142]. Referring to economics, a number of mathematical models describing different phenomena have been introduced. Namely, since fractional operators are non local, they are suitable for constructing models characterized by memory effect. This is the reason why fractional-order difference equations, when describing economic phenomena over large time periods of time, perform better with respect to integer-order discrete-time systems, respectively [143].

Very recently, attention has been focused on the presence of chaotic phenomena in economic systems described using integer-order difference or differential equations. Unlike continuous-time systems, very few papers regarding chaotic phenomena in economic systems described by discrete-time dynamics have been published to date. These economic systems, which usually involve concepts from Cournot game theory applied to oligopolistic markets, generate complex dynamics that lead to the existence of bifurcations and chaos [145]. The behaviors of an oligopoly game are much complicated because firms must consider not only the market demand, but also the strategies of the competitors. Our purpose here is to bring together two independent lines of research in applied mathematics and industrial economics: fractional-order difference equations and Cournot equilibria. We reconsider the Cournot problem in the light of the theory for long memory by proposing a fractional-order discrete Cournot game model with three firms producing differentiated products compete over a common market, which allows participants to make decisions while making full use of their historical information.

5.8.1 Fractional Cournot game model with long memory

To construct the Cournot game model, we have considered a monopolistic market where three firms produce different products. The inverse demand function is given by

$$p_i = \alpha - q_i - \beta \sum_{\substack{j=1 \\ j \neq i}}^{3} q_i, \quad i = 1, 2, 3, \tag{5.20}$$

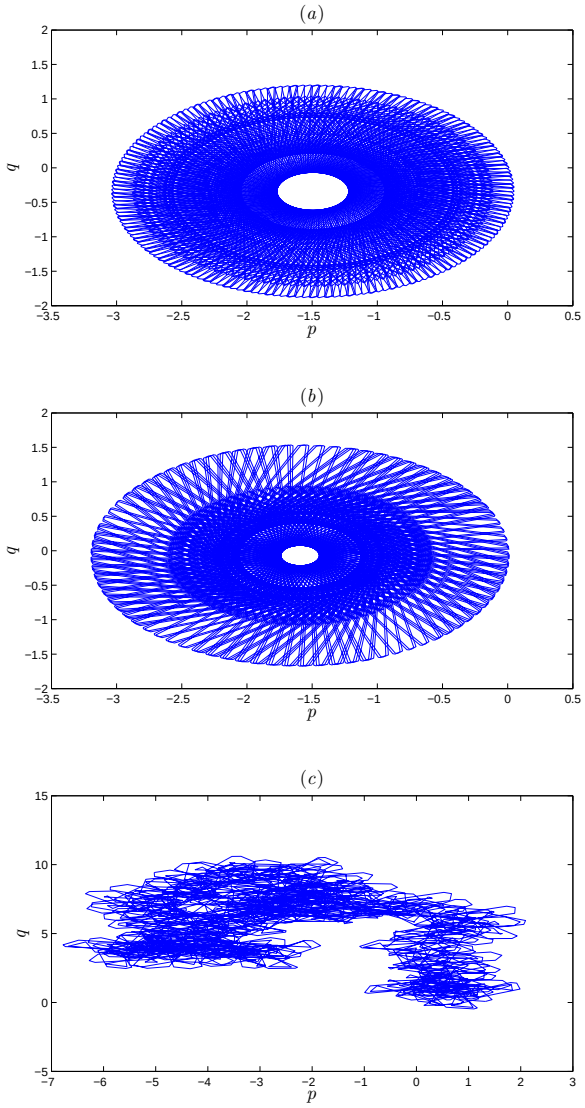

Figure 5.42: 0-1 test of the fractional Grassi–Miller map with $\nu = 0.98$ and $\beta = 0.1$: (a) bounded like trajectories for $\alpha = 0.7$, (b) bounded like trajectories for $\alpha = 1$, (c) bounded like trajectories for $\alpha = 1.375$, (d) Brownian–like trajectories for $\alpha = 1.55$.

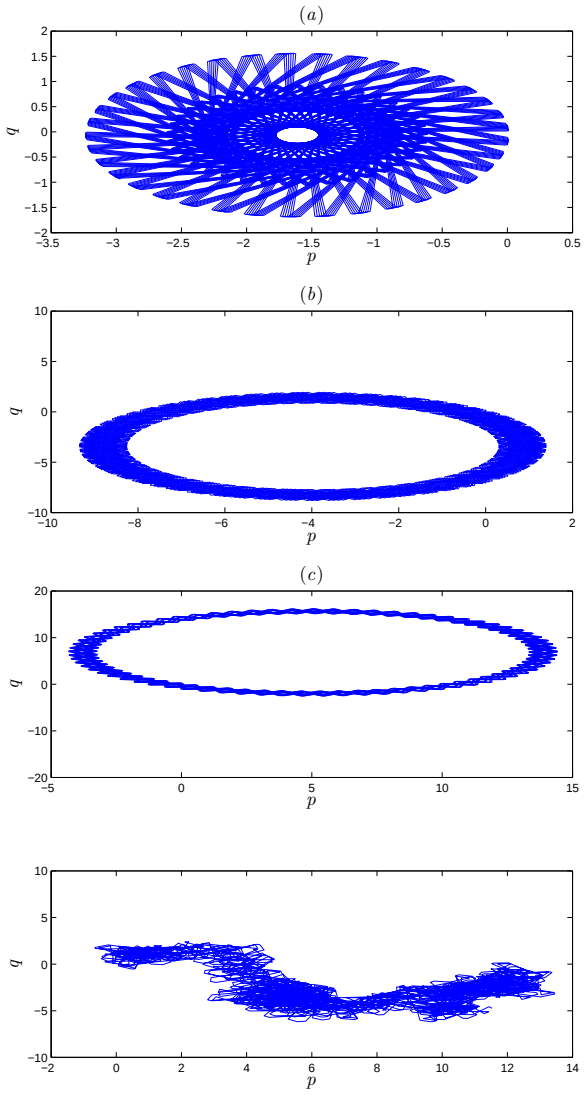

Figure 5.43: 0-1 test of the fractional Grassi–Miller map with $\alpha = 1.3$ and $\beta = 0.1$: (a) bouned like trajectories for $\nu = 1$, (b) bounded like trajectories for $\nu = 0.755$, (c) Brownian–like trajectories for $\nu = 0.775$.

in which q_i denote the outputs of products produced by the three firms, and the constants $\alpha > 0$, $0 < \beta < \sqrt{0.5}$ are the coefficients of the market demand function.
Now, assume that the cost function of these firms is proposed in the nonlinear form

$$C_i(q_i) = \gamma_i q_i + \delta_i \sum_{\substack{j=1 \\ j\neq i}}^{3} q_i q_j, \quad i = 1, 2, 3, \tag{5.21}$$

where γ_i and δ_i are two positive constants. In this setting, firms i relative profit is given by the difference between the absolute profit of the i firm and the sum of the other firms profit

$$\Pi_i(q_1, q_2, q_3) = \left[q_i \left(\alpha - q_i - \beta \sum_{\substack{j=1 \\ j\neq i}}^{3} q_i \right) - \gamma_i q_i - \delta_i \sum_{\substack{j=1 \\ j\neq i}}^{3} q_i q_j \right] - \sum_{\substack{j=1 \\ j\neq i}}^{3} p_j(q_1, q_2, q_3) q_j + C_j(q_j),\ i = 1, 2, 3. \tag{5.22}$$

Through substituting equation (5.20) and equation (5.21) into equation (5.22), the relative profit functions can be given as:

$$\begin{aligned}
\Pi_1(q_1, q_2, q_3) &= \alpha(q_1 - q_2 - q_3) - q_1^2 + q_2^2 + q_3^2 + 2\beta q_2 q_3 - \gamma_1 q_1 + \gamma_2 q_2 \\
&\quad + \gamma_3 q_3 - \delta_1(q_1 q_2 + q_1 q_3) + \delta_2(q_1 q_2 + q_2 q_3) + \delta_3(q_1 q_3 + q_2 q_3), \\
\Pi_2(q_1, q_2, q_3) &= \alpha(q_2 - q_1 - q_3) - q_2^2 + q_1^2 + q_3^2 + 2\beta q_1 q_3 - \gamma_2 q_2 + \gamma_1 q_1 \\
&\quad + \gamma_3 q_3 - \delta_2(q_1 q_2 + q_2 q_3) + \delta_1(q_1 q_2 + q_1 q_3) + \delta_3(q_1 q_3 + q_2 q_3), \\
\Pi_3(q_1, q_2, q_3) &= \alpha(q_3 - q_1 - q_2) - q_3^2 + q_1^2 + q_2^2 + 2\beta q_1 q_2 - \gamma_2 q_3 + \gamma_1 q_1 \\
&\quad + \gamma_2 q_2 - \delta_3(q_1 q_3 + q_2 q_3) + \delta_1(q_1 q_2 + q_1 q_3) + \delta_2(q_1 q_2 + q_2 q_3).
\end{aligned} \tag{5.23}$$

With this assumption, the maximizing profit is obtained by setting $\frac{\partial \Pi_i}{\partial q_i} = 0$. In order to construct the integer order dynamical system of this game, assume that each firm try to use information based on the marginal profit $\frac{\partial \Pi_i}{\partial q_i}$. The mathematical model is written as follows

$$q_i(n+1) = q_i(n) + \varepsilon_i q_i(n) \frac{\partial \Pi_i}{\partial q_i}, \ \ i = 1, 2, 3, \tag{5.24}$$

ε_i is a positive constant which is referring to the speed of adjustment. This game model agrees well with the model proposed by Al-Khedhairi, et al., which has been studied in [144].

Based on the dynamical system (5.24), we propose a new generalized model by introducing the Caputo–like difference operator on the system (5.24). Specifically, our main interest is to study the dynamics of three bounded rationality firms with relative profit maximization and long memory of output decision. The new game model with fractional difference operator is described by

$$\begin{aligned}
{}^{C}\Delta_a^{\nu} q_1(t) &= \varepsilon_1 q_1(t-1+\nu)(\alpha - \gamma_1 - 2q_1(t-1+\nu) \\
&\quad -(\zeta_1 - \zeta_2) q_2(t-1+\nu) - (\zeta_1 - \zeta_3) q_3(t-1+\nu)), \\
{}^{C}\Delta_a^{\nu} q_2(t) &= \varepsilon_2 q_2(t-1+\nu)(\alpha - \gamma_2 - 2q_2(t-1+\nu) \\
&\quad -(\zeta_2 - \zeta_1) q_1(t-1+\nu) - (\zeta_2 - \zeta_3) q_3(t-1+\nu)), \\
{}^{C}\Delta_a^{\nu} q_3(t) &= \varepsilon_3 q_3(t-1+\nu)(\alpha - \gamma_3 - 2q_3(t-1+\nu) \\
&\quad -(\zeta_3 - \zeta_1) q_1(t-1+\nu) - (\zeta_3 - \zeta_2) q_1(t-1+\nu)),
\end{aligned} \tag{5.25}$$

where $\nu \in (0,1]$and $\zeta_i = \beta + \delta_i$. To study the dynamics of the three bounded rationality with long memory we need to define the discrete version of the game model, for that we need to replace a by zero and q_i by x_i. According to Theorem 1.15 the equivalent discrete formula is defined by

$$\begin{cases} x_1(n) = x_1(0) + \frac{1}{\Gamma(\nu)} \sum_{j=1}^{n} \frac{\Gamma(n-j+\nu)}{\Gamma(n-j+1)} (\varepsilon_1 x_1(j-1)(\alpha - \gamma_1 \\ \qquad -2x_1(j-1) - \theta_{12} x_2(j-1) - \theta_{13} x_3(j-1))), \\ x_2(n) = x_2(0) + \frac{1}{\Gamma(\nu)} \sum_{j=1}^{n} \frac{\Gamma(n-j+\nu)}{\Gamma(n-j+1)} (\varepsilon_2 x_2(j-1)(\alpha - \gamma_2 \\ \qquad -2x_2(j-1) - \theta_{12} x_1(j-1) - \theta_{23} x_3(j-1))), \\ x_3(n) = x_3(0) + \frac{1}{\Gamma(\nu)} \sum_{j=1}^{n} \frac{\Gamma(n-j+\nu)}{\Gamma(n-j+1)} (\varepsilon_3 x_3(j-1)(\alpha - \gamma_3 \\ \qquad -2x_3(j-1) - \theta_{13} x_1(j-1) - \theta_{23} x_2(j-1))), \end{cases} \tag{5.26}$$

where $\theta_{ij} = \zeta_i - \zeta_j, \ \forall i,j = 1,2,3.$

5.8.2 Stability analysis

For calculating the equilibrium points of the fractional game model (5.25), we assign its left hand side to zero

$$\begin{cases} \varepsilon_1 x_1(\alpha - \gamma_1 - 2x_1 - \theta_{12} x_2 - \theta_{13} x_3) = 0, \\ \varepsilon_2 x_2(\alpha - \gamma_2 - 2x_2 - \theta_{12} x_1 - \theta_{23} x_3) = 0, \\ \varepsilon_3 x_3(\alpha - \gamma_3 - 2x_3 - \theta_{13} x_1 - \theta_{23} x_2) = 0. \end{cases} \tag{5.27}$$

By algebraic computation, we obtain the following fixed points:

$$\begin{gathered} F_1 = (0,0,0),\ F_2 = (0, 0.5(\alpha - \gamma_2), 0),\ F_3 = (0.5(\alpha - \gamma_1), 0, 0), F_4 = (0, 0, 0.5(\alpha - \gamma_3)), \\ F_5 = \left(\tfrac{2(\gamma_1 - \alpha) + \theta_{12}(\alpha - \gamma_2)}{\theta_{12}^2 + 4}, \tfrac{2(\alpha - \gamma_2) + \theta_{12}(\alpha - \gamma_1)}{\theta_{12}^2 + 4}, 0 \right), \\ F_6 = \left(0, \tfrac{2(\alpha - \gamma_2) + \theta_{12}(\gamma_3 - \alpha)}{\theta_{23}^2 + 4}, \tfrac{2(\alpha - \gamma_3) + \theta_{23}(\alpha - \gamma_2)}{\theta_{23}^2 + 4} \right), \\ F_7 = \left(\tfrac{2(\alpha - \gamma_1) + \theta_{13}(\gamma_3 - \alpha)}{\theta_{13}^2 + 4}, 0, \tfrac{2(\alpha - \gamma_3) + \theta_{13}(\alpha - \gamma_1)}{\theta_{13}^2 + 4} \right), \\ F_8 = (A_1, A_2, A_3), \end{gathered} \tag{5.28}$$

in which

$$A_1 = \frac{(\alpha - \gamma_3)(\theta_{12}\theta_{23} - 2\theta_{13}) - (\alpha - \gamma_2)(\theta_{13}\theta_{23} + 2\theta_{12}) + (\alpha - \gamma_1)(\theta_{23}^2 + 4)}{2(\theta_{13}^2 + \theta_{23}^2 + \theta_{12}^2 + 4)},$$

$$A_2 = \frac{-(\alpha - \gamma_3)(\theta_{12}\theta_{13} + 2\theta_{23}) + (\alpha - \gamma_2)(\theta_{13}^2 + 4) + (\alpha - \gamma_1)(-\theta_{13}\theta_{23} + 2\theta_{12})}{2(\theta_{13}^2 + \theta_{23}^2 + \theta_{12}^2 + 4)},$$

$$A_3 = \frac{(\alpha - \gamma_3)(\theta_{23}^2 + 4) + (\alpha - \gamma_2)(-\theta_{12}\theta_{13} + 2\theta_{23}) + (\alpha - \gamma_1)(\theta_{12}\theta_{23} + 2\theta_{13})}{2(\theta_{13}^2 + \theta_{23}^2 + \theta_{12}^2 + 4)}.$$

The Jacobian matrix of the fractional order difference equations (5.25) at an arbitrary point (x_1, x_2, x_3), is defined by:

$$M(x_1, x_2, x_3) = \begin{pmatrix} D_1 - 2\varepsilon_1 x_1 & -\varepsilon_1 \theta_{12} x_1 & -\varepsilon_1 \theta_{13} x_1 \\ \varepsilon_2 \theta_{12} x_2 & D_2 - 2\varepsilon_2 x_2 & -\varepsilon_2 \theta_{23} x_2 \\ \varepsilon_3 \theta_{13} x_3 & \varepsilon_3 \theta_{23} x_3 & D_3 - 2\varepsilon_3 x_3 \end{pmatrix}, \tag{5.29}$$

where

$$D_1 = \varepsilon_1(\alpha - \gamma_1 - 2x_1 - \theta_{12}x_2 - \theta_{13}x_3),$$
$$D_2 = \varepsilon_2(\alpha - \gamma_2 - 2x_2 + \theta_{12}x_1 - \theta_{23}x_3),$$
$$D_3 = \varepsilon_3(\alpha - \gamma_3 - 2x_3 + \theta_{13}x_1 + \theta_{23}x_2).$$

To investigate the stability of the fixed points we shall use the following theorem:

Theorem 5.1. *[105] Let x_f be a fixed point of a fractional difference system ${}^{C}\Delta_a^{\nu}F(t) = F(x(t+\nu-1))$ where $x(t) = (x_1(t), x_2(t), .., x_n(t))^T$, and $J(x^f) = \frac{\partial f(x)}{\partial x}\Big|_{x=x^f}$ is the Jacobian matrix at the fixed point x_f. The fixed point x_f is asymptotically stable when all the eigenvalues $(\lambda_i,\ i = 1, .., n)$ of J verifies:*

$$\lambda_i \in \left\{ z \in \mathbb{C} : |z| < \left(2\cos\frac{|\arg z| - \pi}{2-\nu}\right)^{\nu} \quad and \quad |\arg z| > \frac{\mathring{}\beta}{2} \right\},\ \forall i = 1, .., n. \tag{5.30}$$

Now, we turn to investigate the stability of the previous fixed points.

Proposition 22. The fixed point $F_1 = (0, 0, 0)$ is asymptotically stable if the fractional order ν and the game parameters satisfies:

$$\nu > log_2|\varepsilon_i(\alpha - \gamma_i)|, \quad and \quad \alpha < \gamma_i,\ \ i = 1, 2, 3. \tag{5.31}$$

Proof. The Jacobian matrix (5.29) at the fixed point $F_1 = (0, 0, 0)$ can be easily computed as:

$$M_{F_1} = \begin{pmatrix} \varepsilon_1(\alpha - \gamma_1) & 0 & 0 \\ 0 & \varepsilon_2(\alpha - \gamma_2) & 0 \\ 0 & 0 & \varepsilon_3(\alpha - \gamma_3) \end{pmatrix}. \tag{5.32}$$

The associated characteristic equation is defined by:

$$(\varepsilon_1(\alpha - \gamma_1) - \lambda) \times (\varepsilon_2(\alpha - \gamma_2) - \lambda) \times (\varepsilon_3(\alpha - \gamma_3) - \lambda) = 0. \tag{5.33}$$

The Eigenvalues are:

$$\lambda_1 = \varepsilon_1(\alpha - \gamma_1),\ \lambda_2 = \varepsilon_2(\alpha - \gamma_2),\ \lambda_3 = \varepsilon_3(\alpha - \gamma_3).$$

Based on Theorem. 5.1, it is easy to show that the fixed point $F_1 = (0, 0, 0)$ is always asymptotically stable when $\nu > log_2|\varepsilon_i(\alpha - \gamma_i)|$ and $\alpha < \gamma_i\ \forall i = 1, 2, 3$. □

Proposition 23. The conditions of asymptotic stability of the fixed point $F_2 = (0, 0.5(\alpha - \gamma_2), 0)$ are:

- If $\alpha > \gamma_2$ and $\nu > log_2|\varepsilon_2(\gamma_2 - \alpha)|$.
- If $\gamma_1 > \alpha + 0.5\theta_{12}(\gamma_2 - \alpha)$ and $\nu > log_2|\varepsilon_1(\alpha - \gamma_1 + 0.5\theta_{12}(\gamma_2 - \alpha))|$.
- If $\gamma_3 > \alpha + 0.5\theta_{23}(\alpha - \gamma_2)$ and $\nu > log_2|\varepsilon_3(\alpha - \gamma_3 + 0.5\theta_{23}(\alpha - \gamma_2))|$.

Proof. The Jacobian matrix (5.29) at the fixed point $F_2 = (0, 0.5(\alpha - \gamma_2), 0)$ can be easily computed as:

$$M_{F_1} = \begin{pmatrix} \varepsilon_1(\alpha - \gamma_1 - 0.5\theta_{12}(\alpha - \gamma_2)) & 0 & 0 \\ 0.5\theta_{12}\varepsilon_2(\alpha - \gamma_2)) & \varepsilon_2(\gamma_2 - \alpha) & 0 \\ 0 & 0 & \varepsilon_3(\alpha - \gamma_3)(1 + 0.5\theta_{23}) \end{pmatrix}. \tag{5.34}$$

The eigenvalues are:

$$\lambda_1 = \varepsilon_1(\alpha - \gamma_1) + 0.5\varepsilon_1\theta_{12}(\gamma_2 - \alpha)\,, \lambda_2 = \varepsilon_2(\gamma_2 - \alpha), \lambda_3 = \varepsilon_3(\alpha - \gamma_3) + 0.5\varepsilon_3\theta_{23}(\alpha - \gamma_2).$$

Therefore, the eigenvalue $\{\lambda_1, \lambda_2, \lambda_3\}$ ensure the condition (5.30) in Theorem 5.1. □

Using the same steps, we obtain the following results.

Proposition 24. The conditions of asymptotic stability of the fixed point $F_3 = (0.5(\alpha - \gamma_2), 0, 0)$ are:

- If $\alpha > \gamma_1$ and $\nu > log_2|\varepsilon_1(\gamma_1 - \alpha)|$.
- If $\gamma_2 > \alpha + 0.5\theta_{12}(\alpha - \gamma_1)$ and $\nu > log_2|\varepsilon_2(\alpha - \gamma_2 + 0.5\theta_{12}(\alpha - \gamma_1))|$.
- If $\gamma_3 > \alpha + 0.5\theta_{13}(\alpha - \gamma_1)$ and $\nu > log_2|\varepsilon_3(\alpha - \gamma_3 + 0.5\theta_{13}(\alpha - \gamma_1))|$.

Proposition 25. The conditions of asymptotic stability of the fixed point $F_4 = (0, 0, 0.5(\alpha - \gamma_2))$ are

- If $\alpha > \gamma_3$ and $\nu > log_2|\varepsilon_3(\gamma_3 - \alpha)|$.
- If $\gamma_1 > \alpha + 0.5\theta_{13}(\gamma_3 - \alpha)$ and $\nu > log_2|\varepsilon_1(\alpha - \gamma_1 + 0.5\theta_{13}(\gamma_3 - \alpha))|$.
- If $\gamma_2 > \alpha + 0.5\theta_{23}(\gamma_3 - \alpha)$ and $\nu > log_2|\varepsilon_2(\alpha - \gamma_2 + 0.5\theta_{23}(\gamma_3 - \alpha))|$.

Proposition 26. The conditions of asymptotic stability of the fixed point $F_5 = \left(\frac{2(\gamma_1-\alpha)+\theta_{12}(\alpha-\gamma_2)}{\theta_{12}^2+4}, \frac{2(\alpha-\gamma_2)+\theta_{12}(\alpha-\gamma_1)}{\theta_{12}^2+4}, 0\right)$ are

- If $\left[\alpha - \gamma_3 - \theta_{12}\frac{2(\gamma_1-\alpha)+\theta_{12}(\alpha-\gamma_2)}{\theta_{12}^2+4} - \theta_{13}\frac{2(\alpha-\gamma_2)+\theta_{12}(\alpha-\gamma_1)}{\theta_{12}^2+4}\right] < 0$ and $\nu > log_2\left|\varepsilon_3\left(\alpha - \gamma_3 - \theta_{12}\frac{2(\gamma_1-\alpha)+\theta_{12}(\alpha-\gamma_2)}{\theta_{12}^2+4} - \theta_{13}\frac{2(\alpha-\gamma_2)+\theta_{12}(\alpha-\gamma_1)}{\theta_{12}^2+4}\right)\right|$.
- If $-\frac{G}{2} \geq \sqrt{H}$ and $\nu > \log_2 \frac{\sqrt{|G^2-4H|}-G}{2}$ where

$$\begin{aligned} G = {} & \varepsilon_1\left(\alpha - \gamma_1 - 4\frac{2(\gamma_1-\alpha)+\theta_{12}(\alpha-\gamma_2)}{\theta_{12}^2+4} - \theta_{12}\frac{2(\alpha-\gamma_2)+\theta_{12}(\alpha-\gamma_1)}{\theta_{12}^2+4}\right) \\ & + \varepsilon_2\left(\alpha - \gamma_2 - 4\frac{2(\alpha-\gamma_2)+\theta_{12}(\alpha-\gamma_1)}{\theta_{12}^2+4} + \theta_{12}\frac{2(\gamma_1-\alpha)+\theta_{12}(\alpha-\gamma_2)}{\theta_{12}^2+4}\right), \end{aligned}$$

$$\begin{aligned} H = {} & \varepsilon_1\left(\alpha - \gamma_1 - 4\frac{2(\gamma_1-\alpha)+\theta_{12}(\alpha-\gamma_2)}{\theta_{12}^2+4} - \theta_{12}\frac{2(\alpha-\gamma_2)+\theta_{12}(\alpha-\gamma_1)}{\theta_{12}^2+4}\right) \\ & \times\varepsilon_2\left(\alpha - \gamma_2 - 4\frac{2(\alpha-\gamma_2)+\theta_{12}(\alpha-\gamma_1)}{\theta_{12}^2+4}\right. \\ & \left. + \theta_{12}\frac{2(\gamma_1-\alpha)+\theta_{12}(\alpha-\gamma_2)}{\theta_{12}^2+4}\right) - \varepsilon_1\varepsilon_2\theta_{12}^2\frac{2(\gamma_1-\alpha)+\theta_{12}(\alpha-\gamma_2)}{\theta_{12}^2+4} \times \frac{2(\alpha-\gamma_2)+\theta_{12}(\alpha-\gamma_1)}{\theta_{12}^2+4}. \end{aligned}$$

Proposition 27. The conditions of asymptotic stability of the fixed point $F_6 = \left(0, \frac{2(\alpha-\gamma_2)+\theta_{12}(\gamma_3-\alpha)}{\theta_{23}^2+4}, \frac{2(\alpha-\gamma_3)+\theta_{23}(\alpha-\gamma_2)}{\theta_{23}^2+4}\right)$ are

- $\left[\alpha-\gamma_1-\theta_{12}\frac{2(\alpha-\gamma_2)+\theta_{23}(\gamma_3-\alpha)}{\theta_{23}^2+4}-\theta_{13}\frac{2(\alpha-\gamma_3)+\theta_{23}(\alpha-\gamma_2)}{\theta_{23}^2+4}\right]<0$ and $\nu > log_2\left|\varepsilon_1\left(\alpha-\gamma_1-\theta_{12}\frac{2(\alpha-\gamma_2)+\theta_{23}(\gamma_3-\alpha)}{\theta_{23}^2+4}-\theta_{13}\frac{2(\alpha-\gamma_3)+\theta_{23}(\alpha-\gamma_2)}{\theta_{23}^2+4}\right)\right|$.
- If $-\frac{I}{2} \geq \sqrt{J}$ and $\nu > \log_2 \frac{\sqrt{|I^2-4J|}-I}{2}$ where

$$I = \varepsilon_2\left(\alpha-\gamma_3-4\frac{2(\alpha-\gamma_2)+\theta_{23}(\gamma_3-\alpha)}{\theta_{23}^2+4}-\theta_{23}\frac{2(\alpha-\gamma_3)+\theta_{23}(\alpha-\gamma_2)}{\theta_{23}^2+4}\right)+\varepsilon_3\left(\alpha-\gamma_3-4\frac{2(\alpha-\gamma_3)+\theta_{23}(\alpha-\gamma_2)}{\theta_{23}^2+4}+\theta_{23}\frac{2(\alpha-\gamma_2)+\theta_{23}(\gamma_3-\alpha)}{\theta_{23}^2+4}\right),$$

$$J = \varepsilon_2\left(\alpha-\gamma_3-4\frac{2(\alpha-\gamma_2)+\theta_{23}(\gamma_3-\alpha)}{\theta_{23}^2+4}-\theta_{23}\frac{2(\alpha-\gamma_3)+\theta_{23}(\alpha-\gamma_2)}{\theta_{23}^2+4}\right)+\varepsilon_3\left(\alpha-\gamma_3-4\frac{2(\alpha-\gamma_3)+\theta_{23}(\alpha-\gamma_2)}{\theta_{23}^2+4}+\theta_{23}\frac{2(\alpha-\gamma_2)+\theta_{23}(\gamma_3-\alpha)}{\theta_{23}^2+4}\right)-\varepsilon_3\varepsilon_2\theta_{23}^2\frac{2(\alpha-\gamma_2)+\theta_{23}(\gamma_3-\alpha)}{\theta_{23}^2+4}\times\frac{2(\alpha-\gamma_3)+\theta_{23}(\alpha-\gamma_2)}{\theta_{23}^2+4}.$$

Proposition 28. The conditions of asymptotic stability of the fixed point $F_7 = \left(\frac{2(\alpha-\gamma_1)+\theta_{13}(\gamma_3-\alpha)}{\theta_{13}^2+4}, 0, \frac{2(\alpha-\gamma_3)+\theta_{13}(\alpha-\gamma_1)}{\theta_{13}^2+4}\right)$ are:

- $\left[\alpha-\gamma_2+\theta_{12}\frac{2(\alpha-\gamma_1)+\theta_{13}(\gamma_3-\alpha)}{\theta_{13}^2+4}-\theta_{23}\frac{2(\alpha-\gamma_3)+\theta_{13}(\alpha-\gamma_2)}{\theta_{23}^2+4}\right]<0$ and $\nu > log_2\left|\varepsilon_1\left(\alpha-\gamma_1-\theta_{12}\frac{2(\alpha-\gamma_2)+\theta_{23}(\gamma_3-\alpha)}{\theta_{23}^2+4}-\theta_{13}\frac{2(\alpha-\gamma_3)+\theta_{13}(\alpha-\gamma_1)}{\theta_{23}^2+4}\right)\right|$.
- If $-\frac{L}{2} \geq \sqrt{O}$ and $\nu > \log_2 \frac{\sqrt{|L^2-4O|}-L}{2}$ where

$$L = \varepsilon_2\left(\alpha-\gamma_2-4\frac{2(\alpha-\gamma_1)+\theta_{13}(\gamma_3-\alpha)}{\theta_{13}^2+4}-\theta_{23}\frac{2(\alpha-\gamma_3)+\theta_{13}(\alpha-\gamma_1)}{\theta_{13}^2+4}\right)+\varepsilon_3\left(\alpha-\gamma_3-4\frac{2(\alpha-\gamma_3)+\theta_{13}(\alpha-\gamma_1)}{\theta_{13}^2+4}+\theta_{13}\frac{2(\alpha-\gamma_1)+\theta_{13}(\gamma_3-\alpha)}{\theta_{13}^2+4}\right),$$

$$O = \varepsilon_2\left(\alpha-\gamma_2-4\frac{2(\alpha-\gamma_1)+\theta_{13}(\gamma_3-\alpha)}{\theta_{13}^2+4}-\theta_{23}\frac{2(\alpha-\gamma_3)+\theta_{13}(\alpha-\gamma_1)}{\theta_{13}^2+4}\right)+\varepsilon_3\left(\alpha-\gamma_3-4\frac{2(\alpha-\gamma_3)+\theta_{13}(\alpha-\gamma_1)}{\theta_{13}^2+4}+\theta_{13}\frac{2(\alpha-\gamma_1)+\theta_{13}(\gamma_3-\alpha)}{\theta_{13}^2+4}\right)-\varepsilon_2\varepsilon_3\theta_{23}^2\frac{2(\alpha-\gamma_1)+\theta_{13}(\gamma_3-\alpha)}{\theta_{13}^2+4}\times\frac{2(\alpha-\gamma_3)+\theta_{13}(\alpha-\gamma_1)}{\theta_{13}^2+4}.$$

5.8.3 Bifurcation analysis and numerical simulation

Numerical experiments are simulated in this part to show the different route to chaos of the fractional triopoly game (5.25). Its phase portraits, bifurcation diagrams and maximum Lyapunov exponents (MLE) were investigated under different levels of parameters and fractional orders. As explained in [144], there is a stable closed invariant curve around the Nash fixed point $F_8 = (0.8882, 0.4283.0831)$. For instance, when selecting parameters $\alpha = 2, \varepsilon_1 = 1.042811791, \varepsilon_2 = 1.1, \varepsilon_3 = 1.1, \zeta_1 = 0.4, \zeta_2 = 0.8, \zeta_3 = 0.1, \gamma_1 = 0.07, \gamma_2 = 0.03, \gamma_3 = 0.4$ and initial values $x_1(0) = 0.4$, $x_2(0) = 0.2$, $x_3(0) = 0.4$, the stable closed invariant curve on $x_2 - x_3$ plane is represented in Figure 5.44(a). The closed invariant curve is expanded as shown in Figure 5.44. It verifies that the closed invariant curve is affected by the fractional order ν and a chaotic attractor is observed at $\nu = 0.81$. To further observe the dynamical behavior, the system parameters

are fixed as above and the fractional order ν is varied in the range $[0.72, 1]$. Figure 5.45 shows the bifurcation diagram and the maximum Lyapunov exponents of the first player output $x_1(n)$. It shows that the long memory system begins from periodic states where the maximum Lyapunov exponent equal to zero, and then it exhibits chaos at 0.8257. Figures 5.44 and 5.45 shows the strong effect of the long memory on the stability of the equilibrium $F_8 = (0.8882, 0.4283.0831)$. More precisely, the complexity of the model increases around the Nash fixed point and chaos appears as ν decreases. Figures 5.44 and 5.45 shows the strong effect of the long memory on

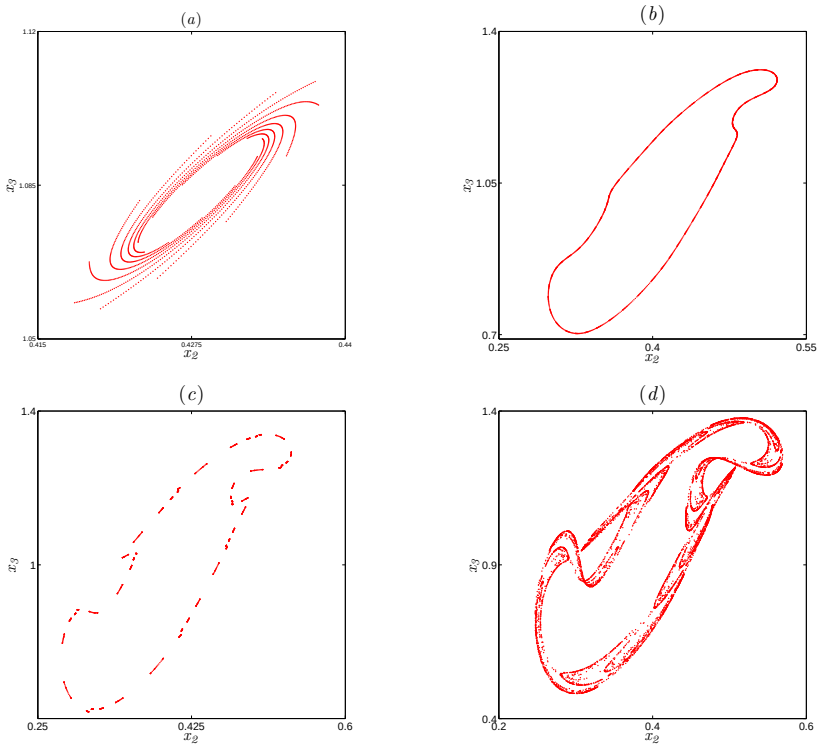

Figure 5.44: The phase portraits of game (5.25) with parameter values $\alpha = 2, \varepsilon_1 = 1.042811791, \varepsilon_2 = 1.1, \varepsilon_3 = 1.1, \zeta_1 = 0.4, \zeta_2 = 0.8, \zeta_3 = 0.1, \gamma_1 = 0.07, \gamma_2 = 0.03, \gamma_3 = 0.4$ for different fractional order values: (a) $\nu = 1, (b)\, \nu = 0.9, (c)\, \nu = 0.865, (d)\, \nu = 0.81$

the stability of the equilibrium $F_8 = (0.8882, 0.4283.0831)$. More precisely, the complexity of the model increases around the Nash fixed point and chaos appears as ν decreases.

Figure 5.46 show the bifurcation diagram with respect to the adjustment parameter ε_1 when $\alpha = 2, \varepsilon_2 = 1.1, \varepsilon_3 = 1.1, \zeta_1 = 0.4, \zeta_2 = 0.8, \zeta_3 = 0.1, \gamma_1 = 0.07, \gamma_2 = 0.03, \gamma_3 = 0.4$. Figure 5.46-(a) and 5.46-(b) are the bifurcation diagrams for $\nu = 0.985$ and $\nu = 0.972$, respectively. As one can see, the two diagrams are similar. A stable Nash fixed point is observed as ε_1 increases from 1 to 1.02 for $\nu = 0.985$ and when ε_1 increases from 1 to 1.007 for $\nu = 0.972$. We can observe that whenever we increased the value of ε_1 the Cournot Nash fixed point losses its stability via

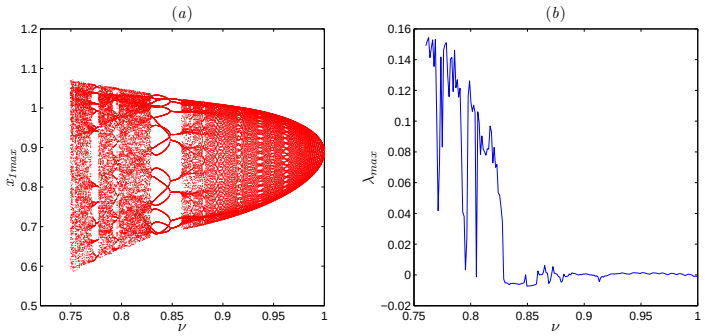

Figure 5.45: (a) Bifurcation diagram versus ν when $\alpha = 2, \varepsilon_1 = 1.042811791, \varepsilon_2 = 1.1, \varepsilon_3 = 1.1, \zeta_1 = 0.4, \zeta_2 = 0.8, \zeta_3 = 0.1, \gamma_1 = 0.07, \gamma_2 = 0.03, \gamma_3 = 0.4$. (b) The maximum Lyapunov exponents with respect to ν corresponding to (a).

Neimark-sacker bifurcation. Moreover, we observe that decreasing the value of the fractional order lead to the disappearance of the chaotic region. When $\nu = 0.985$ the model (5.25) exhibits chaotic behavior at $\varepsilon_1 \in [1.37, 1.443[\cup[1.461.468]$ and for $\nu = 0.972$ the model (5.25) exhibits chaotic behavior for $\varepsilon_1 \in]1.38, 1.431]$. Therefore, it is possible to initially conclude that the speed of adjustment of the first player disestablish the dynamic of the market and make it unpredictable.

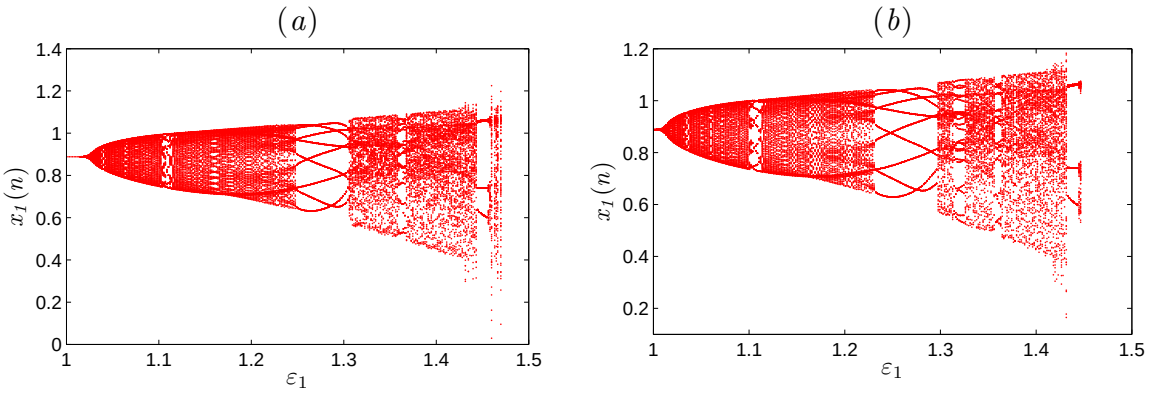

Figure 5.46: (a) Bifurcation diagram versus ε_1 with order $\nu = 0.985$ when $\alpha = 2, \varepsilon_2 = 1.1, \varepsilon_3 = 1.1, \zeta_1 = 0.4, \zeta_2 = 0.8, \zeta_3 = 0.1, \gamma_1 = 0.07, \gamma_2 = 0.03, \gamma_3 = 0.4$. (b) Bifurcation diagram versus ε_1 with order $\nu = 0.972$.

For better observation, we choose to discuss the chaos of the fractional triopoly game for

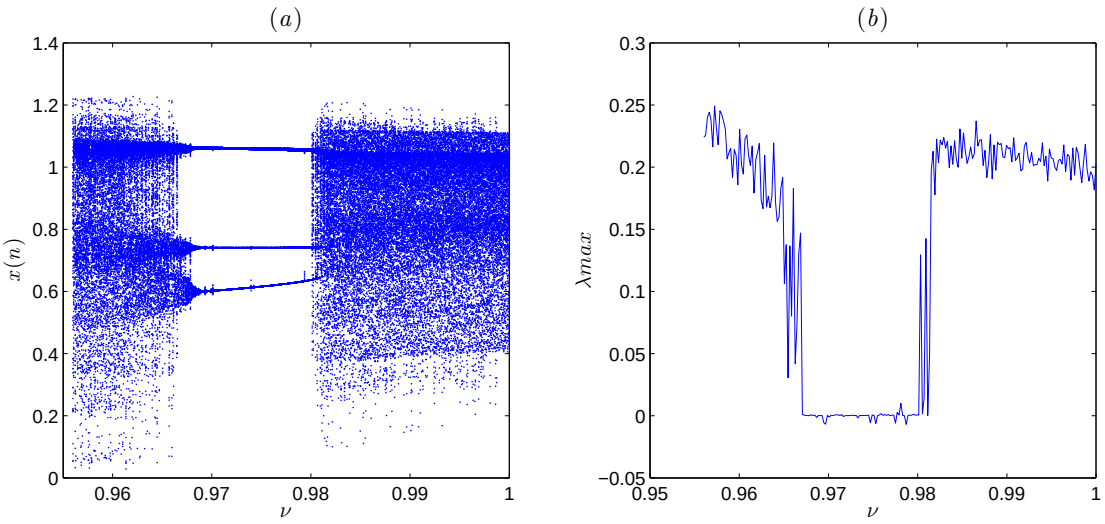

Figure 5.47: (a) Bifurcation diagram versus ν when $\alpha = 2, \varepsilon_1 = 1.44, \varepsilon_2 = 1.1, \varepsilon_3 = 1.1, \zeta_1 = 0.4, \zeta_2 = 0.8, \zeta_3 = 0.1, \gamma_1 = 0.07, \gamma_2 = 0.03, \gamma_3 = 0.4$. (b) The maximum Lyapunov exponents with respect to ν corresponding to (a).

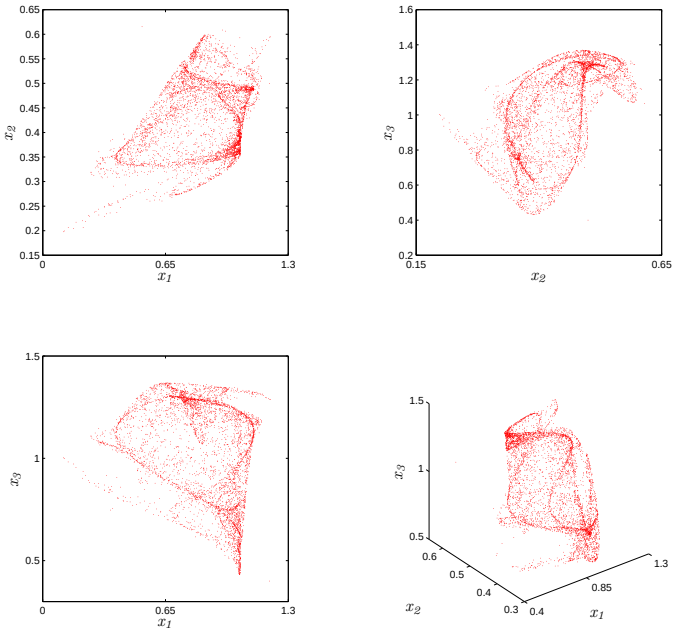

Figure 5.48: Chaotic attractor of the proposed game with $\nu = 0.98$ and for $\alpha = 2, \varepsilon_1 = 1.44, \varepsilon_2 = 1.1, \varepsilon_3 = 1.1, \zeta_1 = 0.4, \zeta_2 = 0.8, \zeta_3 = 0.1, \gamma_1 = 0.07, \gamma_2 = 0.03, \gamma_3 = 0.4$.

$\varepsilon_1 = 1.44$, with ν varying from 0.95 to 1 by the step size $\Delta\nu = 0.6 \times 10^{-4}$. Figure 5.47 shows the bifurcation diagram of x_1 versus ν and the MLE diagram. It illustrates that the states of the long memory system are different as ν decreases. When $\nu \in [0.9562, 0.9673[\cup[0.9809, 1]$ this model is chaotic, where the maximum Lyapunov exponent is positive, and when $\nu \in [0.9562, 0.9809]$ the model is periodic. These results indicate that the long memory decrease the speed of adjustment of the first firm. The chaotic attractor when $\nu = 0.98$ is plotted as shown in Figure 5.48. On the other hand, the periodic behaviour of the proposed system is reported in Figure 5.49 for $\nu = 0.975$, whereas the chaotic attractor obtained for $\nu = 0.96$ is shown in Figure 5.50. Clearly, Figure 5.48, Figure 5.49 and Figure 5.50 confirm both the shape of the bifurcation diagram reported in Figure 5.47(a) and the plot of the maximum Lyapunov exponent reported in Figure 5.47(b).

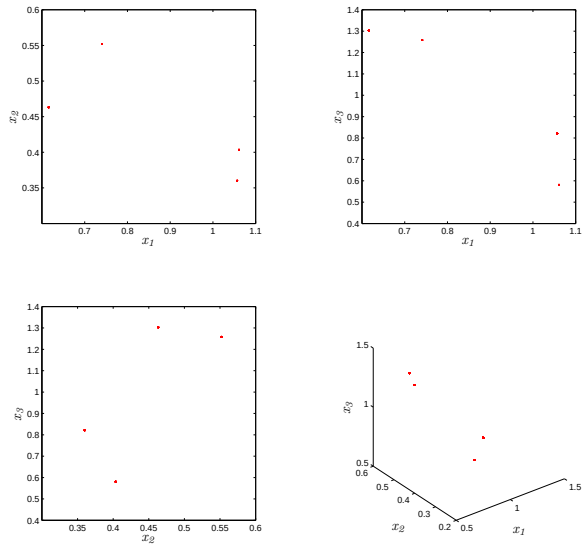

Figure 5.49: Periodic attractor of the proposed game with $\nu = 0.975$ and for $\alpha = 2, \varepsilon_1 = 1.44, \varepsilon_2 = 1.1, \varepsilon_3 = 1.1, \zeta_1 = 0.4, \zeta_2 = 0.8, \zeta_3 = 0.1, \gamma_1 = 0.07, \gamma_2 = 0.03, \gamma_3 = 0.4$.

In [144], Al-kheidari et al showed that for the parameters $\alpha = 1, \varepsilon_2 = 0.9, \varepsilon_3 = 0.9, \zeta_1 = 0.4, \zeta_2 = 0.8, \zeta_3 = 0.1, \gamma_1 = 0.07, \gamma_2 = 0.03, \gamma_3 = 0.4$, a flip bifurcation was observed at $\varepsilon_1 = 2.305628076$ where the equilibrium $F_8 = (0.4451, 0.2384, 0.4502)$ loses its stability . The bifurcation diagram of the first player output $x_1(n)$ versus ε_1 is illustrated in Figure 5.51. Figure 5.51-(a) shows that the Nash equilibrium point undergoes flip bifurcation and period doubling route to chaos. By reducing the value of ν to 0.7635, we obtain the bifurcation diagram shown in Figure 5.51-(b). It was found that chaotic motion exists in the range $\varepsilon_1 \in]2.689, 3]$ with periodic windows at 2.873. The chaotic area increases when $\nu = 0.7635$ as shown in Figure 7.6-(b). In order to confirm the shape of the bifurcation diagram reported in Figure 5.51-(b), we have investigated the system behaviour when $\varepsilon_1 = 2.6$ and $\varepsilon_1 = 2.9$. Namely, Figure 5.52 highlights

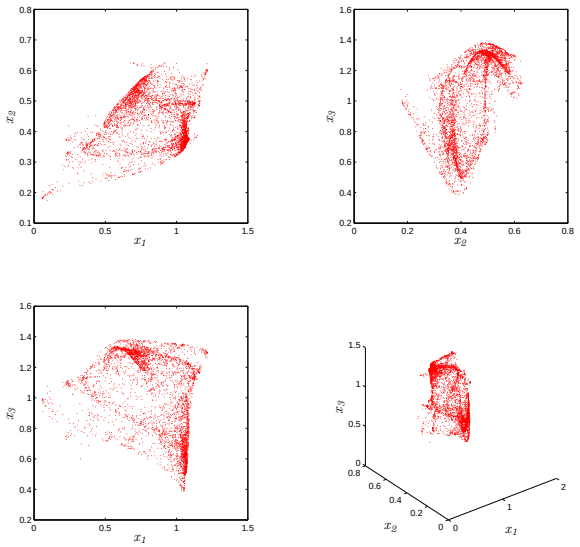

Figure 5.50: Chaotic attractor of the proposed game with $\nu = 0.96$ and for $\alpha = 2, \varepsilon_1 = 1.44, \varepsilon_2 = 1.1, \varepsilon_3 = 1.1, \zeta_1 = 0.4, \zeta_2 = 0.8, \zeta_3 = 0.1, \gamma_1 = 0.07, \gamma_2 = 0.03, \gamma_3 = 0.4$.

the period behaviour of the system obtained for $\varepsilon_1 = 2.6$. The simulation results demonstrate that the long memory increases the speed of adjustment of the first player and the game losses its stability faster.

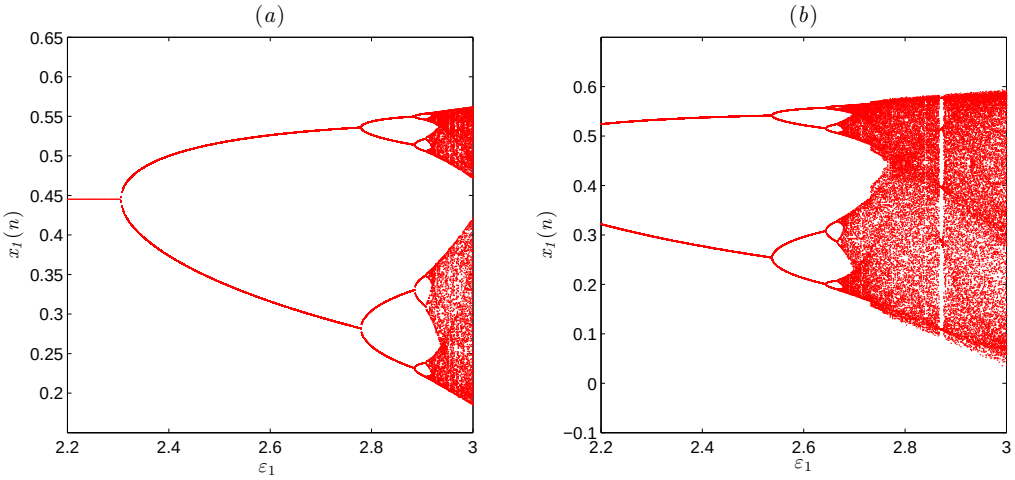

Figure 5.51: (a) Bifurcation diagram versus ε_1 with order $\nu = 1$ when $\alpha = 1, \varepsilon_2 = 0.9, \varepsilon_3 = 0.9, \zeta_1 = 0.4, \zeta_2 = 0.8, \zeta_3 = 0.1, \gamma_1 = 0.07, \gamma_2 = 0.03, \gamma_3 = 0.4$ (b) Bifurcation diagram versus ε_1 with order $\nu = 0.7635$.

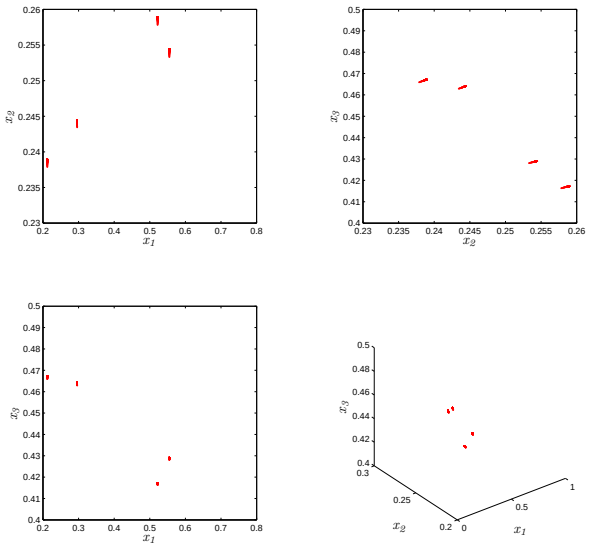

Figure 5.52: Periodic attractor of the proposed game with $\nu = 0.7635$ for $\varepsilon_1 = 2.6$ and $\alpha = 1, \varepsilon_2 = 0.9, \varepsilon_3 = 0.9, \zeta_1 = 0.4, \zeta_2 = 0.8, \zeta_3 = 0.1, \gamma_1 = 0.07, \gamma_2 = 0.03, \gamma_3 = 0.4$.

5.8.4 The 0-1 test for chaos

Here, we applied the 0-1 test method directly to the series data $x_1(n)$ that obtained from the first player to study the influence of the order ν on the dynamics of the market. he results with $\nu = 0.865$ and $\nu = 0.7635$ are shown in Figure 5.53 and Figure 5.54, respectively. In particular, Figure 5.53 depicts bounded trajectories for $\nu = 0.865$, indicating that the suggested game is stable where the output $K = 0.000827$. On the other hand, the unbounded trajectories in Figure 5.54 confirms the chaotic behavior of the game for $\nu = 0.7635$ and the output $K = 0.995$, which clearly confirms the above results.

5.8.5 Entropy

Here, we applied the *ApEn* directly to the series of data $x_3(n)$ that was obtained from the third firm. Figure 5.55 shows the approximate entropy of the proposed game when $\alpha = 2, \varepsilon_1 = 1.042811791, \varepsilon_2 = 1.1, \varepsilon_3 = 1.1, \zeta_1 = 0.4, \zeta_2 = 0.8, \zeta_3 = 0.1, \gamma_1 = 0.07, \gamma_2 = 0.03, \gamma_3 = 0.4$, and for different fractional order values. It is shown in Figure 5.55, that the approximate entropy results agree well with the corresponding bifurcation diagram and MLE in Figure 5.45. It is also shown that the smaller the fractional order ν is, the more complex the game model is. Therefore, we must be aware of the selected fractional order in the game model (5.25) in order to have a relatively high structural complexity.

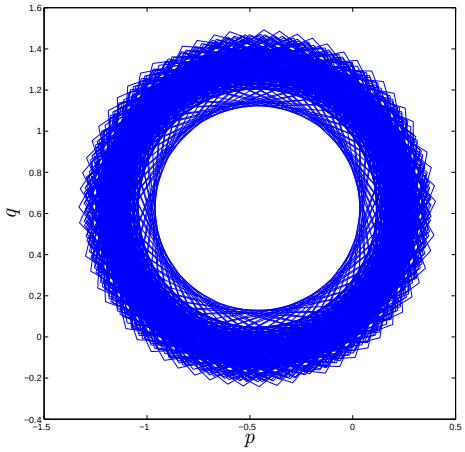

Figure 5.53: 0-1 test: regular dynamics of the translation components (p, q) of the Cournot game (5.25) for $\alpha = 2$,$\varepsilon_2 = 1.1, \varepsilon_3 = 1.1, \zeta_1 = 0.4, \zeta_2 = 0.8, \zeta_3 = 0.1, \gamma_1 = 0.07, \gamma_2 = 0.03, \gamma_3 = 0.4$ with fractional order $\nu = 0.865$.

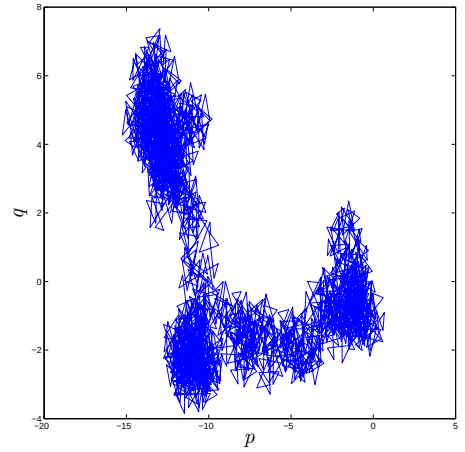

Figure 5.54: 0-1 test: regular dynamics of the translation components (p, q) of the Cournot game (5.25) for $\alpha = 2, \varepsilon_2 = 1.1, \varepsilon_3 = 1.1, \zeta_1 = 0.4, \zeta_2 = 0.8, \zeta_3 = 0.1, \gamma_1 = 0.07, \gamma_2 = 0.03, \gamma_3 = 0.4$ with fractional order $\nu = 0.7635$.

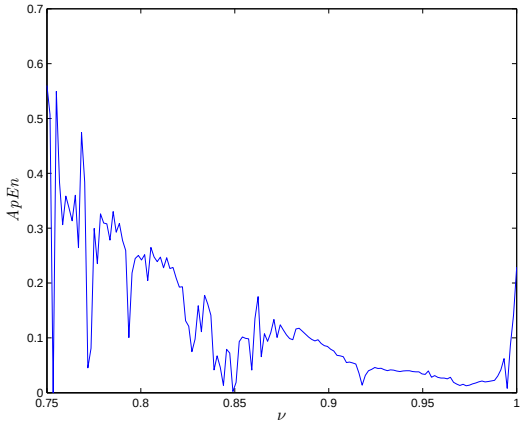

Figure 5.55: $ApEn$ of the game model (5.25) vesrus ν.

5.9 Conclusion

Different three dimensional fractional-order maps have been investigated in this chapter. Such maps can be considered as a generalization of the corresponding integer-order maps where the difference operator is replaced by the Caputo-like difference operator. There are some important concluding remarks to indicate here.

- Compared the fractional case with the integer one, it can be seen that the bifurcation structure of the 3D fractional maps changes qualitatively with the variation of the parameter system parameters and the order ν. Two cases are observed; in the first case the area of the chaotic motion decreases with the augment of the periodic motion as the fractional order decreases. For the second case, the area of the chaotic motion disappears as ν decreases.

- Based on the fractional difference order, the fractional-order Hénon map can display Lorenz-like attractors. We found that as the fractional order decreases the chaotic attractor moves to stable one.

- Both of the fractional-order Grassi-Miller map and the fractional Cournot game model contain rich dynamical behaviors. It is interesting that this maps with integer-order is periodic, but chaos is observed with the decrease of the fractional-order ν

- $ApEn$ and C_0 complexities agree well with LEs and bifurcation diagram results. It shows that complexity analysis is a more convenient method to choose parameters of fractional-order chaotic system in the real applications. We also find that the complexity of the 3D fractional generalized Hénon map decreases as ν decreases.

- The reported results confirm that the discrete-time fractional extensions of chaotic maps can better describe their fractional dynamics.

Chapter 6

Different Families of Fractional Order Discrete Time Systems with Hidden Attractors

6.1 Introduction

Recently, modelling numerous chaotic phenomena in the form of nonlinear dynamical systems, with some special features, examples being particular dynamic behaviors and specific properties related to the system equilibria has drawn the attention of many researchers. Generally speaking, regardless of the type of system (continuous time or discrete-time dynamical systems) chaos can appear in the form of "self-excited attractors" or "hidden attractors", which is a new classification that is defined by Leonov and Kuznetsov in [150]. The self-excited attractors are attractors for which the initial conditions are located close to the saddle points of the chaotic flow [151]. On the other hand, hidden chaotic attractors are attractors in unusual systems, for example, systems with no equilibria or with only one stable equilibrium [154]; for which the initial conditions can only be found via extensive numerical search [152, 153]. Consequently, these types of chaotic attractors are difficult to be discovered [155].

Referring to discrete-time systems, the topic of chaotic discrete-time systems characterized by “hidden attractors" has been only recently investigated [156]. For example, in [157] Jafri et.al. studied a new 1D chaotic discontinuous discrete-time system without equilibrium inspired by the Logistic map, whereas in [156,158] 2D and 3D chaotic discrete-time systems with different types of stable equilibria have been proposed. Moreover, in [159] 2D chaotic quadratic systems without equilibria and with no discontinuity in the right-hand equations have been introduced. Some other examples of chaotic attractors with curve equilibrium were numerically presented in [161]. These studies have proven the significant role of hidden attractors in theoretical problems and engineering applications. For example, hidden attractor can generate unexpected and potentially disastrous responses to perturbations in a structure like a bridge or an airplane wing.

Very recently, the study on fractional-order discrete-time (FODT) systems has received much attention. Actually, FODT systems can much more accurately describe the physical phenomena

than their integer-order ones. To this purpose, several chaotic fractional-order systems have been proposed starting from the chaotic integer-order counterparts (see Chapter 4 and Chapter 5). The well-known chaotic attractors generated from such systems (eg, fractional Lozi map [2], fractional Stefanski map [147], fractional Grassi-Miller map [148], and fractional Duffing map [149] and all the other systems reported in Chapter 4 and Chapter 5) are excited from unstable equilibria. On the other hand, the application of fractional-order calculus to design FODT chaotic systems with hidden dynamics is an emerging discipline of study in which few studies have been performed [163–169]. Which has inspired researcher to devote themselves to the design of new two and three dimensional fractional order discrete-time (FODT) chaotic systems with hidden attractors.

This chapter will present some typical examples of two-dimensional FODT systems and three dimensional FODT systems with hidden chaotic dynamics of equilibrium points, which is a newly introduced category of dynamical systems. FODT systems without equilibruim points, FODT systems with stable equilibruim point, FODT systems with close curve fixed points are reported. The procedure of these designed systems are explained and their dynamical properties are investigated throught phase plots, bifurcation diagrams, largest Lyapunov exponent and 0-1 test. Complexity of the FODT systems is also analyzed by employing approximate entropy and C_0 complexity.

6.2 Two dimensional FODT system with no equilibria and with for non-linearities

The discovery of simple chaotic systems with complex dynamics has always been an interesting research work. Since the field of fractional discrete-time systems (FODT) showing "hidden attractors" is completely unexplored in the literature, we construct a new FODT system with hidden attractors based on a two dimensional iterated system [170] by adding Caputo left operator. Huynh, et al in [170] proposed the following two dimensional iterated system by combining nonlinear functions, as:

$$\begin{cases} x(n+1) = x(n) + y(n), \\ y(n+1) = y(n) - \alpha|y(n)| - x(n)y(n) + \beta(x(n))^2 - \gamma(y(n))^2 + \delta, \end{cases} \tag{6.1}$$

where x and y denote the states of the discrete–time system and α, β, γ and δ are some bifurcation parameters. According to [170], the map has no equilibrium point and exhibits chaos (ie. the system has possesses hidden chaotic attractors). The bifurcation diagram, Lyapunov exponents and phase space are plotted in Figure 6.1 confirming the existence of chaos.

Based on the integer order discrete-time system (6.1), we introduce a new fractional order discrete-time (FODT) system using the left Caputo difference operator. We start by taking the first–order difference as

$$\begin{cases} \Delta x(n) = y(n), \\ \Delta y(n) = -\alpha|y(n)| - x(n)y(n) + \beta x^2(n) - \gamma y^2(n) + \delta. \end{cases} \tag{6.2}$$

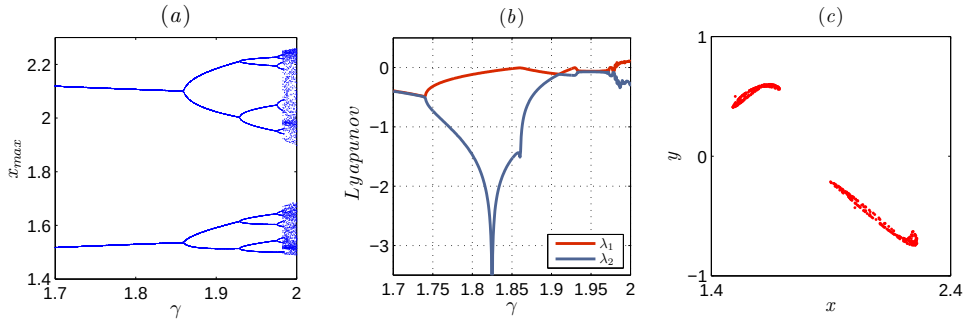

Figure 6.1: (a) Bifurcation diagram of the discrete–time system (6.1) versus γ for $\alpha = 0.01$, $\beta = 0.1$, $\delta = 0.1$; (b) Lyapunov exponent spectrum respect to γ; (c) Hidden chaotic attractor of system (6.1) with $\alpha = 0.01$, $\beta = 0.1$, $\gamma = 2$, $\delta = 0.1$, and initial condition $(x(0), y(0)) = (1.5, 0.5)$.

The new FODT system can be generated by replacing the first–order difference by the left Caputo difference operator. Here, we consider the generalization of system (6.1) for the fractional incommensurate-order model which takes the formas:

$$\begin{cases} {}^{C}\Delta_a^{\nu_1} x(t) = y(t-1+\nu_1), \\ {}^{C}\Delta_a^{\nu_2} y(t) = -\alpha|y(t-1+\nu_2)| - x(t-1+\nu_2)y(t-1+\nu_2) + \beta x^2(t-1+\nu_2) \\ \qquad\qquad\qquad\qquad\qquad\qquad\qquad\qquad -\gamma y^2(t-1+\nu_2) + \delta, \end{cases} \tag{6.3}$$

where $t \in N_{a+1-\nu}$, and a is the starting point.

We denote the equilibrium point of the FODT system (6.3) with (x_f, y_f). Equation (6.3) can be transformed into Equation (6.4) for calculating the fixed points

$$\begin{cases} {}^{C}\Delta_a^{\nu_1} x_f = y_f, \\ {}^{C}\Delta_a^{\nu_2} y_f = -\alpha|y_f| - x_f y_f + \beta x_f^2 - \gamma y_f^2 + \delta, \end{cases} \tag{6.4}$$

and by taking in mind that $\Delta_a^{\nu_1} x_f = \Delta_a^{\nu_2} y_f = 0$, we get

$$\beta x_f^2 + \delta = 0. \tag{6.5}$$

Therefore, the FODT system (6.3) also has no equilibrium points for such positive parameters β, δ and in other words, the attractors generating from system (6.5) are all hidden.

6.2.1 Dynamics analysis

In this subsection, we will employ numerical tools to assess the hidden dynamics of the proposed FODT system (6.3). For that we will need a discrete numerical formula that allows us to evaluate the states of the system in fractional discrete time. Theorem 1.15 provides the basis for the

numerical method. The states solution of the FODT system given in (6.3), for $a = 0$, can be obtained as

$$\begin{cases} x(n) = x(0) + \frac{1}{\Gamma(\nu_1)} \sum_{j=1}^{n} \frac{\Gamma(n-j+\nu_1)}{\Gamma(n-j+1)} y(j-1), \\ y(n) = y(0) + \frac{1}{\Gamma(\nu_2)} \sum_{j=1}^{n} \frac{\Gamma(n-j+\nu_2)}{\Gamma(n-j+1)} (-\alpha|y(j-1)| - x(j-1)y(j-1) + \beta x^2(j-1) \\ \qquad\qquad - \gamma y^2(j-1) + \delta), \end{cases} \tag{6.6}$$

Using the above explicit numerical formula, we are going to explore numerically the action of the fractional order $\nu = (\nu_1, \nu_2)$ on the behavior of the FODT system (6.3). We will mainly discuss the hidden chaotic dynamic of the system by means of bifurcation diagram, largest Lyapunov exponent and phase portrait. To ensure the existence of chaos parameters α, β, δ are set as $\alpha = 0.01, \beta = 0.1, \delta = 0.1$, whereas γ and fractional orders ν_1 and ν_2 are considered as the only bifurcation parameters. Following are the results of our investigations of various cases studied.

6.2.1.1 Commensurate fractional order case ($\nu_1 = \nu_2 = \nu$)

Here, we consider the following cases.

Cas 1 . Let $\nu_1 = \nu_2 = \nu$ and vary γ from 1.7 to 2.05 with the step size $\Delta\gamma = 0.003$. The bifurcation diagram and largest Lyapunov exponent of the FODT system (6.3) without equilibrium points in (γ, x) plane with $\nu = 0.992$ and $\nu = 0.975$ are plotted in Figure 6.2 and Figure 6.3, respectively. The FODT system (6.3) changes from periodic state to chaotic state through period doubling route to chaos. When $\nu = 0.992$ system (6.3) is chaotic at the rang $\gamma \in (1.999, 2.02)$, while when $\nu = 0.975$ the system is chaotic at $\gamma \in (2.025, 2.05)$. Obviously, as the fractional order ν decreases, the bifurcation diagram gradually shifts to the right.

Cas 2 . Let $\gamma = 2$, $\nu_1 = \nu_2 = \nu$ and vary ν from 0.95 to 1 with the step size $\Delta\nu = 0.001$. Figure.6.4(a),(b) shows the bifurcation diagram and the corresponding largest Lyapunov exponent, respectively. It was found that when $\nu > 0.9912$ the largest Lyapunov exponent is positive which indicates that the FODT system without equilibrium point has chaotic behavior. As ν decrease, the chaotic motion disappears and the FODT system (6.3) displays periodic motion from period doubling bifurcation. If we continue decreasing the fractional order ν the system will eventually diverge to infinity.

6.2.1.2 Incommensurate fractional order case ($\nu_1 \neq \nu_2$)

Here, when plotting bifurcation diagrams, two sets of symmetrical initial states and system parameters are considered. The bifurcation diagram is plotted in blue for the initial state $x(0) = 1.5$, $y(0) = 0.5$, and for the system parameters $\alpha = 0.01$, $\beta = 0.1$, $\gamma = 2$, $\delta = 0.1$, while the bifurcation diagram is plotted in red for the initial state $x(0) = -1.5$, $y(0) = -0.5$, and $\alpha = -0.01$, $\beta = -0.1$, $\gamma = -2$, $\delta = -0.1$.

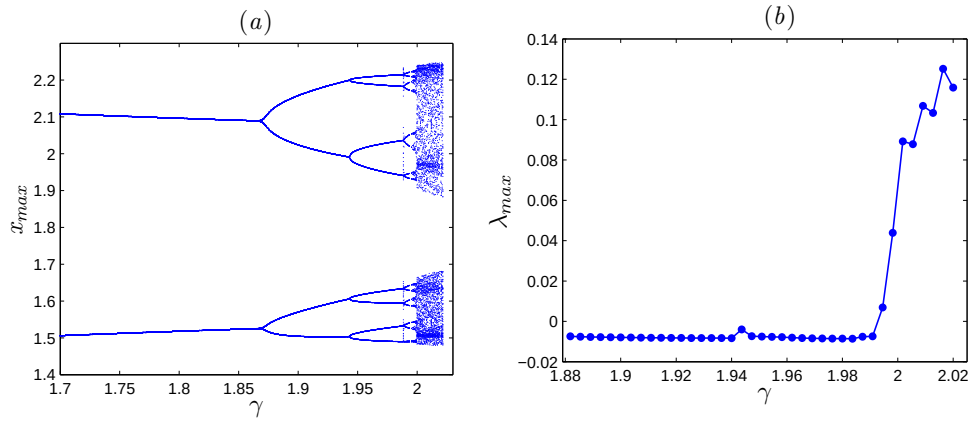

Figure 6.2: (a) Bifurcation diagram of the FODT system (6.3) versus γ. with $\nu = 0.992$ and $\alpha = 0.01$, $\beta = 0.1$, $\delta = 0.1$; (b) largest Lyapunov exponent of the FODT system (6.3) corresponding to (a).

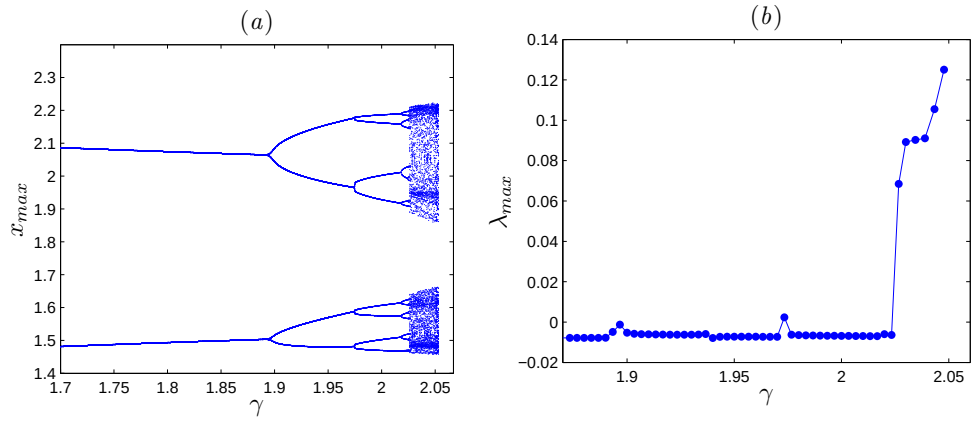

Figure 6.3: (a) Bifurcation diagram of the FODT system (6.3) versus γ, with $\nu = 0.975$ and $\alpha = 0.01$, $\beta = 0.1$, $\delta = 0.1$; (b) largest Lyapunov exponent of the FODT system (6.3) corresponding to (a)

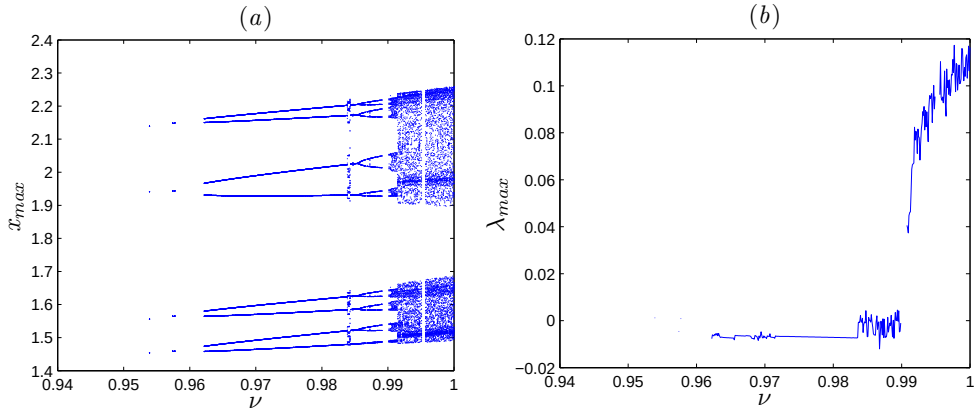

Figure 6.4: Bifurcation diagram and Largest Lyapunov exponent of the FODT system (6.3) with $\nu \in [0.95, 1]$ for $\alpha = 0.01$, $\beta = 0.1$, $\gamma = 2$, $\delta = 0.1$. (a) Bifurcation diagram; (b) Largest Lyapunov exponent

Cas 1 . Let $\gamma = 2$, $\nu_1 = 1$ and vary ν_2 from 0.960215 to 1 with the step size 0.001. The bifurcation diagram for the initial condition $[x(0), y(0)] = [1.5, 0.5]$ is shown in Figure.6.5 (blue diagram). Similarly, the FODT system (6.3) changes from a periodic state to a chaotic state via period-doubling bifurcation. Obviously, the FODT system is chaotic when $\nu_2 \in [0.9915, 1]$, and periodic when $\nu_2 \in [0.960215, 1]$. Now we choose to fix the bifurcation parameters as $\alpha = -0.01$, $\beta = -0.1$, $\gamma = -2$, $\delta = -0.1$ and we vary the value of ν_2 in the interval $[0.960215, 1]$. The bifurcation diagram for the initial condition $[x(0), y(0)] = [-1.5, -0.5]$ is shown in Figure 6.5 (red diagram). From Figure.6.5 we notice that the bifurcation diagrams corresponding to these opposite initial condition and bifurcation parameters had certain symmetrical similarity.

Cas 2 . Let $\gamma = 2$, $\nu_2 = 1$ and vary ν_1 from 0.94645 to 1. The bifurcation diagram for the initial condition $[x(0), y(0)] = [1.5, 0.5]$ are shown in Figure 6.6 (blue diagram). When $\nu_2 < 0.968$ the FODT system (6.3) has a transient state; meaning that the states of the proposed system approaches, some bounded attractor until a minimum number of iterations and then it diverges towards infinity. Similarly, when we choose the parameters $\alpha = -0.01$, $\beta = -0.1$, $\gamma = -2$, $\delta = -0.1$ and initial condition $[x(0), y(0)] = [-1.5, -0.5]$, the red dots show a symmetrical bifurcation diagram.

As shown above, when all the fractional order values of the proposed system (6.3) are varied simultaneously the chaotic region shrink much compared with that when one fractional order values are varied. Figure 6.7 shows the hidden chaotic attractor of the fractional order map (6.3) with fractional order $\nu = 0.992$ for two different initial conditions and bifurcation parameters. The red attractor corresponds to the initial condition $[x(0), y(0)] = [-1.5, -0.5]$ and bifurcation

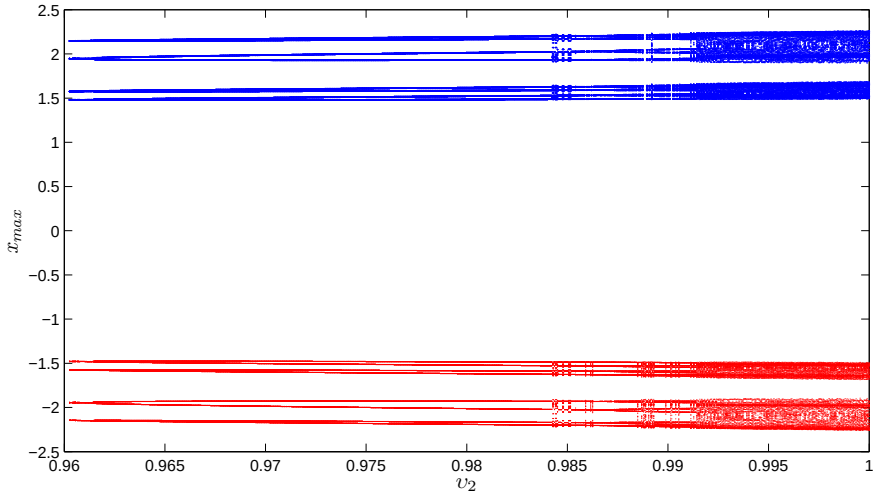

Figure 6.5: Bifurcation diagram versus ν_2 of the FODT system (6.3) for two different initial conditions and bifurcation parameters. Blue diagram $[x(0), y(0)] = [1.5, 0.5]$,$\alpha = 0.01$, $\beta = 0.1$, $\gamma = 2$, $\delta = 0.1$, red diagram $[x_0, y_0] = [-1.5, -0.5]$, $\alpha = -0.01$, $\beta = -0.1$, $\gamma = -2$, $\delta = -0.1$.

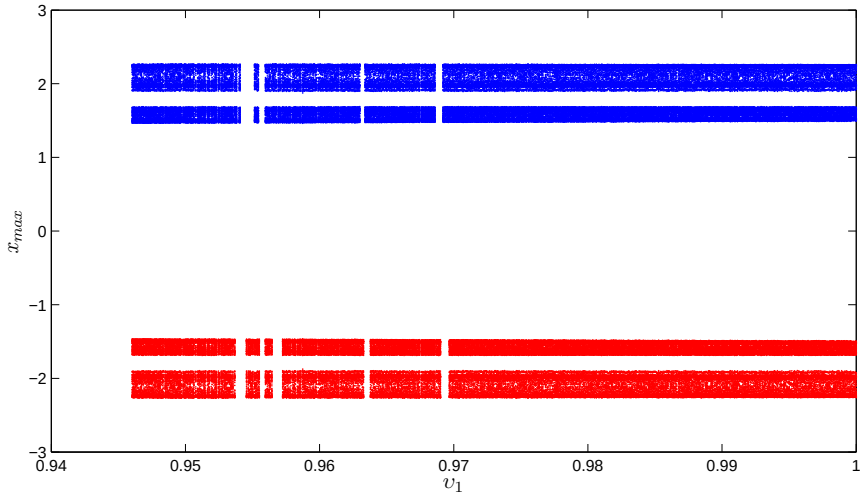

Figure 6.6: Bifurcation diagram versus ν_1 of the FODT system (6.3) for two different initial conditions and bifurcation parameters. Blue diagram $[x(0), y(0)] = [1.5, 0.5]$,$\alpha = 0.01$, $\beta = 0.1$, $\gamma = 2$, $\delta = 0.1$, red diagram $[x(0), y(0)] = [-1.5, -0.5]$, $\alpha = -0.01$, $\beta = -0.1$, $\gamma = -2$, $\delta = -0.1$.

parameters $\alpha = -0.01$, $\beta = -0.1$, $\gamma = -2$, $\delta = -0.1$, while the blue attractor correspond to the initial condition $[x(0), y(0)] = [1.5, 0.5]$ and bifurcation parameters $\alpha = 0.01$, $\beta = 0.1$, $\gamma = 2$, $\delta = 0.1$.

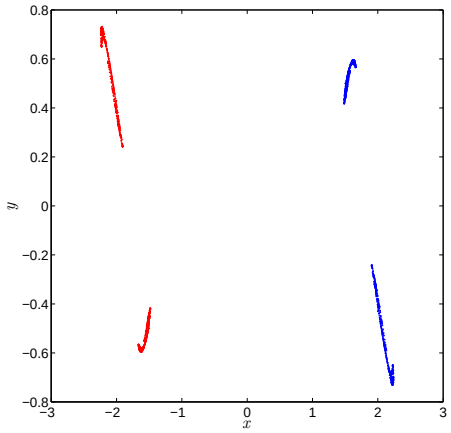

Figure 6.7: The hidden chaotic attractor of the FODT system (6.3) for two different initial conditions and bifurcation parameters. Blue attractor $[x(0), y(0)] = [1.5, 0.5]$,$\alpha = 0.01$, $\beta = 0.1$, $\gamma = 2$, $\delta = 0.1$, red attractor $[x(0), y(0)] = [-1.5, -0.5]$, $\alpha = -0.01$, $\beta = -0.1$, $\gamma = -2$, $\delta = -0.1$.

6.2.2 Complexity analysis

A complexity measure plays important role in analyzing dynamic properties of chaotic systems. In this section we measure the complexity of the FODT system (6.3) by means of approximate entropy algorithm given in Chapter 3 as

$$ApEn = \phi^m(r) - \phi^{m+1}(r), \tag{6.7}$$

where $\phi^m(r)$ is considered as

$$\phi^m(r) = \frac{1}{N-m-1} \sum_{i=1}^{N-m+1} \log C_i^m(r). \tag{6.8}$$

The complexity of the FODT system (6.3) is tested by the ApEn for different fractional order values, results are reported in Table 6.1. The calculated values of ApEn in Table 6.1 validate the chaotic nature of the FODT system (6.3). As shown in Table 6.1, the FODT system (6.3) has higher complexity when $\nu_1 = 0.9995$ and $\nu_2 = 1$ corresponding to the bifurcation diagram in Figure 6.6, and the low complexity region can be found when both values of ν_1 and ν_2 are decreased.

γ	ν_1	ν_2	ApEn
2	1	1	0.2291
2	1	0.9975	0.2131
2	0.9995	1	0.2920
2	0.992	0.992	0.1.942

Table 6.1: Approximate Entropy test

6.3 Fractional order Hénon-like maps with no equilibrium points

Inspired by the Hénon map, the authors Haibo Jiang et.al. in [156] preformed a systematic search to construct two dimensional discrete-time systems with no equilibria or with stable equilibria. The objective was to find the algebraically simplest cases which cannot be further reduced by the removal of terms without destroying the chaos. For each case that was found, a computer search was preformed to find chaotic solutions that are deemed "elegant" in the sense of Sprott [162], by which it means that as many coefficients as possible are set to zero where the others are set to ± 1 or otherwise to a small integer or decimal fraction with the fewest possible digits. In particular, in [156] attention is focused on a class of integer-order Hénon-like map with six real coefficients a_i, $\forall i = \overline{1.6}$, described by

$$\begin{cases} x(n+1) = y(n), \\ y(n+1) = a_1 x(n) + a_2 y(n) + a_3 x^2(n) + a_4 y^2(n) + a_5 x(n) y(n) + a_6. \end{cases} \tag{6.9}$$

The equilibrium point of system (6.9) are obtained by solving

$$\begin{cases} x = y \\ y = a_1 x + a_2 y + a_3 x^2 + a_4 y^2 + a_5 xy + a_6. \end{cases} . \tag{6.10}$$

Therefore, the problem of finding fixed points is transformed into the following equation with respect to x

$$(a_3 + a_4 + a_5)x^2 + (a_1 + a_2 - 1)x + a_6 = 0. \tag{6.11}$$

According to [156], to design an integer-order discrete-time system with no equilibria, we should just find the system parameters a_i, $\forall i = \overline{1.6}$ where the quadratic equation (6.11) has no solution. As a result, the conditions to find the discrete-time systems without equilibria are:

Condition 1 . If $a_3 + a_4 + a_5 = 0$, $a_1 + a_2 - 1 = 0$ and $a_6 \neq 0$.

Condition 2 . If $a_3 + a_4 + a_5 \neq 0$ and $\Delta < 0$ where Δ is the discriminant of equation (6.11) and is given by $\Delta = (a_1 + a_2 - 1)^2 - 4a_6(a_3 + a_4 + a_5)$.

In both cases, for any existence of attractors, they must be hidden as the basin of attractor do not contain any fixed point. By applying the search routine to the general form (6.9) with

Condition 1 infinitely many integer order systems are found. One of the most elegant system is given by

$$\begin{cases} x(n+1) = y(n), \\ y(n+1) = x(n) + a_1 x^2(n) + a_2 y^2(n) - a_3 x(n) y(n) - a_4, \end{cases} \tag{6.12}$$

where a_i, $\forall i = \overline{1.4}$ are real bifurcation parameters. Nonlinear terms in this dynamical system are x^2 , y^2 and xy. Based on what has been reported in [156], the system (6.12) can generate many different hidden chaotic attractors. Here, we give four main hidden attractors depending on the parameters a_i, $\forall i = \overline{1.4}$:

Cas 1 . When $(a_1, a_2, a_3, a_4) = (0.2, 0.71, 0.91, -1.14)$ and initial conditions are $(x(0), y(0) = (0.93, -0.44)$, Lyapunov exponents are $L_1 = 0.0623$, $L_2 = -0.3248$ and the Lyapunov dimension of the map in this case is $\overline{dim_L} = 1.1947$, therefore the map (6.12) displays a chaotic attractor as shown in Figure 6.8-(a).

Cas 2 . When $(a_1, a_2, a_3, a_4) = (-0.6, 0.74, 0.14, -0.33)$ and initial condition $(x(0), y(0) = (-0.78, 0.45)$, Lyapunov exponents are $L_1 = 0.0827$, $L_2 = -0.2349$ and thus the Lyapunov dimension is $\overline{dim_L} = 1.3572$. System (6.12) displays chaotic attractor with no equilibria, as shown in Figure 6.8-(b).

Cas 3 . When $(a_1, a_2, a_3, a_4) = (0.51, 1, 1.51, -0.74)$ and the initial condition $(x(0), y(0) = (-0.81, 0.51)$, the attractor diagrams of system (6.12) is plotted in Figure 6.8-(c), at this time, the corresponding Lyapunov exponents are $L_1 = 0.0886$, $L_2 = -0.2448$, the Lyapunov dimension is $\overline{dim_L} = 1.3649$. Due to fractional dimension and the positive Lyapunov exponent, the map is chaotic.

Cas 4 . When $(a_1, a_2, a_3, a_4) = (0.6, 1, 1.6, -0.72)$ and initial condition $(x(0), y(0) = (-0.26, 0.18)$, so, Lyapunov exponents are as follows $L_1 = 0.1012$, $L_2 = -0.2067$ and the Lyapunov dimension of the map in this case is $\overline{dim_L} = 1.4932$, therefore we have a chaotic attractor. Phase portrait of the map (6.12) is shown in Figure 6.8-(d).

Very recently, based on system (6.12), a novel fractional order Hénon-like map with new hidden chaotic attractors [164] was designed by using the Caputo difference operator ${}^{C}\Delta_a^{\nu}$, as

$$\begin{cases} {}^{C}\Delta_a^{\nu} x(t) = y(t-1+\nu) - x(t-1+\nu), \\ {}^{C}\Delta_a^{\nu} y(t) = x(t-1+\nu) + a_1 x^2(t-1+\nu) + a_2 y^2(t-1+\nu) \\ \qquad\qquad -a_3 x(t-1+\nu) y(t-1+\nu) - a_4 - y(t-1+\nu), \end{cases} \tag{6.13}$$

where $t \in \mathbb{N}_{a+1-\nu}$ and $0 < \nu \leq 1$. Similarly to the previous chapters (Chapter 4 and 5), to examine the dynamics of the fractional order Hénon-like map (6.13), we will use a numerical solution obtained by using Theorem 1.15; which leads to the discrete solution in the form

$$\begin{cases} x(n) = x(0) + \frac{1}{\Gamma(\nu)} \sum_{j=1}^{n} \frac{\Gamma(n-j+\nu)}{\Gamma(n-j+1)} \left(y(j-1) - x(j-1) \right), \\ y(n) = y(0) + \frac{1}{\Gamma(\nu)} \sum_{j=1}^{n} \frac{\Gamma(n-j+\nu)}{\Gamma(n-j+1)} \left(x(j-1) + a_1 x^2(j-1) + a_2 y^2(j-1) \right. \\ \qquad\qquad \left. -a_3 x(j-1) y(j-1) - a_4 - y(j-1) \right), \end{cases} \tag{6.14}$$

in which $x(0)$ and $y(0)$ are the initial conditions. Evaluating (6.14) for $\nu = 1$ we get the classical integer-order discrete time system (6.12) and with some direct calculations, the resulting dynamics of the fractional order Hénon-like map are identical to those of the classical one even though it has a discrete memory effect, i.e. the solution $x(n)$ depends on all previous values $x(0), x(1), ..., x(n-1)$. Now that we have our fractional system (6.13) and the corresponding numerical formulas (6.14), we can study the dynamic behavior of the fractional order Hénon-like map without equilibria.

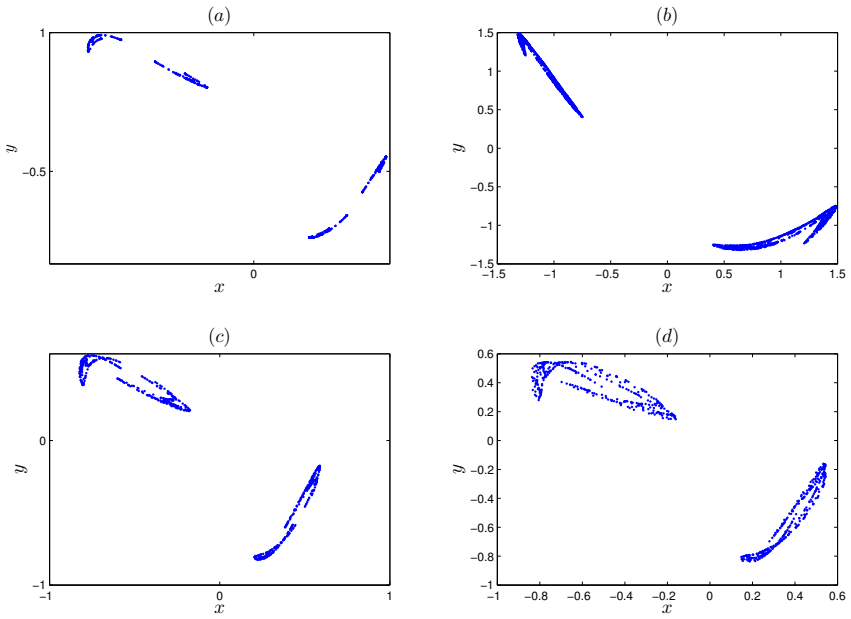

Figure 6.8: Phase plots of the Hénon-like map without fixed point (6.12) for: (a) $(a_1, a_2, a_3, a_4) = (0.2, 0.71, 0.91, 1.14)$ and $(x(0), y(0)) = (0.93, -0.44)$, (b) $(a_1, a_2, a_3, a_4) = (-0.6, 0.74, 0.14, -0.33)$ and $(x(0), y(0)) = (-0.77, 0.45)$, (c) $(a_1, a_2, a_3, a_4) = (0.51, 1, 1.51, 0.74)$ and $(x(0), y(0)) = (-0.81, 0.51)$, (d) $(a_1, a_2, a_3, a_4) = (0.6, 1, 1.6, 0.72)$ and $(x(0), y(0)) = (-0.26, 0.18)$.

Dynamical analysis

To investigate the sensitivity of the fractional order Hénon-like map (6.13), two indicators are used. The first indicator is the bifurcation diagram and the second indicator is the phase portrait. In the following, the system dynamic is analyzed for the fore cases. For each parameter setting the solutions are calculated for a sufficiently long time and the transient is concealed.

Cas 1 . First, we study the effect of the fractional order ν on the dynamics of the Hénon-like map for parameter values $(a_1, a_2, a_3, a_4) = (0.2, 0.71, 0.91, 1.14)$ and the initial conditions $(x(0), y(0)) = (0.93, -0.44)$. When changing the value of order ν from 0.975 to 1 gradually, the bifurcation model of the state variable x is plotted in Figure 6.9. We notice that as ν decreases, the trajectory $x(n)$ remains bounded whereas when $\nu \leq 0.976$, the

chaotic behavior is delayed and the states of the fractional Hénon-like map (6.13) diverge to infinity. The phase diagrams are plotted in Figure 6.10 for different values of ν. Observe from Figure 6.10, one can easily see that the types of these hidden attractors are different from each other. Moreover, this figures indicates that the fractional order ν is another bifurcation parameter.

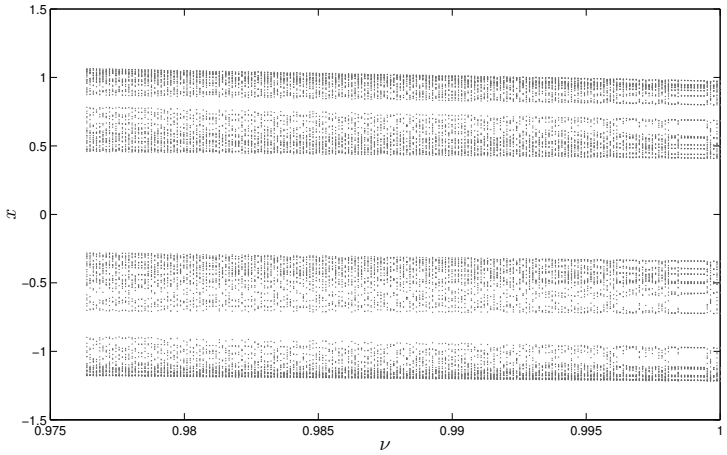

Figure 6.9: Bifurcation diagram of the fractional order Hénon-like map (6.13) versus ν with $(a_1, a_2, a_3, a_4) = (0.2, 0.71, 0.91, 1.14)$ and $(x(0), y(0)) = (0.93, -0.44)$.

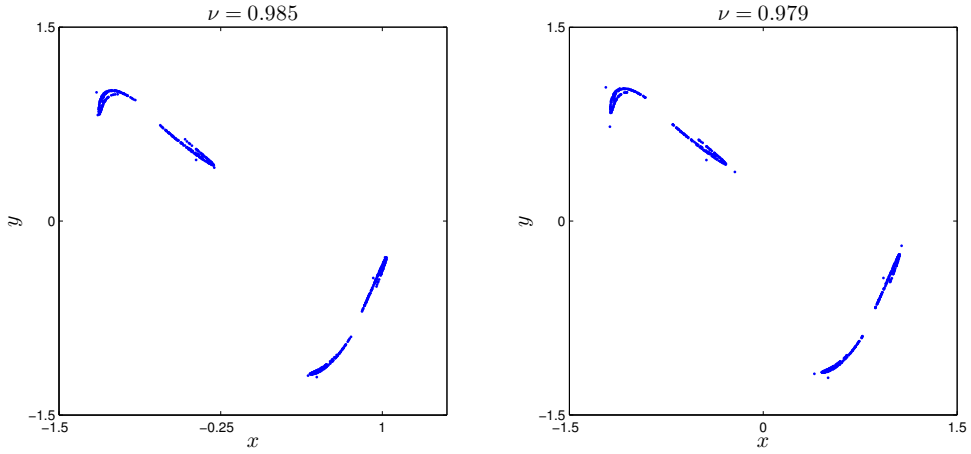

Figure 6.10: The chaotic attractor obtained with $(a_1, a_2, a_3, a_4) = (0.2, 0.71, 0.91, 1.14)$ and $(x(0), y(0)) = (0.93, -0.44)$ for different fractional orders ν.

Cas 2 . Next, we set the parameters (a_1, a_2, a_3, a_4) to $(0.51, 1, 1.51, 0.74)$ and choose the initial values $(x(0), y(0)) = (-0.81, 0.51)$. The bifurcation diagram for the fractional Hénon-like map (6.13) versus order ν is illustrated in Figure 6.11. As can be seen from Figure 6.11, the fractional Hénon-like map (6.13) goes from chaos to period when decreasing the value of ν. It is noticed that the system (6.13) is unbounded for $\nu \leq 0.962$. Figure 6.12

depicts the phase portraits of the fractional order Hénon-like map for the three different fractional orders $\nu = 1$, $\nu = 0.979$, and $\nu = 0.963$. Similarly, when $\nu = 1$, the fractional system (6.13) refers to the classical system. While $0.963 \leq \nu \leq 1$, the fractional Hénon-like map (6.13) exhibits a chaotic behavior.

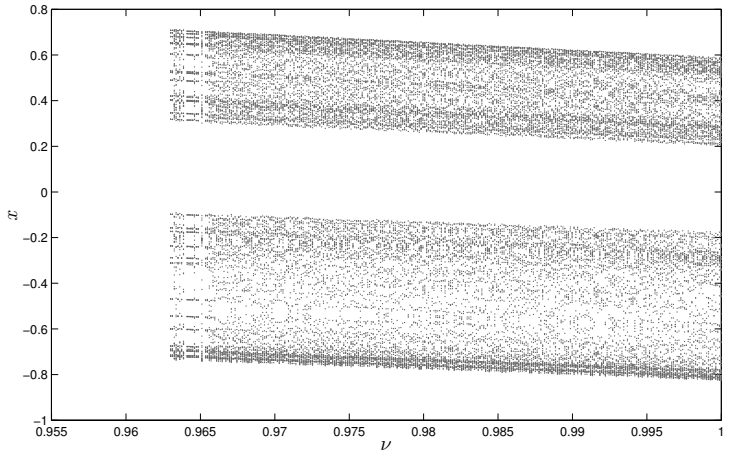

Figure 6.11: Bifurcation diagram of the fractional Hénon-like map (6.13) versus ν with $(a_1, a_2, a_3, a_4) = (0.51, 1, 1.51, 0.74)$ and $(x(0), y(0)) = (-0.81, 0.51)$ for different fractional orders ν.

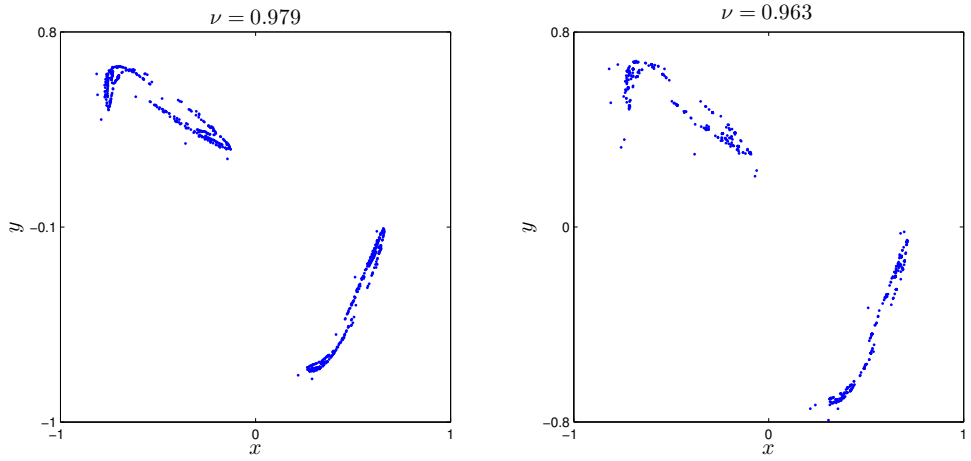

Figure 6.12: The chaotic attractor obtained with $(a_1, a_2, a_3, a_4) = (0.51, 1, 1.51, 0.74)$ and $(x(0), y(0)) = (-0.81, 0.51)$ for different fractional order values ν.

Cas 3 . Let us, now, consider the third set of parameters $(a_1, a_2, a_3, a_4) = (0.6, 1, 1.6, 0.72)$ with initial states $(x(0), y(0)) = (-0.26, 0.18)$. As can be seen in Figure 6.13, the resulting trajectories of the fractional Hénon-like map (6.13) vary with ν. When $\nu < 0.95$, chaos disappears completely.

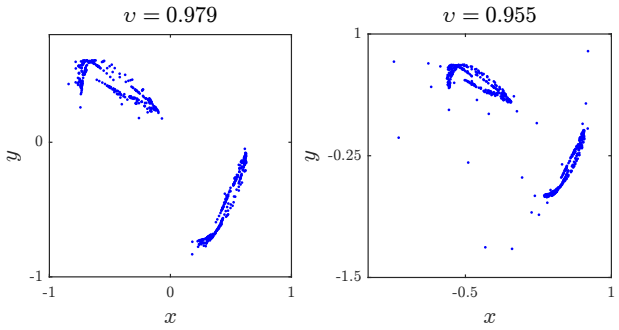

Figure 6.13: The chaotic attractor obtained with $(a_1, a_2, a_3, a_4) = (0.6, 1, 1.6, 0.72)$ and $(x(0), y(0)) = (-0.26, 0.18)$ for different fractional orders ν.

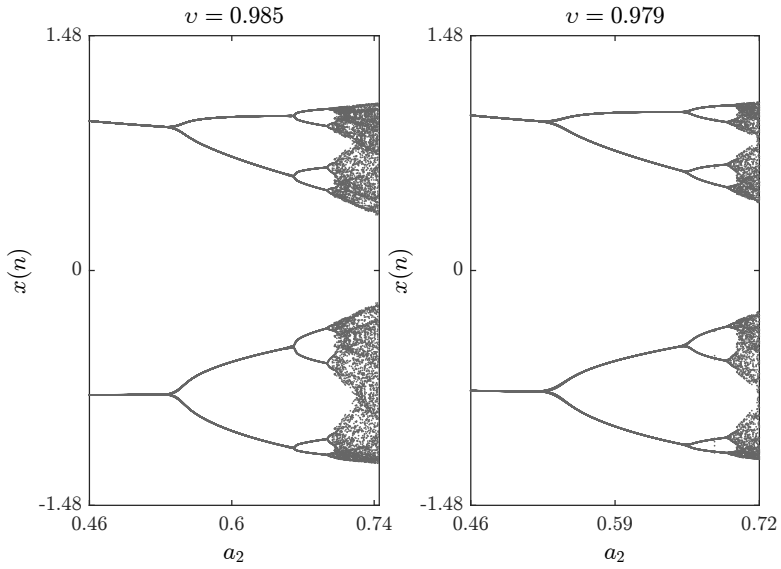

Figure 6.14: Bifurcation diagrams with a_2 as the critical parameter and $(a_1, a_3, a_4) = (0.2, 0.91, 1.14)$ and $(x(0), y(0)) = (0.93, -0.44)$ for different fractional orders ν.

The bifurcation diagrams for different parameters (a_1, a_2, a_3, a_4) are shown in Figures 6.14, 6.15, and 6.16, respectively. First we fix parameters (a_1, a_3, a_4) to $(0.2, 0.91, 1.14)$ and vary a_2 along the interval $[0.46, 0.75]$. Clearly, decreasing the fractional order ν affects the interval over which chaos is exhibited. In Figure 6.15, the bifurcation diagram is obtained with $(a_2, a_3, a_4) = (1, 1.51, 0.74)$ and the critical parameter a_1 being varied in steps of $\Delta a_1 = 0.0006$. In this case, when we decrease the fractional order ν, the opposite is observed as the chaotic band expands and the 8–period stage disappears. Finally, Figure 6.16 is obtained for $(a_2, a_3, a_4) = (1, 1.6, 0.72)$ with a_1 as the critical parameter. We see that a slight change in the fractional order has a considerable effect on the dynamics of the system. For completeness, the time evolution of the

states belonging to the fractional-order Hénon-like map (6.13) are displayed in Figure 6.17 for $\nu = 0.979$.

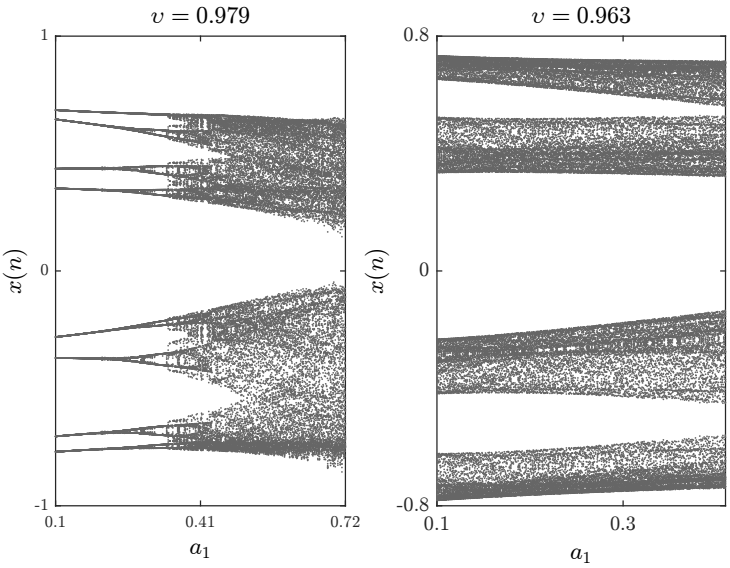

Figure 6.15: Bifurcation diagrams with a_1 as the critical parameter and $(a_2, a_3, a_4) = (1, 1.51, 0.74)$ and $(x(0), y(0)) = (-0.81, 0.51)$ for different fractional orders υ.

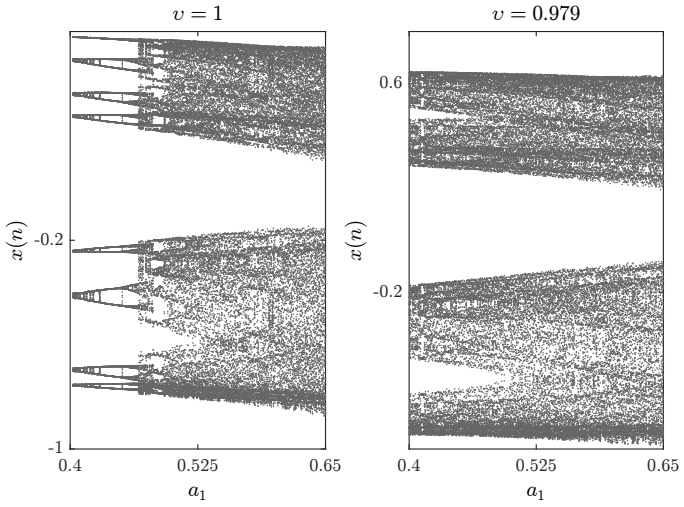

Figure 6.16: Bifurcation diagrams with a_1 as the critical parameter and $(a_2, a_3, a_4) = (1, 1.6, 0.72)$ and $(x(0), y(0)) = (-0.26, 0.18)$ for different fractional orders υ.

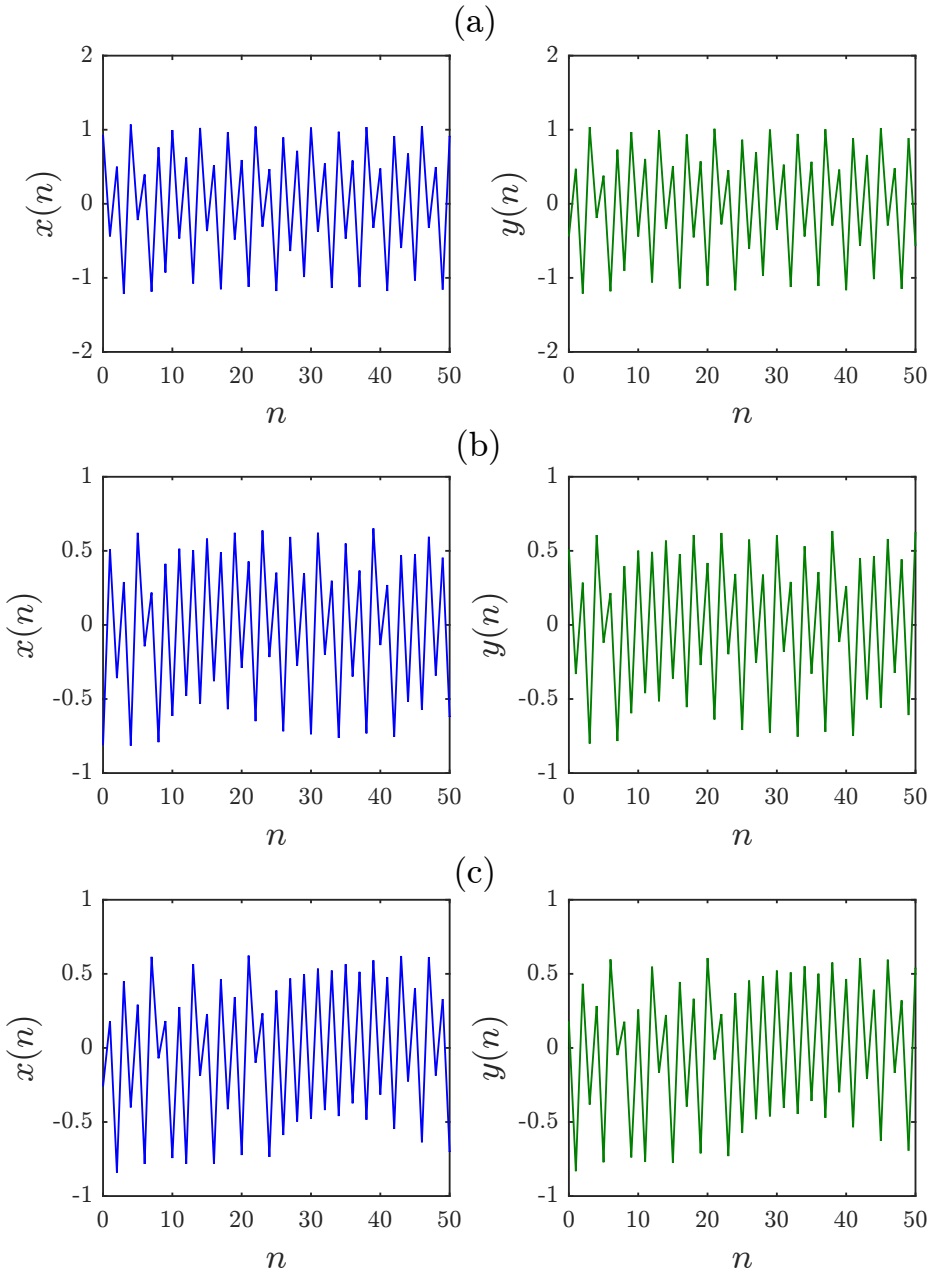

Figure 6.17: Time evolution of states for $\nu = 0.979$ and: (a) $(a_1, a_2, a_3, a_4) = (0.2, 0.71, 0.91, 1.14)$ and $(x(0), y(0)) = (0.93, -0.44)$, (b) $(a_1, a_2, a_3, a_4) = (0.51, 1, 1.51, 0.74)$ and $(x(0), y(0)) = (-0.81, 0.51)$, (c) $(a_1, a_2, a_3, a_4) = (0.6, 1, 1.6, 0.72)$ and $(x(0), y(0)) = (-0.26, 0.18)$.

6.4 Fractional order Hénon-like map with stable equilibria

In this segment, we introduce a simple two-dimensional fractional order discrete-time system with one stable equilibrium point and consider its various numerical analysis. What interest us is that this newly presented system has stable equilibrium point but it can also exhibit rich dynamics including chaos and coexisting hidden attractors. We adopt closely the schematic method developed by Jianget al. in [156], in which the authors preformed a search to find the accuracy initial values that led to hidden attractors in a new two-dimensional chaotic discrete-time system with stable equilibrium point inspired by the Hénon map. The general 2D Hénon-like map with six coefficients is given by

$$\begin{cases} x(n+1) = y(n), \\ y(n+1) = a_1 x(n) + a_2 y(n) + a_3 x^2(n) + a_4 y^2(n) + a_5 x(n) y(n) + a_6. \end{cases} \tag{6.15}$$

To obtain the equilibrium points (x_f, y_f) of the integer order system (6.15) , we solve the following system of equation:

$$\begin{cases} x_f = y_f, \\ y_f = a_1 x_f + a_2 y_f + a_3 x_f^2 + a_4 y_f^2 + a_5 x_f y_f + a_6, \end{cases} \tag{6.16}$$

in which $a_3 + a_4 + a_5 = 0$ and $a_1 + a_2 - 1 \neq 0$. System (6.15) has only one equilibrium point at $(x_f, y_f) = (\frac{-a_6}{a_1+a_2-1}, \frac{-a_6}{a_1+a_2-1})$ with eigenvalues λ that satisfy

$$\lambda^2 - Tr(J)\lambda + Det(J) = 0, \tag{6.17}$$

where $Det(J) = -(a_1 + 2a_3 x_f + a_5 y_f)$ is the determinant of the matrix J and $Tr(J) = a_2 + 2a_4 y_f + a_5 x_f$ is the trace of the Jacobian matrix. According to the stability criterion for the integer order maps the equilibrium point (x_f, y_f) is stable if the roots λ_1 and λ_2 of the characteristic equation (6.18) satisfy that $|\lambda_i| < 1 \ \forall i = \overline{1.2}$. Thus, to design the chaotic map with stable equilibrium, we should just choose suitable bifurcation parameters in a way that one of the roots λ_1, λ_2 of the characteristic equation (6.18) are superior or equal to one.

Motivated by this strategy, we remove and added some terms to the difference equations (6.15) to obtain the following two dimensional fractional Hénon-like map:

$$\begin{cases} {}^{C}\Delta_a^{\nu} x(t) = y(t+\nu-1) - x(t+\nu-1), \\ {}^{C}\Delta_a^{\nu} y(t) = a_1 x(t+\nu-1) + a_2 y(t+\nu-1) + a_3 x^2(t+\nu-1) + a_4 y^2(t+\nu-1) \\ \qquad\qquad + a_5 x(t+\nu-1) y(t+\nu-1) + a_6, \end{cases} \tag{6.18}$$

where $a_3 + a_4 + a_5 = 0$ and $a_1 + a_2 - 1 \neq 0$. For the considered assumptions on parameters, an extensive numerical search involving millions of random combinations of the coefficients a_i, $i = \overline{1.6}$ and initial conditions subject to the integer order case in equation (6.18) has successfully given the following dynamical system

$$\begin{cases} {}^{C}\Delta_a^{\nu} x(t) = y(t+\nu-1) - x(t+\nu-1), \\ {}^{C}\Delta_a^{\nu} y(t) = -0.33 x(t+\nu-1) + A y(t+\nu-1) - 0.48 x^2(t+\nu-1) + 0.47 y^2(t+\nu-1) \\ \qquad\qquad + 0.01 x(t+\nu-1) y(t+\nu-1) - 0.9, \end{cases} \tag{6.19}$$

with state variables x and y, and system parameter A. $0 < \nu \leq 1$ denotes the fractional order. For calculating the equilibrium points of the fractional Hénon-like map (6.19), we assign its left hand side to zero

$$\begin{cases} 0 = y - x, \\ 0 = -0.33x + Ay - 0.48x^2 + 0.47y^2 + 0.01xy - 0.9. \end{cases} \tag{6.20}$$

From system of equation (6.20) it follows

$$(-0.33 + A)x - 0.9 = 0. \tag{6.21}$$

It is easy to verify that the fractional Hénon-like map (6.19) has a unique equilibrium point when $A \neq 0.33$. The Jacobian matrix of system (6.19) at an arbitrary point (x, y), is given by:

$$J = \begin{pmatrix} -1 & 1 \\ -0.33 - 1.29x + 0.01y & A + 0.94y + 0.01x \end{pmatrix}. \tag{6.22}$$

The associated characteristic equation is defined in terms of the trace $(Tr(J))$ and determinant $(Det(J))$ of the matrix J by:

$$det(\lambda I - J) = \lambda^2 - Tr(J)\lambda + Det(J) = 0, \tag{6.23}$$

where $Tr(J) = -1 + A + 0.94y + 0.01x$ and $Det(J) = -A + 0.3 - 0.95y + 1.28x$.

To investigate the stability of the equilibrium point we shall use the following lemma, which is a special version of Theorem 2.6 in Cahpter 2.

Lemma 8. [55] Let $Tr(J) = -1 + A + 0.94y + 0.01x$ and $Det(J) = -A + 0.3 - 0.95y + 1.28x$. Then, the two dimensional fractional map (6.19) is locally asymptotically stable if

$$\frac{-Tr(J)}{2} \geq \sqrt{Det(J)},$$

$$\text{and} \tag{6.24}$$

$$\nu > log_2 \frac{\sqrt{Tr(J)^2 - 4Det(J)} - Tr(J)}{2}.$$

For $A = -0.83$, the fractional Hénon-like map (6.19) has a unique equilibrium point $E = (\frac{-0.9}{1.16}, \frac{-0.9}{1.16})$. Based on Lemma 8 the equilibrium point E is stable when $\nu > log_2 \frac{\sqrt{Tr(J)^2 - 4Det(J)} - Tr(J)}{2}$. By simple calculation it is easy to verify that the equilibruim point E is asymptotically stable when the fractional order $\nu > 0.1430$. In this case, the fractional Hénon-like map (6.19) belongs to the family of chaotic systems having hidden attractors with stable equilibrium point.

Dynamical analysis

In order to investigate the variety of dynamics behavior that can be observed in the fractional Hénon-like map (6.19) near to the stable equilibrium point E, it is important to present at

first the corresponding numerical formula. The fractional Hénon-like map (6.19) with stable equilibrium is changed to

$$\begin{cases} x(n) = x(0) + \frac{1}{\Gamma(\nu)} \sum\limits_{j=1}^{n} \frac{\Gamma(n-j+\nu)}{\Gamma(n-j+1)} (y(j-1) - x(j-1)), \\ y(n) = y(0) + \frac{1}{\Gamma(\nu)} \sum\limits_{j=1}^{n} \frac{\Gamma(n-j+\nu)}{\Gamma(n-j+1)} (-0.33x(j-1) + Ay(j-1) - 0.48x^2(j-1) + \\ \qquad\qquad 0.47y^2(j-1) + 0.01x(j-1)y(j-1) - 0.9), \end{cases} \tag{6.25}$$

where $x(0)$ and $y(0)$ are the initial conditions. When selecting parameter $A = -0.83$, the fractional order $\nu = 0.999$ and initial condition $(x_0, y_0) = (0.32, -1.85)$ system (6.19) has hidden attractor with stable equilibrium point. The Lyapunov exponents (LEs) of the system (6.19) are $LE_1 = 0.0107$. $LE_2 = -0.0279$. Since the maximum Lyapunov exponent is larger than zero, we can determine that the hidden attractor is chaotic. Figure 6.18 presents the phase portrait of the hidden chaotic attractor with stable equilibrium.

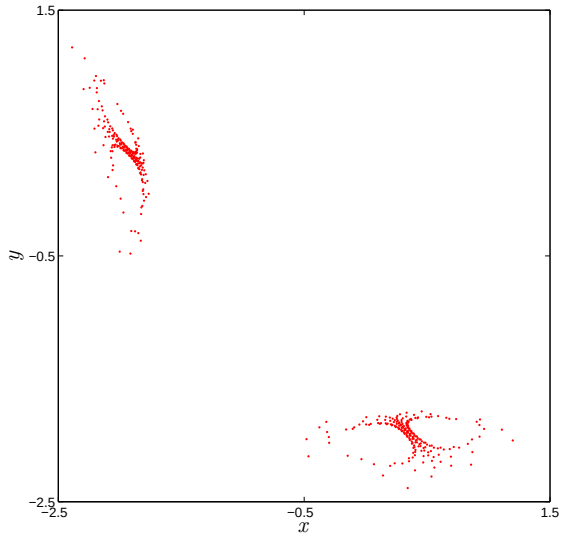

Figure 6.18: Strange attractor of the 2-dimensional fractional map (6.19) for $\nu = 0.999$ and $A = -0.83$.

Based on the numerical formula (6.25) of the fractional Hénon map with stable equilibrium, we focus on the analyze of the influence of the parameter ν.

Bifurcation versus fractional order ν

In the following, the coexisting of hidden attractors in the fractional Hénon-like map (6.25) with stable equilibrium point are revealed by phase portraits and bifurcation diagrams. For

$A = -0.83$, the dynamic evolution of the fractional Hénon-like map (6.25) versus ν is given via plotting its bifurcation diagram (see Figure 6.19). The bifurcation diagram is obtained by plotting the local maximum value of the variable x for two sets of initial conditions. The blue diagram begins with the initial condition $(x(0), y(0)) = (0.32, -1.85)$ and the red diagram begins with the initial condition $(x(0), y(0)) = (-0.32, -1.85)$. When the fractional order ν varies from 1 to 0.999, our fractional system (6.19) generates chaos with transient states. As ν decreases further a coexisting hidden periodic orbits are obtained. The coexisting hidden attractors with different values of ν are shown in Figure 6.20. Two hidden periodic attractors coexist for $\nu = 0.9989$, $\nu = 0.9987$, $\nu = 0.9984$ with initial values $(x(0), y(0)) = (0.32, -1.85)$ and $(x(0), y(0)) = (-0.32, -1.85)$ as shown in Figure 6.20(b)-(d). Also, a hidden chaotic attractor is observed with order $\nu = 0.9996$. It is noticed that the type of hidden attractors not only depend on the value of ν but also on the initial conditions.

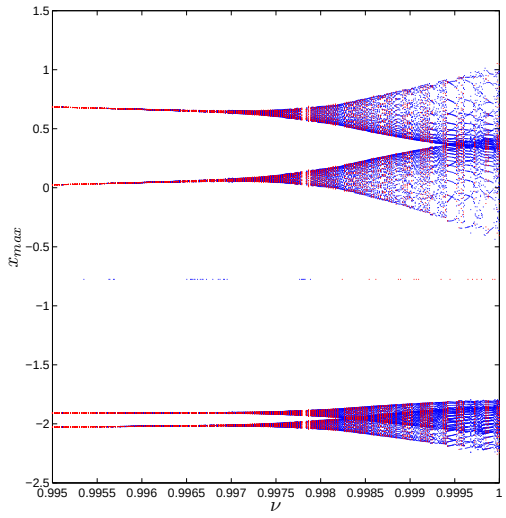

Figure 6.19: Bifurcation diagram of the two dimensional fractional Hénon-like map (6.19) with stable equilibrium point versus ν for $A = -0.83$.

The 0-1 test

To confirm the property of coexisting attractors of the proposed fractional Hénon-like map (6.19), we plot the $p - q$ trajectories of the 0–1 test using Matlab program. As it has been reportedin Chapter 3, unbounded $p - q$ trajectories implies chaotic behavior whereas bounded trajectories implies regular behavior. As in Figure 6.20 we choose to fix the system parameter A to $A = -0.83$ and vary the fractional order ν. Figure 6.21 shows the $p - q$ plots with $\nu = 0.9996$ and $\nu = 0.9984$, where the blue plots are obtained for the initial values $(x(0), y(0)) = (0.32, -1.85)$ and the red plots are obtained for $(x(0), y(0)) = (-0.32, -1.85)$. In particular, Figure 6.21(a) shows Brownian like trajectories in p versus q plan for both initial conditions, confirming that

the dynamic of the fractional system (6.19) with stable equilibrium are chaotic for both initial values and fractional order value $\nu = 0.9996$. When $\nu = 0.9984$ Figure 6.21(b) depicts bounded like trajectories in p versus q plane for both initial conditions, which confirms the coexisting of hidden periodic orbits.

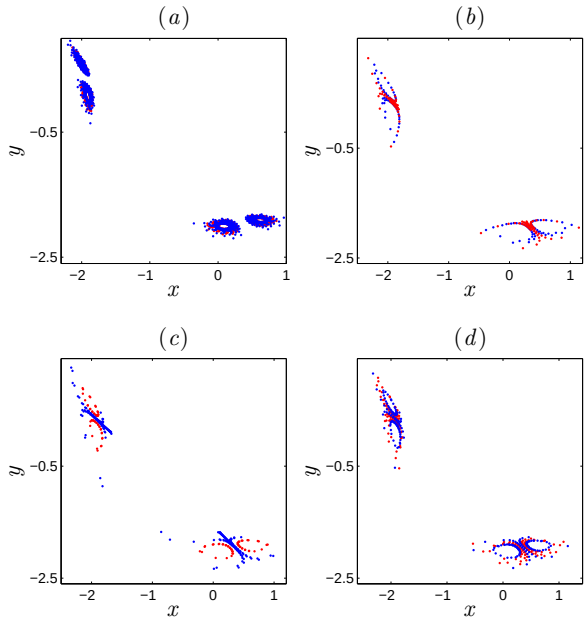

Figure 6.20: The coexisting hidden attractors of two dimensional fractional Hénon-like map (6.19) with stable equilibrium point for system parameter $A = -0.83$ and initial condition $(-0.32, -1.85)$ for red attractors and $(0.32, -1.85)$ for blue attractors, with fractional order varying: (a) $\nu = 0.9996$, (b) $\nu = 0.9989$, (c) $\nu = 0.9987$, (d) $\nu = 0.9984$.

6.5 A quadratic two dimensional fractional map without equilibria

Inspired from the work of Panahi et al. [155] and discrete fractional calculus, in this part, we consider a simple fractional order quadratic map with no discontinuity in the right-hand of equations and without equilibrium points. The system shows a number of hidden attractors for different values of the fractional order in the difference equations. The presence of the chaotic hidden attractors is validated via the bifurcation diagrams, the computation of the maximum Lyapunov exponent and the 0-1 test. Additionally, the complexity (that reflects the irregularity in the discrete data) and the entropy (that quantify the amount of regularity and the unpredictability of fluctuations in the data) are carefully evaluated and analyzed. We start by presenting a simple detailed explanation about the procedure of designing such systems. Let

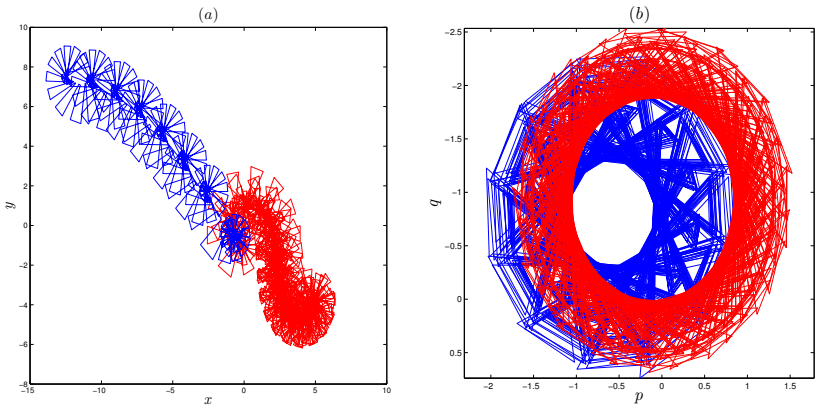

Figure 6.21: The 0-1 test of the two dimensional fractional Hénon-like map (6.19) with stable equilibrium point. (a) Brownian like trajectories for both initial conditions with $\nu = 0.9996$, (b) bounded trajectories for bowth initial condition with $\nu = 0.9984$.

us consider the following general parametric form

$$\begin{cases} x(n+1) = y(n) + x(n), \\ y(n+1) = F\left(x(n), y(n)\right) + y(n)\left[a_1 x(n) + a_2 y(n) + a_3\right] + y(n), \end{cases} \tag{6.26}$$

recently proposed by Panahi et al. [155] where $F(.,.)$ is a continue function that determines the type of system we want to design. x, y are dynamical variables and a_1, a_2, a_3 are three bifurcation parameters. The equilibrium points (x_f, y_f) can be found by solving:

$$\begin{cases} x_f = y_f + x_f, \\ y_f = F\left(x_f, y_f\right) + y_f\left[a_1 x_f + a_2 y_f + a_3\right] + y_f. \end{cases} \tag{6.27}$$

From equation (6.27), we have

$$y_f = 0, \quad and \quad F\left(x_f, y_f\right) = 0. \tag{6.28}$$

Therefore, to design the chaotic map with no equilibrium, we should just choose $F(x_f, y_f)$ in a way that it cannot become zero. In order to illustrate the presence of hidden attractors we discuss the case where $F(x(n), y(n))$ is a second degree equation and $\Delta < 0$, in this case the system defined by equations (6.27) does not allow for the existence of any equilibrium point; neither stable nor unstable.

The systematically exhaustive search for "elegant" systems developed in [162] was performed by Panahi et al. [155] and applied to the two dimensional system (6.27) with quadratic nonlinearities function:

$$F\left(x(n), y(n)\right) = a_4 x(n)^2 + a_5 x(n) + a_6, \tag{6.29}$$

and the condition $a_5^2 - 4a_4a_6 < 0$. The simplest case obtained from the search procedure [155], is

$$\begin{cases} x(n+1) = y(n) + x(n), \\ y(n+1) = 0.1x^2(n) + 0.1 + y(n)[-x(n) - by(n)] + y(n), \end{cases} \tag{6.30}$$

where b is the bifurcation parameter. In its most general form, the system has six parameters. However, two of these parameters are set up to zero and still obtain hidden chaotic behavior of the form, shown in Figure Figure 6.22-(c). The bifurcation diagram and Lyapunov exponents are plotted in Figure 6.22(a) and Figure 6.22(b), respectively, confirming the existence of chaos.

By introducing the Caputo like difference operator ${}^C\Delta_a^\nu$ in the integer order difference equations (6.30), Ouannas et.al. [169] introduced a new fractional-order quadratic two dimensional fractional map without equilibria with order $\nu \in]0, 1]$, as follows

$$\begin{cases} {}^C\Delta_a^\nu x(t) = y(t-1+\nu), \\ {}^C\Delta_a^\nu y(t) = 0.1x^2(t-1+\nu) - by^2(t-1+\nu) - x(t-1+\nu)y(t-1+\nu) + 0.1, \end{cases} \tag{6.31}$$

where a is the starting point and $t \in N_{a+1-\nu}$. The proposed fractional difference equations exploit the Caputo operator and do not contain any discontinuity in their right-hand side. It can be seen that the fractional model possesses three quadratic nonlinearties x^2, y^2 and xy.

We denote the equilibrium point of the quadratic fractional-order map (6.31) with (x_f, y_f). The equilibrium point of (6.31) can be found by solving

$$\begin{cases} {}^C\Delta_a^\nu x_f = y_f, \\ {}^C\Delta_a^\nu y_f = 0.1x_f^2 - by_f^2 - x_f y_f + 0.1, \end{cases} \tag{6.32}$$

and by taking in mind that the Caputo–like delta difference of constant is equal to zero, one can get

$$0.1\left(x_f^2 + 1\right) = 0. \tag{6.33}$$

Therefore, from the above equation, we can easily confirm that the quadratic fractional order map (6.31) has no equilibriua point; which means the attractors produced by system (6.31) are all hidden attractors.

6.5.1 Dynamic analysis

To continue with the analysis of the quadratic fractional map (6.31), we need to define the numerical formula of the proposed system. Using Theorem 1.15 and assuming that $a = 0$, the system (6.31) is converted to

$$\begin{cases} x(n) = x(0) + \frac{1}{\Gamma(\nu)} \sum_{j=1}^{n} \frac{\Gamma(n-j+\nu)}{\Gamma(n-j+1)} \left(y(j-1)\right), \\ y(n) = y(0) + \frac{1}{\Gamma(\nu)} \sum_{j=1}^{n} \frac{\Gamma(n-j+\nu)}{\Gamma(n-j+1)} \\ \qquad \times \left(0.1x^2(j-1) - by^2(j-1) - x(j-1)y(j-1) + 0.1\right). \end{cases} \tag{6.34}$$

This numerical formula will allow us to investigate the existence of hidden attractors of the quadratic fractional-order map (6.31) in detail. Simulation of phase portraits, bifurcation diagram, largest Lyapunov exponents and 0-1 test will help us to analyze its dynamic features.

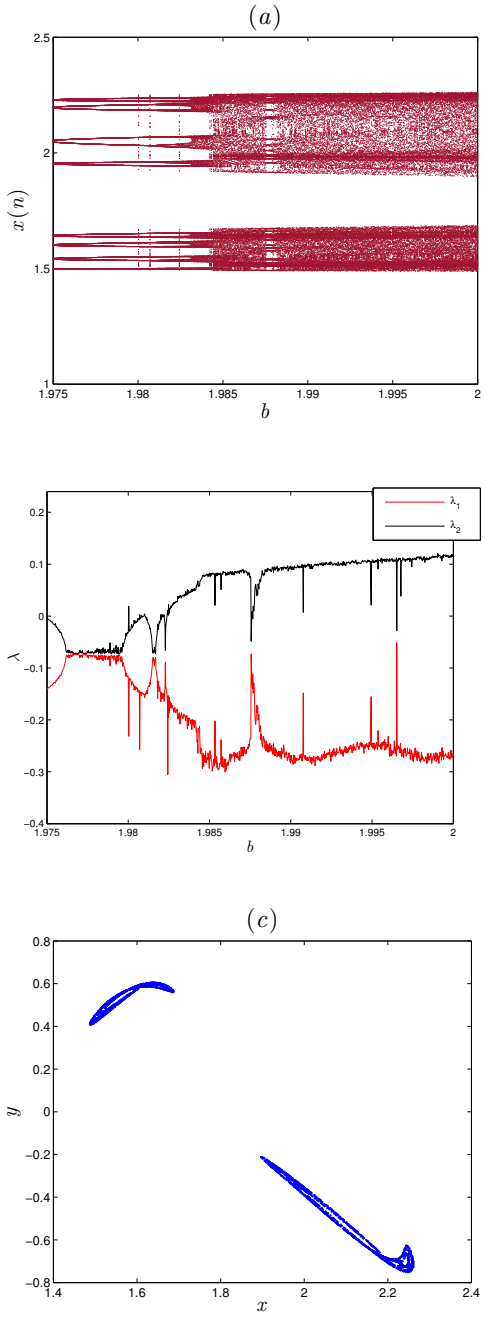

Figure 6.22: Numerical analysis of the quadratic fractional map without equilibria (6.30) with $[x_0, y_0] = [1.7 - 0.39]$: (a) Bifurcation diagram with the variation of b; (b) Lyapunov exponents with variation of b; (c) hidden chaotic attractor for $b = 2$.

Bifurcation diagrams and maximum Lyapunov exponents

Consider the dynamic evolution of system (6.31) with respect to parameter b under the given initial condition $(x_0, y_0) = (1.7, -0.39)$. With the change of the fractional order ν, the system can be tracked in different states. The bifurcation diagrams of the quadratic fractional–order map (6.31) for two different values of ν are shown in Figure 6.23. As it can be seen, the variation of order ν has a critical impact on the states of the quadratic fractional-order map (6.31). Figure 6.23(a) is the bifurcation diagram of system (6.31) with order $\nu = 1$. When $b \in [1.975, 1.983[$ a series of periodic windows is observed. As the value of b increases from 1.983 to 2, the states of the fractional-order map (6.31) displays chaotic dynamics. In the bifurcation diagram of Figure 6.23(b), the fractional order value ν is set to 0.7457. In this case the route leading to chaos is a period doubling bifurcation. Compared this diagrams it can be seen that the area of chaotic motions decreases as the order ν varied.

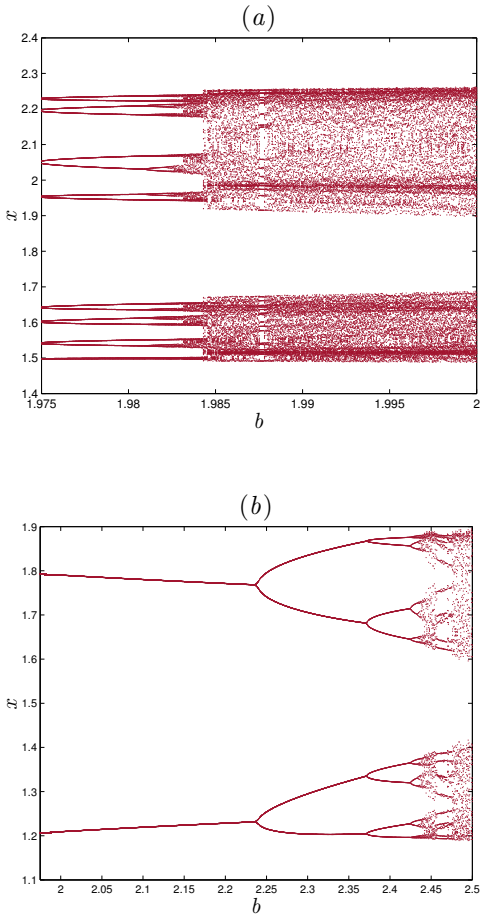

Figure 6.23: Bifurcation diagrams of the quadratic fractional–order map (6.31) when the parameter b is varied with the different values of order ν: (a) for $\nu = 1$; (b) for $\nu = 0.7457$.

To study the dynamics further, the bifurcation diagram of the quadratic fractional-order map (6.31) versus ν for $b = 2$ is considered. Figure 6.24 shows the resulting bifurcation diagram. Clearly, a period doubling scenario route to chaos is observed as ν decreases. In this case the quadratic fractional-order map is chaotic when $\nu \in]0.01, 0.1962[\cup[0.996, 1]$ while is regular in the remaining interval. To valid this, the maximum Lyapunov exponent is calculated using the Jacobian matrix algorithm (See Chapter 3). As is well known a system is verified to be chaotic when the maximum Lyapunov exponent (LE) is positive. The maximum LE diagram which is associated with Figure 6.24 is reported with a red line. In Figure 6.24, the maximum Lyapunov exponent is equal to zero or negative over most of the rang $(0.1962, 0.996)$, which implies that the fractional–order map is periodic. For small values of ν the fractional-order map is more complex, because the corresponding maximum LE is larger. The phase diagrams with several specified values of fractional order are plotted in Figure 6.25. From Figure 6.25, it is clear that there are different and new hidden chaotic attractors, which consistent with the results in Figure 6.24.

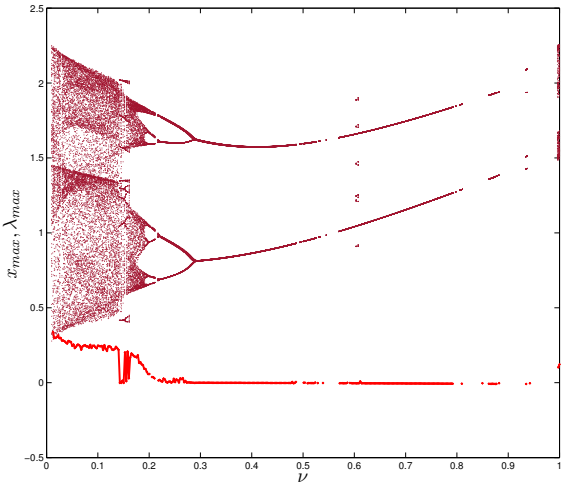

Figure 6.24: Bifurcation diagram and largest Lyapunov exponent of the quadratic fractional–order map (6.31) when the value of the fractional order ν is varied with $b = 0.2$.

0-1 test

Finally, the existence of chaos is justified by means of 0-1 test method. As it has been reported before, the 0-1 test for chaos can apply directly to a series of data and does not require phase space reconstruction. Table 6.2 and Figure 6.26 depicts the results of the test for different values of ν with $b = 2$. First, we observe that when $\nu = 0.06767, \nu = 0.0852$ and $\nu = 0.998$, the asymptotic growth rate K of the quadratic fractional order map are $K = 0.996$, $K = 0.901$ and $K = 0.7633$, respectively. Second, the unbounded behavior of the translation component in the $p - q$ plane (Figure 6.26) shows Brownian-like trajectories which indicates chaos. This

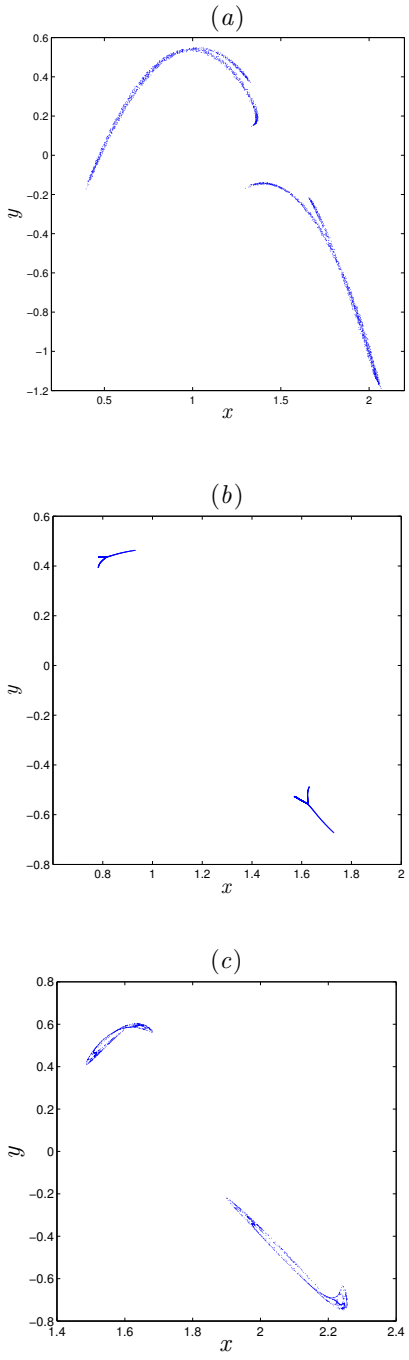

Figure 6.25: Hidden attractors for different values of ν: (a) Hidden chaotic attractor for $\nu = 0.0852$, (b) Hidden periodic attractor for $\nu = 0.2931$, (c) Hidden chaotic attractor for $\nu = 0.998$.

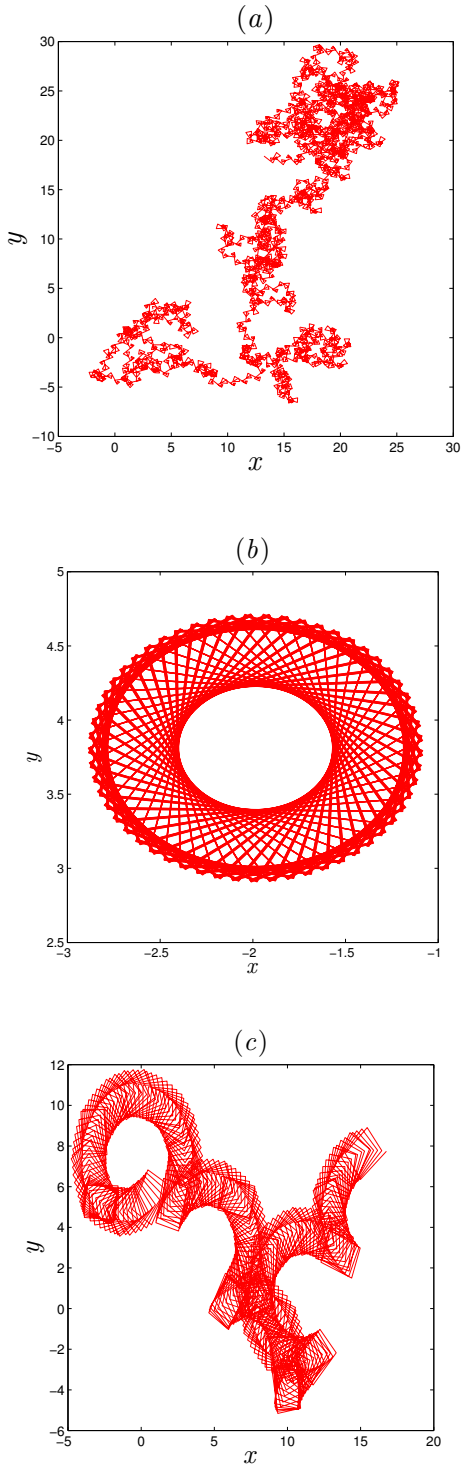

Figure 6.26: Dynamics of the translation components $p - q$ for the quadratic fractional order map (6.31) different values of ν: (a) $\nu = 0.0852$, (b) $\nu = 0.2931$, (c) $\nu = 0.998$.

results agrees well with the phase diagrams in Figure 6.25. Conversely, for $\nu = 0.2931$ the 0-1 test approaches 0 and returns bounded trajectories as shown in Figure 6.26(b) confirming that the quadratic fractional order map is periodic for $\nu = 0.2931$.

Table 6.2: Results of 0-1 test for the quadratic fractional order map (6.31) with different fractional order values

ν	0.06767	0.0852	0.2931	0.4244	0.998
K	0.996	0.901	-0.0015	-0.00762	0.7633

6.5.2 Complexity analysis

C_0 complexity analysis

The C_0 complexity is an index which can describe the random degree of a discrete data. This algorithm is described as in Chapter 3. The C_0 complexity of state $x(n)$ of the numerical formula (6.34) is calculated versus order ν as shown in Figure 6.27. Figure 6.27 shows that the complexity of the fractional order map (6.31) decrease with the increment of the quadratic fractional order ν, which much well with the results in Figure 6.24.

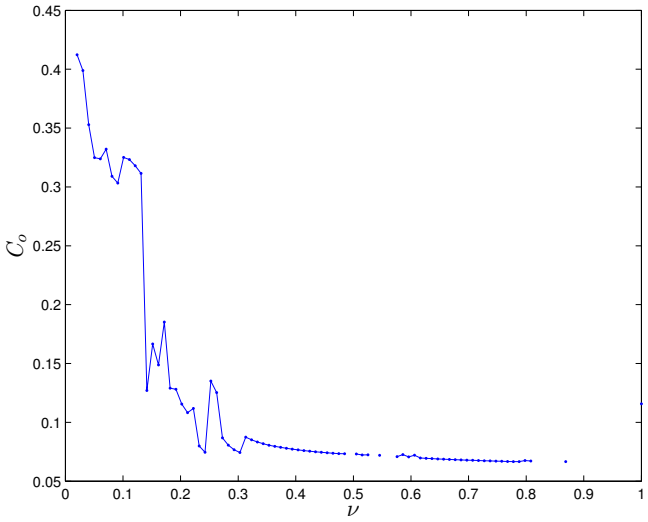

Figure 6.27: C_o complexity of the quadratic fractional order map (6.31) with ν varying and $b = 2$.

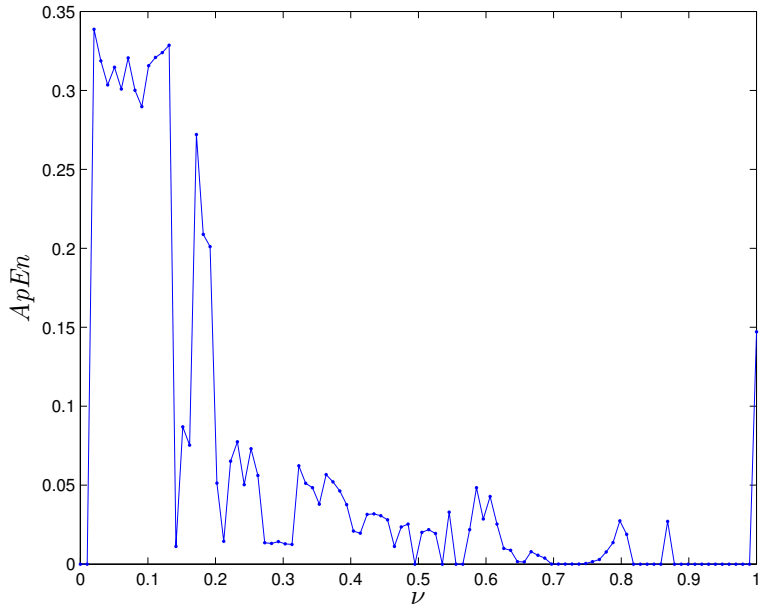

Figure 6.28: ApEn of the quadratic fractional–order map (6.31) with ν varying and $b = 2$.

Approximate entropy

Now, the complexity of the quadratic fractional-order map (6.31) is described by employing approximate entropy (ApEn), which is briefly described in Chapter 3. Let $b = 2$ and $[x_0, y_0] = [1.7, -0.39]$, Figure 6.28 shows the ApEn of the proposed fractional–order map (6.31) for different fractional order values. As one can see, the complexity of the fractional–order map (6.31) varied as we vary ν. Therefore, we must be aware of the selected fractional order in order to have a relatively high structural complexity. The quadratic fractional–order map (6.31) is more complex when $\nu \in (0.1253, 0.1353)$.

This results illustrates that the quadratic fractional-order chaotic map show more complex chaotic behaviors than its integer order counterpart, which can be seen from C_0 complexity, approximate entropy, bifurcation diagram, and largest Lyapunov exponents. The fractional form of system has high complexity when the fractional order is smaller, so it plays an important role in the field of communication encryption. In particular, the complexity of the quadratic fractional-order chaotic map is not only related to the parameters of the system itself, but also related to the fractional order of the map.

6.6 Fractional-order discrete-time systems with closed curve fixed points

With the further research of chaos, scientist found that some nonlinear dynamic systems with special features of the equilibrium points can produce chaos. Here we introduce a new class of fractional-order discrete-time systems with closed curve equilibrium points. Different shapes of equilibria like a square, a rectangle, a circular, and a rounded-suare equilibrium points are shown by choosing proper parameters of nonlinear function. Interestingly, such special systems are classified as systems with "hidden attractors" from the computational point of view. The mathematical model of these fractional systems are formulated by combining Caputo like difference operator and a class of integer order discrete-time systems reported in [161].

Recently, Jiang Haibo et al. [161] have suggested a class of integer-order difference equations to discover two-dimensional discrete time systems with closed curve equilibrium points. Such an interesting system is proposed as:

$$\begin{cases} x(n+1) &= x(n) + a_1 f\left(x(n), y(n)\right), \\ y(n+1) &= y(n) + f\left(x(n), y(n)\right)\left(a_2 x(n) + a_3 y(n) + a_4 x^2(n) + a_5 y^2(n)\right. \\ & \qquad \left. + a_6 x(n) y(n) + a_7\right), \end{cases} \tag{6.35}$$

where $x(n)$, $y(n)$ are the state variables and a_i, $i = \overline{1.7}$ are real constant while $f\left(x(n), y(n)\right)$ is a nonlinear function. Similarly, the equilibrium points (x_f, y_f) of system (6.35) must satisfy:

$$\begin{cases} x_f &= x_f + a_1 f\left(x_f, y_f\right), \\ y_f &= y_f + f\left(x_f, y_f\right)\left(a_2 x_f + a_3 y_f + a_4 x_f^2 + a_5 y_f^2 + a_6 x_f y_f + a_7\right). \end{cases} \tag{6.36}$$

Thus, it is simple to verify that the equilibrium points of the system (6.35) are located on a curve described by $f(x_f, y_f) = 0$. Jiang Haibo et al. [161] used the nonlinear function

$$f\left(x(n), y(n)\right) = \left(\frac{x(n)}{m}\right)^p + \left(\frac{y(n)}{k}\right)^p - r^2, \tag{6.37}$$

in which m, k, r are three strictly positive real constant and p is an integer order such that $p \geq 2$. A summary of fractional-order discrete time systems with different shapes of equilibrium points based on the nonlinear function $f(x, y)$ is given in the following subsections.

6.6.1 Fractional-order discrete time system with square–shaped fixed points

Motivated by the discovery of discrete time systems with closed curve equilibrium points, Hadjabi Fatima et al. [163] introduced a new fractional-order discrete time (FODT) system with square–shaped equilibrium. System (6.35) under the ν–Caputo like difference becomes a FODT system with square–shaped equilibrium, when $m = 1$, $n = 1$, $p = 12$, and $r = 1$. In this case, the system is described by

$$\begin{cases} {}^{C}\Delta_a^{\nu_1} x(t) &= -\alpha\left(x^{12}(t-1+\nu_1) + y^{12}(t-1+\nu_1) - 1\right), \\ {}^{C}\Delta_a^{\nu_2} y(t) &= \beta x(t-1+\nu_2) y(t-1+\nu_2)\left(x^{12}(t-1+\nu_2) + y^{12}(t-1+\nu_2) - 1\right), \end{cases} \tag{6.38}$$

where ν_1, ν_2 are the fractional order and α, β are the bifurcation parameters. The square shaped equilibrium points of the FODT system (6.38) is described as

$$F = \left\{(x, y) \in \mathbb{R}^2 \mid x^{12} + y^{12} - 1 = 0\right\}. \tag{6.39}$$

This fractional map is invariant under transformation $y \to -y$ for all values of parameters α, β and order ν. This property will be reflected in the equilibria and attractors of system (6.38). In the following, we will study the dynamical behavior of the FODT system (6.38) for some specific parameters and initial values.

Dynamical analysis

In order to further investigate the dynamical behavior of the new FODT system (6.38), we need to determine the corresponding numerical formula. Using Theorem 1.15, the equivalent numerical formula of the FODT system (6.38) with square–shaped fixed points can be written as:

$$\begin{cases} x(n) = x(0) - \frac{\alpha}{\Gamma(\nu_1)} \sum_{j=1}^{n} \frac{\Gamma(n-j+\nu_1)}{\Gamma(n-j+1)} (x^{12}(j-1) + y^{12}(j-1) - 1), \\ y(n) = y(0) + \frac{\beta}{\Gamma(\nu_2)} \sum_{j=1}^{n} \frac{\Gamma(n-j+\nu_2)}{\Gamma(n-j+1)} \left(x(j-1)y(j-1)\left(x^{12}(j-1) + y^{12}(j-1)\right)\right). \end{cases} \tag{6.40}$$

where $x(0)$ and $y(0)$ are the initial conditions. Based on the integer-order system (6.35) and the condition (6.39), by performing a systematic search [162], [163] and focusing on elegant cases, the FODT system (6.35) exhibits complex behavior for $\alpha = 0.2, \beta = 2.4$, and initial conditions $(x(0), y(0)) = (0.26, -0.14)$ for the commensurate order $\nu_1 = \nu_2 = 1$, as shown in Figure 6.29-(a) where the black points represent the square-shaped fixed points. Figure 6.29-(b) shows the time evolution of x and y. It can be seen that the system (6.38) has two symmetrical states. Following are the results of our investigations of various cases studied.

Cas 1 . Commensurate order $\nu_1 = \nu_2 = \nu$. We study the dynamics of the FODT system (6.35) with square–shaped equilibrium points by numerical simulation. In this simulation, the initial conditions are taken as $[x(0), y(0)] = [0.26, -0.14]$ to ensure the existence of chaos. For $\nu = 1$, the bifurcation plots with respect to α and β are illustrated in Figures 6.29-(c) and 6.29-(d), respectively. These diagrams are constructed for 50 initial points. We see that the maximum chaotic range is observed for $\alpha \approx 0.35$ and $\beta \approx 2.455$. Also, we notice that the range of β for which we obtain a chaotic behavior is very short. Hence, it is more interesting to visualize the effect of α on the map's dynamics.
For that the system was calculated numerically against $\alpha \in [0, 0.35]$, while the parameter β is fixed to $\beta = 2.4$. The bifurcation diagrams and largest Lyapunov exponents under the fractional order values $\nu_1 = \nu_2 = 0.95$ and $\nu_1 = \nu_2 = 0.9$ are given in Figure 6.30. By comparing fiigures 6.30-(a) and 6.30-(b) with figures 6.30–(c) and 6.30(d), we find that the interval where chaos exists shrinks as ν decreases. In particular, when the value of $\nu = \nu_1 = \nu_2$ changes from 0.95 to 0.9, the areas of chaotic motion shrinks from $[1.022, 1.116] \cup [1.164, 1.216]$ to $[0.2405, 0.2429] \cup [0.3126, 0.3423]$.

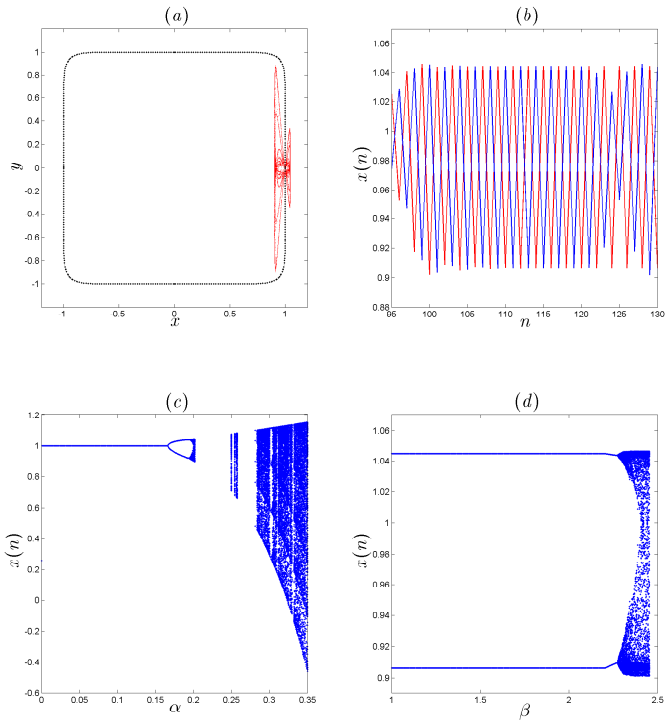

Figure 6.29: Numerical analysis of the FODT system (6.38) with square–shaped equilibrium points in the commensurate case $\nu_1 = \nu_2 = \nu = 1$. (a) Square-shaped fixed point of the fractional-order map in black dots and hidden chaotic attractor in red color. (b) Evolution states of the fractional–order map (6.38) of x and y. (c) Bifurcation diagram of the FODT system (6.38) versus α for $\beta = 2.4$. (d) Bifurcation diagram of the fractional–order map (6.38) versus β for $\alpha = 0.2$.

Cas 2 . Incommensurate order $\nu_1 \neq \nu_2$. In this case, we reset the parameter $\beta = 2.2$ and keep the parameter α as $\alpha = 0.2$, Figure 6.31 shows the bifurcation diagram of the FODT system (6.38) with the decreasing of ν_2 where $\nu_1 = 1$. When ν_2 decreased from 1 the FODT system (6.38) with square–shaped equilibrium points goes into periodic state and it goes into chaos at 0.9035. It is also noticed that the periodic state of the integer order system becomes chaotic as ν_2 decreases. Another interesting dynamic is observed if we increase the value of α to 0.23 and decrease the value of β to 0.5. In this case, two chaotic attractors are observed in the fractional–order map with respect to the fractional orders $\nu_1 = 1$ and $\nu_2 = 0.01$, as shown in Figure 6.32, where the red color attractor is yielded from initial value $(0.1, 0.3)$ and blue color attractor is yielded from initial value $(0.1, -0.3)$. Therefore, we conclude that the fractional orders improve the complexity of the chaotic motion of the original system (6.35) with square-shaped fixed point.

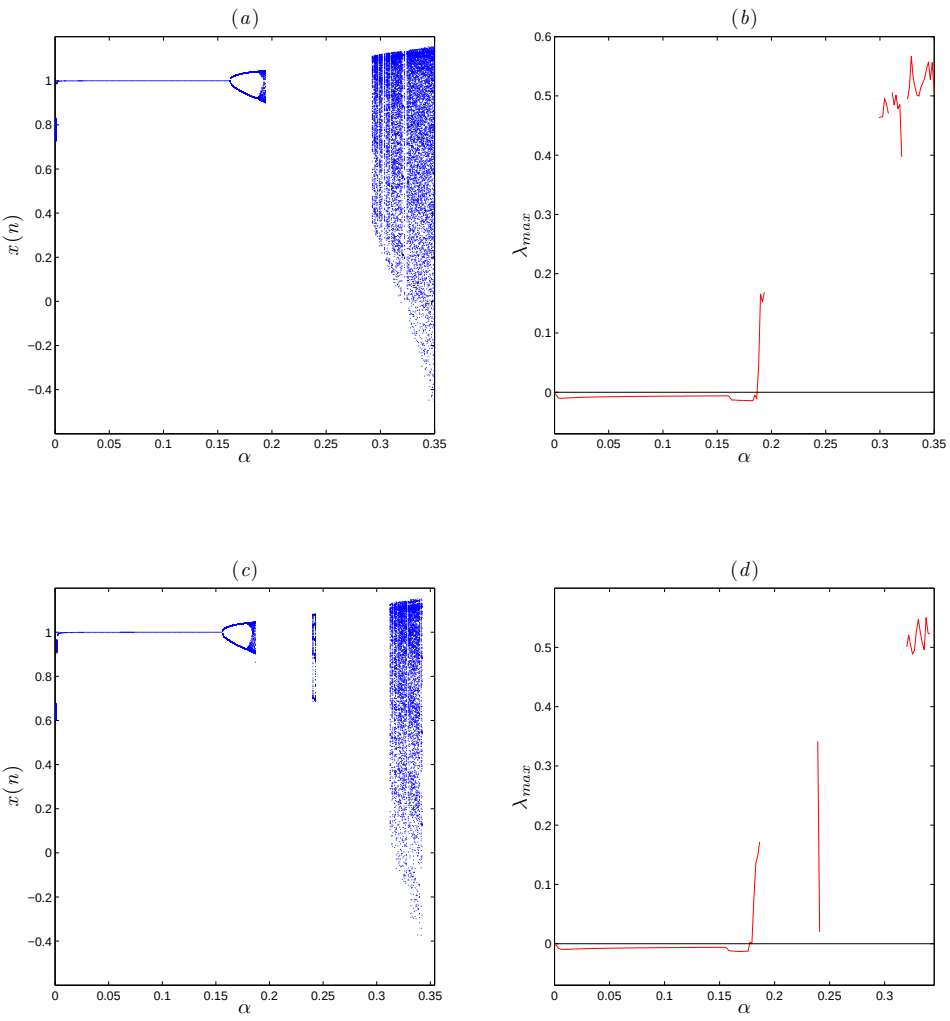

Figure 6.30: (a) Bifurcation diagram of the FODT system (6.38) with square–shaped equilibrium points versus α for $\nu_1 = \nu_2 = 0.95$. (b) Largest Lyapunov exponents corresponding to (a). (c) Bifurcation diagram of the FODT system (6.38) versus α for $\nu_1 = \nu_2 = 0.9$. (d) Largest Lyapunov exponents corresponding to (c).

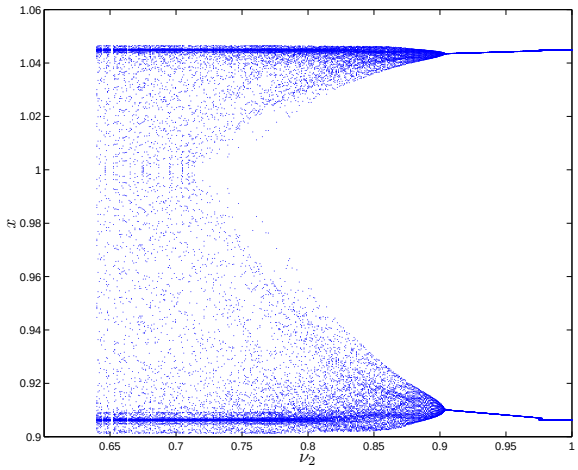

Figure 6.31: Bifurcation diagram of the FODT system (6.38) with square–shaped equilibrium points in the $x - \nu_2$ plane for $\alpha = 0.2$ and $\beta = 2.2$.

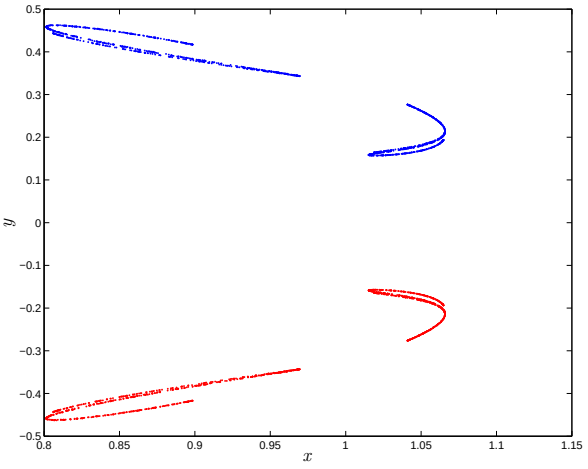

Figure 6.32: Coexisting chaotic attractor of the the FODT system (6.38) with square–shaped equilibrium points for $\alpha = 0.2$ and $\beta = 2.2$.

6.6.2 Fractional-order discrete time system with rectangle shaped equilibrium points

Now, we consider system (6.35) when $m = 5$, $n = 1$, $p = 12$, $r = 1$. In this case we have the following system

$$\begin{cases} x_{k+1} &= x_k + ((\frac{x_k}{5})^{12} + y_k^{12} - 1), \\ y_{k+1} &= y_k + \alpha y_k((\frac{x_k}{5})^{12} + y_k^{12} - 1), \end{cases} \tag{6.41}$$

where x and y are the system variables. Using the same argument as with the previous system, we obtain the following fractional order map

$$\begin{cases} {}^{C}\Delta_a^{\nu_1} x(t) = \left(\frac{x(t-1+\nu_1)}{5}\right)^{12} + y^{12}(t-1+\nu_1) - 1, \\ {}^{C}\Delta_a^{\nu_2} y(t) = \alpha y(t-1+\nu_2)((\frac{x(t-1+\nu_2)}{5})^{12} + y^{12}(t-1+\nu_2) - 1), \end{cases} \tag{6.42}$$

where $\nu \in (0, 1)$ is the fractional order. The fixed point of the new fractional–order map (6.42) are obtained by solving the following system of equation:

$$\begin{cases} (\frac{x}{5})^{12} + y^{12} - 1 &= 0, \\ \alpha y((\frac{x}{5})^{12} + y^{12} - 1) &= 0. \end{cases} \tag{6.43}$$

Thus, we must have

$$(\frac{x}{5})^{12} + y^{12} - 1 = 0. \tag{6.44}$$

Therefore, the novel fractional–order map (6.42) has rectangle-shaped equilibrium points. To study the dynamical behavior of the novel fractional–order map (6.42), we define the numerical formula as

$$\begin{cases} x(n) = x(0) + \frac{1}{\Gamma(\nu_1)} \sum_{j=1}^{n} \frac{\Gamma(n-j+\nu_1)}{\Gamma(n-j+1)} \left(\left(\frac{x(j-1)}{5}\right)^{12} + \left(\frac{y(j-1)}{12}\right)^{12} - 1 \right) \\ y(n) = y(0) + \frac{\alpha}{\Gamma(\nu_2)} \sum_{j=1}^{n} \frac{\Gamma(n-j+\nu_2)}{\Gamma(n-j+1)} \left(y(j-1) \left(\left(\frac{x(j-1)}{5}\right)^{12} + y^{12}(j-1) - 1 \right) \right). \end{cases} \tag{6.45}$$

where $x(0)$ and $y(0)$ are the initial conditions.

Dynamical analysis

In this section we investigate the dynamical behavior of the FODT system(6.42) rectangle-shaped fixed points using numerical simulations. When $\alpha = 2.2$ the system (6.42) shows hidden chaotic attractor as depicts in Figure 6.33. It can be shown that it also has a symmetry with respect to the x-axis. Figure 6.34 shows the bifurcation diagrams and largest Lyapunov exponents of the FODT systems (6.42). According to Figure 6.34, it is very clear that the dynamical behavior of system (6.42) goes from periodic state to chaotic state with the increasing of control parameter α. Obviously, as the fractional order values in the commensurate case $\nu = \nu_1 = \nu_2$ decreases from 0.998 to 0.995, the bifurcation diagram gradually shrinks to the left.

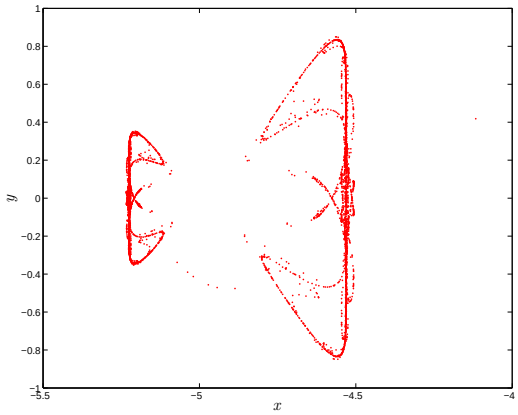

Figure 6.33: Chaotic attractor of the FODT (6.42) with rectangle shaped equilibrium points for $\alpha = 2.2$.

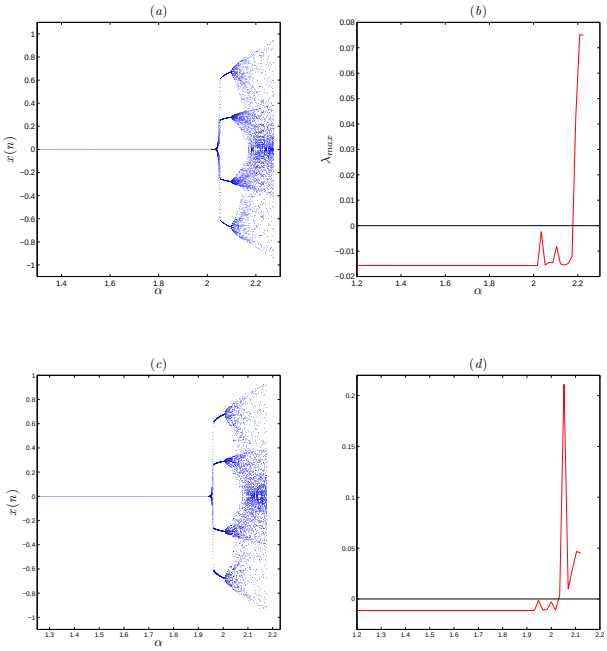

Figure 6.34: (a) Bifurcation diagram of the FODT (6.42) with rectangle shaped equilibrium points versus α for $\nu_1 = \nu_2 = 0.988$. (b) Largest Lyapunov exponents corresponding to (a). (c) Bifurcation diagram of the FODT system (6.38) versus α for $\nu_1 = \nu_2 = 0.995$. (d) Largest Lyapunov exponents corresponding to (c).

6.7 A new 2D-FoDs

This part considers the following 2D-difference system [190]

$$\begin{cases} {}^{C}\Delta_{a}^{\gamma}x(t) = y(t-1+\gamma) - x(t-1+\gamma), \\ {}^{C}\Delta_{a}^{\gamma}y(t) = -\alpha y(t-1+\gamma) - 0.37y^{2}(t-1+\gamma) + 0.81x(t-1+\gamma)y(t-1+\gamma) + 1.79, \end{cases} \tag{6.46}$$

where x and y stand for state variables of the FoDs, α is the system's parameter, and ${}^{C}\Delta_{a}^{\gamma}$ is the Caputo-like difference operator of fractional-order γ, where $\gamma \in (0,1)$.
In the following, some numerical methods are adopted to examine the complex dynamics of the proposed FoDs. First of all, we discuss the equilibrium points of the model at hand. Actually, the equilibrium points can be determined by finding the solution of the following system

$$\begin{cases} y - x = 0, \\ -\alpha y - 0.37y^{2} - 0.81xy + 1.79 = 0. \end{cases} \tag{6.47}$$

From system (6.47), it follows that:

$$-\alpha y - 1.18y^{2} + 1.79 = 0. \tag{6.48}$$

Thus, FoDs (6.46) has no equilibrium point when $-2.9067 < \alpha < 2.9067$. This result shows that FoDs (6.46) is able to produce chaotic hidden attractor for appropriate choice of initial conditions and fractional order as well.

Secondly, we present the numerical formulae corresponding to all equations given in FoDs (6.46):

$$\begin{cases} x(n) = x_{0} + \frac{1}{\Gamma(\gamma)}\sum_{\kappa=1}^{n}\frac{\Gamma(n-\kappa+\gamma)}{\Gamma(n-\kappa+\gamma)}(y(\kappa-1) - x(\kappa-1)), \\ y(n) = y_{0} + \frac{1}{\Gamma(\gamma)}\sum_{\kappa=1}^{n}\frac{\Gamma(n-\kappa+\gamma)}{\Gamma(n-\kappa+\gamma)}(-\alpha y(\kappa-1) - 0.37y^{2}(\kappa-1) \\ \qquad\qquad + 0.81x(\kappa-1)y(\kappa-1) + 1.79), \end{cases} \tag{6.49}$$

where x_0 and y_0 are the initial states. According to the discrete equation (6.49), the proposed fractional system (6.46) has memory effects, which means that the iterated solutions x and y are determined by all the previous states. In the next section, some dynamic characteristics of the novel 2D-FoD system are analyzed numerically.

6.7.1 Bifurcations and LLEs

When plotting bifurcation diagrams, two sets of symmetrical initial states are considered. The bifurcation diagram is plotted in blue for the initial state $x_0 = 1.78$, $y_0 = -0.79$, and red for the initial states $x_0 = -1.78$, $y_0 = 0.79$.

Bifurcation and LLEs versus the system's parameter α

Firstly, the bifurcation diagram of FoDs (6.46) is studied as α varies from 1.35109 to 1.9199. Besides, the bifurcation diagrams and LLEs of the state variable $x(n)$ are also studied corresponding to two distinct fractional-order values of γ as exhibited in Fig. 6.35 and Fig. 6.36. It

can be seen that the states of FoDs (6.46) changes qualitatively with the variation of α and γ. In particular, the bifurcation diagram of FoDs (6.46) is illustrated in Fig. 6.35(a), for $\gamma = 0.9362$. When α increases from 1.35109 to 1.9199, the states of the system goes, via period doubling bifurcation, to chaotic motion. It is noteworthy that FoDs (6.46) exhibits chaotic behavior in larger intervals for the initial condition $x_0 = 1.78$, $y_0 = -0.79$. As shown in Fig. 6.36, when γ is increased starting from 0.9362 up to 0.992, then FoDs (6.46) shows chaotic motion over most of the range $(1.7387, 1.9136)$.

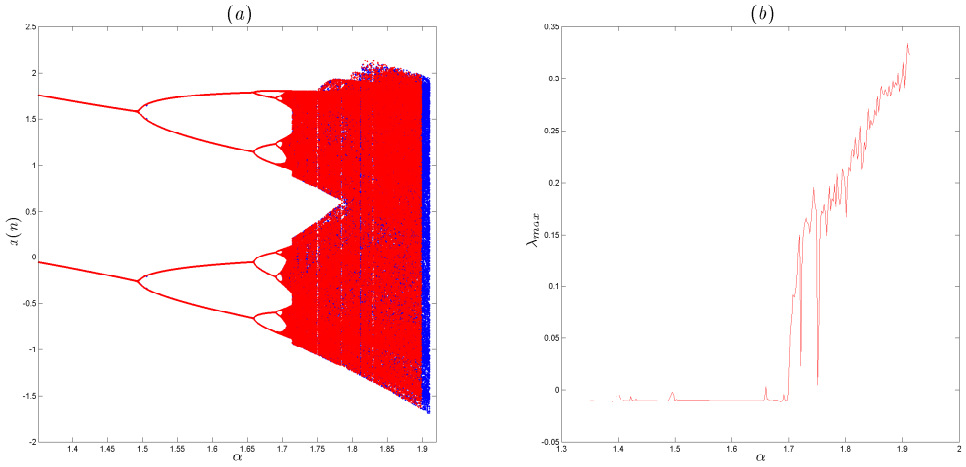

Figure 6.35: (a) Bifurcation diagrams of FoDs (1) vs. α, when $\gamma = 0.9362$, (b) LLE diagram according to (a).

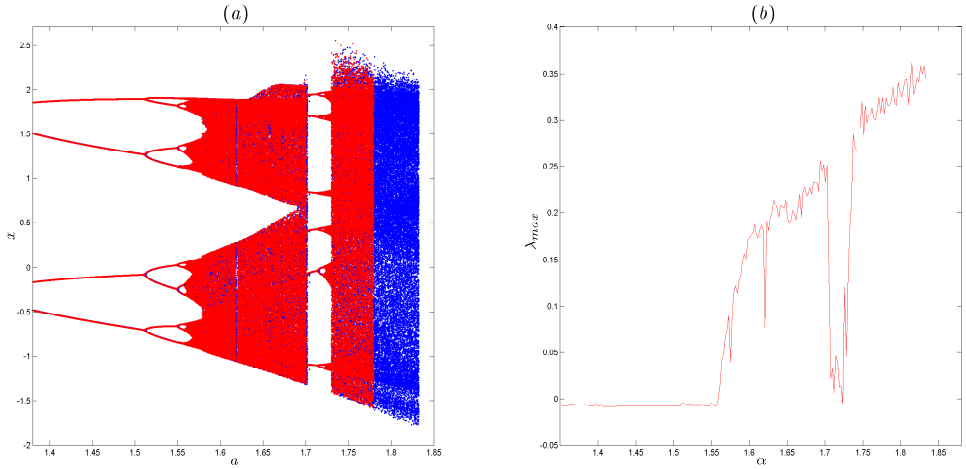

Figure 6.36: (a) Bifurcation diagrams of FoDs (1) vs. α, when $\gamma = 0.992$, (b) LLE diagram according to (a).

Bifurcation versus fractional-order γ

In order to highlight the effect of γ on the dynamic behavior of FoDs (6.46), its bifurcation with respect to γ too is considered. We fix the parameter α to be equal 1.73, and change γ within $[0, 1]$. The bifurcation diagram and the LLE are illustrated in (a) and (b) of Fig. 6.38, respectively. As one can see, the system has positive LE when γ takes the smallest values, indicating that FoDs (6.46) is chaotic. Besides, when $\gamma \in [0.9362, 0.9402] \cup]0.9816, 0.9834]$; the FoDs (6.46) shows chaotic behavior. The phase diagrams are ploted in Figure 6.37 for different values of γ. From these diagrams, it is clear that as the value of γ increases, different chaotic attractors id observed. Moreover, this figures indicates that the fractional order γ is another bifurcation parameter.

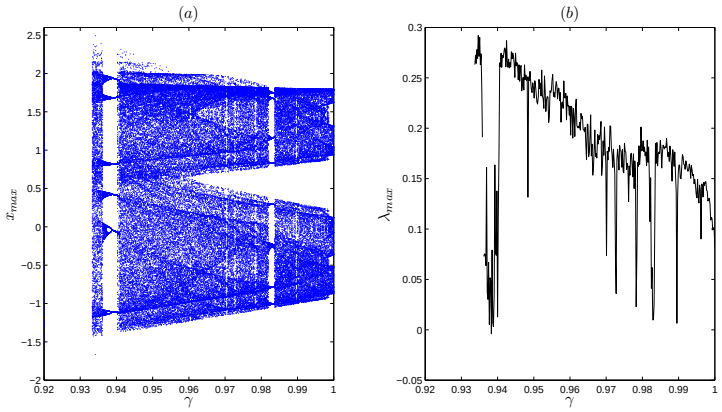

Figure 6.37: Phase diagrams of fractional order map (6.46) for different values of fractional order.

6.7.2 Coexisting chaotic attractors

Herein, the dynamics of FoDs (6.46) are analyzed using the phase portraits, obtained by fixing the parameter α and by considering the two previous different sets of initial conditions. For $\gamma = 0.992$, as shown in Fig. 6.39 (a), the FoDs (6.46) highlights the coexistence of hidden chaotic attractor corresponding to the two initial conditions $(1.78, -0.79)$. Similarly, when the order γ is selected to be equal 0.9992 in FoDs (6.46), Fig. 6.39(b) highlights the coexistence chaotic hidden attractors corresponding to the two initial conditions $(-1.78, 0.79)$ and $(1.78, -0.79)$, respectively. Finally, when γ is taken to be equal 0.96, the coexisting chaotic hidden attractors are plotted in Fig. 6.39(c). One might deduce that the dynamic behavior of the new FoDs given in (6.46) is complex and interesting, by virtue of the presence of different types of coexisting hidden chaotic attractors.

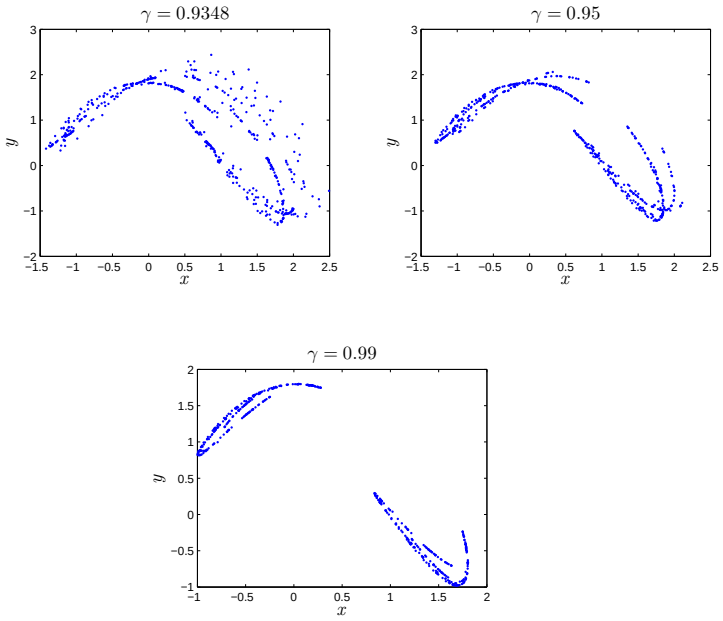

Figure 6.38: (a) Bifurcation diagram vs. γ, when $\alpha = 1.73$, (b) LLE according to diagram (a).

6.7.3 0-1 test for chaos and approximate Entropy

In the following section, we present the influence of both fractional order and initial conditions on the dynamical behavior of the suggested discrete time system by considering 0-1 test method. Then we introduce the approximate entropy to further investigate the complexity of the fractional order discrete time system (6.46).

0-1 test for chaos

To reflect the sensitivity of the FoDs, the 0-1 test is considered. Figure 6.40, however, depicts the results of the test for different values of fractional order μ, in which $(x_0,\ y_0) = (-1.78, 0.79)$. Based on this figure; one can observe that the output K has appeared in a similar manner to the results of the maximum LE and bifurcation diagram, shown in Fig. 6.38, which clearly confirms the above results.

Next the translations functions p and s of the 0-1 test for different fractional order values are plotted in Figure 6.41, and it fits well with the phase diagrams in Fig. 6.37. In particular, Fig. 6.41 depicts the Brownian like trajectories for all the three fractional order values indicating that the suggested map is chaotic in this cases. To further confirm the results we choose to plot a 3D view of the asymptotic growth rate K of the 0-1 test when $1.3 < \alpha \leq 1.9$ and by varying γ from 0.92 to 1. It is clear that the dynamics of system (6.46) shift to small intervals of α as the fractional order γ decreases, and disappears as the fractional order and system parameter α values decreases.

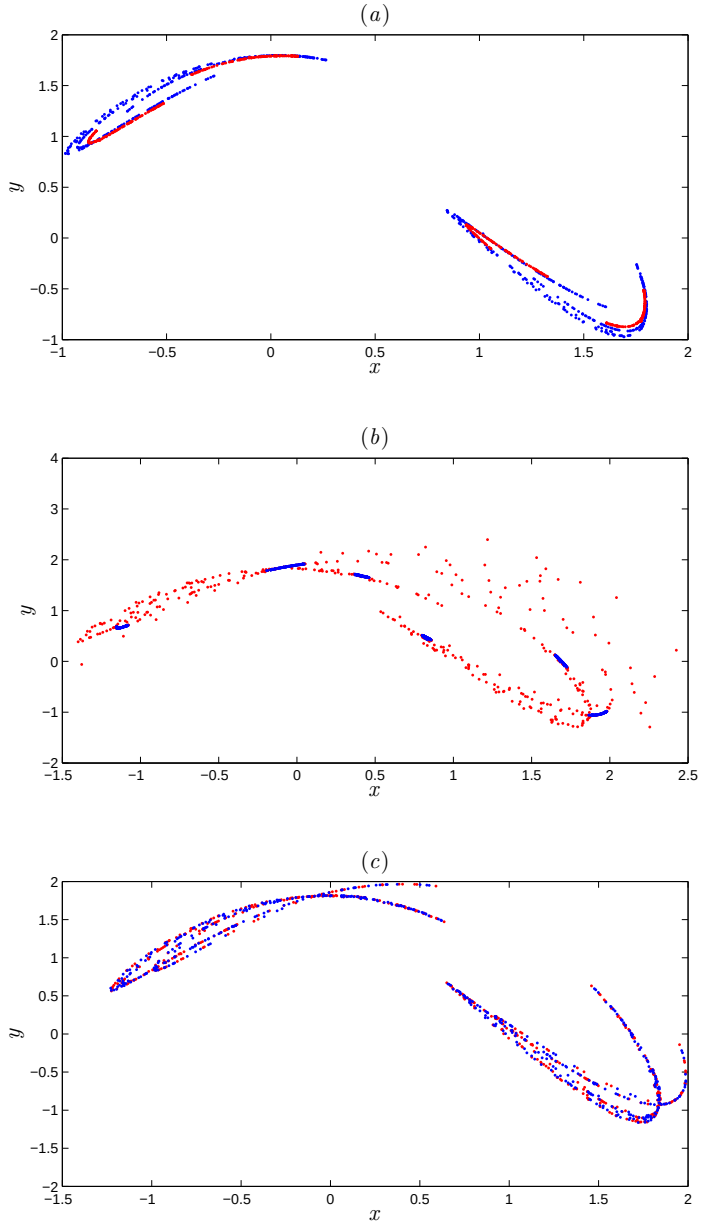

Figure 6.39: The coexisting attractors of FoDs (6.46) with $\alpha = 1.73$ and subject to the two initial conditions (-1.78,0.79) and (1.78,-0.79) for the red and the blue attractors, respectively; (a) $\gamma = 0.9992$; (b) $\gamma = 0.9362$; (c) $\gamma = 0.96$.

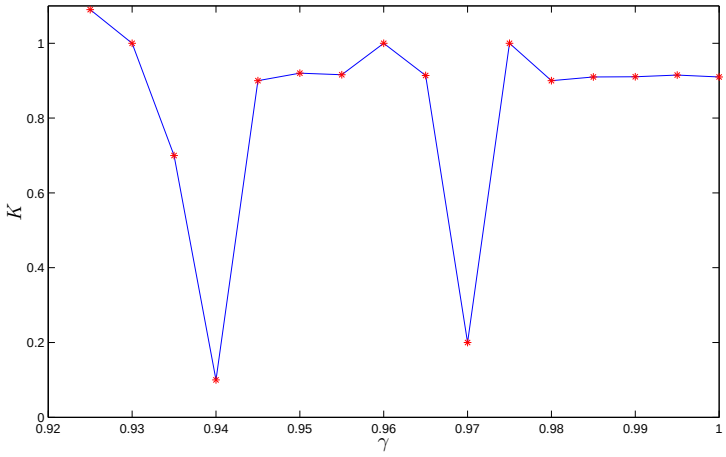

Figure 6.40: Asymptotic growth rate K vs. γ, when $\alpha = 1.73$.

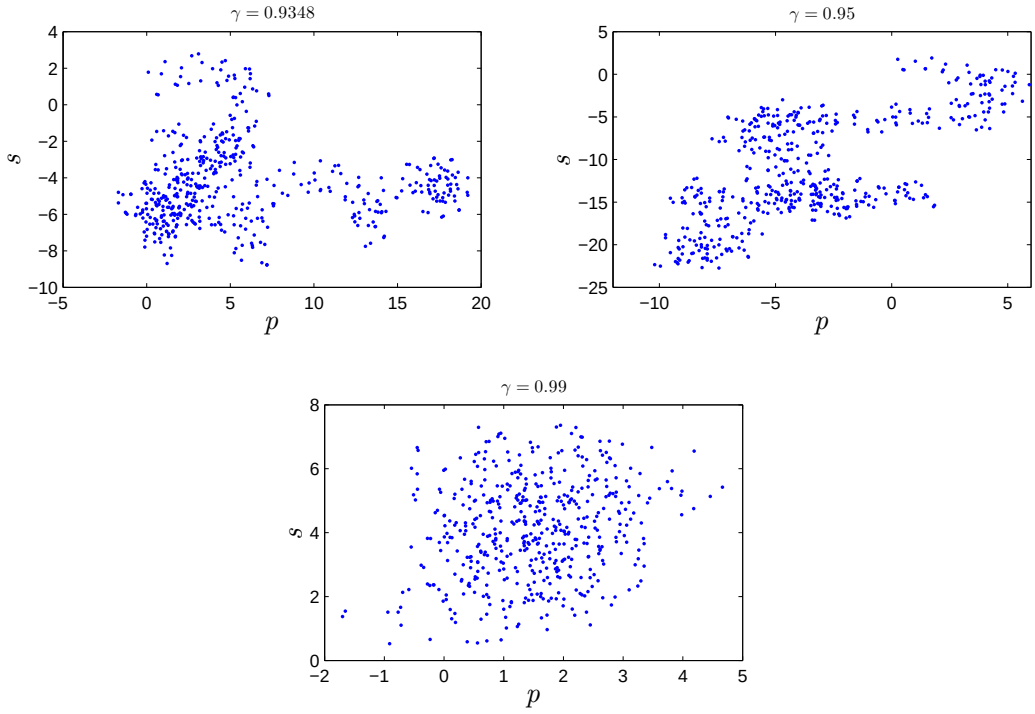

Figure 6.41: 0-1 test of the FoDs (6.46) for $\alpha = 1.73$ and subject to the initial conditions (-1.78,0.79) and for different values of γ.

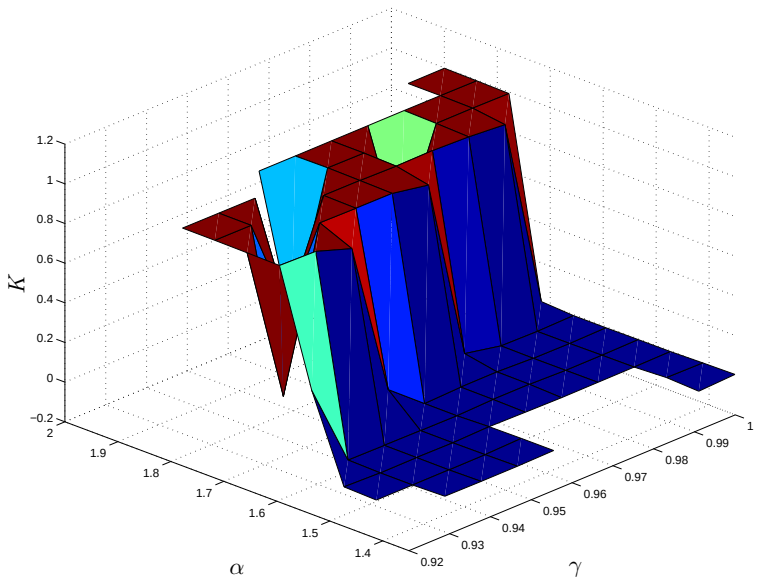

Figure 6.42: Asymptotic growth rate of the 0-1 test method of the fractional-order map (6.46) in three-dimensional space with the variation of system parameter α and fractional order γ.

Approximate Entropy

Herein, the structural complexity of the FoDs (6.46) is analysed by varying the control parameter α and the fractional order γ are reported in Fig. 6.43 and Fig. 6.44 . In particular, the approximate entropy ApEn diagrams with two different initial conditions are plotted in Fig. 6.43. It can be seen that the complexity of the FoDs (6.46) strongly depends on the variations of γ and α. In particular, Fig.6.44 highlights that there are some combined values of α and γ for which the approximate entropy ApEn is high, indicating that the FoDs (6.46) is characterized by complex dynamic behaviors for both initial conditions. The results agree will with the bifurcation diagrams in Fig. 6.35 and 6.36 .

6.8 Three dimensional FODT system with no equilibria and with two non-linearities

In the chaos literature, there is an active interest in the study of systems without equilibrium points due to its importance in engineering application. Compared with continues-time fractional system with no equilibria, the fractional-order discrete counterpart is relatively new. In this section, we consider a new three-dimensional fractional-order discrete system without equilibrium and we focus on the study of the effect of fractional order on the dynamic behaviors of

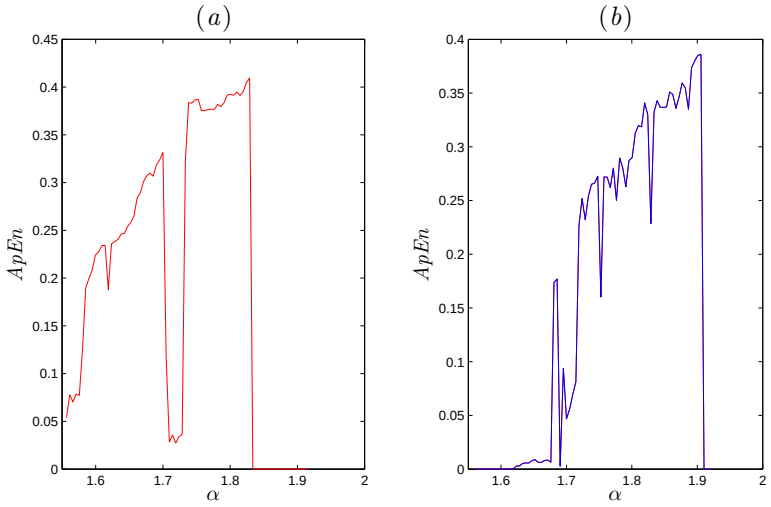

Figure 6.43: The approximate entropy ApEn of the FoDs (6.46) versus α, for: (a) $\gamma = 0.9362$, (b) $\gamma = 0.992$.

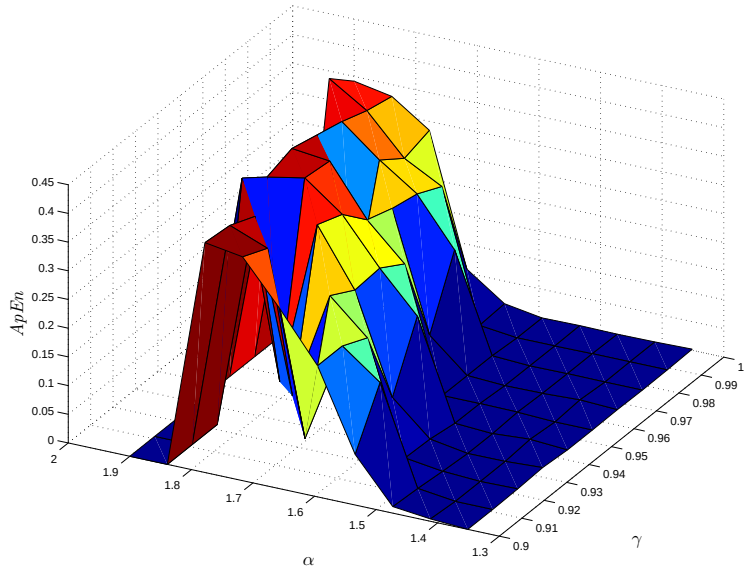

Figure 6.44: The approximate entropy ApEn of the fractional-order map (6.46) in three-dimensional space with the variation of system parameter α and fractional order γ.

this new system. The proposed fractional system can be considered "elegant" in the seance of Sprott [162]. Of particular interest is that this new three-dimensional system has no equilibrium points, which indicates that its attractor are all hidden.
Following up the discovery of two-dimensional fractional maps with different kind of equilibria in the integer order case, Jiang et al. performed an effective approach to find three-dimensional maps with Jerk-like structure and different kind of equilibrium [158].

In particular, in [158] attention is focused on the class of integer order chaotic systems described by the difference equations:

$$\begin{cases} x(n+1) = y(n), \\ y(n+1) = z(n), \\ z(n+1) = a_1x(n) + a_2y(n) + a_3z(n) + a_4x^2(n) + a_5y^2(n) + a_6z^2(n) \\ \qquad\qquad +a_7x(n)y(n) + a_8x(n)z(n) + a_9y(n)z(n) + a_{10}. \end{cases} \tag{6.50}$$

where a_i, $\forall i = \overline{1.6}$ are system parameters to be determine later. By applying the search routine into the general form (6.50), many systems can be found. Based on previous considerations, we propose the following new elegant fractional order discrete-time system:

$$\begin{cases} {}^C\Delta_a^\nu x(t) = y(t-1+\nu) - x(t-1+\nu), \\ {}^C\Delta_a^\nu y(t) = z(t-1+\nu) - y(t-1+\nu), \\ {}^C\Delta_a^\nu z(t) = a_1x(t-1+\nu) + a_2z(t-1+\nu) + a_3x(t-1+\nu)y(t-1+\nu) \\ \qquad\qquad + a_4z^2(t-1+\nu) + a_5 - z(t-1+\nu), \end{cases} \tag{6.51}$$

where $0 < \nu \leq 1$, a is the starting point, and a_1, a_2, a_3, a_4, a_5 are some bifurcation parameters. The system (6.51) has two quadratic nonlinear terms xy and z^2. The novel system can be transformed into a system without fixed point by introducing a condition of hidden attractor into the equilibrium points. The equilibrium points (x_f, y_f) of the fractional order discrete-time system (6.51) are found by solving the following system of equations:

$$\begin{cases} y_f - x_f = 0, \\ z_f - y_f = 0, \\ a_1x_f + a_2z_f + a_3x_fy_f + a_4z_f^2 + a_5 - z_f = 0. \end{cases} \tag{6.52}$$

By using simple calculation, equation (6.52) can be transformed into

$$(a_3 + a_4)x_f^2 + (a_1 + a_2 - 1)x_f + a_5 = 0. \tag{6.53}$$

Here, we want to construct a three-dimensional fractional order discrete time system with no equilibrium points, for that we only need to determine the cases where the second order equation (6.53) has no solution. In particular, two cases are considered:

Cas 1 . when $a_3 + a_4 = 0$, $a_1 + a_2 - 1 = 0$ and $a_5 \neq 0$, equation (6.53) has no solution. Therefore, there is no any equilibrium in the fractional order discrete-time system (6.51).

Cas 2 . when $(a_2 + a_1 - 1)^2 - 4a_5(a_3 + a_4) < 0$ and $a_3 + a_4 \neq 0$, equation (6.53) has no solution. Similarly, there is no any equilibrium in the fractional order discrete-time system (6.51).

Therefore, all the periodic and chaotic attractors generated from the proposed simple fractional discrete system are all hidden in both cases.

Dynamic analysis

Similarly, using Theorem 1.15, the numerical solution of the fractional order discrete-time system (6.53) can be obtained as

$$\begin{cases} x(n) = x(0) + \frac{1}{\Gamma(\nu)} \sum\limits_{j=1}^{n} \frac{\Gamma(n-j+\nu)}{\Gamma(n-j+1)}(y(j-1) - x(j-1)), \\ y(n) = y(0) + \frac{1}{\Gamma(\nu)} \sum\limits_{j=1}^{n} \frac{\Gamma(n-j+\nu)}{\Gamma(n-j+1)}(z(j-1) - y(j-1)), \\ z(n) = z(0) + \frac{1}{\Gamma(\nu)} \sum\limits_{j=1}^{n} \frac{\Gamma(n-j+\nu)}{\Gamma(n-j+1)}(a_1 x(j-1) + a_2 z(j-1) + a_3 x(j-1)y(j-1) \\ \qquad\qquad +a_4 z^2(j-1) + a_5 - z(j-1)), \end{cases} \tag{6.54}$$

where $x(0)$, $y(0)$ and $z(0)$ are the initial states. With this numerical formulas, the sensitivity of the fractional order discrete-time system can be numerically investigated by employing the bifurcation diagrams, largest Lyapunov exponent (LLE), phase portraits and 0-1 test.

Bifurcation and Lyapunov exponents

Cas 1 . Here, the fractional order discrete-time system generate chaotic attractor when $a_1 = 1.7$, $a_2 = -0.7$, $a_3 = 1$, $a_4 = -1$ and $a_5 = -0.3$, with initial condition $x_0 = 0.84$, $y_0 = 1.25$, $z_0 = 1.46$, and fractional order $\nu = 0.9762$. Figure 6.45 display the hidden chaotic attractor in different phase space projections. We investigate the dynamics of the system as the order ν is varied. The bifurcation diagram and the corresponding largest Lyapunov exponent in the $x - \nu$ plane are shown in Figure 6.46. Note that the largest Lyapunov exponents are approximated in a similar manner to the states in Jacobian matrix algorithm 3.5.2. Figure 6.46 shows that the fractional order discrete-time system (6.51) displays chaotic behavior at most of the rang $[0.9732, 0.985] \cup [0.9908, 1]$ with small periodic windows at $\nu = 0.9832$. To obtain a global view, we plot the phase portraits for $\nu = 1$, $\nu = 0.9928$, $\nu = 0.9832$, and $\nu = 0.9762$ in the $x - y$ plane, the results are shown in Figure 6.47. This illustrates that when $\nu = 1$, $\nu = 0.9928$ and $\nu = 0.9762$ the fractional order discrete-time system (6.51) generates hidden chaotic attractors, which consist very well with the corresponding bifurcation diagram and largest Lyapunov exponents in Figure 6.46.
Now, we consider the effect of a_5 on the dynamic behavior of the fractional order discrete-time system (6.51) for fractional order value $\nu = 0.9762$. Figure 6.48(a) shows the bifurcation diagrams of the system. We find that the states of the fractional order discrete-time system (6.51) changes qualitatively with the variation of a_5 and ν. As the fractional order ν decreases to 0.9762, the chaotic motion decreases and new periodic windows are observed in the interval $[-0.2, -0.1]$. This implies that the fractional order stabilize the states of the fractional order discrete-time system. Although bifurcation plots are a useful tool in determining the existence of chaos and quantifying it, the most agreed upon tool is largest Lyapunov exponents. Figure 6.48(b) shows the estimated largest Lyapunov exponent for $\nu = 0.9762$ to further confirm the results, the corresponding largest Lyapunov exponent is positive, which confirms that the fractional order discrete-time system has hidden chaotic attractor in this case.

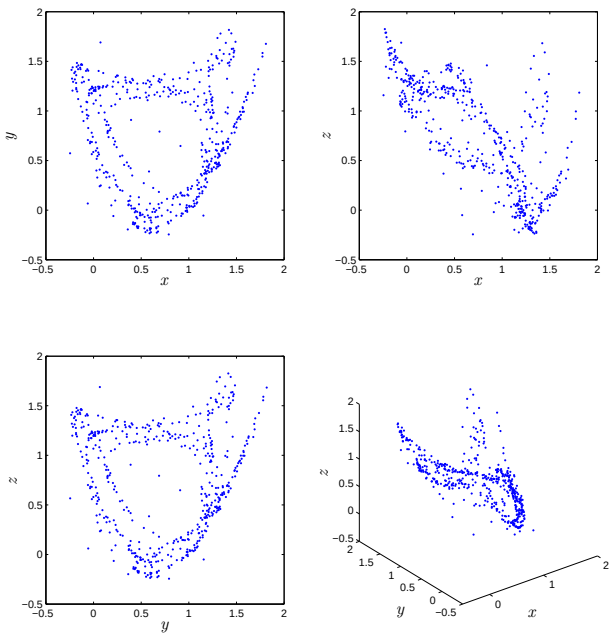

Figure 6.45: Hidden chaotic attractor of the fractional-order discrete-system (6.51) without equilibrium points for $\nu = 0.9762$.

Cas 2 . When the system parameters are fixed as $a_1 = 1$, $a_2 = 0$, $a_3 = 0.3$, $a_4 = -0.2$, $a_5 = 1$, and for $\nu = 1$, the fractional order discrete-time system has no equilibria and behaves chaotically. To investigate the sensitivity of the novel system with respect to the fractional order, we fix $a_1 = 1$, $a_2 = 0$, $a_3 = 0.3$, $a_4 = -0.2$, $a_5 = 1$, and we vary ν in the range $0.6 \leq \nu \leq 1$. The bifurcation diagram and the largest Lyapunov exponent are shown in Figure 6.49. As ν passes through 0.9904, system (6.51) become totally periodic. When $\nu \in (0.6344, 0.8731)$ the system is stabilized to a periodic points. In this case the lowest order ν for which the fractional order discrete-time system generates chaos is 0.9904.

0-1 test

The chaotic nature of the fractional order discrete-time system (6.51) with no equilibrium is validated using the 0-1 test for chaos, which has been proposed and applied to fractional-order discrete time systems in Chapter 3. As mentioned in Chapter 3 when the system is chaotic the output K approaches 1, and when the system is periodic the output K approaches 0. In addition, the dynamics of the components $p_c(n) = \sum_{j=1}^{n} x(j) \cos jc$ and $q_c(n) = \sum_{j=1}^{n} x(j) \sin jc$, provides a visual test. Basically, if the dynamic is regular then the behavior of trajectories in the $(p - q)$

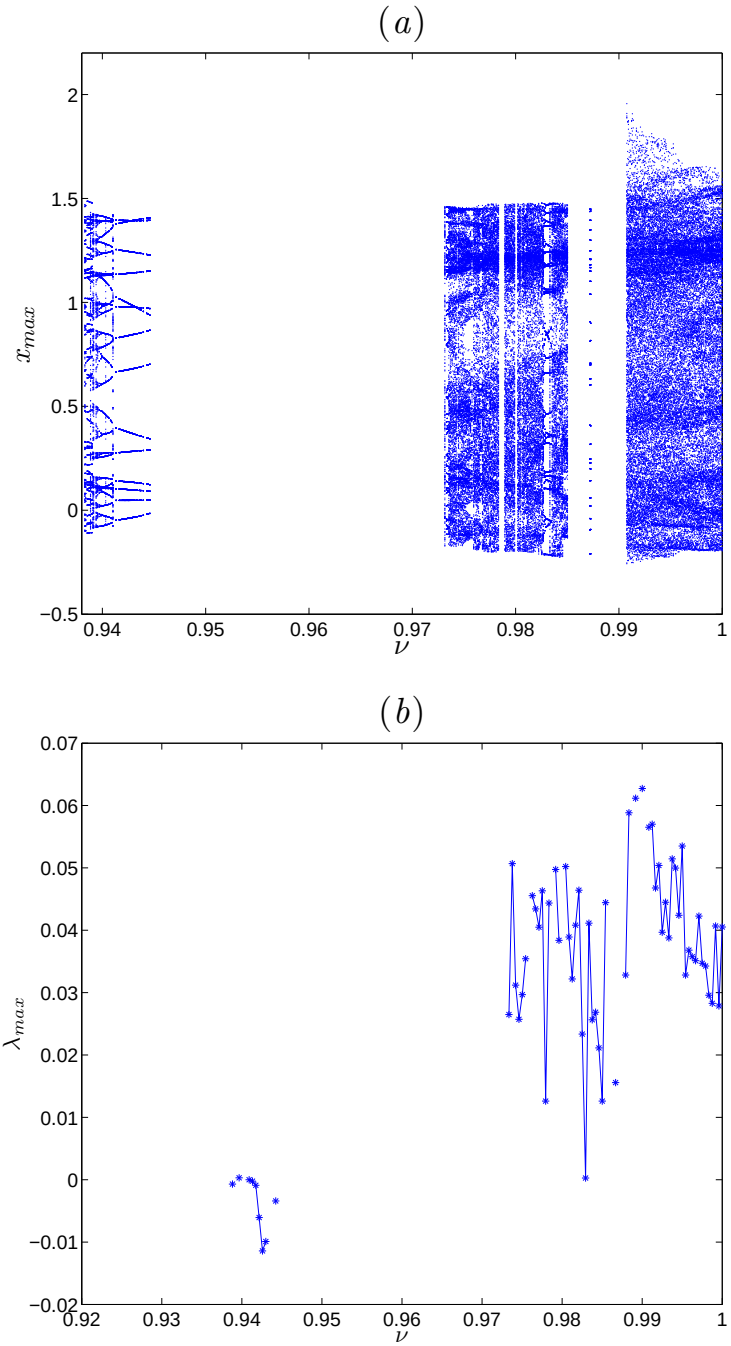

Figure 6.46: (a) Bifurcation diagram of the fractional order discrete-time system (6.51) versus ν for $a_1 = 1.7$, $a_2 = -0.7$, $a_3 = 1$,$a_4 = -1$, $a_5 = -0.3$ and $[x(0), y(0), z(0)] = [0.84, 1.25, 1.46]$. (b) largest Lyapunov exponent versus ν.

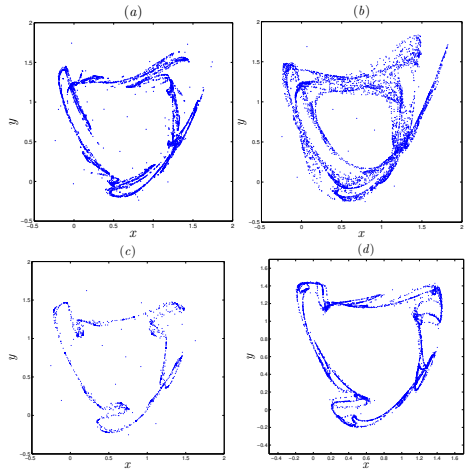

Figure 6.47: Phase diagrams of fractional discrete-time system (6.51) using the parameter values $a_1 = 1.7$, $a_2 = -0.7$, $a_3 = 1$,$a_4 = -1$, and initial condition $\{x_0, y_0, z_0\} = \{0.84, 1.25, 1.46\}$ for (a) $\nu = 1$; (b) $\nu = 0.9928$; (c) $\nu = 0.9832$; (d) $\nu = 0.9762$.

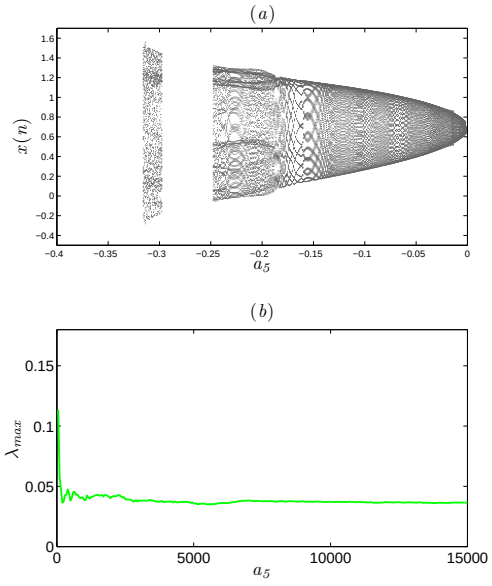

Figure 6.48: Fractional order discrete-time system without fixed point (6.51) with varying parameter a_5 and setting the parameter values $a_1 = 1.7$, $a_2 = -0.7$, $a_3 = 1$,$a_4 = -1$, for order $\nu = 0.9762$ shows (a) the bifurcation diagram and (b) estimated Lyapunov exponents of the fractional order discrete-time system for the same bifurcation parameters and order $\nu = 0.9762$.

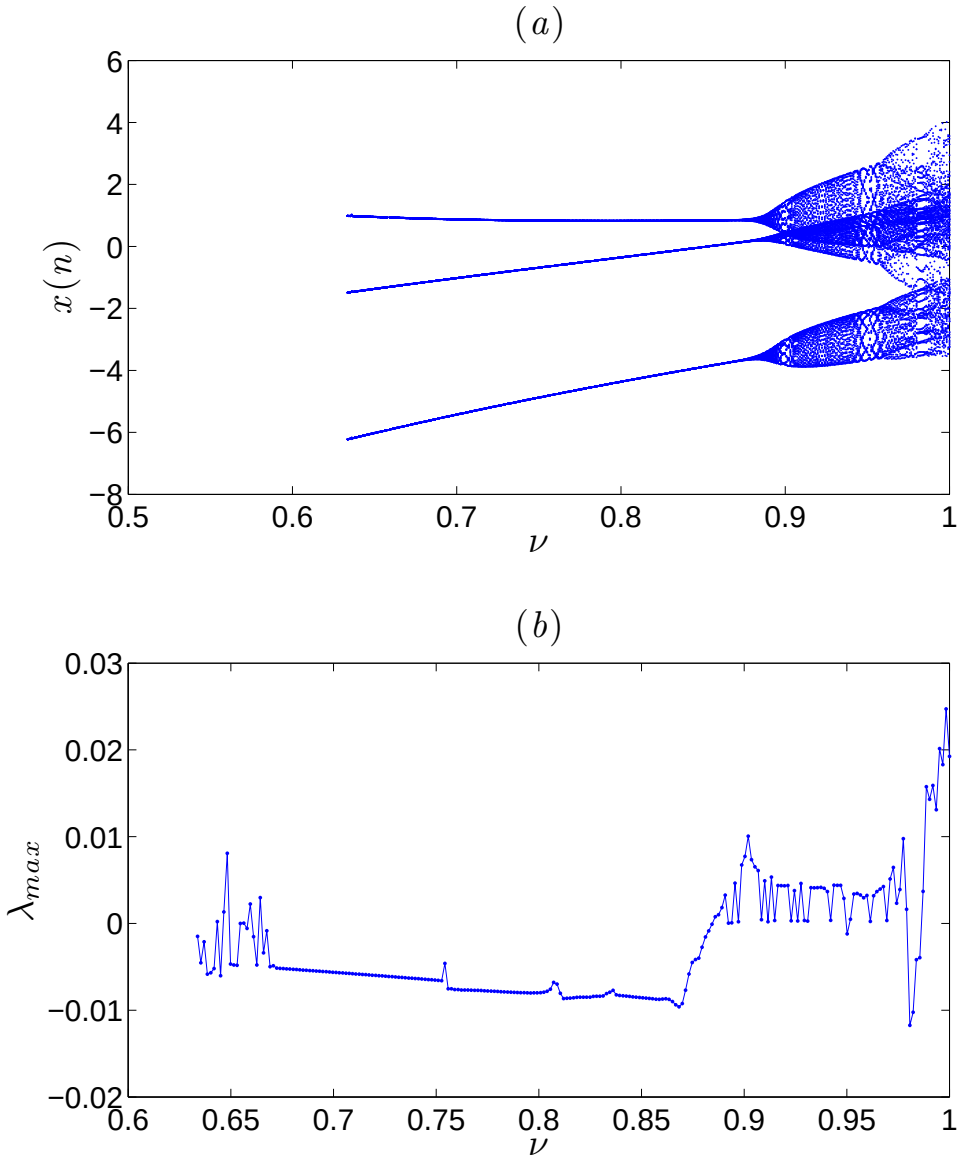

Figure 6.49: (a) Bifurcation diagram of the fractional order discrete-time system (6.51) versus ν for $a_1 = 1$, $a_2 = 0$, $a_3 = 0.3$, $a_4 = -0.2$, $a_5 = 1$ and $[x_0, y_0, z_0] = [1.1, 1.28, -1.78]$, (b) largest Lyapunov exponent versus ν.

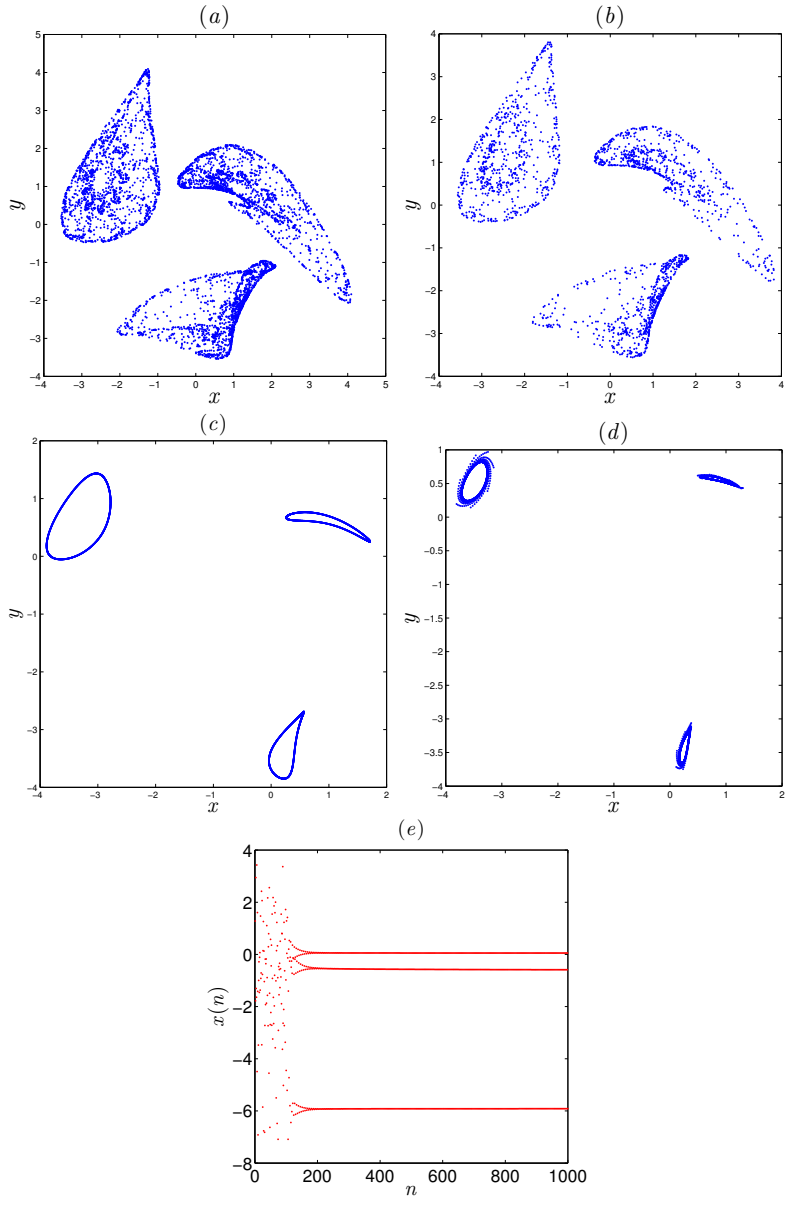

Figure 6.50: The phase diagrams of the fractional order discrete-time system (6.51) using the parameter values $a_1 = 1$, $a_2 = 0$, $a_3 = 0.3$,$a_4 = -0.2$, $a_5 = 1$, and initial condition $[x_0, y_0, z_0] = [1.1, 1.28, -1.78]$ for (a) $\nu = 1$; (b) $\nu = 0.9871$; (c) $\nu = 0.9084$; (d) $\nu = 0.894$, (e) evolution of state $x(n)$ for $\nu = 0.6546$.

plane is bounded, whereas if the dynamic is chaotic then the $(p-q)$ trajectories depict Brownian like behavior. Here, the test has been applied directly to the series data obtained from the

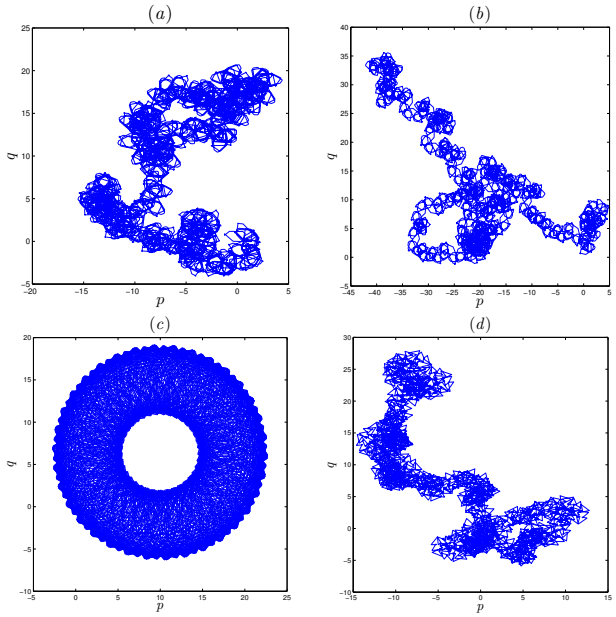

Figure 6.51: Dynamics of the translation components (p, q) of the fractional order discrete-time system for (a) $\nu = 1$; (b) $\nu = 0.9928$; (c) $\nu = 0.9832$; (d) for $\nu = 0.9762$.

numerical formula (6.54), with order $\nu = 0.95$ and system parameters $a_1 = 1.7$, $a_2 = -0.7$, $a_3 = 1$, $a_4 = -1$ and $a_5 = -0.3$. The translation component $(p-q)$ of the fractional order discrete-time system (6.51) with no equilibrium are calculated and illustrated in Figure 6.51(b)-(d). As it can be seen the trajectories in the $p-q$ plane depicts Brownian behavior for $\nu = 0.9928$ and $\nu = 0.9762$, which confirms the chaotic behavior of the fractional order discrete-time system. On the other hand, Figure 6.52 depicts the plot of K versus n for the fractional order value $\nu = 0.998$ and system parameters $a_1 = 0$, $a_2 = 0$, $a_3 = -0.57$, $a_4 = 0.35$, $a_5 = -1.27$. It shows that the asymptotic growth rate K approaches 1 as n increases, indicating that the new system is chaotic. The corresponding hidden chaotic attractor is shown in Figure 6.53.

Successively, the 0-1 test is applied to the system (6.51) when $a_1 = 1$, $a_2 = 0$, $a_3 = 0.3$, $a_4 = -0.2$, $a_5 = 1$, and $\{x_0, y_0, z_0\} = \{1.1, 1.28, -1.78\}$. The translation component $(p-q)$ depicts Brownian-like trajectories for $\nu = 0.9904$ and bounded trajectories for $\nu = 0.9084$ and $\nu = 0.894$ (see Fig. 6.54). These pictures along with the phase diagrams reported in Figure 6.50 indicate that the fractional order discrete-time system (6.51) has hidden chaotic attractor for $\nu = 0.9904$, and regular behavior for $\nu = 0.894$ and $\nu = 0.9084$, which confirms very well the results.

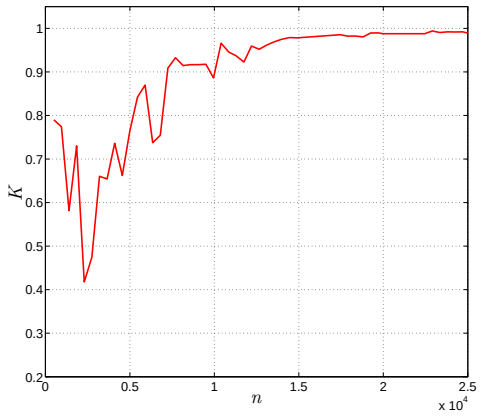

Figure 6.52: The 0-1 test of the fractional order discrete-time system: asymptotic growth rate K versus n for $\nu = 0.998$ with bifurcation parameters $a_1 = 0, a_2 = 0, a_3 = -0.57, a_4 = 0.35, a_5 = -1.27$ and initial condition $[x_0, y_0, z_0] = [-0.14, -0.7, 0.06]$

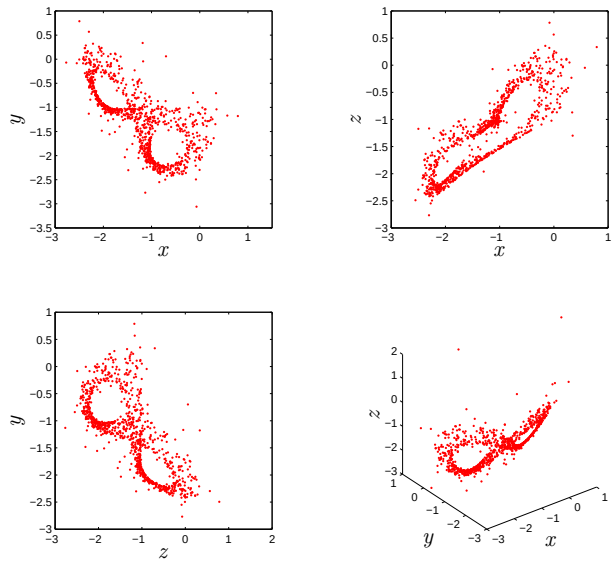

Figure 6.53: Hidden chaotic attractor of the fractional order discrete-time system for $\nu = 0.998$.

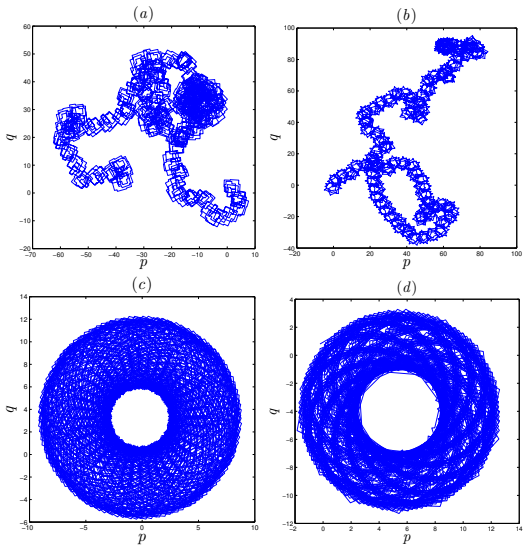

Figure 6.54: Dynamics of the translation components (p, q) of the fractional order discrete-time system for $a_1 = 1$, $a_2 = 0$, $a_3 = 0.3$,$a_4 = -0.2$, $a_5 = 1$ with (a) $\nu = 1$; (b) $\nu = 0.9928$; (c) $\nu = 0.9832$; (d) $\nu = 0.9762$.

6.9 Three dimensional FODT system with no equilibria and with three non-linearities

In the following, the above-described method is applied to construct a fractional Jerk like map with no equilibrium points and with two nonlinearties. The system is described by a set of three dimensional fractional-order difference equation [167], as follows

$$\begin{cases} {}^{C}\Delta_a^{\nu} x(t) = y(t-1+\nu) - x(t-1+\nu), \\ {}^{C}\Delta_a^{\nu} y(t) = z(t-1+\nu) - y(t-1+\nu), \\ {}^{C}\Delta_a^{\nu} z(t) = -a_1 z^2(t-1+\nu) + a_2 x(t-1+\nu) y(t-1+\nu) \\ \qquad\qquad + a_3 x(t-1+\nu) z(t-1+\nu) + a_4 - z(t-1+\nu), \end{cases} \tag{6.55}$$

where a is the starting point, $0 < \nu < 1$ is the fractional order, x, y, z are the state variables, and a_1, a_2, a_3, a_4 are bifurcation parameters. As shown above, the equilibrium points (x_f, y_f, z_f) of the fractional-order discrete system (6.55) are found by solving the following system of equation

$$\begin{cases} y_f - x_f = 0, \\ z_f - y_f = 0, \\ -a_1 z_f^2 + a_2 x_f y_f + a_3 x_f z_f + a_4 - z_f = 0, \end{cases} \tag{6.56}$$

from Equation (6.56) we have the simplified form

$$(-a_1 + a_2 + a_3) z_f^2 + a_4 - z_f = 0. \tag{6.57}$$

6.9 Three dimensional FODT system with no equilibria and with three non-linearities

The aim is to demonstrate that the fractional-order discrete system (6.55) can generate hidden chaotic attractor, for that we only need to determine the cases where Equation (6.57) has no solution. In particular, when $-a_1 + a_2 + a_3 \neq 0$ and $1 \leq 4a_4(-a_1 + a_2 + a_3)$ Equation (6.57) has no solution, which means that the system (6.55) has no equilibrium. We must therefore impose the condition (6.57) on the system parameters a_i in order to obtain hidden attractors.

6.9.1 Dynmical analysis

To continue with our analysis, we need to define the numerical formula of the system (6.55). Using Theorem 1.15 which is mentioned in Chapter 1, the state solution of the fractional-order discrete system (6.55) can be obtained as follows

$$\begin{cases} x\left(t\right) = x\left(a\right) + \frac{1}{\Gamma(\nu)} \sum_{s=a+1-\nu}^{t-\nu} \left(t - \sigma\left(s\right)\right)^{(\nu-1)} \left(y(s+\nu-1) - x(s+\nu-1)\right), \\ y\left(t\right) = y\left(a\right) + \frac{1}{\Gamma(\nu)} \sum_{s=a+1-\nu}^{t-\nu} \left(t - \sigma\left(s\right)\right)^{(\nu-1)} \left(z(s+\nu-1) - y(s+\nu-1)\right), \\ z\left(t\right) = z\left(a\right) + \frac{1}{\Gamma(\nu)} \sum_{s=a+1-\nu}^{t-\nu} \left(t - \sigma\left(s\right)\right)^{(\nu-1)} \left(-a_1 z^2(s+\nu-1) + a_2 x(s+\nu-1) y(s+\nu-1)\right. \\ \qquad\qquad \left. + a_3 x(s+\nu-1) z(s+\nu-1) + a_4 - z(s+\nu-1)\right). \end{cases} \tag{6.58}$$

Replacing the discrete kernel function $\frac{(t-\sigma(s))^{(\nu-1)}}{\Gamma(\nu)}$ by $\frac{\Gamma(t-s)}{\Gamma(\nu)\Gamma(t-s-\nu+1)}$ and assuming that $a = 0$, the above equation is converted to

$$\begin{cases} x(n) = x(0) + \frac{1}{\Gamma(\nu)} \sum_{j=1}^{n} \frac{\Gamma(n-j+\nu)}{\Gamma(n-j+1)} (y(j-1) - x(n-1)), \\ y(n) = y(0) + \frac{1}{\Gamma(\nu)} \sum_{j=1}^{n} \frac{\Gamma(n-j+\nu)}{\Gamma(n-j+1)} (z(j-1) - y(j-1)), \\ z(n) = z(0) + \frac{1}{\Gamma(\nu)} \sum_{j=1}^{n} \frac{\Gamma(n-j+\nu)}{\Gamma(n-j+1)} (-a_1 z^2(j-1) + a_2 x(j-1) y(j-1) \\ \qquad\qquad + a_3 x(j-1) z(j-1) + a_4 - z(j-1)), \end{cases} \tag{6.59}$$

where $x(0), y(0)$ and $z(0)$ are the initial conditions. For the system parameters choice $a_1 = 1, a_2 = 0.7, a_3 = 1$, $a_4 = 0.7$, and initial conditions $x(0) = 1.5$, $y(0) = 2.84$, $z(0) = -1.2$, and fractional order $\nu = 0.998$, system (6.55) can display hidden attractor as exhibited in Figure 6.55. More basic characteristics of this fractional-order discrete system will be given in the following subsection.

Bifurcation diagrams and largest Lyapunov exponents

To fully understand the dynamic characteristic of the fractional order discrete-time system (6.55), standard nonlinear analysis technics, such us, bifurcation diagrams, largest Lyapunov exponents and phase portraits. Firstly, we investigate the bifurcation diagrams of the fractional-order discrete system (6.55) as the system parameter a_1 is varied when the other parameters are taken as $a_2 = 0.7, a_3 = 1, a_4 = 0.7$. The bifurcation diagrams are obtained by plotting the local maxima of the state $x(n)$ in term of system parameter a_1 for three different values of ν as shown in Figure 6.56. By comparing Figure 6.56(a) with Figure 6.56(b) and 6.56(c), we find that the interval where chaos exists shrinks as ν decreases. In particular, when the value of ν changes from 0.9935 to 0.9434, the areas of chaotic motion shrinks from $[1, 1.008] \cup [1.66, 1.267] \cup]1.045, 1.196[$

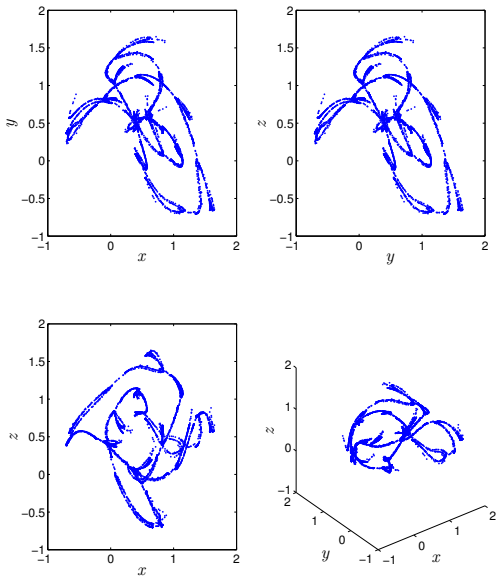

Figure 6.55: The hidden chaotic attractor of the fractional-order discrete system for $\nu = 0.998$.

to $[1.022, 1.116] \cup [1.164, 1.216]$.
When the parameter values are assigned as $a_1 = 1, a_2 = 0.7, a_4 = 0.7$, bifurcation diagrams with a_3 varying are shown in Figure. 6.57. By comparing this diagrams it can be seen that the bifurcation structure is apparently the same. When the value of ν reduces to 0.9434, the fractional-order discrete system (6.55) becomes totally periodic at the interval $[1, 1.141]$.
Next, the dynamic behavior of the fractional-order discrete system (6.55) while parameter a_4 varied is studied in Figure 6.58(a) and Figure 6.59(a). It can be seen that the states of system (6.55) changes qualitatively with the variation of order ν and parameter a_4. The bifurcation diagram of the fractional-order discrete system (6.56) with $\nu = 0.9935$ is plotted in Figure 6.58(a). As can be seen, when $0.87 \leq \nu \leq 0.8$ system (6.55) exhibits chaotic behavior. A serie of period windows occurs at the region $(0.7, 0.8)$ as the value of ν reduces to 0.9434 (see Figure 6.59(a)). Although bifurcation plots are a useful tool in determining the existence of chaos and quantifying it, the most agreed upon tool is Lyapunov exponents. The largest Lyapunov exponent of this new fractional-order discrete system are calculated by Jacobian matrix algorithm. Figure 6.58(b) and Figure 6.59(b) shows the estimated largest Lyapunov exponent for $\nu = 0.9935$, $a_4 = 0.7$, and for $\nu = 0.9434$, $a_4 = 0.7$, respectively. Obviously, when we select $\nu = 0.9935$, the corresponding largest Lyapunov exponent is positive, which implies that system (6.55) is in chaotic state. And when the fractional order is set to $\nu = 0.9434$, the largest Lyapunov exponent is zero, which implies that system (6.55) is in periodic state.

In order to observe the influence of the fractional order ν on the dynamic of the fractional-order discrete system, we fix the system parameters $a_1 = 1$, $a_2 = 0.7$, $a_3 = 1$, $a_4 = 0.7$, and we vary ν in the interval $]0.8, 1]$. Figure 6.60 shows that the fractional-order discrete system display limit cycles, periodic and chaotic motions with the variation of order ν. In particular,

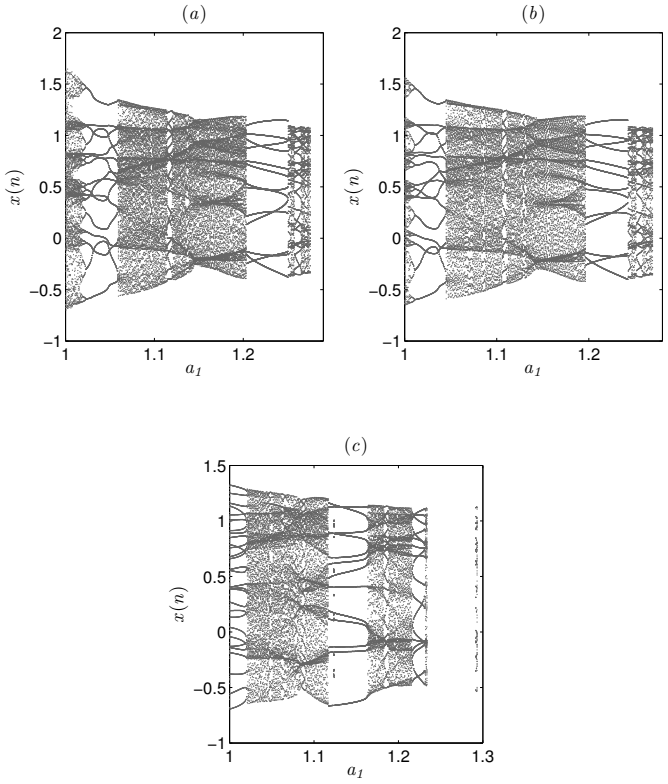

Figure 6.56: Bifurcation diagrams of the fractional-order discrete system (6.55) versus a_1 for (a) $\nu = 1$, (b) $\nu = 0.9935$, and (c) $\nu = 0.9434$.

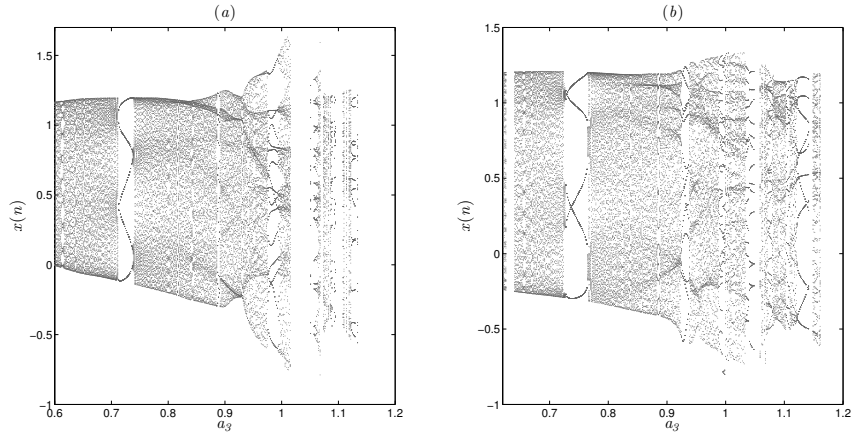

Figure 6.57: Bifurcation diagrams of the fractional-order discrete system (6.55) versus a_3 for (a) $\nu = 0.9935$, and (b) $\nu = 0.9434$.

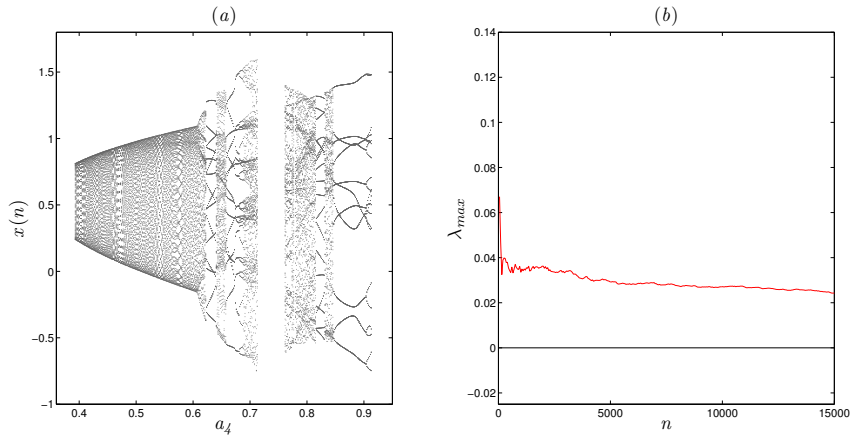

Figure 6.58: (a) Bifurcation diagrams of the fractional-order discrete system (6.55) versus a_4 for $\nu = 0.9935$, (b) estimated latgest Lyapunov exponent of the fractional-order discrete system for $\nu = 0.9935$ and $a_4 = 0.7$.

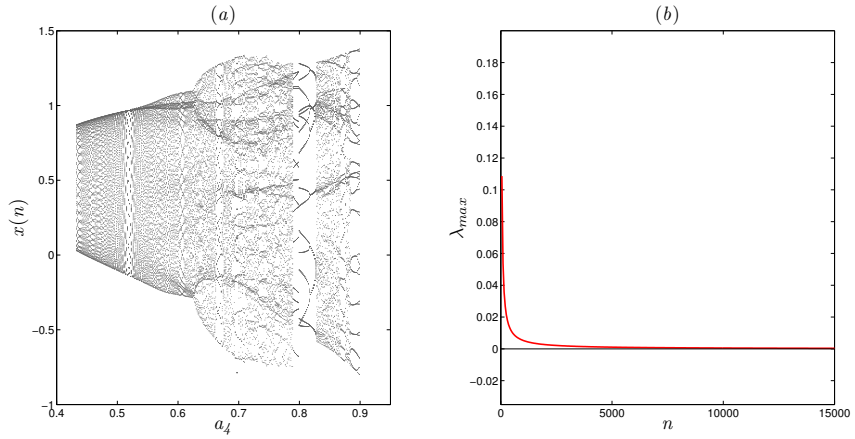

Figure 6.59: (a) Bifurcation diagrams of the fractional-order discrete system (6.55) versus a_4 for $\nu = 0.9434$, (b) estimated largest Lyapunov exponent of the fractional-order discrete system for $\nu = 0.9434$ and $a_4 = 0.7$.

we find that when $0 \leq \nu \leq 0.81$ the system diverge to infinity. When $\nu \in [0.9153, 0.9339] \cup [0.9429, 0.9726] \cup [0.9883, 1]$ the largest Lyapunov exponent changes its values quickly between negative and positive, which implies that there are periodic windows in the chaotic region. When ν is decreased from 0.915 the fractional-order discrete system converges to a periodic orbite. When $\nu \in [0.8211, 0.8467[$ system has a more complex hidden chaotic attractors as it largest Lyapunov exponent takes the highest values. The phase portraits in the $x - y$ plane for different values of order ν are shown in Figure 6.61

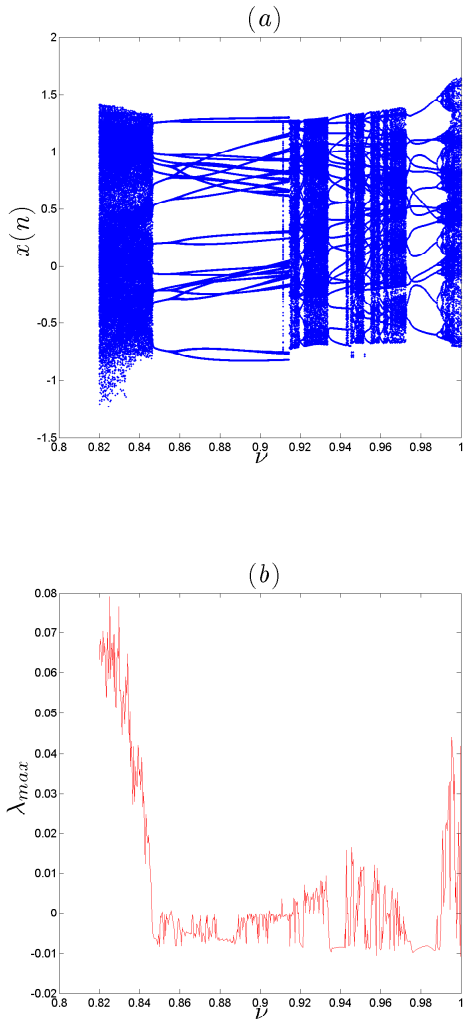

Figure 6.60: (a) Bifurcation diagram versus ν for $a_1 = 1, a_2 = 0.7, a_3 = 1$, and $a_4 = 0.7$, (b) Largest Lyapunov exponent diagram corresponding to diagram (a).

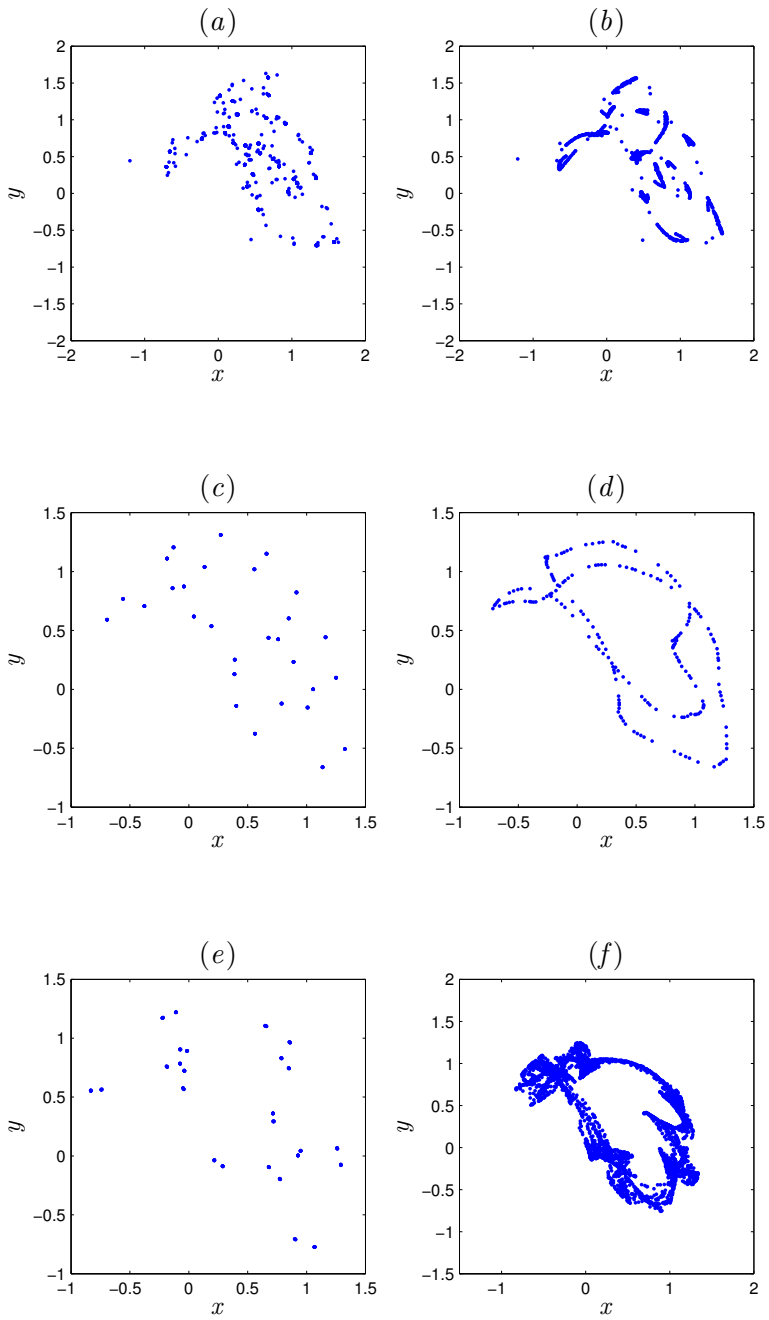

Figure 6.61: Phase portraits of the fractional-order discrete system (6.55): (a) periodic orbit for $\nu = 0.9996$, (b) chaotic hidden attractor for $\nu = 0.9935$, (c) periodic attractor for $\nu = 0.9434$, (d) two limit cycles for $\nu = 0.9177$, (e) periodic orbit for $\nu = 0.895$, (f) hidden chaotic attractor for $\nu = 0.84$.

0-1 test

Now, we apply the 0-1 test to the discrete series data $x(n)$ for different values of ν where the system parameters are assigned as $a_1 = 1$, $a_2 = 0.7$, $a_3 = 1$, $a_4 = 0.7$. The translation components $(p-q)$ of the fractional-order discrete system (6.55) are calculated and illustrated in Figure. 6.62. In particular, when $\nu = 0.9996$, $\nu = 0.9434$, $\nu = 0.895$ and $\nu = 0.9177$, where the trajectories in $(p-q)$ plan shows bounded behavior, system (6.55) is in periodic state. And when ν is set to $\nu = 0.9935$ and $\nu = 0.84$, where the trajectories in $(p-q)$ plan shows unbounded trajectories, system (6.55) is chaotic, which confirms very well the results in Figure 6.62.

6.9.2 Complexity analysis

C_o complexity

In order to observe the effect of fractional order ν on the dynamic properties of the fractional-order discrete system (6.55), we measure the complexity of the new system using C_0 algorithm. For the first state $\{x(j); j = 0, 1, .., N-1\}$, the C_0 complexity is given as

$$C_0 = \frac{\sum_{k=0}^{N-1} |x(k) - \bar{x}(k)|^2}{\sum_{k=0}^{N-1} |x(k)|^2}. \tag{6.60}$$

Fixing system parameters to $a_1 = 1$, $a_2 = 0.7$, $a_3 = 1$, $a_4 = 0.7$ and $\nu \in [0.8, 1]$, the result of C_o complexity is plotted in Figure 6.63. We notice that the complexity of the fractional-order discrete increases when ν passes to the range $[0.8211, 0.8467[$, which agrees well with the result in Figure 6.61.

Approximate entropy

Now, the complexity of fractional-order discrete system (6.55) is described by employing approximate entropy (ApEn). We define the approximate entropy by

$$ApEn = \phi^m(r) - \phi^{m+1}(r), \tag{6.61}$$

where $\phi^m(r)$ is considered as

$$\phi^m(r) = \frac{1}{n-m-1} \sum_{i=1}^{n-m+1} \log C_i^m(r). \tag{6.62}$$

Figure 6.64 shows the ApEn of the proposed fractional-order discrete system (6.55) for different fractional order values and when $a_1 = 1$, $a_2 = 0.7$, $a_3 = 1$, $a_4 = 0.7$. As one can see, the complexity of the fractional- order discrete system (6.55) varied as we vary ν. When $\nu \in [0.8211, 0.8467[$, the system (6.55) is more complex. Therefore, we must be aware of the selected fractional order in order to have a relatively high structural complexity.

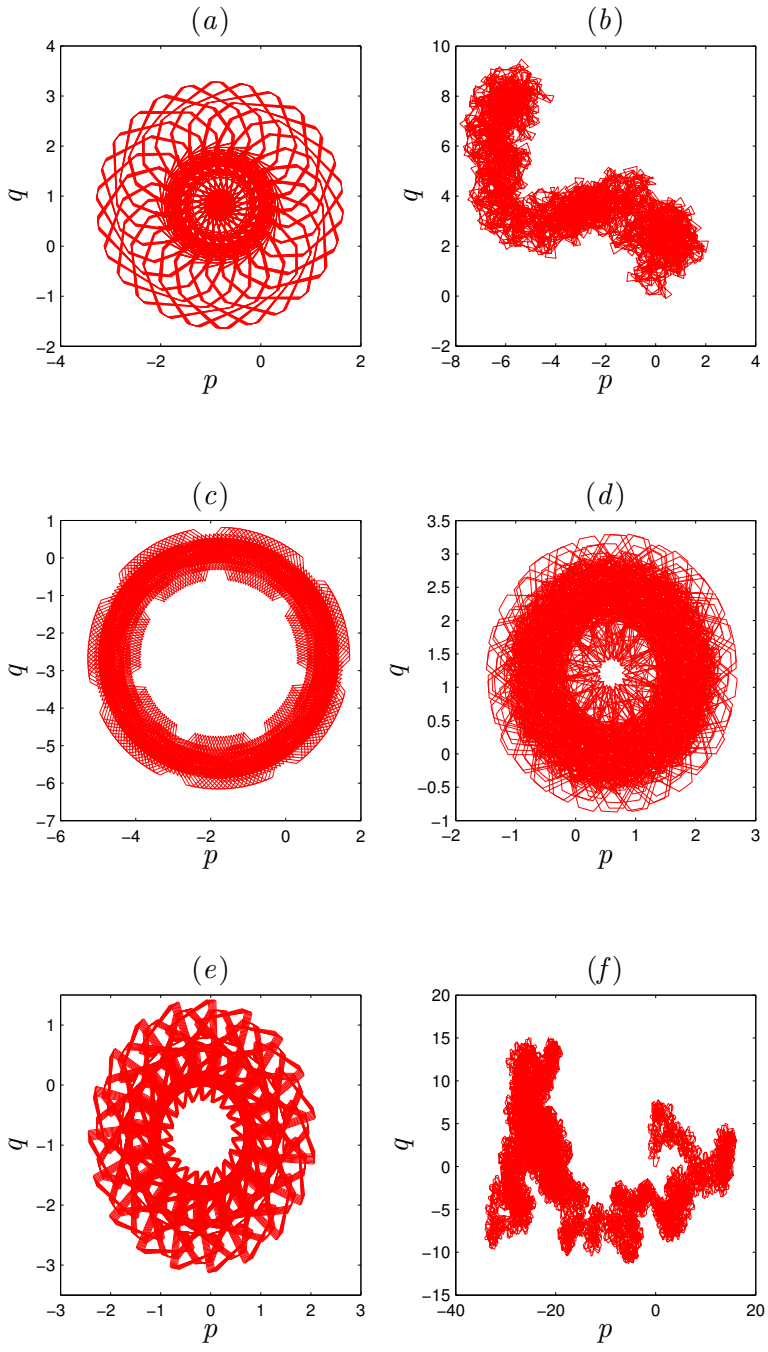

Figure 6.62: The 0-1 test of the fractional-order discrete system (6.55): (a) for $\nu = 0.9996$, (b) for $\nu = 0.9935$, (c) for $\nu = 0.9434$, (d) for $\nu = 0.9177$, (e) $\nu = 0.895$, (f) for $\nu = 0.84$.

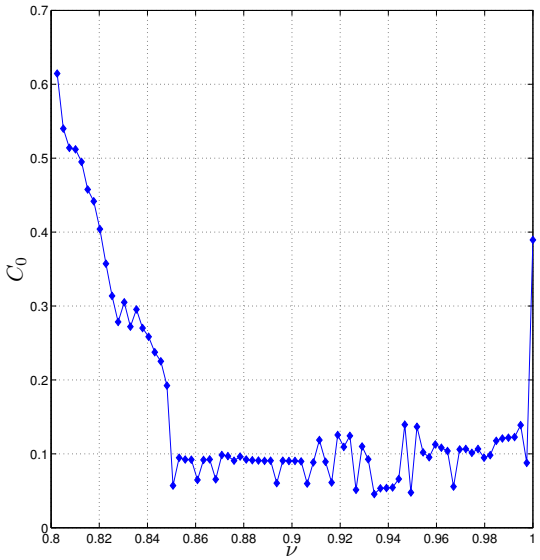

Figure 6.63: C_0 complexity of the fractional-order discrete system (6.55) versus ν with $a_1 = 1$, $a_2 = 0.7$, $a_3 = 1$, and $a_4 = 0.7$.

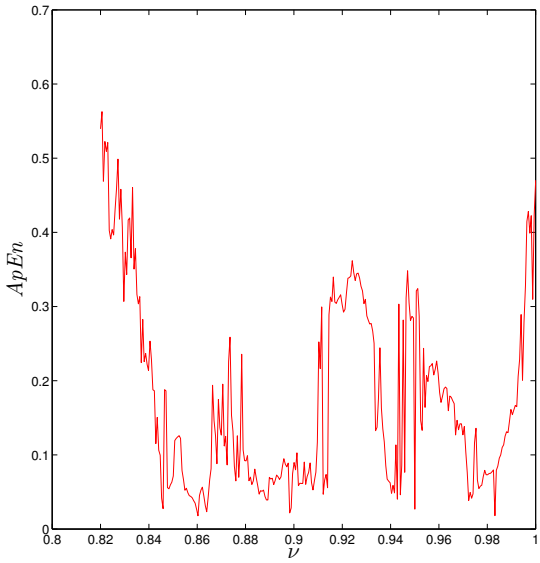

Figure 6.64: Approximate entropy of the fractional-order discrete system (6.55) versus ν with $a_1 = 1$, $a_2 = 0.7$, $a_3 = 1$, and $a_4 = 0.7$.

6.10 Three dimensional fractional order discrete-time system with stable equilibrium point

Recently, hidden attractors with stable equilibria have received considerable attention in chaos theory and nonlinear dynamic systems. Based on discrete fractional calculus, we introduce here a simple three-dimensional fractional-order discrete time system with stable equilibria and hidden coexisting attractors. The system displays an "elegant" mathematical structure and experiences extremely complex dynamics. The mathematical model of the system is

$$\begin{cases} {}^{C}\Delta_a^{\nu} x(t) = y(t+\nu-1) - x(t+\nu-1), \\ {}^{C}\Delta_a^{\nu} y(t) = z(t+\nu-1) - y(t+\nu-1), \\ {}^{C}\Delta_a^{\nu} z(t) = -y(t+\nu-1) - 0.4z(t+\nu-1) - 0.1x(t+\nu-1)z(t+\nu-1) \\ \qquad\qquad +0.1y(t+\nu-1)z(t+\nu-1) + 1, \end{cases} \tag{6.63}$$

where ν is the fractional order in which $0 < \nu \leq 1$. For calculating the equilibrium points (x_f, y_f) of the fractional system (6.63) we solve the following difference equations:

$$\begin{cases} y_f = x_f, \\ z_f = y_f, \\ -y_f - 0.4z_f - 0.1x_f z_f + 0.1y_f z_f + 1 = 0, \end{cases} \tag{6.64}$$

from Equation (6.64) we have the simplified form

$$-1.4x_f + 1 = 0. \tag{6.65}$$

It is obvious that the point $E_f = (\frac{1}{1.4}, \frac{1}{1.4}, \frac{1}{1.4})$ is the only equilibrium point and it is stable. Hence, this system could display hidden attractors in view of appropriate selections of the initial conditions and the fractional-order values as well.

Dynamical analysis

In order to investigate this remarkable property, some numerical formula is designed as:

$$\begin{cases} x(n) = x(0) + \frac{1}{\Gamma(\nu)} \sum\limits_{j=1}^{n} \frac{\Gamma(n-j+\nu)}{\Gamma(n-j+1)} (y(j-1) - x(j-1)), \\ y(n) = y(0) + \frac{1}{\Gamma(\nu)} \sum\limits_{j=1}^{n} \frac{\Gamma(n-j+\nu)}{\Gamma(n-j+1)} (z(j-1) - y(j-1)), \\ z(n) = z(0) + \frac{1}{\Gamma(\nu)} \sum\limits_{j=1}^{n} \frac{\Gamma(n-j+\nu)}{\Gamma(n-j+1)} (-y(j-1) - 0.4z(j-1) \\ \qquad\qquad -0.1x(j-1)z(j-1) + 0.1y(j-1)z(j-1) + 1). \end{cases} \tag{6.66}$$

Here, $x(0), y(0)$ and $z(0)$ are the initial states. Taking advantage of numerical solution (6.66), numerical simulation can be performed to show the basic properties of the novel system (6.63).

6.10 Three dimensional fractional order discrete-time system with stable equilibrium point

Bifurcation and largest Lyapunoc exponents

Here, the dynamical behaviours of the newly established system given in (6.63) are studied by detailed simulation analysis using two indicators: The bifurcation diagrams and the largest Lyapunov exponent (LLE). To evaluate the dynamic properties, the initial condition need to set as $[x(0), y(0), z(0)] = [-0.26, 3.83, -2.22]$. The three dimensional fractional-order discrete time system (6.63) with stable equilibrium point display strange attractor for $\nu = 0.999$ as shown in Figure 6.65. Here, the largest Lyapunove exponent (λ_{max}) of the fractional order discrete time system (6.63) is calculated as $\lambda_{max} = 0.0488$, so the strange attractor in Figure 6.65 is chaotic.

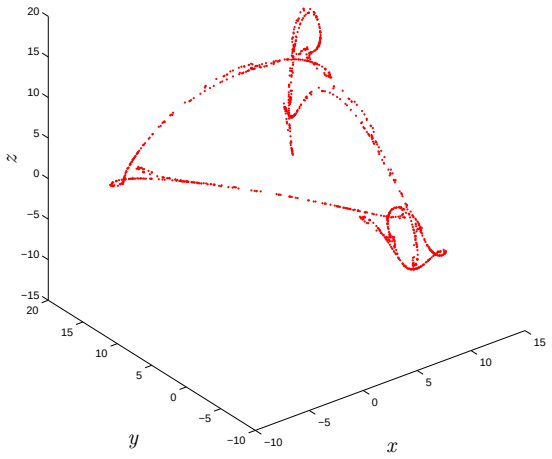

Figure 6.65: Strange attractor of the three–dimensional fractional-order discrete system (6.63).

Bifurcation diagram can help us to observe the dynamic behaviours of the fractional order discrete time system (6.63). The fractional order ν is considered as the only bifurcation parameter in this subsection. Changing ν from 0.95 to 1 and setting two different initial conditions we can obtain the bifurcation diagram in Figure 6.66, where the blue color diagram and the red color diagram are yielded from the initial conditions $[x(0), y(0), z(0)] = [-0.26, -3.83, -2.22]$ and $[x(0), y(0), z(0)] = [-0.26, 3.83, -2.22]$, respectively. When $\nu \in (0.9503, 0.9922)$ coexisting fixed point attractors are observed. When the fractional order increases from 0.9922 to 0.9975, we can observe coexisting periodic windows. For $0.9957 < \nu \leq 1$, the states of the fractional order discrete time system go from periodic behavior to chaos.

0-1 test

The coexistence of the different dynamic behaviours of the proposed system (6.63) with stable equilibrium is confirmed with phase portrait and $p - q$ plots of the 0-1 test for different values of ν.

Figure 6.67 shows the phase portraits of the system while Figure 6.68 shows the $p-q$ plots for the same fractional orders where the blue plots are obtained for the initial values $[x(0), y(0), z(0)] = [-0.26, -3.83, -2.22]$ and the red plots are obtained for $[x(0), y(0), z(0)] = [-0.26, 3.83, -2.22]$. Figure 6.68-(a) depicts bounded like trajectories, which confirms the periodic phenomena of the hidden attractor in Figure 6.67-(a) for $\nu = 0.993$. For $\nu = 0.9984$, a hidden attractor coexists as shown in Figure 6.67, whose Brownian like trajectories can be seen in Figure 6.68.

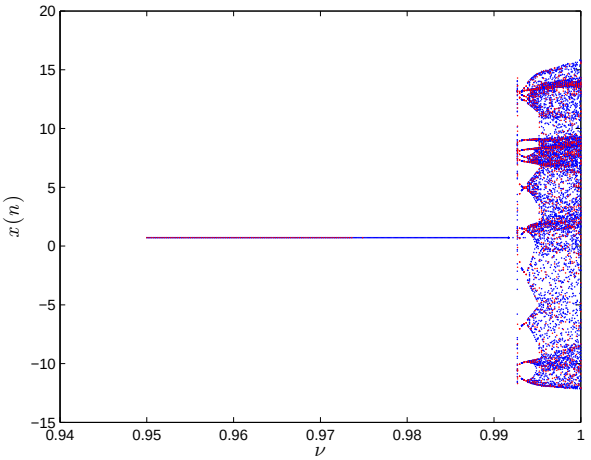

Figure 6.66: Bifurcation diagram of the 3–dimensional fractional map (15) versus ν.

6.11 Conclusion

This chapter provides a brief summarization of fractional-order discrete time systems with hidden attractors. We have presented the hidden attractor and its presence in different classes of two-dimensional and three dimensional maps. Three main families of systems with hidden attractors, systems with stable equilibrium, systems with no equilibrium points, and systems without closed curve equilibrium, have been introduced. Mathematical models of systems with hidden attractors are reported. The schematic method to construct such systems are illustrated also.

Results show that the fractional-order three-dimensional and two dimensional maps of commensurate and incommensurate order can exhibit hidden chaotic attractors. The presented approach can be successfully implemented also for other systems of fractional order. By theoretical analysis and simulating experiments, it can be found that the system has multiple complex characteristics, such as transient period, coexisting attractors and hidden attractors. The phenomena of coexisting attractors also knows as multistability means the coexistence of different kind of attractors in nonlinear systems for different initial conditions with fixed system parameters. The coexistence peculiarity can be used for generating multi-pseudo signals. So the chaotic system has potential applications in electronic measurement, secure communications,

information encryption and other fields.

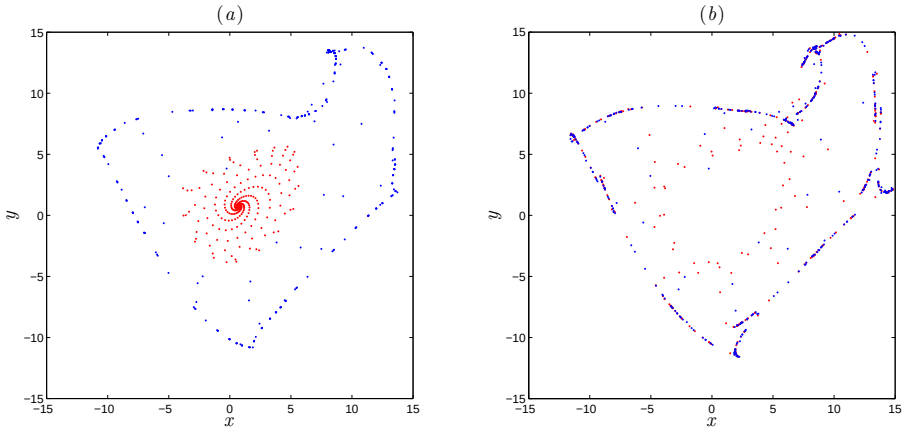

Figure 6.67: Coexisting hidden attractors of three–dimensional fractional-order discrete system (6.63) with initial condition $[-0.26, 3.83, -2.22]$ for red attractor and $[-0.26, -3.83, -2.22]$ for blue attractor, (a) for fractional order $\nu = 0.993$, (b) for fractional order $\nu = 0.9984$.

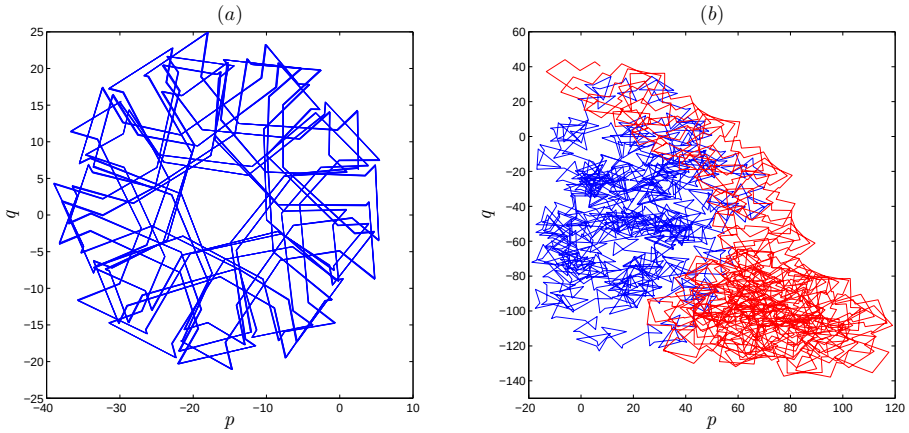

Figure 6.68: $p - q$ plots of the three–dimensional fractional-order discrete system (6.63), (a) Bounded trajectories for $\nu = 0.993$, (b) Brownian like trajectories for both initial conditions with $\nu = 0.9984$.

Chapter 7

Control of Different Dimensional Fractional Chaotic Discrete-Time Systems

7.1 Introduction

When dealing with chaotic dynamical systems in general, particular interest is paid to our ability to control or stabilize these systems. By control, we refer to the addition of new adaptively updated terms to the chaotic system in order to force its states towards zero asymptotically. One of the applications of this topic is in robotics where the control of the chaotic motion of a rigid body is considered.

This chapter suggest different linear and nonlinear stabilization controllers to stabilize the chaotic trajectories of seven of the proposed fractional maps with self-excited and hidden attractors, i.e, the fractional Hénon-Lozi map (4.19), the fractional Duffing map (4.29), the fractional Stefanski map (5.2), the fractional Rossler map (5.5), the fractional Wang map (5.8), the two dimensional fractional map with no equilibria (6.3) and the three dimensional fractional map without equilibria (6.51). By considering the following general fractional discrete-time system

$$ {}^{C}\Delta_{a}^{\nu}\mathbf{x}(t) = f(\mathbf{x}(t+\nu-1)), \tag{7.1} $$

where $\mathbf{x}(t) = \{x_1(t), x_2(t), \ldots, x_m(t)\}$ are the state vector, and ${}^{C}\Delta_{a}^{\nu}$ is the Caputo fractional difference operator where $0 < \nu \leq 1$ is the fractional order value. The purpose of controlling the fractional discrete-time system (7.1) is to derive an adaptive control law such that all states of the fractional order maps converge to zero asymptotically. The controlled fractional discrete-time system (7.1) is given by

$$ {}^{C}\Delta_{a}^{\nu}\mathbf{x}(t) = f(\mathbf{x}(t+\nu-1)) + U, \tag{7.2} $$

where $U(t)$ is adaptive controller. By adding control laws to the states of the fractional-order nonlinear map the system will become linear

$$ {}^{C}\Delta_{a}^{\nu}x\left(t\right) = Mx\left(t+\nu-1\right). $$

In order to establish the convergence of the system states to zero, we use the stability theory of linear fractional discrete–time system to guarantee the asymptotic stability of the zero equilibrium. First, let us recall the following theorem reported in Chapter 2, which identifies the asymptotic stability conditions of the zero solution to a fractional order map.

Theorem 7.1. *Given a vector–valued function* $F(t) = (f_1(t), ..., f_n(t))^T$, *a fractional order* $0 < \nu \leq 1$, *and a matrix* $M \in \mathbb{R}^{n\times n}$, $\forall t \in \mathbb{N}_{a+1-\nu}$, *the zero equilibrium of the linear fractional–order discrete–time system*

$$ {}^{C}\Delta_a^{\nu} F(t) = MF(t+\nu-1), \tag{7.3}$$

is asymptotically stable if the eigenvalues λ *of* M *satisfy*

$$\lambda \in \left\{ z \in \mathbb{C} : \ |z| < \left(2\cos\frac{|\arg z| - \pi}{2-\nu} \right)^{\nu} \ \text{and} \ |\arg z| > \frac{\nu\pi}{2} \right\}. \tag{7.4}$$

7.2 Stabilization control of the fractional Hénon-Lozi map

In this section a novel theorem is proved, which enables to stabilize the dynamics of the above mentioned fractional Hénon-Lozi map to zero asymptotically. We derive one dimensional control law such that both of the map trajectories are controlled to zero asymptotically. We can state the following theorem.

Theorem 7.2. *The fractional Hénon-Lozi map can be controlled under the one–dimensional control law*

$$u_x(t) = \alpha S_{\varepsilon}(x(t)) - y(t) - 1. \tag{7.5}$$

Proof. The controlled fractional order Hénon-Lozi map involves the time–varying control parameter $u_x(t)$ and is given by

$$\begin{cases} {}^{C}\Delta_a^{\nu} x(t) = 1 - \alpha S_{\varepsilon}(x(t-1+\nu)) + y(t-1+\nu) - x(t-1+\nu), + u_x(t-1+\nu), \\ {}^{C}\Delta_a^{\nu} y(t) = \beta x(t-1+\nu) - y(t-1+\nu). \end{cases} \tag{7.6}$$

Substituting the proposed control law (7.5) into (7.6) yields the simplified dynamics

$$\begin{cases} {}^{C}\Delta_a^{\nu} x(t) = -x(t-1+\nu), \\ {}^{C}\Delta_a^{\nu} y(t) = \beta x(t-1+\nu) - y(t-1+\nu). \end{cases} \tag{7.7}$$

The aim is to show that the zero equilibrium of (7.7) is asymptotically stable, which means that the system states converge towards zero as time progresses. The error system can be written in the compact form

$$ {}^{C}\Delta_a^{\nu} (x(t), y(t))^T = \mathbf{M} \times (x(t-1+\nu), y(t-1+\nu))^T, \tag{7.8}$$

where

$$\mathbf{M} = \begin{pmatrix} -1 & 0 \\ \beta & -1 \end{pmatrix}.$$

Now, it is easy to see that all the eigenvalues λ_1 and λ_2 of the matrix $\mathbf{M}$ satisfy the stability condition (7.4). From Theorem 7.4, it is evident that the zero solution of (7.7) is asymptotically stable and, therefore, the system is stabilized. □

A numerical simulation was carried out to illustrate the result of Theorem 7.2. We chose parameters $(\alpha, \beta) = (1.7, 0.5)$, initial conditions $[x(0), y(0)] = [1, 0]$, and fractional order $\nu = 0.95$. Assuming $a = 0$, the evolution of states towards zeros is depicted in Figure 7.1, which confirms the theoretical control proposed in Theorem 7.2.

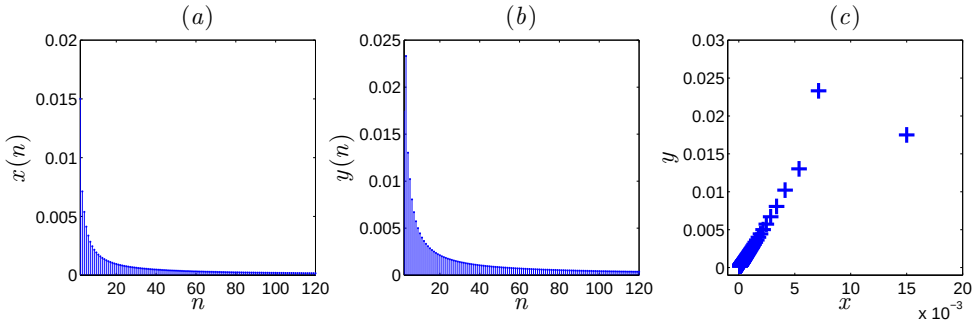

Figure 7.1: The time evolution of the controlled states for the fractional Hénon-Lozi map.

7.3 Stabilization control of the fractional chaotic Duffing map

To control the fractional duffing map, reported in Chapter 4 Section 4.7, given by

$$\begin{cases} {}^{C}\Delta_a^{\nu} x(t) = y(t-1+\nu) - x(t-1+\nu), \\ {}^{C}\Delta_a^{\nu} y(t) = -\beta x(t-1+\nu) + (\alpha - 1) y(t-1+\nu) - y^3(t-1+\nu), \end{cases} \tag{7.9}$$

we need the following theorem that presents the designed adaptive controller.

Theorem 7.3. *The two–dimensional fractional Duffing map is stabilized under the one–dimensional control law described by*

$$u_y(t) = -\alpha y(t) + y^3(t) + \beta x(t). \tag{7.10}$$

Proof. First, let us define the controlled fractional Duffing map by

$$\begin{cases} {}^{C}\Delta_a^{\nu} x(t) = y(t-1+\nu) - x(t-1+\nu), \\ {}^{C}\Delta_a^{\nu} y(t) = -\beta x(t-1+\nu) + (\alpha - 1) y(t-1+\nu) \\ \qquad\qquad -y^3(t-1+\nu) + u_y(t-1+\nu), \end{cases} \tag{7.11}$$

for some adaptive controller $u_y(t)$. The idea is to design a suitable controller $u_y(t)$ such that both states of the system (7.11) reported in Chapter 3 are controlled towards zero. By subtracting equation (7.10) into the system (7.11), we get the following linear equations

$$\begin{cases} {}^{C}\Delta_a^{\nu} x(t) = -x(t-1+\nu) + y(t-1+\nu), \\ {}^{C}\Delta_a^{\nu} y(t) = -y(t-1+\nu), \end{cases} \tag{7.12}$$

which can be described in matrix form by

$$ {}^{C}\Delta_{a}^{\nu}\left(x\left(t\right),y\left(t\right)\right)^{T}=M\left(x\left(t-1+\nu\right),y\left(t-1+\nu\right)\right)^{T}, \tag{7.13} $$

where

$$ M=\begin{pmatrix} -1 & 1 \\ 0 & -1 \end{pmatrix}. \tag{7.14} $$

Based on the stability theorem of linear fractional discrete-time system (Theorem 7.1), the zero equilibrium point is asymptotically stable if the eigenvalues $\lambda_1=\lambda_2=-1$ satisfy (7.4). Clearly, (7.4) is fulfilled, which means that the zero equilibrium of (7.11) is asymptotically stable. Hence, the states are guaranteed to converge to zero asymptotically. □

In order to illustrate the validity and applicability of the proposed control law (7.10), one can set the fractional order as $\nu=0.98$, the bifurcation parameters as $\alpha=2.77$, $\beta=0.2$, and the initial values as $x(0)=0.3$, $y(0)=0.1$. Figure 7.2 shows the time evolution of the controlled states. Clearly, in all cases the states converge towards zero confirming the successful stabilization.

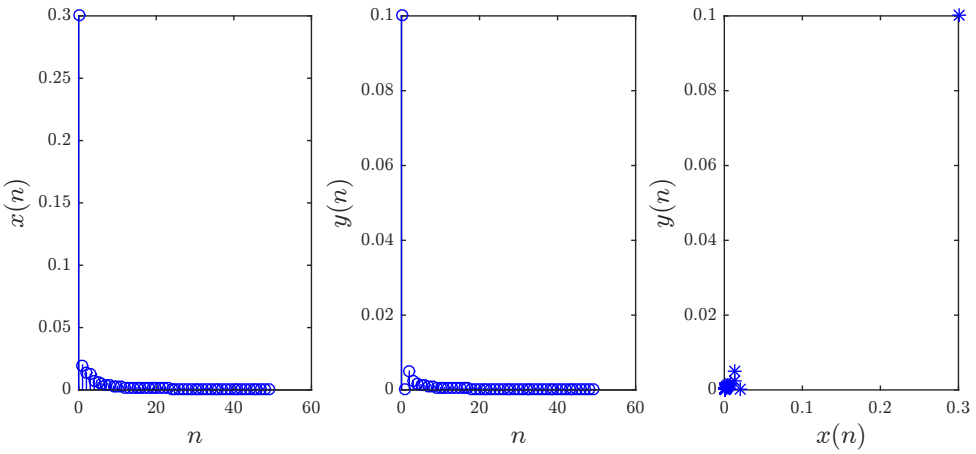

Figure 7.2: Stabilized states of the controlled fractional Duffing map (7.9) with $(\alpha,\beta)=(2.77,0.2)$, $(x\left(0\right),y\left(0\right))=(0.3,0.1)$, and the fractional order $\nu=0.98$.

7.4 Stabilization control of the fractional chaotic Stefanski map

In this section a two-dimensional linear control law is illustrated, with the aim to stabilize at zero the chaotic dynamics of the fractional Stefanski map. The fractional Stefanski system is a three dimensional nonlinear discrete–time system that can exhibit a chaotic behavior. In Section 5.2, the fractional discrete Stefanski map has been studied and discussed. The ν–Caputo which

is defined as:

$$\begin{cases} {}^{C}\Delta_a^{\nu} x(t) = 1 + z(t-1+\nu) - \alpha y^2(t-1+\nu) - x(t-1+\nu), \\ {}^{C}\Delta_a^{\nu} y(t) = 1 + (\beta-1)\, y(t-1+\nu) - \alpha x^2(t-1+\nu), \\ {}^{C}\Delta_a^{\nu} z(t) = \beta x(t-1+\nu) - z(t-1+\nu). \end{cases} \tag{7.15}$$

The following theorem proposes control laws for the fractional–order Stefanski map.

Theorem 7.4. *The 3D fractional–order Stefanski map (7.15) is stable under the 2D control law*

$$\begin{cases} u_x(t) = \alpha y^2(t) - z(t) - 1, \\ u_y(t) = \alpha x^2(t) - 1. \end{cases} \tag{7.16}$$

Proof. Adding two control terms $u_x(t)$ and $u_y(t)$ to the fractional–order Stefanski map (7.15) results in the modified system

$$\begin{cases} {}^{C}\Delta_a^{\nu} x(t) = 1 + z(t-1+\nu) - \alpha y^2(t-1+\nu) - x(t-1+\nu) \\ \qquad\qquad +u_x(t-1+\nu), \\ {}^{C}\Delta_a^{\nu} y(t) = 1 + (\beta-1)\, y(t-1+\nu) - \alpha x^2(t-1+\nu) \\ \qquad\qquad +u_y(t-1+\nu), \\ {}^{C}\Delta_a^{\nu} z(t) = \beta x(t-1+\nu) - z(t-1+\nu). \end{cases} \tag{7.17}$$

Substituting the control law (7.16) yields the new dynamics

$$\begin{cases} {}^{C}\Delta_a^{\nu} x(t) = -x(t-1+\nu), \\ {}^{C}\Delta_a^{\nu} y(t) = (\beta-1)\, y(t-1+\nu), \\ {}^{C}\Delta_a^{\nu} z(t) = \beta x(t-1+\nu) - z(t-1+\nu), \end{cases} \tag{7.18}$$

which can be described more compactly as

$${}^{C}\Delta_a^{\nu} \left(x(t), y(t), z(t)\right)^T = \mathbf{M} \left(x(t), y(t), z(t)\right)^T, \tag{7.19}$$

with

$$\mathbf{M} = \begin{pmatrix} -1 & 0 & 0 \\ 0 & \beta-1 & 0 \\ \beta & 0 & -1 \end{pmatrix}. \tag{7.20}$$

We aim to show that the zero solution of (7.19) is globally asymptotically stable, which guarantees that all states converge towards zero at infinite time. In order to do so, we make use of the stability theory of linear fractional–order maps as described in Theorem 7.1. Simply, we can show that the eigenvalues of the matrix $\mathbf{M}$ are $\lambda_1 = \lambda_3 = -1$ and $\lambda_2 = \beta - 1$. It is easy to see that all the eigenvalues of the matrix $\mathbf{M}$ satisfy

$$|\arg \lambda_i| = \pi > \frac{\nu\pi}{2} \quad \text{and} \quad |\lambda_i| < \left(2\cos\frac{|\arg\lambda_i| - \pi}{2-\nu}\right)^{\nu},$$

for $i = 1, 2, 3$. According to Theorem 7.1, the zero solution of (7.19) is globally asymptotically stable. Hence, the system is stabilized by means of control laws (7.16). □

In order to verify the result of Theorem 7.4, we implemented it numerically in Matlab. The discrete–time states are shown in Figure 7.3. Clearly, the system is asymptotically stable and its states converge towards zero.

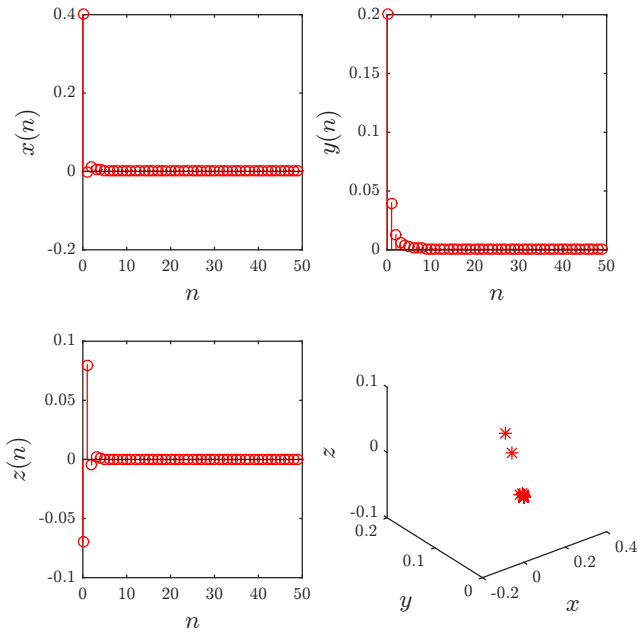

Figure 7.3: The time evolution of the controlled states for the fractional Stefanski map.

7.5 Stabilization control of the fractional chaotic Rössler map

In much the same way followed in the previous section, let us now realize stabilization of the Rössler map by inserting three time varying parameters to the three states $x_1(n), x_2(n), x_3(n)$. Referring to the fractional Rössler map, it was constructed in Section 5.3 based on the ν-Caputo and is given by

$$\begin{cases} {}^{C}\Delta_a^{\nu} x(t) = b_1 x(t-1+\nu)(1-x(t-1+\nu)) \\ \qquad\qquad -b_2((z(t-1+\nu)+b_3)(1-2y(t-1+\nu))) - x(t-1+\nu), \\ {}^{C}\Delta_a^{\nu} y(t) = b_4 y(t-1+\nu)(1-y(t-1+\nu)) + b_5 z(t-1+\nu) \\ \qquad\qquad -y(t-1+\nu), \\ {}^{C}\Delta_a^{\nu} z(t) = b_6(1-b_7 x(t-1+\nu)) \\ \qquad\qquad [(z(t-1+\nu)+b_3)(1-2y(t-1+\nu))-1] - z(t-1+\nu), \end{cases} \tag{7.21}$$

To obtain our results, the following theorem is presented:

Theorem 7.5. *The fractional–order Rössler map (7.21) becomes asymptotically stable subject to the control laws*

$$\begin{cases} u_x(t) = -b_1 x(t) + b_1 x^2(t) - 2b_2 z(t) y(t) + b_2 b_3, \\ u_y(t) = -b_4 y(t) + b_4 y^2(t), \\ u_z(t) = 2b_6 b_3 y(t) + 2b_6 z(t) y(t) + b_6(1-b_3) + b_6 b_7 x(t) z(t) \\ \qquad\qquad - 2b_6 b_7 x(t) y(t) z(t) - 2b_3 b_6 b_7 x(t) y(t). \end{cases} \tag{7.22}$$

Proof. The controlled system corresponding to (7.21) is of the form

$$\begin{cases} {}^{C}\Delta_a^{\nu} x(t) = b_1 x(t-1+\nu)(1-x(t-1+\nu)) \\ \qquad\qquad -b_2((z(t-1+\nu)+b_3)(1-2y(t-1+\nu))) \\ \qquad\qquad -x(t-1+\nu)+u_x(t-1+\nu), \\ {}^{C}\Delta_a^{\nu} y(t) = b_4 y(t-1+\nu)(1-y(t-1+\nu)) + b_5 z(t-1+\nu) \\ \qquad\qquad -y(t-1+\nu)+u_y(t-1+\nu), \\ {}^{C}\Delta_a^{\nu} z(t) = b_6(1-b_7 x(t-1+\nu)) \\ \qquad\qquad [(z(t-1+\nu)+b_3)(1-2y(t-1+\nu))-1] \\ \qquad\qquad -z(t-1+\nu)+u_z(t-1+\nu). \end{cases} \tag{7.23}$$

Substituting the control parameters stated in (7.22) yields the system dynamics

$${}^{C}\Delta_a^{\nu}(x(t), y(t), z(t))^T = \mathbf{M}(x(t), y(t), z(t))^T, \tag{7.24}$$

where

$$\mathbf{M} = \begin{pmatrix} -1 & 2b_2b_3 & -b_2 \\ 0 & -1 & b_5 \\ 0 & 0 & b_6-1 \end{pmatrix}. \tag{7.25}$$

It is easy to see that the eigenvalues of $\mathbf{M}$ satisfy stability condition (7.4). By means of Theorem 7.1, we know that the zero solution is asymptotically stable and thus the system is stabilized. □

Theorem 7.5 was put to the test using the same parameters and initial conditions stated at the beginning of this section and the control laws (7.22). Figure 7.4 shows the time evolution of the states, which clearly converge towards zero indicating successful stabilization.

7.6 Stabilization control of the fractional chaotic Wang map

The following theorem presents the control laws to stabilize the fractional Wang map (5.8). The proof has been omitted as it follows the same lines of Theorems 7.4 and 7.5. It suffices to say that the eigenvalues of the resulting linear fractional error system is stable as a result of Theorem 7.1 for specific parameter values including the parameter set considered earlier in this section.

Theorem 7.6. *The fractional–order Wang map (5.8) is stabilized subject to the control laws*

$$\begin{cases} u_x(t) = 2x(t), \\ u_y(t) = -a_1 x(t) - y(t), \\ u_z(t) = z(t) - a_6 y(t) z(t) - a_5. \end{cases} \tag{7.26}$$

Figure 7.5 depicts the time evolution of the states for the controlled fractional–order discrete–time Wang system. The states are observed to converge towards zeros asymptotically indicating that the system is stabilized.

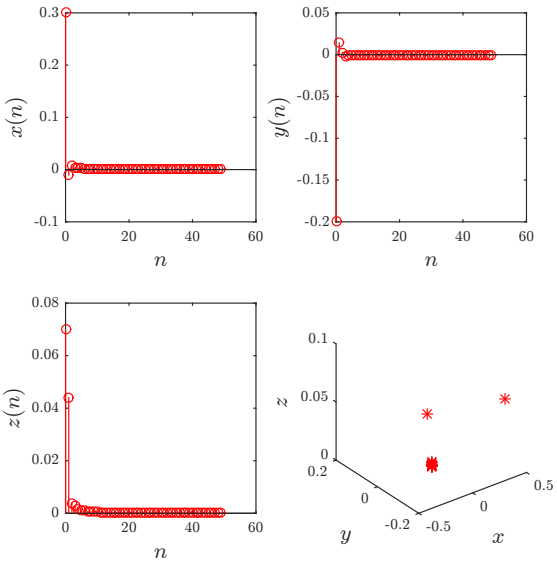

Figure 7.4: The time evolution of the controlled states for the fractional Eössler map.

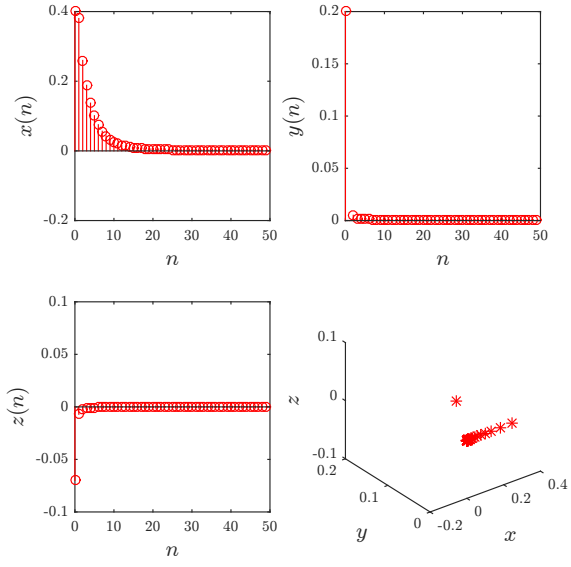

Figure 7.5: The time evolution of the controlled states for the fractional Wang map.

7.7 Stabilization of two dimensional FODT system with no equilibria and with for non-linearities

Here, we design an active controller with the aim of stabilizing the FODT system with no equilibria, reported in Chapter 6 Section 6.2. In general, the stabilization control problem is concerned with finding a suitable adaptive control law such that all of the system's states converge towards zero asymptotically. The following theorem provides the main results to force the system's states converge towards zero asymptotically.

Theorem 7.7. *the FODT system with no equilibria can be controlled under the control law*

$$\begin{cases} u_1(t) = -\frac{1}{2}x(t), \\ u_2(t) = -\frac{1}{2}y(t) + \alpha|y(t)| + x(t)y(t) - \beta x^2(t) + \gamma y^2(t) - \delta. \end{cases} \tag{7.27}$$

Proof. The controlled FODT system with no equilibria is of the form

$$\begin{cases} {}^{C}\Delta_a^{\nu} x(t) = y(t-1+\nu) + u_1(t), \\ {}^{C}\Delta_a^{\nu} y(t) = -\alpha|y(t-1+\nu)| - x(t-1+\nu)y(t-1+\nu) \\ \qquad\qquad + \beta x^2(t-1+\nu) - \gamma y^2(t-1+\nu) + \delta + u_2(t-1+\nu), \end{cases} \tag{7.28}$$

where u_1 and u_2 are the desired controllers. We start by substituting the proposed control law (7.27) into our controlled system (7.28) to obtain the new dynamics

$$\begin{cases} {}^{C}\Delta_a^{\nu} x(t) = -\frac{1}{2}x(t-1+\nu) + y(t-1+\nu), \\ {}^{C}\Delta_a^{\nu} y(t) = -\frac{1}{2}y(t-1+\nu). \end{cases} \tag{7.29}$$

Next, we show that the zero equilibrium of (7.29) is globally asymptotically stable. In order to do so, we can write the error system in the following compact form

$${}^{C}\Delta_a^{\nu}\left(x(t), y(t)\right)^T = \mathbf{M} \times \left(x(t-1+\nu), y(t-1+\nu)\right)^T, \tag{7.30}$$

where

$$\mathbf{M} = \begin{pmatrix} -\frac{1}{2} & 1 \\ 0 & -\frac{1}{2} \end{pmatrix} \tag{7.31}$$

This fulfils the criterion of Theorem 7.4, which means that the zero equilibrium of (7.30) is globally asymptotically stable. Hence, the states are guaranteed to converge to zero asymptotically. □

The proposed control law (7.27) applied to the fractional map (7.27) has been tested numerically for $\nu = 0.998$, $\nu = 0.992$ given the same parameters and initial conditions assumed previously. Figure.7.6 and Figure.7.7 shows how the states indeed converge towards zero by means of time–evolution and phase space plots.

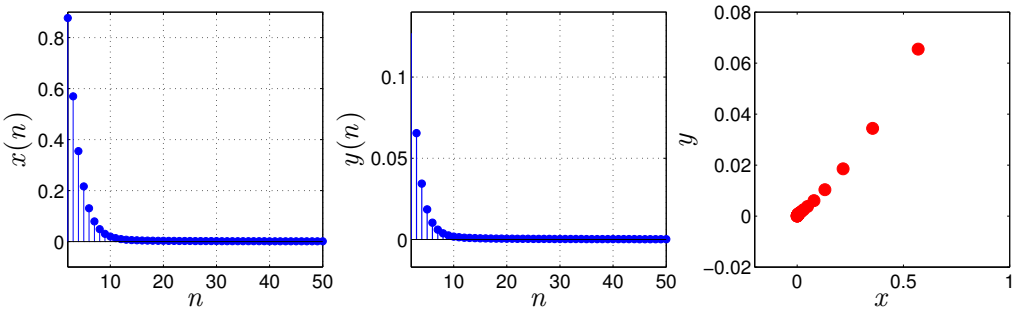

Figure 7.6: Stabilization of states and attractor of the fractional-order map for $\nu = 0.998$.

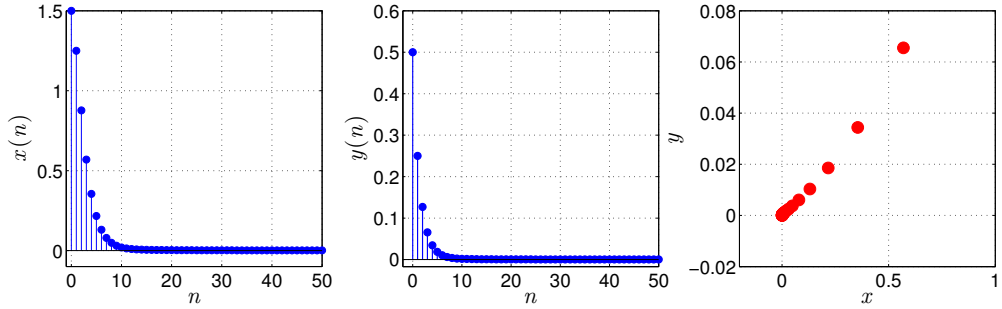

Figure 7.7: Stabilization of states and attractor of the fractional-order map for $\nu = 0.992$.

7.8 Control of three dimensional FODT system with no equilibria

Here, we will realize stabilization of the 3D-FODT system with no equilibria and with two non-linearities, which was proposed in Section 6.9, by inserting a one dimensional time-varying parameter to the state $x(t)$. Recalling that the FODT system equations are given by

$$\begin{cases} {}^{C}\Delta_a^{\nu} x(t) = y(t-1+\nu) - x(t-1+\nu), \\ {}^{C}\Delta_a^{\nu} y(t) = z(t-1+\nu) - y(t-1+\nu), \\ {}^{C}\Delta_a^{\nu} z(t) = a_1 x(t-1+\nu) + a_2 z(t-1+\nu) + a_3 x(t-1+\nu) y(t-1+\nu) \\ \qquad\qquad + a_4 z^2(t-1+\nu) + a_5 - z(t-1+\nu), \end{cases} \tag{7.32}$$

where x_0, y_0 are initial states and $\nu \in (0, 1]$. Now, we can give the following theorem to stabilize the proposed new fractional order discrete-time system.

Theorem 7.8. *The three-dimensional fractional order discrete-time system (7.32) can be stabilized under the one–dimensional control law*

$$u(t) = -a_1 x(t) - a_2 z(t) - a_3 x(t) y(t) - a_4 z^2(t) - a_5. \tag{7.33}$$

Proof. The controlled fractional order discrete-time system (7.32) involves the time–varying control parameter $u(t)$ and is given by

$$\begin{cases} {}^{C}\Delta_a^{\nu} x(t) = y(t-1+\nu) - x(t-1+\nu), \\ {}^{C}\Delta_a^{\nu} y(t) = z(t-1+\nu) - y(t-1+\nu), \\ {}^{C}\Delta_a^{\nu} z(t) = a_1 x(t-1+\nu) + (a_2-1)\, z(t-1+\nu) \\ \qquad\qquad +a_3 x(t-1+\nu) y(t-1+\nu) \\ \qquad\qquad +a_4 z^2(t-1+\nu) + a_5 + u(t-1+\nu). \end{cases} \tag{7.34}$$

Substituting the proposed control law (7.33) into (7.34) yields the simplified dynamics

$$\begin{cases} {}^{C}\Delta_a^{\nu} x(t) = y(t-1+\nu) - x(t-1+\nu), \\ {}^{C}\Delta_a^{\nu} y(t) = z(t-1+\nu) - y(t-1+\nu), \\ {}^{C}\Delta_a^{\nu} z(t) = -z(t-1+\nu). \end{cases} \tag{7.35}$$

The system (7.35) can be written in the compact form

$${}^{C}\Delta_a^{\nu} \left(x(t), y(t), z(t)\right)^T = \mathbf{M} \times \left(x(t-1+\nu), y(t-1+\upsilon), z(t-1+\nu)\right),^T \tag{7.36}$$

where

$$\mathbf{M} = \begin{pmatrix} -1 & 1 & 0 \\ 0 & -1 & 1 \\ 0 & 0 & -1 \end{pmatrix} \tag{7.37}$$

The aim is to show that the zero equilibrium of (7.36) is asymptotically stable, which means that the system states converge towards zero as time progresses. Asymptotic stability can be established using the stability theory of linear fractional discrete-time system as described in Theorem 7.8. Now, it is easy to see that the eigenvalues of the matrix (7.37) are: $\lambda_1 = \lambda_2 = \lambda_3 = -1$ and satisfy $|\arg \lambda_i| = \pi > \frac{\nu\pi}{2}$ and $|\lambda_i| < \left(2\cos\frac{|\arg\lambda_i|-\pi}{2-\nu}\right)^{\nu}$, for $i = 1, 2, 3$. From Theorem 7.1, it is evident that the zero solution of (7.36) is asymptotically stable and, therefore, the three dimensional FODT system (7.32) is stabilized. □

A numerical simulation was carried out to illustrate the result of Theorem 7.1. We choose $a = 0$, initial conditions $(x(0), y(0), z(0)) = (1.5, 2.84, -1.2)$, and fractional order $\nu = 0.98$. The evolution of states towards zeros is depicted in Figure 7.8, which confirms the theoretical control proposed in Theorem 7.8.

7.9 Conclusion

This chapter provides a contribution to the topic by presenting nonlinear and linear control laws to stabilize the dynamics of two and three dimensional fractional maps with self-excited and hidden attractors that have been introduced in the previous chapters. The stabilization task consists by updating one or more of the system's states in order to force all the system states to converge to an equilibrium point. The convergence of the states is established by means of the stability theory of linear fractional order discrete-time systems and verified numerically. The

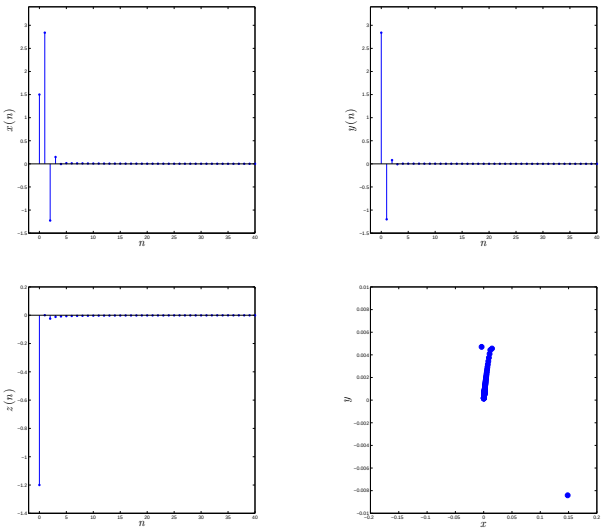

Figure 7.8: The time evolution of the controlled states for the three dimensional FODT system (7.32).

main aventage of the control laws is that they fall with in the feedback linearisation type, which is very simple to implement in realistic applications. Moreover, the proposed control schemes require less control efforts with respect to the nonlinear approach introduces in the literature.

Chapter 8

Different Synchronization Schemes Between Fractional Chaotic Discrete-Time Systems

8.1 Introduction

Due to the many reported advantages of fractional chaotic maps reported in Chapter 4, 5 and 6, we found ourselves compelled to examine their synchronization. Synchronization of chaos in fractional order discrete-time systems regarded as the most interesting topics. From the control point of view, synchronization issue deals with the synchronization of a pair of systems named the master and the slave systems. The objective is to force the states of the slave chaotic system towards that of a master chaotic system. In this case, the synchronization error converges towards zero as $t \to +\infty$. It is not always possible or desirable to completely synchronize two chaotic systems but rather to introduce a more generalized synchronization. There are few literature that has taken into account the dynamics synchronization problems in fractional-order systems in the field of discrete fractional calculus [172–175]. In [172], the authors discuss the dynamics of the fractional logistic map and propose a simple synchronization scheme for a pair of identical maps. The work in [173] concerns identical synchronization, and reference [175] deals with the chaotic synchronization of linearly coupled discrete fractional Hénon maps. Furthermore, synchronization via control technique has been applied in different practical applications, especially secure communication in which direct coupling cannot be done.

Based on the stability theory of linear fractional difference systems reported in Chapter 2, this chapter presents different methods of synchronization between fractional-order chaotic maps described by the left Caputo difference operator. Some nonlinear controller are designed, which enable synchronization to be achieved between different fractional order chaotic maps with different dimensions. We consider different types of synchronisation, namely we introduce two approaches to the *generalized synchronized synchronization* and the *inverse generalized synchronization* of fractional discrete-time chaotic systems with non-identical dimensions, we then introduce the *full-state hybrid projective synchronisation* (FSHPS) for a fractional-order master

and an integer-order slave system. An *inverse FSHPS* laws is also proposed for a fractional-order master and an integer-order slave. Moreover, we propose two control strategies for the $Q-S$ *synchronization* of fractional-order discrete-time chaotic systems. In this scheme two functions Q and S are used such that limit $||Q(Y(t))-S(X(t))||=0$, where $X(t)$ and $Y(t)$ are the drive and response systems. Furthermore, a combined synchronization between two different dimensional fractional discrete time systems is also presented. Finally, the synchronization of the systems with hidden attractors is illustrated through designing nonlinear controller. A detailed description of these synchronisations will be shown in the following sections along with the proposed control laws and the proofs of their convergence. Also, numerical examples are used to illustrate the validity of the proposed synchronisation schemes.

8.2 Generalized synchronization

Generalized synchronization is one of the most widely studied synchronization types. It refers to the existence of a functional relationship between the drive states and the response states [177]. Instead of the conventional definition of synchronization, which stipulates that the difference between the drive and response trajectories tends to zero as $t\to\infty$, *generalized synchronization* forces the difference between the slave states and a function of the master states to zero. This allows for more flexibility and has proven useful in many applications including secure communications [178]. This results has been published in our manuscript [176]. It is important to note that the novelty of the results reported in this section stems from the fact that the *generalized synchronization* scheme achieved is a generalization of a number of different synchronization types including complete synchronization, anti-synchronization, projective synchronization, matrix projective synchronization, and functional matrix projective synchronization.

The set-up is easily demonstrated by considering, the drive and response systems described by

$$ {}^{C}\Delta_{a}^{\nu}X\left(t\right)=f\left(X\left(t+\nu-1\right)\right), \tag{8.1a}$$

$$ {}^{C}\Delta_{a}^{\nu}Y\left(t\right)=BY\left(t+\nu-1\right)+g\left(Y\left(t+\nu-1\right)\right)+U, \tag{8.1b}$$

where $t\in\mathbb{N}_{a+\nu-1}$, $X(t)=(x_1(t),...,x_n(t))^T$ and $Y(t)=(y_1(t),...,y_m(t))^T$ are the corresponding state vectors, $0<\nu\leq 1$, $f:\mathbb{R}^n\to\mathbb{R}^n$, B is an $m\times m$ matrix of parameters, $g:\mathbb{R}^m\to\mathbb{R}^m$, and $U=(u_i)_{1\leq i\leq m}$ is the vector controller to be determined by means of the synchronization process.

Definition 24. Generalization synchronization between master fractional map (8.1a) and slave fractional (8.1b) is achieved if there is a functional relation between both variables X and Y, i.e, if there exists a a map $h:\mathbb{R}^n\to\mathbb{R}^m$ and a controller $U=(u_i)_{1\leq i\leq m}$ such that

$$\lim_{t\to+\infty}\|e\left(t\right):=Y\left(t\right)-h\left(X\left(t\right)\right)\|=0. \tag{8.2}$$

Normally, in order to establish that a certain control law achieved a given type of synchronization, we must prove that the zero solution of the error system is asymptotically stable.

8.2.1 Synchronization scheme

The following theorem proposes a controller U such that the zero solution to the system of equations $e(t)$ as defined in (8.2) is asymptotically stable, meaning that the error tends to 0 as $t \to \infty$. In order to establish the asymptotic stability of the control law described below, we require fractional stability methods. Let us start by stating the following theorem related to the linear stability of fractional maps.

Theorem 8.1. *The master fractional map (8.1a) and the slave fractional map (8.1b) are globally generalized synchronized, under the following control law*

$$U(t) = -CY(t+\nu-1) - g(Y(t+\nu-1)) + (C-B)h(X(t+\nu-1)) + {}^{C}\Delta_a^{\nu} h\left(X(t+\nu-1)\right), \tag{8.3}$$

where $t \in \mathbb{N}_{a+1-\nu}$ *and*

$$C = \begin{pmatrix} c_{11} & b_{12} & \cdots & b_{1m} \\ b_{21} & c_{22} & \cdots & b_{2m} \\ \vdots & \vdots & \ddots & \vdots \\ b_{m1} & b_{m2} & \cdots & c_{mm} \end{pmatrix}, \tag{8.4}$$

and the constants control c_{ii} *are chosen such that*

$$-2^{\nu} < |b_{ii} - c_{ii}| < 0, \quad i = 1, 2, ..., m, \tag{8.5}$$

Proof. The error system (8.2) leads to

$${}^{C}\Delta_a^{\nu} e(t) = BY(t+\nu-1) + g(Y(t+\nu-1)) - {}^{C}\Delta_a^{\nu} h\left(X(t)\right) + U. \tag{8.6}$$

Substituting (8.3) into (8.6) yields the simplified form

$${}^{C}\Delta_a^{\nu} e(t) = (B-C)\, e(t+\nu-1). \tag{8.7}$$

where

$$B - C = \begin{pmatrix} b_{11} - c_{11} & 0 & \cdots & 0 \\ 0 & b_{22} - c_{22} & \cdots & 0 \\ \vdots & \vdots & \ddots & \vdots \\ 0 & 0 & \cdots & b_{mm} - c_{mm} \end{pmatrix}, \tag{8.8}$$

It is easy to see that the eigenvalues ($\lambda_i = b_{ii} - c_{ii}$, $i = 1, 2, ..., m$) of $B - C$ satisfai the following conditions

$$|\lambda_i| < \left(2\cos\frac{|\arg\lambda_i| - \pi}{2-\nu}\right)^{\nu} \quad \text{and} \quad |\arg\lambda_i| > \frac{\nu\pi}{2}.$$

It, therefore, follows immediately from Theorem 7.1 that the zero solution of (8.7) is asymptotically stable and the pair of fractional maps (8.1a) and (8.1b), respectively, is generalized synchronized. □

8.2.2 Numerical simulation

We will put the control laws proposed in Theorem 8.1 to the test by considering a *3D generalized synchronization*. Firstly, we consider the fractional Hénon map as the master system. As reported in Section 3.5.2, the master fractional map is described by

$$\begin{cases} \Delta_{\alpha}^{\nu} x_1(t) = 1 - a_1 x_1^2(t-1+\nu) + x_2(t-1+\nu) - x_1(t-1+\nu), \\ \Delta_{\alpha}^{\nu} x_2(t) = b_1 x_1(t-1+\nu) - x_2(t-1+\nu), \end{cases} \tag{8.9}$$

for $t \in \mathbb{N}_{a+1-\nu}$, which exhibits a chaotic attractor, for instance, when $(a_1, b_1) = (1.4, 0.3)$, $a = 0$, and $\nu = 0.984$.

As for the response system, we consider the 3D fractional generalized Hénon map. The system is described for $t \in \mathbb{N}_{a+1_\nu}$ as

$$\begin{cases} \Delta_{\alpha}^{\nu} y_1(t) = -y_1(t+\nu-1) - b_2 y_3(t+\nu-1) + u_1(t+\nu-1), \\ \Delta_{\alpha}^{\nu} y_2(t) = b_2 y_3(t+\nu-1) + y_1(t+\nu-1) - y_2(t+\nu-1) + u_2(t+\nu-1), \\ \Delta_{\alpha}^{\nu} y_3(t) = 1 + y_2(t+\nu-1) - a_2 y_3^2(t+\nu-1) - y_3(t+\nu-1) + u_3(t+\nu-1), \end{cases} \tag{8.10}$$

where u_1, u_2, and u_3 are controllers. Subject to $(a_2, b_2) = (0.99, 0.2)$, $a = 0$, and $\nu = 0.984$, the uncontrolled fractional map (8.10) with $u_1 = u_2 = u_3 = 0$ is chaotic as shown in Figure 8.1. It

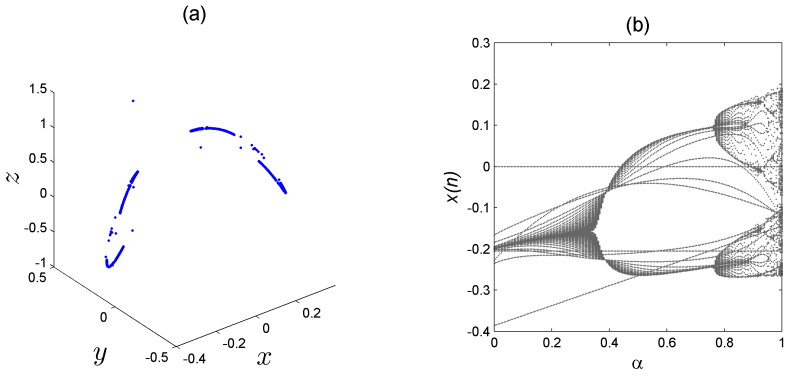

Figure 8.1: 3D chaotic attractor and bifurcation diagram versus parameter α of the generalized Hénon map (8.10) with $(a_2, b_2) = (0.99, 0.2)$ and $\nu = 0.984$.

is easy to see that the linear part of the response system (8.10) is given by

$$B = \begin{pmatrix} -1 & 0 & -b_2 \\ 1 & -1 & b_2 \\ 0 & 1 & -1 \end{pmatrix}. \tag{8.11}$$

Based on the proposed approach described in Section 8.2, the error system corresponding to the generalized synchronization strategy is defined as

$$\left(e_1(t), e_2(t), e_3(t)\right)^T = \left(y_1(t), y_2(t), y_3(t)\right)^T - h\left(x_1(t), x_2(t)\right), \tag{8.12}$$

where

$$h\left(x_1(t), x_2\left(t\right)\right) = \left(x_1\left(t\right), x_2\left(t\right), x_1\left(t\right) x_2\left(t\right)\right)^T. \tag{8.13}$$

According to Theorem 8.1, there exists a control matrix C such that $B - C$ is negative–definite. One can, for instance, choose the case

$$C = \begin{pmatrix} -2 & 0 & -b_2 \\ 1 & -\frac{1}{2} & b_2 \\ 0 & 1 & -\frac{4}{3} \end{pmatrix}, \tag{8.14}$$

which clearly satisfies the conditions (8.4) and (8.5), and by extension systems (8.9) and (8.10) are generalized synchronized in 3D. Now that matrices B and C and function h are known, it is rather easy to construct the control law according to (8.3). The resulting error system is of the form

$$\begin{cases} {}^{C}\Delta_a^{\nu} e_1\left(t\right) = e_1\left(t + \nu - 1\right), \\ {}^{C}\Delta_a^{\nu} e_2\left(t\right) = -\frac{1}{2} e_2\left(t + \nu - 1\right), \\ {}^{C}\Delta_a^{\nu} e_3\left(t\right) = \frac{1}{3} e_3\left(t + \nu - 1\right). \end{cases} \tag{8.15}$$

The time evolution of the errors is depicted in Figure 8.2. Clearly, synchronization is achieved as the errors converge to zero in sufficient time. Similar to the generalized synchronization, a number of different types considered in the literature fall under the *inverse generalized synchronization* type including inverse synchronization, anti-synchronization, inverse projective synchronization, inverse matrix projective synchronization, and inverse functional matrix projective synchronization.

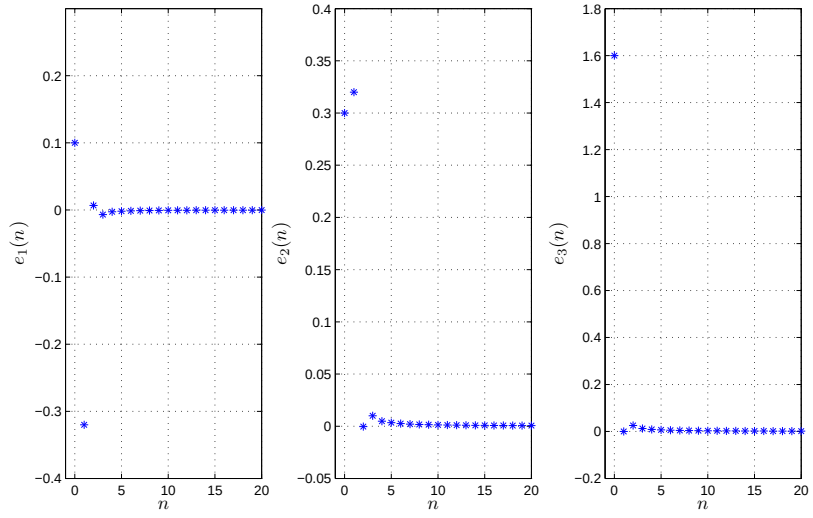

Figure 8.2: Time evolution of the generalized synchronization errors $e_1(t)$, $e_2(t)$, and $e_3(t)$ with $\nu = 0.984$ and $a = 0$.

8.3 Inverse generalized synchronization

Inverse generalized synchronization is the natural reversal of generalized synchronization, i.e., the error is the difference between the master states and a function of the slave states. Our aim in this section is to establish the convergence of the proposed *inverse generalized synchronization* schemes for a pair of fractional discrete systems by means of asymptotic stability results reported in Chapter 2. Thus this type of inverse generalized synchronization has been considered in our research paper [194].

Now, let us consider the master and the response fractional chaotic systems of the form

$$ {}^{C}\Delta_{a}^{\nu}X\left(t\right)=AX\left(t+\nu-1\right)+f\left(X\left(t+\nu-1\right)\right), \tag{8.16a} $$

$$ {}^{C}\Delta_{a}^{\nu}Y\left(t\right)=g\left(Y\left(t+\nu-1\right)\right)+U, \tag{8.16b} $$

where $t\in\mathbb{N}_{a+1-\nu}$. $X(t)=(x_1(t),...,x_n(t))^T$ and $Y(t)=(y_1(t),...,y_m(t))^T$, $0<\nu\leq 1$, $A\in\mathbb{R}^{n\times n}$, $f:\mathbb{R}^n\to\mathbb{R}^n$ is a nonlinear function, $g:\mathbb{R}^m\to\mathbb{R}^m$, and $U=(u_i)_{1\leq i\leq m}$.

Note here that the master and slave systems in (8.16a) and (8.17) are of non identical dimensions given by n and m, respectively, such that $n\leq m$.

Definition 25. The fractional maps (8.16a) and (8.17) are said to be *inverse generalized synchronized* with respect to φ if there exist a controller $U=(u_i)_{1\leq i\leq m}$ and a map $\varphi:\mathbb{R}^m\longrightarrow\mathbb{R}^n$ such that no matter what the initial conditions are, the trajectories of the two systems satisfy the following property

$$ \lim_{t\longrightarrow+\infty}\left\|e\left(t\right):=X\left(t\right)-\varphi\left(Y\left(t\right)\right)\right\|=0. \tag{8.17} $$

8.3.1 The scheme of synchronization

In order to realize the generalized synchronization between the master fractional map (8.16a) and the slave fractional map (8.17), let us suppose that φ can be written as

$$ \varphi\left(Y\left(t\right)\right)=HY\left(t\right)+h\left(Y\left(t\right)\right), \tag{8.18} $$

where $H\in\mathbb{R}^{n\times m}$ and $h:\mathbb{R}^m\to\mathbb{R}^n$ is a nonlinear function. The error dynamics between the master and slave systems can be derived for $t\in\mathbb{N}_{a+1-\nu}$ as:

$$ \begin{aligned} {}^{C}\Delta_{a}^{\nu}e\left(t\right) &= {}^{C}\Delta_{a}^{\nu}X(t)-{}^{C}\Delta_{a}^{\nu}\varphi\left(Y\left(t\right)\right)\\ &= AX\left(t+\nu-1\right)+f\left(X\left(t+\nu-1\right)\right)-H\times{}^{C}\Delta_{a}^{\nu}Y\left(t\right)-{}^{C}\Delta_{a}^{\nu}h\left(Y\left(t\right)\right)\\ &= AX\left(t+\nu-1\right)+f\left(X\left(t+\nu-1\right)\right)-H\times g\left(Y\left(t+\nu-1\right)\right)\\ &\quad-{}^{C}\Delta_{a}^{\nu}h\left(Y\left(t\right)\right)-H\times U. \end{aligned} \tag{8.19} $$

For $i>n$, we can simply choose

$$ u_i=0,\quad i=n+1,\ n+2,....,m. \tag{8.20} $$

This way, (8.19) can be written as follow

$$ {}^{C}\Delta_{a}^{\nu}e\left(t\right)=\left(A-L\right)e\left(t+\nu-1\right)+R-\hat{H}\times\hat{U},\quad t\in\mathbb{N}_{a+1-\nu}, \tag{8.21} $$

where $\hat{U} = (u_1, ..., u_n)^T$, $\hat{H}$ is an invertible $n \times n$ matrix,

$$R = LX(t) + (A-L)HY(t) + (A-L)h\left(Y(t)\right) + f\left(X(t)\right) - Hg\left(Y(t)\right) - {}^{C}\Delta^{\nu} h\left(Y(t)\right), \quad (8.22)$$

and $L \in \mathbb{R}^{n\times n}$ is a control matrix chosen such that all the eigenvalues λ_i, $i = 1, \ldots, n$, of $A - L$ satisfy the conditions

$$|\lambda_i| < 2^{\nu} \quad and \quad |\arg(\lambda_i)| = \pi, \quad i = 1, 2, \ldots, n. \quad (8.23)$$

In order to achieve inverse generalized synchronization, our choice of the remaining control parameters can be made as follows

$$\hat{U} = \hat{H}^{-1} \times R, \quad (8.24)$$

where $\hat{H}^{-1} \in \mathbb{R}^{n\times n}$ is the inverse of matrix $\hat{H}$. By substituting (8.22) into (8.21), the error dynamics can be described as

$${}^{C}\Delta_a^{\nu} e(t) = (A-L)\, e(t+\nu-1), \quad t \in \mathbb{N}_{a+1-\nu}, \quad (8.25)$$

With this dynamic, can follow the same steps as in the proof of Theorem 8.1 to establish the following result.

Theorem 8.2. *Subject to control laws (8.20) and (8.24) and by selecting the control matrix L according to (8.23), the pair (8.16a) and (8.17) are globally inverse generalized synchronized with respect to φ.*

8.3.2 Numerical simulation

Consider the *two-dimensional inverse generalized synchronization* between the 2D fractional Hénon map and the 3D fractional generalized Hénon map. Here, the fractional generalized Hénon map is considered as the master system which is given as

$$\begin{cases} \Delta_{\alpha}^{\nu} y_1(t) = -y_1(t+\nu-1) - b_2 y_3(t+\nu-1), \\ \Delta_{\alpha}^{\nu} y_2(t) = b_2 y_3(t+\nu-1) + y_1(t+\nu-1) - y_2(t+\nu-1), \\ \Delta_{\alpha}^{\nu} y_3(t) = 1 + y_2(t+\nu-1) - a_2 y_3^2(t+\nu-1) - y_3(t+\nu-1). \end{cases} \quad (8.26)$$

The slave system is considered as the 2D fractional Hénon map which is given as

$$\begin{cases} \Delta_{\alpha}^{\nu} x_1(t) = 1 - a_1 x_1^2(t-1+\nu) + x_2(t-1+\nu) - x_1(t-1+\nu) + u_1(t-1+\nu), \\ \Delta_{\alpha}^{\nu} x_2(t) = b_1 x_1(t-1+\nu) - x_2(t-1+\nu) + u(t-1+\nu). \end{cases} \quad (8.27)$$

For the 2D inverse generalized scenario, the linear part of the slave system is

$$A = \begin{pmatrix} -1 & 1 \\ b_1 & -1 \end{pmatrix}. \quad (8.28)$$

Following the synchronization process described in Section 8.3, the error system is given by

$$\left(e_1(t), e_2(t)\right)^T = \left(x_1(t), x_2(t)\right)^T - \varphi\left(y_1(t), y_2(t), y_3(t)\right), \quad (8.29)$$

where

$$\varphi\left(y_1\left(t\right),y_2\left(t\right),y_3\left(t\right)\right)=\left(y_1\left(t\right)-2y_2\left(t\right),y_1\left(t\right)+y_3^2\left(t\right)\right)^T. \tag{8.30}$$

The function φ can be written as

$$\varphi\left(y_1\left(t\right),y_2\left(t\right),y_3\left(t\right)\right)=H\times\left(y_1\left(t\right),y_2\left(t\right),y_3\left(t\right)\right)^T+h\left(y_1\left(t\right),y_2\left(t\right),y_3\left(t\right)\right), \tag{8.31}$$

where

$$H=\begin{pmatrix}1&-2&0\\0&1&0\end{pmatrix}, \tag{8.32}$$

and

$$h\left(y_1\left(t\right),y_2\left(t\right),y_3\left(t\right)\right)=\left(0,y_3^2\left(t\right)\right)^T. \tag{8.33}$$

Using the steps of Section 8.3, we have

$$\hat{H}=\begin{pmatrix}1&-2\\0&1\end{pmatrix}\quad\text{and}\quad\hat{H}^{-1}=\begin{pmatrix}1&2\\0&1\end{pmatrix}. \tag{8.34}$$

According to Theorem 8.2, there exists a control matrix L can be selected as

$$L=\begin{pmatrix}0&0\\b_1-1&-2\end{pmatrix}, \tag{8.35}$$

which clearly satisfies the conditions (8.23). Recall from (8.22) that the controller requires us to determine $\hat{H}^{-1}$ and R, which may be calculated using L as in (8.35) and A as in (8.28). Constructing the controllers is, therefore, straightforward and is governed by (8.20) and (8.22). As a result, systems (8.26) and (8.27) are inverse generalized synchronized in two dimensions. Figure 8.3 depicts the convergence of the errors, which belong to the fractional system

$$\begin{cases}{}^C\Delta_a^\nu e_1\left(t\right)=-e_1\left(t+\nu-1\right)+e_2\left(t+\nu-1\right),\\{}^C\Delta_a^\nu e_2\left(t\right)=-\frac{3}{4}e_1\left(t+\nu-1\right)+e_2\left(t+\nu-1\right).\end{cases} \tag{8.36}$$

8.4 The FSHP synchronisation between integer master and fractional slave maps

This section further investigate the full state hybrid projection synchronization (FSHPS) of a fractional-order master and an integer-order slave chaotic maps with different dimensions. For two pair of discrete–time systems given by

$${}^C\Delta_a^\nu X\left(t\right)=f\left(X\left(t+\nu-1\right)\right),\quad t\in\mathbb{N}_{a+\nu-1}, \tag{8.37a}$$

where $X\left(t\right)=\left(x_1\left(t\right),...,x_n\left(t\right)\right)^T$ represent the states of the master system with fractional order $\nu\in\left(0,1\right]$ and $f:\mathbb{R}^n\longrightarrow\mathbb{R}^n$ is a continuous vector function. A slave system is given by

$$Y\left(t+1\right)=BY\left(t\right)+g\left(Y\left(t\right)\right)+U,\quad t\in\mathbb{N}, \tag{8.37b}$$

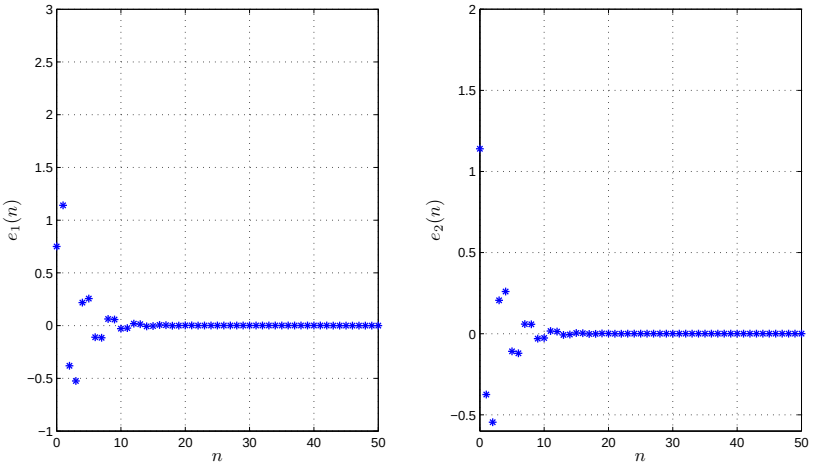

Figure 8.3: Time evolution of the inverse generalized synchronization errors $e_1(t)$ and $e_2(t)$ with $\nu = 0.984$ and $a = 0$.

in which $Y(t) = (y_1(t), ..., y_m(t))^T$ is the state of vector and $B = (b_{ij})_{m\times m}$, $g : \mathbb{R}^m \longrightarrow \mathbb{R}^m$ is a vector of nonlinear function, and $U = (u_i)_{1\leq i\leq m}$ are control parameters to be identified by means of the synchronization strategy. Note that the slave system is an integer–order system with linear and nonlinear parts. Let us now define what is meant by full–state hybrid projective synchronization (FSHPS).

Definition 26. The fractional–order master system and the integer–order slave system described by (8.37a) and (8.37b), respectively, are said to be FSHP synchronized if for an initial conditions, there exists a controller U and a constant matrix $\theta = (\theta_{ij})_{m\times n}$ such that the synchronization errors

$$e_i(t) = y_i(t) - \sum_{j=1}^{n} \theta_{ij} x_j(t), \quad i = 1, 2, .., m, \quad t \in \mathbb{N}, \tag{8.38}$$

satisfy the asymptotic rule

$$\lim_{t\to\infty} e_i(t) = 0, \quad i = 1, 2, .., m. \tag{8.39}$$

Hence the FSHP synchronization problem becomes the stability of error dynamics (8.38). The asymptotic convergence of the synchronisation errors to zero is proved by means of the conventional integer-order direct Lyapunov method.

8.4.1 FSHP synchronization scheme

Here, we give a principle to find suitable feedback controller U such that the fractional-order master and the integer-order slave maps are FSHP synchronized. Therefore, we have the following theorem.

Theorem 8.3. *The master and slave systems in (8.37a) and (8.37b) are FSHP–synchronized give*

$$U = (B - C)\, e(t) - BY(t) - g(Y(t)) + \theta X(t+1), \tag{8.40}$$

where $C \in \mathbb{R}^{m\times m}$ is a control matrix satisfying the condition that matrix

$$(B - C)^T (B - C) - I, \tag{8.41}$$

is negative–definte.

Proof. From (8.38), we have

$$e_i(t+1) = y_i(t+1) - \sum_{j=1}^{n} \theta_{ij} x_j(t+1), \quad i = 1, .., m, \tag{8.42}$$

can be described more compactly as

$$e(t+1) = BY(t) + g(Y(t)) + U - \theta X(t+1). \tag{8.43}$$

After using the control law (8.40), the error system (8.43) yields the simplified system

$$e(t+1) = (B - C)\, e(t). \tag{8.44}$$

The resulting system (8.44) is integer order and thus its stability is classical. As a result, by using the Lyapunov function $V(e(t)) = e^T(t)\, e(t)$, we have

$$\begin{aligned} \Delta V(e(t)) &= e^T(t+1)\, e(t+1) - e^T(t)\, e(t) \\ &= e^T(t)\, (B - C)^T (B - C) e(t) - e^T(t)\, e(t) \\ &= e^T(t) \left[(B - C)^T (B - C) - I \right] e(t). \end{aligned}$$

Since $(B - C)^T (B - C) - I$ is negative definite, it simply follows that

$$\Delta V(e(t)) \leq 0,$$

and by integer–order Lyapunov stability theory, we have

$$\lim_{t \longrightarrow +\infty} e_i(t) = 0, \quad i = 1, 2, ..., m.$$

Hence, by Definition 26 the pair (8.37a), (8.37b) are FSHP synchronized. □

8.4.2 Application of the FSHP synchronization scheme

In order to verify the result of Theorem 8.3, let us take the fractional Hénon chaotic map and the fractional 3D Hénon map to show the full state FSHP synchronization. Similarly to the generalized synchronization results given in Section 8.2.2, we consider the 2D fractional Hénon

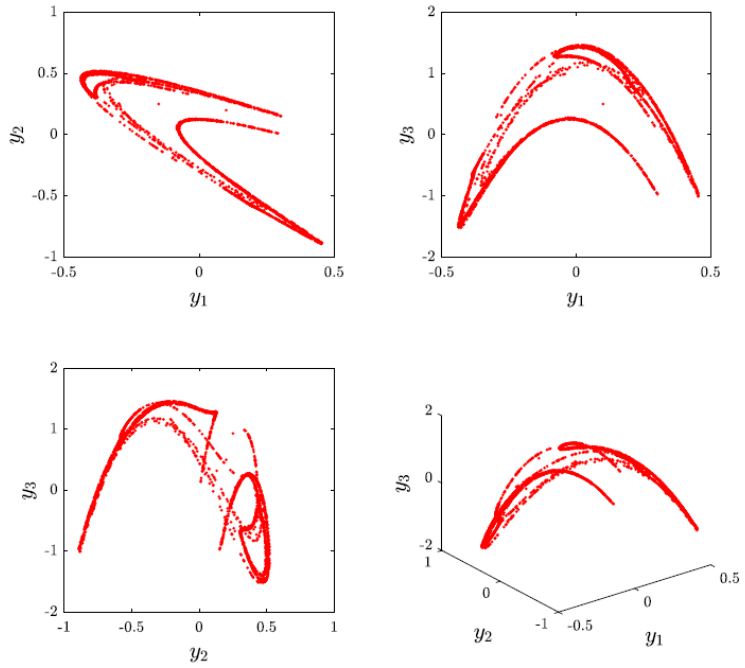

Figure 8.4: Phase portraits for the generalised 3D Hénon map with $(a_2, b_2) = (1.07, 0.3)$ and $(y1(0), y2(0), y3(0)) = (0.1, 0.2, 0.5)$.

map (8.9) as a master system. As for the slave system, we consider a 3D integer–order generalized Hénon map proposed in [179], which is of the form

$$\begin{cases} y_1(t+1) = -b_2 y_3(t) + u_1, \\ y_2(t+1) = b_2 y_3(t) + y_1(t) + u_2, \\ y_3(t+1) = 1 + y_2(t) - a_2 y_3^2(t) + u_3, \end{cases} \tag{8.45}$$

where u_1, u_2, u_3 are controllers. For $u_1 = u_2 = u_3 = 0$, it exhibits a chaotic behavior, for instance, when $(a_2, b_2) = (1.07, 0.3)$. This behavior is depicted in Figure 8.4.
The linear part of the slave is given by

$$B = \begin{pmatrix} 0 & 0 & -b_2 \\ 1 & 0 & b_2 \\ 0 & 1 & 0 \end{pmatrix}. \tag{8.46}$$

We aim to determine the controllers $u_i, i = 1, 2, 3$, that will drive the slave system (8.45) to synchronize with the master system (8.9) under Definition 26. We start by formulating the error system (8.43)

$$\begin{aligned} (e_1(t), e_2(t), e_3(t))^T = (y_1(t), y_2(t), y_3(t))^T \\ -\theta \times (x_1(t), x_2(t))^T, \end{aligned} \tag{8.47}$$

where

$$\theta = (\theta_{ij}) = \begin{pmatrix} 1 & 2 \\ 0 & 3 \\ -1 & 1 \end{pmatrix}. \tag{8.48}$$

Next, according to Theorem 1, we find a suitable control matrix C such that $(B-C)^T(B-C) - I$ is negative definite. It can be easily verified that

$$C = \begin{pmatrix} \frac{-1}{\sqrt{6}} & \frac{-1}{2} & -b_2 - \frac{1}{2\sqrt{3}} \\ 1 + \frac{1}{\sqrt{6}} & \frac{-1}{2} & b_2 - \frac{1}{2\sqrt{3}} \\ \frac{-1}{\sqrt{6}} & 1 & -\frac{1}{\sqrt{3}} \end{pmatrix}, \tag{8.49}$$

is sufficient. The last step is to calculate the control vector $U = (u_i)_{1\le i\le 3}$ according to (8.40) and use it to drive the slave system. The resulting error system is given by

$$\begin{cases} e_1(t+1) = \frac{1}{\sqrt{6}} e_1(t) + \frac{1}{2} e_2(t) - \frac{1}{2\sqrt{3}} e_3(t), \\ e_2(t+1) = \frac{-1}{\sqrt{6}} e_1(t) + \frac{1}{2} e_2(t) + \frac{1}{2\sqrt{3}} e_3(t), \\ e_3(t+1) = \frac{1}{\sqrt{6}} e_1(t) + \frac{1}{\sqrt{3}} e_3(t). \end{cases} \tag{8.50}$$

Figure 8.5 depicts the time evolution of the errors (8.50). Clearly, the errors decay to zero in sufficient time, which means that the master and slave systems (8.9) and (8.45) are synchronized.

Remark 17. Usually, when dealing with continuous- or discrete-time systems, the computational complexity is an important aspect. For continuous-time chaotic systems that represent the dynamics of a nonlinear circuit, complexity can be estimated via integration in a transient period or similar to [180]. However, in discrete-time systems, such an approach is not applicable [196]. One may assess the complexity of the proposed control rule (8.40) in terms of the number of multiply accumulate (MAC) operations required for a single iteration of the controller. Since the number of MACs is dependent on the nonlinear function g, itmay not be estimated in the general case. For the example at hand, we have

$$g(Y(t)) = \begin{pmatrix} 0 \\ 0 \\ 1 - a_2 y_3^2(t) \end{pmatrix}. \tag{8.51}$$

Hence, the number of MACs required to evaluate one iteration of (8.40) is $2m^2 + mn + 5 = 29$.

8.5 IFSHP synchronization between fractional master and integer slave maps

We, now, look at the inverse full-state hybrid projective synchronisation (IFSHP) synchronization of a fractional–order master system and an integer–order slave system; that is the dimension of the response system is greater than that of the master system. Consider the pair

$$\begin{cases} X(t+1) = F(X(t)), & t \in \mathbb{N}, \\ {}^{C}\Delta_a^{\nu} Y(t) = BY(t+\nu-1) + g(Y(t+\nu-1)) + U(t+\nu-1), & t \in \mathbb{N}_{\nu-1}, \end{cases} \tag{8.52}$$

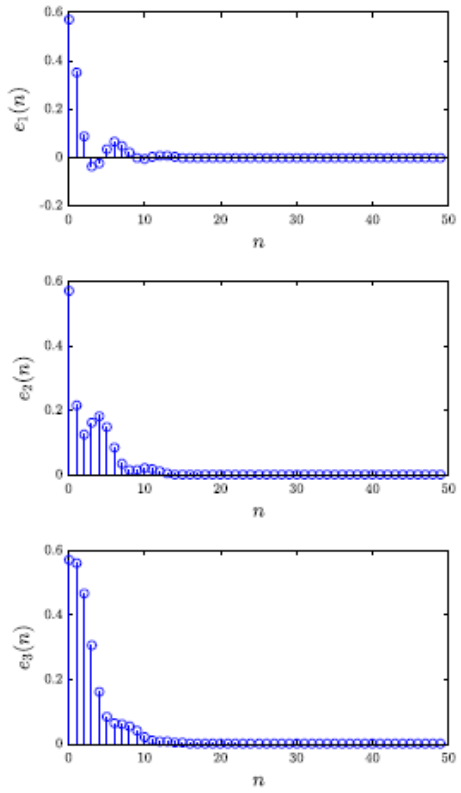

Figure 8.5: The evolution of errors over time for the first example as in (8.50).

where $X(t) = (x_1(t), ..., x_n(t))^T$ and $Y(t) = (y_1(t), ..., y_m(t))^T$ are the master and slave state vectors, respectively, $f : \mathbb{R}^n \longrightarrow \mathbb{R}^n$, $g : \mathbb{R}^m \longrightarrow \mathbb{R}^m$ are nonlinear functions and $U = (u_i)_{1 \leq i \leq m}$ is a control vector. In this case, we assume that $n < m$. The following definition describes the type of synchronization considered in this section.

Definition 27. The master–slave pair (8.52) is said to be inverse full state hybrid projective synchronized if there exists a control vector U and a scaling constant matrix $\gamma = (\gamma_{ij})_{n \times m}$ such that the synchronization errors

$$\lim_{t \to \infty} \left| e_i(t) := x_i(t) - \sum_{j=1}^{m} \gamma_{ij} y_j(t) \right| = 0, \tag{8.53}$$

for $i = 1, 2, .., n$.

8.5.1 IFSHP synchronization scheme with different order

In order to achieve IFSHP synchronization, we take the fractional difference equation of the error vector $e(t) = (e_1(t), ..., e_n(t))^T$ yielding

$${}^{C}\Delta_a^{\nu} e(t) = {}^{C}\Delta^{\nu} X(t) - \gamma B Y(t + \nu - 1) - \gamma g(Y(t + \nu - 1)) - \gamma U, \tag{8.54}$$

For simplicity, we append the control vector U with zeros for $i > n$, i.e.

$$u_i = 0, \quad i = n+1,\ n+2, ..., m. \tag{8.55}$$

Using (8.55), the error system (8.54) simplifies to

$${}^{C}\Delta^{\nu} e\left(t\right) = R - \hat{\gamma}\hat{U}, \tag{8.56}$$

where

$$R = {}^{C}\Delta^{\nu} X\left(t\right) - \gamma BY\left(t+\nu-1\right) - \gamma g\left(Y\left(t+\nu-1\right)\right), \tag{8.57}$$

$\hat{U} = \left(u_1, ..., u_n\right)^T$ and $\hat{\gamma} = \left(\gamma_{ij}\right)_{n\times n}$ is assumed to be an $n \times n$ invertible matrix with its inverse being denoted by $\hat{\gamma}^{-1}$.
In order to achieve IFSHP synchronization between systems (8.52), we may choose the vector controller $\hat{U} = \left(u_1, ..., u_n\right)^T$ as follow:

$$\hat{U} = \hat{\gamma}^{-1}\left[\left(L - \hat{B}\right)\left(X\left(t\right) - \gamma Y\left(t\right)\right) + R\right], \tag{8.58}$$

where $\hat{B} = \left(b_{ij}\right)_{n\times n}$ and $L \in \mathbb{R}^{n\times n}$ is an appropriate control matrix selected such that all the eigenvalues of $\hat{B} - L$ satify

$$-2^{\nu} < \lambda_i < 0,\ i = 1, 2, ..., n. \tag{8.59}$$

Substituting (8.58) into (8.56) yields the new error dynamics

$${}^{C}\Delta^{\nu} e\left(t\right) = \left(\hat{B} - L\right) e\left(t+\nu-1\right). \tag{8.60}$$

In order to show that the zero solution of (8.60) is globally asymptotically stable, we use the stability theory of linear fractional-order maps as described in Theorem 7.1. According to condition (8.59), it is easy to see that all the eigenvalues of the matrix $\hat{B} - L$ satisfy

$$\left|\arg\lambda_i\right| = \pi > \frac{\nu\pi}{2} \quad \textit{and} \quad \left|\lambda_i\right| < \left(2\cos\frac{\left|\arg\lambda_i\right| - \pi}{2-\beta}\right)^{\beta}, \tag{8.61}$$

for $i = 1, 2, ..., n$. Hence, using Theorem 2.6, the zero solution of (8.60) is globally asymptotically stable and the master–slave pair (8.52) are IFSHP–synchronized. The following theorem summarizes the control strategy.

Theorem 8.4. *The master and slave pair (8.52) are IFSHP–synchronized subject to a matrix L being selected such that all the eigenvalues of $\hat{B} - L$ satify (8.59) and control vector U being chosen as described in (8.55) and (8.58).*

8.5.2 Application of the FSHP synchronization scheme

A numerical example is also provided to illustrate the control strategy described the previous section. Let us consider as master the 2D integer-order Hénon map described by

$$\begin{cases} x_1\left(t+1\right) = x_2\left(t\right) + 1 - a_1 x_1^2\left(t\right), \\ x_2\left(t+1\right) = b_1 x_1\left(t\right). \end{cases} \tag{8.62}$$

This system is well known and has a chaotic attractor as reported in Chapter 3. As for the slave, we consider the 3D fractional-order generalized Hénon map proposed in Section 8.2.2 and given by equation (8.10).
The linear part of the slave system can be written in matrix form as

$$B = \begin{pmatrix} -1 & 0 & -b_2 \\ 1 & -1 & b_2 \\ 0 & 1 & -1 \end{pmatrix}. \tag{8.63}$$

So, the matrix $\hat{B}$ is given by

$$\hat{B} = \begin{pmatrix} -1 & 0 \\ 1 & -1 \end{pmatrix}. \tag{8.64}$$

We start by defining the synchronization errors (8.53) as

$$\begin{aligned} \left(e_1(t), e_2(t)\right)^T = & \left(x_1(t), x_2(t)\right)^T \\ & -\gamma \times \left(y_1(t), y_2(t), y_3(t)\right)^T, \end{aligned} \tag{8.65}$$

where

$$\gamma = (\gamma_{ij}) = \begin{pmatrix} 2 & 0 & 4 \\ 0 & 3 & 1 \end{pmatrix}. \tag{8.66}$$

In order to find the suitable controls (8.58), we must first take the reduced matrix

$$\hat{\gamma} = \begin{pmatrix} 2 & 0 \\ 0 & 3 \end{pmatrix}, \tag{8.67}$$

and make sure it is invertible, which it clearly is. Its inverse is simply given by

$$\hat{\gamma}^{-1} = \begin{pmatrix} 1/2 & 0 \\ 0 & 1/3 \end{pmatrix}. \tag{8.68}$$

According to Theorem 8.4, there exists a control matrix L such that the eigenvalues of $(\hat{B} - L)$ satisfy (8.61).We simply choose achieved with

$$L = \begin{pmatrix} 0 & 9/16 \\ 0 & -3/2 \end{pmatrix}, \tag{8.69}$$

leading to

$$\hat{B} - L = \begin{pmatrix} -1 & -9/16 \\ 1 & 1/2 \end{pmatrix},$$

It is easy to see that all the eigenvalues of $\hat{B} - L$ satisfy condition (8.61). All that remains is to calculate matrix R according to (8.57), vector $\hat{U}$ according to (8.58), and append it with a zero at the end as specified in (8.55). The resulting synchronisation error system is of the form

$$\begin{cases} {}^{C}\Delta_a^{\nu} e_1(t) = -e_1(t+\nu-1) - \frac{9}{16} e_2(t+\nu-1), \\ {}^{C}\Delta_a^{\nu} e_2(t) = e_1(t+\nu-1) + \frac{1}{2} e_2(t+\nu-1). \end{cases} \tag{8.70}$$

Given the initial errors $(e_1(0), e_2(0)) = (-1, -2)$, Figure 8.6 depicts the time evolution of the errors (8.70). The errors clearly converge towards the zero solution in sufficient time indicating successful synchronisation between the master and the slave maps.

Remark 18. Similar the the FSHP synchronization the computational complexity involved in the calculation of R according to (8.57) and then $\hat{U}$ according to (8.58) can be shown to be $m^2 + 2n^2 + 4nm = 41$ the number of multiply accumulate operations per iteration.

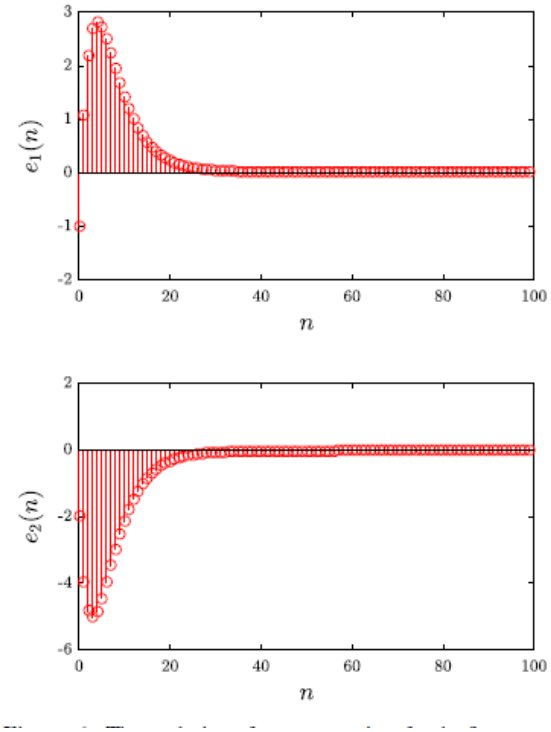

Figure 8.6: The evolution of errors over time for the first example as in (8.70).

8.6 $Q-S$ synchronization of fractional-order discrete-time systems

We are concerned with the $Q-S$ synchronization of fractional-order discrete-time chaotic systems with different dimensions and non-identical orders. In this scheme, two functions Q and S are used to condition the slave and master states, respectively, such that different values for Q and S lead to different types of synchronization. The $Q-S$ comes from a more general synchronization definition, which was presented by Yan in 2005 [181] for continuous-time dynamical systems. The author developed a backstepping approach with a strict feedback form to synchronize two identical systems. The author, then, extended the $Q-S$ scheme to discrete-time systems [182]. Because $Q-S$ focuses on the state of coupled systems, it has been studied by

many researchers. Several algorithms were proposed for the $Q-S$ synchronization of integer-order continuous-time systems including [184–186]. Several studies also looked at the fractional continuous-time case such as [183]. Finally, in [188, 189], the authors investigated $Q-S$ synchronization between integer-order and fractional-order continuous-time systems with different dimensions. In this spirit, we can go ahead and investigate the $Q-S$ synchronization of two chaotic fractional discrete-time systems, i.e for master and response dynamical maps described as

$$\begin{cases} {}^{C}\Delta_{a}^{\nu}X(t)=AX(t+\nu-1)+f(X(t+\nu-1)), & \forall t\in\mathbb{N}_{a+1-\nu}, \\ {}^{C}\Delta_{a}^{\alpha}Y(t)=BY(t+\alpha-1)+g(Y(t+\alpha-1))+U, & \forall t\in\mathbb{N}_{a+1-\alpha}, \end{cases} \tag{8.71}$$

where $X(t)=(x_1(t),...,x_n(t))^T$ and $Y(t)=(y_1(t),...,y_m(t))^T$ denote the master and slave state vectors, respectively, $A\in\mathbb{R}^{n\times n}$, $B\in\mathbb{R}^{m\times m}$, $f:\mathbb{R}^n\to\mathbb{R}^n$, $g:\mathbb{R}^m\to\mathbb{R}^m$ are nonlinear functions and $U=(u_i)_{1\leq i\leq m}$ is a vector controller to be determined by the control laws of the synchronization scheme. Note that $\alpha,\beta\in(0,1]$.

With these notations in mind, the definition of $Q-S$ synchronization of our master-response pair is given a head. The following definition was reported by Ouannas et.al in [190].

Definition 28. The drive-response pair (7.3) is $Q-S$ synchronized in the d^{th} dimension if there exist a controller $U=(u_i)_{1\leq i\leq m}$ and two functions $Q:\mathbb{R}^m\to\mathbb{R}^d$ and $S:\mathbb{R}^n\to\mathbb{R}^d$ such that

$$\lim_{t\longrightarrow+\infty}\|e(t):=Q(Y(t))-S(X(t))\|=0. \tag{8.72}$$

Remark 19. From Definition 28 the depending on our choice of the pair $(Q(Y(t)),S(X(t)))$, we may end up with one of many synchronization types, namely:

$$\begin{array}{ll} (Y(t),X(t)) & \to \text{ Complete synchronization,} \\ (Y(t),-X(t)) & \to \text{ Anti synchronization,} \\ (Y(t),\theta X(t)),\ \theta\in\mathbb{R}^* & \to \text{ Projective synchronization,} \\ (Y(t),MX(t)),\ M\in\mathbb{R}^{m\times n} & \to \text{ Matrix projective synchronization,} \\ (MY(t),X(t)),\ M\in\mathbb{R}^{n\times m} & \to \text{ Inverse matrix projective synchronization,} \\ (Y(t),S(X(t))) & \to \text{ Generalized synchronization,} \\ (Q(Y(t)),X(t)) & \to \text{ Inverse generalized synchronization.} \end{array}$$

For reasons that will become clear later on, suppose that Q can be divided into two parts

$$Q(Y(t))=\mathbf{Q}Y(t)+\mathbf{q}(Y(t)), \tag{8.73}$$

where $\mathbf{Q}$ is an invertible $d\times d$ matrix and and $\mathbf{q}:\mathbb{R}^d\to\mathbb{R}^d$ is a nonlinear function. In the following two sections, we will present two distinct synchronization schemes of dimensions $d=m$ and $d=n$, respectively. We assume an n-dimensional master map and an m-dimensional slave map with the condition $m>n$. Two different control laws will be derived and the asymptotic stability of their zero solution will be investigated through the linearization method.

8.6.1 $Q-S$ Synchronization scheme in dimension m

The $Q-S$ synchronization error defined in (8.72) can be written in the form

$$e(t)=\mathbf{Q}Y(t)+\mathbf{q}(Y(t))-S(X(t)), \tag{8.74}$$

where $\mathbf{Q}$ is an invertible $m \times m$ matrix, $\mathbf{q}: \mathbb{R}^m \to \mathbb{R}^m$, and $S: \mathbb{R}^n \to \mathbb{R}^m$. The α-th order Caputo fractional of (8.74) is of the form

$$\begin{aligned}
{}^{C}\Delta_a^{\alpha} e(t) &= {}^{C}\Delta_a^{\alpha}\left[\mathbf{Q}Y(t) + \mathbf{q}(Y(t)) - S(X(t))\right] \\
&= {}^{C}\Delta_a^{\alpha}\left[\mathbf{Q}Y(t)\right] + {}^{C}\Delta_a^{\alpha}\mathbf{q}(Y(t)) - {}^{C}\Delta_a^{\alpha} S(X(t)) \\
&= \mathbf{Q}\,{}^{C}\Delta_a^{\alpha} Y(t) + {}^{C}\Delta_a^{\alpha}\mathbf{q}(Y(t)) - {}^{C}\Delta_a^{\alpha} S(X(t)) \\
&= \mathbf{Q}\left[BY(t+\alpha-1) + g(Y(t+\alpha-1)) + U\right] + {}^{C}\Delta_a^{\alpha}\mathbf{q}(Y(t)) - {}^{C}\Delta^{\alpha} S(X(t)) \\
&= \mathbf{Q}BY(t+\alpha-1) + \mathbf{Q}g(Y(t+\alpha-1)) + \mathbf{Q}\times U \qquad (8.75) \\
&\quad + {}^{C}\Delta^{\alpha}\mathbf{q}(Y(t)) - {}^{C}\Delta_a^{\alpha} S(X(t)). \qquad (8.76)
\end{aligned}$$

This can be further simplified to

$$ {}^{C}\Delta_a^{\alpha} e(t) = (B-C)\, e(t+\alpha-1) + R + \mathbf{Q}\times U, \tag{8.77}$$

where $C \in \mathbb{R}^{m\times m}$ is an appropriately chosen control matrix and

$$\begin{aligned}
R &= (C-B)\, e(t) + \mathbf{Q}BY(t) + \mathbf{Q}g(Y(t)) \\
&\quad + {}^{C}\Delta^{\beta}\mathbf{q}(Y(t)) - {}^{C}\Delta^{\alpha} S(X(t)).
\end{aligned} \tag{8.78}$$

Remark 20. Note that our aim in synchronization is to find a suitable controller U that forces the synchronization error to zero asymptotically. Since U is part of the response system, the function $Q(Y(t))$ hinders our process. To overcome this problem, we assumed that $Q(Y(t))$ can be decomposed into a linear part (matrix $\mathbf{Q}$) and some other nonlinear function $\mathbf{q}(Y(t))$. The reasoning behind this is that matrix $\mathbf{Q}$ is constant and thus may be factored out of the fractional difference operator.

Theorem 8.5. *The drive–response pair (8.71) is globally Q–S synchronized in dimension m subject to*

$$ U = -\mathbf{Q}^{-1} \times R, \tag{8.79}$$

where $\mathbf{Q}^{-1}$ is the inverse of $\mathbf{Q}$.and the control matrix C is selected such that all the eigenvalues λ of $B-C$.satisfies the condition

$$ -2^{\alpha} < \lambda < 0. \tag{8.80}$$

Proof. By substituting (8.79) into (8.77), we obtain a new formulation for the error system

$$ {}^{C}\Delta^{\alpha} e(t) = (B-C)\, e(t+\alpha-1). \tag{8.81}$$

Now, it is easy to see that all the eigenvalues λ satisfy $|\arg\lambda| = \pi > \frac{\alpha\pi}{2}$ and

$$ |\lambda| < \left(2\cos\frac{|\arg\lambda| - \pi}{2-\alpha}\right)^{\alpha}. \tag{8.82}$$

Therefore, by means of Theorem 7.1, we establish the global asymptotic stability of the zero solution. Consequently, the master–slave maps (8.71) are globally $Q-S$ synchronized in dimension m. □

8.6.2 $Q-S$ Synchronization scheme in dimension n

This second case is not too different from the first one. We define

$$\mathbf{Q} \in \mathbb{R}^{n\times m},\ \mathbf{q}:\mathbb{R}^m \to \mathbb{R}^n,\ \text{and}\ S:\mathbb{R}^n \to \mathbb{R}^n.$$

We set the last $m-n$ controller components to zero, i.e.

$$u_i = 0 \quad \text{for} \quad n < i \leq m. \tag{8.83}$$

Then, the error system reduces to

$$\begin{aligned} {}^{C}\Delta^{\alpha} e\left(t\right) &= \mathbf{Q}BY\left(t+\alpha-1\right)+\mathbf{Q}g\left(Y\left(t+\alpha-1\right)\right) \\ &\quad +\hat{\mathbf{Q}}\times\hat{U}+\ {}^{C}\Delta_a^{\alpha}\mathbf{q}\left(Y\left(t\right)\right)-\ {}^{C}\Delta_a^{\alpha}S\left(X\left(t\right)\right), \end{aligned} \tag{8.84}$$

where $\hat{\mathbf{Q}}$ is an invertible $n\times n$ matrix and $\hat{U}=\left(u_1,...,u_n\right)^T$. This can be further simplified to

$${}^{C}\Delta^{\alpha} e\left(t\right) = \left(A-L\right)e\left(t\right)+\mathbf{T}+\hat{\mathbf{Q}}\times\hat{U}, \tag{8.85}$$

where $L\in\mathbb{R}^{n\times n}$ is an appropriate control matrix and

$$\begin{aligned} \mathbf{T} &= \left(L-A\right)e\left(t\right)+\mathbf{Q}BY\left(t\right)+\mathbf{Q}g\left(Y\left(t\right)\right) \\ &\quad +\ {}^{C}\Delta^{\alpha}\mathbf{q}\left(Y\left(t\right)\right)-\ {}^{C}\Delta^{\alpha}S\left(X\left(t\right)\right). \end{aligned} \tag{8.86}$$

To achieve Q–S synchronization between the master–slave maps (8.71) in dimension n, we propose choosing

$$\hat{U} = -\hat{\mathbf{Q}}^{-1}\mathbf{T}. \tag{8.87}$$

Substituting (8.87) into (8.85) yields the error dynamics

$${}^{C}\Delta_a^{\alpha} e\left(t\right) = \left(A-L\right)e\left(t+\alpha-1\right). \tag{8.88}$$

The following theorem can be proven in the exact same way as Theorem 8.5.

Theorem 8.6. *By selecting control matrix L such that all the eigenvalues λ of $A-L$.satisfy: $-2^{\alpha}<\lambda<0$, the master and slave maps (8.71) are globally $Q-S$ synchronized in dimension n subject to (8.83) and (8.87).*

8.6.3 Application of the $Q-S$ synchronization

In order to show the validity of the proposed control strategies, let us consider some numerical examples. The 2D fractional Hénon map (8.9) as proposed in Section 8.2.2 is chosen as the master map. In order to unify the notation, the fractional Hénon map (8.9) can be rewritten as

$${}^{C}\Delta^{\nu} X\left(t\right) = AX\left(t\right)+f\left(X\left(t\right)\right), \tag{8.89}$$

where

$$A=\begin{pmatrix} -1 & 1 \\ b_1 & -1 \end{pmatrix}\ \text{and}\ f=\begin{pmatrix} 1-a_1x_1^2(t) \\ 0 \end{pmatrix}. \tag{8.90}$$

As for the response map, we choose the 3D fractional-order generalized Hénon map, which is of the form

$$\begin{cases} {}^{C}\Delta^{\alpha} y_1(t) = -y_1(t+\alpha-1) - b_2 y_3(t+\alpha-1) + u_1(t+\alpha-1), \\ {}^{C}\Delta^{\alpha} y_2(t) = b_2 y_3(t+\alpha-1) + y_1(t+\alpha-1) - y_2(t+\alpha-1) + u_2(t+\alpha-1), \\ {}^{C}\Delta^{\alpha} y_3(t) = 1 + y_2(t+\alpha-1) - a_2 y_3^2(t+\alpha-1) - y_3(t+\alpha-1) + u_3(t+\alpha-1). \end{cases} \tag{8.91}$$

This system can be rewritten as

$${}^{C}\Delta^{\alpha} Y(t) = BY(t) + g(Y(t)), \tag{8.92}$$

where

$$B = \begin{pmatrix} -1 & 0 & -b_2 \\ 1 & -1 & b_2 \\ 0 & 1 & -1 \end{pmatrix} \quad \text{and} \quad g = \begin{pmatrix} 0 \\ 0 \\ 1 - a_2 y_3^2(t) \end{pmatrix}. \tag{8.93}$$

We will take 3 and 2 dimensional Q–S synchronization cases separately following the control laws of Theorems 8.5 and 8.6, respectively.

Example 1 . 3-dimensional $Q-S$ synchronization

Based on the approach stated in Section 8.6.1, the error system is given by

$$(e_1(t), e_2(t), e_3(t))^T = Q(y_1(t), y_2(t), y_3(t)) - S(x_1(t), x_2(t)), \tag{8.94}$$

where

$$Q(y_1(t), y_2(t), y_3(t)) = (y_1(t), y_1(t) + y_2(t), y_3(t)(3 + y_2(t)))^T,$$

and

$$S(x_1(t), x_2(t)) = (x_1(t), x_2(t), x_1(t) + x_2(t)).$$

We may rewrite Q in the form

$$Q(y_1(t), y_2(t), y_3(t)) = \mathbf{Q} \times (y_1(t), y_2(t), y_3(t))^T + \mathbf{q}(y_1(t), y_2(t), y_3(t)) \tag{8.95}$$

where

$$\mathbf{Q} = \begin{pmatrix} 1 & 0 & 0 \\ 1 & 2 & 0 \\ 0 & 0 & 3 \end{pmatrix} \tag{8.96}$$

and

$$\mathbf{q}(y_1(t), y_2(t), y_3(t)) = (0, 0, y_2(t) y_3(t))^T. \tag{8.97}$$

It is easy to see that

$$\mathbf{Q}^{-1} = \begin{pmatrix} 1 & 0 & 0 \\ -\frac{1}{2} & \frac{1}{2} & 0 \\ 0 & 0 & \frac{1}{3} \end{pmatrix}. \tag{8.98}$$

According to our approach described in Section 8.6.1, there exists a control matrix C such that all the eigenvalues $B-C$ satisfy the condition of Theorem 8.5. We may simply choose the following

$$C=\begin{pmatrix}0&0&0\\1&0&0\\0&1&0\end{pmatrix}. \tag{8.99}$$

It is clear that all the eigenvalues $B-C$ satisfy the condition of Theorem 8.5. We start by calculating $\mathbf{R}$ by means of (8.78) and then U by means of (8.79). The resulting error system is given by

$$\begin{cases} {}^{C}\Delta^{\alpha}e_1(t)=-e_1(t+\alpha-1)-b_2e_3(t+\alpha-1),\\ {}^{C}\Delta^{\alpha}e_2(t)=-e_2(t+\alpha-1)+b_2e_3(t+\alpha-1),\\ {}^{C}\Delta^{\alpha}e_3(t)=-e_3(t+\alpha-1). \end{cases} \tag{8.100}$$

The time evolution of the errors is depicted in Figure 8.7 for the initial values

$$\begin{pmatrix}e_1(0)\\e_2(0)\\e_3(0)\end{pmatrix}=\begin{pmatrix}0.1\\0.3\\1.6\end{pmatrix}.$$

The errors clearly converge to zero in sufficient time indicating that the master map (8.91) and the response map (8.9) become $Q-S$ synchronized in 3D.

Example 2 . 2-dimensional $Q-S$ synchronization

As for the two dimensional case, we follow the approach described in Section 8.6.2. The error system is given by

$$(e_1(t),e_2(t),e_3(t))^{T}=Q(y_1(t),y_2(t),y_3(t))-S(x_1(t),x_2(t)), \tag{8.101}$$

where

$$Q(y_1(t),y_2(t),y_3(t))=\left(y_1(t)+2y_2(t)+y_3^2(t),-y_1(t)+3y_3(t)\right)^{T},$$

and

$$S(x_1(t),x_2(t))=(x_1(t),x_2(t)).$$

We can write

$$Q(y_1(t),y_2(t),y_3(t))=\mathbf{Q}\times(y_1(t),y_2(t),y_3(t))^{T}+\mathbf{q}(y_1(t),y_2(t),y_3(t)), \tag{8.102}$$

where

$$\mathbf{Q}=\begin{pmatrix}1&2&0\\-1&0&3\end{pmatrix}, \tag{8.103}$$

and

$$\mathbf{q}(y_1(t),y_2(t),y_3(t))=\left(y_3^2(t),0\right)^{T}. \tag{8.104}$$

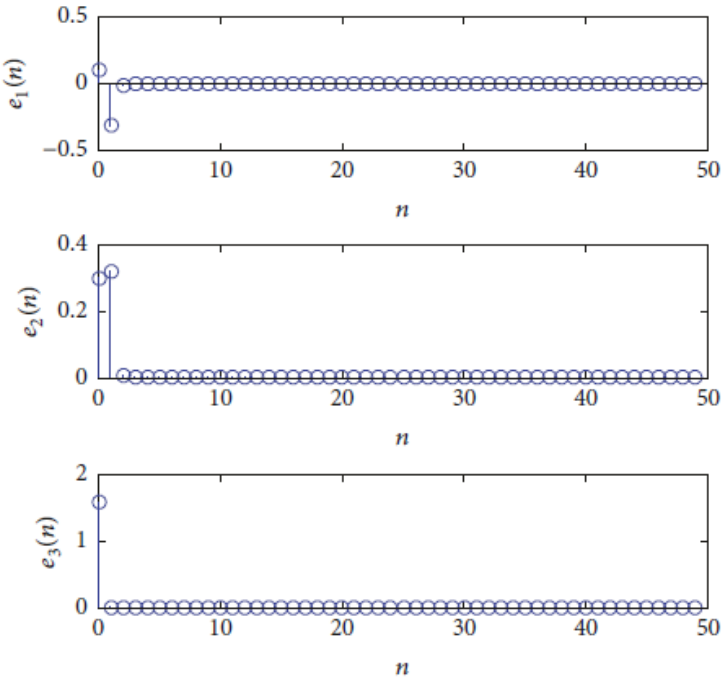

Figure 8.7: The evolution of errors over time for Example 1.

This yields

$$\hat{\mathbf{Q}} = \begin{pmatrix} 1 & 2 \\ -1 & 0 \end{pmatrix} \quad \text{and} \quad \hat{\mathbf{Q}}^{-1} = \begin{pmatrix} 1 & 2 \\ -1 & 0 \end{pmatrix}.$$

According to Theorem 8.6, the control matrix L can be selected as

$$L = \begin{pmatrix} 0 & 0 \\ 4 - b_1 & 3 \end{pmatrix}, \tag{8.105}$$

which clearly satisfies the condition of Theorem 8.6. Next, we calculate $\mathbf{T}$ as specified in (8.86) and $\hat{U}$ as in (8.87). The complete control vector U is formed by appending a zero to the end of $\hat{U}$. The resulting error system is given by

$$\begin{cases} {}^{C}\Delta^{\alpha} e_1(t) = -e_1(t+\alpha-1) + e_2(t+\alpha-1), \\ {}^{C}\Delta^{\alpha} e_2(t) = -4e_1(t+\alpha-1) + 3e_2(t+\alpha-1). \end{cases} \tag{8.106}$$

The convergence of the errors to zero is depicted in Figure 8.8 for the initial conditions

$$\begin{pmatrix} e_1(0) \\ e_2(0) \end{pmatrix} = \begin{pmatrix} 0.75 \\ 1.14 \end{pmatrix}.$$

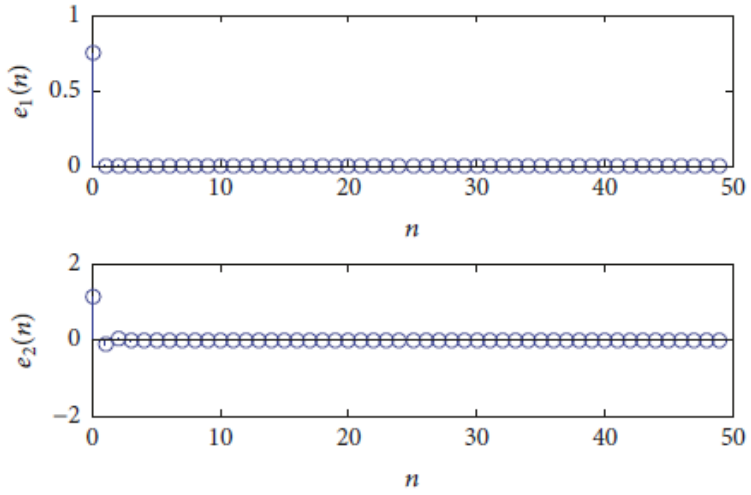

Figure 8.8: The evolution of errors over time for Exemple 2

8.7 The Co–existence of different synchronization types in fractional–order discrete–time chaotic systems with non–identical dimensions

Recently, there has been increasing interest in achieving multiple synchronization types simultaneously for the states of the response system. The idea is to show that multiple types of synchronization may exist simultaneously for a pair of chaotic systems. This phenomenon is commonly referred to as the co-existence of synchronization types. In the following, some control strategy are proposed to examine the phenomenon and develop suitable control laws for various types co-existing for fractional-order discrete-time chaotic systems with different dimensions. In particular, we show that through appropriate nonlinear control, projective synchronization (PS), full state hybrid projective synchronization (FSHPS), and generalized synchronization (GS) can be achieved simultaneously. A second nonlinear control scheme is developed whereby inverse full state hybrid projective synchronization (IFSHPS) and inverse generalized synchronization (IGS) are shown to co-exist.

8.7.1 The problem formulation

In order to estabilish the co–existence of different synchronization types in fractional order discrete–time chaotic systems, we consider the generic n–dimensional drive and response pair of the form

$$\begin{cases} {}^{C}\Delta_{a}^{\nu} x_i(t) = F_i(X(t+\nu-1)), \\ {}^{C}\Delta_{a}^{\nu} y_i(t) = G_i(Y(t+\nu-1)) + u_i, \end{cases}, \quad t \in \mathbb{N}_{a+1-\nu} \tag{8.107}$$

where $X(t) = (x_1(t), ..., x_n(t))^T$, $Y(t) = (y_1(t), ..., y_n(t))^T$ represent the states of the master and slave systems, respectively, F_i, G_i are functions from $\mathbb{R}^n$ to $\mathbb{R}$ for $1 \leq i \leq n$, and $u_i, 1 \leq i \leq$

n, denote control parameters to be identified by means of the synchronization strategy.

Let us, now, define the types of synchronization with which we are interested in our study. The idea is to show that multiple types of synchronization may exist simultaneously for a pair of fractional-order discrete-time chaotic systems.

Definition 29. If there exists a controller $U = (u_i)_{1\leq i\leq n}$ and either constants $\gamma \in \mathbb{R}^*$, a matrix Φ, a map $\phi : \mathbb{R}^n \longrightarrow \mathbb{R}^n$, a matrix Θ, or a map $\varphi : \mathbb{R}^n \longrightarrow \mathbb{R}^n$ such that

$$\begin{aligned}
&\lim_{t\to+\infty} \|Y(t) - \gamma X(t)\| = 0 && \Longrightarrow \text{ Pair (8.107) is projective synchronized (PS).}\\
&\lim_{t\to+\infty} \|Y(t) - \Phi X(t)\| = 0 && \Longrightarrow \text{ Pair (8.107) is full state hybrid projective synchronized (FSHPS).}\\
&\lim_{t\to+\infty} \|Y(t) - \phi(Y(t))\| = 0 && \Longrightarrow \text{ Pair (7.3) is generalized synchronized (GS).}\\
&\lim_{t\to+\infty} \|X(t) - \Theta Y(t)\| = 0 && \Longrightarrow \text{ Pair (8.107) is inverse full state hybrid projective synchronized (IFSHPS).}\\
&\lim_{t\to+\infty} \|X(t) - \varphi(Y(t))\| = 0 && \Longrightarrow \text{ Pair (8.107) is inverse generalized synchronized (IGS).}
\end{aligned}$$

Note that in Definition 29 above, γ is a constant used to scale the master state vector. Matrices ϕ and θ represent linear transformation of the master and slave state vectors, respectively, and are usually referred to as scaling matrices. The terms φ and ϕ denote some arbitrary maps from $\mathbb{R}^n$ towards $\mathbb{R}^n$. In general, these are nonlinear maps that represent scaling functions. We are now ready to present the different synchronization schemes, which has been recently presented by Bendoukha et.al [191].

8.7.2 Co–existence of projective synchronization, FSHPS and genaralized synchronization

Let us consider the 2–dimensional drive system and a 3–dimensional response system given, respectively, by

$$^{C}\Delta_a^{\nu} x_i(t) = f_i(X(t+\nu-1)), \quad i = 1, 2, \tag{8.108}$$

and

$$^{C}\Delta_a^{\nu} y_i(t) = \sum_{j=1}^{3} b_{ij} y_j(t+\nu-1) + g_i(Y(t+\nu-1)) + u_i, \quad i = 1, 2, 3, \tag{8.109}$$

where $t \in \mathbb{N}_{a+1-\nu}$, $0 < \nu \leq 1$, $f_i : \mathbb{R}^2 \longrightarrow \mathbb{R}, 1 \leq i \leq 2$, $(b_{ij}) \in \mathbb{R}^{3\times 3}$ is the linear part of the drive system, $g_i : \mathbb{R}^3 \longrightarrow \mathbb{R}, 1 \leq i \leq 3$, are nonlinear functions, and u_i, $i = 1, 2, 3$, are controllers to be designed. Based on Definition 29, we may define the co–existence of projective synchronization (PS), FSHPS and generalized synchronization (GS) for the coupled systems (8.108) and (8.109) as follows.

Definition 30. It is said that PS, FSHPS and GS co–exist in the synchronization of the drive system (8.108) and the response systems (8.109) if there exist a controller $U = (u_i)_{1\leq i\leq 3}$, a constant $\gamma \in \mathbb{R}^*$, a constant matrix $\Phi = (\Phi_{ij})_{1\times 2}$, and nonlinear map $\phi : \mathbb{R}^2 \longrightarrow \mathbb{R}$ such that the synchronization errors

$$\begin{cases}
e_1(t) = y_1(t) - \gamma x_1(t), \\
e_2(t) = y_2(t) - \Phi \times (x_1(t), x_2(t))^T, \\
e_3(t) = y_3(t) - \phi(x_1(t), x_2(t)),
\end{cases} \tag{8.110}$$

all satisfy the asymptotic rule

$$\lim_{t\to+\infty}\|e_i(t)\|=0 \quad \text{for } i=1,2,3. \tag{8.111}$$

Remark 21. From the error system (8.110), it is obvious that states y_1 and x_1 are projective synchronized, y_2 is full state hybrid projective synchronized with x_1 and x_2, and y_3 is generalized synchronized with x_1 and x_2.

Next, we propose control laws that achieve the co–existence rule (8.110). Let us define the matrix $B=(b_{ij})_{3\times3}$.

Theorem 8.7. *PS, FSHPS and GS co–exist for the pair (8.108)–(8.109) subject to*

$$\begin{cases} u_1=\sum_{j=1}^{3}(c_{1j}-b_{1j})e_j(t)-\sum_{j=1}^{3}b_{1j}y_j(t)-g_1(Y(t+\nu-1))+\gamma f_1(X(t+\nu-1)),\\ u_2=\sum_{j=1}^{3}(c_{2j}-b_{2j})e_j(t)-\sum_{j=1}^{3}b_{2j}y_j(t)-g_2(Y(t+\nu-1))+\Phi_1 f_1(X(t+\nu-1))\\ \qquad\qquad +\Phi_1 f_2(X(t+\nu-1)),\\ u_3=\sum_{j=1}^{3}(c_{3j}-b_{3j})e_j(t)-\sum_{j=1}^{3}b_{3j}y_j(t)-g_3(Y(t+\nu-1))+{}^{C}\Delta^{\nu}\phi(x_1(t),x_2(t)), \end{cases} \tag{8.112}$$

where $C=(c_{ij})_{3\times3}$ is a constant matrix chosen such that all the eigenvalues λ_i of $B-C$ satisfies

$$-2^{\nu}<\lambda_i<0, \quad i=1,2,3. \tag{8.113}$$

Proof. The difference equations corresponding to the error system (8.110) are given by

$$\begin{cases} {}^{C}\Delta_a^{\nu}e_1(t)={}^{C}\Delta_a^{\nu}y_1(t)-\gamma\,{}^{C}\Delta_a^{\nu}x_1(t),\\ {}^{C}\Delta_a^{\nu}e_2(t)={}^{C}\Delta_a^{\nu}y_2(t)-\Phi\,{}^{C}\Delta_a^{\nu}(x_1(t),x_2(t))^{T},\\ {}^{C}\Delta_a^{\nu}e_3(t)={}^{C}\Delta_a^{\nu}y_3(t)-{}^{C}\Delta_a^{\nu}\phi(x_1(t),x_2(t)). \end{cases} \tag{8.114}$$

Substituting the system nonlinearities yields

$$\begin{cases} {}^{C}\Delta_a^{\nu}e_1(t)=\sum_{j=1}^{3}b_{1j}y_j(t+\nu-1)+g_1(Y(t+\nu-1))+u_1-\gamma f_1(X(t+\nu-1)),\\ {}^{C}\Delta_a^{\nu}e_2(t)=\sum_{j=1}^{3}b_{2j}y_j(t+\nu-1)+g_2(Y(t+\nu-1))+u_2-\Phi_1 f_1(X(t+\nu-1)),\\ {}^{C}\Delta_a^{\nu}e_3(t)=\sum_{j=1}^{3}b_{3j}y_j(t+\nu-1)+g_3(Y(t+\nu-1))+u_3-{}^{C}\Delta_a^{\nu}\phi(x_1(t),x_2(t)). \end{cases} \tag{8.115}$$

Substituting the proposed control law (8.112) in (8.115) yields

$$\begin{cases} {}^{C}\Delta_a^{\nu}e_1(t)=\sum_{j=1}^{3}(b_{1j}-c_{1j})e_j(t+\nu-1),\\ {}^{C}\Delta_a^{\nu}e_2(t)=\sum_{j=1}^{3}(b_{2j}-c_{2j})e_j(t+\nu-1),\\ {}^{C}\Delta_a^{\nu}e_3(t)=\sum_{j=1}^{3}(b_{3j}-c_{3j})e_j(t+\nu-1). \end{cases} \tag{8.116}$$

In order to show that the zero solution of (8.117) is globally asymptotically stable, we use the linearization method as described in Theorem 8.7. The error system (8.116) can be written in the compact form

$${}^{C}\Delta_a^{\nu}e(t)=(B-C)e(t+\nu-1). \tag{8.117}$$

where $e(t)=(e_1(t),e_2(t),e_3(t))^{T}$. According to condition (8.113), it is easy to see that all the eigenvalues of the matrix $B-C$ satisfy $|\arg\lambda_i|=\pi>\frac{\nu\pi}{2}$ and $|\lambda_i|<\left(2\cos\frac{|\arg\lambda_i|-\pi}{2-\nu}\right)^{\nu}$, for $i=1,2,3$. It, then, follows immediately from Theorem 7.1 that the zero solution of (8.117) is globally asymptotically stable and consequently, systems (8.108) and (8.109) are synchronized in 3–dimensions according to Definition 30. □

8.7.3 Co–existence of IFSHPS and inverse generalized synchronization

We, now, would like to achieve similar results for the inverse synchronization types listed in Definition 29. Consider the drive and response pair of the form

$$\begin{cases} {}^{C}\Delta_{a}^{\nu}x_{i}\left(t\right)=\sum_{j=1}^{2}a_{ij}x_{j}\left(t+\nu-1\right)+f_{i}\left(X\left(t+\nu-1\right)\right), & i=1,2,\\ {}^{C}\Delta_{a}^{\nu}y_{i}\left(t\right)=g_{i}\left(Y\left(t+\nu-1\right)\right)+u_{i}, & i=1,2,3, \end{cases} \tag{8.118}$$

where $t\in\mathbb{N}_{a+1-\nu}$, $A=(a_{ij})\in\mathbb{R}^{2\times2}$ and $f_{i}:\mathbb{R}^{2}\rightarrow\mathbb{R}$, $1\leq i\leq2$, are nonlinear functions.and $g_{i}:\mathbb{R}^{3}\rightarrow\mathbb{R}$, $1\leq i\leq3$. Based on Definition 29, we can state what is meant by the co–existence of IFSHPs and inverse generalized synchronization (IGS) for (8.118) as summarized in the following definition.

Definition 31. IFSHPS and IGS are said to co–exist in the synchronization of the pair (8.118) if there exist controllers u_{i}, $i=1,2,3$, a constant matrix $\Theta=(\Theta_{ij})_{1\times3}$, and a map $\varphi:\mathbb{R}^{3}\longrightarrow\mathbb{R}$ such that the synchronization errors

$$\begin{cases} e_{1}\left(t\right)=x_{1}\left(t\right)-\Theta\times\left(y_{1}\left(t\right),y_{2}\left(t\right),y_{3}\left(t\right)\right)^{T},\\ e_{2}\left(t\right)=x_{2}\left(t\right)-\varphi\left(y_{1}\left(t\right),y_{2}\left(t\right),y_{3}\left(t\right)\right), \end{cases} \tag{8.119}$$

all satisfy the asymptotic rule

$$\lim_{t\rightarrow+\infty}e_{i}\left(t\right)=0\ \text{ for }i=1,2. \tag{8.120}$$

Remark 22. From the error system (8.119), it is apparent that x_{1} is inverse full state hybrid projective synchronized with $y_{1}\left(t\right)$, $y_{2}\left(t\right)$ and $y_{3}\left(t\right)$, and that $x_{2}(t)$ is inverse generalized synchronized with $y_{1}\left(t\right)$, $y_{2}\left(t\right)$ and $y_{3}\left(t\right)$.

Suppose that the function φ can be factorized in the form

$$\varphi\left(y_{1}\left(t\right),y_{2}\left(t\right),y_{3}\left(t\right)\right)=\sum_{j=1}^{3}\theta_{j}y_{j}\left(t\right)+\psi\left(y_{1}\left(t\right),y_{2}\left(t\right),y_{3}\left(t\right)\right), \tag{8.121}$$

where $\theta_{j},j=1,2,3$, are real numbers and $\psi:\mathbb{R}^{3}\rightarrow\mathbb{R}$ is a nonlinear function. The error dynamics (8.119) yield the difference equations

$$\begin{cases} {}^{C}\Delta_{a}^{\nu}e_{1}\left(t\right)= {}^{C}\Delta_{a}^{\nu}x_{1}\left(t\right)-\Theta_{1}\ {}^{C}\Delta_{a}^{\nu}y_{1}\left(t\right)-\Theta_{2}\ {}^{C}\Delta_{a}^{\nu}y_{2}\left(t\right)\\ \qquad\qquad -\Theta_{3}\ {}^{C}\Delta_{a}^{\nu}y_{3}\left(t\right),\\ {}^{C}\Delta_{a}^{\upsilon}e_{2}\left(t\right)= {}^{C}\Delta_{a}^{\nu}x_{2}\left(t\right)-\theta_{1}\ {}^{C}\Delta_{a}^{\nu}y_{1}\left(t\right)-\theta_{2}\ {}^{C}\Delta_{a}^{\nu}y_{2}\left(t\right)\\ \qquad\qquad -\theta_{3}\ {}^{C}\Delta_{a}^{\nu}y_{3}\left(t\right)-\ {}^{C}\Delta_{a}^{\nu}\psi\left(y_{1}\left(t\right),y_{2}\left(t\right),y_{3}\left(t\right)\right). \end{cases} \tag{8.122}$$

To simplify the equations, we can define

$$R_{1}=\sum_{j=1}^{2}a_{1j}x_{j}\left(t\right)+f_{1}\left(X\left(t\right)\right)-\sum_{j=1}^{3}\Theta_{j}g_{i}\left(Y\left(t\right)\right), \tag{8.123}$$

and

$$R_2 = \sum_{j=1}^{2} a_{2j} x_j \left(t+\nu-1\right) + f_2\left(X\left(t\right)\right) - \sum_{j=1}^{3} \theta_j g_i\left(Y\left(t\right)\right) - \ {}^{C}\Delta_a^{\nu}\psi\left(y_1\left(t\right), y_2\left(t\right), y_3\left(t\right)\right). \tag{8.124}$$

Using (8.123) and (8.124), (8.122) may be written in the reduced form

$$\begin{cases} {}^{C}\Delta_a^{\nu} e_1\left(t\right) = R_1 - \sum_{j=1}^{3} \Theta_j u_j, \\ {}^{C}\Delta_a^{\nu} e_2\left(t\right) = R_2 - \sum_{j=1}^{3} \theta_j u_j, \end{cases} \tag{8.125}$$

or more compactly as

$${}^{C}\Delta_a^{\nu} e\left(t\right) = R - M \times \left(u_1, u_2\right)^T - \left(\Theta_3 u_3, \theta_3 u_3\right)^T, \tag{8.126}$$

where $R = \left(R_1, R_2\right)^T$ and

$$M = \begin{pmatrix} \Theta_1 & \Theta_2 \\ \theta_1 & \theta_2 \end{pmatrix}. \tag{8.127}$$

To establish the co–existence of IFSHPS and IGS, we assume that M is invertible and denote its inverse by M^{-1}. The control law is, then, given by

$$\left(u_1, u_2\right)^T = M^{-1} \times \left[\left(L - A\right) e\left(t\right) + R\right] \text{ and } u_3 = 0, \tag{8.128}$$

where $L \in \mathbb{R}^{2\times 2}$ is a control matrix to be determined. Substituting (8.128) into equation.(8.126), we get

$${}^{C}\Delta_a^{\nu} e\left(t\right) = \left(A - L\right) e\left(t+\nu-1\right). \tag{8.129}$$

The following result follows in a similar manner to Theorem 8.7. The proof has been omitted as it can be infered direct from that of Theorem 8.7.

Theorem 8.8. *If the control matrix L is chosen such that all the eigenvalues of $A - L$ such that $-2^{\nu} < \lambda_i < 0,\ \ i = 1, 2$, then IFSHPS and IGS co–exist for (8.118) as described in (8.119) subject to control law (8.128)*

8.7.4 Application of the co–existence synchronization

We will now put the theoretical results presented in Sections 8.7.2 and 8.7.3 to the test. Similar to the previous schemes, we consider the 2D fractional Hénon map (8.9) as the master system the 3D fractional–order generalized Hénon map (8.10) as the slave system.

The linear and nonlinear parts of the master system (8.9) and the slave system (8.10) are given by, respectively,

$$A = \begin{pmatrix} -1 & 1 \\ b_1 & -1 \end{pmatrix},\ f = \begin{pmatrix} -a_1 x_1^2\left(t\right) + 1 \\ 0 \end{pmatrix},$$

and

$$B = \begin{pmatrix} -1 & 0 & -b_2 \\ 1 & -1 & b_2 \\ 0 & 1 & -1 \end{pmatrix},\ g = \begin{pmatrix} 0 \\ 0 \\ 1 - a_2 y_3^2\left(t\right) \end{pmatrix}.$$

8.7 The Co–existence of different synchronization types in fractional–order discrete–time chaotic systems with non–identical dimensions

Example 1 . Application of the PS, FSHPS and GS synchronization

The error system for the PS, FSHPS and GS synchronization scheme was described in Definition 30. We let

$$\gamma = 3,\ \Phi = (1,3) \quad \text{and} \quad \phi\left(x_1\left(t\right), x_2\left(t\right)\right) = \left(x_1(t)x_2\left(t\right)\right). \tag{8.130}$$

Theorem 8.7 requires the selection of a control matrix C such that all the eigenvalues of $B - C$ satisfies condition (8.113). For instance, the control matrix C can be chosen as

$$C = \begin{pmatrix} 0 & 0 & 0 \\ 1 & 0 & 0 \\ 0 & 1 & 0 \end{pmatrix}. \tag{8.131}$$

Simply, we can show that all eigenvalues of $B - C$ are: $\lambda_1 = \lambda_2 = \lambda_3 = -1$ and therefore condition of Theorem 8.7 is satisfied. We can use the matrix C to construct the following controllers

$$\begin{cases} u_1 = -e_1\left(t\right) - b_2 e_3\left(t\right) + y_1\left(t\right) + b_2 y_3\left(t\right) + 3x_2\left(t\right) \\ \qquad\qquad -3x_1\left(t\right) + 3 - 3a_1 x_1^2\left(t\right), \\ u_2 = -e_2\left(t\right) + b_2 e_3\left(t\right) - b_2 y_3\left(t\right) - y_1\left(t\right) + y_2\left(t\right) - 2x_2\left(t\right) \\ \qquad\qquad + \left(3b_1 - 1\right) x_1\left(t\right) + 1 - a_1 x_1^2\left(t\right) \\ u_3 = -e_3\left(t\right) - 1 - y_2\left(t\right) + a_2 y_3^2\left(t\right) + y_3\left(t\right) \\ \qquad\qquad + {}^{C}\Delta_a^{\nu} x_1(t) x_2\left(t\right). \end{cases} \tag{8.132}$$

These controllers leads to the simplified error system

$$\begin{cases} {}^{C}\Delta_a^{\nu} e_1\left(t\right) = -e_1\left(t+\nu-1\right) - b_2 e_3\left(t+\nu-1\right), \\ {}^{C}\Delta_a^{\nu} e_2\left(t\right) = -e_2\left(t+\nu-1\right) + b_2 e_3\left(t+\nu-1\right), \\ {}^{C}\Delta_a^{\nu} e_3\left(t\right) = -e_3\left(t+\nu-1\right). \end{cases} \tag{8.133}$$

Figure 8.9 shows the errors as functions of time for the initial values $\left(e_1\left(0\right), e_2\left(0\right), e_3\left(0\right)\right) = \left(0.1, 0.2, 0.5\right)$. Clearly, the errors converge towards the zero solution implying that the three slave states are PS–FSHPS–GS synchronized.

Example 2 . Application of of IFSHPS and IGS

The second case is concerned with the co–existence of IFSHPS and IGS in 2D. The error system is defined according to Definition 31 where

$$\Theta = (1,0,3) \text{ and } \varphi\left(y_1\left(t\right), y_2\left(t\right), y_3\left(t\right)\right) = y_1\left(t\right) + y_2\left(t\right) + y_3^2\left(t\right). \tag{8.134}$$

Following the approach of Section 8.7.3, we start with a factorization of φ as

$$\varphi\left(y_1\left(t\right), y_2\left(t\right), y_3\left(t\right)\right) = \sum_{j=1}^{3} \theta_j y_j\left(t\right) + \psi\left(y_1\left(t\right), y_2\left(t\right), y_3\left(t\right)\right). \tag{8.135}$$

It can be easily shown that

$$\left(\theta_1, \theta_2, \theta_3\right) = (1,2,0) \text{ and } \psi\left(y_1\left(t\right), y_2\left(t\right), y_3\left(t\right)\right) = y_3^2\left(t\right), \tag{8.136}$$

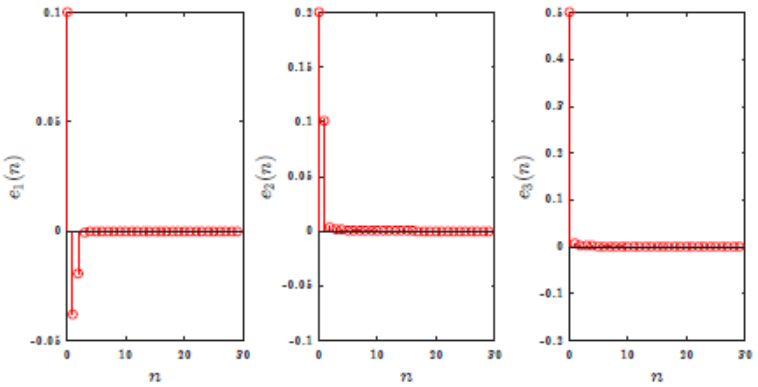

Figure 8.9: The evolution of errors over time for Example 1

are sufficient. The proposed synchronization scheme rearranges Θ and $(\theta_1, \theta_2, \theta_3)$ into the matrix

$$M = \begin{pmatrix} 1 & 0 \\ 1 & 2 \end{pmatrix}, \tag{8.137}$$

which is invertible with inverse

$$M^{-1} = \begin{pmatrix} 1 & 0 \\ -\frac{1}{2} & \frac{1}{2} \end{pmatrix}. \tag{8.138}$$

Theorem 8.8 requires the choice of a matrix L. This may be achieved with

$$L = \begin{pmatrix} 1 & \frac{13}{4} \\ b_1 - 1 & -2 \end{pmatrix}. \tag{8.139}$$

The controllers can, thus, be constructed according to (8.128) based on R_1 and R_2 defined in (8.123) and (8.124), respectively. We end up with

$$\begin{cases} u_1(t) = -2e_1 - \frac{9}{4}e_2 + x_2(t) - x_1(t) - a_1 x_1^2(t) + y_1(t) \\ \qquad\qquad + (b_2+3)\, y_3(t) - 2 - 3y_2(t) + 3a_2 y_3^2(t), \\ u_2(t) = \frac{3}{2}e_1 + \frac{13}{8}e_2 - y_1(t) + \frac{5}{2}y_2(t) - \left(\frac{3}{2} + b_2\right) y_3(t) \\ \qquad\qquad -x_2(t) + \frac{(b_1+1)}{2}x_1(t) + \frac{1}{2}a_1 x_1^2(t) \\ \qquad\qquad -\frac{3a_2}{2}y_3^2(t) - \frac{1}{2}{}^{C}\Delta^{\nu} y_3^2(t) + 1, \\ u_3(t) = 0. \end{cases} \tag{8.140}$$

and

$$\begin{cases} {}^{C}\Delta_a^{\nu} e_1(t) = -2e_1(t+\nu-1) - \frac{9}{4}e_2(t+\nu-1), \\ {}^{C}\Delta_a^{\nu} e_2(t) = e_1(t+\nu-1) + e_2(t+\nu-1). \end{cases} \tag{8.141}$$

It is easy to from Figure 8.10 that the errors converge towards zero in sufficient time proving that the controllers (8.140) in fact achieve IFSHPS–IGS synchronization for the pair (8.9)-(8.10). The initial conditions for (8.141) were set to $(e_1(0), e_2(0)) = (-1.6, -0.325)$.

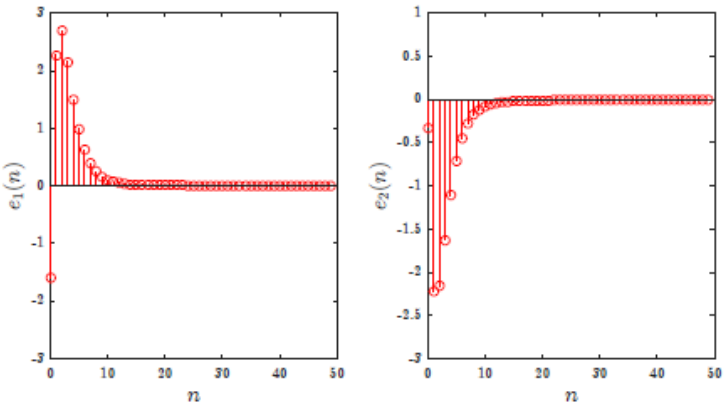

Figure 8.10: The evolution of errors over time for Example 2

8.8 Combined synchronization of two-dimensional fractional maps

8.8.1 Master system and slave systems

Based on previous considerations regarding the synchronization of fractional discrete-time systems, in this chapter we study the combined synchronization between fractional chaotic maps in 2D and 3D. Based on stability of linear fractional-order discrete-time systems and nonlinear control laws, combined synchronization schemes are presented. In this paragraph a master-slave systems based on two-dimensional fractional maps is considered. In particular, we consider the slave system as a combination between the fractional Lorenz map and the fractional flow map, where the fractional Lozi map is considered as the master system. We will indicate to the states of the master and slave systems by m and s respectively.

In the following, we consider the fractional Lozi map as the master system. The Lozi map is a two dimensional fractional map, which has been proposed in Section 4.2 as an example of fractional discrete–time system that can display chaotic behavior:

$$\begin{cases} {}^{C}\Delta_{a}^{\nu} x_{1m}(t) = -\alpha_1 \left| x_{1m}(t-1+\nu) \right| + x_{2m}(t-1+\nu) + 1 - x_{1m}(t-1+\nu), \\ {}^{C}\Delta_{a}^{\nu} x_{2m}(t) = \alpha_2 x_{1m}(t-1+\nu) - x_{2m}(t-1+\nu), \end{cases} \tag{8.142}$$

where x_{1m}, x_{2m} are the states of the master system and α_1, α_2 are parameter values. This fractional map was introduced by replacing the integer order difference operator with the μ-Caputo delta difference operator. According to Section 4.2, the proposed fractional Lozi map (8.147) has memory effects, which means that the iterated solution x_m is determined by all the previous states. Different dynamic behaviors including chaos periodic windows are observed in the fractional Lozi map (8.142).

Then, the equations of the Lorenz slave system are given by

$$\begin{cases} {}^{C}\Delta_{a}^{\nu} x_{1s_1}(t) = \beta_1\beta_2 x_{1s_1}(t-1+\nu) - \beta_2 x_{2s_1}(s-1+\mu)\, x_{1s_1}(t-1+\nu) + L_1(s-1+\mu), \\ {}^{C}\Delta_{a}^{\mu} x_{2s_1}(s) = -\beta_2 x_{2s_1}(t-1+\nu) + \beta_2 x_{1s_1}^{2}(t-1+\nu) + L_2(t-1+\nu), \end{cases} \tag{8.143}$$

where x_{1s_1} and x_{2x_1} are the system states, whereas L_1 and L_2 denote the synchronization controller. When $L_1 = L_2 = 0$ then system (8.143) degenerates into the fractional Caputo Lorenz map. This two dimensional map has been studied in Section using the μ-Caputo difference operator.

Similarly, the indices s_2 is used to denote the states of the fractional flow map, thus are given by:

$$\begin{cases} {}^{c}\Delta_a^{\nu} x_{1s_2}(t) = x_{2s_2}(t-1+\nu) + (\gamma_1 - 1)x_{1s_2}(t-1+\nu) + L_3(t-1+\nu), \\ {}^{c}\Delta_a^{\nu} x_{2s_2}(t) = \gamma_2 + x_{1s_2}^2(t-1+\nu) - x_{2s_2}(t-1+\nu) + L_4(t-1+\nu), \end{cases} \tag{8.144}$$

where the parameters $L_3(t)$ and $L_4(t)$, denote the synchronization controllers. The system (8.144) has been studied extensively in the literature and is known to exhibit a chaotic behavior for the bifurcation parameters $\gamma_1 = -0.1$, and $\gamma_2 = -1.7$.

8.8.2 Synchronization scheme

In order to made the master system (8.142) and the slave systems states (8.143)–(8.144) achieve combination synchronization, we need to define a proper controller functions $L_i \ \forall i = \overline{1.4}$. Below we are providing the combination synchronization scheme.

Definition 32. The fractional Lozi map (8.142) and the slave systems, fractional Lorenz map (8.143) and fractional flow map (8.144) are said to be combination synchronized if there exists controllers $L_i(s), i = 1, 2, 3, 4$, such that

$$\begin{cases} \lim_{s\to+\infty} ||e_1(s)|| = \lim_{s\to+\infty} ||x_{1s_1}(s) + x_{1s_2}(t) - x_{1m}(t)|| = 0, \\ \lim_{t\to+\infty} ||e_2(t)|| = \lim_{t\to+\infty} ||x_{2s_1}(t) + x_{2s_2}(t) - x_{2m}(t)|| = 0, \end{cases} \tag{8.145}$$

with $t \in \mathbb{N}_{\nu+1}$.

We propose the fallowing control law for this type of synchronization.

Theorem 8.9. *If the following control laws hold, the master system (8.142) and the combined slave systems (8.143)–(8.144) will achieve combined synchronized for any initial states:*

$$\begin{cases} L_1(t) = -(1+\beta_1\beta_2)x_{1s_1}(t) + x_{2s_1}(t) + \beta_2 x_{2s_1}(t)x_{1s_1}(t) - \alpha_1|x_{1m}(t)| + 1, \\ L_2(t) = \frac{-9}{16}x_{1s_1}(t) + \left(\alpha_2 + \frac{9}{16}\right)x_{1m}(t) + \left(\beta_2 + \frac{1}{2}\right)x_{2s_1}(t) - \beta_2 x_{1s_1}^2(t), \\ L_3(t) = -\gamma_1 x_{1s_2}(t), \\ L_4(t) = \frac{-9}{16}x_{1s_2}(t) + \frac{3}{2}x_{2s_2}(t) - \frac{3}{2}x_{2m}(t) - \gamma_2 - x_{1s_2}^2(t). \end{cases} \tag{8.146}$$

Proof. The synchronization error system (8.145) has the following form:

$$\begin{cases} {}^{C}\Delta_a^{\nu} e_1(t) = \beta_1\beta_2 x_{1t_1}(t-1+\nu) - \beta_2 x_{2s_1}(t-1+\nu)x_{1s_1}(t-1+\nu) + L_1(t-1+\nu) \\ \qquad\qquad + x_{2s_2}(t-1+\nu) + (\gamma_1 - 1)x_{1s_2}(t-1+\nu) + L_3(t-1+\nu) \\ \qquad\qquad + \alpha_1|x_{1m}(t-1+\nu)| - x_{2m}(t-1+\nu) - 1 + x_{1m}(t-1+\nu), \\ {}^{C}\Delta_a^{\nu} e_2(t) = -\beta_2 x_{2s_1}(t-1+\nu) + \beta_2 x_{1s_1}^2(t-1+\nu) + L_2(t-1+\nu) \\ \qquad\qquad + \gamma_2 + x_{1s_2}^2(t-1+\nu) - x_{2s_2}(t-1+\nu) + L_4(t-1+\nu) \\ \qquad\qquad - \alpha_2 x_{1m}(t-1+\nu) + x_{2m}(t-1+\nu). \end{cases} \tag{8.147}$$

Substituting equation (8.146) into the error system (8.147) yields the following error system:

$$\begin{cases} {}^{C}\Delta_a^{\nu} e_1(t) = -x_{1s_1}(t-1+\nu) - x_{1s_2}(t-1+\nu) + x_{1m}(t-1+\nu) \\ \qquad\qquad +x_{2s_1}(t-1+\nu) + x_{2s_2}(t-1+\nu) - x_{2m}(t-1+\nu), \\ {}^{C}\Delta_a^{\nu} e_2(t) = \frac{9}{16}\left[x_{1s_1}(t-1+\nu) + x_{1s_2}(t-1+\nu) - x_{1m}(t-1+\nu)\right] \\ \qquad\qquad +\frac{1}{2}\left[x_{2s_1}(t-1+\nu) + x_{2s_2}(t-1+\nu) - x_{2m}(t-1+\nu)\right], \end{cases} \tag{8.148}$$

and then we have:

$$\begin{cases} {}^{C}\Delta_a^{\nu} e_1(t) = -e_1(t-1+\nu) - e_2(t-1+\nu), \\ {}^{C}\Delta_a^{\nu} e_2(t) = \frac{9}{16} e_1(t-1+\nu) + \frac{1}{2} e_2(t-1+\nu). \end{cases} \tag{8.149}$$

Now, the design process reduces to demonstrate if the equilibrium $(0,0,0)$ of (8.149) is globally asymptotically stable. The two dimensional dynamical system (8.149) reduces to

$${}^{C}\Delta_a^{\nu}\left(e_1(t), e_2(t)\right)^T = A \times \left(e_1(t-1+\nu), e_2(t-1+\nu)\right)^T, \tag{8.150}$$

where

$$A = \begin{pmatrix} -1 & -1 \\ \frac{9}{16} & \frac{1}{2} \end{pmatrix}. \tag{8.151}$$

The characteristic equation of matrix A is:

$$\lambda^2 + \frac{1}{2}\lambda + \frac{1}{16} = 0. \tag{8.152}$$

It is easy to see that the eigenvalues λ_i of matrix A are negative real number, that is:

$$|\arg \lambda_i| = \pi > \frac{\nu\pi}{2}, \tag{8.153a}$$

and

$$|\lambda_i| < \left(2\cos\frac{|\arg\lambda_i| - \pi}{2-\nu}\right)^{\nu}, \quad \text{for} \;\; i = 1, 2. \tag{8.153b}$$

With Theorem 7.1 one can find that the equilibrium point $(0,0)$ is asymptotically stable. This indicate that the combined slave systems (8.143)–(8.144) are synchronized to the fractional Lozi map. The proof is thus completed. □

Here, some numerical experiments are considered to verify the effectiveness of the combined synchronization. First, the numerical solution of the two–dimensional error system is given as:

$$\begin{cases} e_1(n) = e_1(0) + \frac{1}{\Gamma(\nu)} \sum_{i=1}^{n} \frac{\Gamma(n-i+1)}{\Gamma(n-i+1)}(-e_1(i) - e_2(i)), \\ e_2(n) = e_2(0) + \frac{1}{\Gamma(\nu)} \sum_{i=1}^{n} \frac{\Gamma(n-i+1)}{\Gamma(n-i+1)}(\frac{9}{16} e_1(i) + \frac{1}{2} e_2(i)). \end{cases} \tag{8.154}$$

The bifurcation parameters are considered as above to ensure chaos. The initial value of the fractional Lozi map is set as $x_{1m}(0) = 0$, $x_{2m}(0) = 0$, and the initial values of the fractional

Lorenz map and Flow map are considered as $x_{1s_1} = 0.3, x_{2s_1} = 0.4$; $x_{1s_2} = 1, x_{2s_2} = 0.2$, respectively.

Figure 8.11 illustrate the synchronization error system (8.149) with $\mu = 0.98$. It is very clear that the error states e_1, e_2 can converge to zero when the controller functions L_1, L_2 are added to the slave systems, which implies that the combination synchronization between the master system (fractional Lozi map) is realized. Furthermore, we plot the evolution of states of the master and slave systems for the fractional order value $\nu = 0.98$. Figure 8.12 illustrates the results. Clearly, the states variable of the master and slave systems are synchronized completely. Thus, the numerical results show very well the effectiveness of the proposed combined synchronization for fractional order discrete-time systems.

8.9 Synchronization of the 2D fractional maps with no-equilibrium

Another interesting aspect in synchronization is to synchronize 2D fractional maps with no-equilibrium.
Here, we consider the fractional order discrete time system with hidden attractor presented in Section 6.3 and described by the following equation:

$$\begin{cases} {}^{C}\Delta_a^{\nu} x_m(t) = y_m(t-1+\nu) - x_m(t-1+\nu), \\ {}^{C}\Delta_a^{\nu} y_m(t) = x_m(t-1+\nu) + a_1 x_m^2(t-1+\nu) + a_2 y_m^2(t-1+\nu) \\ \qquad\qquad - a_3 x_m(t-1+\nu) y_m(t-1+\nu) - y_m(t-1+\nu) - a_4, \end{cases} \tag{8.155}$$

where a_1, a_2, a_3, a_4 are bifurcation parameters, $\nu \in (0, 1]$ is the fractional order and $t \in \mathbb{N}_{a+1-\nu}$. In the following, we refer to equation (8.155) as the master system where the subscript m in the states x and y stand for the master system. It has been shown in Section 6.3, that the fractional order discrete-time system (8.155) exhibit chaotic behaviors with no fixed points.
The slave system, thus, is given by

$$\begin{cases} {}^{C}\Delta_a^{\nu} x_s(t) = y_s(t-1+\nu) + u_1, \\ {}^{C}\Delta_a^{\nu} y_s(n) = -\alpha |y_s(t-1+\nu)| - x_s(t-1+\nu) y_s(t-1+\nu) \\ \qquad\qquad + \beta x_s^2(t-1+\nu) - \gamma y_s^2(t-1+\nu) + \delta + u_2. \end{cases} \tag{8.156}$$

Similarly, the subscripts s are used to denote the states of the slave system and the functions u_i, $i = 1, 2$, is a controller to be determined later.

In the following we present a complete synchronization scheme by designing a proper controller u, such that the error between master system (8.155) and slave system (8.156) is asymptotically stable.

8.9.1 Synchronization scheme

The aim of the synchronization process is to force the error between the master system (8.155)and slave system (8.156), defined as

$$\begin{cases} e_1 = x_s - x_m, \\ e_2 = y_s - y_m, \end{cases} \tag{8.157}$$

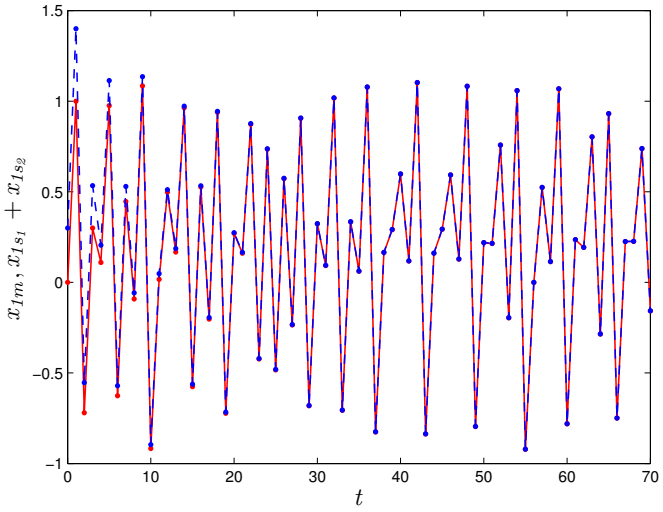

(a)

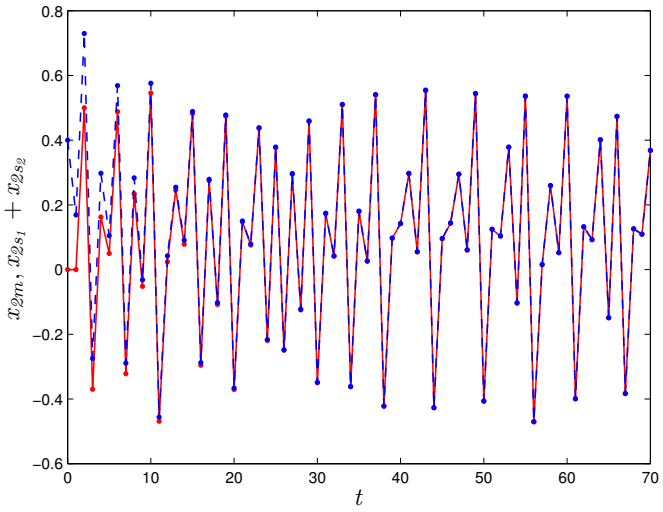

(b)

Figure 8.11: Combined synchronization error between the fractional Lozi map (8.142) and fractional Lorenz (8.143) and flow maps (8.144) with $\mu = 0.98$: (a) the first error state $e_1(s)$, (b) the second error state $e_2(s)$.

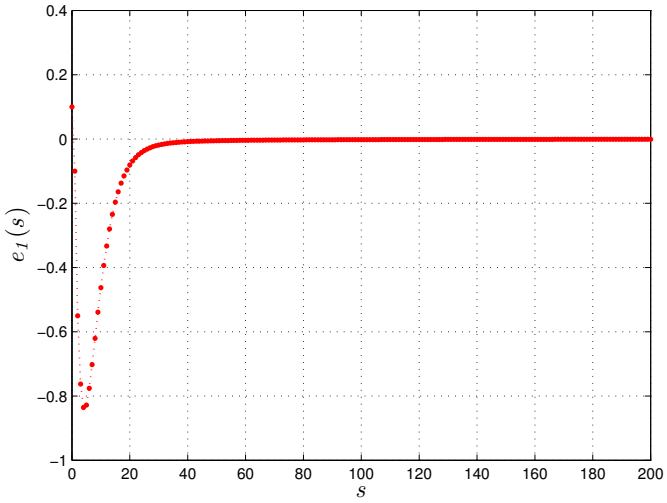

(a)

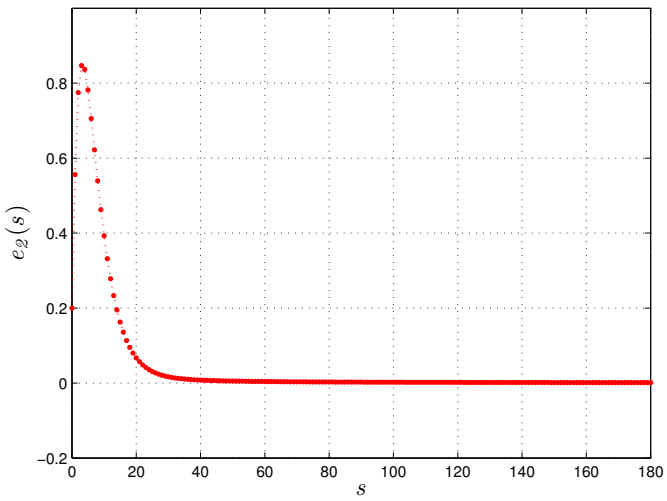

(b)

Figure 8.12: The time histories of the master system (8.142) and the slave systems (8.143)–(8.144) with $\nu = 0.98$: (a) the first state of the master system and the combined slave system. (b) The second state of the master system and the combined slave system.

to zero. To realize complete synchronization between the master and slave systems given in (8.155)- (8.156), we discuss the asymptotical stable of zero solution of synchronization error system given in (8.157). That is we find the controllers u_1 and u_2, such that the solution of the error system (8.157) go to 0 as t goes to $+\infty$. The following theorem presents our main result.

Theorem 8.10. *The master system (8.155) and the slave system (8.156) are synchronized under the following control law*

$$\begin{cases} u_1 = x_s - 2x_m, \\ u_2 = -\frac{9}{4}x_s + \frac{13}{4}x_m - 2y_s + y_m + \alpha|y_s| + x_s y_s - \beta x_s^2 \\ \qquad +\gamma y_s^2 - \delta + a_1^2 x_m + a_2 y_m^2 - a_3 x_m y_m - a_4. \end{cases} \tag{8.158}$$

Proof. The error system (8.157) has the fractional Caputo differences

$$\begin{cases} {}^C\Delta_a^\nu e_1(t) = y_s(t-1+\nu) + u_1(t) - y_m(t-1+\nu) + x_m(t-1+\nu), \\ {}^C\Delta_a^\nu e_2(t) = -\alpha|y_s(t-1+\nu)| - x_s(t-1+\nu)y_s(t-1+\nu) \\ \qquad + \beta x_s^2(t-1+\nu) - \gamma y_s^2(t-1+\nu) + \delta + u_2(t) \\ \qquad -x_m(t-1+\nu) - a_1^2 x_m(t-1+\nu) - a_2 y_m^2(t-1+\nu) \\ \qquad + a_3 x_m(t-1+\nu)y_m(t-1+\nu) + y_m(t-1+\nu) + a_4. \end{cases} \tag{8.159}$$

Substituting the control law (8.158) into (8.159) yields the reduced dynamics

$$\begin{cases} {}^C\Delta_a^\nu e_1(t) = e_1(t-1+\nu) + e_2(t-1+\nu), \\ {}^C\Delta_a^\nu e_2(t) = -\frac{9}{4}e_1(t-1+\nu) - 2e_2(t-1+\nu). \end{cases} \tag{8.160}$$

Next, we investigate that the zero equilibrium of (8.160) is globally asymptotically stable. To do that, we rewrite system (8.160) in the following compact form

$${}^C\Delta_a^\nu \left(e_1(t), e_2(t)\right)^T = \mathbf{M} \times \left(e_1(t-1+\nu), e_2(t-1+\nu)\right)^T, \tag{8.161}$$

where

$$\mathbf{M} = \begin{pmatrix} 1 & 1 \\ -\frac{9}{4} & -2 \end{pmatrix}. \tag{8.162}$$

It is easy to see that the eigenvalues of the matrix $\mathbf{M}$ satisfy the stability condition, and by means of Theorem 7.1, we know that the zero solution of (8.161) is globally asymptotically stable and consequently, the systems (8.155)–(8.156) are synchronized. □

The control laws stated in Theorem 8.10 are confirmed through numerical simulations. Figure 8.13 depcits the time evolution of the states of the master and slave systems (8.155)–(8.156) after control. Also, Figure.8.14 shows the time evolution of the error system (8.160). It is clear that the described synchronization is successful.

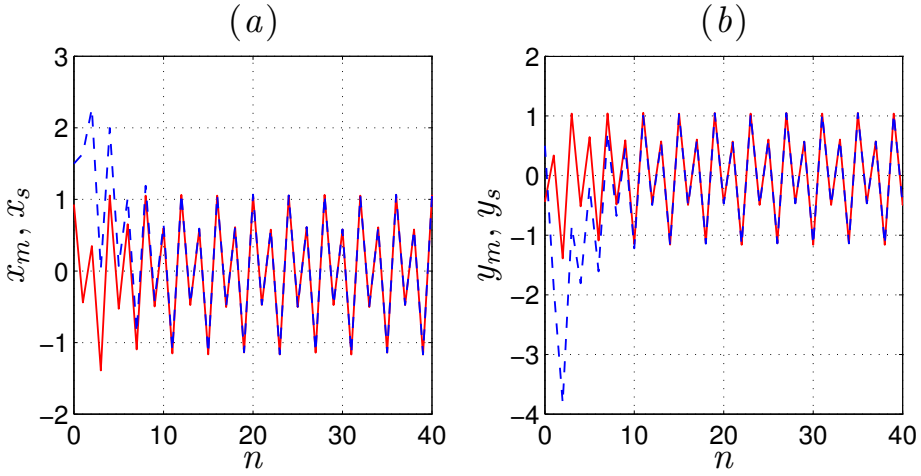

Figure 8.13: The time evolution of the states of the master and slave systems (8.155)-(8.156) after control

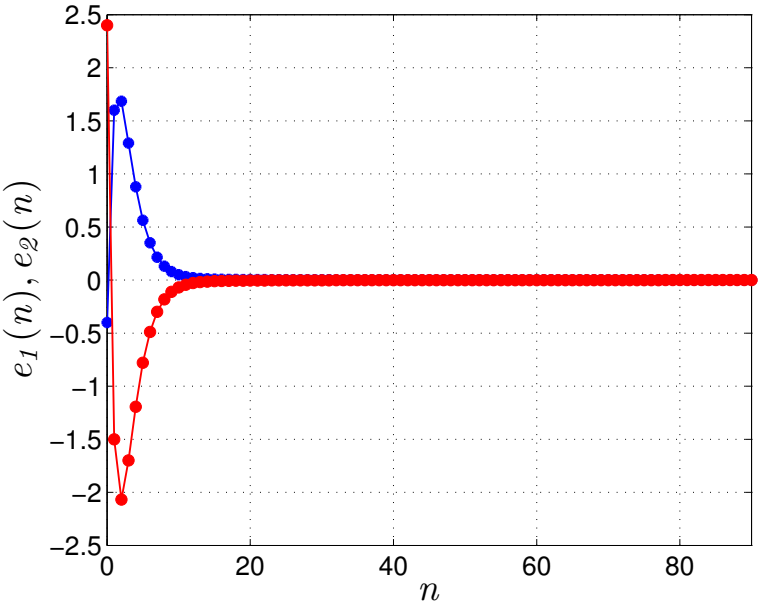

Figure 8.14: The time evolution of the error system (8.160)

8.10 Synchronization of fractional maps with no-equilibria and non identical dimensions

In this section, we discover the synchronization of three-dimensional fractional order discrete-time system with a two-dimensional fractional order discrete-time system with hidden chaotic attractors, by using an adaptive controller.
Let us consider the master system described for $t \in \mathbb{N}_{a+1-\nu}$ by

$$\begin{cases} {}^{C}\Delta_a^{\nu} x_m(t) = y_m(t-1+\nu) - x_m(t-1+\nu), \\ {}^{C}\Delta_a^{\nu} y_m(t) = x_m(t-1+\nu) + b_1 x_m^2(t-1+\nu) + b_2 y_m^2(t-1+\nu) \\ \qquad\qquad - b_3 x_m(t-1+\nu) y_m(t-1+\nu) - y_m(t-1+\nu) - b_4. \end{cases} \tag{8.163}$$

Note that the subscript m in the states refers to the master.

Similarly, the subscripts s are used to denote the states of a three-dimensional fractional order discrete-time system; which was reported in Section 6.8. The slave, thus, is given by

$$\begin{cases} {}^{C}\Delta_a^{\nu} x_s(t) = y_s(t-1+\nu) - x_s(t-1+\nu) + u_1(t-1+\nu), \\ {}^{C}\Delta_a^{\nu} y_s(t) = z_s(t-1+\nu) - y_s(t-1+\nu) + u_2(t-1+\nu), \\ {}^{C}\Delta_a^{\nu} z_s(t) = a_1 x_s(t-1+\nu) + (a_2 - 1)\, z_s(t-1+\nu) \\ \qquad\qquad + a_3 x_s(t-1+\nu) y_s(t-1+\nu) \\ \qquad\qquad + a_4 z_s^2(t-1+\nu) + a_5 + u_3(t-1+\nu), \end{cases} \tag{8.164}$$

where the functions $u_i\,(t)$ for $i = 1, 2, 3, 4$, denote the synchronization controllers. To synchronize the two-dimensional master system (8.163) and the three-dimensional slave system (8.164), we propose a new scheme of synchronization where the error system is defined as follow

$$\begin{cases} e_1\,(t) = x_s\,(t) - x_m\,(t)\,, \\ e_2\,(t) = y_s\,(t) - y_m\,(t)\,, \\ e_3\,(t) = z_s\,(t) - x_m\,(t) - y_m\,(t)\,. \end{cases} \tag{8.165}$$

The master system (8.163) and the slave system (8.164) are said to be synchronized if there exist controllers $u_1(t), u_2(t), u_3(t)$ such that $\lim_{t\to\infty} |e_i\,(t)| = 0, \quad i = 1, 2, 3$, with $t \in \mathbb{N}_{a+1-\nu}$.

The following theorem presents the proposed control law for this type of synchronization.

Theorem 8.11. *Subject to*

$$\begin{cases} u_1\,(t) = 0, \\ u_2\,(t) = -z_s(t) + x_m(t) + a_1 x_m^2(t) + a_2 y_m^2(t) - a_3 x_m(t) y_m(t) - a_4, \\ u_3\,(t) = x_m\,(t) - y_m\,(t) + b_1 x_s(t) - b_2 z_s(t) - b_3 x_s(t) y_s(t) - b_4 z_s^2(t) \\ \qquad\qquad - b_5 + a_1 x_m^2(t) + a_2 y_m^2(t) - a_3 x_m(t) y_m(t) - a_4, \end{cases} \tag{8.166}$$

the master system (8.163) and the slave system (8.164) are synchronized.

Proof. The error system (8.165) has the fractional order Caputo differences

$$\begin{cases} {}^{C}\Delta_a^{\nu} e_1(t) = y_s(t-1+\nu) - x_s(t-1+\nu) + u_1(t-1+\nu) \\ \qquad\qquad -y_m(t-1+\nu) + x_m(t-1+\nu), \\ {}^{C}\Delta_a^{\nu} e_2(t) = z_s(t-1+\nu) - y_s(t-1+\nu) + u_2(t-1+\nu) \\ \qquad\qquad -x_m(t-1+\nu) - \alpha_1^2 x_m(t-1+\nu) - \beta_2 y_m^2(t-1+\nu) \\ \qquad\qquad + \gamma_3 x_m(t-1+\nu) y_m(t-1+\nu) + y_m(t-1+\nu) + \delta_4, \\ {}^{C}\Delta_a^{\nu} e_2(t) = a_1 x_s(t-1+\nu) + (a_2-1) z_s(t-1+\nu) \\ \qquad\qquad +a_3 x_s(t-1+\nu) y_s(t-1+\nu) \\ \qquad\qquad +a_4 z_s^2(t-1+\nu) + a_5 + u_3(t-1+\nu)_1^2 x_m(t-1+\nu) \\ \qquad\qquad -a_1 - a_2 y_m^2(t-1+\nu) + a_3 x_m(t-1+\nu) y_m(t-1+\nu) \\ \qquad\qquad +a_4. \end{cases} \tag{8.167}$$

Substituting the control law (8.166) into (8.167) yields the reduced dynamics

$${}^{C}\Delta_a^{\nu} \left(e_1(t), e_2(t), e_3(t)\right)^T = \mathbf{M} \times \left(e_1(t-1+\nu), e_2(t-1+\nu), e_3(t-1+\nu)\right)^T, \tag{8.168}$$

where

$$\mathbf{M} = \begin{pmatrix} -1 & 0 & 0 \\ 0 & -1 & 0 \\ 0 & 0 & -1 \end{pmatrix}. \tag{8.169}$$

It is easy to see that the eigenvalues of the matrix $\mathbf{M}$ satisfy the stability condition in Theorem 7.1, we know that the zero solution of (8.168) is globally asymptotically stable and consequently, the systems (8.163)–(8.164) are synchronized. □

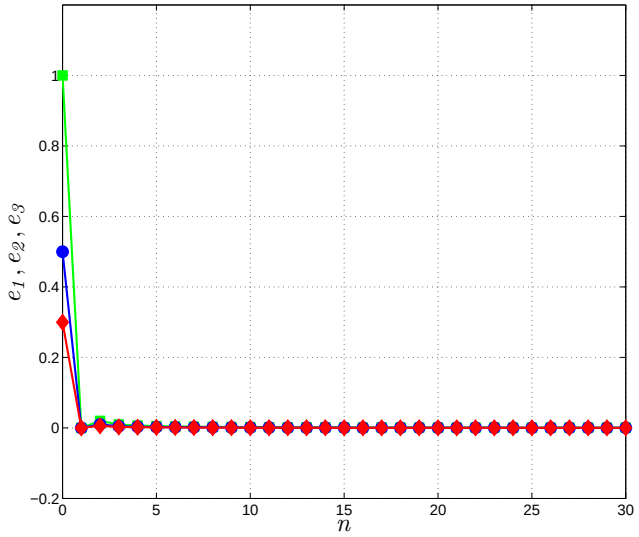

Figure 8.15: Time evolution of the synchronization errors for $\nu = 0.98$.

The control laws stated in Theorem 8.11 are confirmed through numerical simulations. Figure 8.15 depicts the time evolution of the fractional errors (8.168) subject to control law (8.166). The errors clearly converge towards zero indicating that the described combined synchronization is successful.

8.11 Conclusion

In this chapter, we have proposed control strategies for different distinct synchronization types dedicated to discrete-time fractional-order chaotic systems characterized by different dimensions. The synchronization approaches introduced in this chapter has more advantages than synchronization between one master discrete-time system and one slave discrete-time system. Also, this method can be applied to any chaotic fractional discrete-time systems define in the literature. Computer simulation results have been presented. The errors have been shown to converge towards zero in sufficient time.

General Conclusion

In this thesis, we have considered different classes of fractional order discrete time systems with *self-exited* and *hidden* attractors, and with several types of nonlinearties, for example unified and rational functions. Chaos and stability analysis in these fractional maps are investigated by the phase portraits, as well as the bifurcation diagrams and the estimation of Lyapunov exponents. The 0-1 test method is also used to confirm the chaotic regions of the systems. Furthermore, the complexity of these maps where analyzed by means of approximate entropy and C_0 algorithm. It has been found that the complexity of the proposed maps strongly depends on the variation of fractional order ν. Series of attractors of the fractional maps in different forms, including equilibrium points, limit cycles, chaotic attractors, and hyperchaotic attractors are plotted. Furthermore, bifurcations with the simultaneous variation system parameters and fractional order values are also analyzed in the three-dimensional space and the two dimensional space. It shows that both control parameter and fractional order can be treated as bifurcation parameters, but the effective chaotic range of the fractional-order system increase as the decrease of the fractional order value ν. The minimum order to yield chaos is $\nu = 0.03$, which was found for the fractional Ikeda map. Moreover, fractional order discrete time systems show rich intriguing behaviors including period-doubling route to chaos, symmetrical route to chaos, complex phase space trajectory, extreme multistability, transient states, and coexisting attractors. Also the unusual inversion property is also observed. Dynamics and complexity of the conceived maps have been analyzed in details for commensurate and incommensurate fractional order via numerical simulations.

Fractional maps have a major advantage over their conventional counterparts due to the infinite memory they feature, which allows for more flexibility in modelling and leads to a higher degree of chaotic behavior. In addition, fractional maps usually exhibit a chaotic attractor over a range of fractional orders. Namely, since fractional operators are non local, they are suitable for constructing models characterized by memory effect. This is the reason why fractional difference equation are suitable for describing economic systems based on the game theory. In Chapter 5 we have presented a novel fractional-order triopoly game with bounded rationality. By considering suitable values of the fractional order, the conducted analysis has shown that the stability of the Nash equilibrium is lost via a Neimark-Sacker bifurcation or via a flip bifurcation. It is worth noting that the introduction of more realistic models of game theory, such as the considered triopoly game based on fractional calculus, might lead to a better understanding of the economic implications in industrial organization, international trade and business cycles.

Secondly, three main families of systems with hidden attractors, systems with stable equi-

librium, systems with closed curve equilibrium points, and systems without equilibrium, have been introduced. Mathematical models of systems with hidden attractors are reported. Results show that the fractional-order three-dimensional and two dimensional maps of commensurate and incommensurate order can exhibit hidden chaotic attractors and rich complex dynamical behaviour such as coexisting hidden chaotic attractors. For instance, in Section 6.5 bifurcations and route to chaos in a fractional quadratic map without equilibria have been analyzed in details. In Section 6.6 the symmetry properties of fractional maps with rectangle shaped and square-shaped equilibria have been studied, whereas in Section 6.10 the chaotic dynamics of a three dimensional fractional map without equilibria have been studied.

Thirdly, based on the stability theory of fractional-order discrete maps, the chaos of the fractional is controlled by the stabilization controllers. Different linear and nonlinear controller laws were proposed to control the fractional Hénon lozi map and the fractional Duffing maps fractional the Stefanski map, the fractional Rössler map and the fractional Wang map. Moreover, two dimensional and three dimensional fractional order maps whith hidden attractors have been also stabilized.

Finally, Numerous types of synchronization and control strategies have been proposed in Chapter 8 in relation to fractional order discrete time systems with self exited and hidden attractors via nonlinear control laws. We have design some nonlinear controllers, which enable synchronization to be achieved between different fractional order chaotic maps with different dimensions and different orders. Nnamely we have introduce two approaches to the *generalized synchronized synchronization* and the *inverse generalized synchronization* of fractional discrete-time chaotic systems with non-identical dimensions, we then we have introduced the *full-state hybrid projective synchronisation* (FSHPS) for a fractional-order master and an integer-order slave system. Furthermore, we have also presented, combined synchronization and $Q - S$ synchronization between two different dimensional fractional discrete time systems. We have then investigated the synchronization of fractional maps with hidden attractors via nonlinear control. The convergence of the stabilized states as well as the synchronization errors towards zero was illustrated by means of numerical simulation results. The obtained results clearly show that the proposed chaos synchronization controllers are powerful in that it encompasses numerous different synchronization schemes in relation to integer-order discrete-time systems.

It is well known that chaos is closely related to secure communications and data encryption. This is mainly attributed to the random-like nature of the chaotic states and trajectories. Throughout the last three decades a vast amount of literature has erupted in relation to the use of chaos in encryption. Numerous studies have demonstrated the feasibility of using chaotic maps in the generation of pseudo-random keys that may be used with conventional encryption schemes such as the data encryption standard (DES), the advanced encryption standard (AES), etc. Fractional chaotic maps come with the added dimension of the fractional order and thus lead to a higher degree of chaotic random-like behavior. In a future work, the proposed fractional maps will be utilized to encrypt data and images and demonstrate the importance of this kind of systems. Also, due to the memory effect, the fractional calculus has been intensively used in neural networks and complex dynamic systems. Hence, in our future work we will explore potential applications of fractional chaotic neural networks, including image encryptions and pseudo-random number generators.

Bibliography

[1] Strogatz, S. H. (2018). Nonlinear dynamics and chaos with student solutions manual: With applications to physics, biology, chemistry, and engineering. CRC press.

[2] Lozi, R. (1978). Un attracteur étrange (?) du type attracteur de Hénon. Le Journal de Physique Colloques, 39(C5), C5-9.

[3] Hénon, M. A. (1976). two-dimensional mapping with a strange attractor. Comms. Math. Phys. 50, 69–77.

[4] Lorenz, E.N. (1963). Deterministic nonperiodic fow. J. Atmos. Sci.20(2), 130-141.

[5] Stefanski, K. (1998). Modelling chaos and hyperchaos with 3D maps. Chaos Solitons & Fractals **9**, 83–93.

[6] Chen, G., Mao, Y., & Chui, C. K. (2004). A symmetric image encryption scheme based on 3D chaotic cat maps. Chaos, Solitons & Fractals, 21(3), 749-761.

[7] Itoh, M., Yang, T. & Chua, L. (2001). Conditions for impulsive synchronization of chaotic and hyperchaotic systems. Int. J. Bifurcation Chaos 11, 551–558.

[8] Miller, D. A., & Grassi, G. (2001, August). A discrete generalized hyperchaotic Hénon map circuit. In Proceedings of the 44th IEEE 2001 Midwest Symposium on Circuits and Systems. MWSCAS 2001 (Cat. No. 01CH37257) (Vol. 1, pp. 328-331). IEEE.

[9] Wang, X.Y. (2003). Chaos in Complex Nonlinear Systems. Publishing House of Electronics Industry, Beijing.

[10] Aziz-Alaoui, M. A., Robert, C., & Grebogi, C. (2001). Dynamics of a Hénon–Lozi-type map. Chaos, Solitons & Fractals, 12(12), 2323-2341.

[11] Ikeda, K. (1979). Multiple-valued stationary state and its instability of the transmitted light by a ring cavity system. Optics communications, 30(2), 257-261

[12] Elhadj, Z., & Sprott, J. C. (2008). A two-dimensional discrete mapping with C^∞ multifold chaotic attractors. Electron J Theor Phys, 5(17), 107-20.

[13] Wang, X.& Chen, G. (2013). Constructing a chaotic system with any number of equilibria. Nonlinear Dyn. 71, 429–436

[14] Wang, Z., Khalaf, A. J. M., Tian, H., Alsaedi, A., & Hayat, T. (2020). A chaotic map with infinite number of equilibria in a bounded domain. The European Physical Journal Special Topics, 229, 1109-1116.

[15] Ouannas, A., & Odibat, Z. (2015). Generalized synchronization of different dimensional chaotic dynamical systems in discrete time. Nonlinear Dynamics, 81(1), 765-771.

[16] Ouannas, A., Azar, A. T., & Vaidyanathan, S. (2017). A robust method for new fractional hybrid chaos synchronization. Mathematical Methods in the Applied Sciences, 40(5), 1804-1812.

[17] Ouannas, A., & Odibat, Z. (2015). Generalized synchronization of different dimensional chaotic dynamical systems in discrete time. Nonlinear Dynamics, 81(1), 765-771.

[18] Ouannas, A., & Al-sawalha, M. M. (2016). Synchronization between different dimensional chaotic systems using two scaling matrices. Optik, 127(2), 959-963.

[19] Sprott, J.C. (2010). Elegant Chaos: Algebraically Simple Chaotic Flows; World Scientific: Singapore.

[20] Tusset, A. M., Balthazar, J. M., Rocha, R. T., Ribeiro, M. A. & Lenz, W. B. (2020). On suppression of chaotic motion of a nonlinear MEMS oscillator. Nonlinear Dyn. 99, 537-557.

[21] Bassinello, D. G., Tusset, A. M., Rocha, R. T. & Balthazar, J. M. (2018). Dynamical analysis and control of a chaotic microelectromechanical resonator model. Shock Vibration 2018, 4641629.

[22] Sambas, A., Vaidyanathan, S., Tlelo-Cuautle, E., Zhang, S., Guillen-Fernandez, O., Hidayat, Y. S. & Gundara, G. (2019). A novel chaotic system with two circles of equilibrium points: Multistability, electronic circuit and FPGA realization. Electronic, 8, 1211.

[23] Berviller, Y., Tisserand, E., Poure, P. & Rabah, H. (2020). Design and implementation of a digital dual orthogonal outputs chaotic oscillator. Electronis 2020, 9, 264.

[24] Kocarev . L & Lian. S. (2011). Chaos-based cryptography: Theory, algorithms and applications (Springer-Verlag, Berlin, Heidelberg, 2011)

[25] Cuomo, K. M, Oppenheim, A. V., & Strogatz, S. H., (1993). Synchronization in chaotic systems. Phys. Rev. Lett, 71, 65.

[26] Millerioux, G., & Daafouz, J. (2004). Unknown input observers for message-embedded chaos synchronization of discrete-time systems. Int. J. Bifurc. Chaos 14, 1357-1368.

[27] Dedieu, H., Kennedy, M. P., & Hasler, M. (1993). IEEE Trans. Circuits Syst. II: Analog Digital Signal Process. 40, 634.

[28] Tse, K. K., Ng, R. M., Chung, H. S. & S Y Ron Hui, IEEE Trans. Ind. Electron. 50, 171 (2003)

[29] Goodrich, C. & Peterson, A.C. (2015). Discrete Fractional Calculus; Springer: Berlin, Germany, ISBN 978-3-319-79809-7

[30] Ostalczyk, P. (2016). Discrete Fractional Calculus: Applications in Control and Image Processing. World Scientific.

[31] Diaz, J. B, Olser, T. J. (1974). Differences of fractional order. Math. Comput. 28, 185-202

[32] Atici, F. M., & Eloe, P. W. (2007). A transform method in discrete fractional calculus. International Journal of Difference Equations, 2(2).

[33] Agarwal, R. P. (2000). Difference equations and inequalities: theory, methods, and applications. CRC Press.

[34] Atici, F., & Eloe, P. (2009). Initial value problems in discrete fractional calculus. Proceedings of the American Mathematical Society, 137(3), 981-989.

[35] Miller, K. S., & Ross, B. (1988, May). Fractional difference calculus. In Proceedings of the international symposium on univalent functions, fractional calculus and their applications (pp. 139-152).

[36] Atici, F. M., & Sengul, S. (2010). Modeling with fractional difference equations. Journal of Mathematical Analysis and Applications, 369(1), 1-9.

[37] Abdeljawad, T. (2013). On delta and nabla Caputo fractional differences and dual identities. Discrete Dynamics in Nature and Society, 2013.

[38] Bohner, M., & Peterson, A. C. (Eds.). (2002). Advances in dynamic equations on time scales. Springer Science & Business Media.

[39] Holm, M. T. (2011). The theory of discrete fractional calculus: Development and application.

[40] Abdeljawad, T. & Baleanu, D. (2011). Fractional Differences and Integration by Parts. Journal of Computational Analysis & Applications, 13(3).

[41] Abdeljawad, T. (2011). On Riemann and Caputo fractional differences. Computers & Mathematics with Applications, 62(3), 1602-1611.

[42] Caputo, M. (1967). Linear models of dissipation whose Q is almost frequency independent–II. Geophysical Journal International, 13(5), 529-539.

[43] Anastassiou, G. A. (2011). About discrete fractional calculus with inequalities. In Intelligent mathematics: computational analysis (pp. 575-585). Springer, Berlin, Heidelberg.

[44] Mozyrska, D., & Girejko, E. (2013). Overview of fractional h-difference operators. In Advances in harmonic analysis and operator theory (pp. 253-268). Birkhäuser, Basel.

[45] Ferreira, R. A., & Torres, D. F. (2011). Fractional h-difference equations arising from the calculus of variations. Applicable Analysis and Discrete Mathematics, 110-121.

[46] Elaydi, S. N. (2000). An Introduction to Difference Equations. Springer Nature.

[47] Mozyrska, D., & Wyrwas, M. (2015). The-transform method and delta type fractional difference operators. Discrete Dynamics in Nature and Society, 2015.

[48] Fulai, C., Xiannan, L., & Yong, Z. (2011). Existence results for nonlinear fractional difference equation. J. Advances in Difference Equations, 2011(1), 1-12.

[49] Mozyrska, D., Girejko, E., & Wyrwas, M. (2013). Comparison of h-Difference Fractional Operators. In Advances in the theory and applications of non-integer order systems, 191-197.

[50] Bohner, M., & Peterson, A. (2001). Dynamic equations on time scales: An introduction with applications. Springer Science & Business Media.

[51] Holm, M. T. (2011). The Laplace transform in discrete fractional calculus. Computers & Mathematics with Applications, 62(3), 1591-1601.

[52] Kelley, W. G., & Peterson, A. C. (2001). Difference equations: an introduction with applications. Academic press.

[53] Mozyrska, D., & Girejko, E. (2013). Overview of fractional h-difference operators. In Advances in harmonic analysis and operator theory (pp. 253-268). Birkhäuser, Basel.

[54] Verhulst, F. (2006). Nonlinear differential equations and dynamical systems. Springer Science & Business Media.

[55] Cermák, J., Gyori, I., & Nechvátal, L. (2015). On explicit stability conditions for a linear fractional difference system. Fractional Calculus and Applied Analysis, 18(3), 651.

[56] Wu, G. C., Baleanu, D., & Luo, W. H. (2017). Lyapunov functions for Riemann-Liouville-like fractional difference equations. Applied Mathematics and Computation, 314, 228-236.

[57] Wu, G. C., Baleanu, D., & Huang, L. L. (2018). Novel Mittag-Leffler stability of linear fractional delay difference equations with impulse. Applied Mathematics Letters, 82, 71-78.

[58] Abu-Saris, R., & Al-Mdallal, Q. (2013). On the asymptotic stability of linear system of fractional-order difference equations. Fractional Calculus and Applied Analysis, 16(3), 613-629.

[59] Chen, F. (2011). Fixed points and asymptotic stability of nonlinear fractional difference equations. Electronic Journal of Qualitative Theory of Differential Equations, 2011(39), 1-18.

[60] Dzielinski, A., & Sierociuk, D. (2005, November). Adaptive feedback control of fractional order discrete state-space systems. In International conference on computational intelligence for modelling, control and automation and international conference on intelligent agents, web technologies and internet commerce (cimca-iawtic'06) (Vol. 1, pp. 804-809). IEEE.

[61] Baleanu, .D, Wu, G. C, Bai, Y. R. & Chen, F. L. (2017). Stability analysis of Caputo–like discrete fractional systems, Commun Nonlinear Sci Numer Simulat, 48, 520-530.

[62] Petras, I. (2011). Fractional-order nonlinear systems: modeling, analysis and simulation. Springer Science & Business Media.

[63] Ott, E. (2002). Chaos in dynamical systems. Cambridge university press.

[64] Vulpiani, A., Cecconi, F., & Cencini, M. (2009). Chaos: from simple models to complex systems (Vol. 17). World Scientific.

[65] Ruelle, D. (Ed.). (1995). Turbulence, strange attractors and chaos (Vol. 16). World Scientific.

[66] Eckmann, J. P., & Ruelle, D. (1985). Ergodic theory of chaos and strange attractors. The theory of chaotic attractors, 273-312.

[67] Zaslavsky, G. M. (2005). Long way from the FPU-problem to chaos. Chaos: An Interdisciplinary Journal of Nonlinear Science, 15(1), 015103.

[68] Devaney, R. L., Siegel, P. B., Mallinckrodt, A. J., & McKay, S. (1993). A first course in chaotic dynamical systems: theory and experiment. Computers in Physics, 7(4), 416-417.

[69] Banks, J., Brooks, J., Cairns, G., Davis, G., & Stacey, P. (1992). On Devaney's definition of chaos. The American mathematical monthly, 99(4), 332-334.

[70] Gleick, J. (2011). Chaos: Making a new science. Open Road Media.

[71] Effah-Poku, S., Obeng-Denteh, W., & Dontwi, I. K. (2018). A Study of Chaos in Dynamical Systems. Journal of Mathematics, 2018.

[72] Lorenz, E. N. (1963). Deterministic nonperiodic flow. Journal of atmospheric sciences, 20(2), 130-141.

[73] Moysis, L., & Azar, A. T. (2017). New discrete time 2D chaotic maps. International Journal of System Dynamics Applications (IJSDA), 6(1), 77-104.

[74] Ruelle, D. (1981). Small random perturbations of dynamical systems and the definition of attractors. Communications in Mathematical Physics, 82(1), 137-151.

[75] Verhulst, P. F. (1845). Recherches mathématiques sur la loi d'accroissement de la population. Journal des économistes, 12, 276.

[76] Peitgen, H. O., Jurgens, H. & Saupe, D. (2004). Chaos and Fractals New Frontiers of Science, Springer.

[77] Lyapunov, A. M. (1992). The general problem of the stability of motion. International journal of control, 55(3), 531-534.

[78] Oseledec, V. I. (1968). Multiplicative ergodic theorem.

[79] Benettin, G., Galgani, L., Giorgilli, A. et al. Lyapunov Characteristic Exponents for smooth dynamical systems and for hamiltonian systems; a method for computing all of them. Part 1: Theory. Meccanica 15, 9–20 (1980).

[80] Benettin, G., Galgani, L., Giorgilli, A. et al. Lyapunov Characteristic Exponents for smooth dynamical systems and for hamiltonian systems; A method for computing all of them. Part 2: Numerical application. Meccanica 15, 21–30, (1980)

[81] De Souza, S. L., & Caldas, I. L. (2004). Calculation of Lyapunov exponents in systems with impacts. Chaos, Solitons & Fractals, 19(3), 569-579.

[82] Eckmann, J. P., & Ruelle, D. (1992). Fundamental limitations for estimating dimensions and Lyapunov exponents in dynamical systems. Physica D: Nonlinear Phenomena, 56(2-3), 185-187.

[83] Wolf, A., Swift, J. B., Swinney, H. L., & Vastano, J. A. (1985). Determining Lyapunov exponents from a time series. Physica D: Nonlinear Phenomena, 16(3), 285-317.

[84] Vallejo, J. C., Sanjuan, M. A., & Sanjuan, M. A. (2017). Predictability of chaotic dynamics. Springer International Publishing.

[85] Geist, K., Parlitz, U., & Lauterborn, W. (1990). Comparison of different methods for computing Lyapunov exponents. Progress of theoretical physics, 83(5), 875-893.

[86] Wu, G. C., & Baleanu, D. (2015). Jacobian matrix algorithm for Lyapunov exponents of the discrete fractional maps. Communications in Nonlinear Science and Numerical Simulation, 22(1-3), 95-100.

[87] Wang, X. (2013). Calculation of negative Lyapunov exponents using a time series for potentially stable robotic systems.

[88] Hu, T. (2014). Discrete chaos in fractional Hénon map. Applied Mathematics, 2014.

[89] Gottwald, G. A., & Melbourne, I. (2004). A new test for chaos in deterministic systems. Proceedings of the Royal Society of London. Series A: Mathematical, Physical and Engineering Sciences, 460(2042), 603-611.

[90] Gottwald, G. A., & Melbourne, I. (2016). The 0-1 test for chaos: A review. Chaos detection and predictability, 221-247.

[91] Gottwald, G. A., & Melbourne, I. (2009). On the implementation of the 0–1 test for chaos. SIAM Journal on Applied Dynamical Systems, 8(1), 129-145.

[92] Cafagna, D., & Grassi, G. (2008). Bifurcation and chaos in the fractional-order Chen system via a time-domain approach. International Journal of Bifurcation and Chaos, 18(07), 1845-1863.

[93] En-hua, S., Zhi-jie, C., & Fan-ji, G. (2005). Mathematical foundation of a new complexity measure. Applied Mathematics and Mechanics, 26(9), 1188-1196.

[94] Cai, Z. J. & Sun, J. (2008). Modified C_0 complixity and applications. Journal of Fudan University. 47(6), 791-79

[95] He, S., Sun, K., & Wang, H. (2016). Solution and dynamics analysis of a fractional-order hyperchaotic system. Mathematical Methods in the Applied Sciences, 39(11), 2965-2973.

[96] Ran, J. (2018). Discrete chaos in a novel two-dimensional fractional chaotic map. Advances in Difference Equations, 2018(1), 1-12.

[97] Eckmann, J. P. & Ruelle, D. (1985). Ergodic theory of chaos and strange attractors. The theory of chaotic attractors, 273-312.

[98] Pincus, S. M. (1991). Approximate entropy as a measure of system complexity. Proceedings of the National Academy of Sciences, 88(6), 2297-2301.

[99] Pincus, S. (1995). Approximate entropy (ApEn) as a complexity measure. Chaos: An Interdisciplinary Journal of Nonlinear Science, 5(1), 110-117.

[100] Wang, C., & Ding, Q. (2018). A new two-dimensional map with hidden attractors. Entropy, 20(5), 322.

[101] Xu, G., Shekofteh, Y., Akgül, A., Li, C.,& Panahi, S. (2018). A new chaotic system with a self-excited attractor: entropy measurement, signal encryption, and parameter estimation. Entropy, 20(2), 86.

[102] Restrepo, J. F., Schlotthauer, G., & Torres, M. E. (2014). Maximum approximate entropy and r threshold: A new approach for regularity changes detection. Physica A: Statistical Mechanics and its Applications, 409, 97-109.

[103] Wu, G. C., & Baleanu, D. (2014). Discrete fractional logistic map and its chaos. Nonlinear Dynamics, 75(1), 283-287.

[104] Gottwald, G. A., & Melbourne, I. (2009). On the implementation of the 0-1 test for chaos. SIAM Journal on Applied Dynamical Systems, 8(1), 129-145.

[105] Khennaoui, A. A., Almatroud, O. A., Ouannas, A., Al-sawalha, M. M., Grassi, G. & Pham, V. T. (2021). The effect of caputo fractional difference operator on a novel game theory model. Discrete & Continuous Dynamical Systems-B, 22(11).

[106] Edelman, M., Macau, E. E., & Sanjuan, M. A. (Eds.). (2018). Chaotic, fractional, and complex dynamics: new insights and perspectives. Springer International Publishing.

[107] Peng, Y., Sun, K., He, S.,Wang, L. (2019). Comments on "Discrete fractional logistic map and its chaos" [Nonlinear Dyn. 75, 283–287 (2014)]. Nonlinear Dyn., 97(1), 897-901.

[108] Ge, Z. M., & Ou, C. Y. (2007). Chaos in a fractional order modified Duffing system. Chaos, Solitons & Fractals, 34(2), 262-291.

[109] Hartley, T. T., Lorenzo, C. F., & Qammer, H. K. (1995). Chaos in a fractional order Chua's system. IEEE Transactions on Circuits and Systems I: Fundamental Theory and Applications, 42(8), 485-490.

[110] Zeraoulia, E.; Sprott, J.C. A unified piecewise smooth chaotic mapping that contains the Hénon and the Lozi systems. Ann. Rev. Chaos Theory Bifurcations Dyn. Syst. 2012, 1, 50-60.

[111] Khennaoui, A. A., Ouannas, A., Bendoukha, S., Wang, X.,& Pham, V. T. (2018). On chaos in the fractional-order discrete-time unified system and its control synchronization. Entropy, 20(7), 530.

[112] Botella-Soler, V., Castelo, J. M., Oteo, J. A., & Ros, J. (2011). Bifurcations in the Lozi map. Journal of Physics A: Mathematical and Theoretical, 44(30), 305101.

[113] Elhadj, Z. (2013). Lozi Mappings: Theory and Applications. CRC Press.

[114] Elhadj, Z., & Sprott, J. C. (2009). The discrete hyperchaotic double scroll. International Journal of Bifurcation and Chaos, 19(03), 1023-1027.

[115] Parks, P. C. (1986). JMT Thompson, HB Stewart, Non-Linear Dynamics and Chaos, John Wiley & Sons, Chichester (1986), 376; Price 16.

[116] Dignowity, D., Wilson, M., Rangel-Fonseca, P., & Aboites, V. (2013). Duffing spatial dynamics induced in a double phase-conjugated resonator. Laser Physics, 23(7), 075002.

[117] Mahdi, A., Jawad, A. K., & Hreshee, S. S. (2016). Digital chaotic scrambling of voice based on duffing map. International Journal of Information and Communication Sciences, 1(2), 16-21.

[118] Ouannas, A., Khennaoui, A. A., Wang, X., Pham, V. T., Boulaaras, S., & Momani, S. (2020). Bifurcation and chaos in the fractional form of Hénon-Lozi type map. The European Physical Journal Special Topics, 229(12), 2261-2273.

[119] Hasan, M. M., Faruqi, T. M., Tazrean, M., & Chowdhury, T. H. (2017, September). Biometric encryption using Duffing map. In 2017 4th International Conference on Advances in Electrical Engineering (ICAEE) (pp. 737-742). IEEE.

[120] Ouannas, A., Khennaoui, A. A., Momani, S., & Pham, V. T. (2020). The discrete fractional duffing system: Chaos, 0-1 test, C 0 complexity, entropy, and control. Chaos: An Interdisciplinary Journal of Nonlinear Science, 30(8), 083131.

[121] Sprott, J. C., & Xiong, A. (2015). Classifying and quantifying basins of attraction. Chaos: An Interdisciplinary Journal of Nonlinear Science, 25(8), 083101.

[122] Gasri, A., Ouannas, A., Khennaoui, A. A., Bendoukha, S., & Pham, V. T. (2020). On the dynamics and control of fractional chaotic maps with sine terms. International Journal of Nonlinear Sciences and Numerical Simulation, 21(6), 589-601.

[123] Ikeda, K., Daido, H., & Akimoto, O. (1980). Optical turbulence: chaotic behavior of transmitted light from a ring cavity. Physical Review Letters, 45(9), 709.

[124] Ouannas, A., Khennaoui, A. A., Odibat, Z., Pham, V. T., & Grassi, G. (2019). On the dynamics, control and synchronization of fractional-order Ikeda map. Chaos, Solitons & Fractals, 123, 108-115.

[125] Lu, J. A., Wu, X., Lu, J., & Kang, L. (2004). A new discrete chaotic system with rational fraction and its dynamical behaviors. Chaos, Solitons & Fractals, 22(2), 311-319.

[126] Rulkov, N. F. (2002). Modeling of spiking-bursting neural behavior using two-dimensional map. Physical Review E, 65(4), 041922.

[127] Chen, G., Mao, Y., & Chui, C. K. (2004). A symmetric image encryption scheme based on 3D chaotic cat maps. Chaos, Solitons & Fractals, 21(3), 749-761.

[128] Wang, C. & Ding, Q. (2018). A New Two-Dimensional Map with Hidden Attractors, Entropy, 20, 2018.

[129] Khennaoui, A. A., Ouannas, A., Grassi, G., Pham, V. T., & Volos, C. (2019, May). On Fractional Forms of Modified and Generalized Arnold Mappings. In 2019 8th International Conference on Modern Circuits and Systems Technologies (MOCAST) (pp. 1-4). IEEE.

[130] He, S., Sun, K., & Wang, H. (2015). Complexity analysis and DSP implementation of the fractional-order Lorenz hyperchaotic system. Entropy, 17(12), 8299-8311.

[131] Ouannas, A., Khennaoui, A. A., Bendoukha, S., Wang, Z., & Pham, V. T. (2020). The Dynamics and Control of the Fractional Forms of Some Rational Chaotic Maps. Journal of Systems Science and Complexity, 33(3), 584-603.

[132] Chang, L., Lu, J., & Deng, X. (2005). A new two-dimensional discrete chaotic system with rational fraction and its tracking and synchronization, Chaos, Solitons & Fractals, 24, 1135-1143.

[133] Zeraoulia, E., & Sprott, J. (2011). On the dynamics of a new simple 2D rational discrete mapping, Int. J. Bifur. Chaos. 21(1): 1–6.

[134] Jouini, L., Ouannas, A., Khennaoui, A. A., Wang, X., Grassi, G., & Pham, V. T. (2019). The fractional form of a new three-dimensional generalized Hénon map. Advances in Difference Equations, 2019(1), 1-12.

[135] Zheng, J., Wang,Z., Li, Y., & Wang, J. Bifurcations and chaos in a three-dimensional generalized Hénon map.

[136] Gonchenko, S. V., Ovsyannikov, I. I., Simó, C. & Turaev, D. V. (2005). Three-dimensional Hénon-like map and wild Lorenz-like attractors. International Journal of Bifurcation and Chaos, 15(11), 3493–3508.

[137] Gonchenko, S. V., Gonchenko, V. S. & Tatjar, J. C. (2007). Bifurcation of three-dimensional diffeomorphisms non-simple quadratic homoclinic tangencies and generalized Hénon maps, Regul. Chaotic Dyn. 12(3), 233-266.

[138] Gonchenko, S. V., Shilnikov, L. P., & Turaev, D. V. (2009). On global bifurcations in three-dimensional diffeomorphisms leading to wild Lorenz-like attractors, Regul. Chaotic Dyn. 14(1), 137-147.

[139] Ouannas, A., Khennaoui, A. A., Grassi, G., & Bendoukha, S. (2019). On chaos in the fractional-order Grassi-Miller map and its control. Journal of Computational and Applied Mathematics, 358, 293-305.

[140] Ouannas A. & Grassi G. (2016). A new approach to study co-existence of some synchronization types between chaotic maps with different dimensions, Nonlinear Dynamics.86 (2) , 1319-1328.

[141] Ouannas, A., Azar, A.T & Abu-Saris, R. (2017) A new type of hybrid synchronization between arbitrary hyperchaotic maps, Intenational journal of Learning Machine and Cybernitic, 8 , 1887.

[142] Sun H, Zhang Y, Baleanu D, Chen W, Chen Y (2018) A new collection of real world applications of fractional calculus in science and engineering. Communications in Nonlinear Science and Numerical Simulation 64:213–231

[143] Xin, B., Peng, W., & Kwon, Y. (2019). A fractional-order difference Cournot duopoly game with long memory. arXiv preprint arXiv:1903.04305.

[144] Al-khedhairi, A. (2019). Differentiated Cournot duopoly game with fractional-order and its discretization. Engineering Computations.

[145] Cournot A. Researches into the principles of the theory of wealth, Engl. Trans., Irwin Paper Back Classics in Economics (Chapter VII). Paris: Hachette, 1963.

[146] Khennaoui, A. A., Ouannas, A., Bendoukha, S., Grassi, G., Lozi, R. P., & Pham, V. T. (2019). On fractional–order discrete–time systems: Chaos, stabilization and synchronization. Chaos, Solitons & Fractals, 119, 150-162.

[147] Khennaoui, A. A., Ouannas, A., Bendoukha, S., Grassi, G., Wang, X., Pham, V. T., & Alsaadi, F. E. (2019). Chaos, control, and synchronization in some fractional-order difference equations. Advances in Difference Equations, 2019(1), 1-23.

[148] Ouannas, A., Khennaoui, A. A., Grassi, G., & Bendoukha, S. (2019). On chaos in the fractional-order Grassi–Miller map and its control. Journal of Computational and Applied Mathematics, 358, 293-305.

[149] Ouannas, A., Khennaoui, A. A., Momani, S., & Pham, V. T. (2020). The discrete fractional duffing system: Chaos, 0-1 test, C_0 complexity, entropy, and control. Chaos: An Interdisciplinary Journal of Nonlinear Science, 30(8), 083131.

[150] Leonov, G. A., Kuznetsov, N. V., & Vagaitsev, V. I. (2012). Hidden attractor in smooth Chua systems. Physica D: Nonlinear Phenomena, 241(18), 1482-1486.

[151] Leonov, G. A., Kuznetsov, N. V., Kiseleva, M. A., Solovyeva, E. P., & Zaretskiy, A. M. (2014). Hidden oscillations in mathematical model of drilling system actuated by induction motor with a wound rotor. Nonlinear Dynamics, 77(1-2), 277-288.

[152] Leonov, G. A., & Kuznetsov, N. V. (2013). Hidden attractors in dynamical systems. From hidden oscillations in Hilbert-Kolmogorov, Aizerman, and Kalman problems to hidden chaotic attractor in Chua circuits. International Journal of Bifurcation and Chaos, 23(01), 1330002.

[153] Sharma, P. R., Shrimali, M. D., Prasad, A., Kuznetsov, N. V., & Leonov, G. A. (2015). Controlling dynamics of hidden attractors. International Journal of Bifurcation and Chaos, 25(04), 1550061..

[154] Wei, Z. (2011). Dynamical behaviors of a chaotic system with no equilibria. Physics Letters A, 376(2), 102-108.

[155] Panahi, S., Sprott, J. C., & Jafari, S. (2018). *Two simplest quadratic chaotic maps without equilibrium.* International Journal of Bifurcation and Chaos, 28(12), 1850144.

[156] Jiang, H., Liu, Y., Wei, Z., & Zhang, L. (2016). Hidden chaotic attractors in a class of two-dimensional maps. Nonlinear dynamics, 85(4), 2719-2727.

[157] Jafari, S., Pham, V. T., Golpayegani, S. M. R. H., Moghtadaei, M., & Kingni, S. T. (2016). The relationship between chaotic maps and some chaotic systems with hidden attractors. International Journal of Bifurcation and Chaos, 26(13), 1650211.

[158] Jiang, H., Liu, Y., Wei, Z., & Zhang, L. (2016). A new class of three-dimensional maps with hidden chaotic dynamics. International Journal of Bifurcation and Chaos, 26(12), 1650206.

[159] Panahi, S., Sprott, J. C., & Jafari, S. (2018). Two simplest quadratic chaotic maps without equilibrium. International Journal of Bifurcation and Chaos, 28(12), 1850144.

[160] Khennaoui, A. A., Ouannas, A., Odibat, Z., Pham, V. T., & Grassi, G. (2020). On the Three-Dimensional Fractional-Order Hénon Map with Lorenz-Like Attractors. International Journal of Bifurcation and Chaos, 30(11), 2050217.

[161] Jiang, H., Liu, Y., Wei, Z., & Zhang, L. (2019). A New Class of Two-Dimensional Chaotic Maps with Closed Curve Fixed Points. International Journal of Bifurcation and Chaos, 29(07), 1950094.

[162] Sprott, J. C. (2010). Elegant chaos: algebraically simple chaotic flows. World Scientific.

[163] Hadjabi, F., Ouannas, A., Shawagfeh, N., Khennaoui, A. A., & Grassi, G. (2020). On Two-Dimensional Fractional Chaotic Maps with Symmetries. Symmetry, 12(5), 756.

[164] Ouannas, A., Wang, X., Khennaoui, A. A., Bendoukha, S., Pham, V. T., & Alsaadi, F. E. (2018). Fractional form of a chaotic map without fixed points: Chaos, entropy and control. Entropy, 20(10), 720.

[165] Khennaoui, A. A., Ouannas, A., Boulaaras, S., Pham, V. T., & Taher Azar, A. (2020). A fractional map with hidden attractors: chaos and control. The European Physical Journal Special Topics, 229, 1083-1093.

[166] Ouannas, A., Khennaoui, A. A., Momani, S., Grassi, G., & Pham, V. T. (2020). Chaos and control of a three-dimensional fractional order discrete-time system with no equilibrium and its synchronization. AIP Advances, 10(4), 045310.

[167] Ouannas, A., Khennaoui, A. A., Momani, S., Pham, V. T., & El-Khazali, R. (2020). Hidden attractors in a new fractional–order discrete system: Chaos, complexity, entropy, and control. Chinese Physics B, 29(5), 050504.

[168] Ouannas, A., Almatroud, O. A., Khennaoui, A. A., Al-sawalha, M. M., Baleanu, D., Huynh, V. V., & Pham, V. T. (2020). Bifurcations, Hidden Chaos and Control in Fractional Maps. Symmetry, 12(6), 879.

[169] Ouannas, A., Khennaoui, A. A., Momani, S., Grassi, G., Pham, V. T., El-Khazali, R., & Vo Hoang, D. (2020). A Quadratic Fractional Map without Equilibria: Bifurcation, 0–1 Test, Complexity, Entropy, and Control. Electronics, 9(5), 748.

[170] Huynh, V. V., Ouannas, A., Wang, X., Pham, V. T., Nguyen, X. Q., & Alsaadi, F. E. (2019). Chaotic map with no fixed points: entropy, implementation and control. Entropy, 21(3), 279. tems with non-identical dimensions. Advances in Difference Equations, 2018(1), 1-14.

[171] T. Hu, Discrete Chaos in Fractional Henon Map, Appl. Math., Vol. 5 (2014), pp. 2243–2248.

[172] Wu, G. C., & Baleanu, D. (2014). Chaos synchronization of the discrete fractional logistic map. Signal processing, 102, 96-99.

[173] Liu, Y. (2016). Chaotic synchronization between linearly coupled discrete fractional Hénon maps. Indian Journal of Physics, 90(3), 313-317.

[174] Wu, G. C., Baleanu, D., Xie, H. P., & Chen, F. L. (2016). Chaos synchronization of fractional chaotic maps based on the stability condition. Physica A: Statistical Mechanics and its Applications, 460, 374-383.

[175] Shukla, M. K., & Sharma, B. B. (2017). Investigation of chaos in fractional order generalized hyperchaotic Henon map. AEU-International Journal of Electronics and Communications, 78, 265-273.

[176] Khennaoui, A. A., Ouannas, A., Bendoukha, S., Grassi, G., Wang, X., & Pham, V. T. (2018). Generalized and inverse generalized synchronization of fractional-order discrete-time chaotic systems with non-identical dimensions. Advances in Difference Equations, 2018(1), 1-14.

[177] Zhang, G., Liu, Z., & Ma, Z. (2007). Generalized synchronization of different dimensional chaotic dynamical systems. Chaos, Solitons & Fractals, 32(2), 773-779.

[178] Terry, J.R., VanWiggeren, G.D. Chaotic communication using generalized synchronization. Chaos Solitons Fractals 12(1), 145–152 (2001)

[179] Hitzl, D. L., & Zele, F. (1985). An exploration of the Hénon quadratic map. Physica D: Nonlinear Phenomena, 14(3), 305-326.

[180] Wang, C., Chu, R., & Ma, J. (2015). Controlling a chaotic resonator by means of dynamic track control. Complexity, 21(1), 370-378.

[181] Yan, Z. (2005). $Q-S$ (lag or anticipated) synchronization backstepping scheme in a class of continuous-time hyperchaotic systems–a symbolic-numeric computation approach. Chaos: An Interdisciplinary Journal of Nonlinear Science, 15(2), 023902.

[182] Yan, Z. (2005). $Q-S$ synchronization in 3D Hénon-like map and generalized Hénon map via a scalar controller. Physics Letters A, 342(4), 309-317.

[183] Ouannas, A., Odibat, Z., & Shawagfeh, N. (2019). A new Q–S synchronization results for discrete chaotic systems. Differential Equations and Dynamical Systems, 27(4), 413-422.

[184] Hu, M., & Xu, Z. (2008). A general scheme for $Q-S$ synchronization of chaotic systems. Nonlinear Analysis: Theory, Methods & Applications, 69(4), 1091-1099.

[185] Zhao, J., & Ren, T. (2010). Q–S synchronization between chaotic systems with double scaling functions. Nonlinear Dynamics, 62(3), 665-672.

[186] Zhao, J., & Zhang, K. (2010). A general scheme for Q–S synchronization of chaotic systems with unknown parameters and scaling functions. Applied Mathematics and Computation, 216(7), 2050-2057.

[187] Ouannas, A., Azar, A. T., & Vaidyanathan, S. (2017). On a simple approach for Q-S synchronisation of chaotic dynamical systems in continuous-time. International Journal of Computing Science and Mathematics, 8(1), 20-27.

[188] Ouannas, A., & Abu-Saris, R. (2015). A Robust Control Method for Synchronization between Different Dimensional Integer-Order and Fractional-Order Chaotic Systems. Journal of Control Science and Engineering, 2015.

[189] Ouannas, A., Pham, V. T., Abdelmalek, S., Ziar, T., & Boubaker, O. (2018, March). Q-S Chaos Synchronization Between Fractional-Order Master and Integer-Order Slave Systems. In 2018 15th International Multi-Conference on Systems, Signals & Devices (SSD) (pp. 1150-1154). IEEE.

[190] Khennaoui, A. A., Almatroud, A. O., Ouannas, A., Al-sawalha, M.M., Grassi, G., Pham, V. T. & Batiha, I. M. (2021). An Unprecedented 2-Dimensional Discrete-Time Fractional-Order System and Its Hidden Chaotic Attractors. Mathematical Problems in Engineering, 2021.

[191] Bendoukha, S., Ouannas, A., Wang, X., Khennaoui, A. A., Pham, V. T., Grassi, G., & Huynh, V. V. (2018). The co-existence of different synchronization types in fractional-order discrete-time chaotic systems with non–identical dimensions and orders. Entropy, 20(9), 710.

[192] Ouannas A. & Al-Sawalha M.M., A new approach to synchronize different dimensional chaotic maps using two scaling matrices, Nonlinear Dynamics and Systems Theory, 2015, 15(4), 400–408.

[193] Ouannas A. & Al–sawalha M.M., Synchronization between different dimensional chaotic systems using two scaling matrices, Optik, 2016, 127, 959–963.

[194] Khennaoui, A. A., Ouannas, A., Bendoukha, S., Grassi, G., Wang, X., & Pham, V. T. (2018). Generalized and inverse generalized synchronization of fractional-order discrete-time chaotic systems with non-identical dimensions. Advances in Difference Equations, 2018(1), 1-14.

[195] Ouannas, A., Khennaoui, A. A., Bendoukha, S., Grassi, G. (2019). On the Dynamics and Control of a Fractional Form of the Discrete Double Scroll International. Journal of Bifurcation and Chaos 29 (06), 1950078.

[196] Ouannas, A., Khennaoui, A. A., Zehrour, ., Bendoukha, S., Grassi, G., Pham, V. T. (2019) . Synchronisation of integer-order and fractional-order discrete-time chaotic systems. Pramana 92 (4), 52.

Abstract

In this graduation thesis entitled as *Chaos, Control and Synchronization of Discrete Fractional Systems*, we have considered different classes of fractional order discrete time systems with *self-excited* and *hidden attractors*. The proposed systems are defined using Caputo-like difference operator, where there dynamics are investigated numerically using, phase portraits, bifurcation diagrams, Lyapunov exponents, 0-1 test, approximate entropy and C_0 complexity. The main motivation behind this thesis is to assess the benefits of the fractional-order maps, where the asymptotic convergence of the states are established by means of the stability theory of linear fractional discrete systems. In addition, we have studied the existence of chaos and its control and synchronization, where different dimensional nonlinear and linear control laws are proposed for stabilizing at the origin the chaotic dynamics of the proposed systems. The design of these control laws are derived based on the linearisation method. Some nonlinear controller are designed, which enable synchronization to be achieved between different fractional order chaotic maps with different dimensions.

As a conclusive remark, we would point out that the main contributions and innovations of the thesis can be summarized as follows, novel fractional-order discrete time systems based on the Caputo ν-difference operator, chaos synchronization using linear and nonlinear control laws, and chaos stabilization based on very simple controllers.

Keywords: Chaos, Control, Synchronization, Discrete fractional calculus, Bifurcation, Hidden dynamics, Caputo-like difference operator

Résumé

Dans cette thèse de fin d'étude, nous avons considéré différentes classes des systèmes discrets d'ordre fractionnaire. Les systèmes proposées sont définis en utilisant l'opérateur de différence "Caputo", où leur comportement est étudier numériquement au moyen de phase portraits, diagrammes de bifurcation, les exposant du Lyapunov, 0-1 test, C_0 complexité et l'entropie approximative. L'objectif essentiel derrière cette thèse consiste à évaluer les avantages des systèmes discrets d'ordre fractionnaire, où la convergence asymptotique des états est établie au moyen de la théorie du stabilité des systèmes linéaires discrets d'ordre fractionnaire. En outre, nous avons étudié l'existence du chaos et son contrôle et sa synchronisation, où différents lois de contrôle linéaire et non linéaire sont proposée pour stabiliser à l'origine le comportements chaotique des systèmes proposer. La conception de ces lois sont dérivé sur la base de la méthode du linéarisation.

On conclusion, nous soulignons que la contributions principale de la thèse peut étre résumée comme suit, nouveaux systèmes discrets d'ordre fractionnaire définir a partir de l'opérateur de différence ν-Caputo, synchronisation du chaos a l'aide des lois du contrôle linéaire et non linéaire et stabilisation du comportement chaotique de tels systèmes en utilisant des lois de contrôle très simple.

Mot-Clés : Chaos, Contrôl, Synchronisation, Calcule fractionnaire discrets, Bifurcation, L'opérateur de différence Caputo.

ملخص

في هذه الأطروحة قمنا بتعريف عدة أنظمة متقطعة ذات أس كسري باستعمال معامل الكسري المتقطع كبوتو, حيث قمنا بدراسة رقميا تأثير الأس الكسري على الخصائص الديناميكية لهذه الأنظمة باستعمال, رسومات الجواذب, التشعبات, أسس ليابونوف, اختبار 0-1 و دراسة تعقيد باستعمال أونتروبي.

إن الهدف الرئيسي من هذه الأطروحة هو تلخيص خصائص هذه الأنظمة المتقطعة ذات الأس الكسري, أين قد استعملنا نظريات الاستقرار للأنظمة الخطية المتقطعة ذات الأس الكسري لدراسة الاستقرار. إضافة لذلك لقد قمنا بدراسة الفوضى و استقرارها و مزامنتها اين قمنا باقتراح عدة قوانين خطية و غير خطية.

كملاحظة ختامية، نود أن نشير إلى أن المساهمات والابتكارات الرئيسية للأطروحة يمكن تلخيصها على النحو التالي، أنظمة زمنية منفصلة ذات ترتيب كسري جديد تعتمد على معامل متقطع كابوتو.

مزامنة الفوضى باستخدام قوانين التحكم الخطية وغير الخطية والتخلص من الفوضى على أساس قوانين تحكم بسيط للغاية.

الكلمات المفتاحية

نضرية الفوضى, تشعبات, جواذب مخفية, مزامنة, الحساب الكسري المتقطع.